OPEN ACCESS

University of BRISTOL

This electronic thesis or dissertation has been downloaded from Explore Bristol Research, http://research-information.bristol.ac.uk

Author:
Anson, Richard

Title:
The study of an active landslide in the Swainswick Valley, north of Bath.

General rights
Access to the thesis is subject to the Creative Commons Attribution - NonCommercial-No Derivatives 4.0 International Public License. A copy of this may be found at https://creativecommons.org/licenses/by-nc-nd/4.0/legalcode This license sets out your rights and the restrictions that apply to your access to the thesis so it is important you read this before proceeding.

Take down policy
Some pages of this thesis may have been removed for copyright restrictions prior to having it been deposited in Explore Bristol Research. However, if you have discovered material within the thesis that you consider to be unlawful e.g. breaches of copyright (either yours or that of a third party) or any other law, including but not limited to those relating to patent, trademark, confidentiality, data protection, obscenity, defamation, libel, then please contact collections-metadata@bristol.ac.uk and include the following information in your message:

• Your contact details
• Bibliographic details for the item, including a URL
• An outline nature of the complaint

Your claim will be investigated and, where appropriate, the item in question will be removed from public view as soon as possible.

THE STUDY OF AN ACTIVE LANDSLIDE IN THE SWAINSWICK VALLEY, NORTH OF BATH

BY

RICHARD ANSON

THESIS SUBMITTED FOR
THE DEGREE OF DOCTOR OF PHILOSOPHY
UNIVERSITY OF BRISTOL
1996

ABSTRACT

This thesis describes both field and laboratory based investigations of an active landslide in the Fuller's Earth adjacent to Soper's Wood, in the Swainswick valley, north of Bath.

A detailed field study and monitoring programme provided evidence of the changing morphology and the controls which affect the rate of movement of an inland landslide. In addition, the effects of landslide activity in enhancing the weathering grade, moisture content and geotechnical indices of the Fuller's Earth was studied. Geochemical analysis of ground water samples demonstrated the dominance of calcium with subordinate magnesium and potassium. It is proposed that these originate from the dissolution of impure calcium carbonate and the depotassification of illite by acidic ground waters. A representative sample of a shear surface was obtained from the landslide to investigate the nature of the failure "plane" and whether chemical weathering was occurring at a greater rate along shear surfaces due to the preferential percolation of acidic ground waters.

To compliment these studies, laboratory based testing was carried out to determine the effects of calcium in pore water on the residual shear strength and Atterberg limits of clays, using "pure" montmorillonite and kaolinite. The results indicate these parameters are sensitive to the concentration of calcium in pore water.

From these investigations, a model for the long term and seasonal stability of the landslide at Soper's Wood has been developed. The model emphasises the dominance of rainfall and ground water levels as the main controls on seasonal slope stability and indicates that the inherent residual shear strength of failure "planes" should be considered a dynamic property, showing seasonal variation dependent on the concentration of calcium in the ground water. In the long term, it is expected that the depotassification of illite and the dissolution of calcite will cause a gradual reduction in the inherent residual shear strength of the failure "planes", which will promote instability.

ACKNOWLEDGEMENTS

I would like to express my gratitude to Dr. Brian Hawkins for providing the opportunity to undertake this research and for his invaluable supervision and editorial expertise. This gratitude is extended to Dr. Chris McDonald for his enthusiasm, help and encouragement throughout the project.

A special thanks is extended to Pete Forrest for his friendship, advice and assistance in the field.

Mr. Gould of View Point Farm is thanked for allowing continual access to the fields adjacent to Soper's Wood.

Thanks to all my field assistants who were often dragged out for surveying at short notice, especially Jo Collins, Matt Hilton, Jonny Keeling, Robby Narbett and Justin Wilson. The work at Soper's Wood has also benefited from Adam Fisher's undergraduate project.

The head of department is acknowledged for the provision of facilities and equipment within the Geology Department. The technical staff have been of considerable help and thanks is extended to Wayne Bowery, Andrew Hook, Mike Overs, Simon Powell, Gary Webber and Fred Wheeler. I would like to thank Tony Kemp for his invaluable advice and support with the geochemistry.

This research has benefited from the loan of surveying equipment from the Department of Civil Engineering and the use of their soil mechanics laboratory. I would particularly like to thank Mike Pope, Roy Samson, Martin Lings, Derek Knight and David Nash.

The department of geography supplied me with essential equipment for ground water analysis and I am very grateful to Richard Newman and Dave King for their help and advice.

I would also like to thank my post graduate colleagues for their friendship and encouragement during the course of this project.

Finally a special thanks to my parents for their encouragement and support.

MEMORANDUM

This thesis is the result of independent research undertaken at the Department of Geology, University of Bristol, under the supervision of Dr. A.B. Hawkins. Any previously published or unpublished work used is given full acknowledgement.

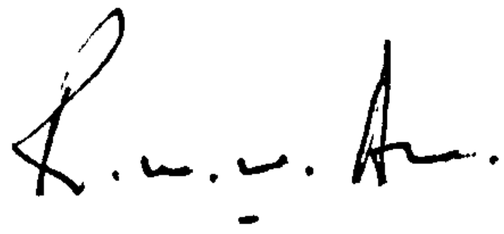

Richard Anson
1996

TABLE OF CONTENTS

	Page
1 A REVIEW OF THE GEOLOGY AND TOPOGRAPHY OF THE SWAINSWICK VALLEY, BATH; WITH EMPHASIS ON THE FULLER'S EARTH FORMATION	
1.1 Introduction	1
1.2 General Geology of the Swainswick valley	1
1.3 A Review of the Geology and Engineering Properties of the Fuller's Earth Formation	7
1.3.1 The Geology of the Fuller's Earth Formation	7
1.3.2 The Clay Mineralogy of the Fuller's Earth Formation	9
1.3.3 The Geotechnical Properties of the Fuller's Earth Formation and the Effects of Weathering	15
1.4 Topographic Setting and the Development of Superficial Structures	19
1.4.1 The Topography of the Swainswick Valley	20
1.4.2 Superficial Structures in the Swainswick valley	22
1.4.3 The Development of the City of Bath	24
1.5 Aims of this Research	25
2 RESIDUAL SHEAR STRENGTH	27
2.1 Introduction	27
2.2 Early Observations of Residual Shear Strength	27
2.3 Later Developments	29
2.4 The Residual Shear Strength of the Landslipped Mudrocks and Clays of the Fuller's Earth Formation	37
2.5 Influences of Pore Water Chemistry on the Residual Shear Strength of Soils	40
2.6 Conclusions	51

3 A DETAILED INVESTIGATION OF AN ACTIVE LANDSLIDE IN THE FIELDS TO THE SOUTH OF SOPER'S WOOD, BATH 52

3.1 Introduction 52
3.1.1 Location 53
3.1.2 Geology 53

3.2 Investigative Techniques 58
3.2.1 Engineering Geomorphological Mapping 58
3.2.2 Surveying Technique 58
3.2.3 Borehole Augering 62
3.2.4 Standpipe Installation 62
3.2.5 Ground Water Sampling 63

3.3 Slip Geomorphology 63
3.3.1 Discussion of Engineering Geomorphological Map (January 1994) 63
3.3.2 Classification of Landslides 69
3.3.3 History of Instability 71
3.3.4 Comparison with Previous Geomorphological Maps 71

3.4 Auger Hole Information 72
3.4.1 Sample Descriptions and Weathering Profile 72
3.4.2 Moisture Content Analysis 78
3.4.3 Comparison of the Index Properties of Boreholes B and C 82
3.4.4. Discussion 86

3.5 Analysis of Landslide Movement 88
3.5.1 Surveying Results 88
3.5.1.1 Summary 94
3.5.2 Comparison of Landslide Movement with Precipitation 94
3.5.2.1 Discussion 102
3.5.3 Piezometric Information 104
3.5.3.1 Discussion 108
3.5.4 Comparison of Slip Movement with Ground Water Level 108
3.5.5 General Discussion 110
3.5.6 Comparison of Geomorphological Maps at the Start and End of Movement 111

3.6 Longitudinal Slope Profile 116

3.7 Ground Water Chemistry 121
3.7.1 Ground Water Analysis 121
3.7.2 Ground Water Chemistry Variation within the Slip 124
3.7.3 Discussion 131

3.8 Conclusions 132

4 A STUDY OF A SHEAR SURFACE IN THE FULLER'S EARTH CLAY 136

4.1 Introduction 136

4.2 Field Technique 136

4.3 Sample Preparation 137

4.4 Moisture Content Analysis 141

4.5 A Comparison of Calcite Content and Moisture Content 143

4.6 Normalisation of the Moisture Content Profiles 143

4.7 Analysis of the Shear Surface by SEM 147

4.8 Mineralogy Across the Shear Surface 148

4.9 Conclusions 157

5 AN INVESTIGATION INTO THE EFFECTS OF CALCIUM IN PORE WATER ON THE RESIDUAL SHEAR STRENGTH OF CLAYS 159

5.1 Introduction 159

5.2 A Review of Clay Structure 159

5.3 Clay Mineral Chemistry 161

5.4 A Review of Calcium Carbonate Dissolution 163

5.5 The Laboratory Simulation of Calcium Carbonate Dissolution 165

5.5.1 Laboratory Technique 166

5.5.2 Experiment 1 166

5.5.3 Experiment 2 168

5.5.4 Experiment 3 168

5.5.5 Discussion of Results 170

5.6 Investigation into a New Ring Shear Technique 170

5.6.1 Multiple Shear Technique 172

5.6.2 Multiple Shear Technique with Staged Consolidation 172

5.6.3 Discussion 174

5.7 The Effects of Calcium Ions on the Residual Shear Strength of Kaolinite and Montmorillonite 174
5.7.1 Preparation of the Clays 174
5.7.1.1 Kaolinite 174
5.7.1.2 Montmorillonite 176
5.7.2 Preparation of Solutions 177
5.7.3 Experimental Technique 177
5.7.3.1 Kaolinite 177
5.7.3.2 Montmorillonite 178
5.7.3.3 Discussion 178
5.7.4 Results 179
5.7.4.1 Kaolinite 179
5.7.4.2 Montmorillonite 184
5.7.5 Discussion 191
5.8 Conclusions 200

6 A MODEL FOR THE STABILITY OF THE LANDSLIDE ADJACENT TO SOPER'S WOOD 202

6.1 Introduction 202

6.2 Long Term Controls on Slope Stability 202

6.3 Slope Stability Analyses of the Soper's Wood Landslide 206
6.3.1 Method of Analysis 206
6.3.1.1 Discussion 210
6.3.2 Conditions and Parameters 211
6.3.3 Results 213
6.3.4 Discussion of Results 213

6.4 A Generalised Model for the Seasonal Control of Slope Stability 214

6.5 Discussion 218

7 SUMMARY AND CONCLUSIONS 220

7.1 Field Investigation 220

7.2 Small Scale Analysis of a Shear Surface 226

7.3 Effects of Calcium in Pore Water on the Residual Shear Strength of Clays 227

7.4 A Model for the Stability of the Landslide Adjacent to Soper's Wood 230
7.4.1 Long Term Stability 230
7.4.2 Seasonal Stability 231

7.5 Avenues for Further Research 233

REFERENCES		235
APPENDIX I	LABORATORY TECHNIQUES	252
APPENDIX II	SURVEY DATA FOR THE LANDSLIDE ADJACENT TO SOPER'S WOOD	256
APPENDIX III	RECORDS OF GROUND WATER LEVELS FOR THE LANDSLIDE ADJACENT TO SOPER'S WOOD	263
APPENDIX IV	ENGINEEERING GEOMORPHOLOGICAL MAP OF THE LANDSLIDE ADJACENT TO SOPER'S WOOD	267

LIST OF FIGURES

		Page
Fig. 1.1	Extract from the 1:50000 "Landranger Series" Ordnance Survey map, Bristol and Bath sheet 172, showing the topography of the Swainswick valley and the surrounding area. The valley is bounded by the roads highlighted in black and the location of the landslide adjacent to Soper's Wood is indicated.	2
Fig. 1.2	Extract from the one inch Geological Survey map of Bath, sheet 265. The horizontal shading indicates foundered strata.	3
Fig. 1.3	Outcrops of the Fuller's Earth in the Bath region and sample locations: DFB = Down Farm borehole; SWB = Soper's Wood borehole; WB = Wellsway borehole; CHM = Combe Hay mine, after Hawkins *et al.* (1988).	10
Fig. 1.4	Stratigraphic log of the Soper's Wood borehole, after Hawkins *et al.* (1988), based on Lawrence (1985).	10
Fig. 1.5	Lithology and sampling levels in the Fuller's Earth Bed seam at Combe Hay mine, after Hawkins *et al.* (1986), based on Jeans *et al.* (1977).	13
Fig. 1.6	Plots showing the variation with depth of the moisture content, Atterberg limits and calcite content of the samples of the Fuller's Earth formation obtained from the Soper's Wood borehole, after Hawkins *et al.* (1988).	13
Fig. 1.7	Plots showing the variation with depth of the moisture content, Atterberg limits and calcite content of the samples of the Fuller's Earth formation obtained from the Down Farm borehole: I - IV represent weathering zones, after Hawkins *et al.* (1988).	16
Fig. 1.8	Plots showing the variation with depth of the moisture content, Atterberg limits and calcite content of the samples obtained from the Fuller's Earth Bed at the Combe Hay mine, after Hawkins *et al.* (1988).	16
Fig. 1.9	Plots of calcite content with plasticity index (A) and liquidity index (B) for the Fuller's Earth clay and the Fuller's Earth Bed, after Hawkins *et al.* (1988): solid circles = fresh to slightly weathered Fuller's Earth clay; open circles = moderately to completely weathered Fuller's Earth clay; open triangles = Fuller's Earth Bed.	18

Fig. 1.10	Plots showing the variation with depth of the Atterberg limits and calcite content of the samples of the Fuller's Earth formation obtained from the borehole at Peasedown St John, after Hawkins & McDonald (1992).	18
Fig. 1.11	Plots showing the relationship between Atterberg limits and calcite content of the samples of the Upper (open) and Lower (solid) Fuller's Earth obtained from the borehole at Peasedown St John, after Hawkins & McDonald (1992).	18
Fig. 1.12	Extract from the 1:25 000 "Pathfinder" Ordnance Survey map, Bath and Keynsham sheet 1183, with topographic cross-section across the Swainswick valley.	21
Fig 2.1	Map showing the outcrop location of the Fuller's Earth formation around Bath.	28
Fig. 2.2	Correlations between residual shear strength and plasticity index, after Lupini *et al.* (1981).	32
Fig. 2.3	Correlations between residual shear strength and clay fraction, after Lupini *et al.* (1981).	32
Fig. 2.4	Graph displaying the results of ring shear tests on sand-bentonite mixtures, after Skempton (1985) based on Lupini *et al.* (1981).	35
Fig. 2.5	Drawings, from thin section analysis, of the residual shear structures seen in the tests conducted on the Happisburgh-London clay mixtures. After Lupini *et al.* (1981).	35
Fig. 2.6	Plot of ultimate residual shear angle against calcite content for the samples obtained from the Peasedown St John borehole, after McDonald (1990).	38
Fig. 2.7	Graph showing the relationship between calcite content and ultimate residual shear angle for a progressively decalcified sample of the Upper Fuller's Earth clay, after Hawkins and McDonald (1992).	38
Fig. 2.8	Graphs showing the residual shear strength, at $\sigma'_n = 250$ kPa, of pure kaolinite and montmorillonite treated with sodium chloride and calcium chloride, after Moore (1991).	47
Fig. 2.9	Graphs showing the effect of sea water concentration upon the residual shear strength, at $\sigma'_n = 250$ kPa, of weathered and unweathered London and Weald clay, after Moore (1991).	48

Fig. 3.1	Enlarged extract (scale approximately 1:17800) from the 1:25000 'Pathfinder' Ordnance Survey map, Bath and Keynsham sheet 1183.	54
Fig. 3.2	Summary geological map of the Soper's Wood area, after Lawrence (1985). Extract from the 1:10560 Geological Survey Sheets, Gloucs. LXXVII and Soms. VIIISW.	56
Fig. 3.3	Lithostratigraphic log for the Soper's Wood borehole, Bath, after Hawkins *et al.* 1986.	57
Fig. 3.4	Map showing the location of the survey stations relative to the field boundaries in the area.	59
Fig. 3.5	Schematic diagram showing the orientation of a survey station and the use of the adapted standpipe.	59
Fig. 3.6	Illustration displaying surveying technique and calculations.	61
Fig. 3.7	Engineering geomorphological map of the landslide adjacent to Soper's Wood, January 1994. (Approximate distances from Colliers Lane are displayed down the right edge.)	64
Fig. 3.8	Geomorphological mapping symbols from Engineering Group Working Party Report (Anon 1972), apart from additional symbols.	65
Fig. 3.9	Engineering geomorphological map of landslide adjacent to Soper's Wood in 1992, after Dalwood 1992. (In order to compare this map with the 1994 map, this map has been inverted.)	73
Fig. 3.10a	Longitudinal section through the Soper's Wood landslip showing the location of the boreholes. An indication of the moisture content profiles is shown, for further details see Figure 3.10b.	79
Fig. 3.10b	Graphs displaying variations in moisture content with depth for the boreholes at Soper's Wood.	80
Fig. 3.11	Graphs comparing moisture content, Atterberg limits, plasticity index and calcite content for Boreholes B and C.	83
Fig. 3.12	Plots displaying the relationship between Atterberg limits and calcite content for boreholes B and C.	87
Fig. 3.13	Plots showing the total cumulative movement of each survey station over the period of surveying (19 January 1994 to 30 June 1994).	90

Fig. 3.14	Histogram showing daily rainfall at Woolley Farm, Bath from 1 November 1993 to 2 August 1994. The left border separating each month represents the first of the month.	96
Fig. 3.15	Graphs comparing the cumulative horizontal movement of each survey station (solid line) with cumulative rainfall (dashed line), for the period of surveying (19 January 1994 to 30 June 1994). Note the variation in vertical axis scale for cumulative horizontal movement.	98
Fig. 3.16	Graphs comparing the cumulative vertical movement of each survey station (solid line) with cumulative rainfall (dashed line), for the period of surveying (19 January 1994 to 30 June 1994). Note the variation in vertical axis scale for cumulative vertical movement.	101
Fig. 3.17	Graphs comparing ground water level (solid line) with cumulative rainfall (dashed line) for each standpipe over the period of monitoring (19 January 1994 to 3 August 1994). Note the variation in vertical axis scale for water table depth.	105
Fig. 3.18	Graphs comparing cumulative horizontal movement for survey stations A2, A3, A4 and A5 (triangle symbols) with ground water level in adjacent standpipes (square symbols) over the period of monitoring (19 January 1994 to 3 August 1994).	109
Fig. 3.19	Comparison of landslide geomorphology in January 1994 (in black) and May 1994 (in red).	112
Fig. 3.20	Transverse crack propagation in the landslide at Soper's Wood.	117
Fig. 3.21	Retrogressive scarp migration in the landslide at Soper's Wood.	117
Fig. 3.22	Longitudinal section through the landslide at Soper's Wood, March 1994.	119
Fig. 3.23	Graphs displaying calcium, magnesium and potassium concentrations in the ground water samples taken from standpipes F, B, E, C and A over the period of study.	122
Fig. 3.24	Graphs comparing the calcium concentration and the temperature of ground water samples from standpipes F, B, E, C and A, with rainfall levels over the period of study.	125

Fig. 3.25	Graphs showing the variation in calcium ion concentration, pH and temperature of the ground water samples taken from standpipes F, B, E, C and A over the period of study.	126
Fig. 3.26	Engineering geomorphological map of the landslide adjacent to Soper's Wood showing the location of the additional standpipes.	128
Fig. 3.27	Graphs showing the variation in calcium concentration, conductivity and pH of ground water samples taken from the standpipes within the landslide on the 27 May 1994.	129
Fig. 3.28	Graphs displaying the variation in calcium, magnesium and potassium levels in the ground water samples taken from the standpipes within the landslide on the 27 May 1994.	130
Fig. 4.1	Schematic plan view of the prepared slab showing the position of the shear surface and the descriptions of the various lithological units. Sample numbers for moisture and calcite content determination and XRD sample units are also displayed.	140
Fig. 4.2	Graph displaying the moisture content profile for the right edge of the "slab".	142
Fig. 4.3	Graph displaying moisture content profiles for the right and left edges of the "slab".	142
Fig. 4.4	Plot comparing the profiles for moisture content and calcite content for the right edge of the "slab".	144
Fig. 4.5	Graph demonstrating the inverse relationship between moisture content and calcite content.	144
Fig. 4.6	Graph comparing the normalised moisture content, according to Trotter (1993), with calcite content.	146
Fig. 4.7	Graph showing the normalised moisture content profile according to the new method described in this study.	146
Fig. 4.8	Clay fraction (< 2μm) x-ray diffractograms for unit C.	154
Fig. 4.9	Clay fraction (< 2μm) x-ray diffractograms for unit E.	154
Fig. 5.1	Graphs showing the variation in calcium concentration and pH for bombs 1, 2 and 3.	167
Fig. 5.2	Graph showing the variation in Ca^{2+} concentration for the second experiment.	169

Fig. 5.3	Graph showing how pH varies with time for the second experiment.	169
Fig. 5.4	Graph showing the variation in Ca^{2+} concentration for the third experiment.	171
Fig. 5.5	Graph showing how pH varies with time for the third experiment.	171
Fig. 5.6	Complete residual failure envelope for kaolinite using the multiple shear technique, with consolidation imposed by instant loading. Note the exaggerated vertical scale.	173
Fig. 5.7	Complete residual failure envelope for kaolinite using the multiple shear technique with staged consolidation. Note the exaggerated vertical scale.	173
Fig. 5.8	Residual failure envelopes for kaolinite treated with solutions of calcium at the concentrations shown. Note the exaggerated vertical scale.	180
Fig. 5.9	Graphs displaying the relationship between calcium concentration and the effective residual shear angle of kaolinite at various effective normal stresses.	181
Fig. 5.10	Graphs showing the relationship between calcium concentration and the effective residual cohesion intercept of kaolinite at various effective normal stresses.	182
Fig. 5.11	Graphs displaying the relationship between calcium concentration and the residual shear strength of kaolinite at six effective normal stresses.	183
Fig. 5.12	Graph showing the relationship between calcium concentration and the Atterberg limits of kaolinite .	185
Fig. 5.13	Residual failure envelopes for montmorillonite treated with solutions of calcium at the concentrations shown. Note the exaggerated vertical scale.	186
Fig. 5.14	Graphs displaying the relationship between calcium concentration and the effective residual shear angle of montmorillonite at various effective normal stresses.	188
Fig. 5.15	Graphs displaying the relationship between calcium concentration and the effective residual cohesion intercept of montmorillonite at various effective normal stresses.	189

Fig. 5.16	Graphs displaying the relationship between calcium concentration and the residual shear strength of montmorillonite at six effective normal stresses.	190
Fig. 5.17	Graph showing the relationship between calcium concentration and the Atterberg limits of montmorillonite.	185
Fig. 5.18	X-ray diffractograms for the samples of kaolinite treated with solutions of calcium at the concentrations shown.	194
Fig. 5.19	X-ray diffractograms for the samples of montmorillonite treated with solutions of calcium at the concentrations shown.	195
Fig. 6.1	Complete residual failure envelope for the remoulded sample of Fuller's Earth clay obtained from within 5 mm either side of the shear surface described in Chapter 4.	205
Fig. 6.2	Complete residual failure envelope for the general homogenised sample of Fuller's Earth clay taken from a wider zone of material through which the shear surface passed.	205
Fig. 6.3	Graph used to obtain the correction factor for use in Janbu's simplified method, after Janbu *et al.* (1956).	208

LIST OF PLATES

		Page
Plate 3.1	View from Solsbury Hill of the west side of the Swainswick valley. Soper's Wood can be seen in the distance to the right of the photograph; the landslide studied is located in the field adjacent to the wood.	55
Plate 3.2	AGA geodimeter and theodolite in use at Soper's Wood.	55
Plate 3.3	View, looking west, of the lower part of the landslide active in 1994 adjacent to Soper's Wood.	67
Plate 3.4	Fresh scarps evident at the head of Slide A.	68
Plate 3.5	Slickenside striations visible on the lateral shear of Slide A.	68
Plate 3.6	Blocks of turf which have remained upright on the saturated clay of the mudflow.	70
Plate 3.7	View upslope showing the very disturbed nature of the intermediate toe in which survey station A2 is located. Survey station A2 is visible just to the right of the piezometer.	70
Plate 3.8	View down the mudflow in Slide B showing the removal of soil by the mudflow from one side of survey station B1.	93
Plate 3.9	View down Slide B showing the enlarged mudflow. Survey station B1 was swept away by it and is visible towards the edge of the mudflow.	93
Plate 3.10	View upslope of the lower mudflow in January 1994.	114
Plate 3.11	View upslope of the lower mudflow in February 1994.	114
Plate 3.12	View across slope of the toe of the large combined mudflow in April 1994.	115
Plate 3.13	View of the right edge of the main translational landslide showing a propagating transverse crack extending off from the lateral shear towards the centre of the landslide.	115
Plate 3.14	Photograph of retrogressive scarp migration seen in the landslide adjacent to Soper's Wood.	118
Plate 4.1	Photograph showing polished surface of the slip plane.	138

Plate 4.2	Photograph of the hand dug trial pit showing the technique used to obtain a block sample containing the shear surface.	138
Plate 4.3	Photograph displaying the fresh clay surface revealed after sawing the boxed sample in half. Notice the location of the shear surface.	139
Plate 4.4	Photograph displaying the sampling technique.	139
Plate 4.5	Scanning electron micrographs of the shear surface obtained from the landslip at Soper's Wood, Bath.	149

LIST OF TABLES

		Page
Table 1.1	Stratigraphic succession in the Swainswick valley, after Chandler *et al.* 1976.	4
Table 1.2	Qualitative XRD mineralogy of <2μm clay smears obtained from the Soper's Wood borehole, after Hawkins *et al.* (1986). Qualitative relative scale; dominant (dom), very strong (> str), strong (str), less strong (< str), present (pr), weak (wk), very weak (v. wk), trace (tr).	12
Table 1.3	Qualitative XRD mineralogy of <2μm clay smears obtained from the Wellsway borehole, after Hawkins *et al.* (1986). Qualitative relative scale as for Table 1.2.	12
Table 1.4	Qualitative XRD mineralogy of <2μm clay smears obtained from the Fuller's Earth Bed at Combe Hay, after Hawkins *et al.* (1986). Qualitative relative scale as for Table 1.2.	12
Table 2.1	Examples of residual shear strength parameters for a variety of materials for which c'_r ranges from 1.5 kN/m^2 to 20 kN/m^2, after Prior & Graham (1974).	43
Table 3.1	Summary of past phases of instability at Soper's Wood.	57
Table 3.2	Weathering scheme for the Fuller's Earth clay, after Lawrence 1985.	77
Table 3.3	Horizontal velocity of each survey station during the five phases of movement.	100
Table 4.1	Qualitative proportion of clay minerals identified in the XRD units.	153
Table 5.1	Qualitative analysis of (001) montmorillonite reflection.	193
Table 6.1	Residual shear angle and residual cohesion intercept corresponding to the effective normal stress at the basal shear surface at Soper's Wood relating to the ground water levels shown.	212
Table 6.2	Factors of safety obtained from infinite slab analyses for the landslide adjacent to Soper's Wood.	213
Table 6.3	Generalised qualitative seasonal model illustrating controls on landslide activity in the Fuller's Earth clay.	215

LIST OF TABLES

		Page
Table 1.1	Stratigraphic succession in the Swainswick valley, after Chandler *et al.* 1976.	4
Table 1.2	Qualitative XRD mineralogy of <2μm clay smears obtained from the Soper's Wood borehole, after Hawkins *et al.* (1986). Qualitative relative scale; dominant (dom), very strong (> str), strong (str), less strong (< str), present (pr), weak (wk), very weak (v. wk), trace (tr).	12
Table 1.3	Qualitative XRD mineralogy of <2μm clay smears obtained from the Wellsway borehole, after Hawkins *et al.* (1986). Qualitative relative scale as for Table 1.2.	12
Table 1.4	Qualitative XRD mineralogy of <2μm clay smears obtained from the Fuller's Earth Bed at Combe Hay, after Hawkins *et al.* (1986). Qualitative relative scale as for Table 1.2.	12
Table 2.1	Examples of residual shear strength parameters for a variety of materials for which c'_r ranges from 1.5 kN/m^2 to 20 kN/m^2, after Prior & Graham (1974).	43
Table 3.1	Summary of past phases of instability at Soper's Wood.	57
Table 3.2	Weathering scheme for the Fuller's Earth clay, after Lawrence 1985.	77
Table 3.3	Horizontal velocity of each survey station during the five phases of movement.	100
Table 4.1	Qualitative proportion of clay minerals identified in the XRD units.	153
Table 5.1	Qualitative analysis of (001) montmorillonite reflection.	193
Table 6.1	Residual shear angle and residual cohesion intercept corresponding to the effective normal stress at the basal shear surface at Soper's Wood relating to the ground water levels shown.	212
Table 6.2	Factors of safety obtained from infinite slab analyses for the landslide adjacent to Soper's Wood.	213
Table 6.3	Generalised qualitative seasonal model illustrating controls on landslide activity in the Fuller's Earth clay.	215

CHAPTER 1

A REVIEW OF THE GEOLOGY AND TOPOGRAPHY OF THE SWAINSWICK VALLEY, BATH; WITH EMPHASIS ON THE FULLER'S EARTH FORMATION

1.1 Introduction

The topography of the Swainswick valley, through which Lam Brook flows southwards to join the River Avon at Bath, is typical of the relief of much of the Bath area (see Figure 1.1). The reactivation of a known landslide in the Fuller's Earth formation in the fields adjacent to Soper's Wood, within the valley, provided an excellent opportunity to further the understanding of the slope stability problems which are characteristic of the formation in the south Cotswolds. The location of the landslide is indicated in Figure 1.1.

This chapter reviews the general geology of the Swainswick valley, including a review of the Fuller's Earth formation of the Bath area, the topography of the valley and discusses how these interrelate in the development of superficial structures. The engineering significance of these structures is then briefly extended to the area of the City of Bath and their influence on its development is discussed.

1.2 General Geology of the Swainswick Valley

Fig 1.2 contains an extract from the 1:63360 geological map of the Bath area (Sheet 265), published in 1965. In contrast to the previous 1:63360 geological map (1873) which indicated a typical sub-parallel outcrop pattern, much of the area in the 1965 map, including the Swainswick valley, is depicted as "Foundered Strata". This was subsequently described by Hawkins & Kellaway (1971) and is due to both colluvial head covering the hill slopes and the cambering of strata, preventing the accurate mapping of the outcrop of individual stratigraphic units. The succession in the Swainswick valley is mainly of Lower and Middle Jurassic age. In order to obtain an accurate assessment of the "undisturbed" geology, in the early 1970's a borehole was drilled near the southwest corner of Charmy Down as part of the A46 engineering studies and proved the thicknesses given in Table 1.1 (Chandler *et al.* 1976).

Fig. 1.1 Extract from the 1:50 000 "Landranger Series" Ordnance Survey map, Bristol and Bath sheet 172, showing the topography of the Swainswick valley and the surrounding area. The valley is bounded by the roads highlighted in black and the location of the landslide adjacent to Soper's Wood is indicated.

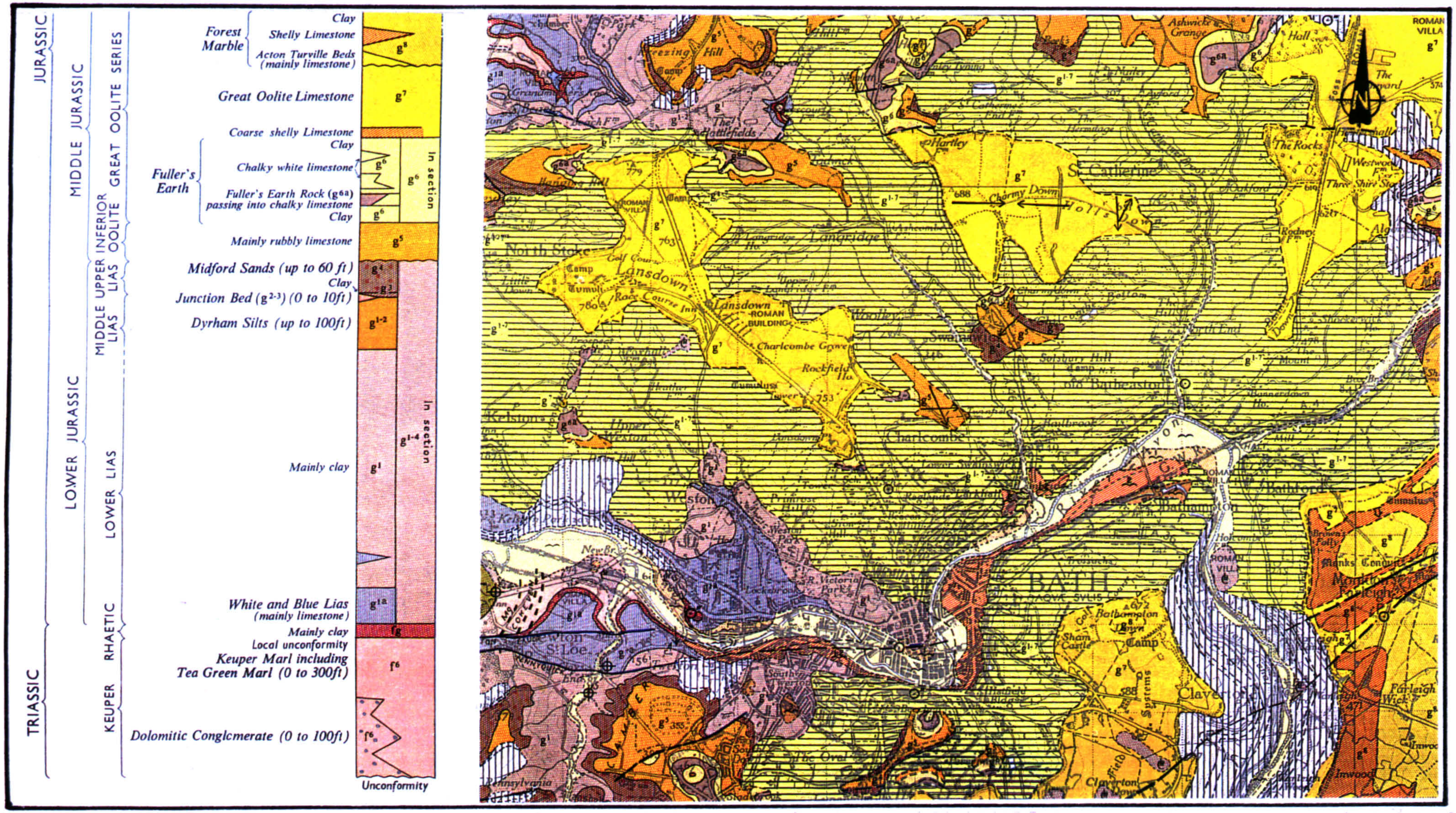

Fig. 1.2 Extract from the one inch Geological Survey map of Bath, sheet 265. The horizontal shading indicates foundered strata.

AGE	STRATIGRAPHIC UNIT	SUBDIVISION	THICKNESS
Middle Jurassic	Great Oolite	Lower Ragstones	
	Fuller's Earth	Upper Fuller's Earth clay	27 m
		Fuller's Earth Rock	4 m
		Lower Fuller's Earth clay	10 m
	Inferior Oolite	Inferior Oolite	15 m
Lower Jurassic	Upper Lias	Midford Sands	31 m
		Junction Bed	1 m
	Middle and Lower Lias	Dyrham Silts	15 m
		Lower Lias clay	65 m

Table 1.1 Stratigraphic succession in the Swainswick valley, after Chandler *et al.* (1976).

Kellaway & Taylor (1948), Green & Donovan (1969), Donovan & Kellaway (1984), Green (1992) and Kellaway & Welch (1993) provide general descriptions of the geology for the Bath and Bristol area. Although Green & Donovan (1969) produced a major paper on the subdivision of the Middle Jurassic, it is not considered necessary to review their paper in detail. However, a general summary of the lithologies is considered essential background for any geotechnical interpretation. For simplicity in this thesis, the stratigraphy is described from youngest to oldest.

Great Oolite

The Great Oolite outcrops over much of the south Cotswold plateau. The nature of the lithology can be seen to the north of the village of Upper Swainswick, near the garage after the three lane section of the A46 (ST 753697). It consists of a moderately strong to strong, shelly, cream coloured, fine to medium grained oolitic limestone. The observed jointing is widely to very widely spaced, such that within the medium bedded strata, large discontinuity bounded blocks dominate the rock mass. The thickness of the Great Oolite varies over the plateau region of Lansdown and Charmy Down, but is generally less than 10 m thick; much of the Bath Oolite, Twinhoe Beds and Combe Down Oolite have been removed by erosion. Thus, now only a relict deposit of the Great Oolite forms the dip slope on the western side of the south Cotswolds and it is not until the Bradford upon Avon area to the east, that the full sequence of the Great Oolite is encountered. In the Lansdown/Charmy Down area, it is generally the more resistant Lower Ragstones which form the cap rock. As a consequence of

the structural geology and topography, this area is in contrast to that found south of the River Avon, as described by Brown (1991) in his study of the disused mines in the Combe Down area.

In view of the Great Oolite forming a thin cap rock around the upper slopes of the valley, the ground water level in this part of the Cotswolds is frequently only just above the base of the Great Oolite. Hence in this area it is not a major aquifer, although to the east of Bath, water is extracted from strata of this age.

Fuller's Earth

In the Lansdown area to the west of the Swainswick valley, the Fuller's Earth has been described by Arkell & Donovan (1952). Both these authors and the subsequent site investigation for the A46 in the 1970's, failed to locate the presence of the montmorillonite rich horizon known as the Fuller's Earth Bed, which is present to the south of Bath. Although later papers by Green & Donovan (1969) and Cave (1977) have indicated the presence of further sub-divisions, especially to the north, in this part of the south Cotswolds the Fuller's Earth can be divided into three main units. In addition to the following summary, further details on the Fuller's Earth are given in Section 1.3, in order to provide a greater background on the main strata type studied in this thesis.

A) *Upper Fuller's Earth*

This consists mainly of a weak to moderately weak, medium grey, calcareous mudrock. The mudrock is interbedded with argillaceous limestone bands, especially towards the top of the sequence near the Great Oolite (Hawkins *et al.* 1986). These act as lines of preferential water flow within the relatively low permeability mudrocks. Near the surface, the mudrock weathers to a fissured brown clay.

B) *Fuller's Earth Rock*

The Fuller's Earth Rock is a moderately strong, rubbly limestone which is often oolitic and shelly. In its unweathered state it is grey, but frequently, because it is a zone of moderate to high permeability, it is unsaturated and in these areas it is brown in colour.

C) *Lower Fuller's Earth*

A sequence of weak to moderately weak, grey, calcareous, fissured mudrock, with occasional argillaceous limestone bands. Chandler *et al.* (1976) notes that it is similar to the Upper Fuller's Earth clay, but less plastic.

Inferior Oolite

As indicated by Arkell (1933), only the Upper Inferior Oolite is present in the Bath area of the south Cotswolds. The Upper Inferior Oolite, seen on the south side of Lansdown (Hawkins 1977a), is mainly a well jointed, permeable, oolitic limestone. The stratigraphic unit has been sub-divided, but it is not considered necessary in this thesis to describe the sequence in detail as it was not encountered during this study.

Midford Sands

These Upper Lias deposits are grey, weakly cemented, silty fine sands. The strata contains frequent 'hard' horizons which are more thoroughly cemented by calcite and form thin to medium beds of moderately strong, calcareous sandstone. On exposure, as normally seen at outcrop, the sands oxidise to a yellow-brown colour.

Junction Bed

This distinct lithology, which acts as a convenient marker bed, forms the base of the Upper Lias. It consists of thin to medium bedded, highly fossiliferous, grey limestones, with iron-stained oolitic and conglomeratic bands and some thin mudrock layers.

Middle and Lower Lias

The Middle Lias is represented by the Dyrham Silts, a silty horizon between the Junction bed and the Lower Lias. The Silts vary in thickness from 0-30 m. In the Swainswick valley, some 5 km south of Dyrham, the type locality, the deposits are some 5-15 m thick.

The Lower Lias is a very weak to weak, grey, fissured mudrock containing occasional argillaceous limestone bands and the interbedded Blue Lias towards the base. Near the surface, the mudrock has weathered to a silty clay.

Structurally, the area is part of the south Cotswolds, in which the general regional dip is between 2° and 5° to the east. However, because of the intensely dissected nature of the area around Bath and the interbedded nature of the geology, the structure is dominated by superficial movements rather than tectonic influences.

The properties of the Fuller's Earth are of particular relevance to this thesis. Hence, it is considered appropriate to provide more detailed information on the Fuller's Earth, in order to assist in the understanding of the superficial structures and as a background to the discussions in Chapter 3.

1.3 A Review of the Geology and Engineering Properties of the Fuller's Earth Formation

1.3.1 The Geology of the Fuller's Earth Formation

The Fuller's Earth formation has been recognised since 1799, when William Smith (Phillips 1844) noted a dominantly mudrock succession, which he termed the Fuller's Earth formation, between the Inferior Oolite and the overlying Great Oolite. Since that time a number of authors have described the stratigraphy of the formation, culminating with the work of Arkell and Donovan (1952) who investigated the detailed stratigraphy in the Bath-Stroud area. More recently Penn *et al.* (1979) described the Fuller's Earth strata between Bath and Frome.

Lonsdale (1832) was the first to describe in any detail the commercially valuable montmorillonite rich Fuller's Earth Bed, which at that time was being worked from a number of small adits in the Bath area. Lonsdale's reference to the Fuller's Earth formation was therefore dominated by the commercial Fuller's Earth Bed. He separated the formation into four units; blue and yellow clay, with nodules of indurated marl; bad Fuller's Earth; good Fuller's Earth; clay containing beds of bad Fuller's Earth and layers of nodular limestone and indurated marl. Lonsdale (1832) was followed by a publication by Woodward (1876) who recorded brief details of the geology exposed at a number of localities. Subsequently, Woodward (1887 and 1894) proposed three main sub-divisions of the formation when attempting to correlate the stratigraphy in the Bath area. He introduced the terms Lower Fuller's Earth, Fuller's Earth Rock and Upper Fuller's Earth and proposed that they were independent sequential formations. However, soon afterwards Buckman (1901), following a detailed study of the ammonites of the Middle Jurassic, realised that the fossils did not necessarily correlate with the lithologies. As the fossils were considered to indicate time related zones, Buckman (1901) correlated the Fuller's Earth Rock of Bath with part of the Great Oolite of Gloucestershire.

Arkell and Donovan (1952) examined the succession of the Fuller's Earth on the south-western spurs of Lansdown, just to the west of the Swainswick Valley, as part of their investigation of the Fuller's Earth formation along the 50 miles of strike from the Avon valley at Bath to the Vale of Moreton at Stow-on-the-Wold. A bomb crater 250 yards (229 m) south-west of Kelston Round Hill (ST 711675) and an exposure at Prospect Stile (ST 713683), just to the south of the race course at Lansdown,

revealed a succession of the Fuller's Earth similar to that described in Section 1.2. However, Arkell and Donovan (1952) showed that further to the north, at Dyrham Wood, the Fuller's Earth Rock separates into two distinct rock bands. These rock bands eventually pass laterally into the Great Oolite of the north Cotswolds, with the wedging out of the clays of the Fuller's Earth, as predicted by Buckman (1901). It is of note that Arkell and Donovan (1952) did not find any evidence of the Fuller's Earth Bed at Lansdown, although it had long been known to be an important commercial deposit to the south of Bath.

The long section, shown by Green (1992), from Burford to the south coast, emphasises the lateral variation of the stratigraphy of the Fuller's Earth formation. Hence, the stratigraphy of the Fuller's Earth formation around the close vicinity of Bath, is only characteristic of this area.

During the period of the Fuller's Earth formation, the Bath area is likely to have been a relatively shallow, quiet water, marine environment in which illitic, kaolinitic and some calcium montmorillonite clays were deposited. Periodically, the marine environment became more calcareous rich, such that the accumulated muds varied from weakly calcareous to highly calcareous, argillaceous limestones. These carbonate rich members occur throughout the Fuller's Earth formation, but are dominant in the Upper Fuller's Earth. The strata now referred to as the Fuller's Earth Rock is likely to have formed as a result of a change in depositional environment, with a shallowing of the seas and less suspended sediment in the water column. In this environment, ooliths formed to produce an oolitic, shell rich sediment which now forms the Fuller's Earth Rock. Towards the top of the Upper Fuller's Earth, the carbonate rich horizons become increasingly oolitic, indicating a shallowing of the seas, such that there is no clear boundary with the overlying Great Oolite. Brown (1991) noted that at Peasedown St John it was not possible, even in a trial trench, to locate the exact boundary between the increasingly oolite rich Upper Fuller's Earth and the overlying Great Oolite.

The origin of the Jurassic Fuller's Earth Bed, which although only about 2.4 m thick, has been the subject of much controversy since the 1930's. Some authorities have suggested a volcanic source and some that the formation may be due to a marine chemical precipitate. Jeans *et al.* (1977) investigated the montmorillonite rich Fuller's Earth Bed present to the south of Bath, but absent in the area of Lansdown and the Swainswick valley. They review the controversy of its origin and, by analysing samples obtained from the face of the commercial seam at the Combe Hay mine

(ST 730610), provide evidence that the Fuller's Earth Bed has been formed by the argillisation of volcanic ash deposited in a shallow marine environment. They found that the Fuller's Earth Bed contained a very small proportion of sand-grade material (0.4%) which consisted largely of pyroclastic minerals and rock particles. In addition, calcitic nodules in the deposit contained a much higher proportion of well preserved pyroclastic material than the surrounding smectite matrix. This is considered to be due to the local precipitation of mineral cement during the early diagenesis of the ash deposit which preferentially preserved the pyroclastic material within the nodules. The pyroclastic fragments show little evidence of abrasion supporting the view that most of the ash was air-borne. The bulk chemical composition of the Fuller's Earth Bed suggests that it is derived from a dominantly trachytic ash and K/Ar isotope analyses indicates a minimum age for the volcanism of 159 Ma. Work undertaken by Penn *et al.* (1979) found a calcareous microfauna existed throughout the bed. This indicated that ash did not accumulate at an abnormally rapid rate and contained sufficient nutrient to support deposit feeders. Thus, although Jeans *et al.* (1977) showed that the Fuller's Earth Bed is of volcanic origin, they recognised that it is not the result of one single catastrophic ashfall deposit which would have destroyed the existing community of microfauna.

1.3.2 The Clay Mineralogy of the Fuller's Earth Formation

Hawkins *et al.* (1986) analysed the clay mineralogy of the Fuller's Earth formation. They obtained samples of the Fuller's Earth Bed from the Combe Hay mine and samples of the Fuller's Earth formation from two localities in the Bath area (Soper's Wood and Wellsway), to compare the clay mineralogy of the Upper and Lower Fuller's Earth with that of the Fuller's Earth Bed. The sample locations are shown in Figure 1.3.

The borehole at Soper's Wood first passed through approximately 2 m of the Great Oolite before extending through the entire succession of the Fuller's Earth formation. The abbreviated log of the borehole, shown in Figure 1.4, indicates approximately 40 m of blue grey, calcareous, randomly fissured, overconsolidated silty claystone, interbedded with occasional argillaceous limestone bands. The Upper Fuller's Earth clay is separated from the Lower Fuller's Earth clay by the Fuller's Earth Rock, a 3 m thick band of shelly oolitic limestone. The borehole log provides no evidence of the Fuller's Earth Bed found to the south of Bath. Samples were taken at 1 m intervals from the core and XRD analyses undertaken on

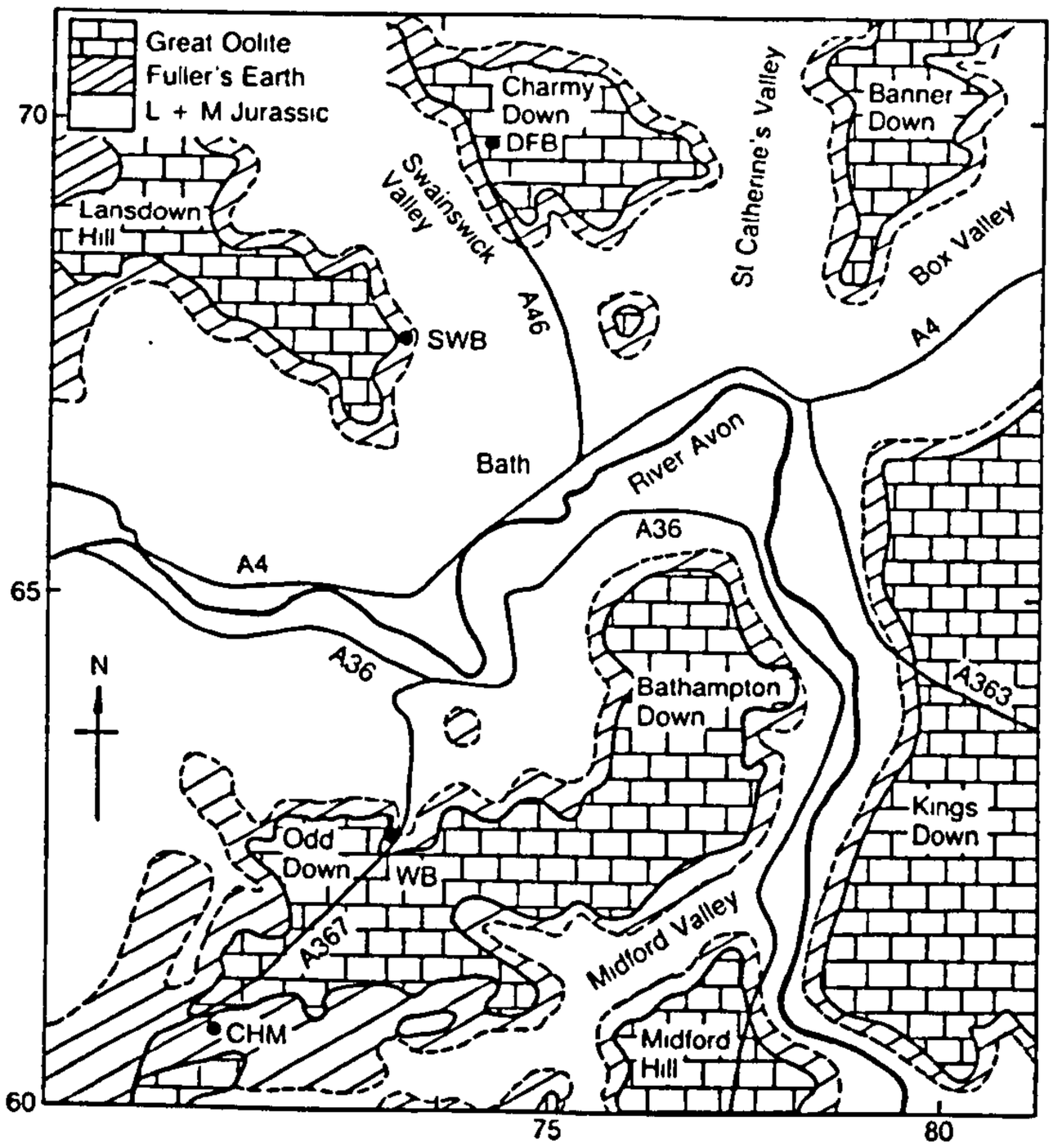

Fig. 1.3 Outcrops of the Fuller's Earth in the Bath region and sample locations: DFB = Down Farm borehole; SWB = Soper's Wood borehole; WB = Wellsway borehole; CHM = Combe Hay mine, after Hawkins *et al.* (1988).

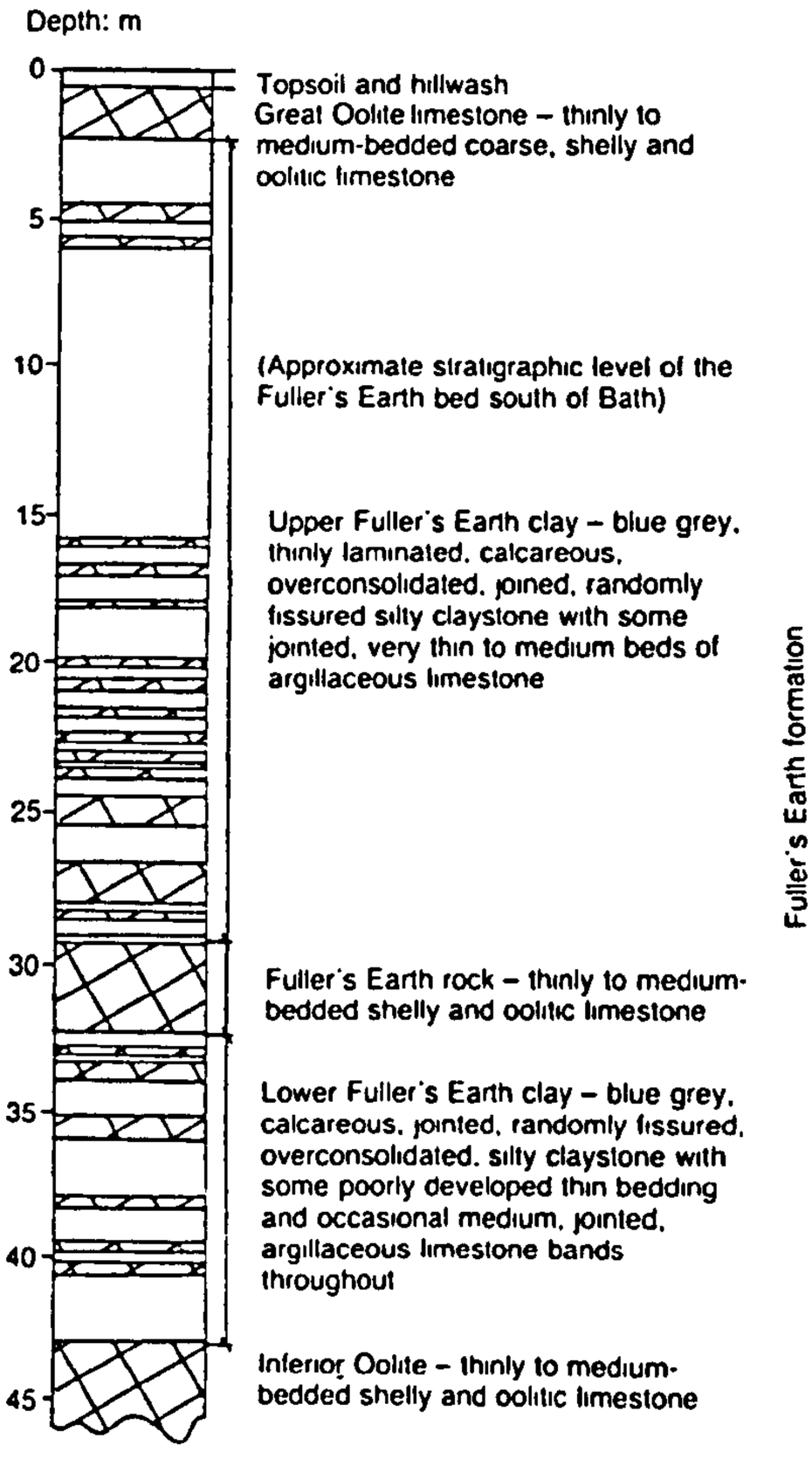

Fig. 1.4 Stratigraphic log of the Soper's Wood borehole, after Hawkins *et al.* (1988), based on Lawrence (1985).

both untreated and glycolated clay smears from the samples. The qualitative mineralogy of the samples is shown in Table 1.2. The Table highlights the dominance of illite, with kaolinite appearing strongly in all samples, however, montmorillonite is only shown to be "weak" or "very weak" on the qualitative scale, except in the uppermost four samples where it has been described as "present".

The Wellsway borehole penetrated the Upper Fuller's Earth which was also sampled at 1 m intervals. The mineralogy of the clay was investigated using the same technique and the results are displayed in Table 1.3. Table 1.3 shows the clay mineralogy to have a very similar distribution to that seen in the Soper's Wood borehole. Illite is again dominant, followed by kaolinite, with generally only a trace of montmorillonite present. However, in the uppermost three samples, the montmorillonite content is shown to be "weak". As in the Soper's Wood borehole, Hawkins *et al.* (1986) note that the Fuller's Earth Bed is absent in the Wellsway borehole, only 2 km north of the once commercial seam at Combe Hay.

Samples of the Fuller's Earth Bed were obtained at 200 mm intervals from the seam at Combe Hay. Figure 1.5 shows the lithological sequence of the Combe Hay seam and the sample locations. The seam has been divided up into a Top Seam and a Whole Seam. The Top Seam was about 0.5 m thick and consisted of a very calcareous silty claystone, with occasional boulder size calcareous nodules. The Whole Seam was dominated by a grey, slightly calcareous claystone, with occasional grey calcareous nodules. The samples were analysed by XRD and the results are again displayed qualitatively in Table 1.4. Hawkins *et al.* (1986) note that the mineralogy is notably different to that seen in the previous two boreholes. Here montmorillonite is the dominant mineral, with only a trace of kaolinite present throughout the seam and illite only present in the uppermost three samples. The calcite content, determined from whole rock powder mounts, clearly reflects the division between the highly calcareous Top Seam and the generally less calcareous Whole Seam, as depicted on the log in Figure 1.5. The peak in calcite content at 1.4 m is related to the thin band of cobble sized, calcareous nodules.

Hawkins *et al.* (1986) compared the XRD diffractograms of the Top Seam with those of the Whole Seam and demonstrated that in the Top Seam the illite is randomly interstratified with montmorillonite. This interstratified illite-montmorillonite is absent in the Whole Seam, apart from in one sample at the top of the Whole Seam (depth 0.6 m), and only

Depth (m)	Illite	Kaolinite	Montmorillonite	Calcite	Quartz
3	dom	str	pr	pr	—
4	dom	str	pr	pr	tr
5	dom	<str	pr	pr	tr
6	dom	str	pr	tr	—
7	dom	str	wk	pr	—
8	dom	<str	v wk	pr	tr
9	dom	str	v wk	pr	tr
10	dom	str	tr	pr	—
11	dom	str	v wk	pr	—
12	dom	str	v wk/tr	pr	tr
13	dom	str	v wk	pr	—
14	dom	<str	v wk	pr	tr
15	dom	str	tr	str	—
16	dom	str	v wk/tr	str	tr
17	dom	str	v wk/tr	str	—
18	dom	str	wk	str	tr
19	dom	str	wk	pr	tr
20	dom	str	tr	str	tr
21	dom	str	wk	str	tr
22	dom	str	wk	str	—
23	dom	str	wk	>str	tr
24	dom	str	v wk/tr	>str	—
25	dom	>str	wk	str	tr
26	dom	str	v wk	pr	tr
27	dom	str	tr	str	—
28	dom	>str	wk	>str	tr
29	dom	str	wk	>str	tr
30	dom	str	v wk/tr	>str	—
31	dom	>str	tr	>str	—
32	dom	>str	v wk/tr	>str	—
33	dom	str	v wk/tr	>str	—
34	dom	str	wk	pr	tr
35	dom	>str	wk	>str	tr
36	dom	>str	wk	pr	—
37	dom	str	wk	pr	tr
38	dom	str	wk	str	tr
39	dom	str	wk	pr	tr
41	dom	str	wk	>str	tr
42	dom	str	wk	pr	tr
43	dom	str	wk	pr	tr

Table 1.2 Qualitative XRD mineralogy of <2μm clay smears obtained from the Soper's Wood borehole, after Hawkins *et al.* (1986). Qualitative relative scale; dominant (dom), very strong (> str), strong (str), less strong (< str), present (pr), weak (wk), very weak (v. wk), trace (tr).

Depth (m)	Illite	Kaolinite	Montmorillonite	Calcite	Quartz
2	dom	pr	wk	pr	—
3	dom	pr	wk	pr	tr
4	dom	pr	wk	pr	tr
5	dom	pr	tr	pr	tr
6	dom	pr	tr	pr	tr
7	dom	pr	tr	str	tr
8	dom	pr	tr	str	tr
9	dom	pr	wk	pr	tr
10	dom	pr	wk	pr	tr
11	dom	pr	v wk/tr	pr	tr
12	dom	pr	—	pr	tr
13	dom	pr	tr	pr	tr
14	dom	pr	tr	pr	tr
15	dom	pr	tr	pr	tr

Table 1.3 Qualitative XRD mineralogy of <2μm clay smears obtained from the Wellsway borehole, after Hawkins *et al.* (1986). Qualitative relative scale as for Table 1.2.

Depth (m)	Illite	Kaolinite	Montmorillonite	Calcite*	Quartz
0·2	str	tr	str	dom	tr
0·4	pr	tr	str	>str	tr
0·6	wk	tr	>str	>str	—
0·8	—	tr	dom	str	—
1·0	—	tr	dom	pr	—
1·2	—	tr	dom	pr	—
1·4	—	tr	dom	>str	—
1·6	—	tr	dom	str	—
1·8	—	tr	dom	str	—
2·0	—	tr	dom	pr	—
2·2	—	tr	dom	pr	—

Table 1.4 Qualitative XRD mineralogy of <2μm clay smears obtained from the Fuller's Earth Bed at Combe Hay, after Hawkins *et al.* (1986). Qualitative relative scale as for Table 1.2.

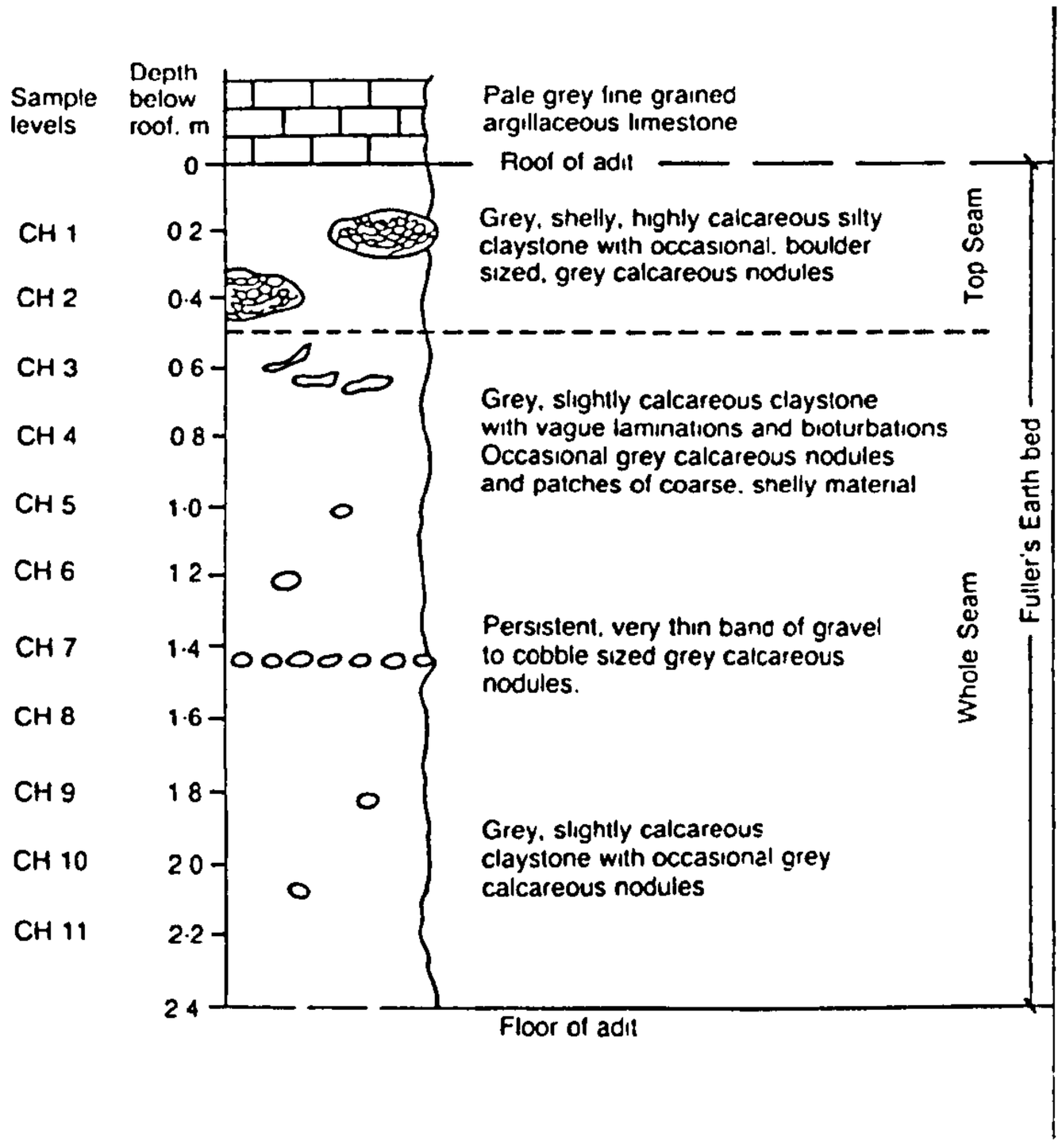

Fig. 1.5 Lithology and sampling levels in the Fuller's Earth Bed seam at Combe Hay mine, after Hawkins *et al.* (1986), based on Jeans *et al.* (1977).

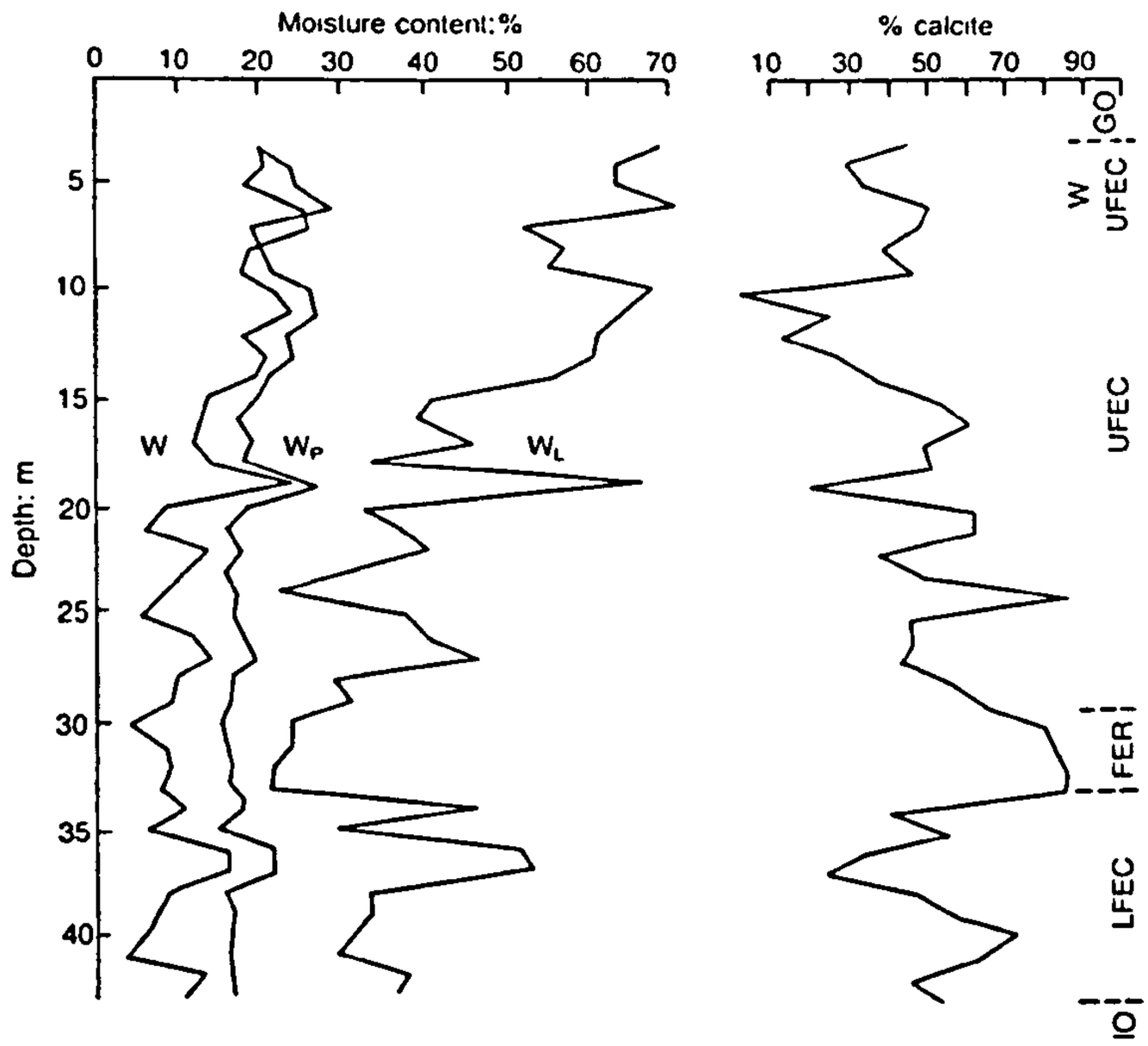

Fig. 1.6 Plots showing the variation with depth of the moisture content, Atterberg limits and calcite content of the samples of the Fuller's Earth formation obtained from the Soper's Wood borehole, after Hawkins *et al.* (1988).
GO = Great Oolite; WUFEC = Weathered Upper Fuller's Earth clay; UFEC = Upper Fuller's Earth clay; FER = Fuller's Earth Rock; LFEC = Lower Fuller's Earth clay; IO = Inferior Oolite

montmorillonite and kaolinite are present (see Table 1.4). Using methods developed by Srodon (1980 and 1981), they quantified the percentage of montmorillonite in the interstratified assemblage and showed that in the Top Seam between 52% and 84% montmorillonite is present, whereas in the Whole Seam, where illite is indicated to be absent in Table 1.4, approximately 98% montmorillonite is present. They suggest that the randomly interstratified illite-montmorillonite in the Top Seam is a possible relic of contemporaneous chemical weathering of the typically illite rich shallow marine deposits, reworked at the time of deposition of a trachytic ash which formed the Whole Seam. They report that Jackson *et al.* (1952) suggest that on chemical weathering, mica is altered to illite, which on further weathering, forms an intermediate interstratified illite-smectite, before developing into a smectite on continued weathering. They propose that on chemical weathering, potassium ions are lost from the interlayer space in illite by leaching and are replaced by calcium ions, with the formation of interstratified illite-smectite. This process of depotassification begins at the edges of the clay mineral and on continued weathering may proceed rapidly inwards.

The work by Hawkins *et al.* (1986) has highlighted the difference in clay mineralogy between the montmorillonite dominated Fuller's Earth Bed and the generally illite rich clay of the Upper and Lower Fuller's Earth. They have shown that in the Top Seam of the Fuller's Earth Bed at Combe Hay, interstratified illite-montmorillonite is present. In addition, they have demonstrated that in the weathered zone of the Upper and Lower Fuller's Earth clay, there is an increase in the proportion of montmorillonite present and diffractogram traces have shown this to be interstratified with illite. In contrast to the relatively high montmorillonite component of the Top Seam, they found the percentage of the montmorillonite component in the weathered Fuller's Earth clay to be between 23% and 39%. However, they relate both the interstratified assemblage in the weathered clay of the Fuller's Earth and that found in the Top Seam of the Fuller's Earth Bed, to the chemical weathering of illite, with the formation of a randomly interstratified illite-smectite.

The detailed analysis of the clay mineralogy has also confirmed the limited aerial extent of the Fuller's Earth Bed. Hence, from an engineering view point, especially with regard to the known landslides that occur in the Fuller's Earth formation, a knowledge of the clay mineralogy and geotechnical properties of the more aerially extensive Upper and Lower Fuller's Earth clays is more important. The process of depotassification has

resulted in the formation of interstratified illite-calcium montmorillonite in the weathered clay along the edge of the Cotswold escarpment, resulting in the material being named after its "fulling" properties.

1.3.3 The Geotechnical Properties of the Fuller's Earth Formation and the Effects of Weathering

The first published data on the geotechnical properties of the Fuller's Earth formation was provided by Chandler *et al.* (1976), following site investigations carried out in the Swainswick valley. Samples obtained from boreholes and trial pits in the Upper Fuller's Earth provided a mean liquid limit of 51% (range 40-65%), a mean plastic limit of 20%, giving a plasticity index of 31%. The Lower Fuller's Earth had a mean liquid limit of 44% (range 35-55%), a mean plastic limit of 17%, giving a plasticity index of 27%. In addition, they report the Atterberg limits of the Head deposits overlying the Fuller's Earth formation. These had a mean liquid limit of 47% (range 30-70%), a mean plastic limit of 19%, giving a plasticity index of 28%. They note that:

"The results call for no particular comment as the Atterberg limits are unexceptional and the natural water contents are, as usual in weathered over-consolidated clays, approximately equal to the plastic limit ".

Hawkins *et al.* (1988) report the moisture contents, Atterberg limits and calcite content of samples of the Fuller's Earth formation obtained from the Soper's Wood borehole and a borehole drilled at Down Farm; and of samples of the Fuller's Earth Bed from the Combe Hay mine (see Figure 1.3 for sample locations).

Figures 1.6, 1.7 and 1.8 show the variation with depth of these indices for the samples obtained from the Soper's Wood borehole, the Down Farm borehole and the Combe Hay mine seam, respectively. Figures 1.6 and 1.7 indicate that, contrary to the opinion expressed by Chandler *et al.* (1976) regarding the Atterberg indices, the moisture content of the unweathered clay is less than the plastic limit. However, near the ground surface, where weathering has taken place, it tends to be greater than the plastic limit. Hawkins *et al.* (1988) relate the effect of weathering on the moisture content-plastic limit relationship, to the increase in the montmorillonite content in the more weathered zones due to the depotassification of illite. In addition, their data from trial pits in the Soper's Wood area, highlights a progressive increase in moisture content and Atterberg limits through the weathering grades. In comparison, Figure 1.8

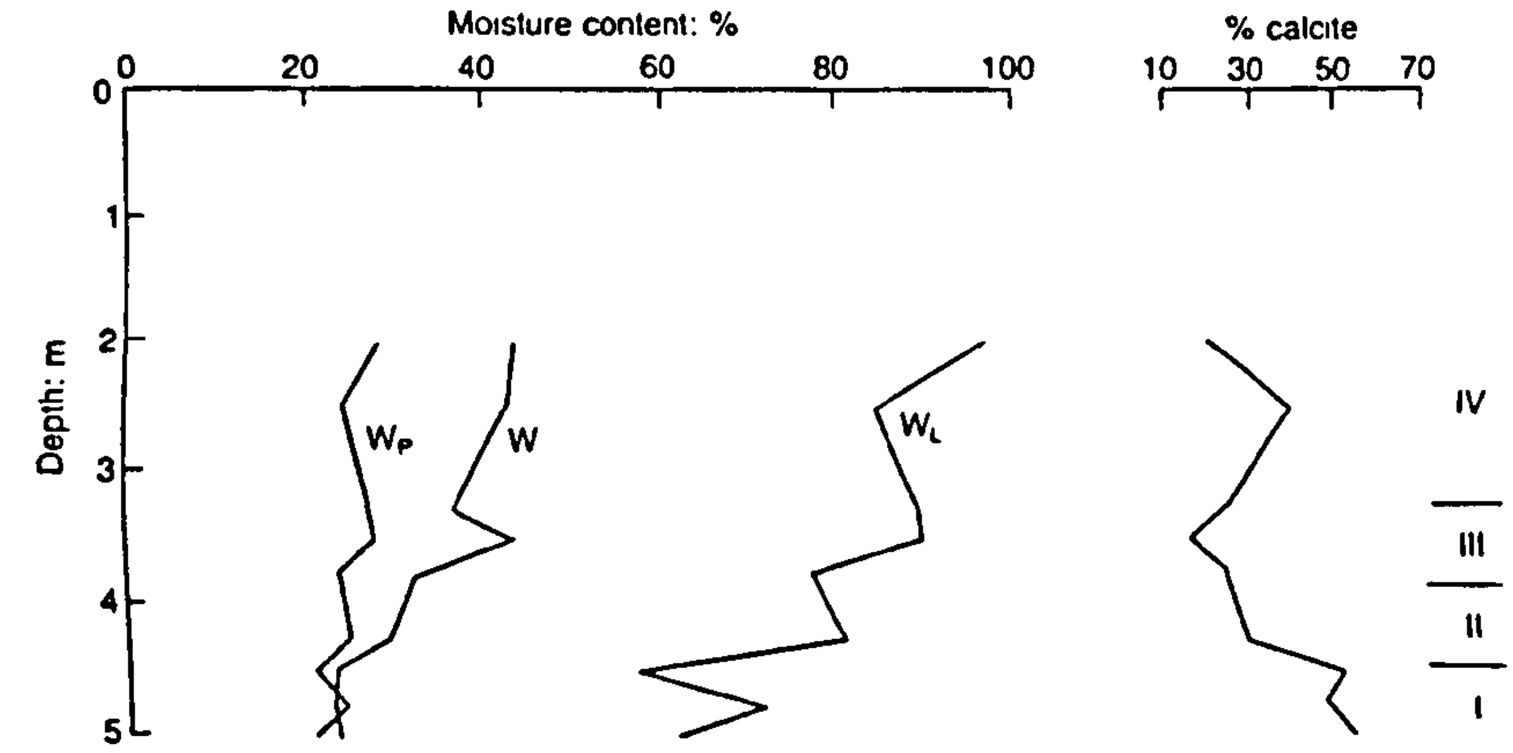

Fig. 1.7 Plots showing the variation with depth of the moisture content, Atterberg limits and calcite content of the samples of the Fuller's Earth formation obtained from the Down Farm borehole: I - IV represent weathering zones, after Hawkins *et al.* (1988).

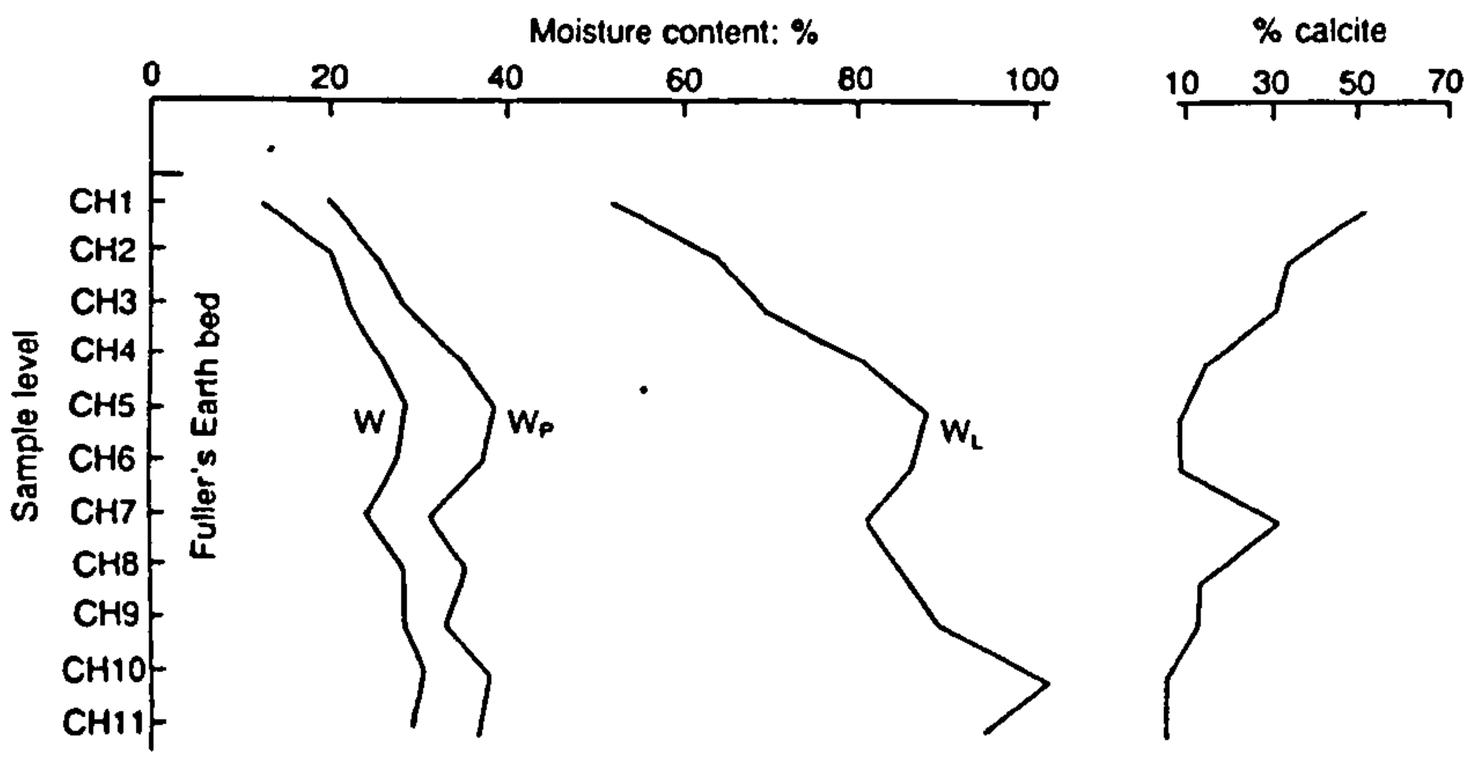

Fig. 1.8 Plots showing the variation with depth of the moisture content, Atterberg limits and calcite content of the samples obtained from the Fuller's Earth Bed in the seam at the Combe Hay mine, after Hawkins *et al.* (1988).

shows the moisture content profile of the unweathered Fuller's Earth Bed to be parallel to the plastic limit, but consistently 10% lower. However, those samples obtained from the Top Seam have lower Atterberg limits and moisture contents, consistent with the decrease in montmorillonite content (compared to the Whole Seam), as discussed in Section 1.3.2.

Analysing the plots of calcite content with depth, Hawkins *et al.* (1988) note that there is a general trend of decreasing calcite content with decreasing depth shown in the samples taken from the Soper's Wood and Down Farm boreholes, displayed in Figures 1.6 and 1.7 respectively. In addition, a comparison of the liquid limit with the calcite content of the samples demonstrates a strong inverse relationship. Although it is less pronounced, this relationship can also be extended to the plastic limit and moisture content. Figure 1.8 also shows this inverse relationship in the samples of the Fuller's Earth Bed obtained from the Combe Hay mine. However, here the liquid limit decreases upwards through the seam, while the calcite content increases. This is to be expected as the calcite rich Top Seam (see Figure 1.5) clearly influences the results.

The inverse relationship between the calcite content and the geotechnical indices is emphasised in Figure 1.9. It is of note that the Fuller's Earth Bed plots in the area of the weathered material in the graph of plasticity index against calcite content, probably due to the increase in montmorillonite content of the more weathered material. The plot of liquidity index against calcite content shows the weathered Fuller's Earth clay to have a positive liquidity index and the unweathered Fuller's Earth clay and Fuller's Earth Bed to have negative liquidity indices. This is due to the fact that although the weathered clay and unweathered Fuller's Earth Bed have similar Atterberg limits, the weathered Fuller's Earth clay has higher moisture contents due to the weathering process and stress release allowing the infiltration of surface water and the hydration of the clay.

Hawkins *et al.* (1988) have shown that two relationships exist in the Fuller's Earth on weathering and have demonstrated the control that the calcite content has on the fundamental geotechnical properties of the clay. They envisaged that stress relief in the near surface strata aids the percolation of acidic ground waters causing chemical weathering. On weathering, calcite is removed and the depotassification of illite results in the formation of a randomly interstratified illite-smectite clay mineral. X-ray diffractometry analyses confirmed that calcite (in addition to quartz, pyrite and feldspars) comprises the bulk of the coarse silt fraction. Hence, the decrease in the proportion of a non-sorptive mineral such as calcite leads to

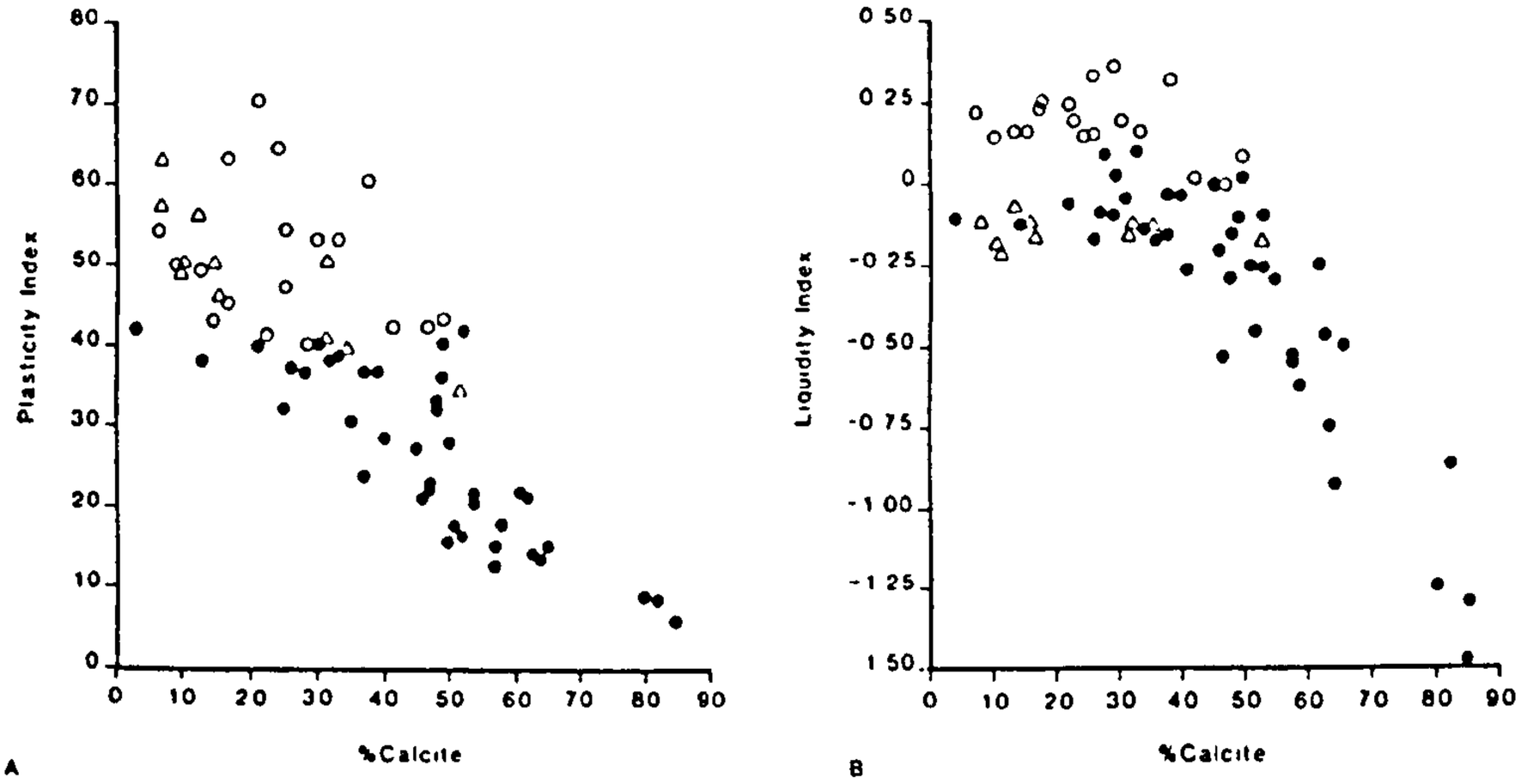

Fig. 1.9 Plots of calcite content with plasticity index (A) and liquidity index (B) for the Fuller's Earth clay and the Fuller's Earth Bed, after Hawkins *et al.* (1988): solid circles = fresh to slightly weathered Fuller's Earth clay; open circles = moderately to completely weathered Fuller's Earth clay; open triangles = Fuller's Earth Bed.

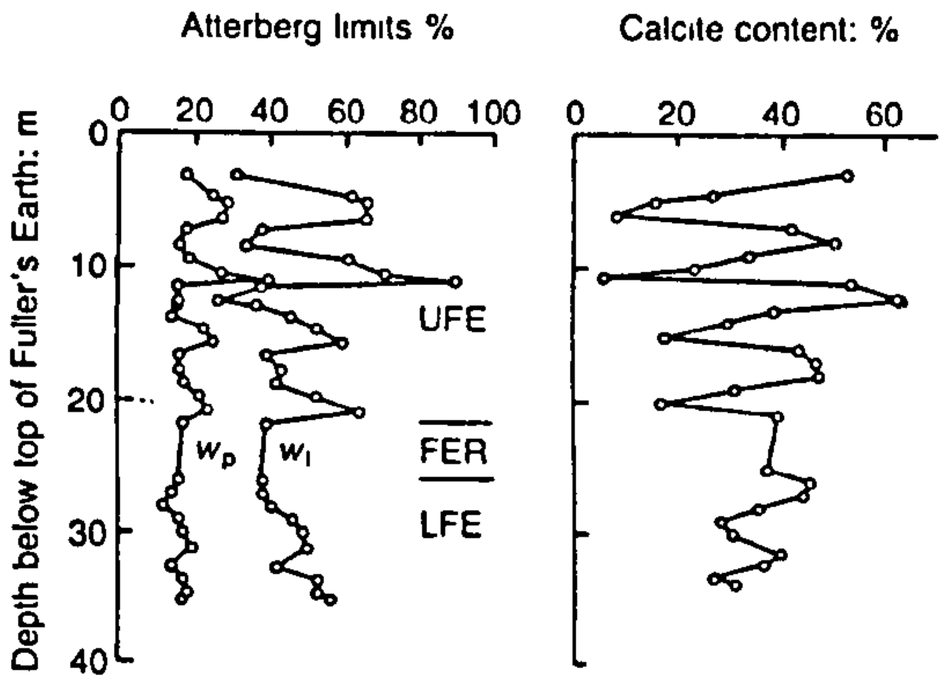

Fig. 1.10 Plots showing the variation with depth of the Atterberg limits and calcite content of the samples of the Fuller's Earth formation obtained from the borehole at Peasedown St John, after Hawkins & McDonald (1992).

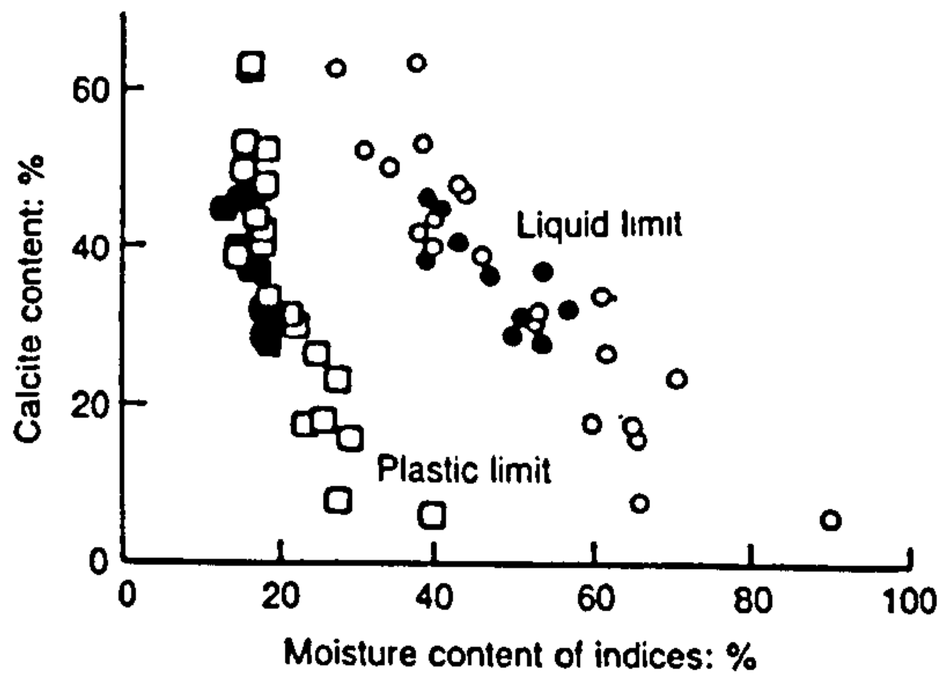

Fig. 1.11 Plots showing the relationship between the Atterberg limits and calcite content of the samples of the Upper (open) and Lower (solid) Fuller's Earth obtained from the borehole at Peasedown St John, after Hawkins & McDonald (1992).

an increase in the clay fraction, with increased plasticity of the clay. This effect is enhanced by the formation of interstratified illite-smectite increasing the proportion of swelling clay in the soil and hence the Atterberg limits are increased. Stress relief in the near surface weathered zone allows the hydration of the interstratified illite-smectite and hence an increase in moisture content results. Visual observations of weathering in the Fuller's Earth formation are indeed evident in the near surface material and Lawrence (1985) constructed a weathering scheme which is applied in Chapter 3.

McDonald (1990) and Hawkins & McDonald (1992) provide further evidence for the inverse relationship between the calcite content and Atterberg limits of the clays of the Fuller's Earth formation. They plotted the variation with depth of the index properties and calcite content of samples obtained at 1 m intervals from a borehole drilled at Peasedown St John, Bath (ST 71125815) which extended through the complete succession of the Fuller's Earth formation (see Figure 1.10). The inverse relationship between the calcite content and the indices is clearly evident, especially when the two are displayed as in Figure 1.11.

1.4 Topographic Setting and the Development of Superficial Structures

Hollingworth *et al.* (1944) were the first to describe superficial structures (cambers, gulls, dip-and-fault structures and valley bulges) in any detail, following the mapping of the Northamptonshire Ironstone. The region consists of a plateau, gently sloping to the east, at an elevation of 150 to 90 m AOD, which has been incised by local rivers to a depth of up to 60 m. The hilltop plateaus are capped by competent Jurassic strata of the Great Oolite and Inferior Oolite series (in many areas the plateaus are blanketed by a deposit of Chalky Boulder-clay), underlain by less competent Upper Lias clay, which in general forms the lower valley slopes. The regional tectonic dip of the strata is sub-horizontal, dipping at approximately 1° to the east.

The authors put forward suggestions for the origin and mode of formation of the superficial structures. They considered that the structures formed as a result of plastic deformation in the Upper Lias clay and indicated that the structures were likely to be present in other parts of the country, where a similar combination of geology (sequences of sub-horizontally bedded competent strata overlying incompetent strata) and topography existed. The work of Hollingworth *et al.* (1944) was followed by

Kellaway & Taylor (1952), who reconsidered the origin of the superficial structures during their study of the east Midlands and proposed that they were formed under periglacial conditions.

Subsequently a number of authors (Ackerman & Cave 1967, Cave 1969, Higginbottom & Fookes 1970 and Horswill & Horton 1976) have described and discussed the formation of superficial structures in various parts of the country, especially in the east Midlands and the north Cotswolds. The combination of the geology and topography within the Swainswick valley in the south Cotswolds has many similarities to that described in Northamptonshire and the north Cotswolds and hence has facilitated the development of superficial structures within the valley.

1.4.1 The Topography of the Swainswick Valley

The dissected nature of the Swainswick valley has a topography typical of the south Cotswolds. Figure 1.12 shows a schematic topographic cross-section across the Swainswick valley between Beckford's Tower near Lansdown, to the west and Solsbury Hill, to the east. The estimated levels of the individual stratigraphic units, from both the authors field knowledge and thicknesses given in the literature, are shown on the cross-section. However, it should be emphasised that these levels are very approximate and that, in reality, the cambering of the stratigraphic units and the presence of landslips have substantially disturbed the strata, such that their dips are valleyward and much of the strata is masked by head deposits.

The Great Oolite forms the cap rock of the broad plateau which drops from approximately 230 m AOD at Lansdown to 200 m AOD at Solsbury Hill, to the east. As Figure 1.12 shows, this competent rock is underlain by a series of incompetent and competent strata. The plateau has been deeply dissected by a number of rivers, in the case of the Swainswick valley, the Lam Brook has produced the steep sided valley. The close spacing of the contours and the topographic cross-section in Figure 1.12 highlights the steepness of the Swainswick valley, which separates the broad plateaus of Lansdown, Charmy Down and Solsbury Hill. The valley sides have varying slopes, the individual slope facets frequently being related to particular stratigraphic units. As a consequence, the valley sides contain slopes as steep as 22°, formed at the edge of the cap rock of the Great Oolite, but are typically 7° to 17° on the Fuller's Earth formation and underlying Liassic strata.

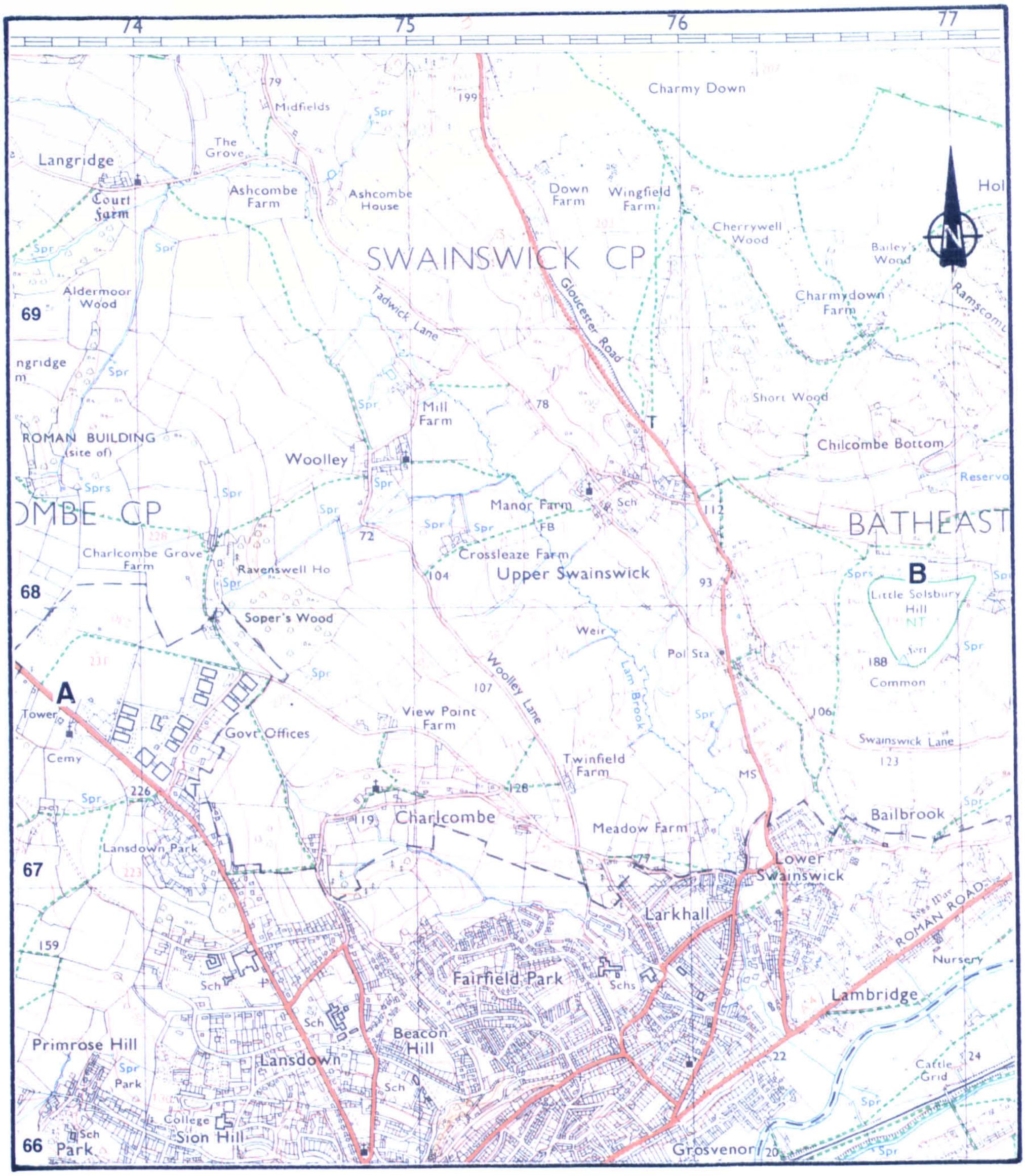

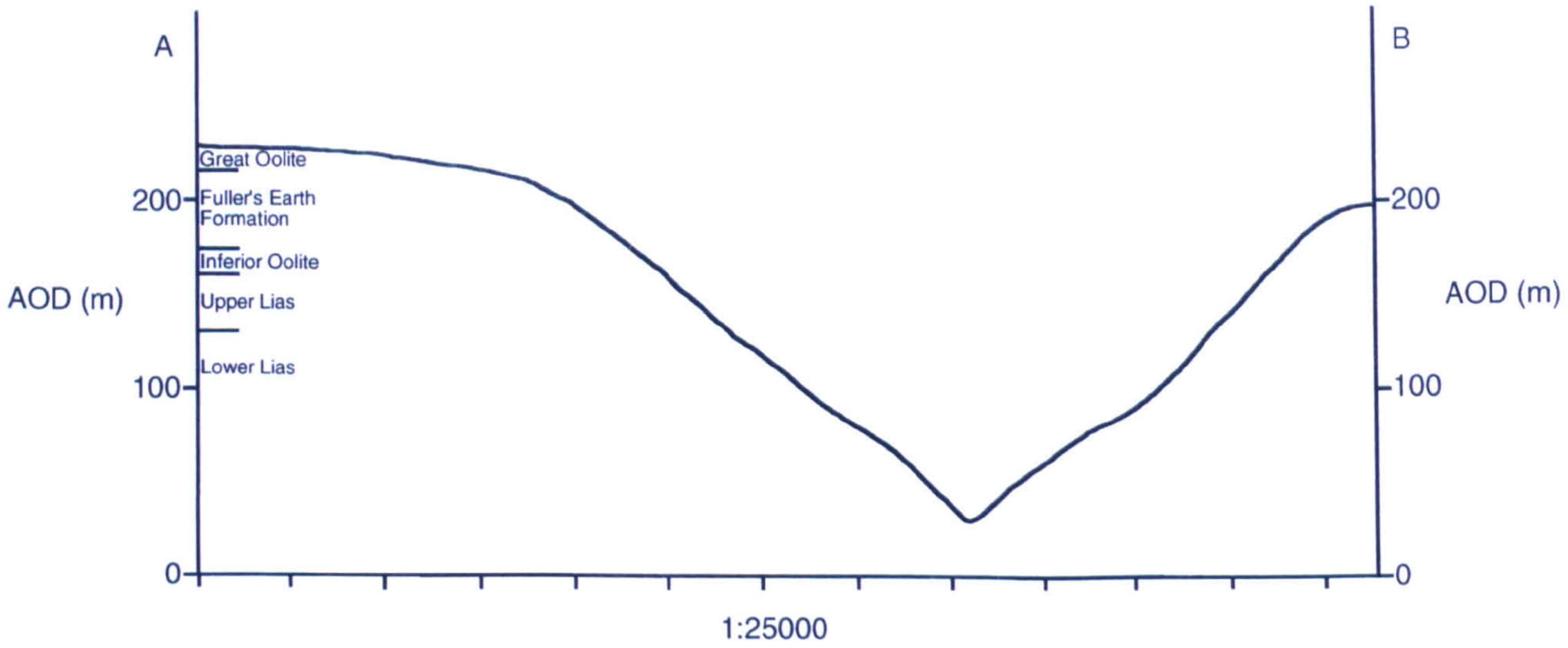

Fig. 1.12 Extract from the 1:25 000 "Pathfinder" Ordnance Survey map, Bath and Keynsham sheet 1183, with topographic cross-section across the Swainswick valley. Note the exaggerated vertical scale on the cross-section.

To the east of the Swainswick valley is the very steep sided valley of Chilcombe Bottom, a tributary valley to that formed by St. Catherine's Brook. A complete explanation for the formation of this over-steepened valley is not known, but it is believed to be related to significant water egress from the central area of Charmy Down, where the geological map indicates the presence of a structural low, as noted by the regional dip arrows.

1.4.2 Superficial Structures in the Swainswick Valley

Harmer (1907) suggested that the Limpley Stoke gorge, south of Bath, is related to glacial diversion and thus the Avon valley in Bath is in part over steepened due to the increased flow of the upper Avon catchment. Although there was clearly an early valley related to By Brook, the major incision of the river valleys would have been related to Quaternary erosion, made worse by the diversion of the upper Avon. The production of steepened metastable valley sides, resulted and still results in extensive landslipping and the development of superficial structures, as described by Kellaway & Taylor (1968).

Shallow landslips and mud flows occur extensively in the Fuller's Earth formation within the Swainswick valley, with deeper rotational slides occurring in the Lower Lias. Chandler *et al.* (1976) noted the presence of cambering, deep-seated landslides, shallow slides and mudflows, within the Swainswick valley, which are typical of the area. Cook (1973) describes an investigation of a landslip that occurred in the Fuller's Earth clay, on a south facing slope of Lansdown (ST 727679), not far from Soper's Wood. Due to the proximity of this landslip, to the landslide adjacent to Soper's Wood investigated during the course of this research, the paper by Cook (1973) is summarised below.

The landslide was initiated by the tipping of rubbish into an old quarry in the Great Oolite. Total downslope movement amounted to approximately 210 m and sterilised about 12 acres (0.05 km^2) of land. The overall slip geometry indicated that a shallow translational slip had occurred, of type 'L" classification, after Hutchinson (1967). Cook (1973) suggested that the blockage of small spring outlets at the base of the Great Oolite contributed to increased pore water pressures, which during a period of heavy rainfall, helped to initiate sliding. Piezometer measurements led him to conclude that the major slips that occurred during the wet season were a consequence of perched water table conditions.

A trial pit within the slip zone revealed a band of soft brown clay containing a distinct shear plane, sandwiched between the fill and the

weathered Fuller's Earth clay. Laboratory tests on the soft brown clay indicated an effective peak angle of friction of 17.4°, with zero cohesion and a residual shear angle of 12°. Slope stability analyses, undertaken using the infinite slab procedure (Skempton & Delory 1957) and assuming a gradient of 8.7° and residual shear strength parameters, demonstrated that the slope was only stable when the perched water table in the slip was greater than 0.5 m below ground level. It is worth noting that no analyses were undertaken using residual shear strength parameters for the steeper gradient of 12.7°, where clearly these analyses would have provided a lower factor of safety.

The investigation by Cook (1973) highlighted the general condition of instability of the slopes of the Fuller's Earth formation in the area. This instability was re-emphasised by Chandler *et al.* (1976). They carried out slope stability analyses of west facing slopes in the Fuller's Earth formation within the Swainswick valley and concluded that the majority of these slopes were in a state of limited equilibrium.

In addition to the extensive shallow translational slides over much of the Fuller's Earth formation and the deeper rotational slides in the upper part of the Lower Lias succession, as described by Kellaway & Taylor (1968), there are numerous mudflows around the egress points of springs, particularly at the edge of the Great Oolite plateau. In these areas, weathering and softening of the mudrock of the Upper Fuller's Earth has decomposed the rock structure to form an engineering soil of silty clay. In the later part of the Wolstonian and Devensian glaciations, this softened material moved as mudflows, frequently infilling the small valleys related to the individual spring outlets. Whilst the mudflows are often difficult to discern on topographic evidence, their presence has been determined during site investigation works. These mudflows are important, as the material forming them does not have the same intact competency exhibited by the general landslipped terrain, which forms in excess of 80% of the hillside slopes of the Fuller's Earth formation.

Cambering has clearly occurred in the Great Oolite, as evidenced by the lateral valley-ward creep and the formation of gulls. However, the gulls are rarely identifiable from surface morphological expression. Hawkins (1977a) notes that gulls are present in the cambered Great Oolite in the cutting at the North Road entrance to Bath University (ST 764650), south of the River Avon. These only develop into cavities about 2 m from ground level, within the medium to thickly bedded strata. Nearer the surface, within the thinly bedded weathered zone, voids tend not to develop as the

tensional strains are accommodated by small fractures and cracks. Hence, in the field above, there is no morphological evidence of the gulls below.

The most pronounced cambered strata is that of the Inferior Oolite, as below this, the calcareous, silty fine sandstones of the Midford Sands have suffered intense decalcification and leaching, with the removal of fine particles in suspension. Although the cambering in the Swainswick valley is not as prominent as the cambered slopes in the 'Newton Brook' valley to the west of Bath (Hawkins & Privett 1979), the lack of a significant topographic feature at the level of the Inferior Oolite is largely a consequence of its disturbance by superficial movement to form a camber drape. Hawkins & Privett (1979) suggest that due to both the likely age of the cambering (Anglian or Wolstonian age) and the non-catastrophic nature of their formation resulting in relatively minor surface geomorphological expression at the time of formation, any morphological evidence of cambering tends to have been smoothed by more recent superficial movement of material valleyward.

Using borehole data in the early 1970's, Chandler *et al.* (1976) produced a number of geological sections in the eastern part of the Swainswick valley, related to the realignment of the A46. Whilst these emphasise the presence of superficial features, it must be noted that these sections are based on relatively sparse information and with further data these would have undoubtedly have been refined. The accurate determination of superficial structures using borehole data frequently misses much of the structural disturbance, even when the analysis is carried out by someone with significant experience.

1.4.3 The Development of the City of Bath

The superficial structures in the Bath area have important engineering implications and have influenced the development of the City of Bath (Kellaway & Taylor 1968). By historic times the valley sides surrounding Bath had experienced a number of phases of landslipping, eg. the Bailbrook, Beacon Hill and Beechen cliff slides. Initially Medieval Bath was built on the alluvium deposits of the valley floor, however as the city grew during the 18th century, buildings spread onto the slipped Jurassic strata of the valley sides. In 1794, during the construction of Camden Crescent, failure of the slope occurred, preventing the full completion of the crescent. Between 1860 and 1870 the area below the crescent was built over, following which the Hedgemead slip, between 1875 and 1885, caused the collapse of 135 houses out of a total of 271, covering an area of

2.5 hectares (Hawkins 1977b). Moore (1880), whilst an alderman of the City of Bath, describes the slip and writes:

"Many small houses in streets and terraces, suitable to residences for the artizan and mechanic classes were built afterwards *(after Camden Crescent)*, some of which almost from the first showed signs of movement, and of late houses of a still better class, which unfortunately only add weight to an insecure surface and help on the creeping movement of all theron towards the valley".

Although Moore was a famous amateur palaeontologist and highly regarded for his work on the Lower Lias, during city council meetings he commented that there were unlikely to be limestone horizons beneath the Hedgemead area (Hawkins 1977b). This was subsequently found not to be the case, with a limestone horizon at 29 feet (8.8 m) below ground level, having a head of water of 11 feet (3.4 m), while a limestone band at 50 feet (15.2 m) below ground level had a recorded head of water of 29 feet (8.8 m). These high water heads on occasions produced pressures greater than the weight of the overlying hillwash such that the soil particles were separated and the effective stress/shear strength reduced. It was noted by a Mr Parfit that the water pressures were clearly significant, although he did not necessarily appreciate the principles of effective stress, subsequently explained by soil mechanics. Parfit noted that when the water level in local wells rose, the hillsides became unstable. Slip movement allowed the egress of water and hence the levels in the wells dropped dramatically and temporary stability developed. Through the subsequent drainage of the area stability was re-established, but rather than rebuild the houses, in 1889 it was decided to create a public garden. Small slips still periodically occur elsewhere in Bath, the three most recent being the Beacon Common slip (1958-1961), the Perfect View slip in 1972 and the St. Magaret slip in 1984.

1.5 Aims of this Research

This chapter has highlighted the steep topographic slopes of the Swainswick valley and drawn attention to the formation of the over steepened Avon valley and its tributaries during the Quaternary. In such dissected topography, where the strata has been shown to be dominated by interbedded limestone (competent strata) and mudrocks/calcareous siltstones (incompetent strata), superficial structures have developed. These superficial structures have important engineering implications and hence influenced the growth of the City of Bath and indeed continue to

cause numerous complications for geotechnical engineers during the present day.

The active landslide in the Fuller's Earth in the fields adjacent to Soper's Wood provided the focus for the research described in this thesis. An investigation was carried out, at both a macro and micro scale, to further the understanding of the slope stability problems which occur in the Fuller's Earth formation around Bath.

On a macro scale, Chapter 3 describes the field work undertaken to gain an insight into the changing geomorphology and rate of movement of an inland landslide in the Fuller's Earth. The effects of rainfall and ground water levels on the rate of movement and slope stability are studied. A comparison of the geotechnical indices of the recently slipped and apparently unslipped ground is undertaken to study the effects of mass movement on weathering rates and the geotechnical parameters of the Fuller's Earth. Ground water samples, taken from both inside and outside the visibly slipped mass, are analysed to investigate the chemistry of the ground water and determine whether active chemical weathering is occurring, with particular emphasis on the dissolution of calcite and the depotassification of illite.

On a micro scale, Chapter 4 describes the analyses of a sample of the shear surface from the landslide using XRD and SEM techniques to investigate whether preferential chemical weathering occurs along the shear surface. In addition, the moisture content and calcite content of the clay surrounding the shear surface is analysed.

To complement this investigation, a series of laboratory experiments and residual shear strength tests were undertaken to study the effects of pore water chemistry on the residual shear strength of clays. This work is described in Chapter 5. The findings of the field work and the laboratory analyses and testing are then brought together in Chapter 6, where a model is put forward for the long term and seasonal controls on the stability of inland landslides in the Fuller's Earth clay around Bath.

CHAPTER 2

RESIDUAL SHEAR STRENGTH

2.1 Introduction

In the Swainswick valley and the surrounding Bath area, the Fuller's Earth formation outcrops on steep hill-slopes, many of which are landslipped as a result of oversteepened valley sides. Figure 2.1 highlights the location of the Fuller's Earth formation on the slopes around Bath and indicates that over 80% of the outcropped Fuller's Earth is landslipped. Thus, due to past failures, it is the residual shear strength of the near surface Fuller's Earth material which is mobilised in resisting movement on the valley-sides. Chandler *et al.* (1976) undertook stability analyses of selected slopes in the Bath area using residual shear strength parameters and showed that the slopes exist in a metastable state of limited equilibrium.

The term residual shear strength (τ_r) describes the minimum shear strength reached by a soil after suffering displacement due to shearing. This Chapter provides a historical review of the development of the understanding of the residual shear strength of soil, with emphasis placed on past work relevant to this thesis.

2.2 Early Observations of Residual Shear Strength

The residual shear strength of clays has been recognised since the 1930's, when measurements of the shear strengths of soils at large displacements were carried out by Hvorslev (1936, 1937 and 1939), Tiedemann (1937) and Haefeli (1938).

Hvorslev (1936), during tests using a ring shear apparatus, noticed a reduction in shear resistance following peak shear strength and suggested that the shear resistance after failure depends on continuing displacement. It is probable that these tests were not fully drained and, in 1937, Tiedemann determined the drained residual shear strength of an undisturbed clay (Weser-Elbe clay), by carrying out drained tests in a ring shear apparatus. He described the strength attained as "pure sliding resistance" and found that the residual shear strength of the clay, when normally consolidated from a slurry, differed little from that of undisturbed, over-consolidated samples.

Haefeli (1938) used the term "Restcherspannung" or "remaining shear strength" to describe the residual shear strength of soils at the

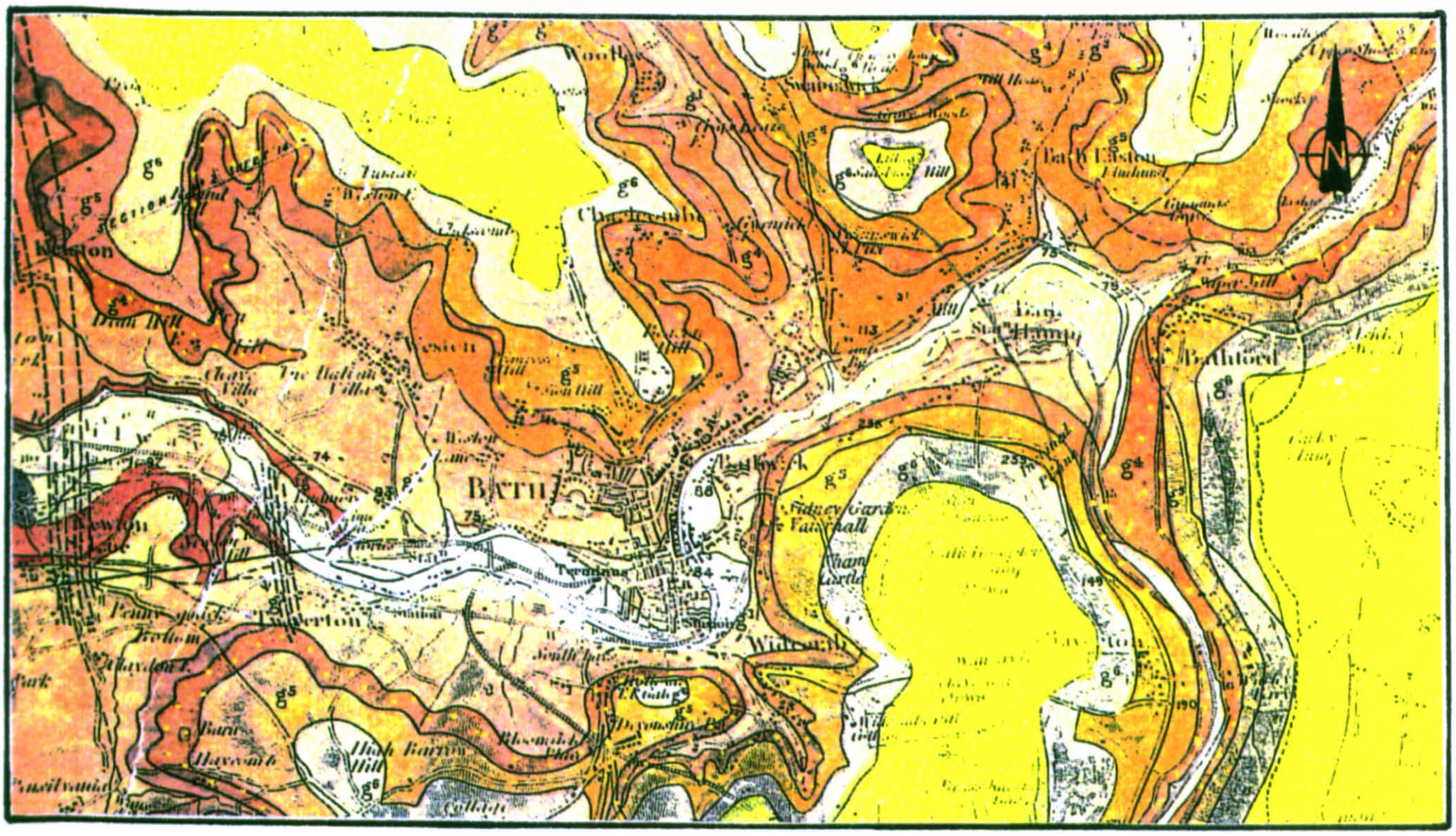
Barn
Widcombe
Bathford
Claverton
Monkton Farleigh
Farleigh Wick
Imwood
Sham Castle
Bathampton Down
Lansdown
ROMAN BUILDING
Charlcombe Copse
Rockfield Ho
Tumulus
Tumulus
Tumulus

ultimate point of the stress-displacement curve, however his stress displacement curves indicate that he did not refer to a lowest strength independent of displacement.

Casagrande (1949) is believed to have been the first to have used the term "residual" in his discussion of a paper by Binger & Thompson (1949). He noted, from laboratory tests, that the stability of a man made slope in Cucaracha Shale could be governed by a strength which is lower than the peak strength.

In 1951, Haefili suggested the term "residual strength" as a translation of "Restcherspannung" and noted that the magnitude of the drop from peak to residual strength increased with liquid limit. However, his tests were not performed with controlled rates of displacement as the shear stress was applied by dead weights, with post peak movements retarded by a spring. This was followed by a paper by Hvorslev (1960), who noted that the shear strains promoted the orientation of clay particles in a direction parallel to the direction of shear, forming slickensided failure surfaces.

2.3 Later Developments

Since the pre 1960's work on residual shear strength, much research has been undertaken into furthering the understanding of the residual shear strength of soils. This section reviews these later developments in residual shear strength.

In 1961, the construction of an embankment for the M6 motorway led to the reactivation of an old landslip at Walton Wood, just north of Madeley, Staffordshire. The landslide occurred in a 10.5 m thick zone of the Upper Coal Measures which had weathered to colluvial clay, in which kaolinite was identified as the dominant clay mineral.

Early & Skempton (1972) give a detailed description of the study of this landslide, which is an important case study in the development of residual shear strength. Preliminary, earlier accounts, are given by Skempton (1964) and Skempton & Petley (1967).

They report the first successful shear tests on samples of a slip surface from the landslide and found the residual shear strength parameters to be $c'_r = 0$ and $\phi'_r = 14°$ (where ϕ'_r is the effective residual shear angle and c'_r is the effective residual cohesion intercept). This was in reasonably good agreement with a conventional back analysis of this old but then still active landslip. Moreover, the residual shear strength of the shear surface was found to be much less than the "fully-softened" or "critical state" strength which was estimated to be $c'_r = 0$ and $\phi'_r = 20°$. In addition,

UNIVERSITY
OF BRISTOL
LIBRARY

residual shear strengths obtained from multiple reversal shear box tests on intact clay were found to be similar to those measured on the slip surfaces.

Following these tests the slip surface was observed in thin section under the polarizing microscope and they noted that the clay platelets were orientated parallel to the shear surface. Hence, they concluded that a clay has a residual shear strength when shear displacements are sufficiently large to cause the development of a continuous slip surface at which the clay platelets are re-orientated by strains so that they are parallel to the direction of movement. Other researchers have since noticed this particle re-orientation (eg. Mitchell 1956 and Morgensten & Tchalenko 1967, who used optical microscope techniques and Yong & McKyes 1971, who used the electron microscope).

In the 4th Rankine lecture, Skempton (1964) presented a number of case histories of landslides and brought the subject of residual shear strength to the engineering public, revitalising interest in the strength of landslipped clays. The residual shear strength tests reported by Skempton (1964), and by some later authors, were carried out using multiple reversal shear box tests, a technique which is likely to provide an over-estimation of the residual shear strength of a soil (Hawkins & Privett 1985). The development of a ring shear apparatus, as reported by Bishop *et al.* (1971) and Bromhead (1979), has overcome some of the problems associated with reversal shear box testing, eg. the continual change of direction of movement causing a realignment of the clay particles and hence peaks in the shear strength at the start of each reversal.

Skempton (1964) emphasised the importance of choice of shear strength parameters in slope stability analyses and concluded that:

" if a failure had already occurred, any movements on the existing slip surface will be controlled by the residual shear strength of the clay, no matter what type of clay is involved".

His lecture highlighted that unlike peak shear strength, where the strength is affected by the previous stress history of the soil, the residual shear strength of a clay is independent of the consolidation history and is dependent only on the nature of the particles. He suggested that if the soil consisted entirely of clay platelets, then the residual shear angle would be comparable to the angle of friction (ϕ_u) of the clay particles. Horn & Deere (1962) measured ϕ_u for different layered minerals including biotite, talc and chlorite and Skempton (1964) proposed that their physical properties may

not be very different from those of the non-swelling clay minerals such as kaolinite and illite.

However, Skempton recognised that the more rotund quartz grains in a sand or silt, cannot orientate themselves in the strain field at a slip surface and proposed that the residual shear angle for sands and silts may be given by the following relationship for particles in random orientation, shearing at constant volume:

$$\tan\phi'_r = \pi/2.\tan\phi_u \qquad \textbf{Equation (2.1)}$$

In the general case of a natural soil (which is likely to consist of silt, sand and clay grade material), he proposes that the non-platy, larger particles will tend to prevent ϕ'_r from being as low as ϕ_u; the larger, rotund particles preventing the full orientation of the clay platelets and contributing a proportion of their own higher residual shear angle to the overall residual shear angle of the soil. Thus, he postulated a general correlation between residual shear strength and clay fraction.

Following the 4th Rankine lecture and prior to the work of Lupini *et al.* (1981), much research was done to explore the relationship between clay fraction and residual shear angle and most authors report a reduction in residual shear angle with increasing clay content/plasticity. Figures 2.2 and 2.3 display some of the relationships found by the various authors which are summarised briefly below.

Borowicka (1965) reported that brittleness increased and residual shear angle decreased with increasing clay fraction, in reversal shear box tests on different artificial clay soils. A similar relationship was found by Blondeau & Josseaume (1976), who investigated the residual shear strength of clays of varying plasticity.

Kenney (1967), from reversal shear tests, concluded that mineralogy was the most important factor affecting the residual shear strength and that he could find no satisfactory relationship between residual shear angle and plasticity index. In a later paper, Kenney (1977) noted the importance of the proportions of clay particles to massive rotund particles present in a mixture. His findings are supported by earlier work reported by Spears & Taylor (1972) who used a shear box to investigate the residual shear strength of mudrocks and found that the residual shear strength was related to the proportions of quartz to clay minerals present.

Chandler (1966 and 1969) used reversal shear box and triaxial tests to study the residual shear strength of the Keuper Marl. He found that the

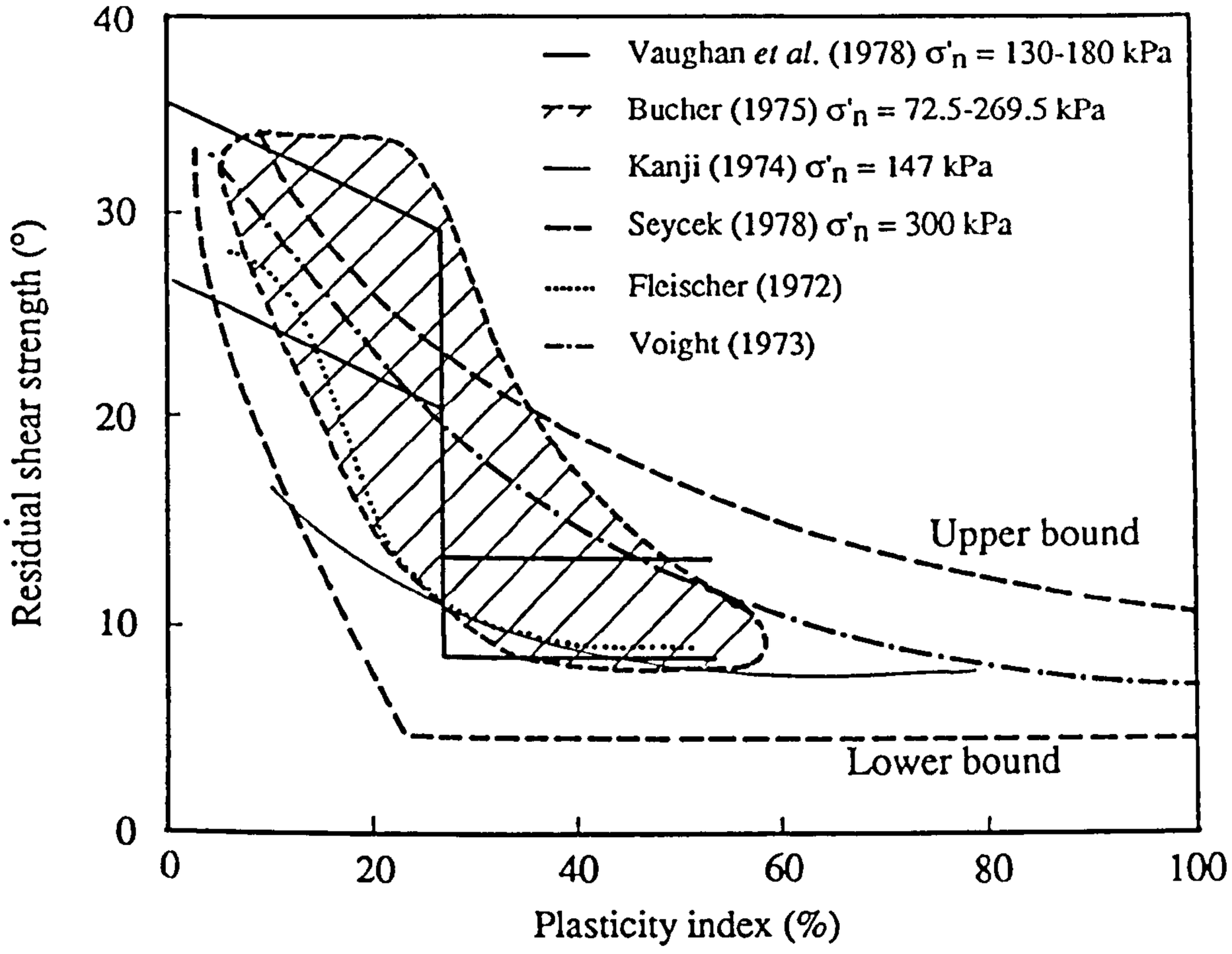

Fig. 2.2 Correlations between residual shear strength and plasticity index, after Lupini *et al.* (1981).

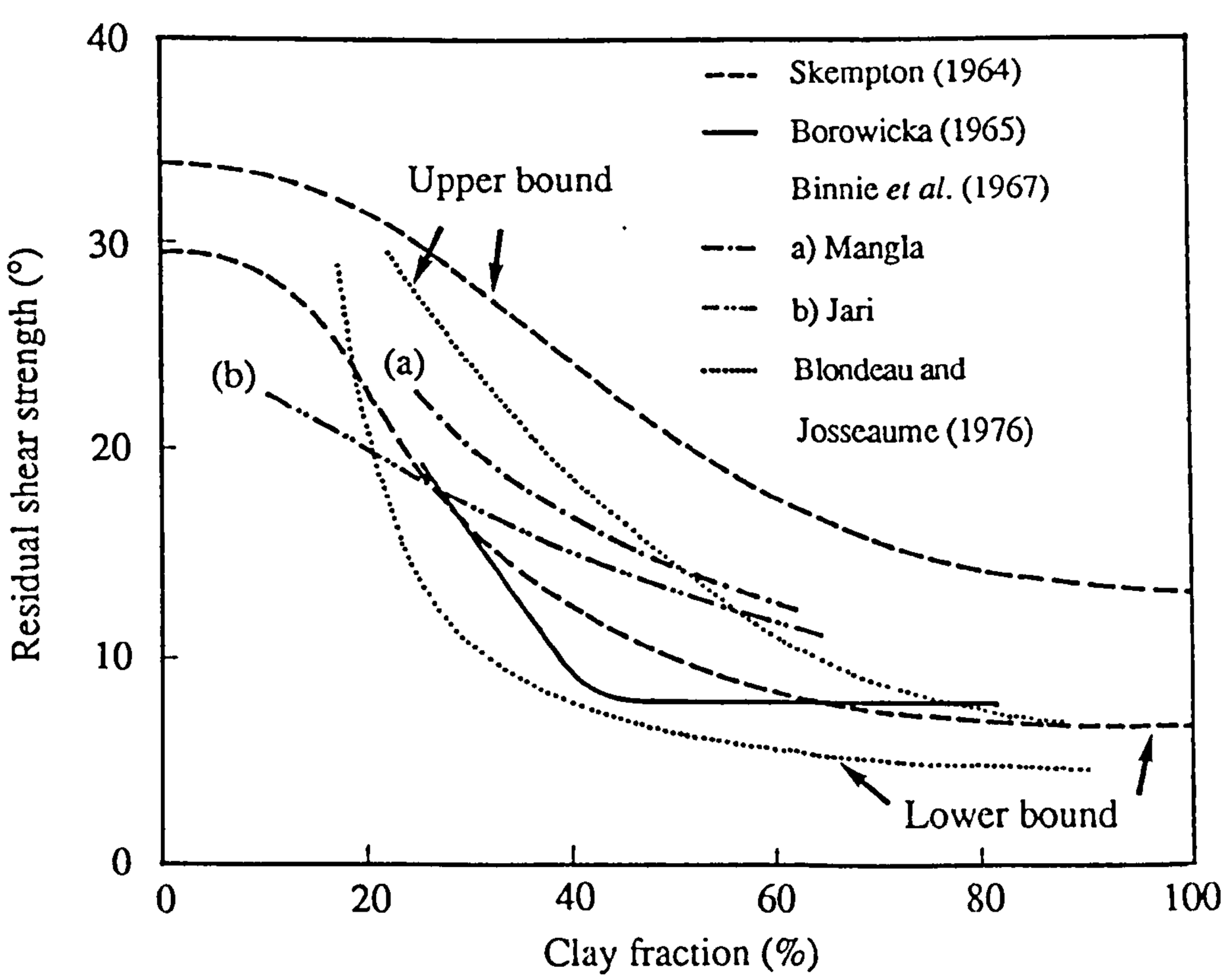

Fig. 2.3 Correlations between residual shear strength and clay fraction, after Lupini *et al.* (1981).

clay fraction at the shear surface was higher than in the adjacent soil, indicating a breakdown during shearing of the silt size aggregations of clay minerals found in the Keuper Marl. Similar observations were made by Hutchinson *et al.* (1973) during their investigation of shear surfaces from a landslide in periglacially disturbed silty mudstones of the Etruria Marl.

La Gatta (1970), Garga (1970) and Bishop *et al.* (1971) all used a strain-controlled ring shear apparatus and found that specimen preparation and stress history did not influence residual shear strength, supporting the conclusions of Skempton (1964) who reported the results of testing using a shear box. In addition, La Gatta (1970) found that the rate of shear had little influence on residual shear strength.

Chattopadhyay (1972), as reported by Mitchell (1976), found that low residual shear angles were associated with platy particles and that sub-angular and needle-shaped particles gave high residual shear angles. This relationship of residual shear strength to particle shape is supported by Wesley (1977), who reported high residual shear strengths from shear tests on highly plastic tropical clays containing allophane and halloysite minerals.

Fleischer (1972), Seycek (1978) and Fleischer & Scheffer (1979) report the results of ring shear tests on various stiff clays and noted a relationship between residual shear angle and plasticity index. This relationship was also found by Voight (1973) from an analysis of previous test data. Kanji (1974) and Kanji & Wolle (1977) report the results of reversal shear box tests on the interfaces between soils and polished rock surfaces and note that the residual shear angle decreases with increased plasticity.

Townsend & Gilbert (1973, 1974 and 1976) measured the residual shear angle of clay-shales and natural soils using reversal shear box tests and a strain-controlled ring shear apparatus. They found that the residual shear angle was independent of initial soil structure and stress history and that it was substantially independent of effective normal stress above 150 kPa. In addition, Townsend & Gilbert (1974) found that for the Dawson clay-shale the residual shear angle increases sharply when the plasticity index falls below a threshold value. This type of relationship was also proposed by Vaughan & Walbancke (1975) and Vaughan *et al.* (1978) who report the results of ring shear tests on clays of medium activity.

In 1981 Lupini *et al.* published their paper titled "The drained residual strength of cohesive soils". They attempted to confirm the results of the work carried out over the preceding 20 years and investigated the

mechanism controlling residual shear. They report the results of three separate series of ring shear tests.

The first series was conducted on medium fine sand and powdered mica mixtures to simulate the properties of natural clay. The second used mixtures of Happisburg and London clay, allowing the clay fraction of naturally occurring clays to be varied between 20% and 48%. Their last set of tests used mixtures of well graded quartz and sodium bentonite to investigate the behaviour of a bentonite-sand mixture rather than the sand-silt-clay mixture of natural clays. They studied the nature of the resulting shear surfaces using thin sections and SEM examination and compared their observations to the value of ϕ'_r obtained for each test.

Lupini *et al.* (1981) observed that three types of residual behaviour can occur depending on the proportion of platy, low friction, clay particles relative to silt and sand grade material present in the sample. Skempton (1985) summarises the three modes in Figure 2.4, with a graph of ϕ'_r against clay fraction.

In soils dominated by non-platy, rounded particles (such as silt and sand), with a clay fraction less than 25%, the material fails by rotation of the particles and hence the failure is said to occur in the *turbulent mode*. Due to the dominance of the silt and sand particles, there is no preferred particle orientation, hence a zone of shear is developed and the residual shear strength is high. In this mode the residual shear angle depends largely upon the shape and packing arrangement of the particles and not on the coefficient of interparticle friction (ϕ_u).

In soils where neither particle shape is dominant, usually with a 25% to 50% clay fraction, residual shearing occurs in the *transitional mode.* The transitional nature means that the residual shear angle is very sensitive to changes in particle size and shape. In this mode, different parts of the zone of shear, depending on the nature of the soil, will display behaviour characteristic of the turbulent and sliding modes.

The *sliding mode* occurs in soils dominated by platy, clay particles, usually with a clay fraction greater than 50% by weight. In this material the clay particles become orientated by the shear displacement and one or more discrete shear planes develop depending on the actual nature of the material. In the sliding mode, in addition to the importance of particle shape and size and the coefficient of interparticle friction, they highlighted the significance of the mineralogy of the clay particles, and the effects of pore water chemistry on the residual shear angle.

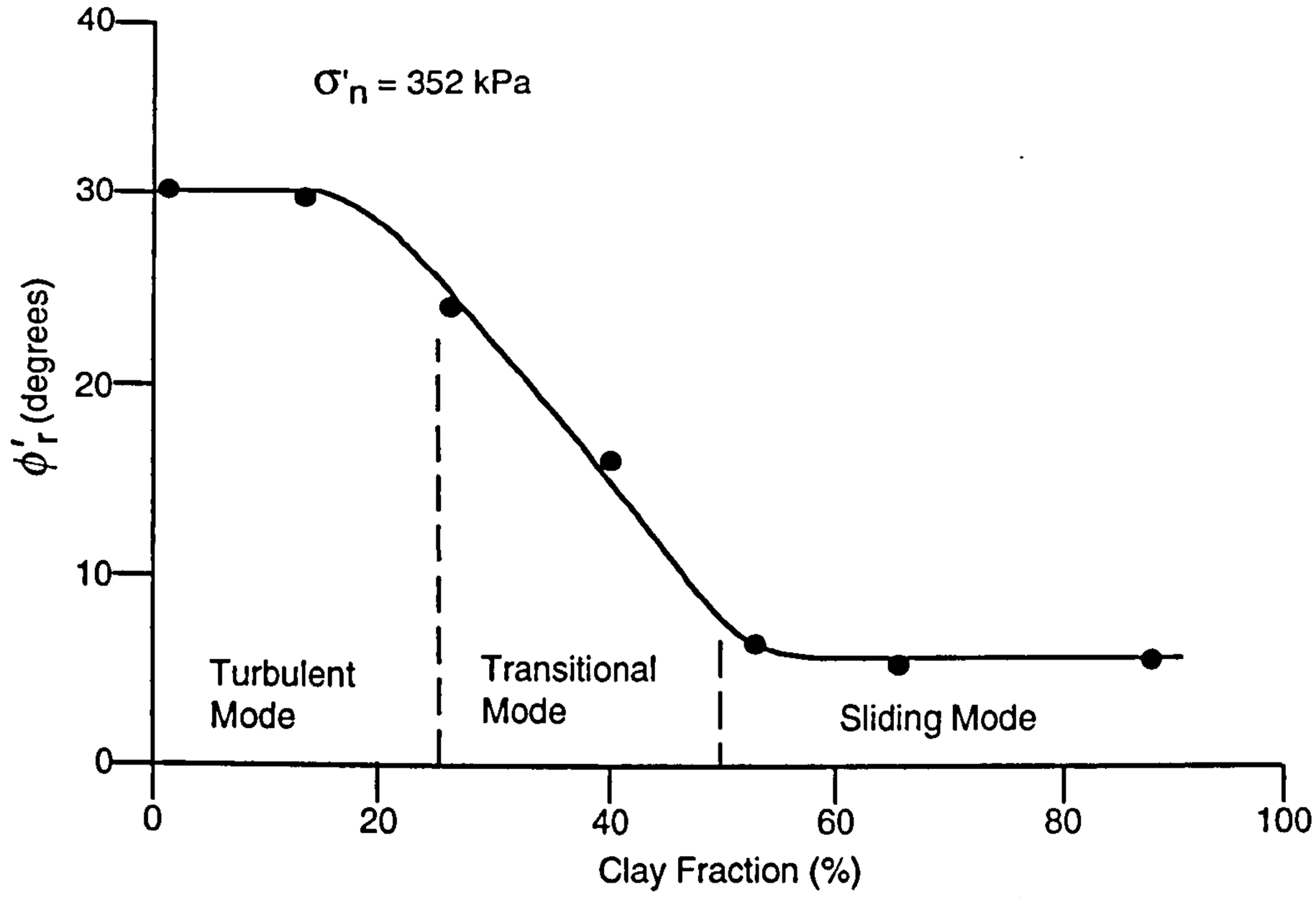

Fig. 2.4 Graph displaying the results of ring shear tests on sand-bentonite mixtures, after Skempton (1985) based on Lupini *et al.* (1981).

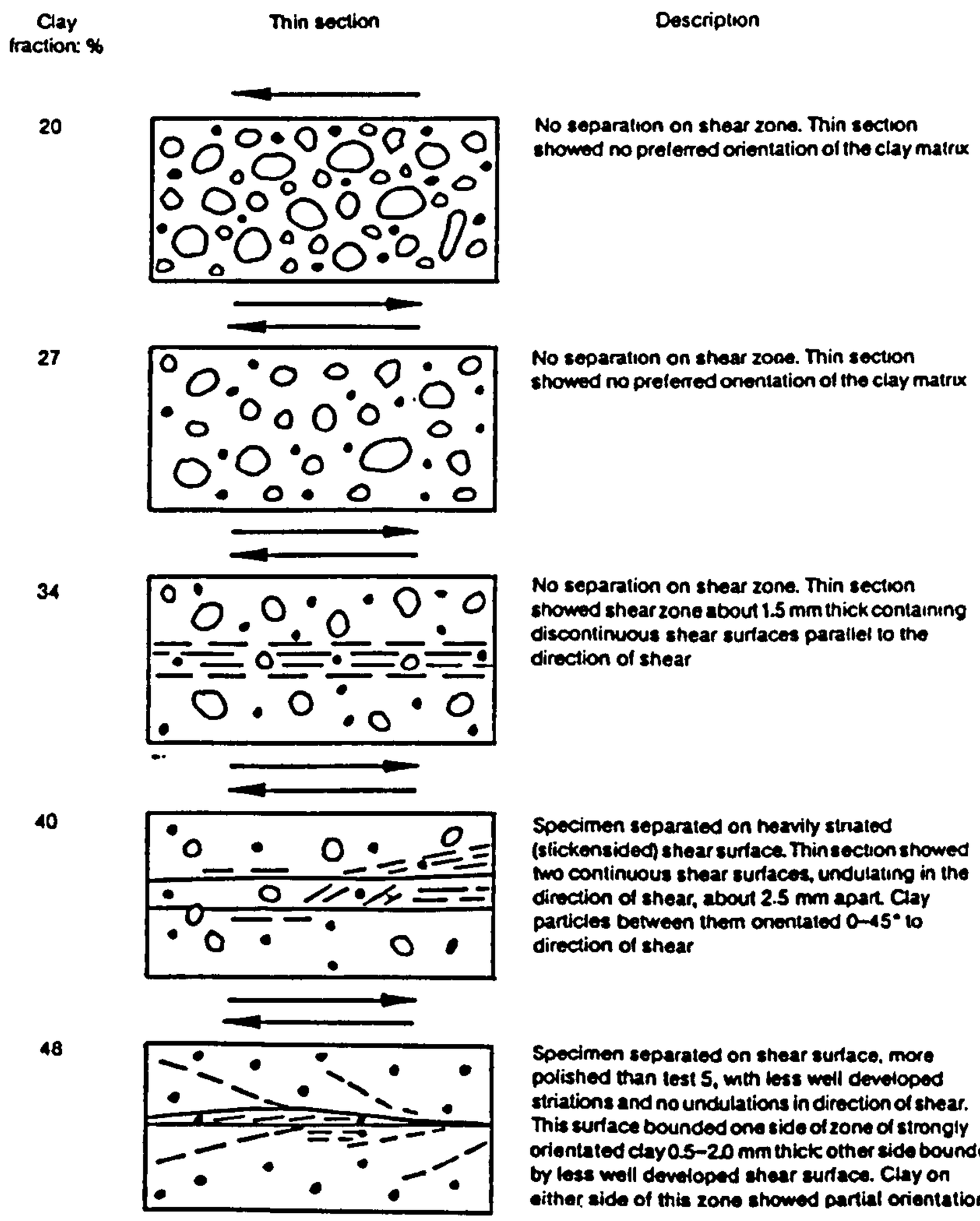

Fig. 2.5 Drawings, from thin section analysis, of the residual shear structures seen in the tests conducted on the Happisburgh-London clay mixtures. After Lupini *et al* (1981).

Figure 2.5 contains sketches by Lupini *et al.* (1981) from their examinations of the shear surfaces created in the tests conducted on Happisburgh-London clay mixtures. These diagrammatically demonstrate the modes of shear described above.

In addition to their conclusions on the modes of residual shear they state that:

"Correlations between residual shear strength and soil index properties and gradings cannot be general. They may be valuable in studying the residual strength of a particular soil deposit, provided that they properly reflect changes in the more fundamental properties of particle shape, grading, mineralogy, pore water chemistry, etc".

Lupini *et al.* (1981) recognised that the residual shear angle is dependent on the normal effective stress and this is highlighted by Hawkins & Privett (1985).

Hawkins & Privett (1985) re-emphasised the curved nature of the failure envelope at low effective normal stresses and noted the importance of establishing the value of ϕ'_r at the effective normal stress relevant to the particular slope stability problem. The determination of the complete failure envelope enables ϕ'_r to be calculated at a variety of effective stresses. The complete residual failure envelope is defined by the Mohr-Coulomb failure criterion:

$$\tau'_r = c'_r + \sigma'_n . \tan\phi'_r \qquad \textbf{Equation (2.2)}$$

where τ'_r is the effective residual shear strength, ϕ'_r is the effective residual shear angle, σ'_n is the effective normal stress and c'_r is the effective residual cohesion intercept.

In view of the initial curved nature of the envelope it is unrealistic to assume that $c'_r = 0$ and it is necessary to include a projected value of the envelope if realistic mathematical solutions are to be obtained. They defined the continuation of the envelope, at high effective normal stresses, as providing a straight line and the "lowest residual shear strength". Hawkins & McDonald (1992) redefined the residual shear angle for this portion of the envelope, as the "ultimate residual shear angle" ($\phi'_{r(ult)}$).

In 1985, Skempton gave a special lecture to the British Geotechnical Society which summarised much of the work put forward by previous authors. He stated that the post-peak drop in drained shear strength of an overconsolidated clay takes place in two stages. At small displacements the shear strength decreases to the fully softened state or critical state due to an increase in water content (dilatancy). After larger displacements, the

strength falls to the residual value owing to the reorientation of the clay minerals. However, in the turbulent mode, where rotund particles dominate he suggests that the critical state strength and residual strength of a soil will be similar.

2.4 The Residual Shear Strength of the Landslipped Mudrocks and Clays of the Fuller's Earth Formation

The individual works of Privett (1980) and Lawrence (1985), summarised by Hawkins *et al.* (1988), demonstrated that, in addition to controlling the index properties of the Fuller's Earth clay (see Chapter 1), the calcite content influenced the residual shear strength of the clay. They showed that samples of the Fuller's Earth Bed with calcite contents greater than 30%, had higher values of residual shear strength compared to samples with calcite contents less than 30%. To confirm the influence of calcite on residual shear strength, a sample with 52% calcite content was decalcified in the laboratory by acetic acid digestion. This produced a considerable reduction in ϕ'_r from 27° to 11° at a normal effective stress of 25 kPa and from 21° to 6° at 400 kPa. McDonald (1990) and Hawkins & McDonald (1992) investigated this relationship and their findings are summarised below.

A series of ring shear tests were conducted on samples of Fuller's Earth clay obtained at 1 m intervals from a borehole drilled near Peasedown St John, Bath (ST 71125815). Figure 2.6 displays $\phi'_{r(ult)}$ of the samples against the calcite content, as measured by titration. The graph shows two pronounced clusters. The upper cluster is defined by samples with a calcite content of 28% and above, with the ultimate residual shear angle having a range between 16° and 39°, generally increasing with calcite content. The second, lower cluster is defined by samples with $\phi'_{r(ult)}$ between 5° and 11°, for calcite contents of 6% to 34%. Hawkins & McDonald (1992) relate the clusters to the work done by Lupini *et al.* (1981) and conclude that the upper cluster is likely to be associated with the transitional mode of failure and the more consistent lower cluster, with the sliding mode of failure.

To investigate this relationship further, a bulk sample of Upper Fuller's Earth clay was progressively decalcified in the laboratory. The sample was taken from the base of the Upper Fuller's Earth in a trial pit, at a depth of 2.5 m, at Peasedown St John (ST 71235802). As the majority of the non-clay fraction consisted of calcitic material, the decalcification would have the effect of increasing the clay fraction. Figure 2.7 graphically

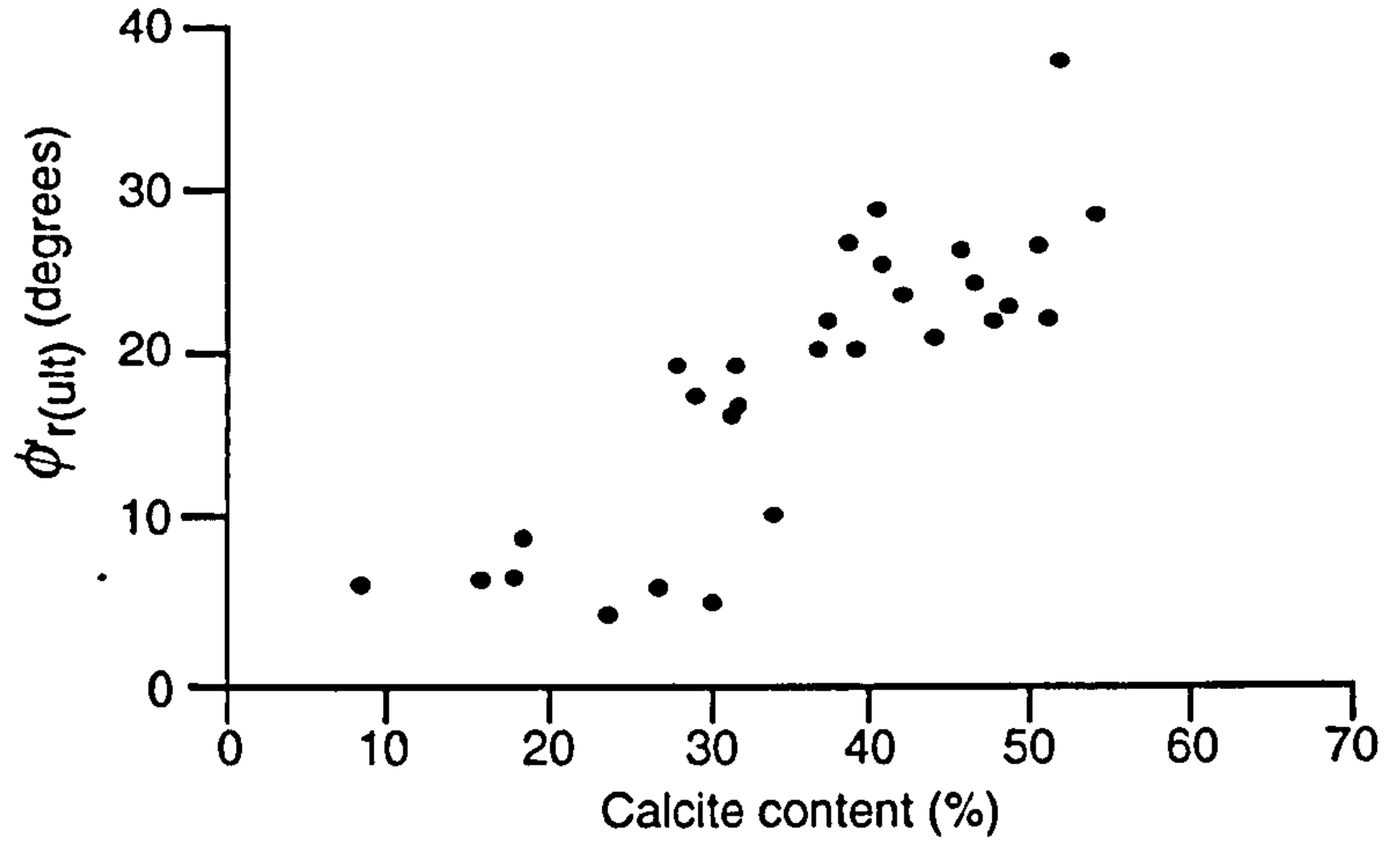

Fig. 2.6 Plot of ultimate residual shear angle against calcite content for the samples obtained from the Peasedown St John borehole, after McDonald (1990).

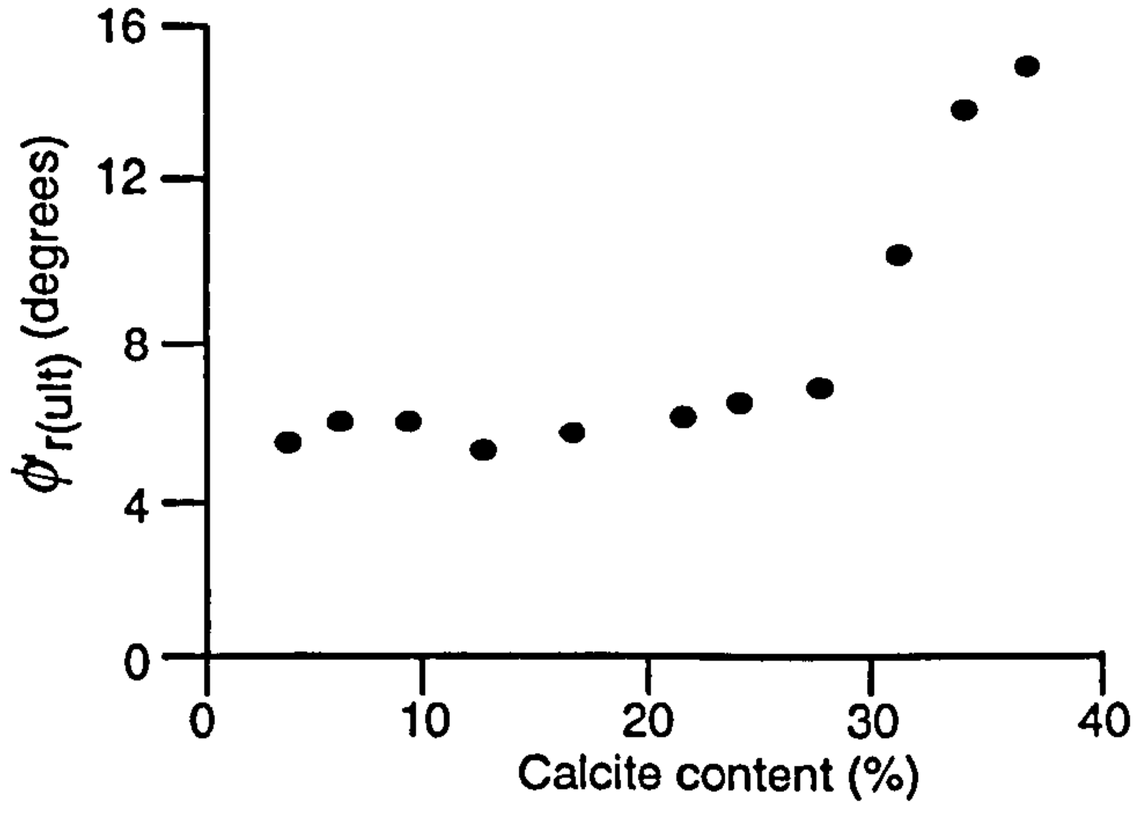

Fig. 2.7 Graph showing the relationship between calcite content and ultimate residual shear angle for a progressively decalcified sample of the Upper Fuller's Earth clay, after Hawkins and McDonald (1992).

displays the effects on $\phi'_{r(ult)}$ when the bulk sample was progressively decalcified. The graph demonstrates that, for the laboratory decalcified samples above a 28% calcite content, any increase in calcite, will increase $\phi'_{r(ult)}$ from about 5°-7°, to a maximum of 16° for the original sample containing 36% calcium carbonate. Below a 28% calcite content, the residual shear angle remains approximately constant. Due to the sensitivity of $\phi'_{r(ult)}$ above a 28% calcite content, Hawkins & McDonald (1992) consider that the results indicate that residual shear occurs in the transitional mode, while below this threshold, shear occurs in the sliding mode.

This relationship was confirmed by SEM examination of the shear surface material retrieved from the ring shear apparatus. Samples of the shear surface with calcite contents above the threshold value displayed a stepped topography in plan section and appeared as a "multilayered stack of aligned clay platelets" when viewed in cross-section. This implied a stacking of shear surfaces across a shear zone. Those samples which had failed in the sliding mode showed "smoothly striated reflective surfaces" in plan section and appeared as discrete shear surfaces with clay minerals aligned parallel to the surface, when viewed in cross-section.

The authors found that owing to the curved nature of the residual shear strength envelope, the threshold between transitional and sliding modes based on ϕ'_r, shifts from approximately a 20% calcite content at 25 kPa effective normal stress, to a 28% calcite content in the ultimate residual condition. When this effect is reconsidered in terms of residual shear strength (τ_r), they found that such a variation in the threshold does not appear and the threshold consistently occurs at a 24% calcite content. This value may therefore be the better threshold for geotechnical considerations in the Fuller's Earth clay of the Bath area.

It is interesting to note that $\phi'_{r(ult)}$ of the progressively decalcified samples with a calcite content above the threshold value is generally less than that of the samples obtained from the Peasedown St John borehole. One possible explanation for this is put forward by Hawkins & McDonald (1992). In the process of preparing a sample with acetic acid, the crystals of calcite may have had there edges rounded and smoothed. Thus, for the same calcite content, the value of $\phi'_{r(ult)}$ will be lower for samples which have been treated with acetic acid, compared to natural samples.

The presence of this threshold has important engineering implications, particularly with regard to the stability of natural slopes and man-made structures in calcareous mudrocks. Chapter 1 has shown that

with increased weathering of the Fuller's Earth clay there is a trend of decreasing calcite content, increasing moisture content and increasing Atterberg limits. In addition, in the weathered zone some of the illite present is transformed to a randomly interstratified illite-smectite. As this section has shown, if the calcite content of the Fuller's Earth clay is above its threshold value, a gradual decalcification of the clay will have a dramatic effect on the residual shear strength.

The dissolution of calcite and the leaching of clay minerals is likely to alter the chemistry of the ground water percolating through a landslide in the Fuller's Earth and, in the sliding mode of shear, Lupini *et al.* (1981) indicated that the chemistry of the pore water is likely to influence the residual shear strength of the soil. Hence, the next section reviews past work conducted on the influence of pore water chemistry on the residual shear strength of soil, with a view to providing background to work undertaken in this thesis.

2.5 Influences of Pore Water Chemistry on the Residual Shear Strength of Soils

The sensitivity of the physical properties of clays to pore water chemistry has been known about since the early half of this century. In 1941, Winterkorn and Moorman studied the effects of cation composition on the geotechnical properties of a grey-brown silty clay from Missouri, known as Putnam clay. From plane and triaxial shear tests they found that the peak shear strength of the clay was influenced by the chemistry of the ions adsorbed to the clay.

Since their work, other authors have investigated the influences of pore water chemistry on the physical properties of clays (eg. Bjerrum 1954, Rosenqvist 1946, Skempton & Northey 1952, Rosenqvist 1953, Matsuo 1957, Moum & Rosenqvist 1961, Olson & Mitronovas 1962 and Warkentin & Yong 1962). However, though the early work investigated the influence of pore water chemistry on shear strength, this was confined to peak shear strength and it is not until Kenney (1967) that the results of investigations into the effects on residual shear strength are reported. Hence, as the testing described in this thesis concentrates on the residual shear strength of pure clays, related to the investigation of an active landslide in the Fuller's Earth clay, this detailed critique focuses on the post 1967 work related to residual shear strength.

Kenney (1967) investigated the influence of mineral composition on the residual shear strength of natural soils. He conducted a series of

reversal shear strength tests on both natural soils and pure minerals, using 2 to 3 mm thick samples placed between carborundum disks in a direct shear machine, at a range of normal stresses from approximately 20 to 80 kN/m^2. In addition, micas and clay minerals were prepared in Na^+, K^+ and Ca^{2+} homoionic states, by repeated washing in the respective solution of NaCl, KCl and $CaCl_2$ to study the effects of pore water chemistry.

Kenney found that the residual shear strength of natural soils is primarily dependent on mineralogy, and to a lesser extent on system chemistry and the magnitude of effective normal stress. From his laboratory tests on pure minerals, he noted the following order of decreasing residual strength: massive minerals, micaceous minerals, kaolinite and montmorillonite. Hence for those soils containing large amounts of montmorillonite the residual shear angle is small compared to those containing large quantities of massive minerals, such as quartz. In addition, he proposed that the residual shear strength of clays and hydrous mica depended not only on the mineralogy of the clay minerals, but also on the type and concentration of cations in the pore water. He found that the residual shear strength of micaceous minerals and montmorillonite was strongly dependent on system chemistry and noted that the residual shear angle was increased by; (i) cations of a higher valency ($Ca^{2+}>K^+=Na^+$), (ii) cations of greater polarizability ($K^+>Na^+$) and (iii) increased ion concentration in the pore fluid. Kenney attributes this increase in residual shear strength to an increase in bond strength and attractive forces between clay minerals and found that at low effective normal stresses these factors have greater influences on the residual shear angle than at high stresses.

Kenney continued to investigate the residual shear strength of clay minerals, mineral mixtures and natural soils and in 1977 published the results of his further work. His conclusions support those of Kenney (1967) with regard to the effects of system chemistry on the residual shear strength of clay minerals. He found that the residual shear strength of a mineral mixture is dependent on the relative contents of massive minerals to clay minerals and on the residual shear strength characteristics of these components. Kenney writes:

"In a mixture of clay-mineral particles, quartz particles and water, the clay minerals and water form a cohesive matrix and the quartz particles are discrete inclusions in the matrix. The strength behaviour of the mixture is dependent on the relative volumes of matrix and inclusions; for small volumes of quartz, the behaviour of the mixture is controlled by the clay-mineral matrix, and increasing volumes of quartz inhibit to an increasing

extent the clay-mineral particles becoming orientated parallel to the direction of shear displacement, thus causing increased shear resistance. Beyond a certain volume the massive minerals will form a continuous structure which resists applied forces and the clay mineral matrix only acts to fill voids".

Thus in natural soils, it can be expected that the pore water chemistry will influence the residual shear strength of the soil as long as the behaviour of the soil is controlled by the clay mineral matrix, this broadly equates to the sliding and transitional modes of shear proposed by Lupini *et al.* (1981).

The work by Kenney (1967) was followed by Ramiah *et al.* (1970), who investigated the effects of chemicals on the residual shear strength of a fine grained soil, containing 7% sand, 85% silt and 8% clay, by weight. Samples of the soil were treated with either a flocculant, calcium hydroxide or with a dispersant, sodium hexameta phosphate; the samples were then subjected to a series of residual shear strength tests in a direct shear box. They found that for both normally and overconsolidated soils treated with the flocculant, the ϕ'_r was higher at 33° compared to the soil treated with the dispersant, where ϕ'_r was 28°. In addition, they reported that increasing the concentration of the flocculant and dispersant had no effect on the residual shear angle in either case. They conclude that their findings are due to the flocculated soil having more interparticle contacts than the dispersed soil and consequently the clay with flocculant exhibits a higher residual shear strength.

These conclusions differ from those of Kenney (1967), who found that for clays an increase in cation concentration increased the residual shear strength. Ramiah *et al.* (1970) fail to determine whether the 85% silt fraction was dominantly non platy minerals, such as quartz, or large platy clay minerals, such as kaolinite. The soil has a liquid limit of 45% and a plastic limit of 28%, indicating that it is likely to be dominated by the larger non-platy less sensitive minerals, such as quartz. This would affect the sensitivity of ϕ'_r to system chemistry, as Moum & Rosenqvist (1961) demonstrated that the attractive forces and bonding between clay minerals is sensitive to pore water chemistry, whereas pore water chemistry will have little or no effect on the more rounded, larger minerals, such as quartz, as noted by Kenney (1967). In addition the dominance of quartz would mean that shear occurred in the transitional or turbulent mode so that no discrete shear plane would form; Lupini *et al.* (1981) concluded that in the turbulent

mode of shear, ϕ'_r depends largely upon the shape and packing arrangement of the particles and not on system chemistry.

Prior & Graham (1974) report the results of reversal shear box testing of intact samples and samples of shear surfaces obtained from landslips in weathered Carboniferous shale. The testing was carried out at a range of low effective normal stresses (c. 20 to 120 kN/m^2) providing a residual failure envelope for this low stress range with c'_r = 5.0 kN/m^2 and ϕ'_r = 8.2°. They do not curve the envelope to the origin, however the results appear to approximate a straight line above σ'_n = 20 kN/m^2 such that their reported values may be equivalent to the "ultimate" case as defined by Hawkins & McDonald (1992).

They note that it is unusual to observe values of c'_r of such magnitude, as many authors state that c'_r should be zero. Thus, from a literature search, they produced Table 2.1 which highlights the residual shear strength parameters of some clays where a residual cohesion intercept was noted, as determined in reversal shear box tests. This table does not give any indication of the percentage of clay minerals, simply the nature of the clay minerals present.

Source	Location and Material	Clay Mineralogy	c'_r kN/m^2	ϕ'_r
Skempton & Petley (1967)	London Clay		1.5	13°
Quigley *et al.* (1971)	Toronto varved clay	illite, chlorite, montmorillonite, vermicullite	20	16°
Chandler (1972)	Uppingham Lias clay	kaolinite, illite, montmorillonite, vermicullite	10	20°
Parry (1972)	Bedford Oxford Clay	vermicullite, montmorillonite, illite	20	12.5°-25°

Table 2.1 Examples of residual shear strength parameters for a variety of materials for which c'_r ranges from 1.5 kN/m^2 to 20 kN/m^2, after Prior & Graham (1974).

They relate residual cohesion to physico-chemical forces and quote from Yong & Warkentin (1966), who wrote:

"Cohesion is a property of the clay soil mass arising from physico-chemical forces of an interatomic, intermolecular and inter-particle nature...and is so dependent upon the interaction of the clay water system that a definitive description as to what constitutes cohesion becomes virtually impossible".

There is currently much debate regarding the presence of cohesion amongst engineering geologists and geotechnical engineers. However, Prior & Graham (1974) have indicated that it is affected by system chemistry and, from stability analyses, that the cohesion plays a part in the stability of the landslip they were studying. Hence, they propose that c'_r is a parameter which cannot be ignored in stability calculations of shallow slip masses.

Steward & Cripps (1983) and Steward (1984) studied the engineering implications of chemical weathering with regard to a landslip in a weathered Namurian pyritic shale, known as Edale Shale, at Mam Tor, Derbyshire. They used a modified ring shear apparatus that enabled the flow of specific chemical solutions through the the sample during shearing. The sample was first consolidated at an effective normal stress of 294 kPa, approximately equivalent to the in situ stress at the depth of the shear surface, and then each test started by establishing the residual condition using distilled water. Once the residual shear stress had reached a constant value, different chemical solutions were fed from a reservoir tank through the sample and a new residual shear strength established. The value of ϕ'_r, at that effective normal stress (294 kPa), was then calculated by assuming c'_r equalled zero.

Their experiments were carried out using solutions of $NaNO_3$ and KNO_3 on the dark grey mudstone. They state that the mudstone had a clay fraction of 40%, the remaining 60% comprised quartz with some feldspar clay minerals and diagenetic pyrite. Of the clay fraction, 50% consisted of expandable mixed layer clays, 21% illite, 23% kaolinite and 6% chlorite. As Figure 2.4 shows, a 40% clay fraction indicates that the mudstone is likely to shear in the transitional mode and hence it is less likely to be sensitive to system chemistry compared to shear in the sliding mode, as noted by Lupini *et al.* (1981). Having obtained the residual shear angle with distilled water, $NaNO_3$ was then fed through the sample and the new residual shear angle measured. The sample was then flushed with distilled water and a solution of KNO_3 fed through. This process negated the effects of any variation due to the use of different samples and was repeated in reverse order to check accuracy. They consider the results to show that ϕ'_r is sensitive to pore water chemistry. Treatment with a solution of 0.1M KNO_3 increased ϕ'_r to 23°, from 22° obtained for distilled water; treatment with 0.1M and 1.0M solutions of $NaNO_3$ decreased it to 20° and 19°, respectively, indicating that ϕ'_r may be sensitive to solution concentration. Their findings correlate with the previous work by Kenney (1967), who found that the residual shear

strength of montmorillonite was lower in the presence of Na^+ ions compared to K^+ ions. Steward & Cripps (1983) found that the changes were rapid and reversible suggesting that ion exchange takes place in the interlayer and on the outer surfaces of the clay minerals, affecting clay swelling and bond energies and thus influencing residual shear strength.

The results were then compared with data from field investigations of the landslip at Mam Tor, Derbyshire. The ground waters were found to be rich in Ca^{2+}, Mg^{2+} and K^+, probably from carbonate dissolution and the leaching of illite by acidic ground waters originating from the oxidation and dissolution of pyrite. They conclude that these mineralogical changes together with pore water composition play a part in determining the residual shear strength and hence the stability of the landslip. In addition, they indicate that other weathering reactions such as void creation (Vear & Curtis 1981) and the expansion of discontinuities, due to the precipitation of minerals from supersaturated solutions, may also occur and are of engineering significance. The volume change, according to Vear & Curtis (1981), may allow access to previously unweathered material by acidic ground waters.

This interesting study related laboratory work on the influence of system chemistry on residual shear strength to weathering of a landslip for the first time. However, there are two issues arising from their technique for establishing the residual shear strength of the shale which should be discussed. The first is that the forcing of solutions across a shear surface may mean that the anisotropic alignment of clay particles parallel to the shear plane is disturbed, affecting the values obtained for residual shear strength. Steward (1984) states that concerns were held over the possibility of a change in effective stress and liquefaction of the clay using this technique. However, confidence was gained as the residual shear strengths obtained in tests performed with distilled water in an unmodified ring shear apparatus, were comparable to values obtained with distilled water under a flow regime.

Secondly, the method used to establish the value of ϕ'_r, where τ_r is only determined at one value of σ'_n and ϕ'_r calculated by assuming c'_r equals zero, is likely to provide an over valued result due to the curved nature of the residual shear strength envelope. The assumption that $c'_r = 0$ is in itself open to discussion, however Steward (1984) states that:

" the value of c'_r is not critical in comparative work where the normal stress is not changed".

In addition, it is interesting to note that Steward (1984) described the shear angle as an "apparent residual friction angle" (ϕ'_{ra}) due to; (i) the constant normal effective stress during testing, hence ϕ'_{ra} values are not true residual shear angles for Edale Shale and (ii) displacement during shearing may have been insufficient to establish a full residual condition. She describes ϕ'_{ra} as probably an "intermediate minimum shear resistance". However, in Steward & Cripps (1983) the same method is used to establish this "intermediary minimum shear resistance" but it is quoted as ϕ'_{r} rather than ϕ'_{ra}.

Moore (1988 and 1991) considered the chemical controls upon the residual shear strength of pure kaolinite, montmorillonite, and weathered and unweathered samples of Weald and London Clay, using the same technique as Steward & Cripps (1983). Sodium and calcium chloride salts were used to conduct a series of ring shear tests on the pure clays, as Ca^{2+} and Na^{+} are important cations in fresh water and salt water systems, respectively. The results showed that both kaolinite and montmorillonite had lower residual shear strengths when treated with sodium chloride compared to calcium chloride (see Figure 2.8). In addition, the concentration of the cation affected τ'_r, but as Figure 2.8 shows, there is no obvious linear trend. It is worth noting that the molarity of the calcium ion used, though broadly comparable with the concentrations found in seawater, is much higher than that found in natural fresh water systems.

Testing on the Weald and London Clay revealed that weathered material has a lower residual shear strength compared to unweathered (see Figure 2.9). In addition, testing the Weald and London Clays using various concentrations of seawater to assess the influence of sea salts, showed that an increase in seawater concentration provided an increase in τ'_r. Figure 2.9 shows this trend, which is relatively linear.

Moore (1991) concluded that in the sliding mode of shear, where clay content is high, residual shear strength is influenced by; (i) the type of clay minerals due to differences in particle size, shape and surface area and (ii) the type, valency and concentration of cations in pore water solutions. In the discussion of his paper, Moore (1992) proposes that an increase in residual shear strength and a decrease in plasticity occurs with increased salt concentration and cation valency, due to an increase in the strength of interparticle bonds. He notes that there should be closer control

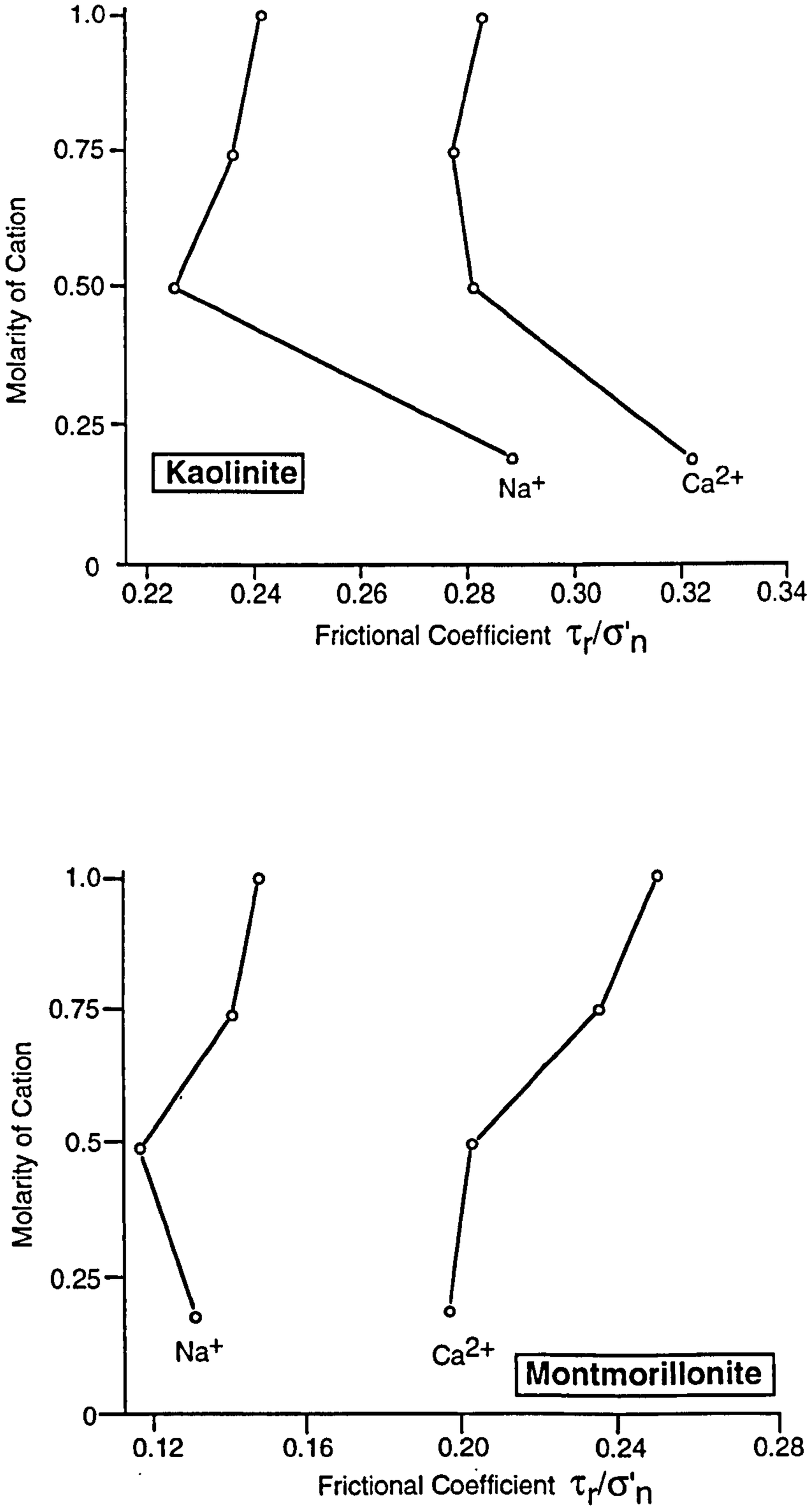

Fig. 2.8 Graphs showing the residual shear strength, at σ'_n = 250 kPa, of pure kaolinite and montmorillonite treated with sodium chloride and calcium chloride, after Moore (1991).

UNIVERSITY
OF BRISTOL
LIBRARY
WILLS M.L.

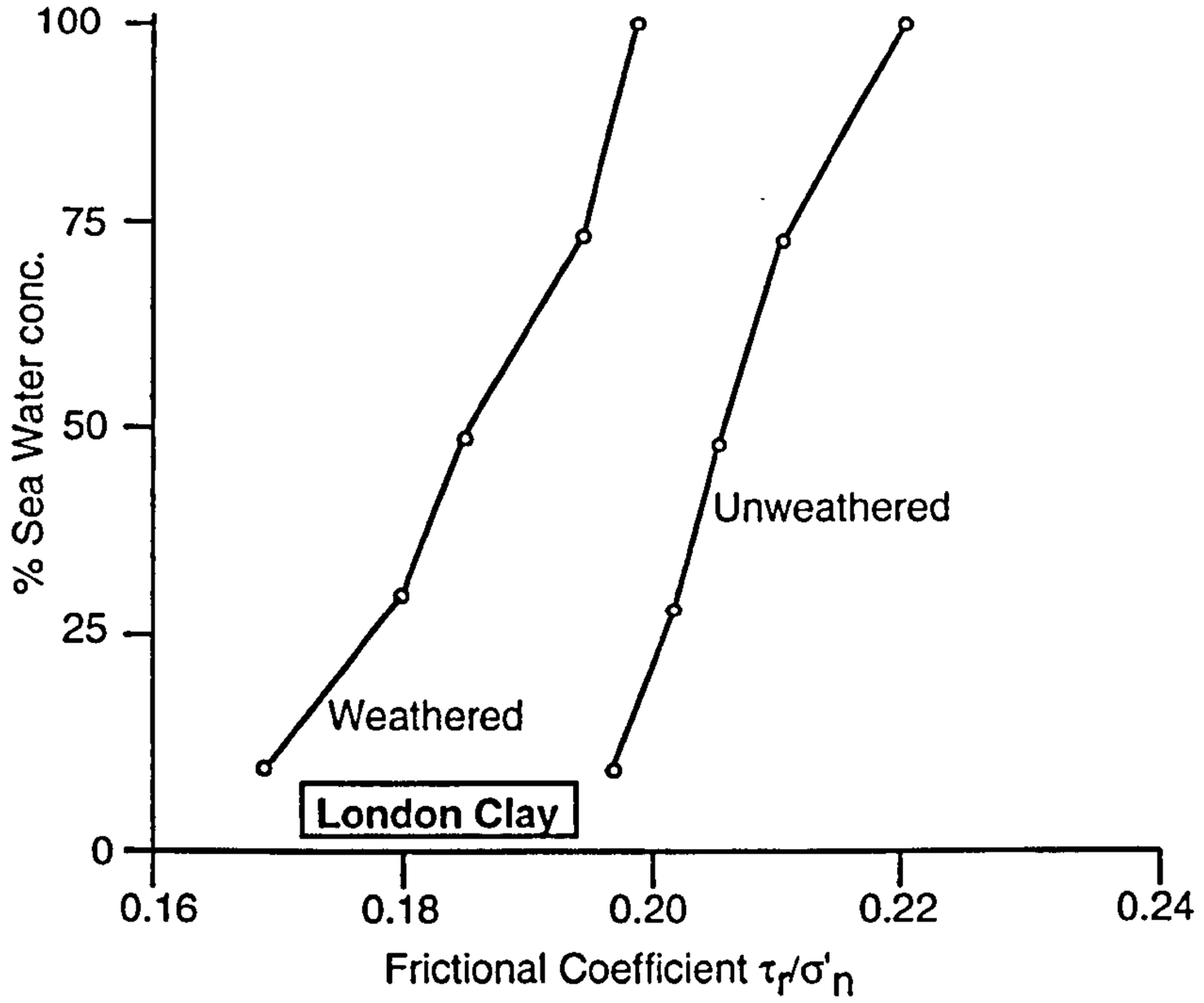

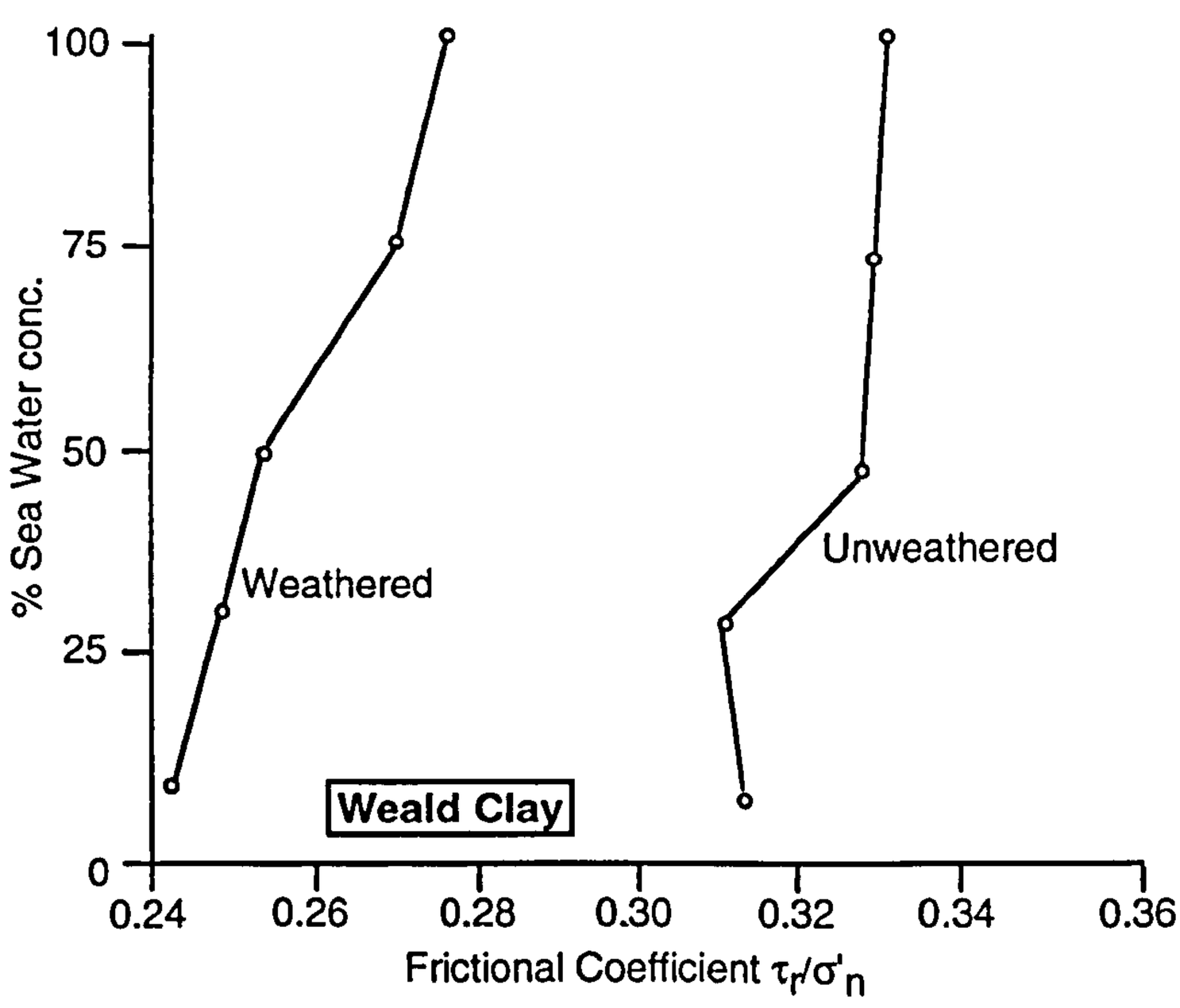

Fig. 2.9 Graphs showing the effect of sea water concentration upon the residual shear strength, at $\sigma'_n = 250$ kPa, of weathered and unweathered London and Weald clay, after Moore (1991).

of chemical conditions during testing procedures and proposes that changes in residual shear strength could be prevented by using naturally occurring ground water from sampling sites.

From the results of these laboratory studies, Moore suggests that seasonal fluctuations in the concentration of salts in pore water can modify the residual shear strength of naturally occurring clays. This concept is expanded by Moore & Brunsden (1996).

Moore & Brunsden (1996) calibrated observed seasonal fluctuations in the pore water concentration of a coastal mudslide in Weald Clay with the changes in residual shear strength reported by Moore (1991). From stability analyses they demonstrated that field observations of pore water pressures and the presence of undrained loading (as described by Hutchinson & Bhandari 1971) were insufficient to cause instability. It was only when variations in the residual shear strength of the clay due to changes in system chemistry were incorporated into the model, that it started to predict the observed behaviour of the mudslide. The correlation of pore water chemistry data obtained from the field with laboratory measured residual shear angles for use in stability analyses is innovative, however caution should be noted as the shear angle measured by Moore (1991) is the apparent residual shear angle as defined by Steward (1984).

Moore & Brunsden (1996) propose a physico-chemical mechanism for the observed seasonal movement as follows:

(1) During the winter months pore water pressures increase in excess of clay bond strength. Initially this results in small "stick-slip movements" in response to the gradual bond braking along the pre-existing shear surface.

(2) Eventually the clay minerals at the shear surface become poorly bonded and have zero cohesion so that "surge behaviour" results. This movement aids the infiltration of air-borne salts deposited by winter storms and together with degradation and weathering processes there is an increase in pore water concentration.

(3) The increase in pore water concentration results in a higher residual shear strength as it allows close range ionic bonding to develop. Thus, the mudslide has a higher residual shear strength at the end of movement compared to at the start. They use this to explain why higher pore pressures were required to trigger subsequent movements and why movement can cease while pore pressures remain high.

(4) During periods of no movement (in their case study this corresponds to the summer months), the pore water becomes progressively more dilute due to the infiltration of rain water. This causes weakening of close range

ionic bonds and thus as winter approaches again, the higher winter pore water pressures increase in excess of clay bond strength and instability is induced.

This physico-chemical explanation for the seasonal movement of coastal mudslides is clearly of interest and there may be a similar explanation for the seasonal movement of inland landslides. However, the control on pore water chemistry in inland slides is likely to be different to that of coastal mudslides, where sea water is washed onto the mudslide by winter storms.

The most recent published work in this field is by Maio & Fenelli (1994). They consider the effects of sodium chloride solutions on the residual shear strength of kaolinite, sodium bentonite and on mixtures of the two clay minerals. The residual shear strength of the clays was established using a Casagrande direct shear box. Initially distilled water was placed in the water bath. However, once the residual shear strength had been established for a particular sample, the distilled water was replaced by a solution of 1M NaCl and the test repeated until a new value for the residual shear strength was obtained. The water bath was then emptied and refilled with a solution of saturated NaCl and the procedure repeated again.

In direct contrast to Moore (1991), they find that the behaviour of kaolinite is not influenced by exposure to either solutions of 1M sodium chloride or saturated sodium chloride. However, they report that the residual shear angle for bentonite increases from about 6 ° in the case of distilled water, to 9° for 1M NaCl solution and to a value as high as 18° when treated with a solution of saturated NaCl.

They conclude that this increase in residual shear strength is due to the increase in true effective inter-particle stresses (Sridaran & Ventakappa Rao 1979 and Chatterji & Morgenstern 1989), which vary with pore water salt concentration because of the existence of significant physico-chemical forces. This interpretation could explain the difference in behaviour of the bentonite and kaolinite samples. It is supported by their investigation of the shear surfaces by SEM which did not reveal any change in the micro-structure of the clays (ie particle aggregation) which might account for the observed changes in residual shear strength. However, it is worth noting that any precipitation of sodium chloride from the saturated solution will undoubtedly increase the residual shear strength of the clay, not as a result of a change in physico-chemical forces, but due to the relative decrease in clay fraction.

2.6 Conclusions

The above reviews indicate that the residual shear strength of clays appears to be very sensitive to changes in pore water chemistry, however there is some lack of consistency between the results of various authors. In addition, previous workers have only observed the residual shear strength at one particular effective normal stress (or at a range of low effective normal stresses in the case of Kenney 1967) rather than defining the complete residual failure envelope for the samples tested. It appears that in general the residual shear strength of clays shearing in the sliding mode and possibly the transitional mode is increased by; (i) cations of a higher valency, (ii) cations of a greater polarizability, and (iii) increased ion concentration in the pore fluid.

While failings in the various experimental techniques have been highlighted, it is worth emphasising the highly complex and sensitive nature of clay chemistry, such that a simplification of the systems is often necessary in order to preserve sample homogeneity. Within the research programme described in Chapter 5, work has been undertaken to investigate the influence of calcium ions in pore water on the complete residual failure envelope of clays, with particular reference to the study of the landslide in the Fuller's Earth adjacent to Soper's Wood.

CHAPTER 3

A DETAILED INVESTIGATION OF AN ACTIVE LANDSLIDE IN THE FIELDS TO THE SOUTH OF SOPER'S WOOD, BATH

3.1 Introduction

The landslides found in the fields to the south of Soper's Wood are known to have been active on several occasions over at least the past 27 years. Fresh scarps were evident in early January 1994 following the very high levels of precipitation in late December 1993, indicating that some of the landslides had become reactivated. Chapter 1 highlights the historical slope stability problems of the Bath area, hence the reactivated landslides in the fields adjacent to Soper's Wood provided an excellent opportunity to undertake a field study of an active landslide.

This chapter describes the field investigation of the reactivated slipped area closest to Soper's Wood. This landslide was chosen as it was the most pronounced reactivation and it had been previously mapped and referred to by Lawrence (1985). Engineering geomorphological mapping and surveying for line and level were undertaken to gain an insight into the changing morphology and rate of movement of an inland landslide in the Fuller's Earth. The rate of movement is then compared to cumulative rainfall and ground water levels observed in standpipes located both inside and outside the visibly slipped mass, to study the effects of precipitation and ground water levels on slip movement rates and slope stability.

Samples of the visibly slipped and unslipped Fuller's Earth clay were obtained from auger holes and logged to study the effects of mass movement on weathering grade. The geotechnical indices of these samples are then compared to study the effects of landslide activity on the geotechnical parameters of the Fuller's Earth. In addition, ground water samples were extracted from the standpipes for chemical analysis, to investigate chemical weathering and determine whether it occurs at preferential rates within the slipped mass, with particular emphasis on the dissolution of calcite and the depotassification of illite.

For convenience, the landslide studied in this thesis will be described as being located "at Soper's Wood" or as the "Soper's Wood landslide". However, as Section 3.1.1 describes, in reality the landslide is located in the field just to the south of the wood. This clarification should prevent any confusion arising with a relict landslide situated within the

wood and with other landslides located to the south of the one investigated, which are not discussed in this thesis .

3.1.1 Location

Soper's Wood (ST 746667) is situated on the west side of the Swainswick valley, approximately 3 km north of the centre of the city of Bath (see Figure 1.1). The landslide investigated during this research is located in the field adjacent to Collier's Lane at the top of the valley, next to the southern boundary of the wooded area (see Figure 3.1 and Plate 3.1). As evident from the close contours in Figure 3.1, the land here is steep and consequently the main farming activity has been grazing. The area contains abundant geomorphological evidence of landslipping, including scarps, transverse cracks and rounded toes of slipped material. These are most clearly visible during the winter months, being masked by vegetation with the onset of summer.

3.1.2 Geology

The general geology of the Swainswick valley is discussed in Chapter 1. Figure 3.2 contains a summary geological map of the Soper's Wood area from the initial unpublished 1:10560 Geological Survey map, Sheets Gloucs. LXXVII and Soms. VIIISW. The map emphasises the limestone plateau of the Great Oolite at the top of the valley and highlights the cambered nature of the margin of the Great Oolite. The landslide under investigation occurs in the Fuller's Earth, below the cambered spur of the Great Oolite, and is depicted on the map as “hummocky clay slips exposing fresh earth scars”.

In 1974, a research borehole (ST 74556774) was drilled approximately 20 m down-slope from Collier's Lane, in an old quarry (about 1.5 m deep) in the small field just to the south of the wood (see Figure 3.2). The detailed log of this borehole has been recorded in Lawrence (1985) and a summary log is shown in Figure 3.3. The borehole proved 26.85 m of the Upper Fuller's Earth, 2.95 m of the Fuller's Earth Rock and 10.85 m of the Lower Fuller's Earth. The summary log indicates that beneath the limestone of the Great Oolite, the Fuller's Earth in the area consists of interstratified claystone and limestone. The Fuller's Earth Bed, important to the south of Bath, is absent in this area; the volcanic ash being of only limited aerial extent.

Although not indicated on the map in Figure 3.2, from the borehole drilled through the “in situ” strata, the projected Fuller's Earth Rock horizon

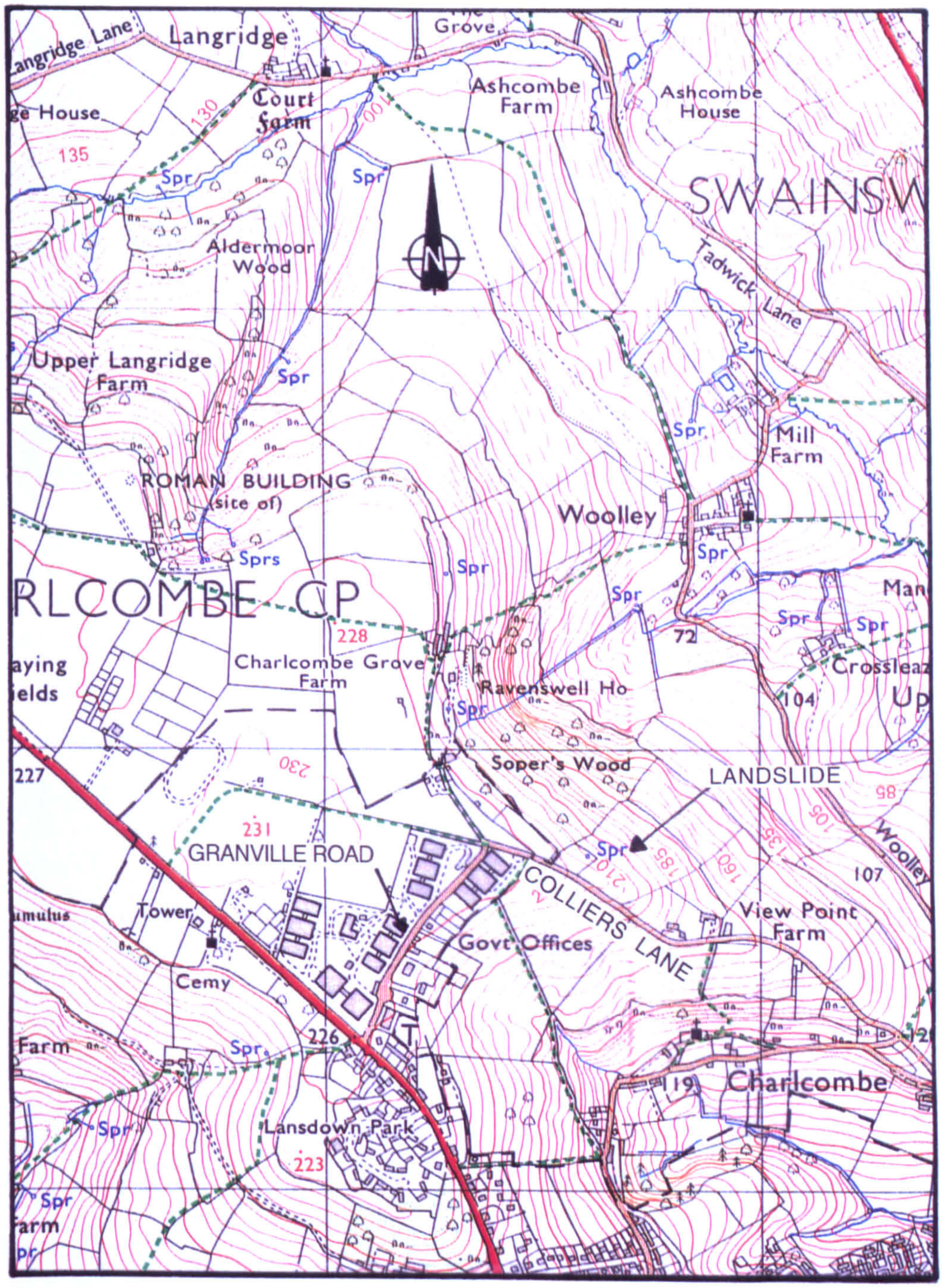

Fig. 3.1 Enlarged extract (scale approximately 1:17800) from the 1:25000 'Pathfinder' Ordnance Survey map, Bath and Keynsham sheet 1183.

Plate 3.1 View from Solsbury Hill of the west side of the Swainswick valley. Soper's Wood can be seen in the distance to the right of the photograph; the landslide studied is located in the field adjacent to the wood.

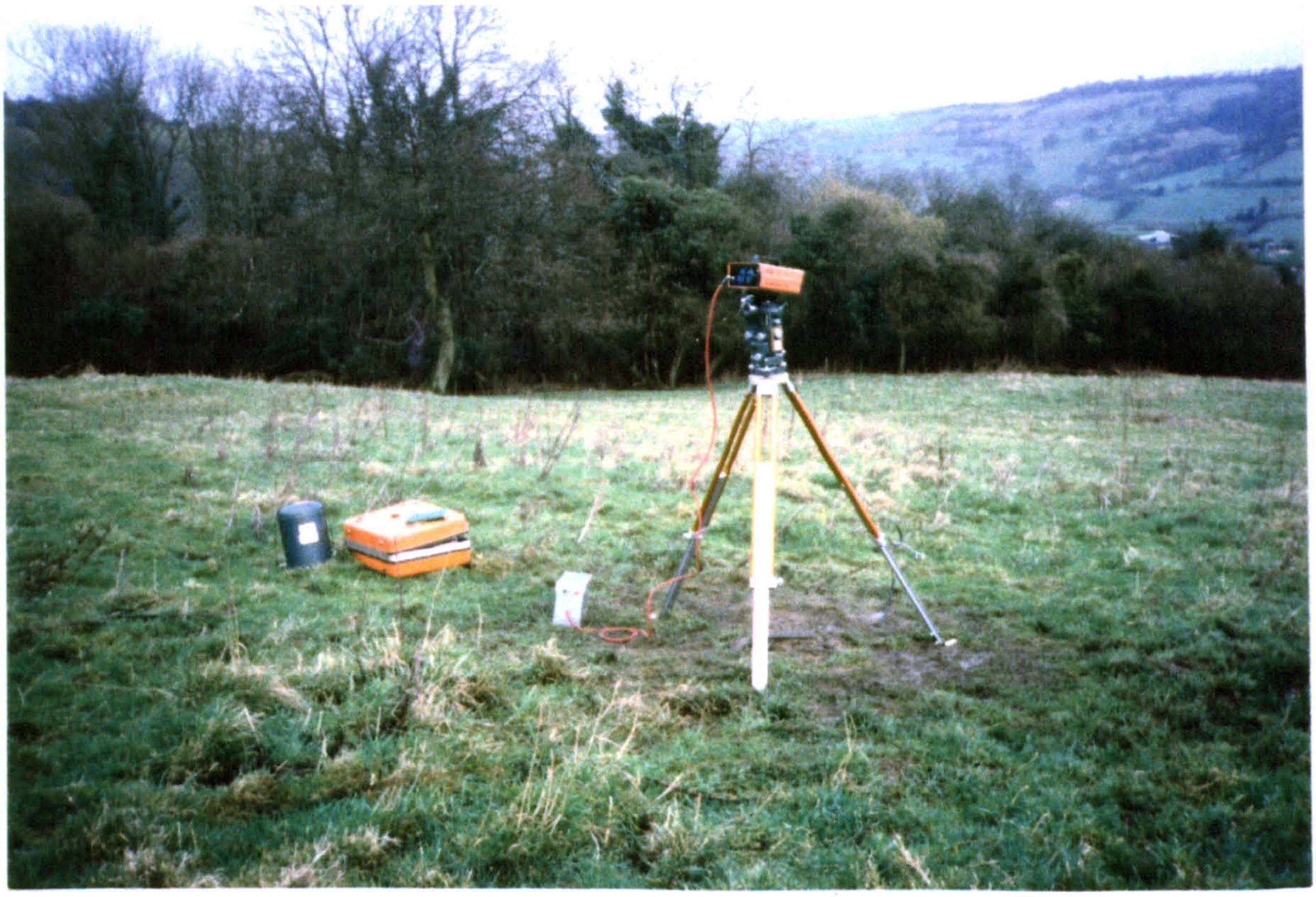

Plate 3.2 AGA geodimeter and theodolite in use at Soper's Wood.

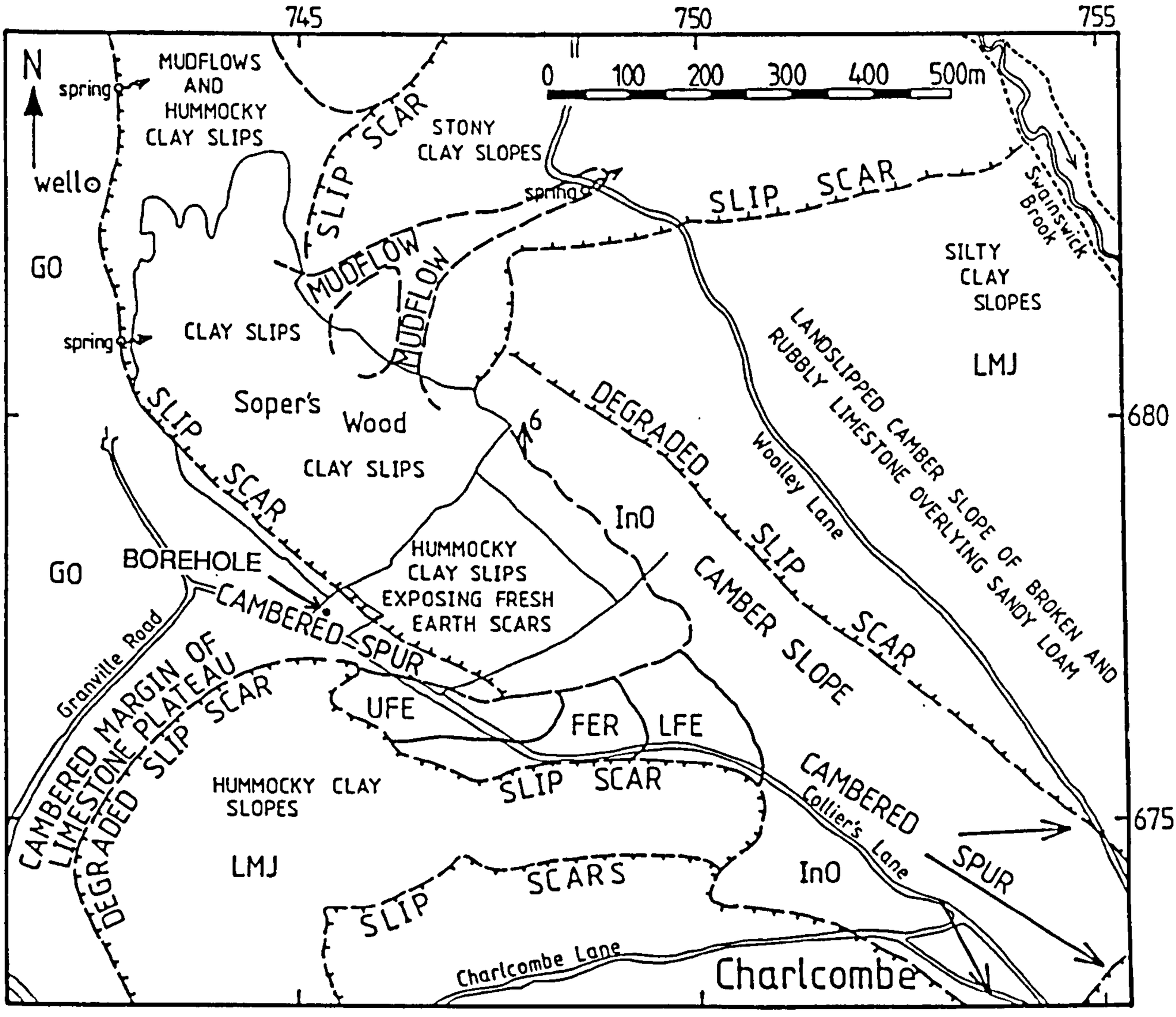

Fig. 3.2 Summary geological map of the Soper's Wood area, after Lawrence (1985). Extract from the 1:10560 Geological Survey Sheets, Gloucs. LXXVII and Soms. VIIISW.

LMJ - slipped Lower and Middle Jurassic; GO - Great Oolite; UFE - Upper Fuller's Earth clay; FER - Fuller's Earth Rock; LFE - Lower Fuller's Earth clay; IO - Inferior Oolite.

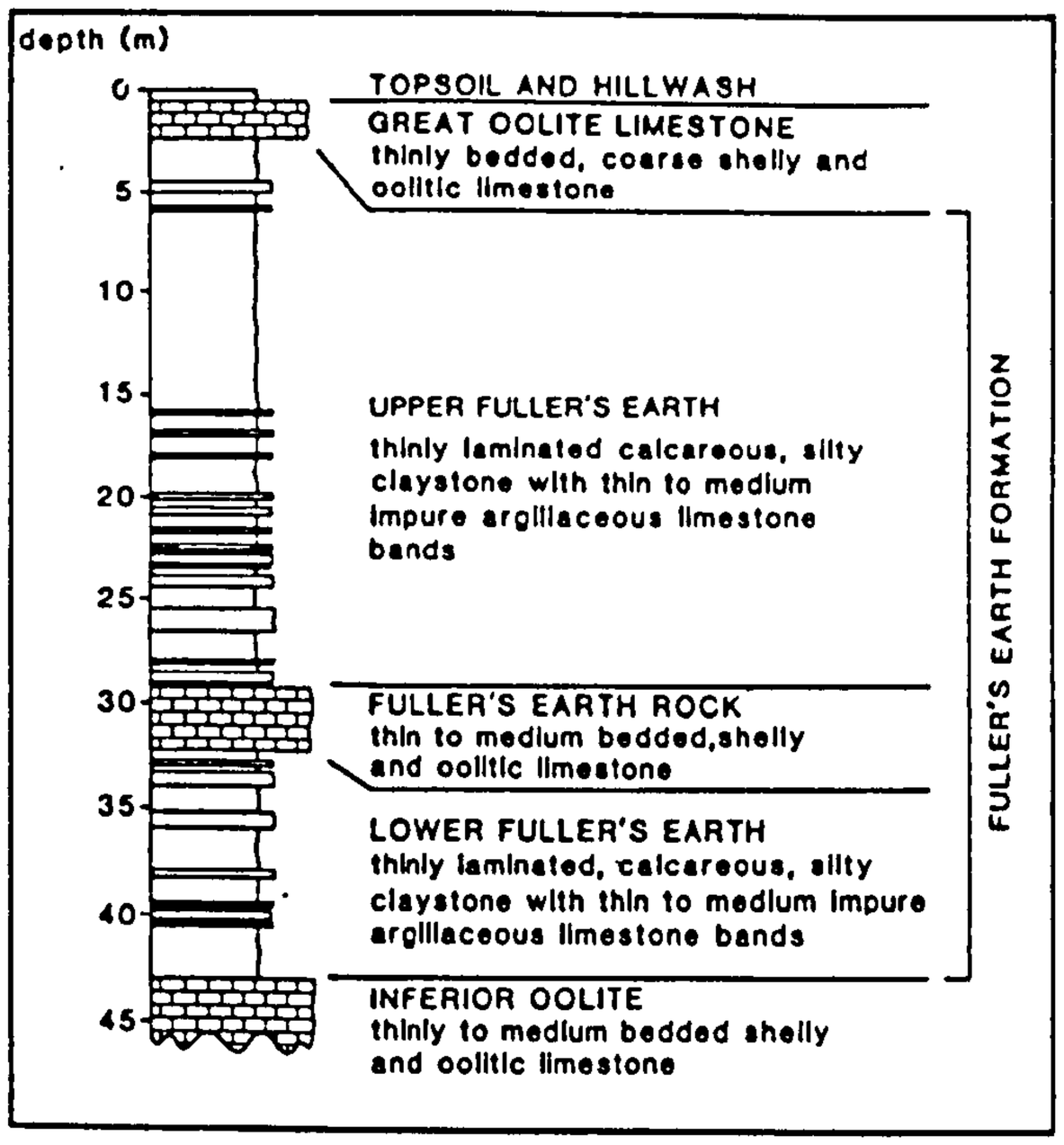

Fig. 3.3 Lithostratigraphic log of the Soper's Wood borehole, after Hawkins *et al.* (1986).

Date	Observation	Author
1978	A 1974 aerial photograph highlighted the broad morphological features of the site and a geomorphological map of the Swainswick valley showed relict landslips and mudflows at Soper's Wood.	Privett (1980)
August 1980	Farmer regrades slope profile with building debris.	Lawrence (1985)
Late September - early October 1980	Renewed instability during period of heavy rainfall, possibly after 23 mm of rain on 20th September.	Lawrence (1985)
March-August 1981	New geomorphological map produced.	Lawrence (1985)
Late August 1981	Slope profile regraded by the farmer.	Lawrence (1985)
11 September 1981	Inspection after regrading revealed gradients of 10° - 11°, with locally steeper slopes of 13°.	Lawrence (1985)
15 September - 15 October 1981	202 mm of rainfall recorded at Batheaston Weather Station.	Lawrence (1985)
15 October 1981	Inspection revealed reactivation of the 1980 slide. Farmer confirmed major movement commenced on 29th September and continued to 2nd October 1981. Following the slide the site was remapped and the slope regraded.	Lawrence (1985)
Late September - mid-December 1982	Renewed movement of the 1981 slip mass during a period of prolonged heavy rainfall.	Lawrence (1985)
Autumn 1983	Following heavy rainfall there was a reactivation of a 1968 slide approximately 60 m down-slope from the principal scarp. Total rain in September and October was 195 mm.	Lawrence (1985)
January - February 1989	Renewed movement of the 1968 slide. Entire length of slipped mass reactivated and lower field boundary fence distorted.	McDonald (1992)
February - March 1992	A new geomorphological map indicated that the landslip had not moved in the preceding two years.	Dalwood (1992)
March 1992 - December 1994	Occasional visits did not reveal any signs of fresh movement.	

Table 3.1 Summary of past phases of instability at Soper's Wood.

can be located approximately half way down the top field towards the head of the currently active landslide (see Figure 3.22). However, it is recognised that some cambering due to creep will have affected the outcrop level of the Fuller's Earth Rock. In the same way, cambering of the Inferior Oolite resulting from the leaching of the Midford Sands has lowered the outcrop position of the Inferior Oolite compared to that expected from an extrapolation of the position of the Inferior Oolite from the borehole log. Hence, its location shown on the map in Figure 3.2 is downslope of the study area. This vertical displacement of the Inferior Oolite will clearly have an effect on the stability of the overlying Fuller's Earth formation, giving the strata an accentuated valleyward dip which may well have exasperated the effect of the slope failure.

3.2 Investigative Techniques

Following the evidence of renewed movement of the landslide in January 1994, a monitoring program was initiated. The field work and monitoring program included engineering geological mapping, surveying, augering, the installation of standpipes and ground water sampling.

3.2.1 Engineering Geomorphological Mapping

Engineering geomorphological mapping has developed as an important tool in ground investigation. Savigear (1965) discusses the technique, with modifications introduced by the Geological Society Engineering Group Working Party (Anon 1972).

In view of the explanations given in these documents and other papers (eg. Brunsden & Jones 1972), the landslipped area adjacent to Soper's Wood was subdivided into a square grid. Twenty eight squares, each 400 m^2, permitted the accurate location of the geomorphological features, which were then plotted in the field onto graph paper to allow maximum accuracy. Gradients were measured using an inclinometer sited onto the head of an individual of similar build.

3.2.2 Surveying Technique

Nine survey stations were set up by eye in two parallel lines within the slipped area (stations A1-A5 and B1-B4), parallel to the expected direction of movement. In order to investigate any movement, the survey stations in each line were compared with a corresponding additional survey station downslope of the line, outside the main slipped area in apparently stable ground (stations AD and BD, respectively). Figure 3.4 shows the

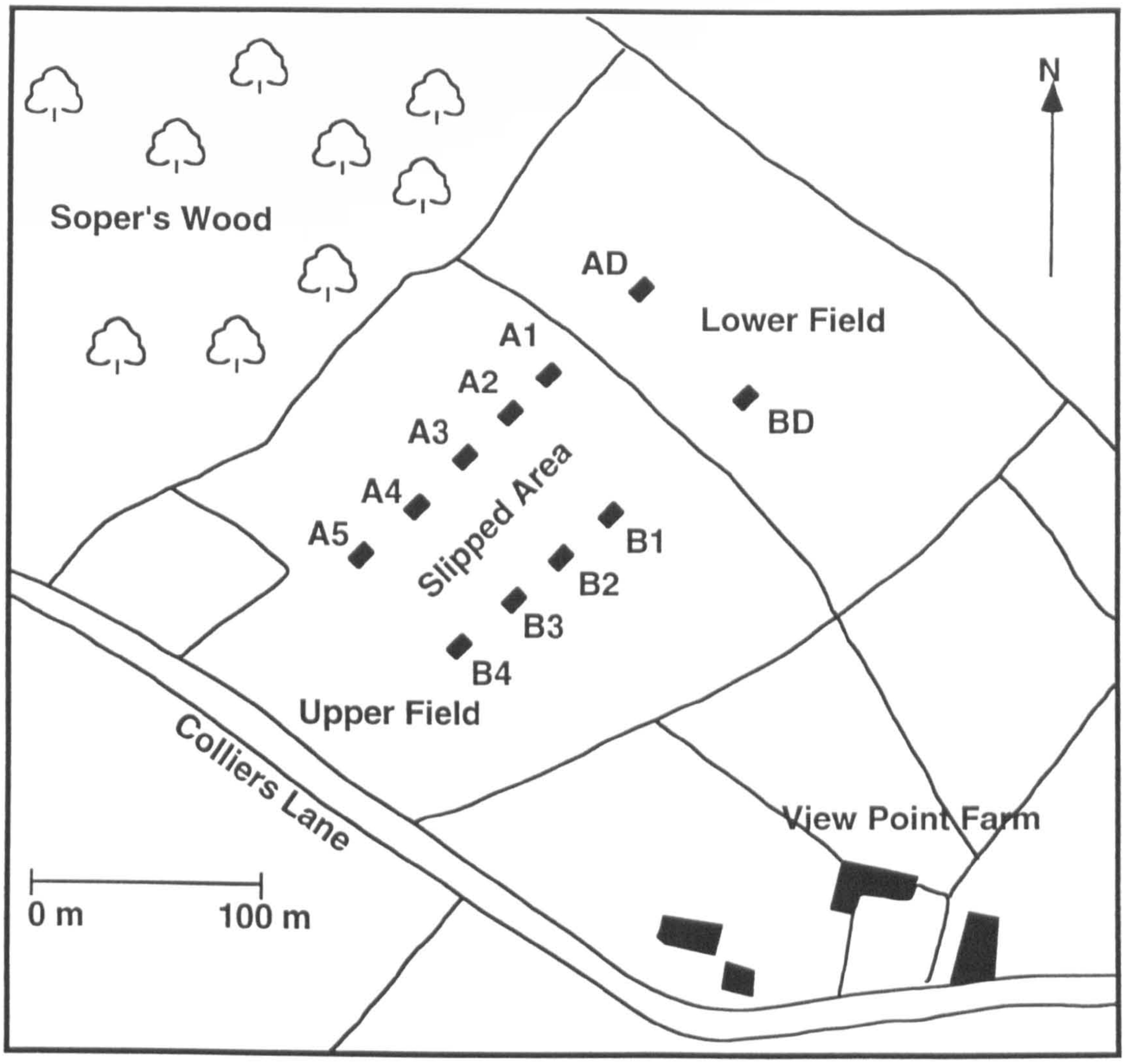

Fig. 3.4 Map showing the location of the survey stations relative to the field boundaries in the area.

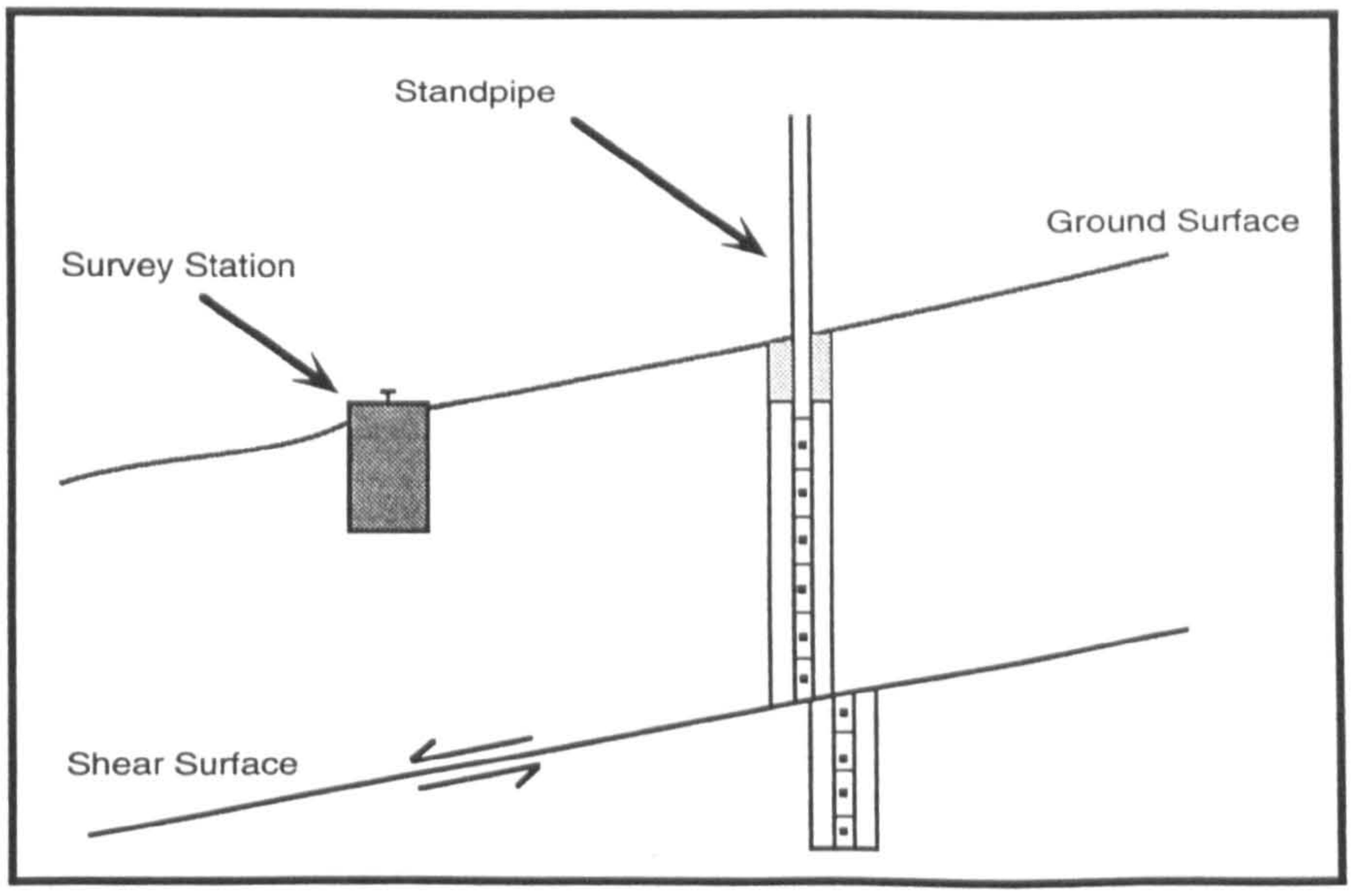

Fig. 3.5 Schematic diagram showing the orientation of a survey station and the use of the adapted standpipe.

approximate locations of the survey stations relative to the field boundaries in the area. It can be seen that stations AD and BD are located in the lower field, downslope of the visibly slipped area.

The survey stations consisted of breeze blocks (450 mm x 225 mm x 100 mm), which were sunk into the ground and a masonry nail hammered into the top of each block to act as a survey datum point (see Figure 3.5). The blocks were installed vertically by some 400 mm in carefully dug pits and great care was taken to pack clay tightly around the blocks. This ensured that they portrayed any movement of near surface material, while at the same time preventing injury to cattle.

An AGA geodimeter and theodolite were used to survey the site at frequent intervals during the winter, spring and summer of 1994 (see Plate 3.2). The geodimeter and theodolite were first levelled above the datum point on survey station AD, which acted as a reference datum for the line of "A" survey stations, and a reflective prism levelled in turn above each of the datum points on the five corresponding "A" survey stations. Once the geodimeter had been corrected for the prevailing temperature and atmospheric pressure, the geodimeter was sited onto the centre of the prism using the telescope within the theodolite. The distance between the geodimeter and prism was then obtained using the electronic distance measurement facility of the geodimeter. Four readings were taken for each survey station and the values averaged. The inclination of the line of site from the geodimeter to the prism from the horizontal was then determined using the built-in inclinometer. Once this procedure had been completed for the line of five "A" survey stations, the geodimeter and theodolite were levelled above the datum point on survey station BD, which acted as a reference datum for the line of four "B" survey stations, and the procedure repeated.

In order to calculate the vertical and horizontal distances of the survey datum points from their corresponding reference datums (AD and BD), it was necessary to measure the heights of the geodimeter and the centre of the prism above their respective datum points. Figure 3.6 summarises the technique and calculations used. A comparison of the horizontal and vertical distances on a weekly basis allowed movement of the various survey stations, and hence of different parts of the slide, to be assessed. The data obtained can be found in Appendix II and the interpretation of the results is discussed in Section 3.5.1.

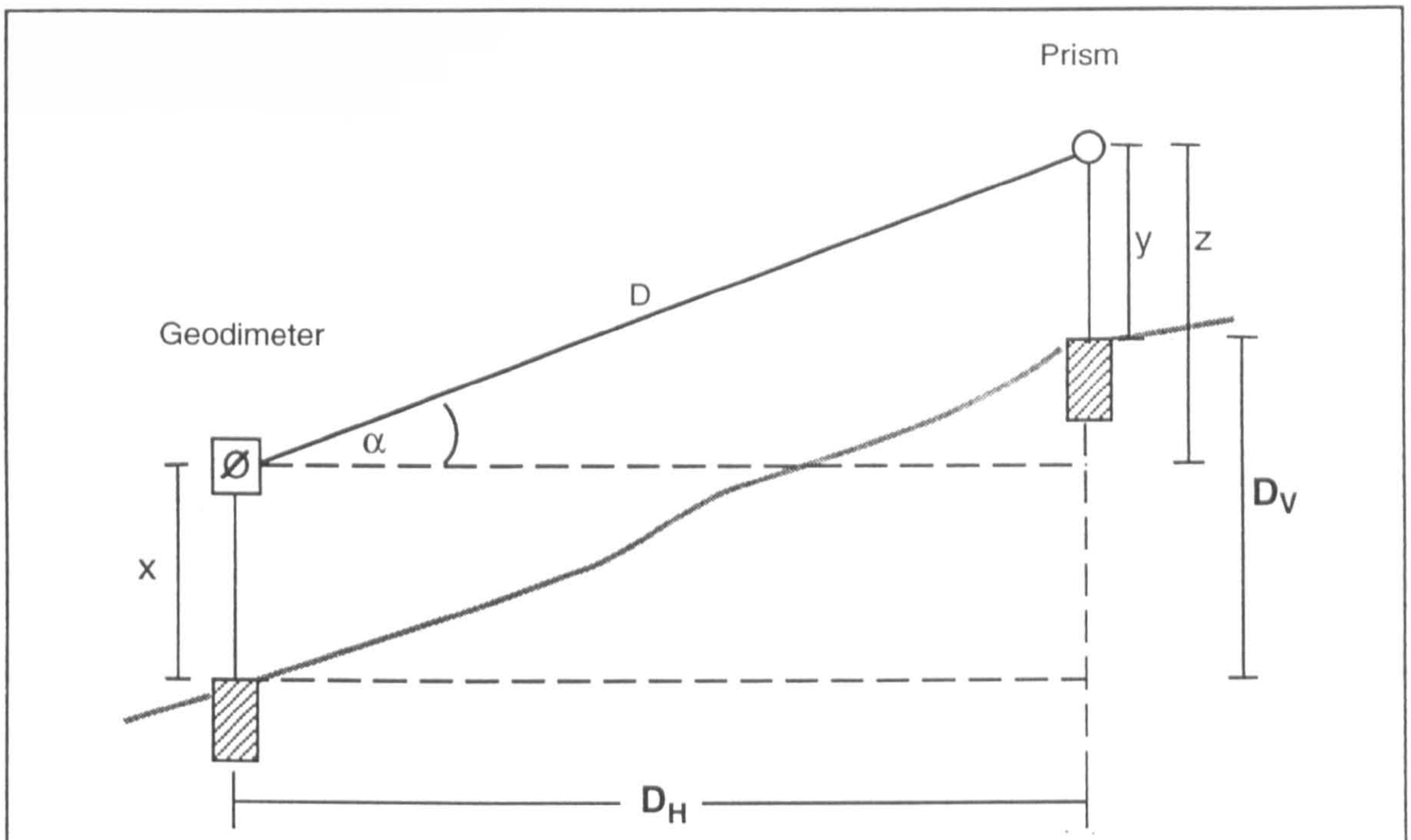

x = measured vertical height of geodimeter from reference datum point

y = measured vertical height of prism from survey datum point

α = measured inclination of prism from geodimeter

D = measured distance between geodimeter and prism

$\mathbf{D_H}$ = calculated horizontal distance between reference datum point and survey datum point

$\mathbf{D_V}$ = calculated vertical distance between reference datum point and survey datum point

z = calculated vertical height from geodimeter to prism

Calculations:

$$\mathbf{D_H} = D.\cos\alpha$$

$$z = D.\sin\alpha$$

$$\mathbf{D_V} = x + (z - y)$$

Fig. 3.6 Illustration displaying surveying technique and calculations.

3.2.3 Borehole Augering

Boreholes were augered using a 20 mm diameter hand auger, with samples taken at 100 mm intervals. The first metre was easily drilled, however with greater depths the suction effect produced by the saturated clay made extraction of the auger difficult, limiting the depth to which each borehole could be extended. As there was some evidence that lateral creep was causing a reduction of the borehole diameter, it was necessary to undertake the augering as quickly as possible, with care being taken to ensure that the clay sampled was always from the undisturbed ground at the base of the borehole. In addition, the presence of fragmented blocks of argillaceous limestone within the Fuller's Earth meant that a number of boreholes had to be abandoned and restarted.

3.2.4 Standpipe Installation

The standpipes consisted of 4 m long plastic pipes (19 mm i.d.) which were plugged at their base. In order to use the standpipes as shear movement indicators, zones of weakness were created in the pipes by scoring them at 50 mm intervals throughout the lower 3 m. Between each score a 2 mm diameter hole was drilled to allow the ingress of water. The standpipes were placed in the boreholes and the top of the borehole carefully sealed with remoulded clay to prevent the ingress of surface run off which would clearly distort the results. To further ensure that there was no ingress of surface water, an inverted cone of clay was created around the top of the borehole to divert surface run off and, where possible, the standpipes were also placed on hummocks.

It was assumed that if the standpipes passed through an active shear surface, then further movement would snap the standpipe at a zone of weakness at the approximate depth of the failure surface. Figure 3.5 displays the way in which the standpipes were used to indicate the depth at which failure takes place. In some instances it was not possible to discern whether the standpipe had snapped or kinked, however both provide an indication of the depth of the shallowest active shear surface. Hence, in the discussions later in this chapter, for simplicity the standpipes are quoted as being "snapped" if they provide an indication of the depth of the failure surface. On a frequent basis over the study period, the ground water level was established using a electronic dipper and the depth of the displacement zone ascertained using a plumb line. The records of this can be found in Appendix III and are discussed in Sections 3.5.3 and 3.6.

3.2.5 Ground Water Sampling

Water was extracted from the standpipes using a hand held pump. The pump arrangement involved the interruption of a plastic extraction pipe by a 250 ml plastic bottle in which a vacuum was created, which extracted water from the standpipes. In general, the standpipes were pumped dry prior to sampling of the ground water. However, due to the relatively long refill time of approximately 3 to 4 days (this period was longer during the late spring/summer), the ground water was often not sampled until a week later (in the late spring/early summer, this interval was up to 3 weeks).

Conductivity, temperature and pH were tested in the field using a WTW L91 conductivity and temperature meter and a Hanna Instrument pH meter. After these tests had been carried out, this initial water sample was disposed of and further water samples taken for return to the laboratory. In the laboratory the waters were immediately filtered, placed in clean plastic bottles and stored in a refrigerator, in order to reduce chemical alteration, prior to analysis by atomic adsorption spectroscopy (see Appendix I).

3.3 Slip Geomorphology

3.3.1 Discussion of Engineering Geomorphological Map (January 1994)

An engineering geomorphological map of the site was produced in January 1994 (See Figure 3.7). In addition to the geomorphological features, the map displays the location of the survey stations and standpipes. The symbols, shown in Figure 3.8, are taken from the Geological Society Engineering Group Working Party report (Anon 1972), although it was necessary to add some additional symbols. An enlarged copy of the map may be found in Appendix IV. The nomenclature used below in discussing the various parts of the landslide is based in part on the terms used by Varnes (1958).

Approaching the site along Granville Road past the Government Offices emphasises the plateau like nature of the Lansdown area (see Figure 3.1). This surface represents the gentle easterly dip of the Great Oolite. To the south of Colliers Lane is the valley of the Charlcombe Brook; the upper part of this valley is terminated on the crest of the cambered spur of the Great Oolite which is present in the top field to the north of Colliers Lane, containing the landslide investigated (see Figure 3.2). This cambered spur creates the anomalous slope at the top of the field adjacent to the lane (see Figure 3.7). North of the crest of the spur, towards the Swainswick valley, the slope gradient gradually increases from 4°, some

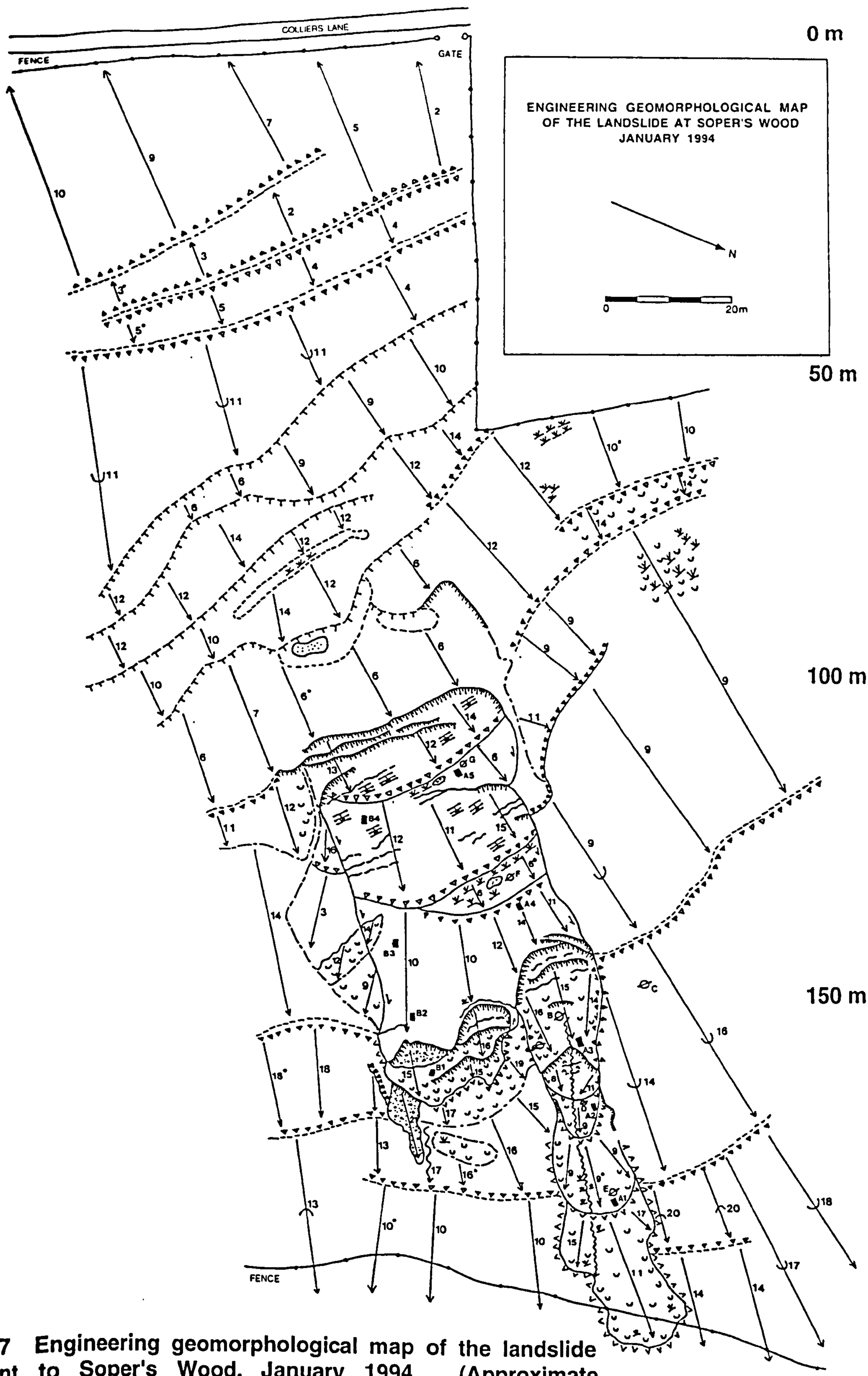

Fig. 3.7 Engineering geomorphological map of the landslide adjacent to Soper's Wood, January 1994. (Approximate distances from Colliers Lane are displayed down the right edge).

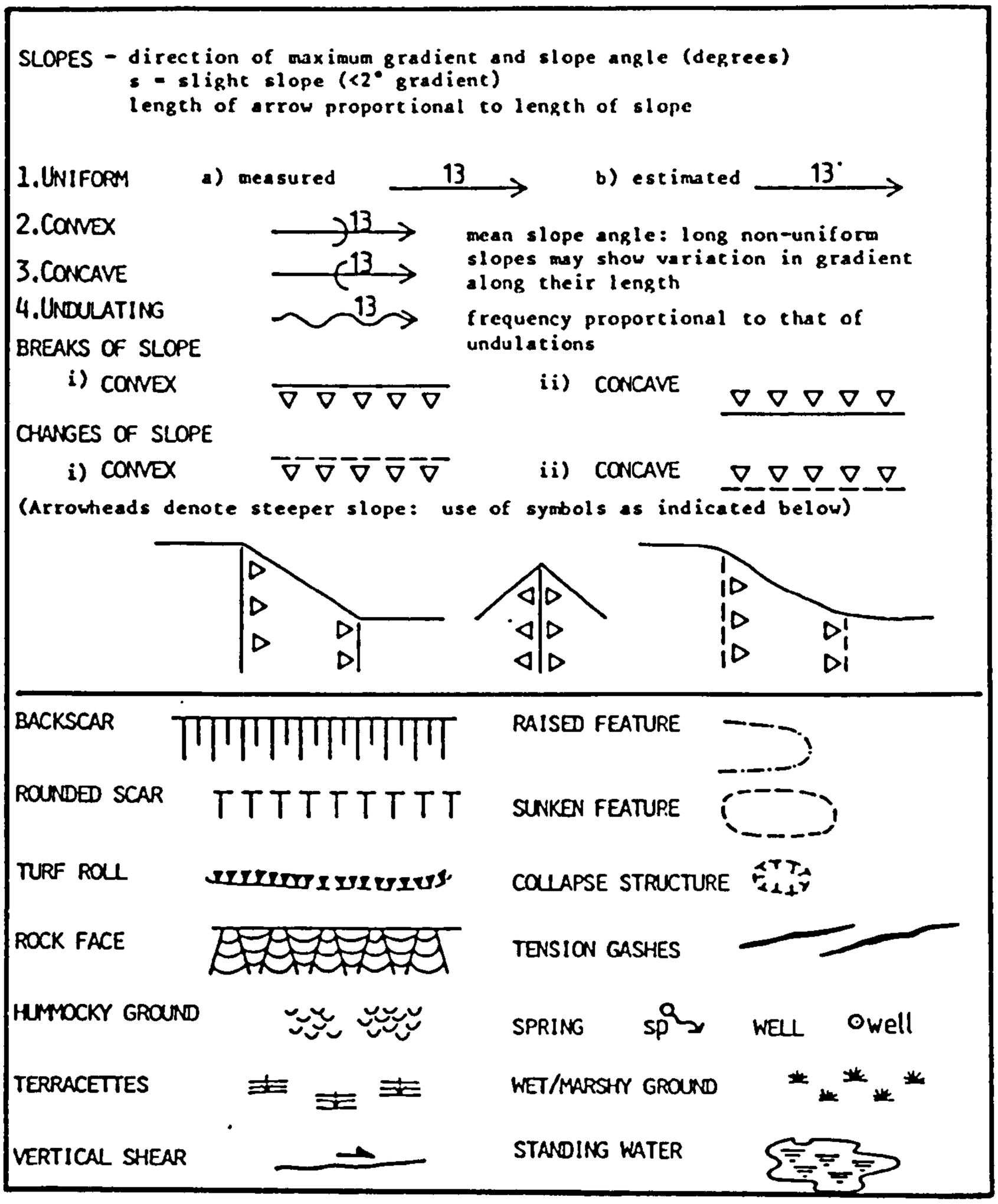

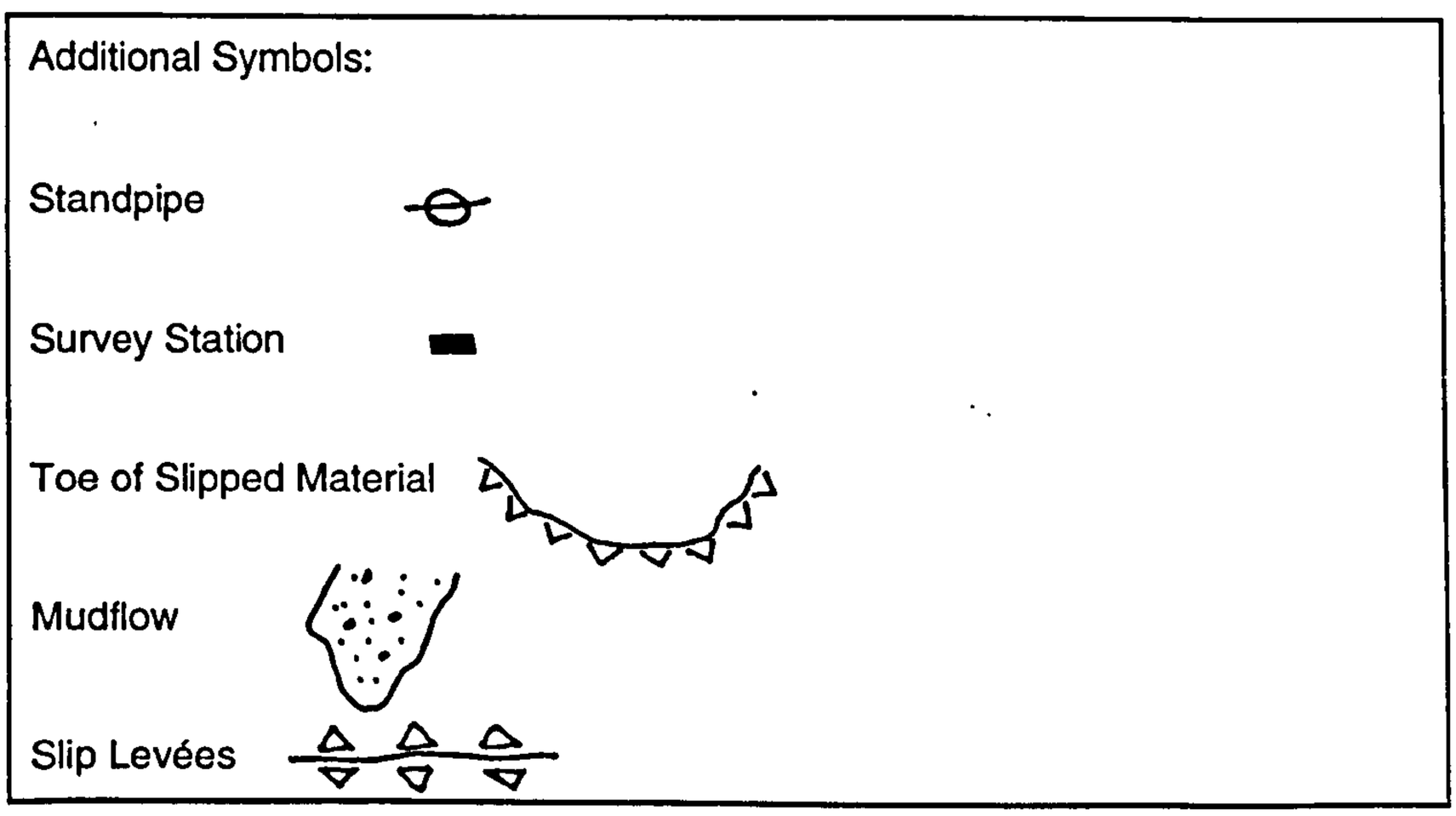

Fig. 3.8 Geomorphological mapping symbols from Engineering Group Working Party Report (Anon 1972), apart from additional symbols.

20 m to 40 m into the field, to 11° where the slope is underlain by the outcrop of the Fuller's Earth formation. From about 50 m from Colliers Lane, the generally smooth morphology of the upper slope is interrupted by pronounced rounded scarps, running approximately SE-NW, parallel with the edge of the Great Oolite plateau. These rounded features are likely to be redundant scarps from earlier phases of movement. Between the scarps there are a number of depressions, probably resulting from the back rotation of landslide units, in which marshy ground is very prevalent and in one case builders rubble can be observed. It is understood that some of this fill material was placed on the hillslope in the late 1960's.

The translational landslide active in 1994, which formed the main area of study, commences about 100 m downslope from Colliers Lane. This is believed to be a reactivation of a 1968 landslide which developed at the time of a very heavy rainstorm, soon after the builders rubble was placed in the hollows at the top of the Fuller's Earth formation (A.B. Hawkins pers comm., 1996). Its general morphology consists of a cluster of well formed scarps at the head of the landslide, about 35 m in length, while downslope the landslide is defined by two sub-parallel lateral shears. In the upper 50 m, within the main body of the landslide, there are numerous terracettes, areas of standing water and visible transverse cracks which extend off from the lateral shears. The general gradients in this part of the slope are between 10° and 15°.

About 150 m down-slope from Colliers Lane, the main translational landslide splits into two distinct morphological features (see Plate 3.3). On the northern side, the main slipped mass has extended downslope as a discrete narrow translational landslide, defined as Slide A, on which survey stations A1 to A3 are placed. On the southern side, the main translational slide has not extended so far valleyward and the lower feature is termed Slide B, on which survey station B1 is situated.

The narrow translational landslide (Slide A) commences with a series of fresh, large scarps (see Plate 3.4). The main body of the landslide contains minor scarps and transverse cracks and is restricted by two sub-parallel lateral shears with clear slickenside striations (see Plate 3.5). The lateral shears form small slide levées which clearly define the edge of the landslide. As can be seen in some places, the lateral shears act as lines of preferential drainage and, although the ground within the landslide was extremely hummocky, it contained a defined drainage channel. At the foot of the landslide, a mudflow lobe of very hummocky and disturbed ground extends from the landslide, indicating a phase of past movement. This is

Plate 3.3 View, looking west, of the lower part of the landslide active in 1994 adjacent to Soper's Wood.

Plate 3.4 Fresh scarps evident at the head of Slide A.

Plate 3.5 Slickenside striations visible on the lateral shear of Slide A.

overridden by the toes of more recent phases of movement. These toes have general gradients of approximately 9° to 11°.

Slide B commences upslope with a 20 m long main scarp, which, in plan section, appears as two joined arcuate scarps. Downslope of these arcuate scarps the slipped ground forms a poorly defined main body, containing minor scarps and transverse cracks, which ends abruptly with a steeply faced toe. This toe rests on an area of hummocky ground which forms a low raised area above the general hillslope terraine and may represent a relict mudflow lobe at the foot of the original 1968 landslide, which has since been superimposed by Slide B. Downslope of the southern arcuate main scarp, the landslide has become so saturated that a portion of the main body has the characteristics of a mudflow. The mudflow contains blocks of turf which have remained upright, appearing to "float" on the highly saturated clay (see Plate 3.6). Downslope of this area a second mudflow has developed, extending from the toe of the landslide. Here there is clear evidence of fresh movement. At the time of the visit in January 1994 the mudflow had formed a thin, partially discontinuous veneer over the grass, flattening blades (see Plate 3.10). On subsequent visits the thickness of the flow had increased and again, upright blocks of turf were observed. Here slope gradients are between 15° and 21°.

3.3.2 Classification of Landslides

Many authors have attempted to provide a classification for landslides (for example Sharpe 1938, Ladd 1935, Ward 1945, Hutchinson 1968, Zaruba & Mencl 1969, Crozier 1973, Blong 1973a and 1973b, Coates 1977 and Varnes 1978) and a good review of these classifications can be found in Hansen (1984). However, due to the ever changing nature of the morphology of landslides and that in reality many are formed of a combination of features, categorising a particular landslide can be a difficult and subjective task.

The landslide active in 1994 at Soper's Wood is best described as a translational landslide of Type L (after Hutchinson 1967 and 1968). In the lower half of the main translational landslide, the landslide splits into two separate features. The southern half has developed into a poorly defined landslide (Slide B), with zones that have become "supercharged with water and reach moisture contents far above their liquid limit" (Allison 1992) and hence are characteristic of mudflows. On the northern side, the main translational landslide has extended downslope to form a narrow, well defined translational landslide (Slide A). However, at the foot of Slide A or

Plate 3.6 Blocks of turf which have remained upright on the saturated clay of the mudflow.

Plate 3.7 View upslope showing the very disturbed nature of the intermediate toe in which survey station A2 is located. Survey station A2 is visible just to the right of the piezometer.

"accumulation zone" (Varnes 1978), the slipped mass has spread out into a lobe, characteristic of a mudflow.

Slide A has some characteristics of a mudslide, as defined by Hutchinson & Bhandari (1971) following Fleming (1878) and Cailleux & Tricart (1950), and has a similar *outline* in plan view to the diagramatic sketches of a typical mudslide shown in Brunsden (1973 & 1984). However, when the total morphology, longitudinal cross-section and apparent movement pattern is taken into account, the author considers that the term narrow translational landslide best describes Slide A. The decision not to classify Slide A as a "mudslide" is strengthened by the comparison of photographs of mudslides in Brunsden (1984) and Allison (1992), which have a different morphology.

Throughout the remainder of this thesis, the author has used the terms "slip", "landslip", "landslide" and "slide" to refer to the translational landslides at Soper's Wood. These are used for convenience and brevity.

3.3.3 History of Instability

The landslides at Soper's Wood have been periodically studied by the Engineering Geology Research Group at the University of Bristol. Table 3.1 summarises the various phases of past instability recorded by previous workers at Bristol University. Movement in 1980, 1981 and 1982 occurred on the now rounded principal main scarp, adjacent to the Great Oolite margin. However, since 1983 there has been renewed activity of a 1968 slide, approximately 60 m down-slope from the rounded principal main scarp. From January 1989, until this study, there have been no observed signs of movement, there thus has been a five year period of inactivity.

3.3.4 Comparison with Previous Geomorphological Maps

A number of geomorphological maps have been produced in the past creating a useful chronological library of the geomorphology of the landslides.

In 1978, Privett (1980) produced a 1:2500 geomorphological map of the Swainswick valley which included the Soper's Wood landslides. Unfortunately, due to the scale of the map, it was not possible to record all the features in great detail. However, the map indicates a large main scarp about 50 m from Colliers Lane. Due to its location this is likely to be the same scarp as the relict principal main scarp shown on the enclosed 1994 map. Valleyward, Privett has indicated areas of hummocky ground whose

outline is similar to that of the slide in this study and may be the remains of the 1968 slide.

Lawrence (1985) produced two maps, one after the 1980 landslide and a second after the 1981 slide. However, the main area of land movement was above the currently active slide and unfortunately Lawrence's maps do not extend downslope sufficiently to include the currently active landslide. Despite the ground being regraded by the farmer before both the 1980 and 1981 phases of slipping, the landslides mapped by Lawrence (1985) have the same gross morphology, supporting the argument that movement occurs along pre-existing shear surfaces.

The last map produced was that by Dalwood (1992) as part of an undergraduate dissertation (see Figure 3.9) and covers a similar area to the 1994 map. Dalwood has recognised a set of relict scarps at the top of the field. Due to their similarity with those depicted on the map in this thesis (allowing for some subjectivity due to personal mapping styles), and the fact that no new phases of movement have appeared on these features since the work done by Lawrence (1985), it is highly probable that this section of the slope has temporarily stabilised. However, with movement further down slope removing supporting material, this state of stability is unlikely to be permanent. The area of study in this thesis has a similar gross morphology to that mapped by Dalwood, providing further evidence that the main movements at Soper's Wood are associated with pre-existing shear surfaces. However, recent movements have resulted in a new toe being superimposed on those displayed on Dalwood's map. In addition, the previously existing single scarp, as mapped by Dalwood, is now part of a cluster of scarps.

3.4 Auger Hole Information

Five boreholes (B,D,E,F and G) were augered in a line from the main scarp to the toe of the translational slide. Boreholes G and F are situated down the left side (northern side) of the main translational slide and boreholes B, D, and E are located down the centre of Slide A. A sixth borehole, C, was augered outside the visibly slipped area to act as a control. See Figure 3.7 for exact locations.

3.4.1 Sample Descriptions and Weathering Profile

The samples obtained were logged and are summarised below in approximate downslope order (except for borehole C). The strengths implied in the descriptions below are comparative strengths giving the best

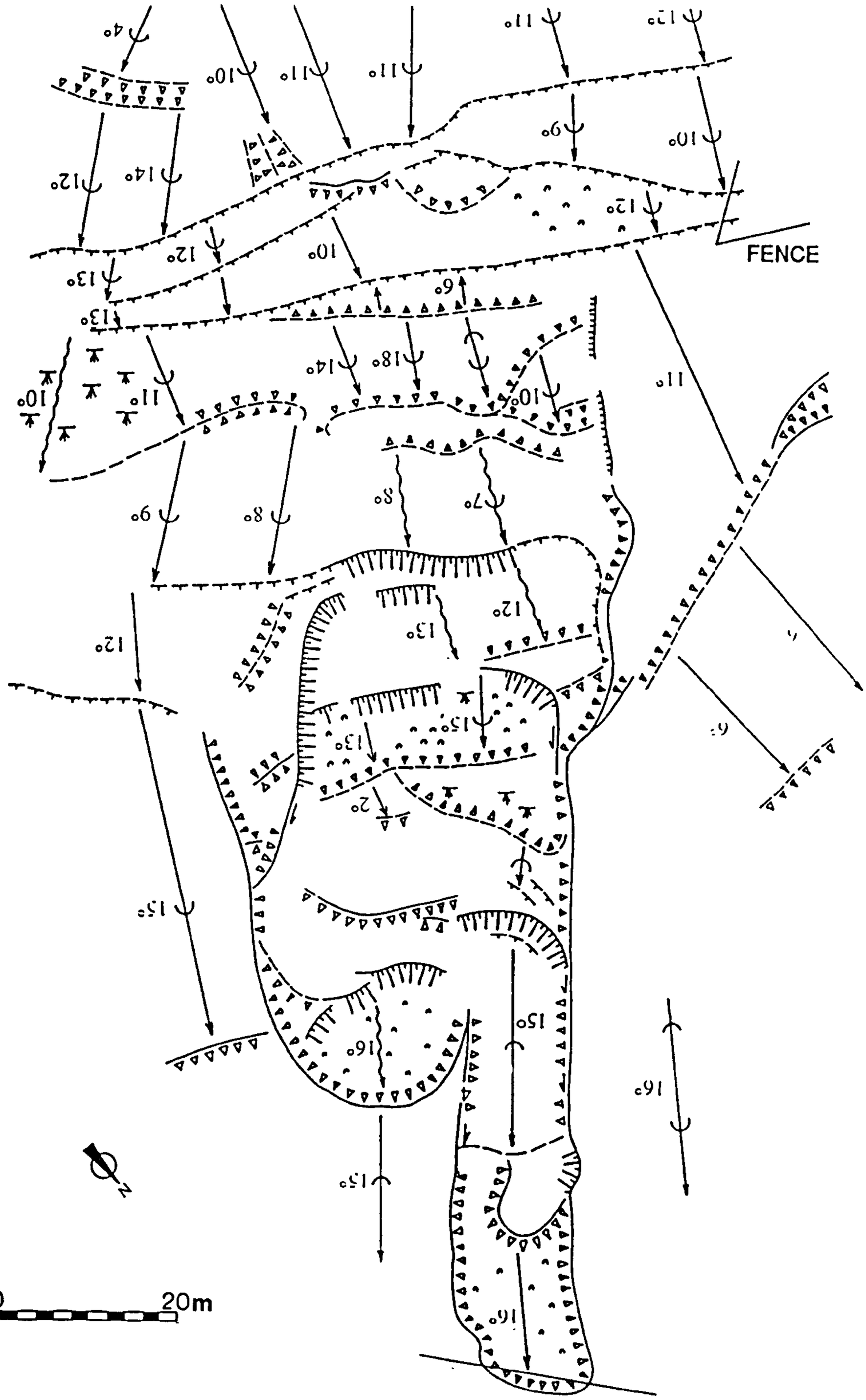

Fig. 3.9 Engineering geomorphological map of the landslide adjacent to Soper's Wood in 1992, after Dalwood 1992. (In order to compare this map with the 1994, this map has been inverted.)

estimate of what in situ strengths would be from samples extracted from a helical auger.

The samples in each borehole are divided into weathering zones according to the weathering scheme developed by Lawrence (1985) for the mudrocks of the Fuller's Earth formation (see Table 3.2). The scheme is based dominantly on the colour changes produced by oxidation.

Depth (m)		Weathering Zone
Borehole G		
0.1 - 0.3	Soft, medium to dark brown, silty CLAY, with occasional roots and occasional fragments of medium gravel.	vi
0.4 - 1.0	Soft, medium brown, silty CLAY, with occasional roots, occasional medium sand and occasional fragments of medium gravel.	v
1.1 -1.3	Firm, medium brown with grey patches, silty CLAY, with occasional medium and coarse sand.	iv
1.4 -1 .5	Firm to stiff, mottled medium grey/orange/brown, silty CLAY, with occasional fine gravel.	iv
1.6 -1 .8	Stiff, mottled medium grey/brown, silty CLAY, with occasional roots.	iii
1.9 - 2.2	Stiff to very stiff, light to medium grey/brown, silty CLAY, with occasional roots.	ii
Borehole F		
0.1 -0.2	Soft to firm, dark brown, silty CLAY, with many roots.	vi
0.3 - 0.7	Soft to firm, medium brown, silty CLAY, with occasional roots.	v
0.8 - 1.0	Soft, light brown, silty CLAY, with occasional fine gravel.	v
1.1 - 1.5	Very soft to soft, light brown, silty CLAY, with occasional fine to medium sand.	v
1.6 - 2.0	Soft to firm, light brown with mottled orange and grey patches, silty CLAY, with occasional medium sand to fine gravel.	v
2.1 - 2.5	Firm, medium grey, silty CLAY, with occasional fine gravel .	iv
2.6 - 2.7	Soft to firm, light brown, silty CLAY, with occasional fine to coarse gravel.	iv
2.8 - 3.2	Firm, light brown with orange grey patches of drier material, silty CLAY, with occasional coarse sand to fine gravel.	iv

Borehole B

0.1 - 0.4	Soft, dark brown, silty CLAY with occasional roots and occasional medium oolitic limestone gravel.	vi
0.5 - 0.9	Very soft to soft, medium brown, silty CLAY.	v
1.0 - 1.1	Firm, light to medium brown, silty CLAY, with occasional fine sand to fine gravel.	v
1.2 - 1.9	Soft to firm, light brown, silty CLAY, with occasional fine sand to coarse sand.	v
2.0 - 2.7	Firm, light brown, silty CLAY, with occasional fine to coarse sand.	iv

Borehole D

0.1 - 0.5	Soft, medium brown, silty CLAY, with occasional roots and coarse sand.	v
0.6 - 1.0	Very soft, medium brown, silty CLAY, with occasional roots and fine gravel.	v
1.1	Soft, medium brown, silty CLAY, with occasional roots.	v
1.2 - 1.6	Soft to firm, medium brown, silty CLAY.	v
1.7 - 2.2	Firm, medium brown, silty CLAY, with occasional medium sand to fine gravel.	iv
2.3 - 2.6	Firm to stiff, medium orange/brown, silty CLAY, with some sand and gravel.	iii
2.7 - 2.8	Very stiff, light grey with mottled orange patches, silty CLAY, with occasional fine gravel.	ii

Borehole E

0.1 - 0.4	Soft to firm, medium brown, silty CLAY, with occasional medium oolitic limestone gravel.	vi
0.5 - 1.0	Soft to firm, medium brown, silty CLAY, with occasional fine to medium sand.	v
1.1 - 1.2	Soft, medium brown, silty CLAY, with some medium sand and occasional medium oolitic limestone gravel.	v
1.3 - 1.6	Very soft, light brown, silty CLAY, with occasional medium sand.	v
1.7 -1.8	Soft, light brown, silty CLAY, with occasional fine to coarse sand.	v
1.9 - 2.1	Very soft, light brown, silty CLAY, with occasional fine to coarse sand.	v
2.2 - 2.6	Soft to firm, light brown, silty CLAY, with some coarse sand.	v

Borehole C

0.1 - 0.3	Soft to firm, dark brown, silty CLAY, with some roots and occasional fine gravel.	v
0.4 -0.5	Soft to firm, medium grey/brown, silty CLAY, with occasional roots.	iv
0.6 - 1.2	Firm, light brown/grey, silty CLAY, with occasional roots.	iii
1.3 -1 .9	Stiff to very stiff, orange/brown, silty CLAY, with much medium sand and occasional medium gravel.	ii
2.0 - 2.7	Very stiff, light grey/orange/brown, silty CLAY.	ii
2.8 - 3.0	Very stiff, medium green/grey, silty CLAY.	

A comparison of the various profiles reveals that all the boreholes within the slip (B, D, E, F and G) contain a large proportion of completely or highly weathered material, down to a known maximum depth of 3.2 m in the case of borehole F. In contrast, the highly weathered material only extended to a depth of 0.5 m in borehole C outside the slip. This indicates that the visibly landslipped terrain has extended depths of weathering within the slipped material, compared to that of the adjacent visibly unslipped material. Such exasperation of weathering is likely to be due to the greater aeration of the slipped material resulting from the dilation of the ground, with the development of minor scarps and transverse cracks allowing deeper oxidation to occur. However, within the visibly unslipped ground, the influx and percolation of surface waters is limited due to the relatively impermeable nature of the clay material.

Borehole B is situated close to a set of active minor scarps and contains only completely or highly weathered soil. Clearly the large amounts of movement associated with this part of the slip, together with the cluster of minor scarps providing avenues for the infiltration of ground waters, has increased the depth of weathering.

Borehole F, situated within the main body of the translational slide, has a similar weathering profile to that of borehole B. The enhanced weathering caused by the presence of shear surfaces within the slip and the dilated nature of the slipped ground has allowed the movement of ground waters and encouraged chemical weathering.

Borehole G is similarly situated within the main body of the translational slide, but upslope of borehole F and closer to the main scarp. Here, however, highly weathered material only extends to a depth of 1.5 m, with the remainder of the weathering profile having similarities to borehole C. At this location the shear surface is believed to be deeper than the base of the borehole. Analysis of the movement of the landslide

Residual soil (hillwash/solifluction)	VI	Soft to firm	In the superficial material, claystone is weathered to a soil in which the original rock fabric is completely destroyed. Mottled yellow-brown oxidation above the ground water level is extensive to complete. Some gleying occurs at shallow depths. Frequently contains many gravel and cobble fragments of weathered Great Oolite limestone derived from higher slopes. Seasonal desiccation features are common.
Completely weathered	V	Soft to firm	Claystone is discoloured and oxidized and completely weathered to a yellow-brown clay soil. Occasional small corestones may preserve relic laminations. Frequent gleyed fissures and root channels. Calcite content variable.
Highly weathered	IV	Firm to stiff	Fissured clay with extensive oxidation discoloration. Fissures are open and may be gleyed on surfaces. Oxidation alteration penetrates deeply from fissures. Lithorelicts (10–40%) indicate some remaining structure. Calcite content variable. Some gypsum crystals on discontinuity surfaces. Many minor striated shear surfaces.
Moderately weathered	III	Firm to stiff	Claystone is partially oxidized and altered to clay. Open fissures and discontinuities are discoloured orange-brown on surfaces. Alteration penetrates into soil mass, becoming yellow and grey-brown along 15 mm wide zones parallel to fissures. Lithorelicts comprise 40–70% of bulk soil. Original soil structure very evident. Calcite content variable. Many large gypsum crystals along fissure and bedding surfaces. Minor shear surfaces present with small displacements, resulting from overburden stress release and swelling.
Slightly weathered	II	Stiff to very stiff	Slightly discoloured claystone, confined to narrow oxidation zones adjacent to discontinuities which may be open and dark brown. Intact unweathered lithorelicts predominate (70–95%) and original structure is largely unaltered. Fissures are very closely to closely spaced. Calcite content variable. Some large selenite crystals, often along major discontinuities.
Fresh	I	Weak to very weak	Parent blue-grey silty claystone showing no oxidation discoloration or any other weathering effects apart from closed stress release fissuring. Occasional open and extensive joints are iron stained. Occasional iron-rich fossil nodules with local brown discoloration zones. Calcite content variable.

Table 3.2 Weathering scheme for the Fuller's Earth clay, after Lawrence (1985).

(see Section 3.5) has demonstrated that this area of the slide is the least active and hence has not been affected by the same level of extensive internal disturbance noted in other boreholes. This is supported by the augering of borehole G, when the clay was stiff making augering difficult. Thus, the depth of weathering has been restricted by the more intact nature of the ground below a depth of 1.5 m.

Boreholes D and E are both situated in superimposed toes in Slide A. Borehole D penetrates highly weathered material down to a depth of 2.2 m reflecting the very disturbed nature of the clay within the toe of the slip. Indeed, the ground here was notably highly fissured. Borehole E is situated on a larger toe and it is noted that it was completely weathered for the full depth of the borehole (2.6 m).

3.4.2 Moisture Content Analysis

The moisture contents of each of the samples extracted in January 1994 were established and the profiles for each borehole are shown in Figure 3.10a and 3.10b. It should be noted that these boreholes are given in approximate downhill profile, with borehole C adjacent to the landslide. It is understood that the majority of the landslips near Soper's Wood have been most active in the wet season (autumn and winter months) and therefore it was considered appropriate to establish the moisture contents during the winter months.

Most of the profiles show that at this time of year there is a general trend of decreasing moisture content with depth. The peaks within the first 0.3/0.4 m indicate an extremely high moisture content which may represent organic rich material, a saturated open texture material or may possibly be due to the infiltration of surface waters aided by the presence of soil cracks.

The upper borehole, G, clearly shows a high moisture content above 0.6 m implying a highly disturbed upper zone which during wet periods experiences a very high moisture content. The log of borehole G indicates that roots are present in the upper zone but they are not considered sufficient to affect moisture content. Below 0.6 m there is a steady decrease in moisture content from approximately 45% to 35%. From the moisture content profile, the logging of the borehole and the topographic setting, it is considered that these moisture contents indicate a dilated upper zone to a depth of approximately 1 m, while the main lower zone shows little evidence of slip disturbance.

The profile of borehole F indicates a high moisture content in the upper 1 m, probably due to similar reasons discussed above. Below 1 m

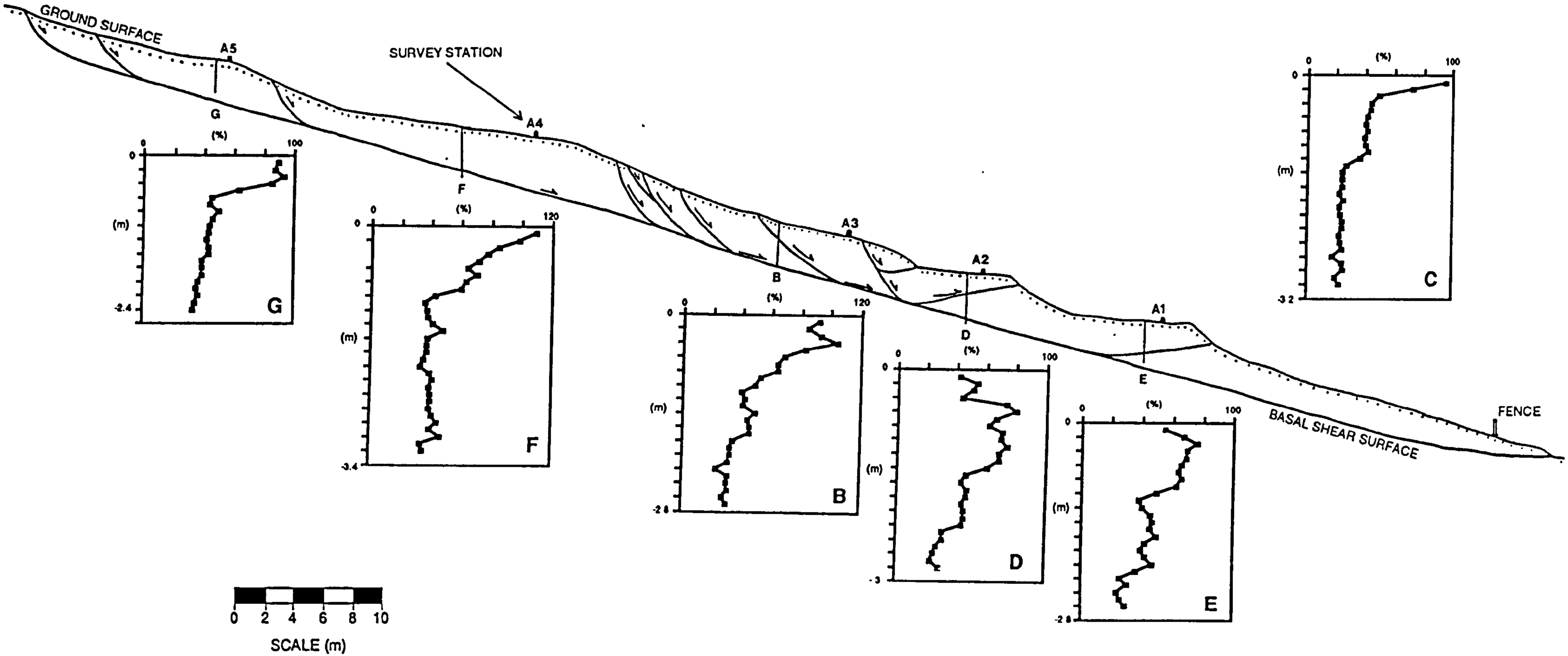

Fig. 3.10a Longitudinal section through the Soper's Wood landslip showing the location of the boreholes. An indication of the moisture content profiles is shown, for further details see Figure 3.10b.

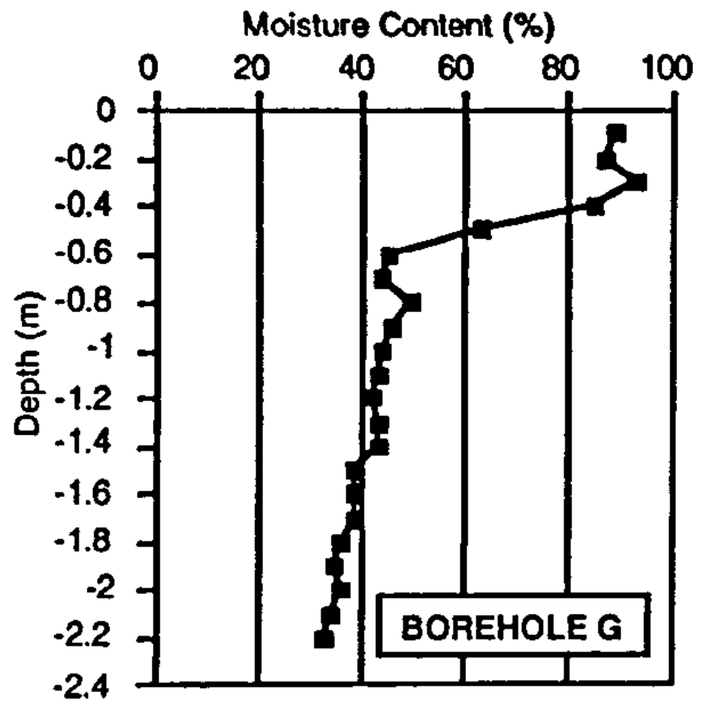

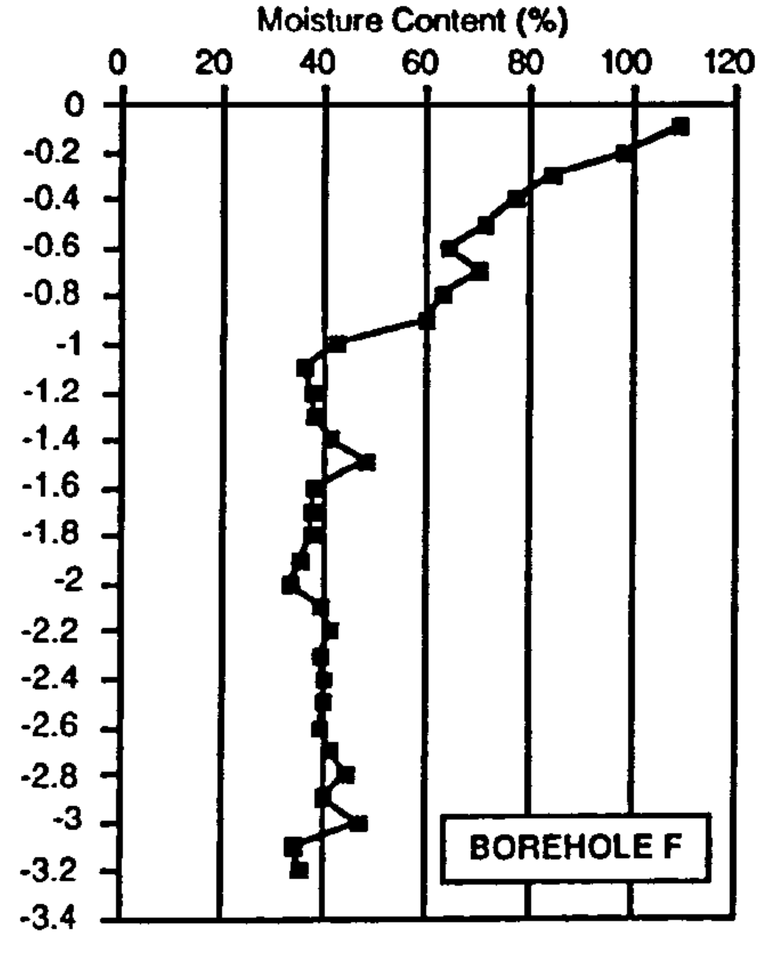

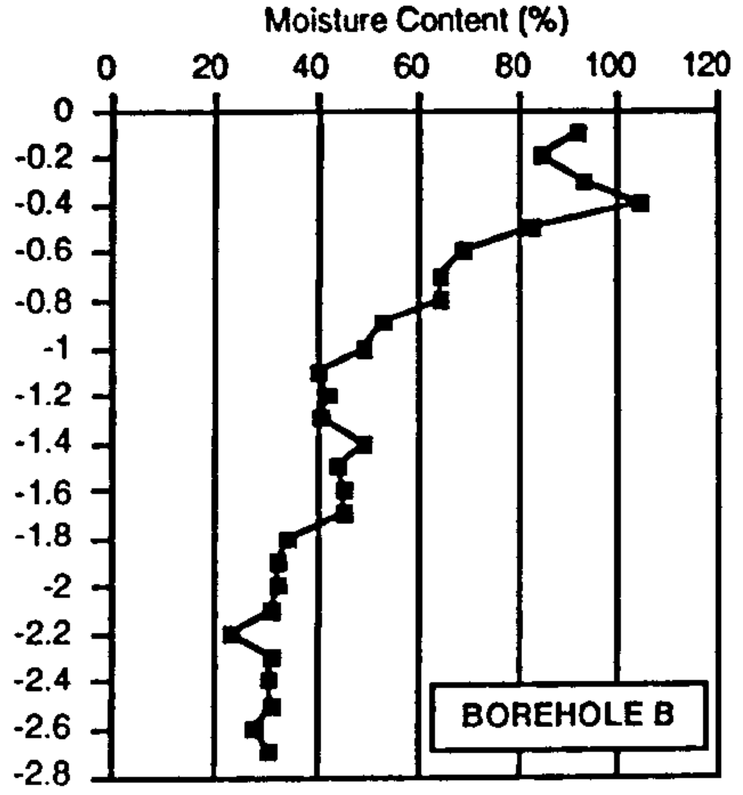

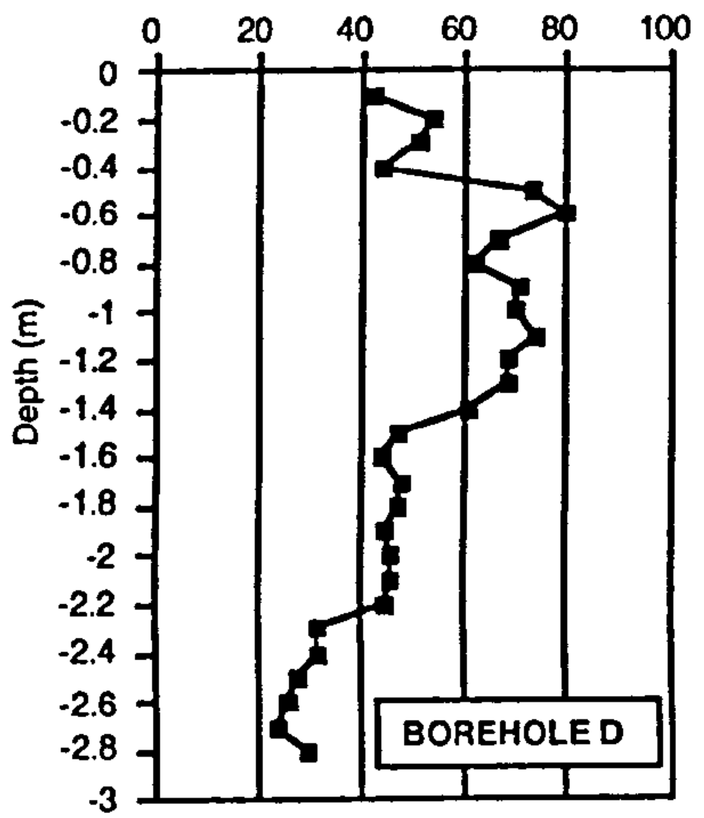

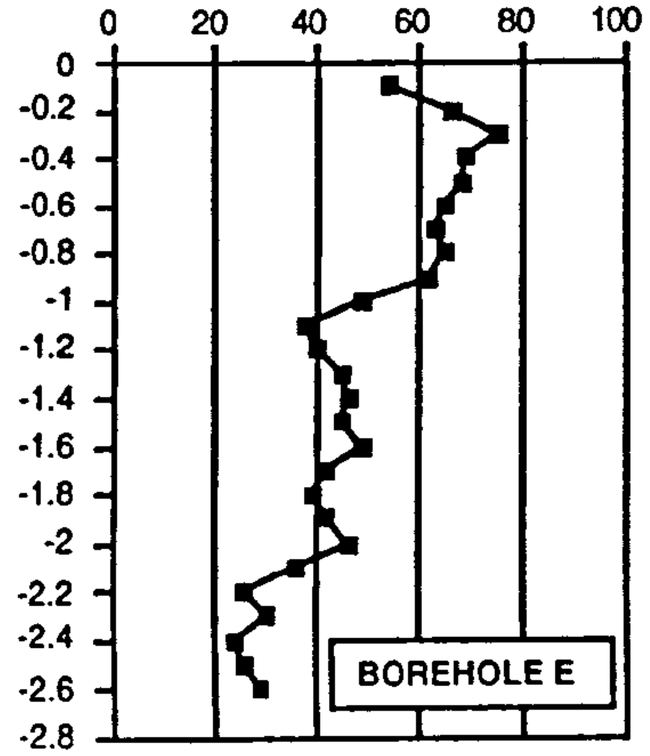

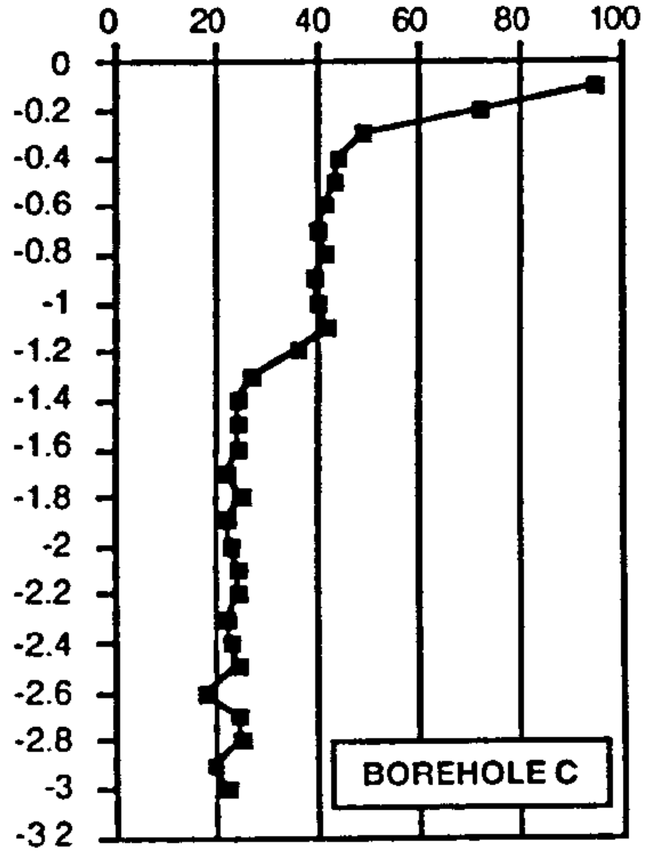

Fig. 3.10b Graphs displaying variations in moisture content with depth for the boreholes at Soper's Wood.

the moisture content tends to remain at approximately 40%. It will be noted that at 1.5 m and 3 m, small zones of increased moisture content are present, while there is also a change at 2 m. These changes may represent zones of disturbance, with the peaks at 1.5 m and 3 m possibly representing the moisture content adjacent to slip surfaces, as noted by Skempton (1964). The two deepest samples below 3 m indicate a decrease in moisture content although at the maximum depth of augering, the moisture content is still at 35%, some 10% to 15% higher than the moisture contents found in the lower zone of borehole C outside the visibly slipped ground.

In borehole B, the upper disturbed zone of high moisture content extends to 1.1 m. It would appear that the high moisture content at 0.4 m may be related to the auger hole passing near a fracture as clearly such high moisture contents at this depth are atypical except in dilated or very organic rich ground. The small peak of 49% at 1.4 m may indicate the presence of a shear surface and the 11% change at 1.8 m suggests that an additional shear surface is encountered at approximately this depth in this borehole position. The lower moisture content of 23% at 2.2 m depth interrupts the general moisture content in the lower zone of approximately 30%. This may represent a better cemented more calcareous band although this was not recorded during logging.

Boreholes D and E are both located in the toes of the slip and the moisture content profiles show sufficient similarity to be treated together, although between the individual profiles there is some 0.3 m to 0.5 m depth difference. This is due to the topographic setting of the boreholes and the position of the boreholes with regard to the toes of slipped material. The boreholes show an upper zone with moisture contents of approximately 50% to 80%, with a layer below having lower moisture contents as a consequence of the auger holes being placed in the toe areas of the slip. A pronounced reduction in moisture content occurs at approximately 1.5 m in borehole D and at about 1 m in borehole E, suggesting that a shear surface may be present at this level. Hence, the material in the toe of the slip above the shear surface is more dilated and thus during the winter period it has a significantly higher moisture content (by approximately 20% to 30%). For the next 0.7 m in borehole D and 1 m in borehole E, the moisture content profile is relatively constant, although notably in borehole E, a minor peak occurs at approximately 1.6 m, suggesting that a shear surface may be present at this depth. At a depth of about 2.2 m in borehole D and a depth of 2 m in borehole E, both moisture content profiles show a second

pronounced reduction. This reduction may be related to the presence of another shear surface.

The profile in borehole C indicates a high moisture content above 0.4 m relating either to creep dilation in the upper zone and/or the presence of fossil root hollows. Below 0.4 m, the moisture content remains at approximately 40% until a depth of 1.3 m, at which point there is a pronounced change in moisture content. The pronounced change at 1.3 m may indicate the presence of a fossil shear surface above which the dilation related to past movement is sufficient to cause the material to have a moisture content some 15% to 20% higher than in the material below. Below a depth of 1.3 m, the moisture contents of 20% to 25% are relatively typical of slightly weathered calcareous mudrocks and it is likely that this zone has suffered little, if any shearing in the past.

It is worth noting that in borehole C, below a depth of only 0.4 m the moisture content is less than or equal to approximately 40%. In comparison, the clay from those boreholes within the landslip has much higher moisture contents at this depth and a moisture content of about 40% is not reached until approximately a depth of 1 m in boreholes F, B and E, 1.5 m in borehole D and 0.6 m in borehole G. In addition, those boreholes within the slipped mass, never show the consistently low moisture content of approximately 20%, exhibited by the clay in borehole C below a depth of 1.3 m.

It is clear from the discussion above and the data provided in Figure 3.10a and 3.10b that there are significant differences in the profiles of the soil moisture content, both downslope within a slipped mass and when the profiles within a slip are contrasted with a profile taken outside the main visibly slipped mass.

3.4.3 Comparison of the Index Properties of Boreholes B and C

In order to obtain a sufficient quantity of sample for index testing, the top sample of each borehole was discarded and the remaining individual samples combined in pairs down the profile of the borehole. Geotechnical index tests were performed on the pairs of samples obtained from Boreholes B and C (which are at approximately the same topographic level) in order to compare the properties of the highly weathered, slipped Fuller's Earth clay and the "relatively fresh" unslipped Fuller's Earth clay. In addition the calcite contents of the sample pairs were determined. The results are displayed in Figure 3.11 and the techniques used are described in Appendix I.

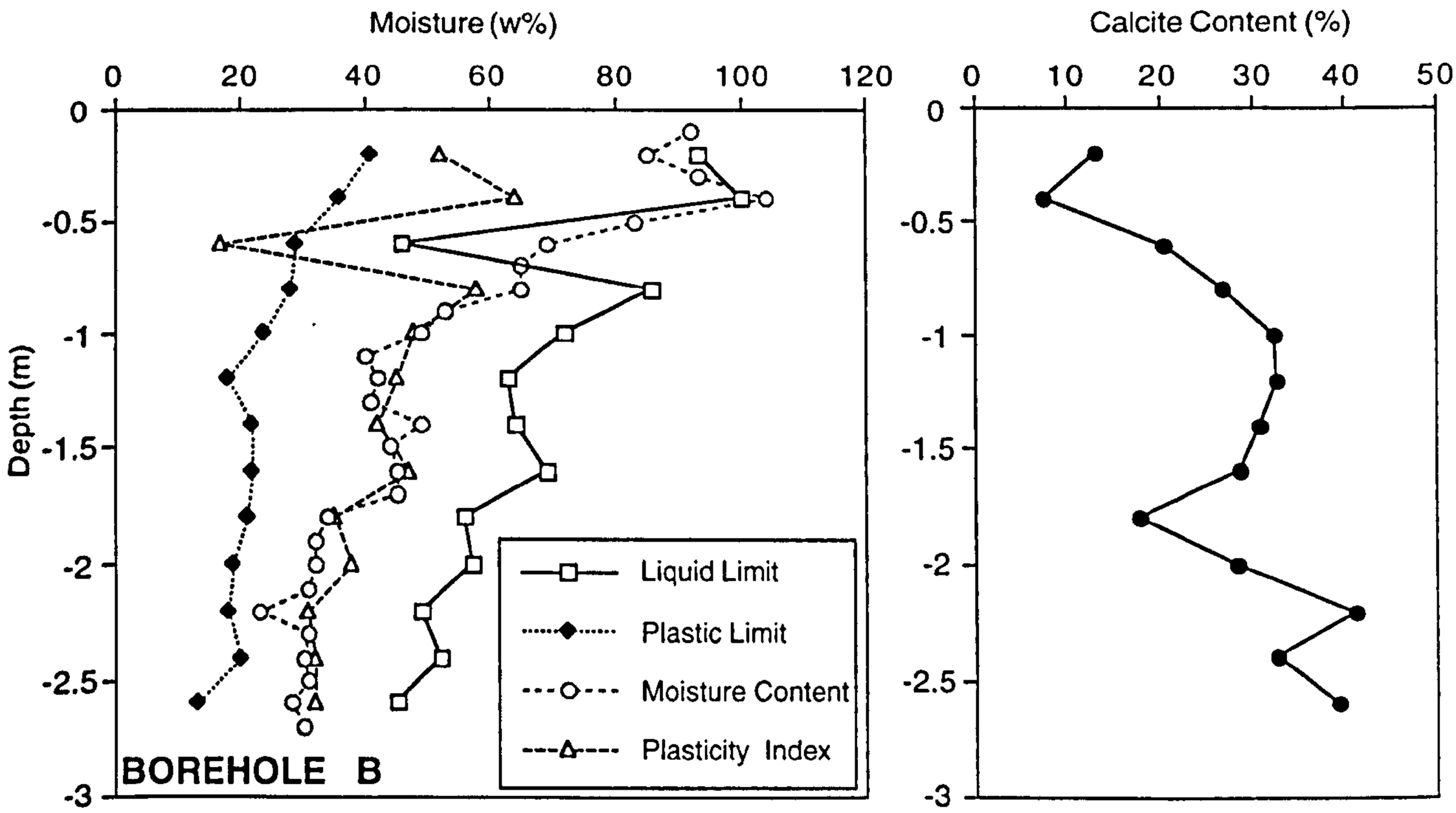

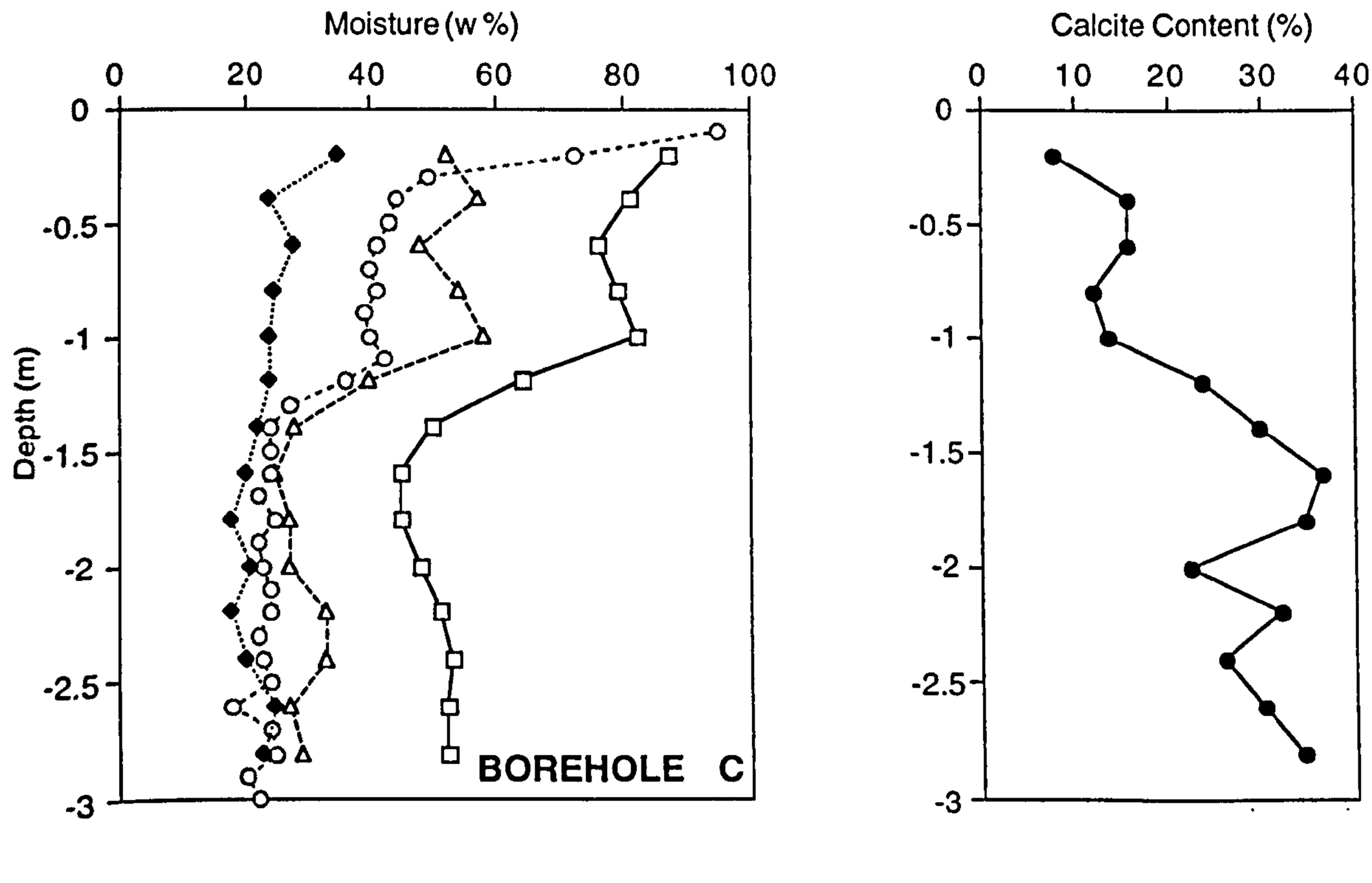

Fig. 3.11 Graphs comparing moisture content, Atterberg limits, plasticity index and calcite contents for boreholes B and C.

Work reported by Chandler *et al.* (1976) on the Upper's Fuller Earth clay in the Swainswick Valley indicated a mean liquid limit of 51% (range 40% to 65%), a mean plastic limit of 20%, giving a plasticity index of 31%. In addition, they found that the Lower Fuller's Earth clay had a mean liquid limit of 47% (range 30-70%), a mean plastic limit of 19%, giving a plasticity index of 28%. In this study, borehole B provided a mean liquid limit of 66% (range 45% to 100%), a mean plastic limit of 24%, giving a plasticity index of 42%. Borehole C provided an average liquid limit of 62% (range 45% to 87%), a mean plastic limit of 24%, giving a plasticity index of 38%. These values are significantly higher than those reported by Chandler *et al.* (1976), especially with regard to the liquid limit.

Hawkins *et al.* (1986 and 1988) discuss the effects of weathering on the geotechnical properties of the Fuller's Earth formation and observed that with an increase in weathering grade there is an increase in the Atterberg limits, moisture content and a decrease in the calcite content (see Chapter 1). The higher limits found at Soper's Wood are thus likely to be due to the relatively weathered nature of the near surface samples obtained, whereas Chandler's work included samples of unweathered Fuller's Earth obtained from a borehole located on the Great Oolite plateau of Charmy Down, some distance away from any slope feature.

Indeed, if the indices of the samples above a depth of 1.3 m are ignored in the calculation of the average indices for borehole C (this corresponds to the change from moderately weathered to slightly weathered shown on the borehole log in Section 3.4.1), this provides an average liquid limit of 51% (range 45% to 64%), a mean plastic limit of 21%, giving a plasticity index of 30%, much closer to the values of Chandler *et al.* (1976). In comparison, if the same treatment is applied to borehole B, where the samples have all been graded at least highly weathered, this provides an average liquid limit of 56% (range 45% to 69%), a mean plastic limit of 19%, giving a plasticity index of 37%, still higher than the values of Chandler *et al.* (1976). This is probably due to the more weathered and dilated nature of the material in borehole B, even at depth.

In Figure 3.11, both boreholes B & C show a strong correlation between moisture content and Atterberg limits and to some extent an inverse relationship with calcite content.

In borehole B, the Atterberg limits and moisture content show a general trend of increasing with decreasing depth and hence, as the logs in Section 3.4.1 show, with increasing weathering grade from “highly weathered” at a depth of 2.7 m to “residual soil” at ground level. In contrast,

the calcite content profile indicates a decreasing trend with decreasing depth and increasing weathering grade. In addition, in the near surface material found in borehole B, the natural moisture contents more closely reflect the high liquid limits and only begin to approach the plastic limit at a depth of approximately 1.1 m. However, at this depth the moisture content is still high at approximately 40%, compared to the plastic limit of about 20% and even at the depth of the borehole (2.7 m), the moisture content is about 30%, still some 10% higher than the plastic limit. This is in contrast to the findings of Chandler *et al.* (1976), who report that the moisture content of the Fuller's Earth was approximately equal to the plastic limit (see Chapter 1).

In borehole C, above a depth of 1.3 m, a similar trend to that indicated by the profiles in borehole B can be observed. However, below 1.3 m, where the log shows the silty clay to be only slightly weathered, the Atterberg Limits and moisture content are approximately constant and the calcite content is more variable showing no particular trend. In contrast to borehole B, in the material found in borehole C, the moisture contents are very similar to the plastic limits below the initial 0.3 m, and notably below a depth of 1.3 m are almost equal, with the moisture content dropping below the plastic limit after a depth of 2.5 m.

These findings support the conclusions of Hawkins *et al.* (1986 and 1988), who suggested that on weathering there is a gradual depotassification of the illite rich Fuller's Earth clay, transforming the illite into a mixed layer illite-smectite. In addition, the percolation of acidic ground waters in the weathered zone may result in the gradual dissolution of the calcite in the near surface deposits. Clearly an increase in the proportion of the mixed layer illite-smectite, coupled with a decrease in the proportion of a non-sorptive mineral such as calcite, will result in an increase in both the liquid and plastic limit. In addition, they suggest that natural moisture contents are generally below the plastic limit in the less weathered material, but above it in the near surface samples where weathering has increased the illite-smectite content and stress release has allowed the infiltration of surface water and the hydration of the clay.

Hence in borehole B, which the log show to be at least heavily weathered for the whole profile and the topography to be highly disturbed due to slipping, the moisture content is higher than the plastic limit and indeed, above a depth of about 1.1 m is closer to the liquid limit. In addition, the calcite content increases with depth. In borehole C, the log shows that less weathered material is reached at 1.3 m, coinciding with the depth at

which the moisture content starts to approximate the plastic limit. Above 1.3 m, dilation due to creep of the near surface material may have allowed the infiltration of ground waters. Hence, above a depth of 1.3 m, there is an increase in Atterberg limits and a decrease in calcite content, due to some near surface weathering, and the moisture content is greater than the plastic limit. However, unlike in borehole B, it is notably less than the liquid limit below the initial 0.3 m.

The graphs of calcite content with depth show an overall inverse relationship with the geotechnical indices, supporting the observations made by Hawkins *et al.* (1986 and 1988) and Hawkins & McDonald (1992), see Chapter 1. This is more clearly shown in Figure 3.12, where both plastic and liquid limits show a decrease with increasing calcite content. Hawkins & McDonald (1992) showed that the silt sized particles within the Fuller's Earth were dominantly calcareous. Hence, an increase in calcite content corresponds to an increase in non-sorptive silt size particles (and a corresponding decrease in the proportion of clay minerals) causing reduced plasticity.

3.4.4. Discussion

At Soper's Wood, the logs of the boreholes have demonstrated the highly weathered nature of the slipped Fuller's Earth clay. These indicate that both the weathering grade and the depth to which weathering occurs are greater in the slipped material compared to the material outside the visibly slipped mass. The moisture content profiles for the slipped material are variable, compared to the smoother decrease with depth in the profile for the visibly unslipped material. In addition, these demonstrate that the slipped material generally has a higher moisture content compared to the unslipped material at a similar depth and that the slipped material never shows a consistently low moisture content at the depth of these boreholes, unlike the material outside the slip.

A comparison of the geotechnical indices of samples from inside and outside the visibly slipped mass has shown the effects of the increased weathering of the slipped material on the geotechnical indices of the Fuller's Earth clay. In addition the study has confirmed the control that calcite has on the Atterberg limits of the Fuller's Earth clay .

Within the slide, the moisture content and Atterberg limits all increase with decreasing depth and increasing weathering grade and the calcite content decreases. In addition, near the surface the moisture content is similar to the liquid limit, although below 1.1 m, it becomes closer to the

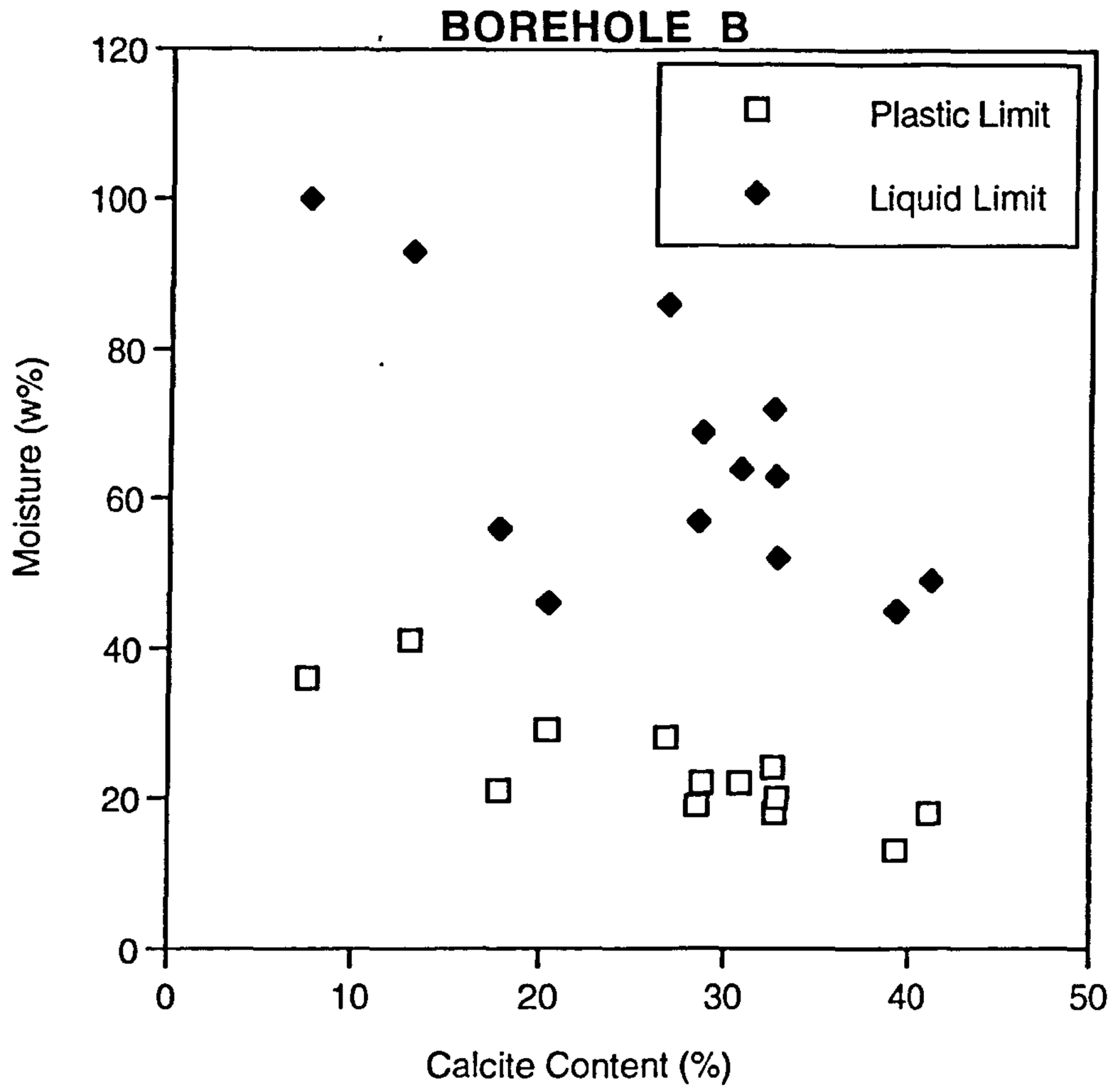

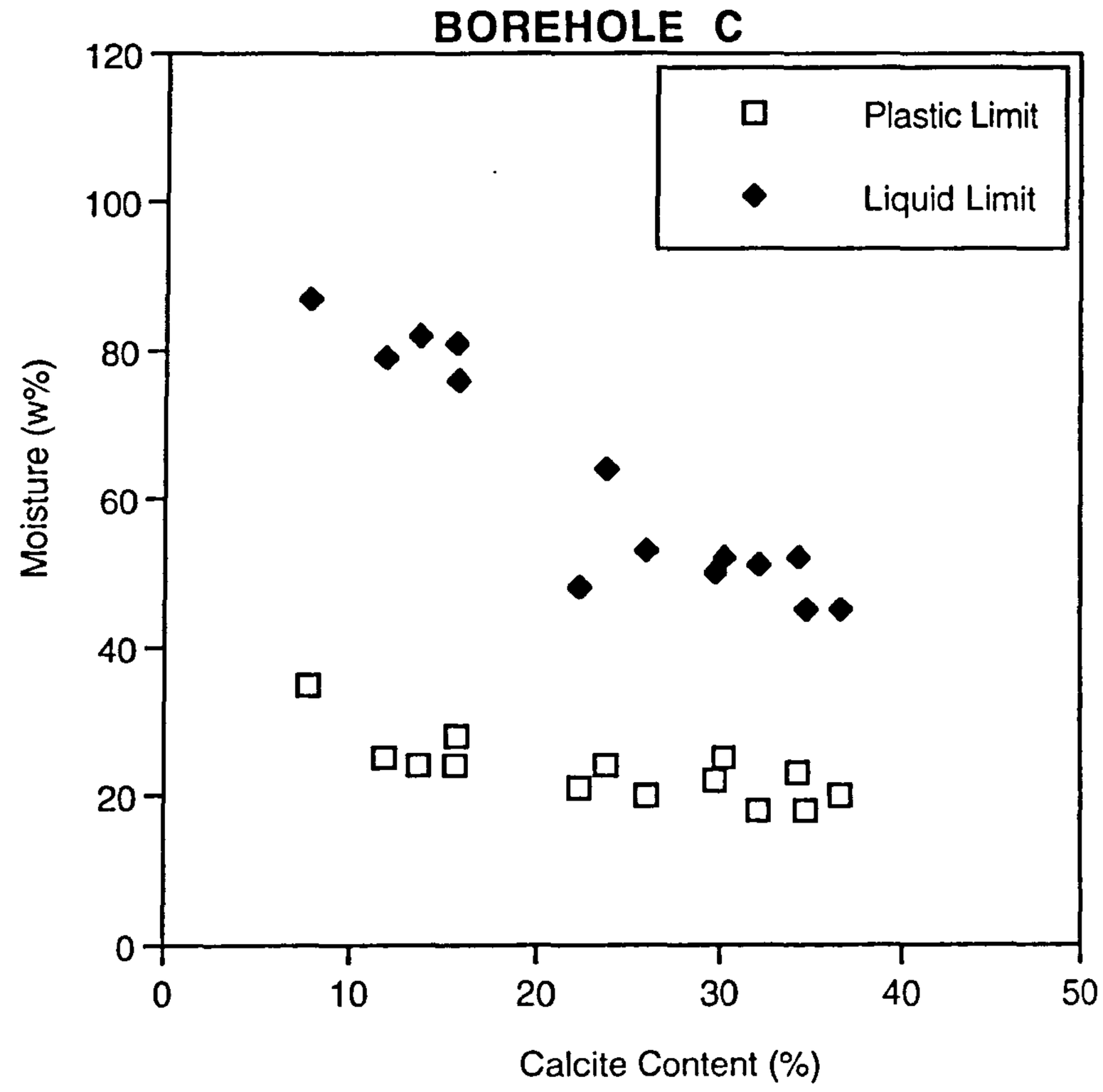

Fig. 3.12 Plots displaying the relationship between Atterberg limits and calcite content for boreholes B and C.

plastic limit. However, even at the base of borehole B (2.7 m), it is still some 10% higher than the plastic limit.

Outside the landslide, above a depth of 1.3 m, there is a similar trend of increasing Atterberg limits and moisture content and a decreasing trend of calcite content, probably due to near surface creep dilation of the soil. However, below the initial 0.3 m the moisture content more closely reflects the plastic limit of the clay. Below 1.3 m, the Atterberg limits and moisture content remain approximately constant with a variable calcite content and the moisture content is shown to be approximately equal to the plastic limit, falling below it at a depth of 2.5 m.

It appears that, as proposed by Hawkins *et al.* (1986 and 1988), the highly fractured nature of the slipped material has aided the infiltration of ground waters into the previously relatively impermeable clay, which has aided chemical weathering. The acidic ground waters have encouraged the transformation of some of the illite rich Fuller's Earth clay into an interstratified illite-smectite and has caused the dissolution of calcite.

Clearly from the above observations there is an interrelationship between the degree of landslipping and the depth and grade of weathering in the Fuller's Earth clay. The increased weathering caused by the landslipping increases the geotechnical indices of the clay, compared to the adjacent unslipped ground. This has important engineering implications, especially if geomorphological evidence of a relict landslip is absent due to erosion, surface creep and the influence of agriculture (Chandler 1970). Thus, there may be no ground surface indication that an area of slipped ground is present, which will have different geotechnical properties compared to the surrounding unslipped material.

3.5 Analysis of Landslide Movement

The landslip was monitored from January to August 1994 to investigate the rate of slip movement, the changing morphology related to slip movement, and whether slip movement could be related to factors such as rainfall and ground water levels. In addition, the analysis aided the identification of those parts of the slip which were most active.

3.5.1 Surveying Results

Surveying was undertaken on 19 occasions from the 19th January 1994 until 30th June 1994, a total of 163 days. Initially it was anticipated that surveying would be carried out at approximately weekly intervals. However, due to the non-availability of the AGA Geodimeter over the Easter

period, a longer interval occurs between the 10th reading (21st March 1994) and the 11th reading (7th April 1994). Unfortunately, this period coincides with a phase of more rapid movement, as discussed below. In addition, from the end of April 1994, surveying was undertaken less frequently as the landslide appeared to have stopped moving. The data can be found in Appendix II.

Figure 3.13 contains plots showing the horizontal and vertical components of cumulative movement of the survey stations over the entire period. It should be noted that they are in upslope order, as seen in Figure 3.7, and each plot corresponds to one days surveying. These plots are displayed to compare the cumulative movement of the various survey stations and, due to some variation in the intervals between surveying, are not meant to provide an indication of the velocity of each survey station throughout the period. The cumulative movement of each survey station is discussed in turn below.

Station A1

A1, located in the toe of Slide A (see Figure 3.7), has remained effectively stationary. It shows no evidence of movement during the current phase of landslide activity, whereas significant movement has occurred elsewhere. This is supported by adjacent standpipe E, approximately 1 m away, which has not snapped.

Station A2

A2 is located in an intermediary toe within Slide A (see Figure 3.7). Initially this rose by 0.15 m with a horizontal movement of 0.2 m. Movement of this survey station then continued as a dominantly translational movement until the 11th reading (7th April 1994). Between the 10th (21st March 1994) and 11th reading, a further 0.4 m of horizontal movement had taken place, although since that period the amount of translational movement has decreased, with a decrease in the level of the ground surface. Total cumulative horizontal and vertical movement was almost 2 m and 0.05 m downwards (ignoring the initial upward movement). The surrounding toe has clearly been active and the initial rise of the station is likely to be due to the curved nature of a shear surface which exists beneath this part of the toe. In the later phases of movement, the gradual decrease in height is most probably due to the station tilting valleyward, due to the development of radial cracks in this part of the toe (see Plate 3.7). Movement is supported by the snapping of adjacent standpipe D, approximately 1 m away.

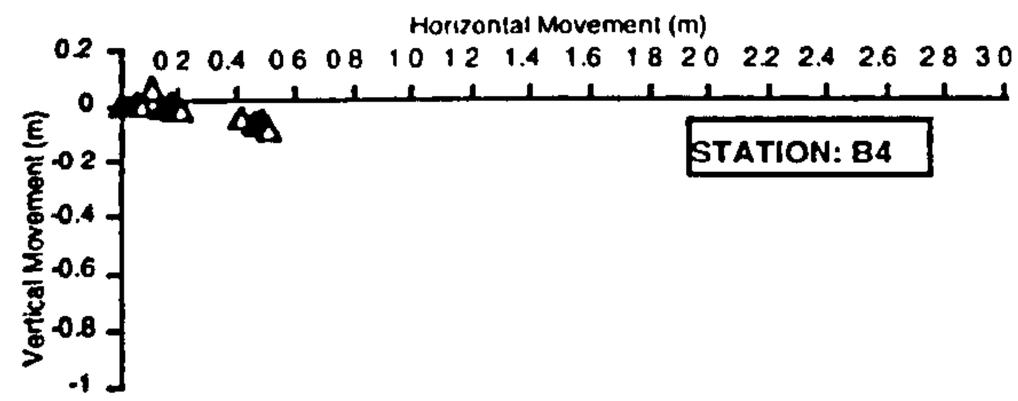

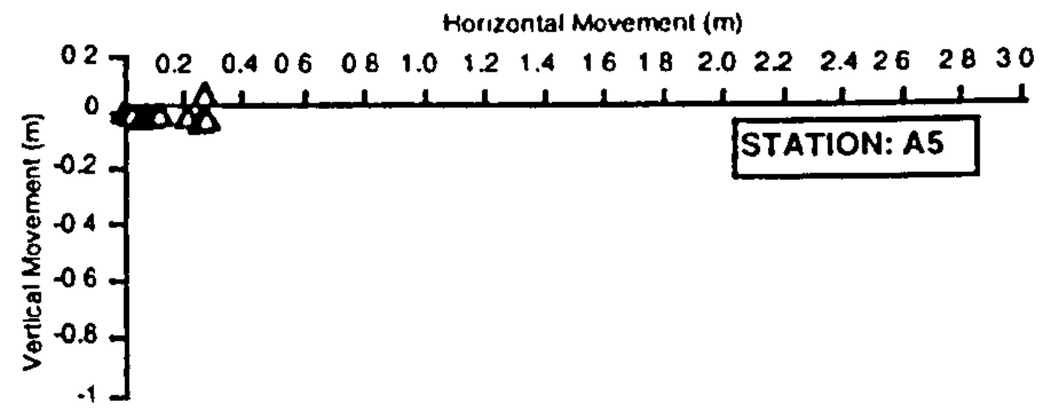

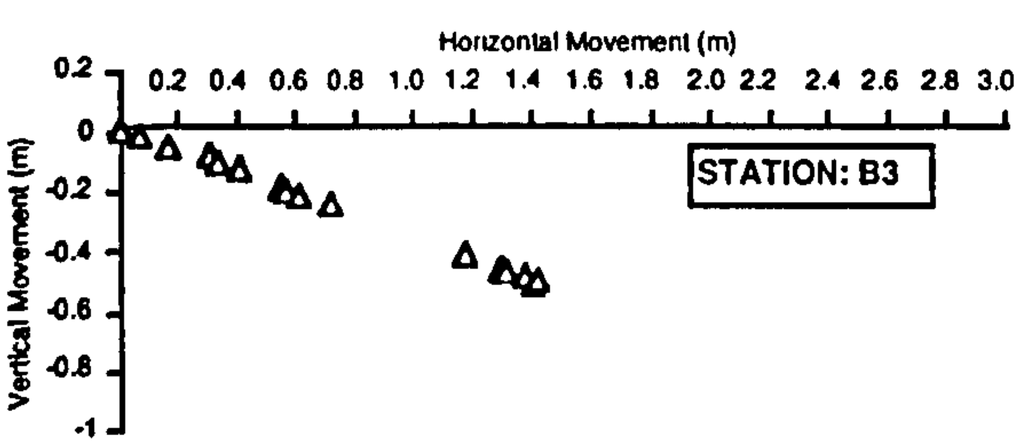

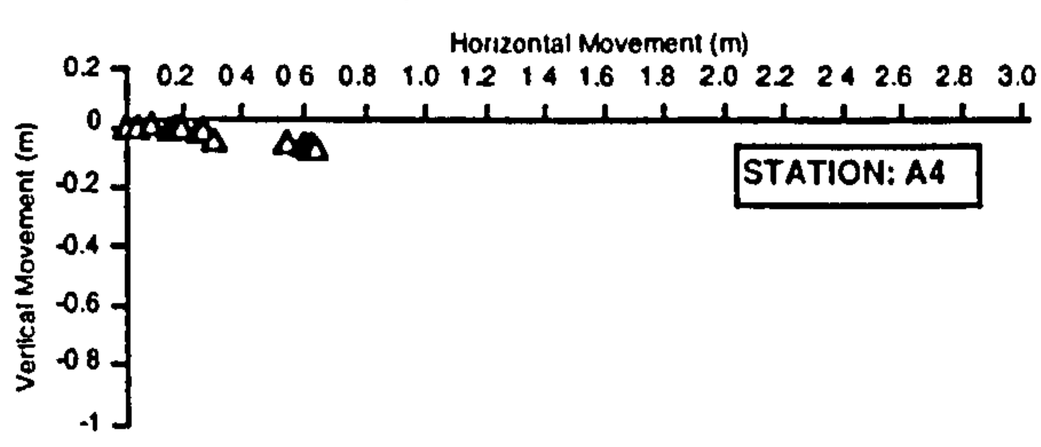

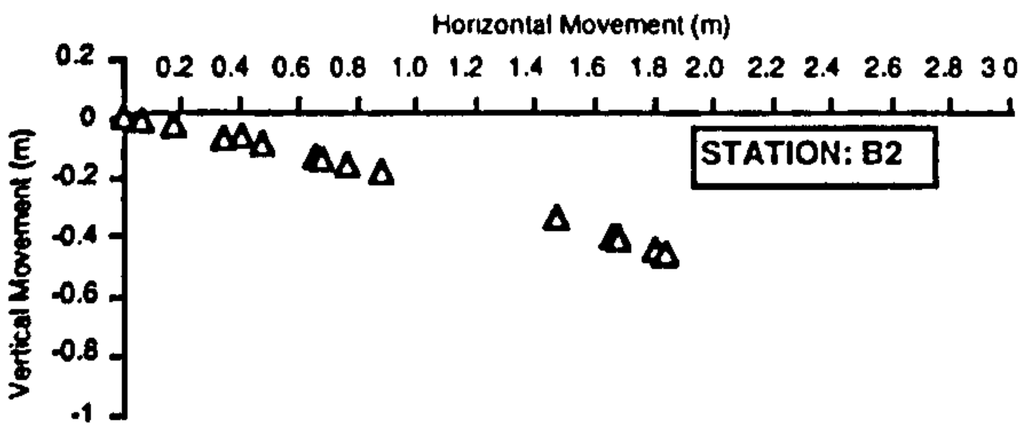

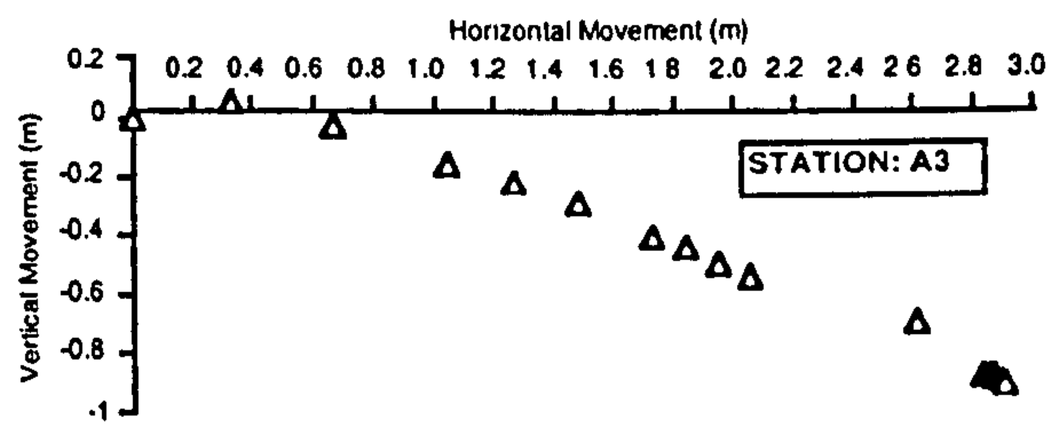

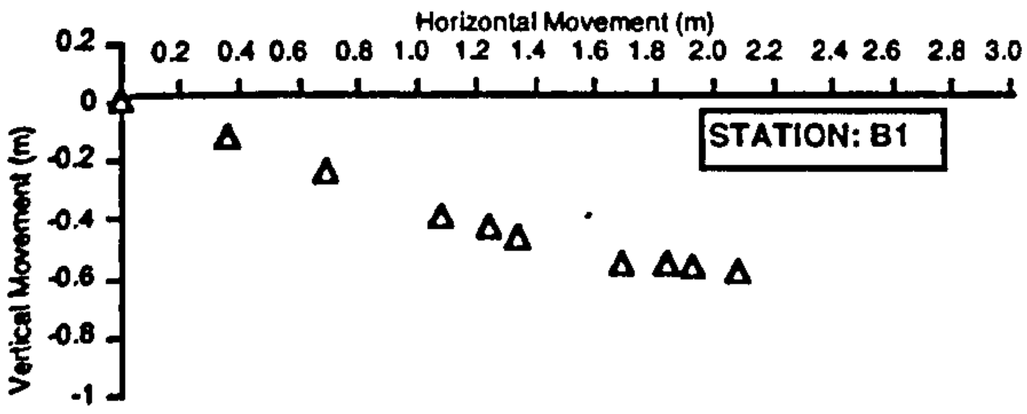

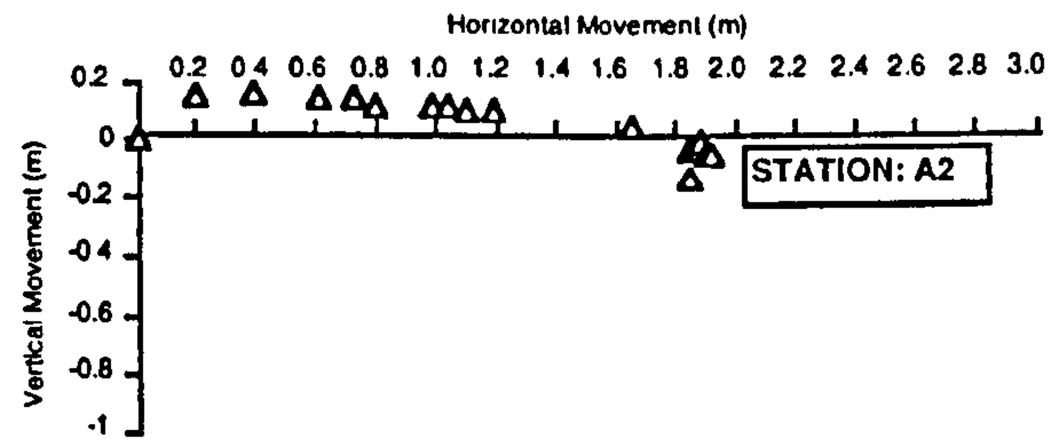

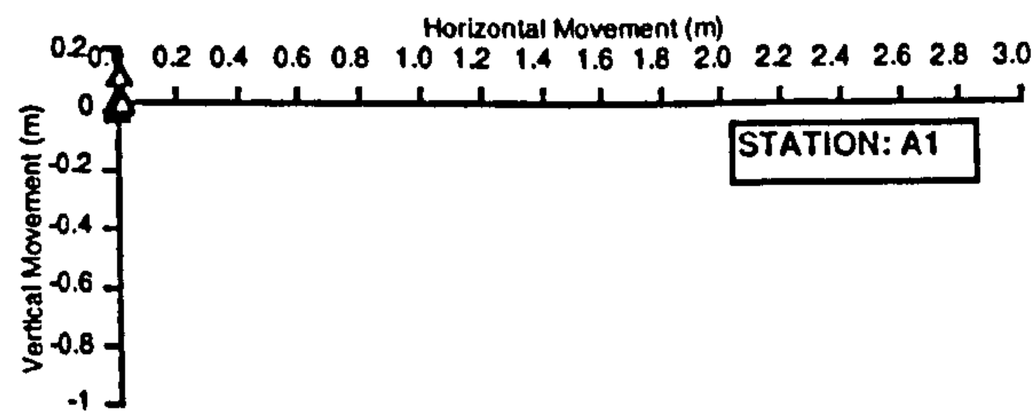

Fig. 3.13 Plots showing the total cumulative movement of each survey station over the period of surveying (19 January 1994 to 30 June 1994).

Station A3

A3, situated in the main body of Slide A (see Figure 3.7), moved a total of 2.9 m horizontally and 0.9 m vertically downwards. As for station A2, there is increased displacement between the 10th and 11th readings. Soon after emplacement a small tension crack appeared right behind station A3. The large amounts of movement were confirmed by the freshness of the adjacent lateral shears and the enlargement of the minor scarps upslope of station A3. Slip movement caused standpipes A and B to be "drawn into" the slipped mass. Standpipe A was "drawn in" by approximately 0.5 m in total. In comparison, standpipe B was "drawn in" by 0.8 m in the first four weeks of monitoring (corresponding to the 4th monitoring point). In order to avoid loosing the standpipe, an extension was made by splicing a length of plastic pipe and attaching the extension with jubilee clips.

Station A4

A4 is located on the left side of the main translational slide (see Figure 3.7) which showed much less movement. The total horizontal and vertical movement was 0.62 m and 0.07 m. The plot shows that movement was generally small and gradual, although again there is increased movement between the 10th and 11th readings. In this part of the slip, movement was confirmed by the snapping of nearby standpipe F, some 6 m upslope. As seen in standpipes A and B, standpipe F was also "drawn into" the landslide by some 0.1 m between the 10th and 11th readings, coinciding with the period of increased movement.

Station A5

A5 is located towards the head of the left side of the main translational slide (see Figure 3.7) and showed comparatively little movement. Total horizontal and vertical movement was 0.28 m and 0.03 m. The single positive reading may be correct but the possibility of a slightly inaccurate reading cannot be dismissed. As in station A4, movement was generally very small and gradual. Initially standpipe G, located about 1 m away, did not snap. However, between the 11th and 12th reading (7th and 13th April 1994) standpipe G appears to have snapped at a depth of approximately 0.9 m. It is thought that the basal shear surface, along which the majority of movement has occurred, is below the maximum depth of standpipe G at this location (see Figure 3.22). The snapping of standpipe G, towards the end of the period during which the majority of movement occurred, is interpreted to have been caused by movement along a minor shear.

Station B1

B1 is situated between the two mudflows in Slide B (see Figure 3.7) and moved a total of 2.07 m horizontally, and 0.59 m downwards. However, this was only for the first nine weeks of monitoring up to reading 10 (21st March 1994). B1's survival for surveying to reading 10 was fortunate, as from reading 7 (3rd March 1994) the material on one side of the station had been removed by movement (see Plate 3.8). When surveying was undertaken on the 7th April 1994 (reading 11) the station had been "swept away" by the enlarged mudflow, formed by the joining of the two pre-existing mudflows (see Plate 3.9). This part of the landslide has clearly been very active as demonstrated by the loss of station B1.

Station B2

B2, situated just behind the scarp of the mudflow in Slide B (see Figure 3.7), moved 1.83 m horizontally and 0.46 m vertically downwards. The amount of movement of this part of the slip is less than that of B1 but is still considerable. Movement was fairly consistent, but again between reading 10 (21st March 1994) and reading 11 (7th April 1994), cumulative movement increases from 0.87 m to 1.46 m horizontally and from 0.19 m to 0.34 m vertically downwards. These dates correspond with the loss of station B1 and so clearly between these dates there was increased slip activity with the joining of the two mudflows. Although station B1 was discontinued after the 21st March (reading 10), the equivalent movement of 2.07 m shown by station B1 was only some 0.9 m in station B2.

Station B3

B3, situated on the right side of the main translational (see Figure 3.7), showed total downslope movement of 1.41 m horizontally and 0.50 m vertically. This is less than for B2, however it is interesting to note that the slip at B3 has moved considerably further than at A4, which is situated at approximately the same topographic level in the main translational slide. In addition, B3 shows a similar increase in movement between readings 10 and 11.

Station B4

B4 is located close to the head of the right side of the main translational slide at a similar topographic level to station A5. Total horizontal and vertical movement were 0.48 m and 0.06 m downwards, respectively. This is considerably less than at B3, but is again greater than the amount of movement seen at A5. In addition, at this location also, there appears to be increased movement between readings 10 and 11.

Plate 3.8 View down the mudflow in Slide B showing the removal of soil by the mudflow from one side of survey station B1.

Plate 3.9 View down Slide B showing the enlarged mudflow. Survey station B1 was swept away and is visible towards the edge of the mudflow.

3.5.1.1 Summary

Along the line of survey stations A1 to A5, the portion of Slide A containing stations A3 and A2 has been the most active, with movement occurring on the cluster of minor scarps behind standpipe B, down to the toe containing station A2. The upper area of the main translational slide containing stations A5 and A4 has shown much less movement.

Along the line of survey stations B1 to B4, the mudflows, towards the bottom of the slope in Slide B, have shown the most movement with the loss of survey station B1. Stations B2 and B3, situated in the body of the main translational slide, showed significant movement, but less than that shown by station B1. The upper area of the main translational slide containing station B4 showed much less movement. From the plots there appears to have been a phase of enhanced movement between the 21st March 1994 (reading 10) and 7th April 1994 (reading 11), although it is recognised that this period also represents an approximately 2 week interval between surveying. This is clearly evident in the cumulative movement shown by the 'B' survey stations, but is also shown to lesser extent by movement of the 'A' stations. In addition, it appears that in the main translational slide, up-slope of where the landslide extends into two features, the side containing survey stations B3 and B4 has shown a greater amount of movement.

3.5.2 Comparison of Landslide Movement with Precipitation

Rainfall is recognised by many workers as a major factor influencing the frequency of landslides. Zaruba & Mencl (1969) provide a review of the relationship between slope movement and precipitation, with examples of particular studies carried out in central Europe. Lichkov (1938) conducted a statistical analysis of 350 landslides and assessed their relationship with rainfall and snow melting in the Kiev area of Ukraine. Schmassmann (1953) assessed the dependence of landslides on the pattern of precipitation in the Basle Canton of Switzerland. However, these works generally relate to the relationship between landslide incidence and precipitation.

In this country, most slope movements display a seasonal pattern, generally occurring in the wet period from October to April. Brunsden (1984) reports that coastal mudslides display a marked seasonal relationship with the incidence of wet and dry periods (as noted by Hutchinson 1970, Brunsden 1973, Prior & Eve 1975, Balteanu 1976 and Craig 1979) and that Prior *et al.* (1968 and 1971) observed that movements of mudslides correlate with 10-day and 30-day cumulative rainfall totals.

However, these investigations into the relationship between movement and rainfall have been concentrated on coastal mudslides and comparatively less work appears to have been carried out on the relationship between the pattern of movement of an inland translational slide and rainfall, during a particular phase of slide activity. Lawrence (1985) observed that renewed movement of the landslides at Soper's Wood appeared to coincide with high levels of precipitation and this research attempts to investigate the relationship between movement rate and rainfall of the inland slide at Soper's Wood.

The histogram in Figure 3.14 shows daily rainfall at Woolley Farm from the 1st November 1993 to the 1st August 1994 inclusive, as recorded by the National Rivers Authority at 9:00 GMT each day using a Tipping Bucket rain gauge attached to a data logger. Woolley Farm (ST 749685) is situated in the Swainswick valley, approximately 750 m to the north of the landslips at Soper's Wood.

The histogram indicates that rainfall was sparse in November 1993, totalling 45.4 mm. While in December 1993 it totalled 142.2 mm, with peaks occurring on the 8th, 12th, 18th and 30th of December, of 11 mm, 13.8 mm, 17 mm and 12.6 mm, respectively. Total monthly rainfall is slightly less in January 1994, but at 117.8 mm is still high, with peaks occurring on the 4th and 17th of January, of 16.4 mm and 11.8 mm, respectively.

Total monthly rainfall was less in February 1994, at 80.8 mm and remains at a similar level through to March 1994 when the monthly total was 82.2 mm. Peaks of 17.4 mm, 11.8 mm and 16.4 mm occur on the 10th and 22nd February and the 31st March, respectively.

The monthly total drops again in April 1994 to 58.8 mm, with 14 mm recorded on the 3rd April and 21.4 mm recorded on the 8th April. In May 1994 total monthly rainfall was back up to 78.6 mm with a peak of 18.2 mm on the 21st May 1994. (Unfortunately due to the failure of the data logger at Woolley farm, information was lost from the 7th May 1994 to the 7th June 1994 and data for this period had to be obtained from the weather station at nearby Bath University (ST 774643)). Monthly totals for June and July 1994 were much lower at 21.6 mm and 44.8 mm, respectively, with peaks of 15.8 mm and 15.2 mm on the 6th and 31st July 1994.

The reactivation of the currently active slide appears to have been caused by the very high levels of near continuous precipitation in late December 1993 and early January 1994, at a time of low evapotranspiration when consequently ground saturation is likely to be most intense. Movement continued through the spring supported by the

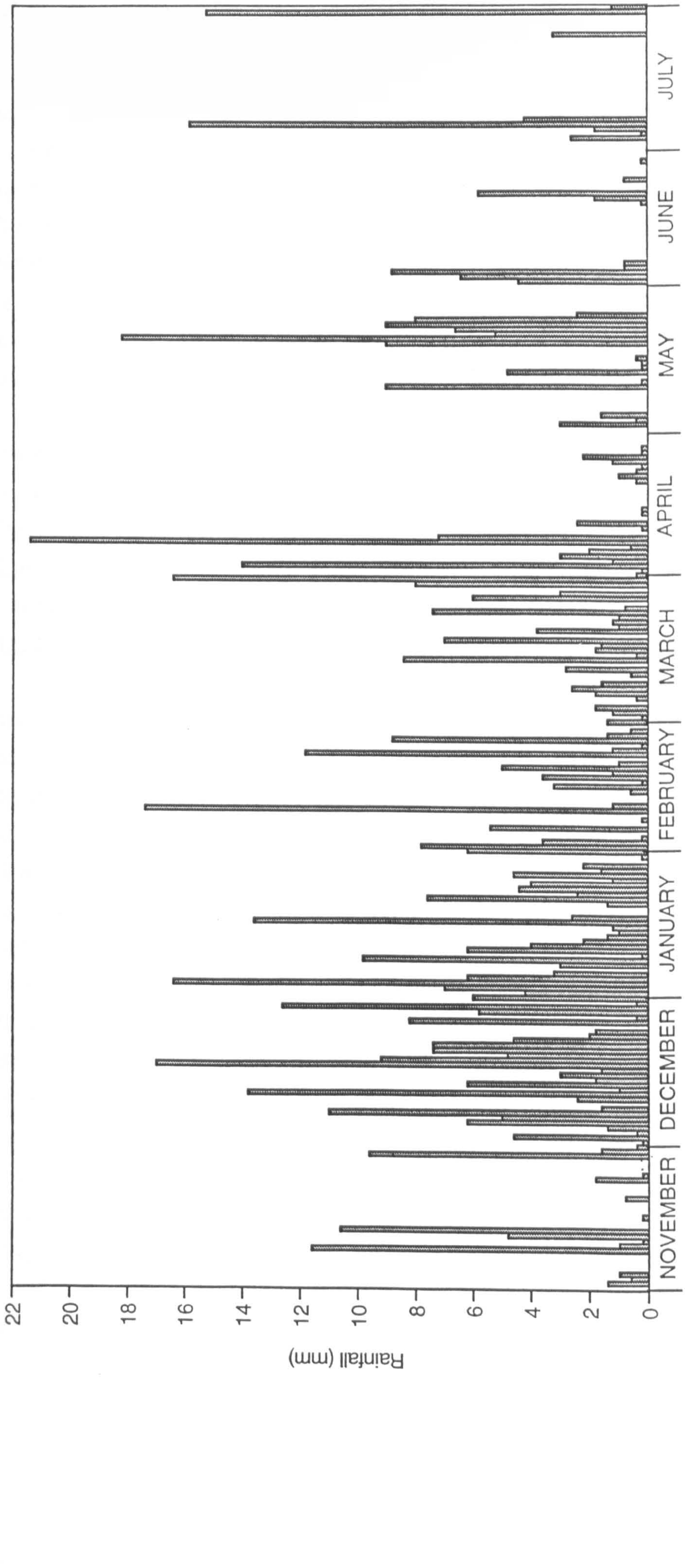

Fig. 3.14 Histogram showing daily rainfall at Woolley Farm, Bath from 1 August 1993 to 1 November 1993 to 1994. The left border separating each month represents the first of the month.

higher levels of rainfall during this period. In order to analyse this relationship in more detail, cumulative rainfall has been plotted against the cumulative horizontal movement of each survey station for the period of surveying (19th January 1994 to 30th June 1994), see Figure 3.15. As the scale of horizontal movement is so different in different parts of the slip, it has been considered necessary to vary the vertical axis scale for the different survey stations. It should be noted that straight lines join adjacent points and there has been no attempt to try and estimate the curve of the line. In addition, stations B4 and A5 show much smaller amounts of movement and therefore inaccuracies in the surveying technique may account for some of the more extreme readings.

Each survey station (apart from that of station A1, which has been shown in the previous section to be effectively stationary) displays a very similar pattern of horizontal movement which is clearly intimately related to rainfall, even with the varying amounts of movement of each station. Five broad phases of horizontal movement which are related to rainfall are evident for each station and these are discussed below.

Phase 1 Monitoring days:0-21 (19th January-9th February)

As demonstrated by the gradients of the two curves, cumulative rainfall increases rapidly at first and cumulative horizontal movement increases at a similarly rapid rate.

Phase 2 Monitoring days:22-43 (10th February - 3rd March)

From the 22nd day of monitoring (10th February), there is a slight lowering in the rate of increase of cumulative precipitation and, from the same day, this decrease is displayed by the rate of horizontal movement. Thus, there appears to be no time lag in the response of the landslide to this small change in rainfall. Horizontal movement then continues at this slightly reduced rate until the 43rd day of monitoring (3rd March 1994), after which there is change in gradient of the profile and the rate of movement decreases further. This reduction in slip movement rate appears to be related to the decrease in precipitation which occurred on the 38th day of monitoring (26th February 1994), after which the rate of increase in cumulative precipitation levels off. There therefore appears to be about a 6 day lag before the change in precipitation levels affects the rate of slip movement. However, this time lag is affected by the surveying interval and can therefore only be approximate.

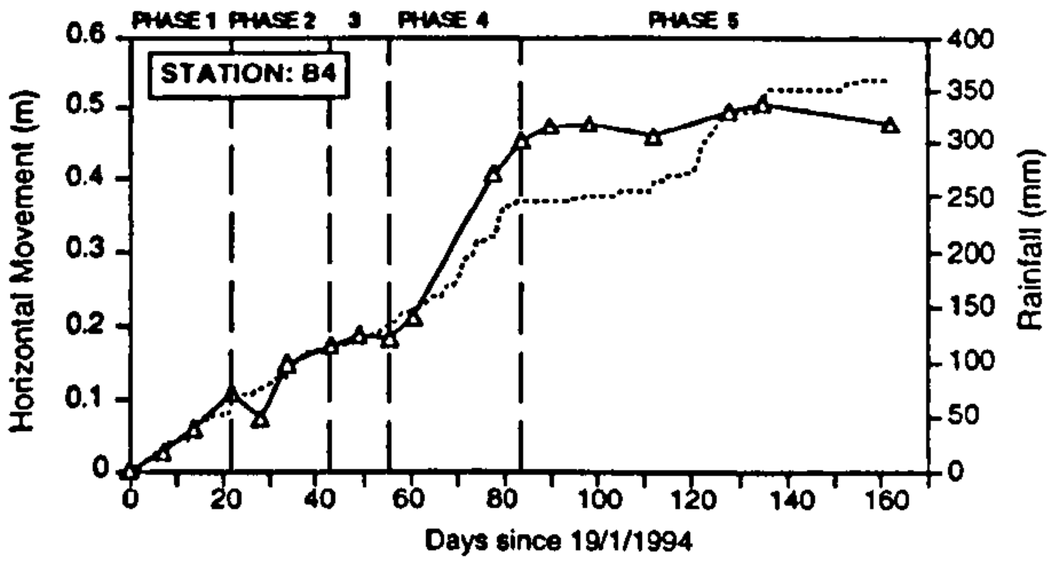

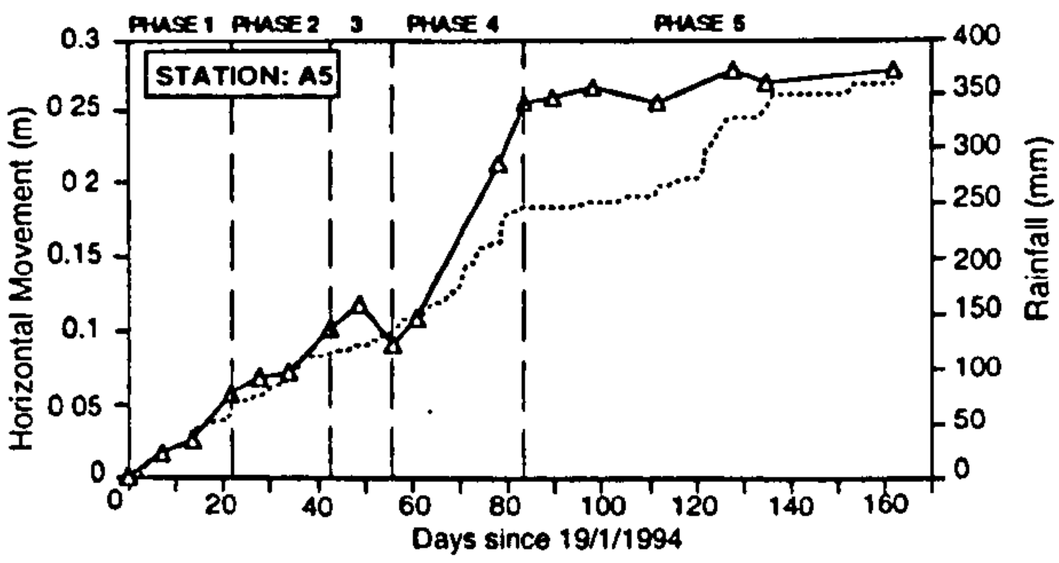

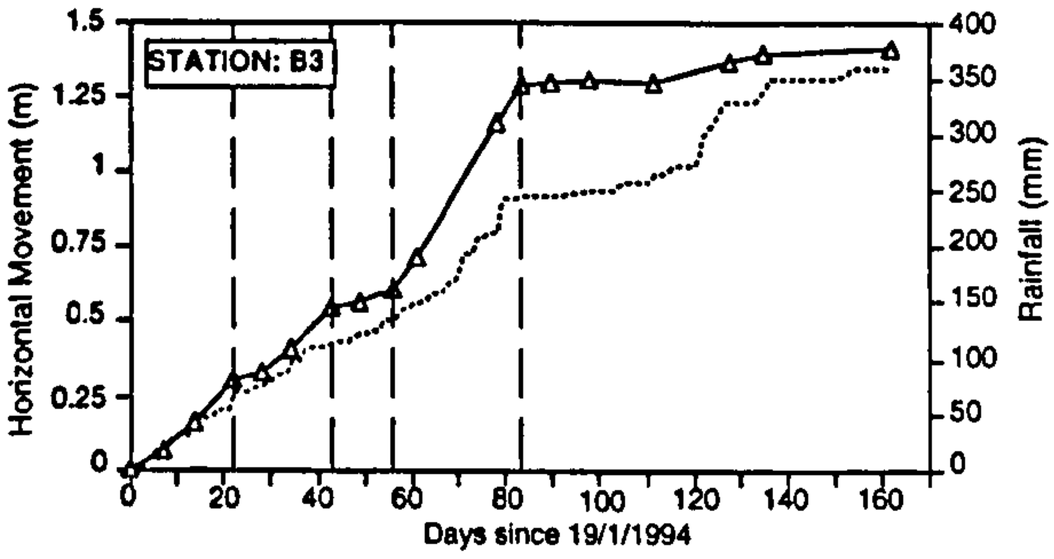

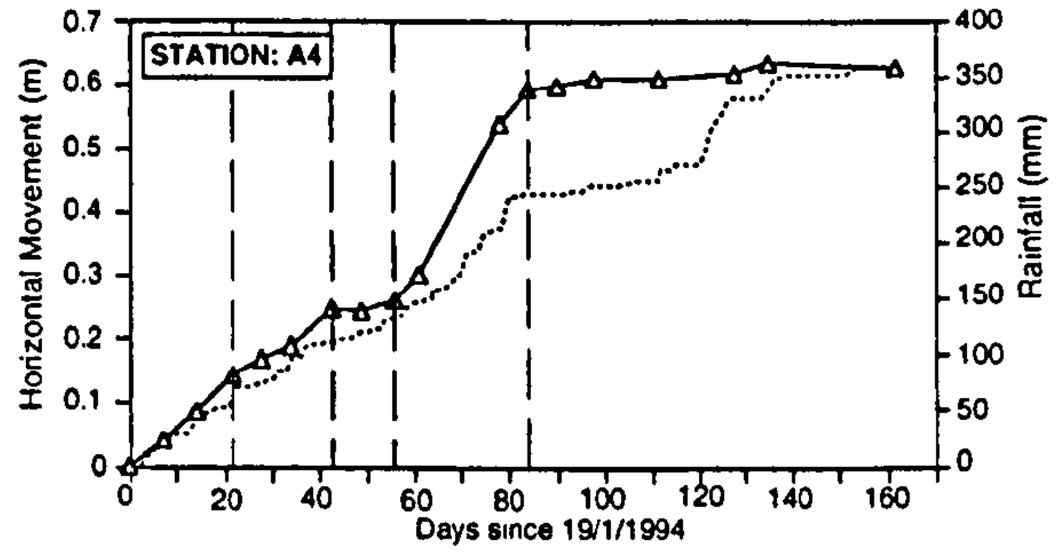

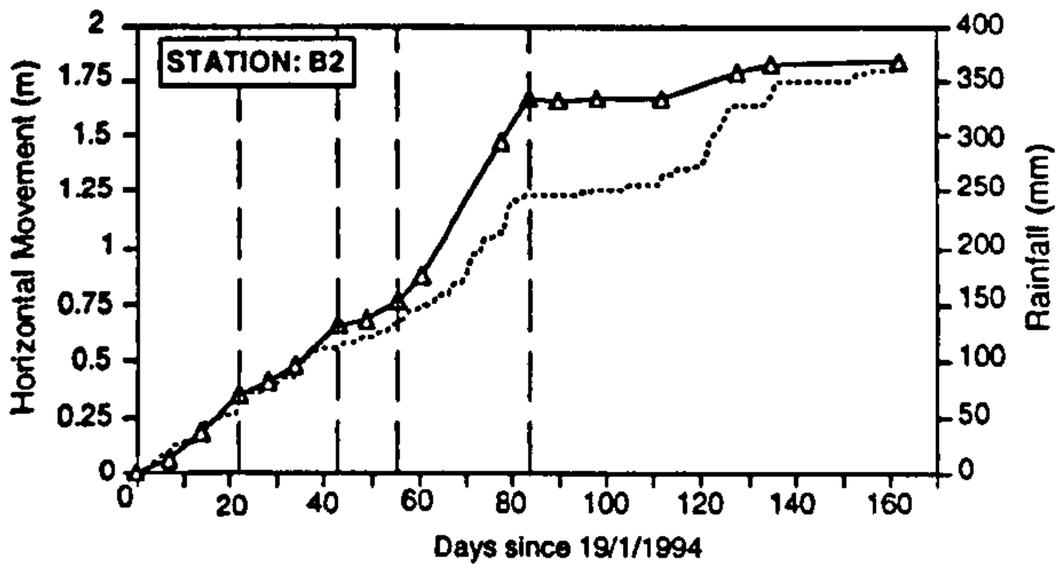

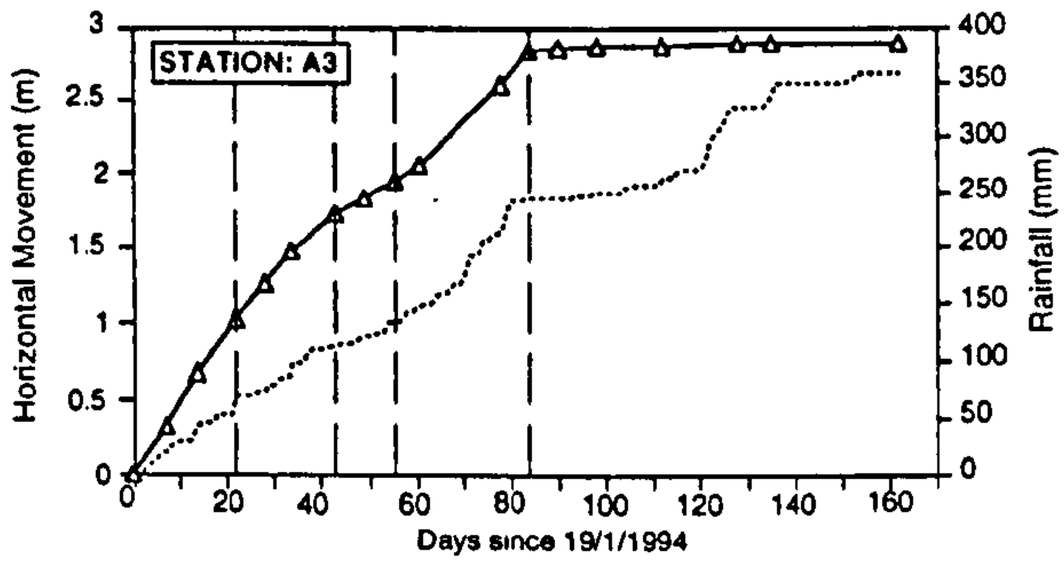

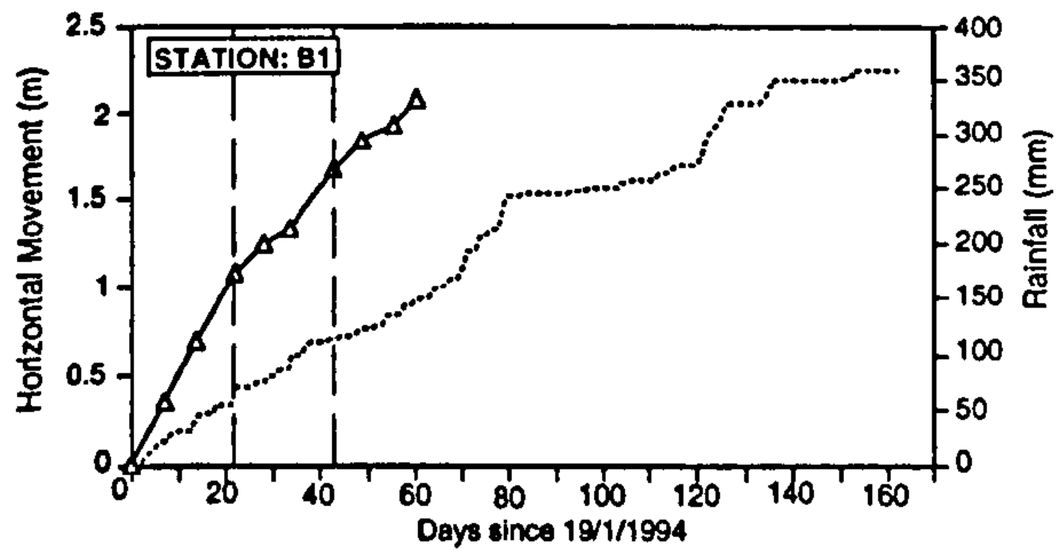

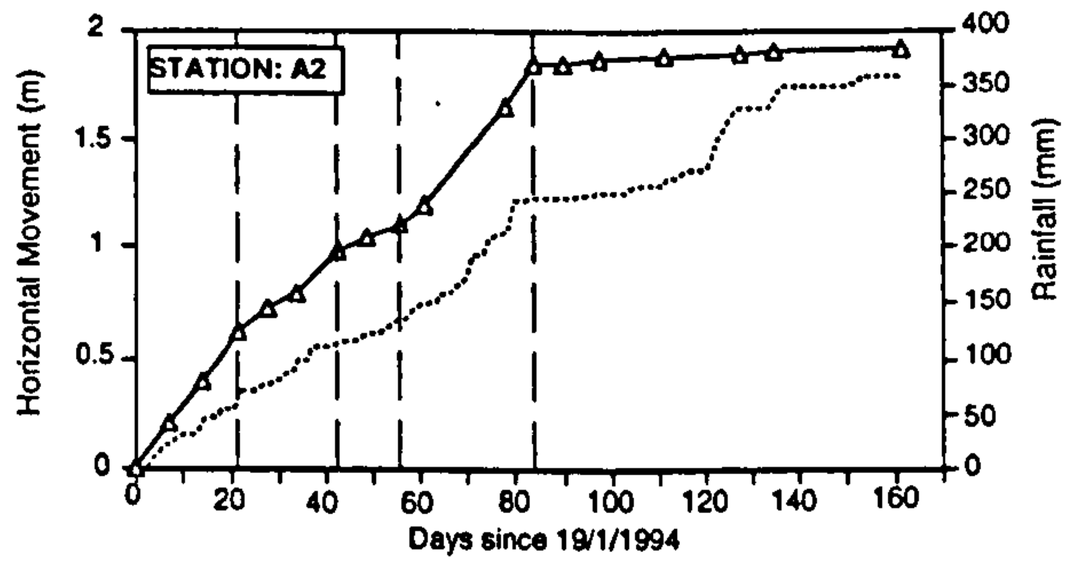

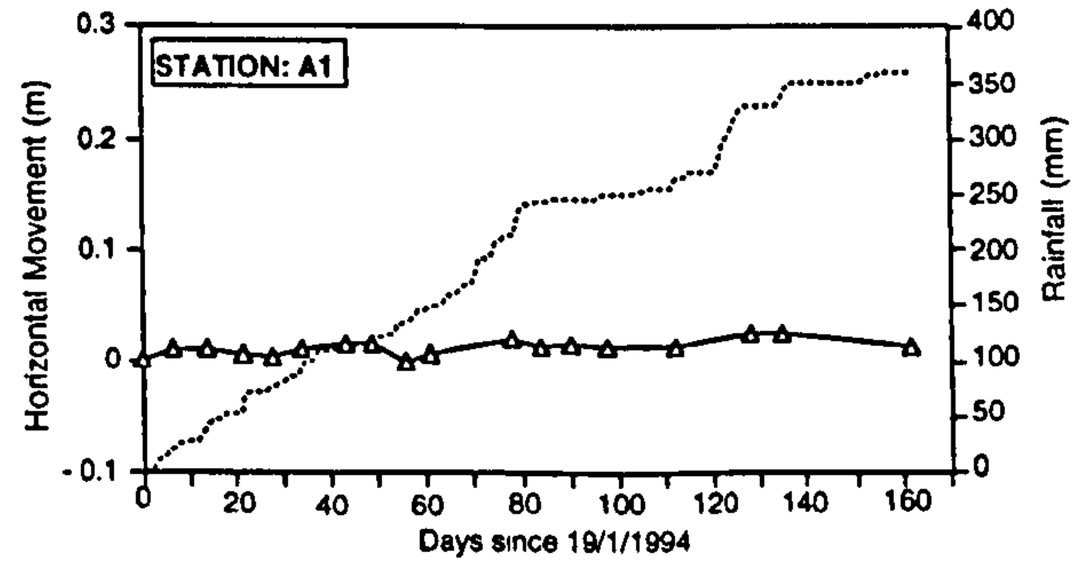

Fig. 3.15 Graphs comparing the cumulative horizontal movement of each survey station (solid line) with cumulative rainfall (dashed line), for the period of surveying (19 January 1994 to 30 June 1994). Note the variation in vertical axis scale for cumulative horizontal movement.

Phase 3 Monitoring days:44-56 (4th March-16th March)

The two profiles then increase at similar reduced gradients until the 56th day of monitoring (16th March 1994) when there is an increase in the rate of horizontal movement. This increase in the rate of slip movement appears to be related to a wetter period which commenced on 54th day of monitoring (14th March 1994). Thus, there appears to be a time lag of 3 days between the increased level of rainfall and the increased rate of slip movement. Again, the effect of the surveying interval is recognised.

Phase 4 Monitoring days:57-84 (17th March-13th April)

Cumulative rainfall and horizontal movement then continue to increase at this much higher rate until the 84th day of monitoring (13th April 1994) when the rate of slip movement drops and the slip effectively stops moving. This cessation of horizontal movement appears to be related to a drier spell of spring weather which commenced on the 81st day of monitoring (10th April 1994). Hence, from the graphs it would appear that the rate of slip movement did not decrease immediately and it is likely that there has been a lag of 4 days.

Phase 5 Monitoring days:85-End (14th April-30th June)

From the 85th day of monitoring (14th April 1994) day until the 112th day of monitoring (11th May 1994) all stations show little evidence of new horizontal movement. Cumulative rainfall levels then increase sharply on the 121st day of monitoring (20th May 1994), before levelling off on approximately the 137th day of study (5th June 1994). However, this increase is only reflected by relatively small amounts of new movement for stations A2, A3, A4, A5, B2, B3 and B4.

Within these five main phases of the horizontal component of movement, each survey station and hence the different parts of the landslide, exhibit different rates of movement and these are displayed in Table 3.3. The rates of horizontal movement for each phase have been determined by calculating the total horizontal distance moved by a particular survey station during each phase and dividing this by the phase duration. Hence, it is recognised that the rates are affected by the choice of phase subdivision.

STATION	LOCATION	PHASE 1 19/1-9/2 (10^{-7} m/s)	PHASE 2 10/2-3/3 (10^{-7} m/s)	PHASE 3 4/3-16/3 (10^{-7} m/s)	PHASE 4 17/3-13/4 (10^{-7} m/s)	PHASE 5 14/4-30/6 (10^{-7} m/s)
A1	Toe of Slide A	0.00	0.00	0.00	0.00	0.00
A2	Toe of Slide A	3.19	1.96	1.06	3.05	0.11
A3	Main Body of Slide A	5.44	3.61	1.95	3.68	0.10
A4	Main Translational Slide	0.75	0.55	0.11	1.37	0.05
A5	Main Translational Slide	0.30	0.24	-0.09*	0.68	0.03
B1	Slide B	5.64	3.16	2.18	-	-
B2	Main Translational Slide	1.80	1.62	0.94	3.78	0.24
B3	Main Translational Slide	1.59	1.25	0.58	2.81	0.19
B4	Main Translational Slide	0.56	0.34	0.10	1.11	0.04

Table 3.3. Horizontal velocity of each survey station during the five phases of movement. ***This negative velocity is likely to be due to surveying errors due to the small movement of station A5 during phase 3.**

Table 3.3 indicates that during all the phases of movement, along the line of the A survey stations, stations A2 and A3 show the greatest horizontal velocity, although the velocities shown by station A3 is greater (apart from in phase 5). Stations A4 and A5 move at significantly slower rates, compared to stations A2 and A3. In addition, station A5 moves at approximately half the rate of station A4. Along the line of the B survey stations, station B1, showed a significantly higher horizontal velocity, comparable to that of station A3. Stations B2 and B3, show comparable velocities, but these are significantly less than that for station B1. As is seen along the line of the A stations, the station at the head of the main translational slide, station B4, shows the lowest horizontal velocities. A comparison of the horizontal velocities of stations B3 and B4, with the velocities of stations A4 and A5, at similar topographic levels, indicates that the right side of the main translational slide is moving at a greater rate than the left side.

Figure 3.16 contains plots of vertical cumulative movement against cumulative precipitation for each survey station for the period of surveying. It should be noted that again the graphs have been drawn to various scales in order to emphasise the relationship between rainfall and movement. Those plots displaying relatively large amounts of vertical cumulative movement (stations A3, B1, B2 and B3) clearly display a similar relationship

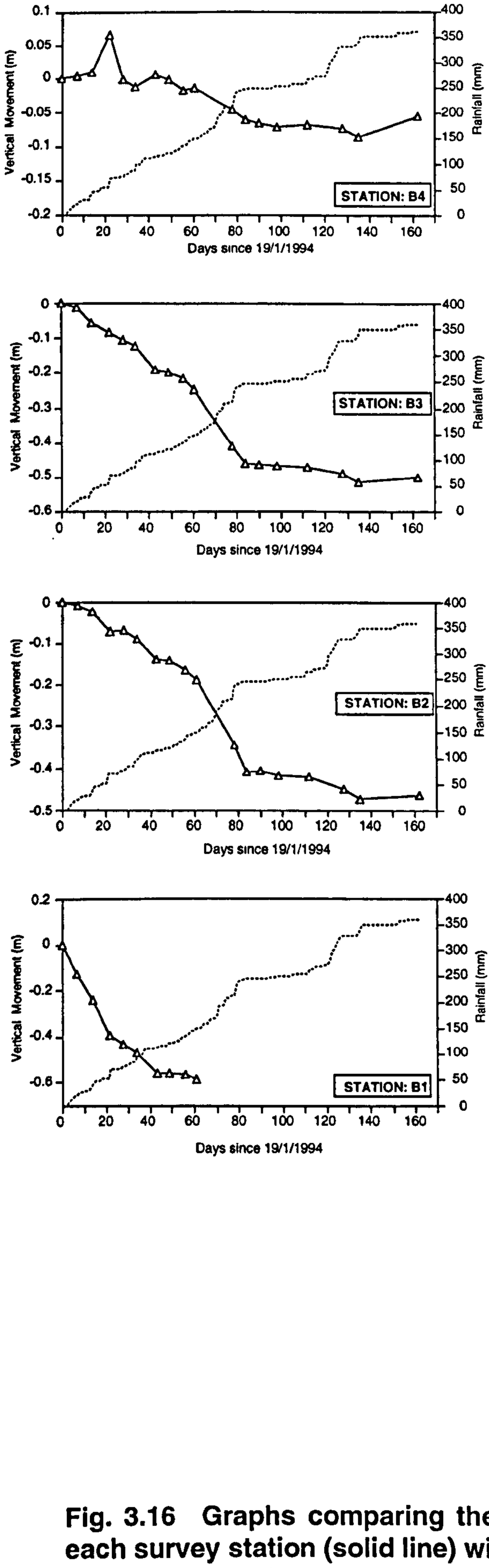

Fig. 3.16 Graphs comparing the cumulative vertical movement of each survey station (solid line) with cumulative rainfall (dashed line), for the period of surveying (19 January 1994 to 30 June 1994). Note the variation in vertical axis scale for cumulative vertical movement.

with cumulative rainfall as that for horizontal cumulative movement and the same five phases of movement can generally be identified. However, where cumulative vertical movement has beèn relatively small, the relationship is less clear (stations A2, A4, A5 and B4). Previously it was concluded that station A1 had not moved, therefore this station can be ignored. It appears that where the topographic effects of slipping has been more dramatic, the scale used shows that a definite relationship exists between cumulative rainfall and cumulative vertical movement, but where the topographic effects of slipping are small and the vertical axis has been exaggerated to an almost unrealistic extent, the relationship is less clear.

The plots in figure 3.16 again indicate that along the line of the A survey stations, the parts of Slide A containing stations A2 and A3 are most active and, along the line of the B survey stations, the parts containing stations B1, B2 and B3 are much more active than the area containing station B4. In addition, a comparison of the total vertical and horizontal distances moved by each station, indicates that, as would be expected in slopes with a gradient in the order of 1:3, the amount of vertical movement is significantly less than the horizontal movement. An attempt was made to determine the vertical velocities of the stations during each phase of movement, but due to the small amounts of displacement and the opposing effects of both upward and downward movement, the results did not provide any useful information. However, due to the significantly greater amount of horizontal movement compared to vertical movement, the horizontal velocities shown in Table 3.3 can be taken to approximate the true velocity of the various parts of the landslide and are indicative of a slow moving landslide.

3.5.2.1 Discussion

The results indicate that once the landslide at Soper's Wood is active, regardless of the amount of movement in different parts of the slip, any significant decrease or increase in the level of precipitation is reflected by the rate of movement. Not withstanding the fact that surveying was not undertaken everyday or more than once a day, from the data presented in this thesis, where there is a dramatic change in rainfall there appears to be a time lag of between 3 and 6 days between the two events. When there is an increase in rainfall levels, the lag time appears to be slightly shorter (c. 3 days). The lag following increased levels of precipitation is likely to be related to the time it takes surface water to infiltrate into the slipped mass via minor scarps, lateral shears and transverse cracks and migrate along shear

surfaces and hence increase pore pressures/reduce shear strength and enhance the rate of slip movement. In addition, the effects of seepage of ground water through the "in situ" geology cannot be ignored. Hence, the time lag is also likely to reflect the time it takes for surface waters to percolate down through the strata and along the sub-horizontal limestone bands within the Fuller's Earth, resulting in increased pore water pressures within the landslide where limestone bands are present. When there is a decrease in the amount of rainfall there appears to be a longer time lag (c. 4-6 days). The lag on a decrease in rainfall levels reflects the time it takes for pore pressures to reduce along shear planes within the slip.

Figure 3.15 shows that the majority of slip movement had been completed by the 13th April 1994 (84th day of monitoring) coincident with a prolonged period of very little rainfall from the 10th April 1994 (81st day of monitoring) until 20th May 1994 (121st day of monitoring). During this period it is likely that, due to increasing insolation at this time of year, evaporation would be more pronounced resulting in a condition of soil moisture deficit. As a consequence there would have been an increase in effective stress. Thus, although renewed rainfall was recorded after the 20th May 1994, little further movement was recorded for most of the survey stations. However, if this increased rainfall had precipitated in the main wet period during movement phases 1 to 4, a substantial increase in movement would be expected. It thus appears that, in a drier period, once the landslide has stopped moving for a prolonged period (phase 5), the landslide becomes insensitive to precipitation levels. Thus, it requires a substantial and prolonged period of rainfall for sustained movement to be restarted. Whereas if the landslide is already moving (phases 1 to 4), the landslide movement rate is very sensitive to precipitation levels. This may be related to a seasonal effect and indirectly, vegetation may play an important role in controlling slip movement.

During the late spring (April/May) vegetation growth increases, particularly on the slipped ground, due to the greater amount of water in this disturbed zone. During the late spring and summer, the increased grass cover over the slipped area will collect rainwater, which will tend to evaporate with the warmer weather, reducing the amount of water available for infiltration compared to the winter period. This effect may be partially balanced by the presence of desiccation cracks which will provide additional avenues for surface water infiltration. In addition, much of the rainfall that infiltrates into the ground will be be taken up by roots and hence moisture penetration will be retarded and possibly halted. Hence, an

equivalent amount of recorded rainfall during the summer and winter will have very different effects. In the winter, due to a relative lack of vegetation cover, most of the recorded rainfall will penetrate into the slipped mass and thus slip movement will be sensitive to recorded rainfall. Whereas in the summer, little of the recorded normal summer rainfall will penetrate into the slipped mass and thus there is a reduced effect, with slip movement appearing to be insensitive to recorded rainfall.

The demand for moisture by the grass roots during the summer months, together with the effects of evaporation, will result in capillary rise further reducing effective pore pressure, increasing effective stress and hence the shear strength of the soil. Indeed, this will be enhanced further by the growth of roots seeking moisture such that the root system will aid the apparent shear strength of the soil mass. Greenway (1987) amongst others, has highlighted the effects of vegetation on slope stability, notably on shrub and tree covered slopes.

3.5.3 Piezometric Information

Standpipes were placed in boreholes B to G and a seventh standpipe, A, emplaced near the right lateral shear at a similar level to standpipe B. For standpipe locations see Figure 3.7. At frequent intervals between the 19th January 1994 and the 3rd August 1994, the ground water level was ascertained (for data see Appendix III). The results for all the standpipes are compared with cumulative rainfall for the period in Figure 3.17. As some of the standpipes were dry at certain periods, dashed lines have been inserted to demonstrate the likely level of the water table during this period.

Considering each of the standpipes in turn:

<u>Standpipe E</u>

Standpipe E was installed in the toe at the bottom of the slope on the 22nd January 1994 to a depth of 2.6 m and after four days a ground water depth of 0.73 m was recorded. Standpipe E is located in a now redundant toe and past movement will have increased the secondary permeability of the clay due to its more open and possibly fractured structure and hence the initial response was fairly rapid. The standpipe shows an almost ideal summer/winter relationship with fluctuations in the ground water level appearing to be caused by rainfall levels.

<u>Standpipe D</u>

Standpipe D was installed on the 4th February 1994 to a depth of 2.8 m, but snapped at an approximate depth of 0.9 m before the first

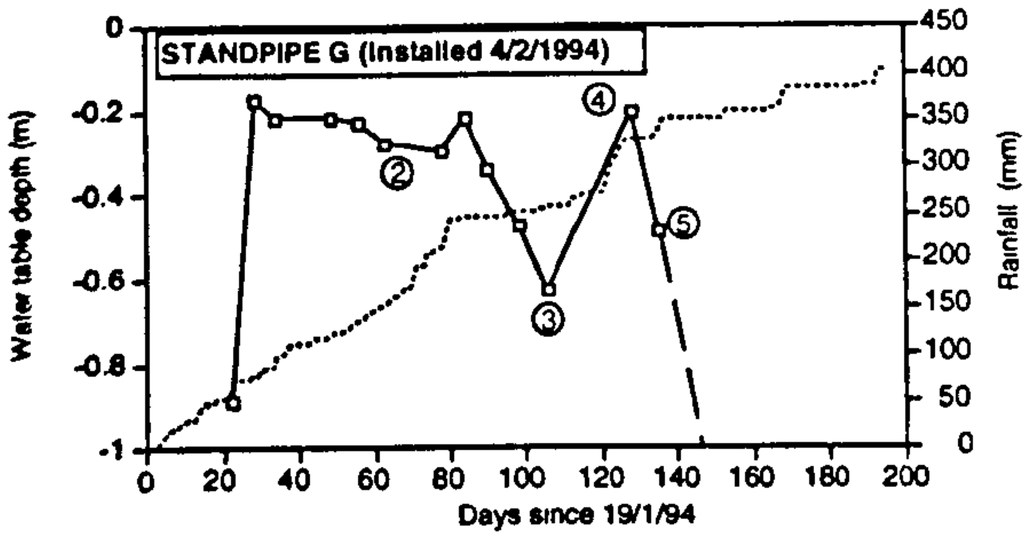

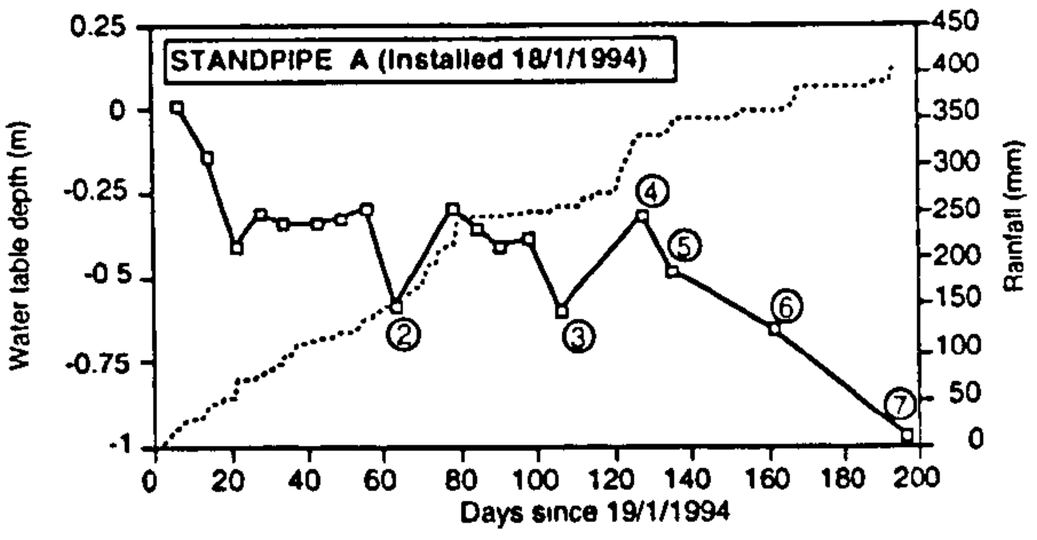

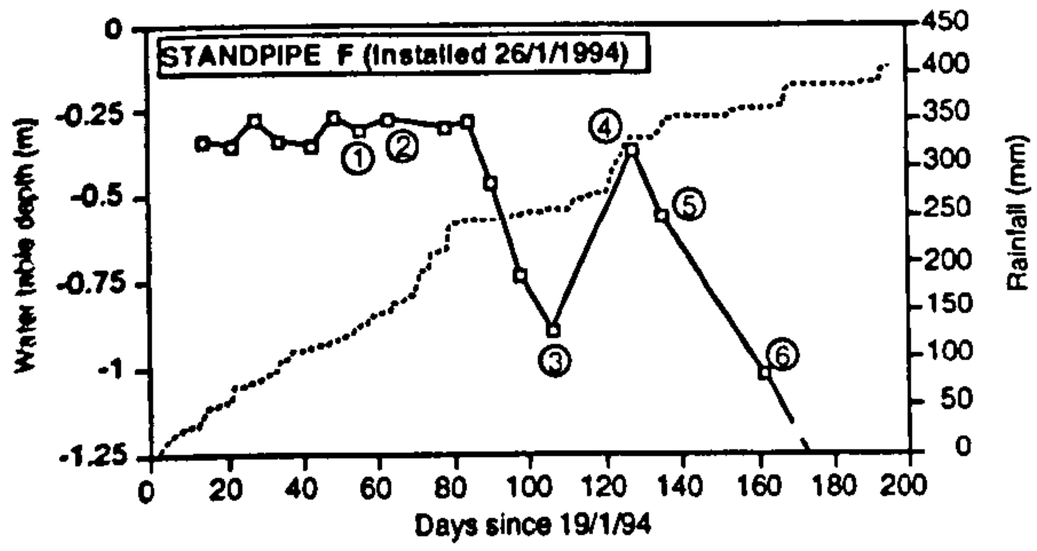

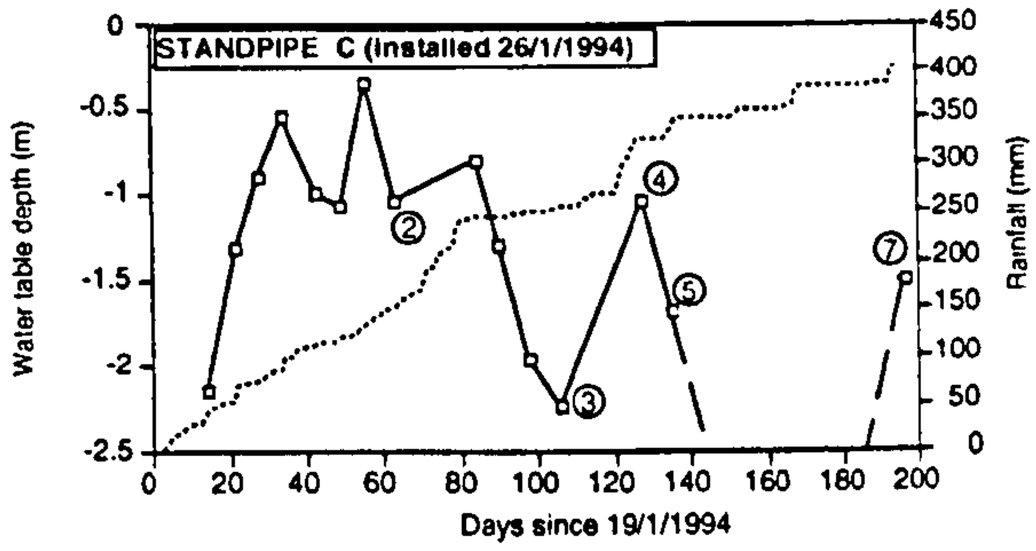

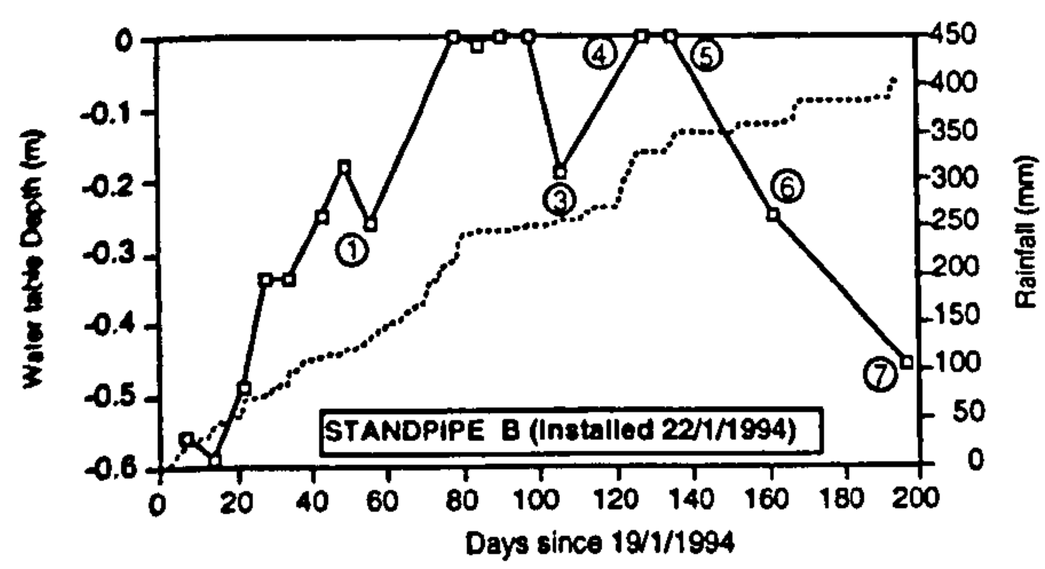

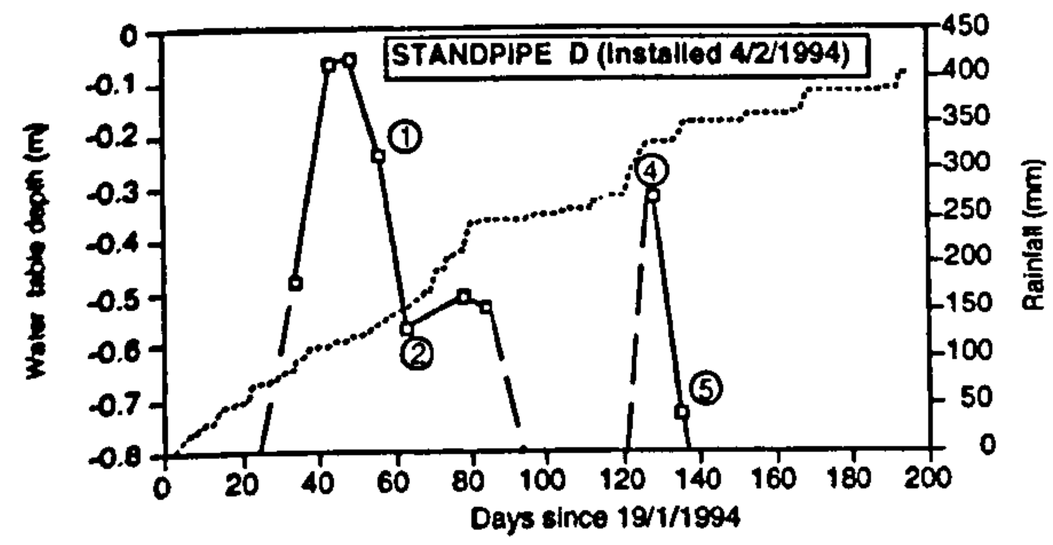

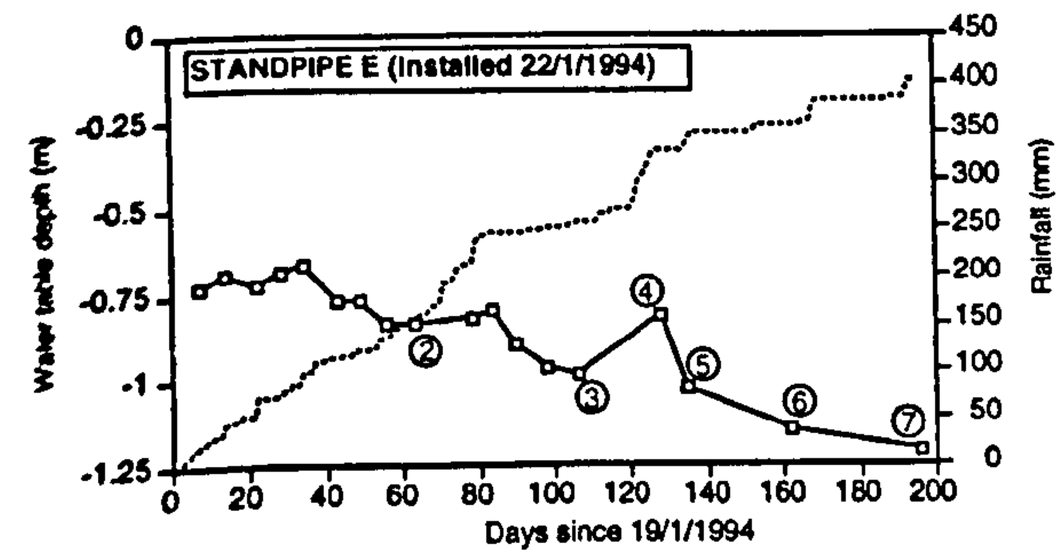

Notes:
The draining of the standpipes prior to extraction of ground water samples may have affected some of the readings and these are highlighted by the numbered circles which refer to the points discussed below.

1. (Date: 16/3/94) Standpipes B, D and F were drained on the 11/3/94. This may account for the decrease in the measured ground water level in these standpipes, however this lower ground water level also coinicides with a period of less rainfall.

2. (Date: 23/3/94) All the standpipes were drained after measurements were taken on the 16/3/94, prior to ground water sampling on the 23/3/94. This is likely to account for the reduced ground water levels measured in the standpipes. In addition, due to the failure of the electronic dipper normally used, a larger diameter dipper was used which would not fit through the spliced section of the additional plastic pipe attached to standpipe B. Hence, no reading was recorded for standpipe B.

3. (Date: 5/5/94). Ground water samples were obtained from the standpipes on the 27/4/94 and this may have enhanced the minima in the measured ground water level. However, this minima also coinicides with a period of little rainfall.

4. (Date: 27/5/94). All the standpipes were drained on the 7/5/94 for ground water sampling on the 11/5/94. However, the majority of standpipes were found to still be dry on the 11/5/94 due to the preceding period of little rainfall and hence no measurements were recorded. Thus, the readings which were made on the 27/5/94 could be affected by the draining of the standpipes on the 7/5/94. However, due to the recent rainfall, the shallow nature of the water level recorded and the long time interval, this is considered unlikely.

5. (Date: 3/6/94). The recorded decrease in the height of the ground water level may be enhanced by the sampling of the ground waters in the standpipes on the 27/5/95.

6. (Date: 30/6/94). All standpipes were drained at the end of measurements on the 3/6/94, prior to ground water sampling on the 30/6/94. This may influence the ground water level recorded on the 30/6/94, although due to the long time interval this is considered unlikely.

7. (Date: 3/8/94). Ground water samples were taken from all standpipes on the 30/6/94, after which the standpipes were drained. However, due to the long time interval, this is considered unlikely to affect the results.

Fig. 3.17 Graphs comparing ground water level (solid line) with cumulative rainfall (dashed line) for each standpipe over the period of monitoring (19 January 1994 to 3 August 1994). Note the variation in vertical axis scale for water table depth.

reading. The initial response of the standpipe was slow and on the 18th day after installation, a ground water depth of 0.48 m was recorded. The piezometric profile shows large fluctuations, which can be broadly correlated with rainfall. This is probably due to the location of D on the active toe of the slip, approximately 1 m above the general level of the hillside, where the ground is likely to be very dilated and fractured due to earlier movement. Hence, Figure 3.17 indicates that the ground water dissipates very quickly from the toe during periods of lower rainfall. Initially the piezometric surface rose to almost ground level, but then dropped almost 0.5 m, most likely due to lower precipitation rates, however slip movement still continued. Thus, the continued movement of the toe may not be directly related to high pore pressures but to the toe being pushed by the unstable ground upslope of this standpipe.

Standpipe B

Standpipe B was installed in the centre of the slip on the 22nd January 1994 to a depth of 2.65 m and after just four days a ground water depth of 0.56 m was recorded. The standpipe snapped at approximately 0.6 m between the 1st and 2nd readings (26th January 1994 and 2nd February 1994). The water table is shallow, even reaching ground level during the middle of the study. In addition, the piezometric surface displays a very broad response to rainfall. It should be noted that the three readings taken after the 78th day of monitoring (7th April 1994), which show the water table at ground level, were probably influenced by the presence of a puddle around standpipe B during this period. Slip movement had caused a depression to form which was filled by surface run off. The puddle was successfully drained on the 90th day (19th April 1994) and it did not refill. After early June 1994, with a decrease in rainfall and an increase in evaporation, as anticipated, the ground water level dropped and was continuing to drop when the study ceased.

Standpipe F

Standpipe F, located in the upper part of the slip, was installed to a depth of 3.20 m on the 26th January 1994 but snapped before the first reading at a depth of approximately 2.6 m. Later in the study, between the 23rd March 1994 and 7th April 1994, standpipe F appeared to have snapped at a shallower depth of about 1.4 m. After seven days a ground water depth of 0.34 m was recorded. The water table stayed at a shallow depth, remaining steady during a period of constant rainfall. When the rainfall profile changes dramatically on the 81st day of monitoring (10th April 1994) there is a corresponding drop in the elevation of the

ground water table. With increased rainfall after the 121st day of monitoring (20th May 1994), ground water level responds temporarily, after which, with a decrease in rainfall and the onset of summer, with both associated evaporation and plant growth, the ground water level dropped.

Standpipe G

Standpipe G was installed on the 4th February 1994 to a depth of 2.20 m and after six days a ground water depth of 0.89 m was recorded. Initially standpipe G did not snap, but between the 7th and 13th April 1994, it snapped at a depth of about 0.9 m. The water table is again shallow and shows a very good response to rainfall, of a similar nature to that shown by standpipe F.

Standpipe A

Standpipe A was installed at the inner edge of Slide A, close to the lateral shear, on the 18th January 1994 to a depth of 2.5 m, but snapped at a depth of approximately 1.2 m before the first reading. After eight days the water level in the standpipe was found to be at ground surface. The water table over the period was shallow, only dropping to a depth of 0.97 m at the end of the study, and shows an approximate response to rainfall. Although initially the ground water level was equivalent to ground surface elevation, within a further eight days, being so close to the side scar, the ground water level showed a general decrease with time as water was able to escape from the lateral extremities of the slip.

Standpipe C

Standpipe C, located outside the landslip, was installed on the 26th January 1994 to a depth of 3.00 m. Even after 7 days the depth of water was still at 2.15 m, indicating a relatively slow response for this standpipe located away from the currently active landslip. The ground water level is deeper than in standpipe B, located at approximately the same topographic level, and there is also a high degree of fluctuation in the profile. During the period of February and March 1994, the rainfall is relatively consistent but fluctuations of about 0.6 m in the ground water level occur. This may in part reflect the effects of ground water sampling. After the 81st day of monitoring (10th April 1994), when there is less rainfall, the ground water level dropped until the later period of rainfall towards the end of May, when the piezometric surface showed an increase of almost 1 m after which it continued to decline. The levels shown between the 140th and 196th day of monitoring are not considered reliable, particularly the final reading. Unfortunately this was not plotted up quickly enough for a further visit to be made to check this value.

3.5.3.1 Discussion

From the readings it is clear that the water table within the visibly slipped ground is considerably shallower than outside the slip, probably due to selective recharge in the disturbed zone. In addition, all the standpipes within the slip had a faster initial response compared to standpipe C, this is most likely due to the increased disturbance and dilation of the soils within the slipped mass caused by the presence of transverse cracks, lateral shears and minor scarps. This increased permeability also enables the ground water level to respond to changes in rainfall, clearly displayed in standpipes F and G and to a lesser extent in standpipes B,D and E. The increased permeability may have also been exasperated by selective percolation along shear surfaces.

The study has highlighted the importance of standpipe location within a landslip, as there is variation in the ground water level between different locations. For example, standpipe D, located in the active toe of the slip, shows very large fluctuations in the ground water level; the presence of radial cracks and the dilated nature of the soil, is likely to allow the rapid dissipation of ground water. In contrast, standpipes G and F, located in the main body of the slip, show less extreme responses and probably more accurately represent the general ground water level in the main body of the slip, for use in slope stability analyses. In addition, if it could have been anticipated where the major movement was going to take place, standpipe B would have been positioned differently, as ground movement caused the ponding of water in a topographic hollow. This would have reduced the reliability of the actual ground water level measured, as the pool of water may have caused localised seepage into the ground.

3.5.4 Comparison of Slip Movement with Ground Water Level

In Figure 3.18 cumulative horizontal movement of survey stations A2, A3, A4 and A5 is compared to the variation in the ground water level in the standpipe nearest to that station. Locations and approximate distances can be scaled from Figure 3.7.

Horizontal movement of station A2 is compared with the level of the ground water table in standpipe D and movement can be very broadly correlated to the ground water level in standpipe D. However, after the initial rise in ground water level to almost ground surface, the water table drops rapidly, but slip movement continues. This may well be an example

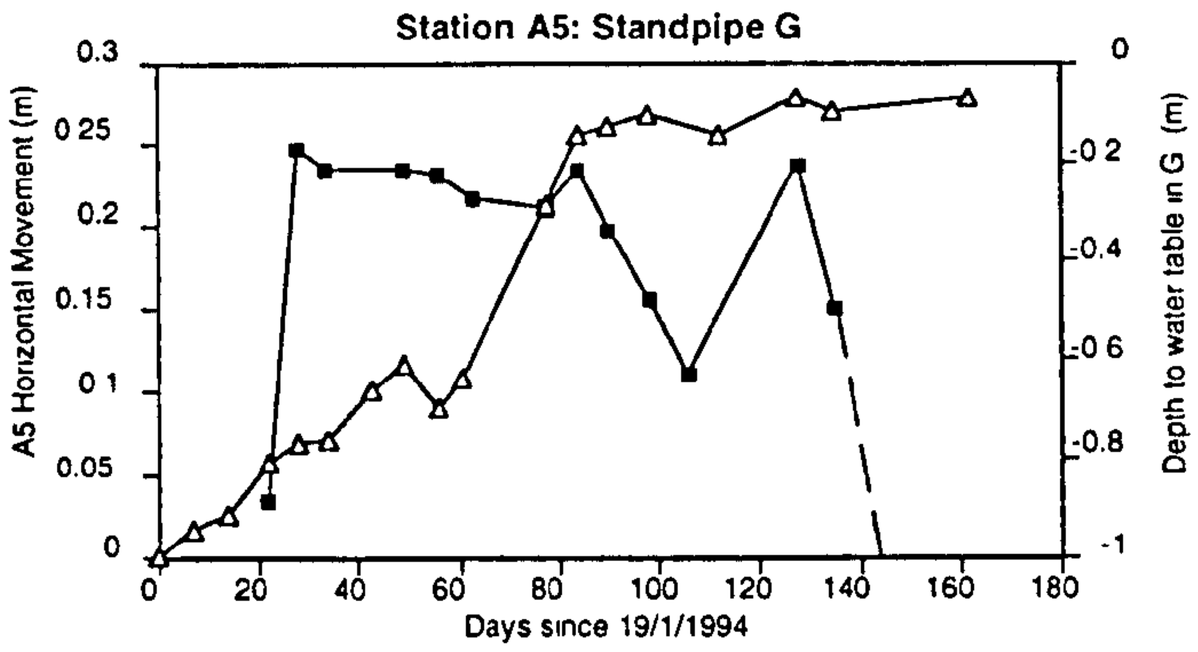

Fig. 3.18 Graphs comparing cumulative horizontal movement for survey stations A2, A3, A4 and A5 (triangle symbols) with ground water level in adjacent standpipes (square symbols) over the period of monitoring (19 January 1994 to 3 August 1994).

of undrained upslope loading, similar to that described by Hutchinson & Bhandari (1971), where movement of the upslope area "pushes" the lower area.

Horizontal movement of Station A3 is compared with the ground water level in standpipe B, and up to the 78th day of monitoring (7th April 1994), an increase in height of the water table corresponds with continued movement, probably due to the increasing pore water pressures along the shear surfaces within the slip. However, due to the problem of ponding, the pattern is less obvious later in the study, but with clear evidence that the ground water level drops towards the end of the study, it is not surprising that the slip has stabilised.

Horizontal movement of Station A4 shows a clear relationship with the ground water level in standpipe F. Up to the 84th day of monitoring (13th April 1994), when the majority of movement occurs, the water table is shallow at approximately 0.3 m below ground level. During this period pore water pressures are high inducing instability. The ground water level then rapidly drops and the slip becomes inactive for a prolonged period, presumably the pore water pressures have fallen below a certain critical value for these particular ground conditions. However, from the 105th day of monitoring (5th May 1994) the plot indicates that there is an increase in the height of the water table to 0.37 m on the 128th day (27th May 1994) and the station shows evidence of very small amounts of movement. The prolonged period of inactivity may have caused the slip to stabilise, however the rapid decrease in the depth to the water table, probably caused pore pressures to temporarily increase and some movement to occur. The water table quickly drops again with the onset of summer and so no renewed movement was sustained.

A comparison of the horizontal movement of station A5 with the ground water level in standpipe G shows a similar relationship to that of station A4 and standpipe F.

3.5.5 General Discussion

This study has shown that once the landslide is moving, movement is sensitive to rainfall and ground water levels and there is a general relationship between rainfall, ground water levels and slip movement, although a lag of some 3 to 6 days is frequently noted. This relationship is particularly clear in the body of the main translational landslide. At the active toe of slide A, undrained loading caused by movement of the main body of the slide is thought to occur.

It appears that in addition to general infiltration, rainfall selectively penetrates into the soil along disturbance zones such as transverse cracks, lateral shears and minor scarps, raising the ground water level, which in turn increases pore pressures and reduces effective stress, encouraging slip movement. This effect will be enhanced by the presence of limestone bands within the Fuller's Earth, along which ground water will preferentially percolate. It is likely that the percolation rate controls the length of delay involved between rainfall and an increase in pore water pressure. With a termination of rainfall, the ground water level drops, resulting in a decrease in pore pressures, with a corresponding increase in effective stress, and the slip stops moving. Again there is a time delay between a reduction in rainfall and the dissipation of pore pressures.

However, this investigation has shown that once the slip has temporarily stabilised for a period of time during a drier period (eg. summer months), increased rainfall, which would have caused a significant increase in the rate of movement of the previously active slide during the wet period (winter months), causes only relatively small amounts of movement which is short lived. This is likely to be due to a combination of the following factors:

(1) During the period of stability, the ground water level has dropped, increasing effective stress and hence the residual shear strength of the landslide.

(2) With the onset of summer, vegetation levels on the slip have increased such that all the recorded rainfall does not infiltrate into the slipped mass but much is lost due to evaporation. Hence, less water is available to increase the height of the water table and promote movement. In addition, if the increase in rainfall is not sustained, the presence of vegetation means that roots will take up moisture, which together with general evaporation, prevents the increase in ground water level from being sustained. Clearly this applies to "normal" levels of summer rainfall and not necessarily to very exceptional levels of summer rainfall, such as that experienced in July 1968 (Hawkins 1973).

3.5.6 Comparison of Geomorphological Maps at the Start and End of Movement

The initial geomorphological map was produced in January 1994 at the start of monitoring. A second geomorphological map was made in May 1994 when it appeared that the main wet season movement had ceased. Figure 3.19 compares the geomorphology of the slip in January 1994 (in black) and May 1994 (in red).

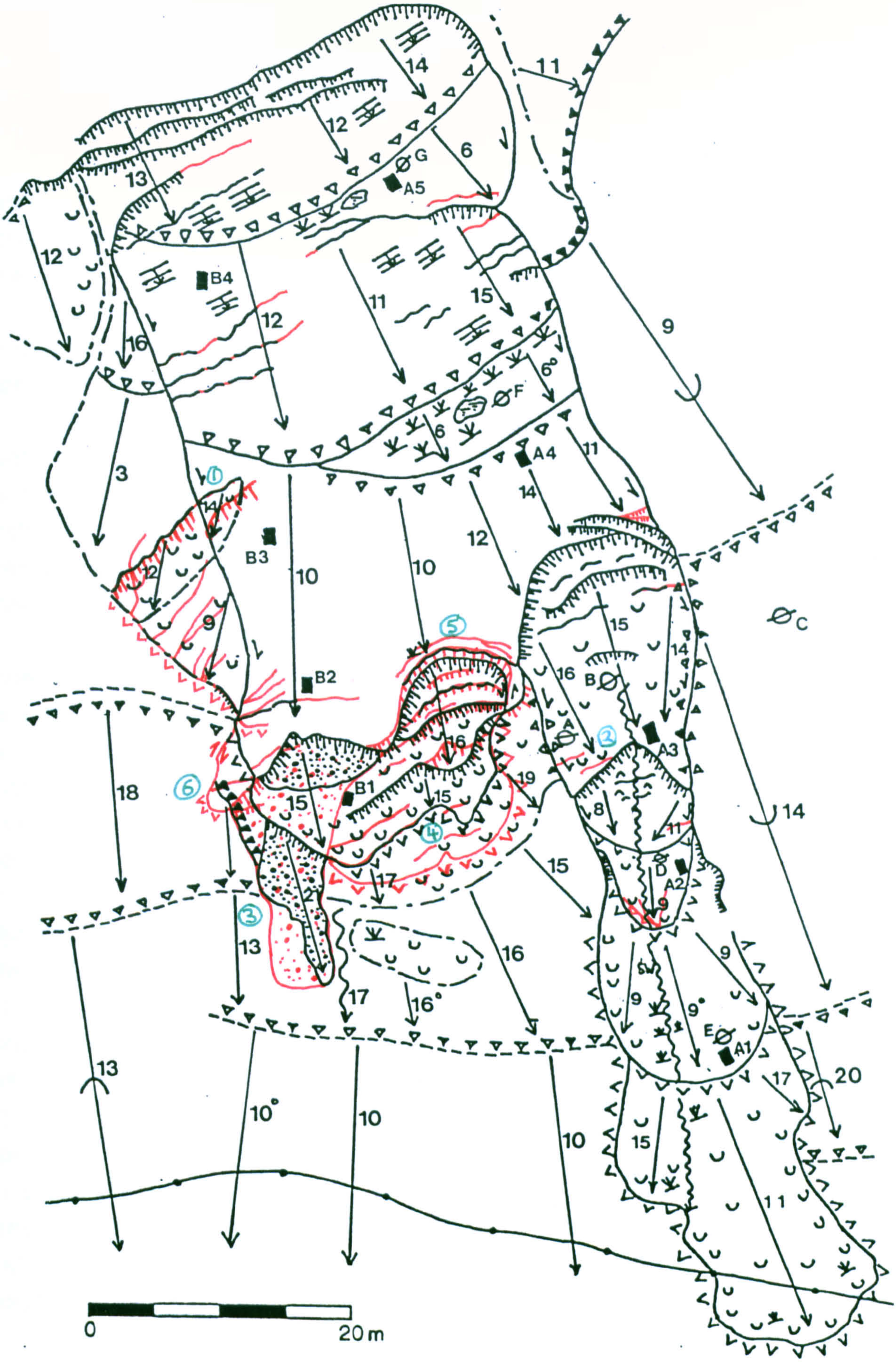

Fig. 3.19 Comparison of landslide geomorphology in January 1994 (in black) and May 1994 (in red).

The main morphological differences are highlighted below (the particular points can be seen on the map in Figure 3.19 by referring to the numbers in the green circles):

(1) In the main translational landslide a number of new transverse cracks have appeared with some pre-existing cracks being extended. In addition, some of the transverse cracks adjacent to the lateral shears, have developed into minor scarps.

(2) Slide A has shown little change in gross morphology, although a number of new transverse cracks are evident and radial cracks have appeared in the toe containing survey station A2.

(3) The morphology of Slide B has changed considerably. The two mudflows existing in January 1994 have combined to form one large mudflow. The clay in the main body of the landslide, between the two existing mudflows, became so saturated with water that it lost all its internal strength and flowed down slope. This occurred between the 21st March 1994 and the 7th April 1994. (See Plates 3.10, 3.11 and 3.12).

(4) The toe of Slide B, adjacent to the mudflow, has extended down-slope with the addition of a number of transverse cracks within the foot of the slide.

(5) A new scarp has appeared in place of an existing crescentic crack, evident in January 1994, in the crown behind the northern arcuate scarp of Slide B. In addition, a new crescentic crack has appeared behind the latest scarp.

(6) The lateral shear on the right flank of the main translational slide, adjacent to the head of the mudflow, has extended with the formation of a new toe.

(7) The ground within the landslides in January 1994 was soft and boggy, whereas in May 1994 the surface was considerably harder and desiccation cracks were evident.

(8) The remapping has highlighted the difference between the mode of movement in the mudflow and landslide. In the mudflow, movement occurs on a grain by grain basis, due to the highly saturated nature of the soil, hence the changing geomorphology. Whereas in the landslide, units of material move along discrete basal shear surfaces and the gross morphology remains relatively constant.

In addition, from the mapping together with continual observation over the period of movement, two patterns of movement were observed:

Plate 3.10 View upslope of the lower mudflow in January 1994.

Plate 3.11 View upslope of the lower mudflow in February 1994.

Plate 3.12 View across slope of the toe of the large combined mudflow in April 1994.

Plate 3.13 View of the right edge of the main translational landslide showing a propagating transverse crack extending off from the lateral shear towards the centre of the landslide.

(A) Transverse Crack Propagation. (See Figure 3.20).

(1) Due to the irregular outline of the lateral shear and the current general gradient, the hill mass moves obliquely against part of the lateral shear. See point (1) in green on Figure 3.19.

(2) This oblique movement causes a transverse crack to form, extending off from the lateral shear towards the middle of the slipped mass.

(3) Continued movement of the slip causes the crack to propagate towards the centre of the main body of the slide and widen, with some dip slip movement occurring due to the shearing motion. See plate 3.13.

(B) Retrogressive Scarp Migration (See Figure 3.21).

(1) Due to the depth of the main scarp, the ground in the crown upslope of the main scarp was unable to fully support it and a crescentic crack appeared. See point (5) in green on Figure 3.19.

(2) Continued movement caused the crescentic crack to grow and eventually the crown gave way to form a new scarp behind the pre-existing main scarp.

(3) Due to the depth of the newly formed main scarp, a new crescentic crack forms in the crown. With continued time and slip movement this can be expected to collapse to form a third scarp behind the pre-existing two. In this way the main scarp migrates up-slope.

It is clear from this observation that at Soper's Wood not only does the landslide increase in length by the slipped mass moving down slope but also by the main scarp migrating up-slope. Plate 3.14 shows retrogressive scarp migration at Soper's Wood.

3.6 Longitudinal Slope Profile

An accurate longitudinal section of the landslide along the axis of Slide A was developed in March 1994 (see Figure 3.22). Along the length of the slip, twenty-nine datums were surveyed with the geodimeter to provide a detailed surface topography. In addition, the standpipes within the slip were also surveyed. The surface topography data were then plotted and the actual profile drawn in from field knowledge together with the details recorded on the geomorphological map made in January 1994. The positions of the standpipes and survey stations are indicated.

Standpipe F snapped at a depth of 2.6 m and, as its location is in the centre of the slip mass, the most likely explanation was that it was snapped by movement along a shear surface, probably the basal shear surface. Later on in the study, standpipe F snapped at a shallower depth of about

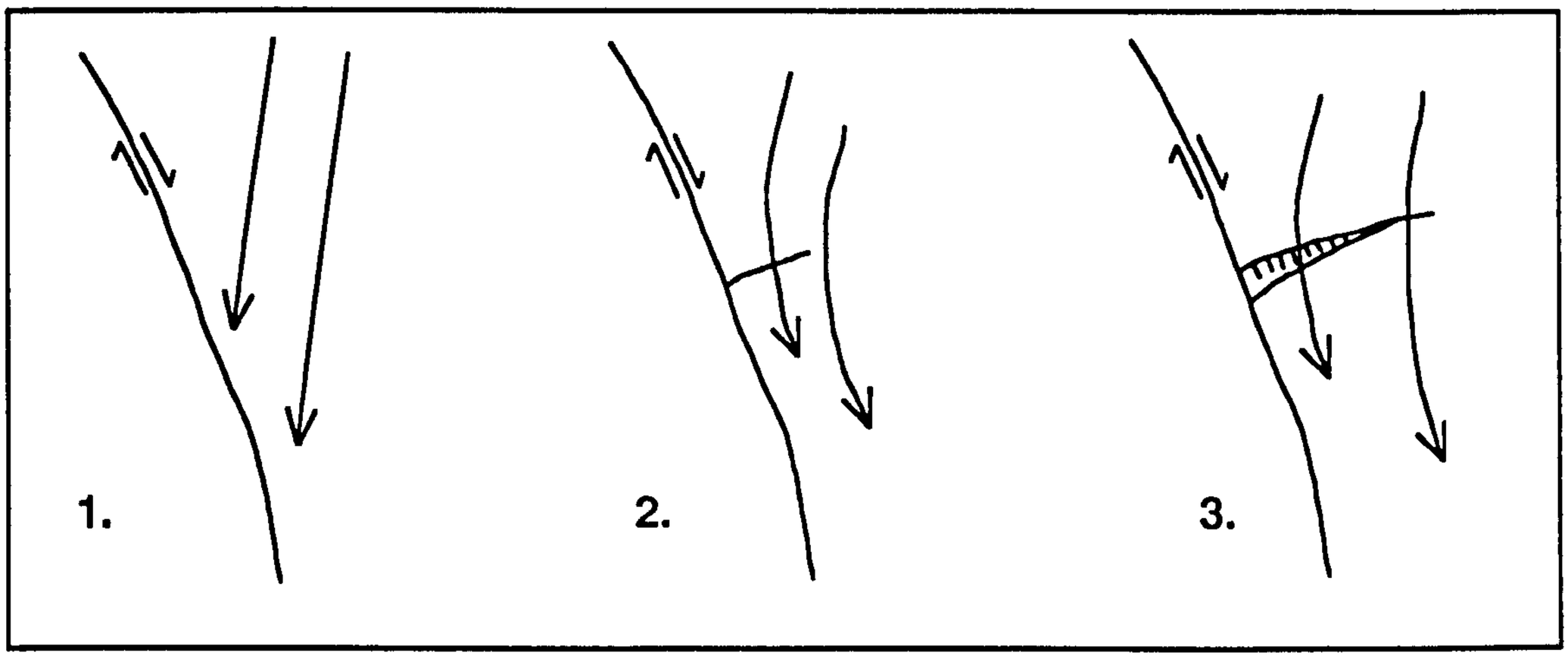

Fig. 3.20 Transverse crack propagation in the landslide at Soper's Wood.

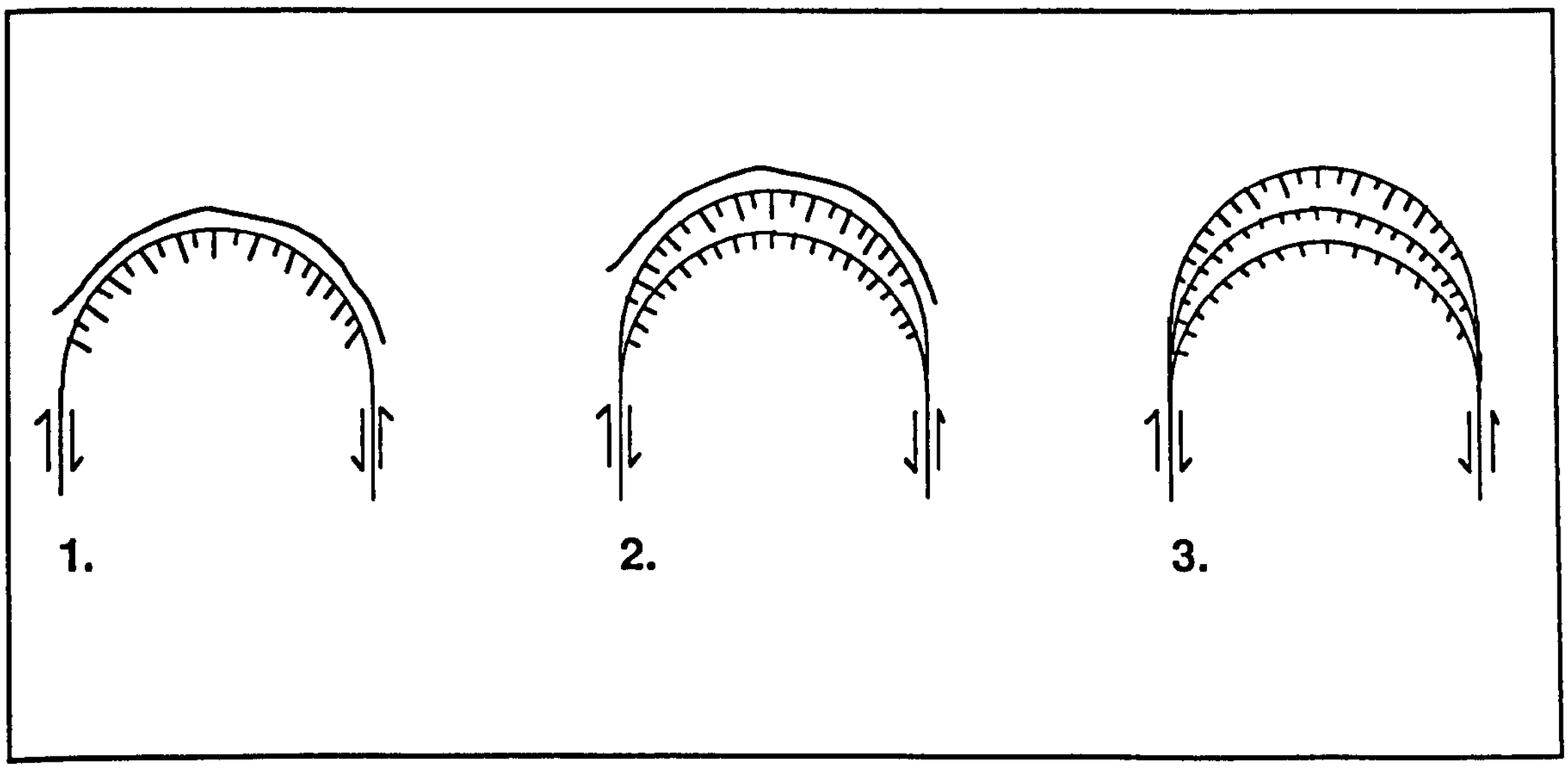

Fig. 3.21 Retrogressive scarp migration in the landslide at Soper's Wood.

Plate 3.14 Photograph of retrogressive scarp migration seen in the landslide adjacent to Soper's Wood.

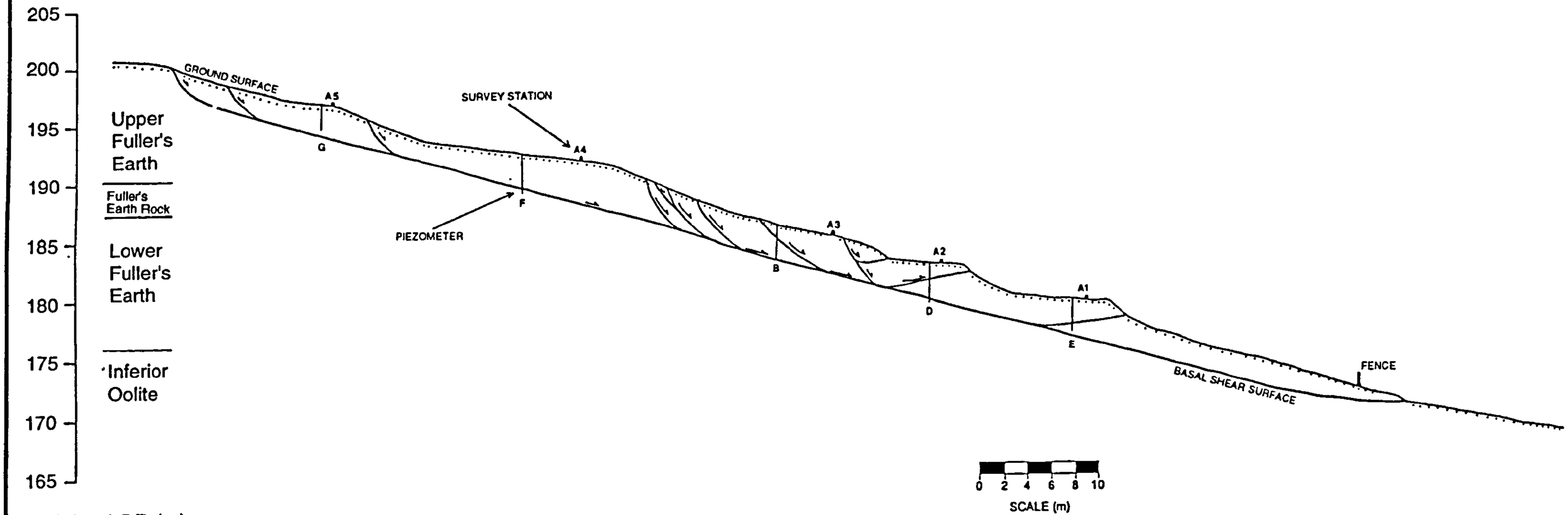

Fig. 3.22 Longitudinal section through the landslide at Soper's Wood, March 1994.

1.4 m, but as no surface expression was evident, it is assumed that the standpipe was snapped by movement along a minor shear within the slipped mass. Hence, it is not indicated on the profile. Due to the orientation of minor scarps and toes, the principal longitudinal basal shear surface was considered to be approximately planar, extending under the length of the slip, with the failure surfaces of minor scarps joining it and the shear surfaces beneath toes bifurcating from it. Field observations have shown the scarps curving downwards at such an angle that they can be expected to join the basal shear surface. Only those surfaces with evidence in the field have been shown on the longitudinal section, although their exact curvature within the slipped ground is not known. Arrows on the shear surface indicate current movement, with the length of the arrow providing a very approximate indication as to the relative amounts of movement.

The other standpipes provided useful information as to the location of other shear surfaces. Initially, standpipe G (depth 2.2 m) did not snap supporting the suggestion discussed above, that the basal shear surface was below the depth of this standpipe at approximately 2.6 m. However, between the 7th April 1994 and the 13th April 1994, towards the end of movement phase 4 when adjacent station A5 showed its highest velocity, standpipe G snapped at an approximate depth of 0.9 m. This is likely to have been caused by small amounts of movement occurring along a minor shear surface present at this depth and has not been shown on the profile, for similar reasons to that discussed for standpipe F above.

Standpipe B snapped at approximately 0.6 m. Due to the presence of a nearby minor scarp, it was deduced that this standpipe was snapped by the shear surface extending down from the scarp, as shown on the section. Standpipe D snapped at 0.9 m, and due to its position in the toe of the slip, the cross-section shows a shear surface bifurcating from the basal shear and cutting through D underneath the toe of the slide. Standpipe E did not snap, however the presence of a relatively large toe means there must be a shear surface beneath it, albeit of some previous period of movement, believed to be 1968. At present no movement is occurring along this shear surface, as supported by the surveying and the non-snapping of standpipe E.

As discussed in Section 3.3.2, this longitudinal section indicates that the slide is a predominantly translational slide and fits into the Type "L" category, according to the classification by Hutchinson (1967). However, as typical in such situations, where an older toe stabilises, newer upper toe

shears ride over the pre-existing toes. The section compares well with the profile produced by Lawrence (1985) of the 1980 landslide further up the slope. He classified the upper part of the 1980 slope movement as a markedly non-circular shallow rotational slip of Type "N" and the lower part as a predominantly shallow translational slide of 1 to 5 m depth, of Type "L".

3.7 Ground Water Chemistry

Section 3.4 has demonstrated that within the visibly slipped mass there is increased weathering compared to within the unslipped ground and showed the effects of this on the geotechnical indices of the Fuller's Earth clay. It was proposed that the change in the geotechnical properties of the clay was as a result of the depotassification of illite and the dissolution of calcite by chemical weathering.

This section investigates the geochemistry of the ground water, both from within the landslide at Soper's Wood and from outside the visibly slipped mass, to determine whether chemical weathering is occurring at present; with particular emphasis on the dissolution of calcite and the depotassification of illite as these are likely to effect slope stability (see Chapter 2). This study was undertaken conscious of the presence of the Fuller's Earth Rock horizon and other "in situ" limestone bands that are present in the Fuller's Earth formation and the effects that their presence may have on ground water chemistry. A review of calcium carbonate equilibria chemistry can be found in Chapter 5.

3.7.1 Ground Water Analysis

Ground waters were sampled from the standpipes at approximately monthly intervals between the 16th March 1994 and the 3rd August 1994. The results of the chemical analyses of the ground water samples obtained from standpipes F, B, E, C, and A over the period have been analysed and these are discussed below. As not enough water samples were obtained from Standpipes G and D for an adequate analysis of the variation in ground water chemistry over the period, the analysis of these water samples is not discussed.

Figure 3.23 displays calcium, magnesium and potassium concentrations for the ground water samples taken from each of the standpipes over the period of study. The following points are noted:

(1) The levels of calcium are significantly higher than those for magnesium and potassium. It is likely that the majority of the calcium originates from the dissolution of calcium carbonate within the Fuller's

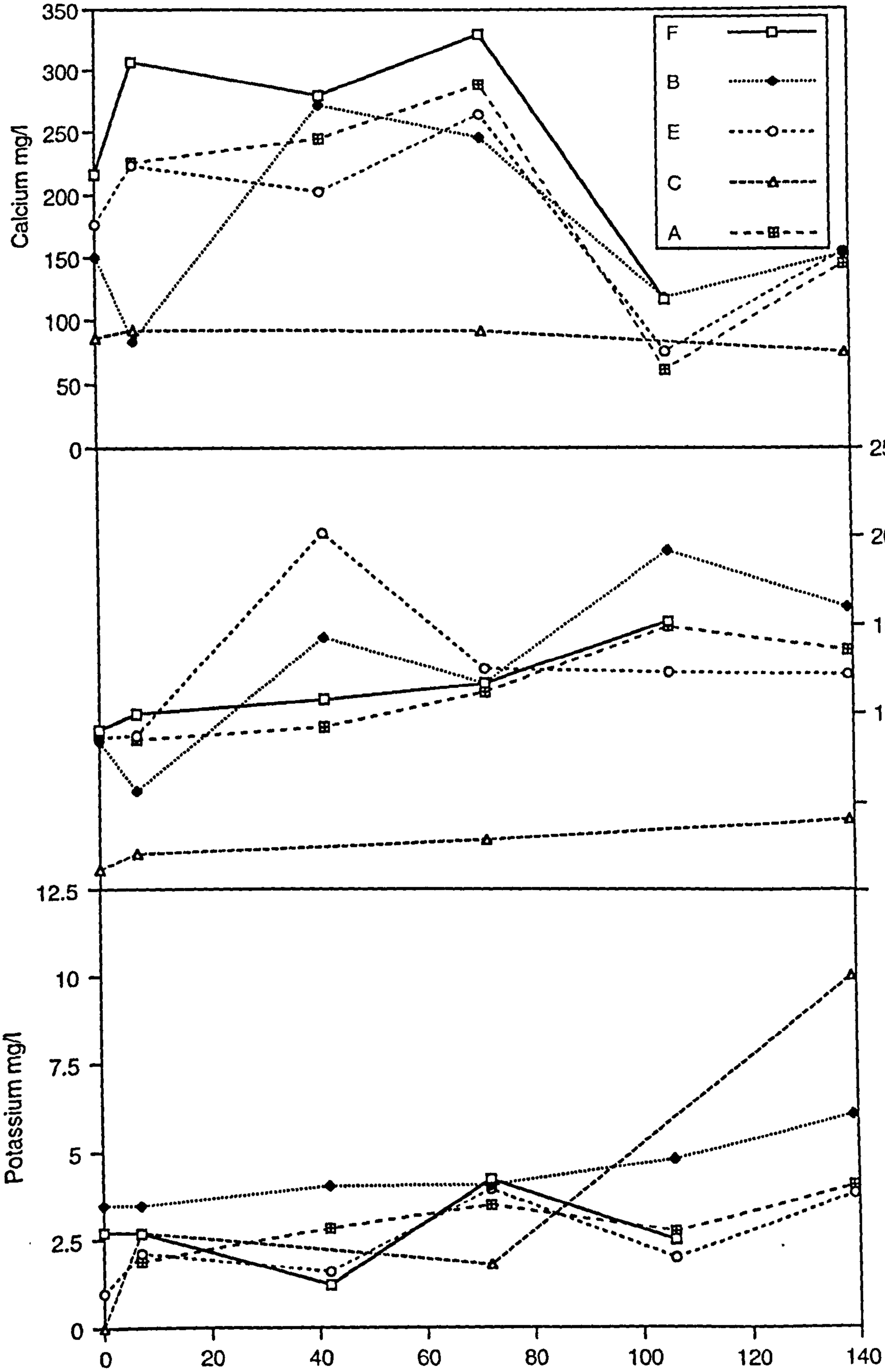

Fig. 3.23 Graphs displaying calcium, magnesium and potassium concentrations in the ground water samples taken from standpipes F, B, E, C and A over the period of study.

Earth. The magnesium found in the ground water samples is likely to originate from the dissolution of impure calcium carbonate. The concentration of potassium in the ground water at Soper's Wood is similar to a potassium concentration of 5.4 mg/l found in the ground waters emerging from a crush zone within a landslide at Mam Tor, Derbyshire, as reported by Vear & Curtis (1981). They attribute the presence of potassium in the ground water to the leaching of potassium ions from illite by acid ground waters originating from the decomposition of pyrite. Hence, the potassium present in the ground water samples is likely to originate from the depotassification of illite caused by chemical weathering of the Fuller's Earth clay.

(2) Calcium concentrations vary between 61 mg/l and 335 mg/l. A calcium level of 335 mg/l is high for natural ground waters; the hardness classification of water (Sawyer & McCarty 1967) classifies water with over 300 mg/l of calcium as very hard. If the calcium is considered to only come from the dissolution of calcium carbonate then the concentration of dissolved calcium carbonate would be between 153 mg/l and 837 mg/l. A calcium carbonate concentration of 837 mg/l is very high for natural fresh water (see Chapter 5) and thus some of the calcium present in the ground water may come from the dissolution of gypsum, although no gypsum was noted during the logging of the auger hole samples. However, Lawrence (1985) noted its presence in trial pits.

(3) Magnesium and calcium levels found in those ground water samples obtained from standpipes within the landslip are higher than in the water samples obtained from standpipe C outside the slipped mass. This observation is less clear for potassium. This implies that enhanced dissolution of calcium carbonate is likely to be occurring within the slipped Fuller's Earth clay, probably due to the increased permeability caused by lateral shears, minor scarps, shear surfaces and transverse cracks allowing the percolation of acidic ground waters. This is supported by water flowing out from the base of the toe of the slip, during the winter and early spring. Outside the slipped mass, the lower permeability of the visibly unslipped ground inhibits the flow of ground water and hence dissolution levels would be lower. However, the presence of the Fuller's Earth Rock and other "in situ" limestone horizons cannot be ignored and the higher levels of calcium found in the ground water within the landslide may be partially caused by ground water flowing from the impure limestone into the disturbed slipped ground. In the visibly undisturbed ground outside the landslide, the lower permeability may hinder the flow of waters from the limestone bands.

(4) Calcium and magnesium concentrations over the period of study vary considerably in those ground water samples obtained from standpipes within the slip, whereas the concentrations found in the ground water samples from standpipe C are much more constant.

Figure 3.24 displays the calcium concentration and temperature of the ground water samples obtained from the standpipes over the period of study together with daily rainfall. From the graphs the following points are evident:

(1) All the profiles for calcium concentration for ground water samples obtained from standpipes within the slip are similar.

(2) For the ground water samples obtained from standpipes within the slip there is a general correlation between calcium concentration and rainfall, although sampling and temperature readings are widely spaced and hence correlation can only be approximate.

(3) For the standpipes within the slip, calcium concentrations appear to show an approximate inverse correlation with temperature. Work done by Picknett *et al.* (1976) demonstrated that in the laboratory there is increased dissolution of calcium carbonate with decreasing temperature. This is due to the increased solubility of carbon dioxide at lower temperatures causing increased acidity (see Chapter 5).

Figure 3.25 displays the calcium concentration, pH and temperature of the ground waters obtained from the standpipes over the period of study and demonstrates that:

(1) The pH of the ground water within the slip is slightly lower at around 7.25 compared to outside the slip where it varies between 7.7 and 8.1. This may indicate more open system conditions within the slipped mass related to the increased dilation of the slipped material, allowing an abundant supply of carbon dioxide. Outside the slip the less permeable nature of the clay may have led to more closed system conditions, with a limited supply of carbon dioxide.

(2) There is little correlation between temperature and pH. This is likely to be due to the buffering effect caused by the dissolution of calcium carbonate.

3.7.2 Ground Water Chemistry Variation within the Slip

On the 5th and 6th May 1994, six additional standpipes (X, Y, Z, W, U, and T) were placed in the northern half of the landslide along the line of the existing standpipes, so that twelve standpipes now formed a profile down the slip from main scarp (standpipe G) to toe (standpipe X). For

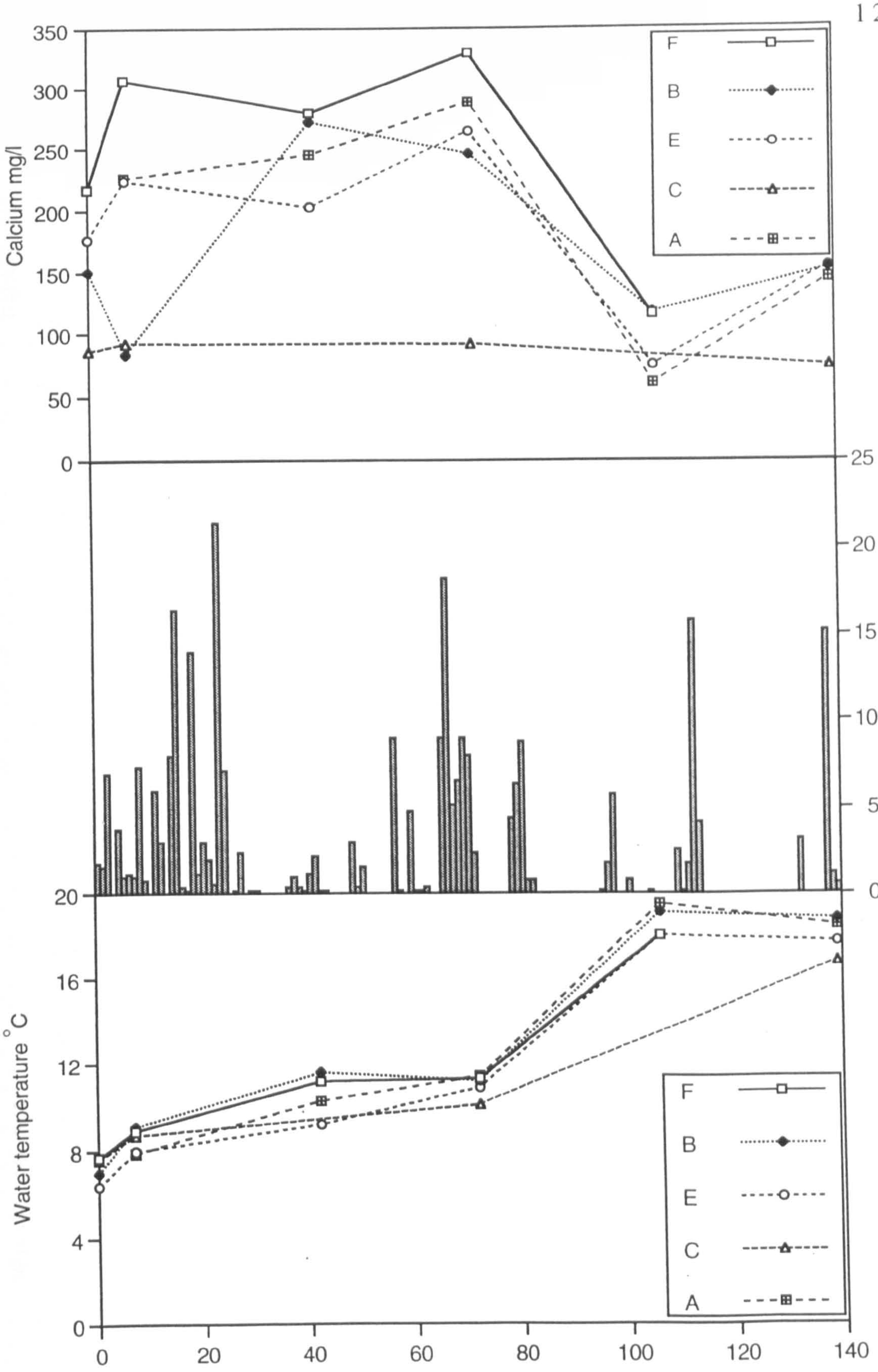

Fig. 3.24 Graphs comparing the calcium concentration and the temperature of ground water samples from standpipes F, B, E, C and A, with rainfall levels over the period of study.

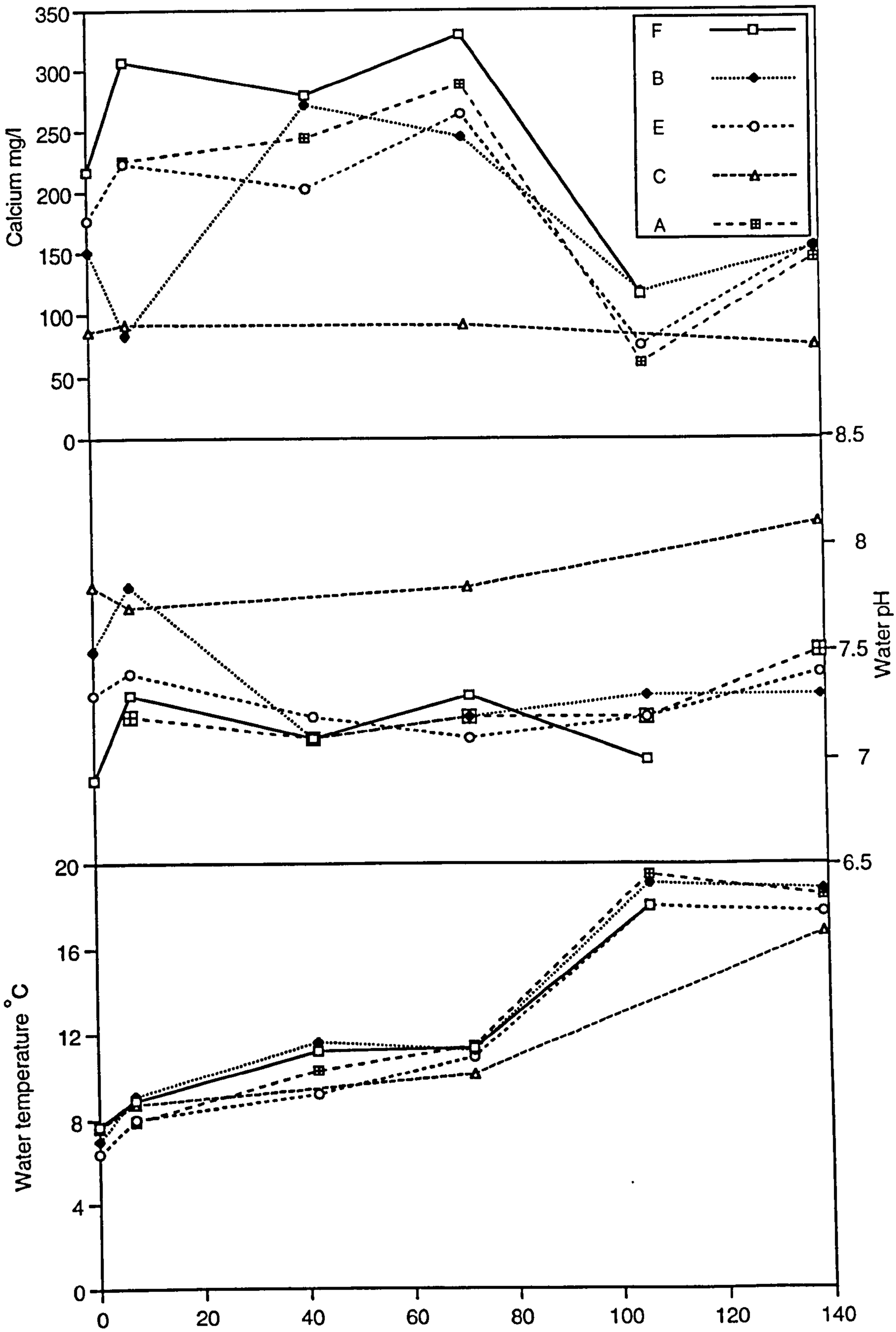

Fig. 3.25 Graphs showing the variation in calcium concentration, pH and temperature of the ground water samples taken from standpipes F, B, E, C and A over the period of study.

standpipe locations see Figure 3.26. Ground water samples were extracted from the standpipes on the 27th May 1994 and the results of the chemical analyses are discussed below.

Figure 3.27 displays the variation in calcium concentration, conductivity and pH of the ground water obtained from the standpipes down the slip profile. Conductivity correlates well with calcium concentration which varies considerably down-slope. In addition, there is a very broad inverse correlation between calcium ion concentration and pH, which varies between 7.1 and 7.6, indicating open system conditions.

Inspection of the graphs in Figure 3.27 reveals that those water samples taken from standpipes F and T, have the highest concentrations of calcium. In standpipe F, this may be due its location in the centre of the main translational slide. Thus, the water sampled has percolated some distance within the slip allowing it to reach its level of maximum dissolution and hence concentrations of calcium are high. In standpipe T, the higher concentrations are likely to be due to its location at the edge of the active toe, where water was observed to egress. Hence, the water has migrated down the length of the slip increasing in calcium concentration as it migrates down-slope. It is recognised that these concentrations may also have been affected by both the lithology and permeability of the in situ bed rock.

This longitudinal profile indicates that where there is an increase in concentration, it is likely that the ground water has not been diluted by recently infiltrated rainfall. Downslope from standpipe F, the presence of the cluster of minor scarps at the head of Slide A has allowed rain water to penetrate, reducing the calcium ion concentration in the ground water, which again rises as the ground water percolates down Slide A dissolving calcite, towards a peak in calcium concentration at standpipe T. The lower values of calcium found in the ground water sampled from standpipes E and X may represent dilution due to the infiltration of rain water in the relict disturbed toes of the slip.

Figure 3.28 displays the downslope variation in levels of calcium, magnesium and potassium in the ground waters sampled. Again calcium levels are significantly higher than those of magnesium and potassium. In addition, there is a very broad correlation with the variation in magnesium concentration down-slope, supporting the suggestion in Section 3.7.1 that the magnesium originates from the dissolution of impure calcium carbonate. There is no correlation with potassium concentrations which show very little

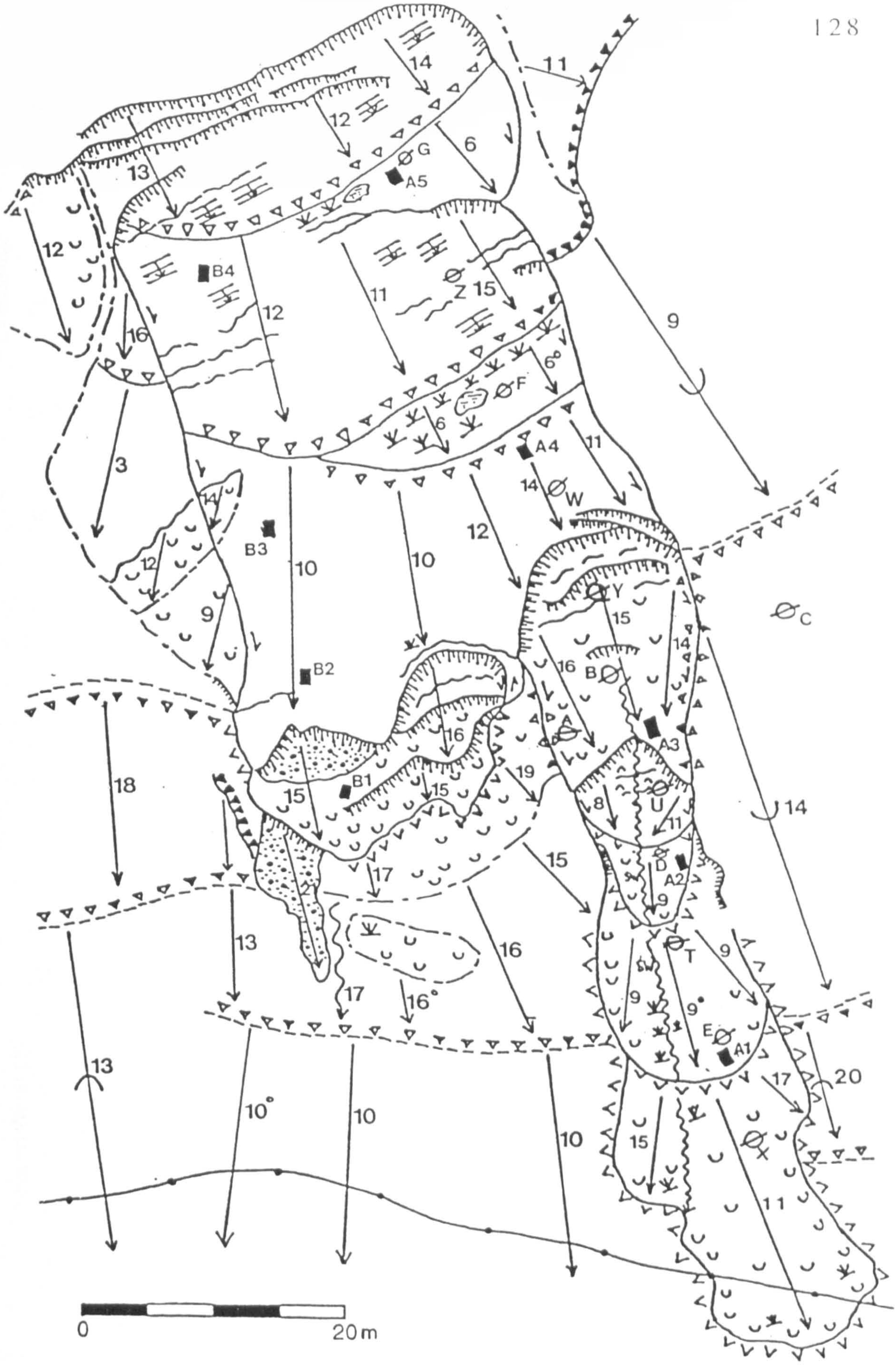

Fig. 3.26 Engineering geomorphological map of the landslide adjacent to Soper's Wood showing the location of the additional standpipes.

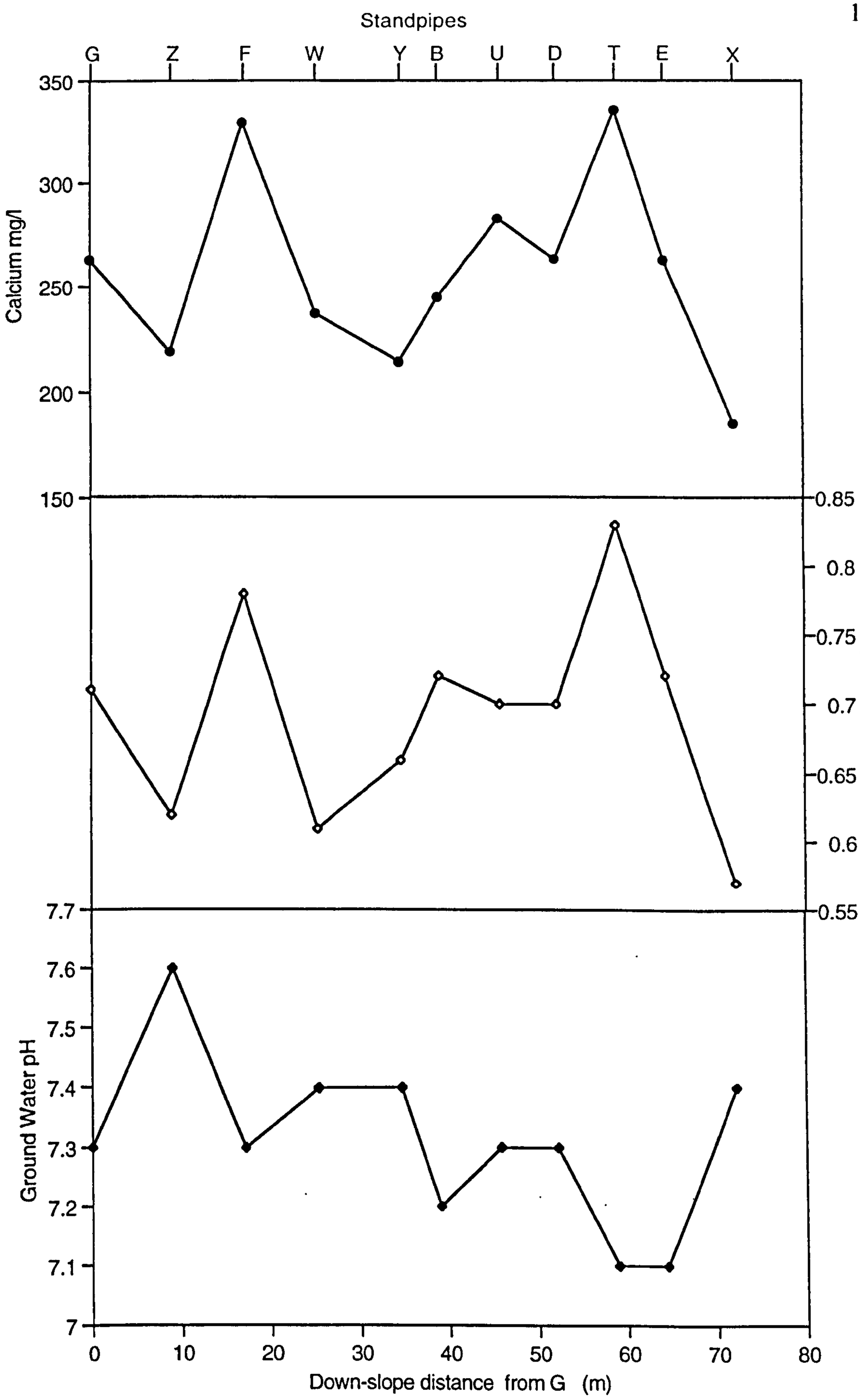

Fig. 3.27 Graphs showing the variation in calcium concentration, conductivity and pH of the ground water samples taken from the standpipes within the landslide on the 27 May 1994.

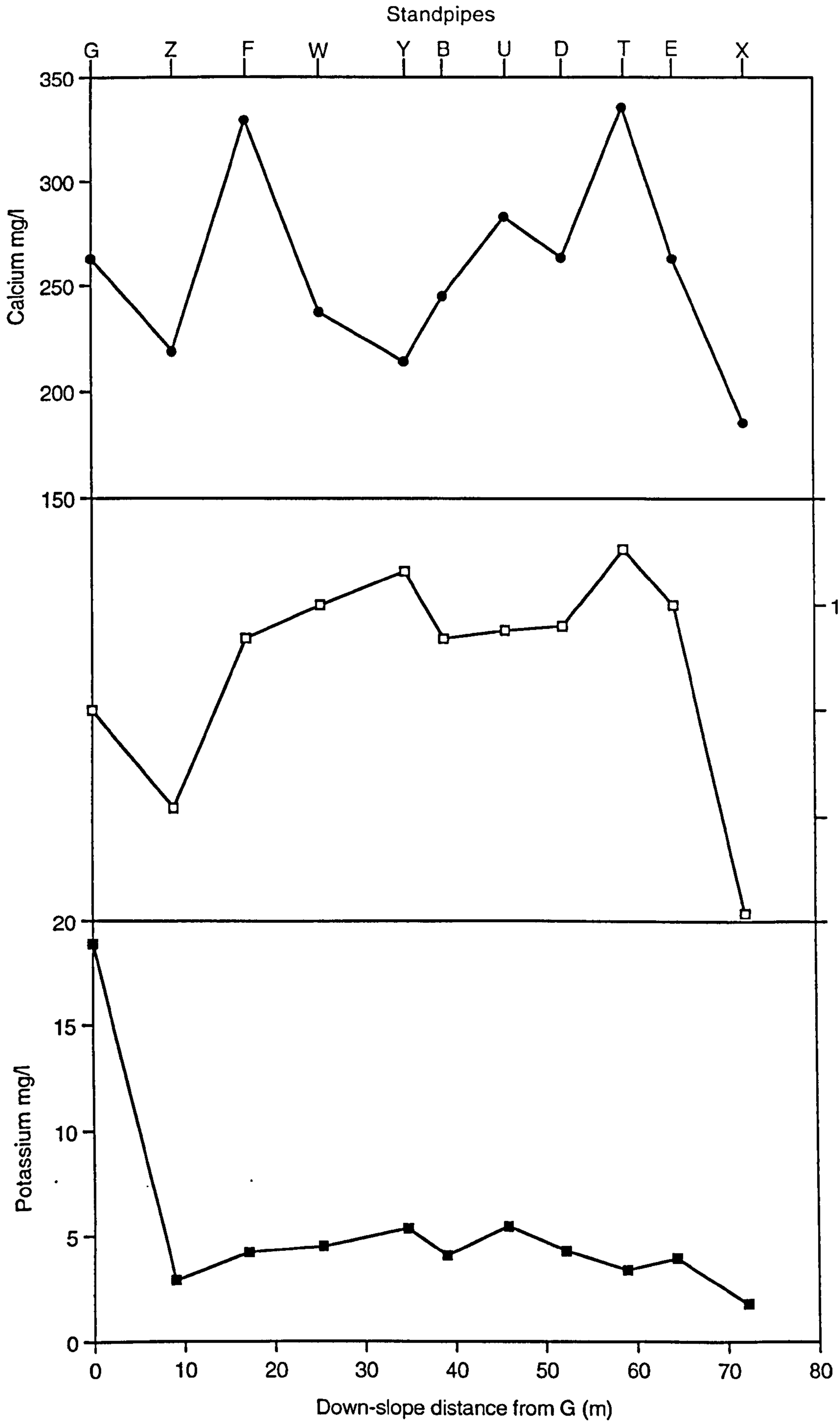

Fig. 3.28 Graphs displaying the variation in calcium, magnesium and potassium levels in the ground water samples taken from the standpipes within the landslide on the 27th May 1994.

variation down slope (apart from in the ground water sample obtained from standpipe G which may be due to an erroneous reading).

3.7.3 Discussion

The dissolution of calcium carbonate within the Fuller's Earth clay is undoubtedly occurring. However, exact levels resulting from the dissolution of disseminated calcite within the clay are difficult to predict as the concentration of calcium in the ground water will also be affected by the dissolution of any gypsum present and the presence of "in situ" argillaceous limestone bands.

The significantly lower calcium concentration in the ground water sampled outside the visibly slipped mass, is likely to indicate that increased dissolution rates of disseminated calcium carbonate are occurring within the more permeable, disturbed Fuller's Earth clay. However, the ground water concentrations may in part reflect water preferentially flowing from the limestone bands to the disturbed area as egress here will be easier than where "in situ" clay cover is present.

The downslope variation in calcium concentration in the ground waters sampled from the standpipes within the slip, as shown in Figure 3.28, indicates that within Slide A, containing standpipes Y to T, there is a significant increase in calcium concentration in the ground water from the cluster of minor scarps (standpipe Y) to toe (standpipe T). This supports the suggestion that the disseminated calcium carbonate in the Fuller's Earth clay is actively being dissolved by the percolation of ground waters downslope within the landslide. Hence, the concentration of calcium in the ground water increases down the landslide. In addition, the magnesium present in the ground water is likely to originate from the dissolution of impure calcium carbonate and, according to Crabtree (1986), this may increase the rate of calcite dissolution.

The knowledge that active dissolution of detrital calcite in the Fuller's Earth clay is occurring within the landslide has important implications for the long term stability of the slope. Hawkins *et al.* (1986 and 1988) and Hawkins & McDonald (1992) have demonstrated that decalcification of the Fuller's Earth clay dramatically reduces the residual shear strength of the clay if shear occurs in the transitional mode. Hence, if failure is occurring in the transitional mode, the dissolution observed at Soper's Wood is likely to reduce the residual shear strength of the landslide and with time the slip may further destabilise, causing renewed movement.

In addition to calcite dissolution, this study has also shown that potassium ions are being leached from the clay minerals in the Fuller's Earth. In Chapter 1 it is proposed that this results in the formation of a randomly interstratified illite-montmorillonite. Chapter 2 reports the work of Kenney (1967) and Chattopadhyay (1972), who note that the residual shear strength of montmorillonite is significantly less than that of illite. Thus, if illite is being transformed to a mixed layer illite-montmorillonite along shear surfaces within the landslide, with time this will result in a decrease in the residual shear strength of the shear surface, additional to the decrease which will occur as a result of calcite dissolution, further promoting instability.

3.8 Conclusions

(1) The production of geomorphological maps of the landslide has indicated that the slide active in 1994 is very likely to be a reactivation of a 1968 slide, supporting the argument that the majority of movement occurs along pre-existing shear surfaces. The upper part of the slide consists of a translational landslide, about 50 m in length, which downslope extends into two distinct morphological features. On the northern side, the main translational landslide has extended to form a well defined narrow translational landslide (Slide A). On the southern side, the main translational landslide has not extended so far valleyward and the lower feature is termed Slide B.

(2) A study of the logs of samples of the Fuller's Earth clay, obtained every 100 mm from auger holes drilled both inside and outside the visibly slipped mass, has demonstrated the highly weathered nature of the slipped Fuller's Earth clay. The logs indicate that both the weathering grade and depth to which weathering occurs are greater in the visibly slipped material compared to in the material outside the landslide.

(3) An analysis of sample moisture contents revealed that there are significant differences in the soil moisture both within the slipped zone and when the slipped zone is contrasted with the moisture content profile of the auger hole drilled outside the visibly slipped mass.

(4) A comparison of the geotechnical indices of samples from inside and outside the landslide has shown the effects of the increased weathering of the slipped material on the geotechnical indices of the Fuller's Earth clay.

In addition, this study has confirmed the control that calcite has on the Atterberg limits of the Fuller's Earth clay.

(5) Along the line of survey stations A1 to A5, the portion of Slide A containing stations A2 and A3 was most active. Station A3 moved a total of 2.9 m horizontally and 0.9 m vertically downwards. Station A1, situated on the lowest toe of the slip, was effectively stationary. The upper area of the main translational landslide containing stations A4 and A5 showed much less movement.

(6) Along the line of the B survey stations, stations B1 and B2 were the most active, with stations B3 and B4 in the upper area of the main translational slide showing less movement. Station B1 moved 2.07 m horizontally and 0.59 m vertically downwards. However, this was only in the first nine weeks of monitoring, as between the 21st March and 7th April 1994, there was an enhanced phase of movement during which time station B1 was swept away by the mudflow.

(7) In the main translational slide up-slope of where the landslide splits into two separate morphological features, the side containing survey stations B3 and B4 has shown a greater amount of movement than the side containing stations A4 and A5.

(8) A comparison of cumulative movement for each survey station with cumulative rainfall reveals that the two are intimately related, even with the varying amounts of movement of each station. Where the change in rainfall levels is dramatic, there appears to be a time lag of 3 to 6 days between the two events.

(9) The majority of slip movement had been completed by the 13th April 1994, coincident with a prolonged period of very little rainfall from the 10th April 1994 to 20th May 1994. Increased levels of rainfall after the 20th May 1994 caused only comparatively small amounts of further movement.

(10) A comparison of ground water levels in the standpipes within the landslide, with ground water levels in the standpipe placed outside the slip as a control, revealed that the water table within the slip is considerably shallower than outside the slip, most likely due to selective recharge in the

slipped mass. In addition, all the standpipes within the slip had a faster initial response, probably related to the increased dilation of the soil within the slipped mass.

(11) The study has highlighted the importance of standpipe location within a landslide, as there is some variation in the ground water level between different locations. This is clearly important when considering slope stability analyses.

(12) A comparison of the geomorphological map produced at the start of monitoring in January 1994, with a second map produced in May 1994 when the majority of movement appeared to have taken place, highlighted two patterns of movement; transverse crack propagation and retrogressive scarp migration.

(13) Geochemical analyses of ground water samples extracted from the standpipes revealed that the concentration of calcium varied between 61 mg/l and 335 mg/l, significantly higher than the levels found for magnesium (2.1 to 14.4 mg/l) and potassium (1.21 to 10.03 mg/l). It is likely that the majority of calcium in the ground water originates from the dissolution of calcium carbonate in the Fuller's Earth. The magnesium found in the ground water samples is probably originating from the dissolution of impure calcium carbonate. The presence of potassium is likely to originate from the depotassification of illite, as noted by Vear & Curtis (1981).

(14) Magnesium and calcium levels found in the ground water taken from those standpipes within the landslip are significantly higher and more variable over the period of study than the levels found in standpipe C outside the visibly slipped mass. This implies enhanced dissolution of calcium carbonate within the slip.

(15) The calcium concentration found in the ground water varied downslope within the landslide. This variation is likely to be related to the positions of the sampling standpipes within the slip relative to the flow of ground water. Hence, at the head of the slip, ground water concentrations of calcium are low and in general increase downslip as the ground water percolates downslope dissolving calcium carbonate.

(16) The knowledge that active dissolution of detrital calcite in the Fuller's Earth clay is occurring within the landslide has important implications for the long term stability of the slope. If shear is occurring in the transitional mode, as described by Lupini *et al.* (1981), the dissolution of calcite observed at Soper's Wood is likely to reduce the residual shear strength of the landslide and with time the slip will further destabilise.

(17) In addition to the dissolution of calcite, this study has also shown that potassium ions are being leached from the clay minerals in the Fuller's Earth. Thus, if illite is being transformed to an illite-montmorillonite along shear surfaces within the landslide, this will also result in a decrease in the residual shear strength of the shear surface, further promoting instability.

CHAPTER 4

A STUDY OF A SHEAR SURFACE IN THE FULLER'S EARTH CLAY

4.1 Introduction

The investigation of the landslide at Soper's Wood described in Chapter 3 demonstrated that both the weathering grade and the depth to which weathering occurs are greater in the ground within the landslide compared to in the material outside the visibly slipped mass. In addition, chemical analyses of ground water samples indicated that; (i) the dissolution of calcite within the Fuller's Earth clay is occurring and (ii) potassium is being leached from illite, the dominant clay mineral within the Upper and Lower Fuller's Earth, which results in the formation of a randomly interstratified illite-montmorillonite.

Through the use of trial pits in the landslide at Soper's Wood, Lawrence (1985) noted the presence of discrete shear planes, although he did not install inclinometers to determine the depths at which movement was taking place. McDonald (1990) demonstrated the increased permeability of shear surfaces within the Fuller's Earth and proposed that the shear surfaces act as preferential zones of ground water percolation within a landslide.

This chapter describes the study of a small sample of Fuller's Earth clay containing a discrete shear surface taken from a trial pit within the landslide at Soper's Wood. The research was intended to investigate whether the dissolution of disseminated calcium carbonate and the chemical weathering of illite is occurring at a greater rate along shear planes within the visibly landslipped Fuller's Earth clay, due to the preferential percolation of acidic ground waters. The detailed morphology of the shear surface has been investigated to gain an understanding of the nature of the shear surfaces within the landslide at Soper's Wood. In addition, the variation of moisture content across the slip surface has been analysed to determine if there is an increase in moisture content at the shear surface due to the percolation of ground waters along it.

4.2 Field Technique

A hand dug trial pit of 1.5 m depth was carefully excavated across the right lateral shear of Slide A at Soper's Wood; this permitted the shear surface to be traced down from ground level. This proved more difficult than

first anticipated and occasionally the shear surface became hard to follow. However, its location was confirmed at a depth of about 0.8 m by the easy removal of the clay above it to reveal a highly polished slip plane (see Plate 4.1). A specially made steel box (85 mm x 245 mm x 160 mm), which had sharp bevelled edges to aid penetration, was then pushed into the wall of the trial pit at the level of the shear surface, so that a portion of the shear surface was contained within the box (see Plate 4.2). The box was then dug out and immediately wrapped in 3 layers of cling film to prevent moisture loss during transportation.

4.3 Sample Preparation

In the laboratory the boxed sample was sawn in half using a high speed rotary blade to obtain a "fresh" clay surface (see Plate 4.3). One of the boxed halves was then put aside as a reference and the second was used for sampling and analysis. A flat piece of wood was placed in the back of the boxed sample to be used for analysis and the clay pushed out so that 10 mm was revealed. This was then sliced off using a "cheese wire" and disposed of to remove any remnants of steel from sawing. A further 10 mm of clay was then pushed through to provide a fresh "slab" of Fuller's Earth clay containing the shear surface.

The "slab" was first divided into broad lithological units which were logged. The initial idea was then to extract a profile of "mini-cores" down the length of the "slab", using a 3 mm diameter cork borer and a perspex template. However, this proved unsuccessful and the edges of the "slab" were then divided into 44, 5 mm wide samples using a razor blade (see Plate 4.4). The samples were carefully cut away and placed in clean, oven dried and pre-weighed 10 ml glass jars for standard moisture content analysis. Following the moisture content analysis the individual samples were ground to a rock flour using a pestle and mortar and the calcite content determined by titration. Finally, the slab was cut up into units for XRD analysis.

Figure 4.1 contains a plan view of the slab showing the lithological units. The position of the 44 samples taken for moisture content and calcite content analysis and the location of the units taken for XRD analysis are also displayed. The shear surface drops from sample numbers 20 and 21 on the left edge to sample number 16 on the right edge of the "slab".

Plate 4.1 Photograph showing polished surface of the slip plane.

Plate 4.2 Photograph of the hand dug trial pit showing the technique used to obtain a block sample containing the shear surface.

Plate 4.3 Photograph displaying the fresh clay surface revealed after sawing the boxed sample in half. Notice the location of the shear surface.

Plate 4.4 Photograph displaying the sampling technique.

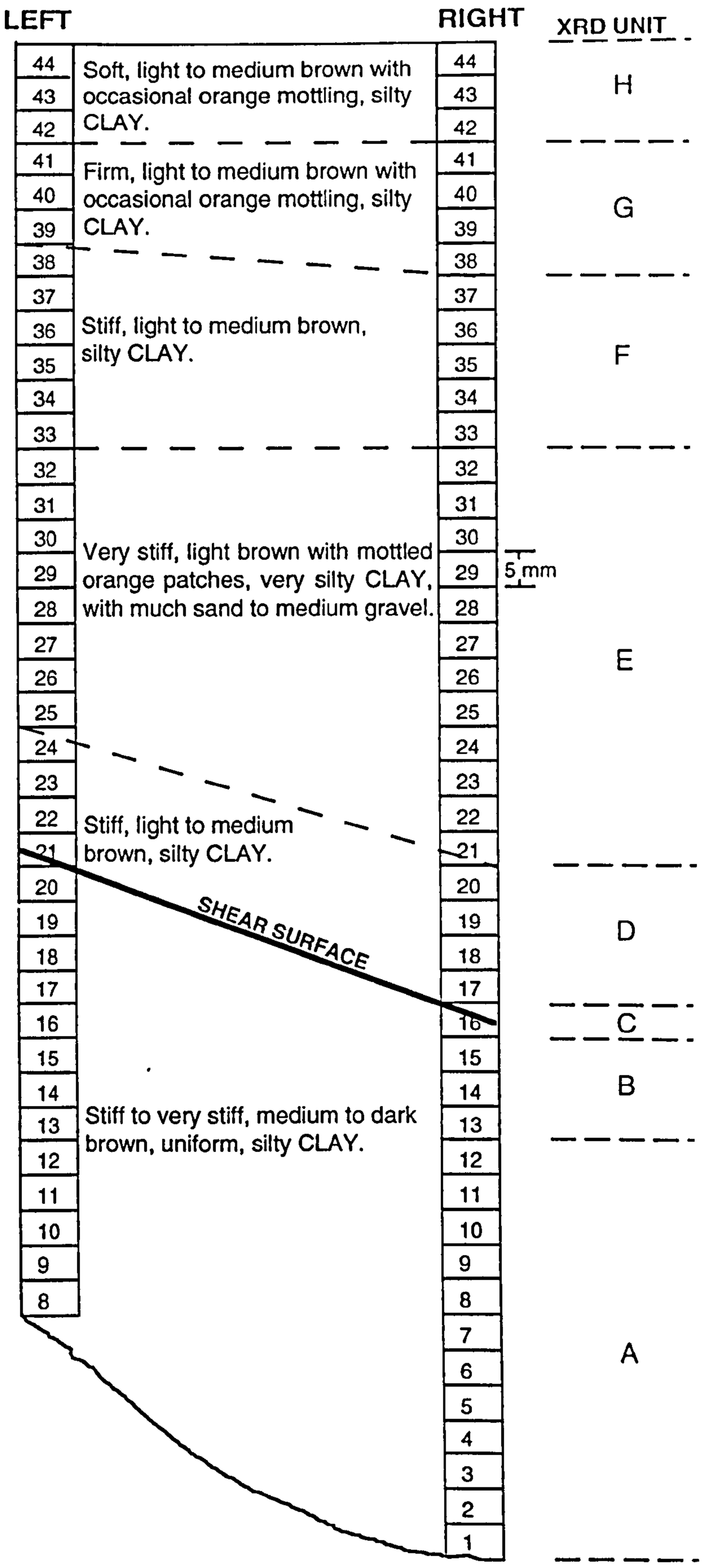

Fig. 4.1 Schematic plan view of the prepared slab showing the position of the shear surface and the discriptions of the various lithological units. Sample numbers for moisture and calcite content determination and XRD sample units are also displayed.

4.4 Moisture Content Analysis

Moisture content analyses were first conducted on the samples obtained from the right edge of the "slab". The profile of the moisture content recorded for each of the 5 mm thick samples is displayed in Figure 4.2. The graph shows a relatively sudden change in the profile between samples 16 and 15, with sample 16 corresponding to the level of the shear surface. Above the shear surface the moisture content of the clay is very varied, whereas below it the profile is relatively uniform at about 63%. This relationship was confirmed by a second moisture content analysis conducted on the samples from the left edge of the "slab". Fig 4.3 compares the two moisture content profiles which are very similar, but are offset from each other due to the dip of the shear surface. The left samples still exhibit the difference in moisture content profile above and below the shear surface which is contained in samples 20 and 21. The generally slightly lower values exhibited by the samples taken from the left edge of the "slab", may be accounted for by the likely loss in moisture during the one day delay between the analysis of the right samples and the left samples, even though the "slab" was wrapped in cling film during the interval.

The moisture content profiles for both the right and left edges of the "slab" indicate a very varied moisture above the shear surface between approximately 23% and 96%, whereas below the shear surface the moisture content is much more uniform at about 58% for the left edge and 63% for the right edge. Above the shear surface, the disturbed and slipped clay is likely to be fractured and more permeable relative to the clay below the shear surface. Ground water will preferentially percolate through such zones, further softening the clay, so that high moisture contents are developed, such as for right sample 43 at 96%. The variable nature of the profiles above the slip plane can also be correlated to the lithology of the clay, with the lower moisture content exhibited by right samples 21 to 32 and left samples 25 to 32, related to the very silty clay unit E, containing much sand and gravel. Clearly where the soil contains a high proportion of sand and gravel, the moisture content will be lower due to the less sorptive nature of sand and gravel sized material compared to clays. The peaks shown by right and left samples 43 correlate well with unit H, described as soft silty clay. Below the shear surface, the recently unslipped clay is lithologically fairly uniform and likely to be less disturbed and hence less permeable, providing a more stable moisture content profile; although the remarkably high values are likely to be related to the generally dilated nature of near surface material as a result of stress relief.

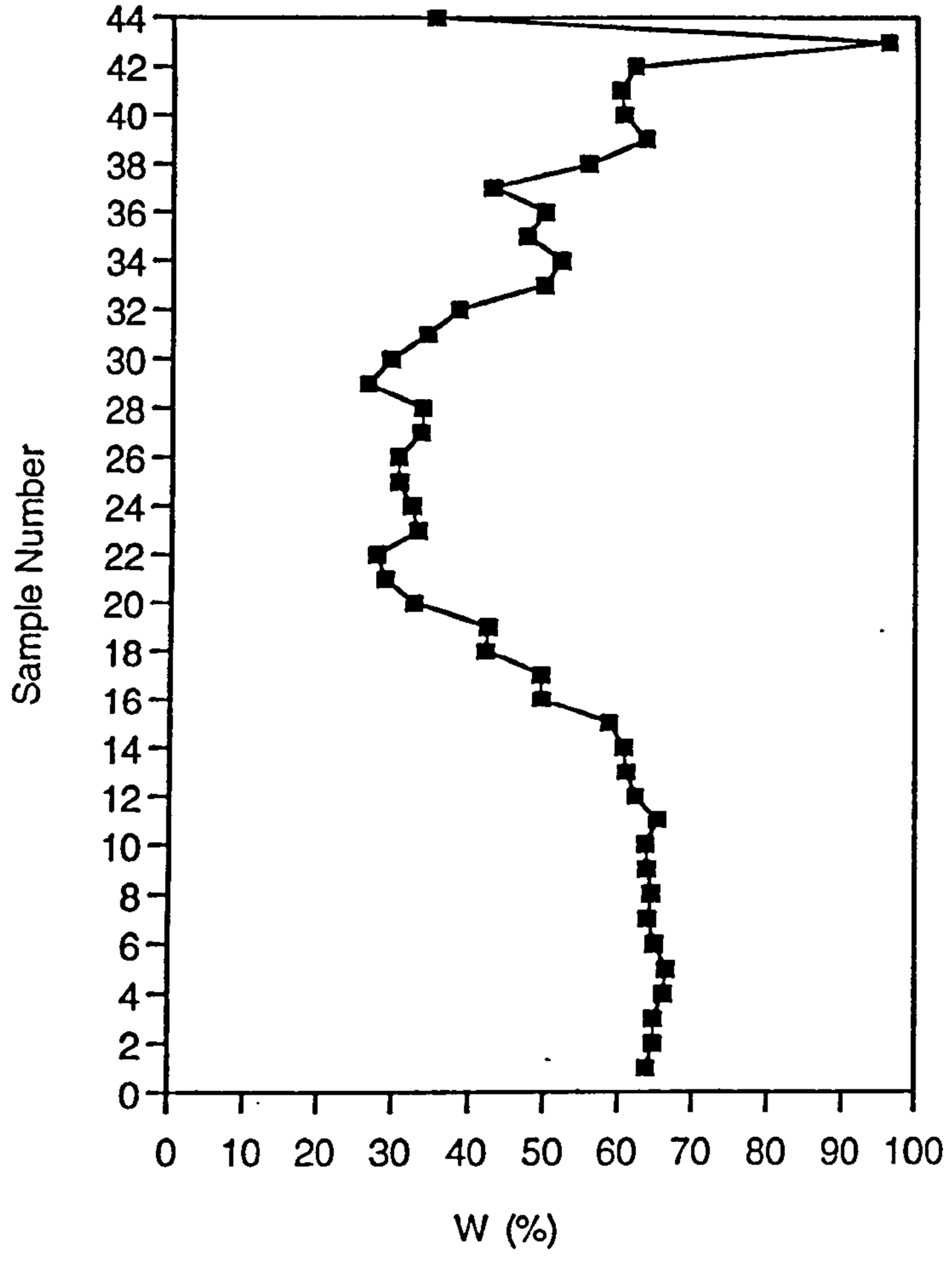

Fig. 4.2 Graph displaying the moisture content profile for the right edge of the "slab".

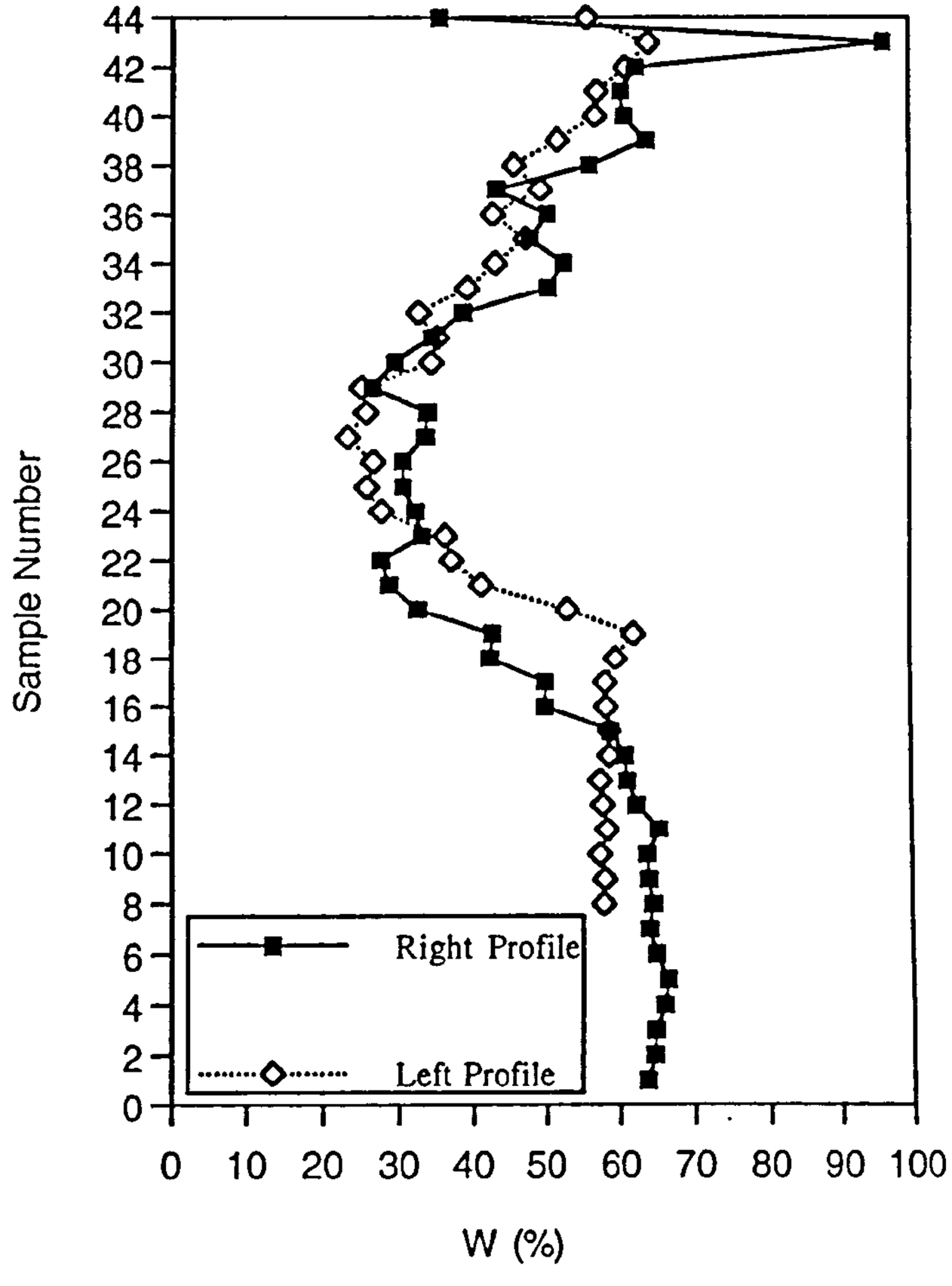

Fig. 4.3 Graph displaying the moisture content profiles for the right and left edges of the "slab".

4.5 A Comparison of Calcite Content and Moisture Content

Calcite contents were determined for the samples obtained from the right edge of the "slab" to establish whether there was a decrease in calcite content at the shear surface due to the percolation of acidic ground waters along it.

Figure 4.4 shows the profiles of calcite content and moisture content for the samples from the right edge of the "slab". The calcite content profile indicates a very varied calcite content above the shear surface of between approximately 11% and 68%, whereas below the shear surface the calcite content is very low and uniform at about 2%. At the level of the shear surface contained in sample 16, the calcite content is approximately 22%, intermediate between the generally higher values found above the shear surface and the very low values below the shear surface. However, the results provide no conclusive evidence that calcium carbonate dissolution is occurring at a preferential rate along the shear surface.

A comparison of the calcite and moisture content profiles shown in Figure 4.4 demonstrates a clear inverse relationship between the two profiles. The nature of this relationship is remarkable considering the very small sample size of this study. Figure 4.5 shows calcite content plotted against moisture content for the samples and emphasises this relationship. The two outliers to the trend represent samples 43 and 44. As shown by the log, the clay here was soft and the very high moisture content of sample 43 is likely to be caused by a portion of saturated clay. Sample 44 is right at the edge of the slab and the lower moisture content of the sample may be as a result of handling and/or the loss of moisture through the "open end" of the top of the sample.

These results provide further evidence that an inverse relationship exists between calcite content and moisture content, as initially demonstrated by Hawkins *et al.* (1986 and 1988), and emphasise the control that calcite content has on the moisture content of the Fuller's Earth clay, even at a very small scale. The control of the moisture content by the percentage of calcite present can be explained by the non-sorptive nature of calcite compared to clay minerals. Hence, a decrease in the calcite content leads to a relative increase in clay fraction and thus moisture content.

4.6 Normalisation of the Moisture Content Profiles

Trotter (1993) studied the weathering properties of an "earthflow" in Tertiary calcareous mudrock in New Zealand. He found that from an

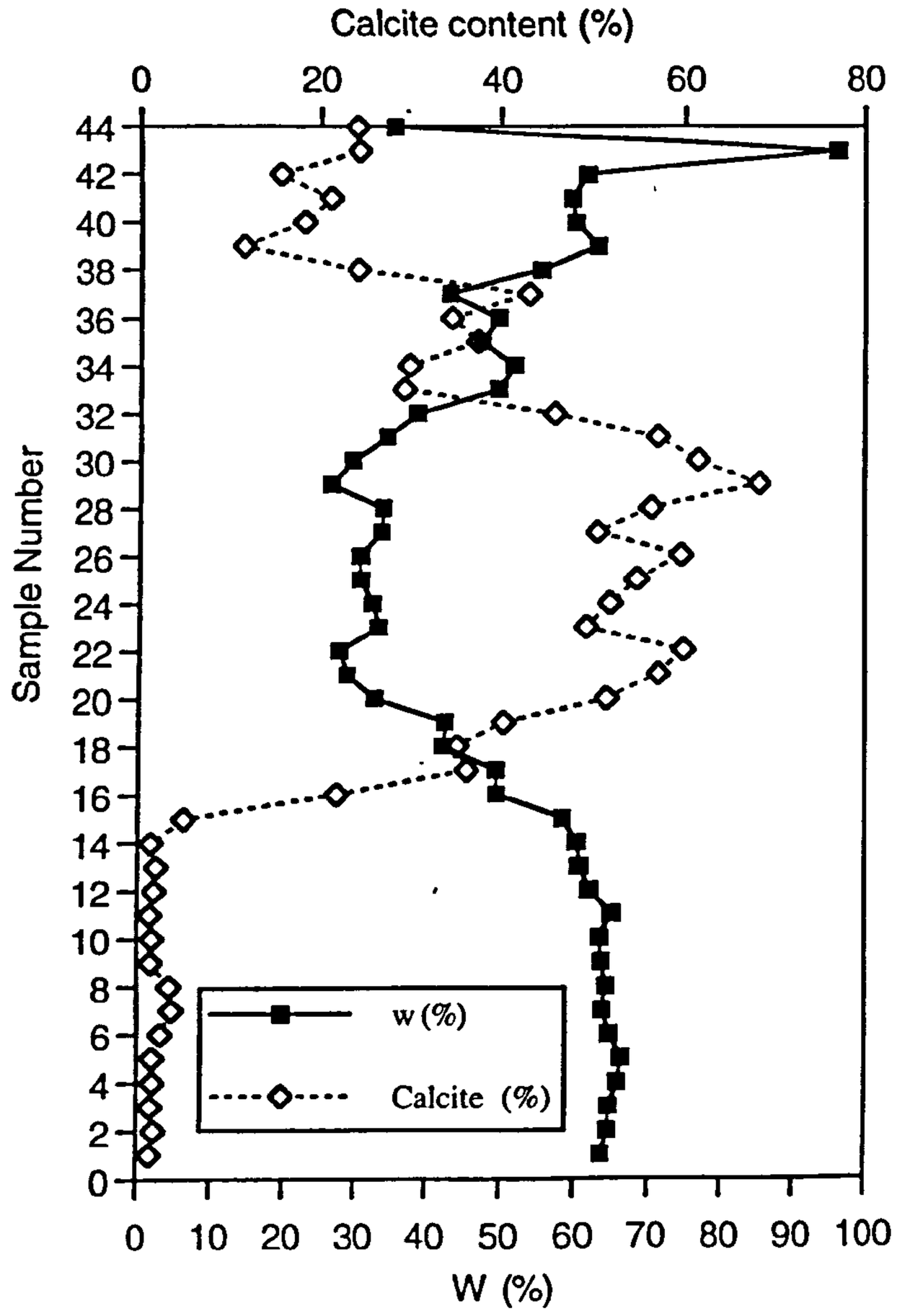

Fig. 4.4 Plot comparing the profiles for moisture content and calcite content for the right edge of the "slab".

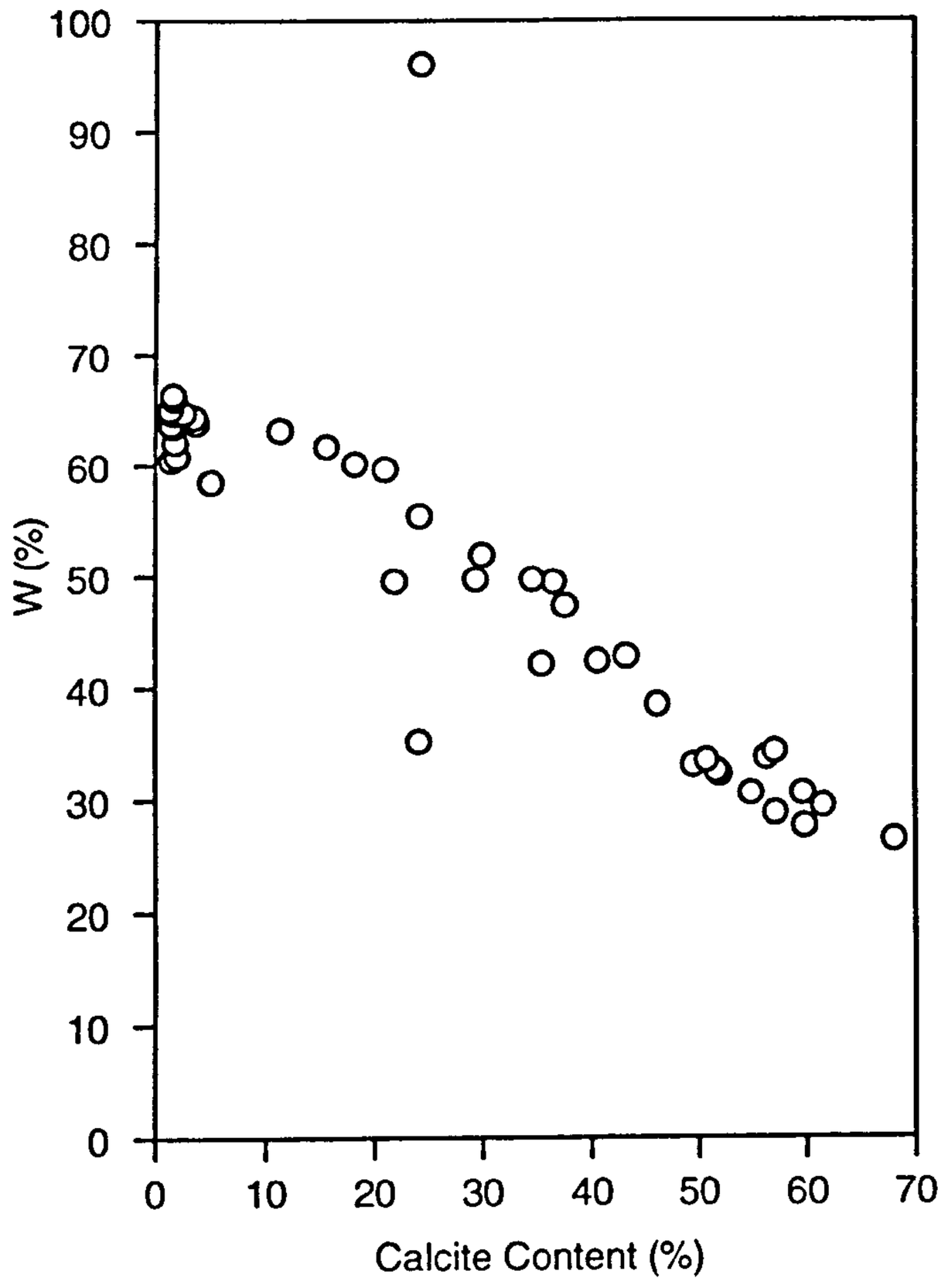

Fig. 4.5 Plot demonstrating the inverse relationship between moisture content and calcite content.

analysis of samples obtained from boreholes both inside and outside the perimeter of the "earthflow", the relationship between the geotechnical properties and the calcite contents of the calcareous mudflow were similar to those reported by Hawkins *et al.* (1986 and 1988) for the Fuller's Earth formation. To study the effects of the variation in the borehole moisture content profiles as a function of weathering alone, he removed the effects of any intra-profile variation in calcite content by normalising the borehole moisture content profiles to a calcite content of zero. He did this by assuming that:

" all the calcite is removed without bulk volume change and that water then occupies the available pore space."

To investigate any variations in the moisture content profile which are not controlled by the variation in calcite content, the moisture content was normalised according to the method described by Trotter (1993). Figure 4.6 graphically displays the normalised moisture content profile for the samples from the right edge of the "slab" according to Trotter's method and compares the profile to the profile for calcite content. Above the shear surface contained in sample 16, the normalised moisture content profile is variable, with values between approximately 54% and 160%, whereas below the shear surface the moisture content is lower and more uniform at about 66%. According to Trotter (1993), this indicates that the material above the shear surface is fissured allowing the percolation of ground waters and weathering to occur. Whereas below the shear surface the lack of fissuring has inhibited the percolation of ground waters and hence the normalised moisture content is more uniform. However, a comparison of the normalised moisture content profile to the calcite content profile, shows that the normalised moisture content profile is simply caused by replacing the calcite with water and does not add significance to this investigation.

As calcite is non-sorptive, it is much more useful to normalise the moisture content so that it reflects that of the clay minerals within the Fuller's Earth alone, without the calcite. This is expected to highlight any change in the moisture content profile of the clay across the shear surface. As a consequence, in this research the moisture content has been normalised to a calcite content of zero, using the following equation:-

Normalised W % = Mass of Water / (Total Dry Mass - Mass of Calcite)

Equation (4.1)

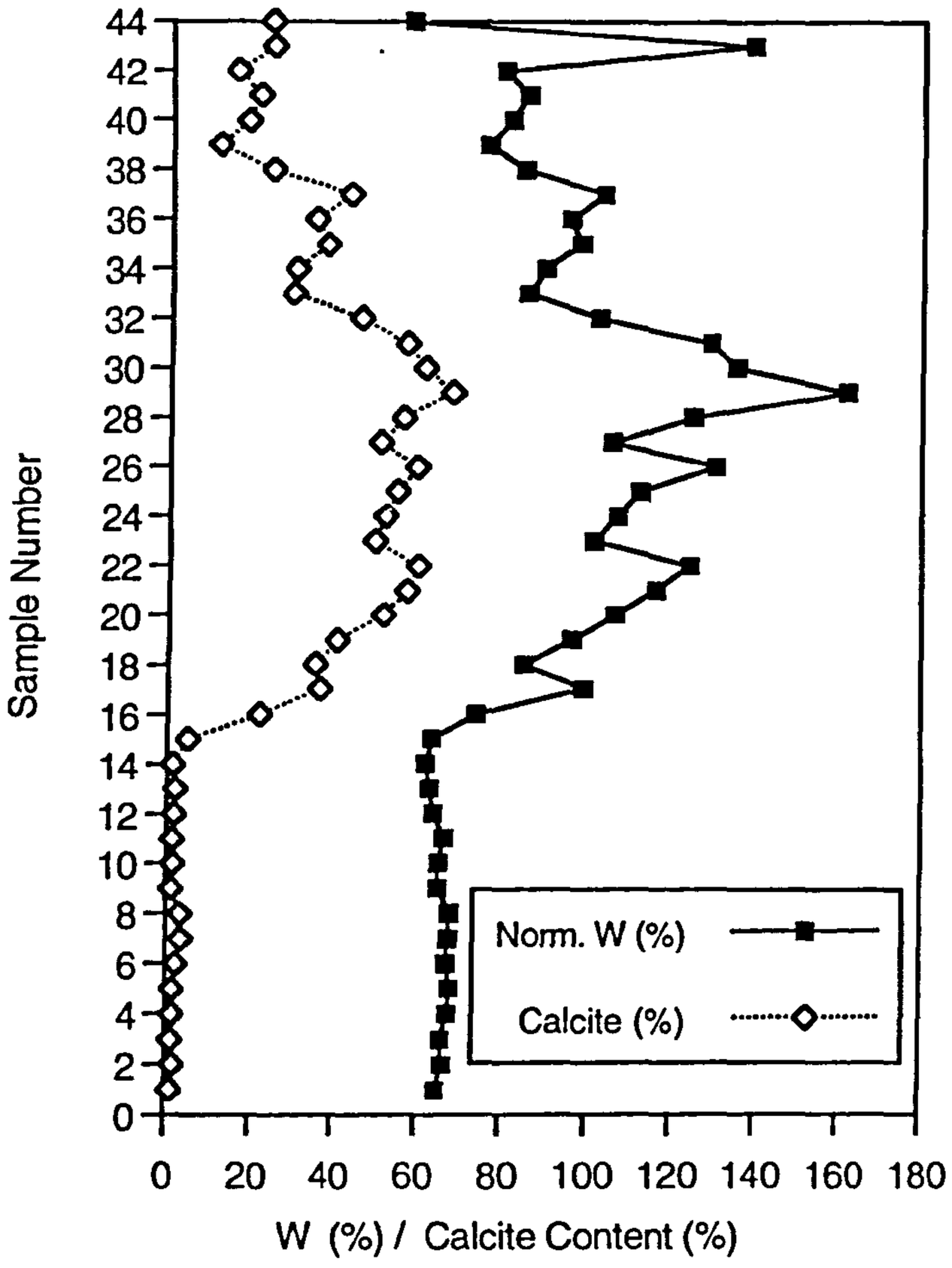

Fig. 4.6 Graph comparing the normalised moisture content, according to Trotter (1993), with calcite content.

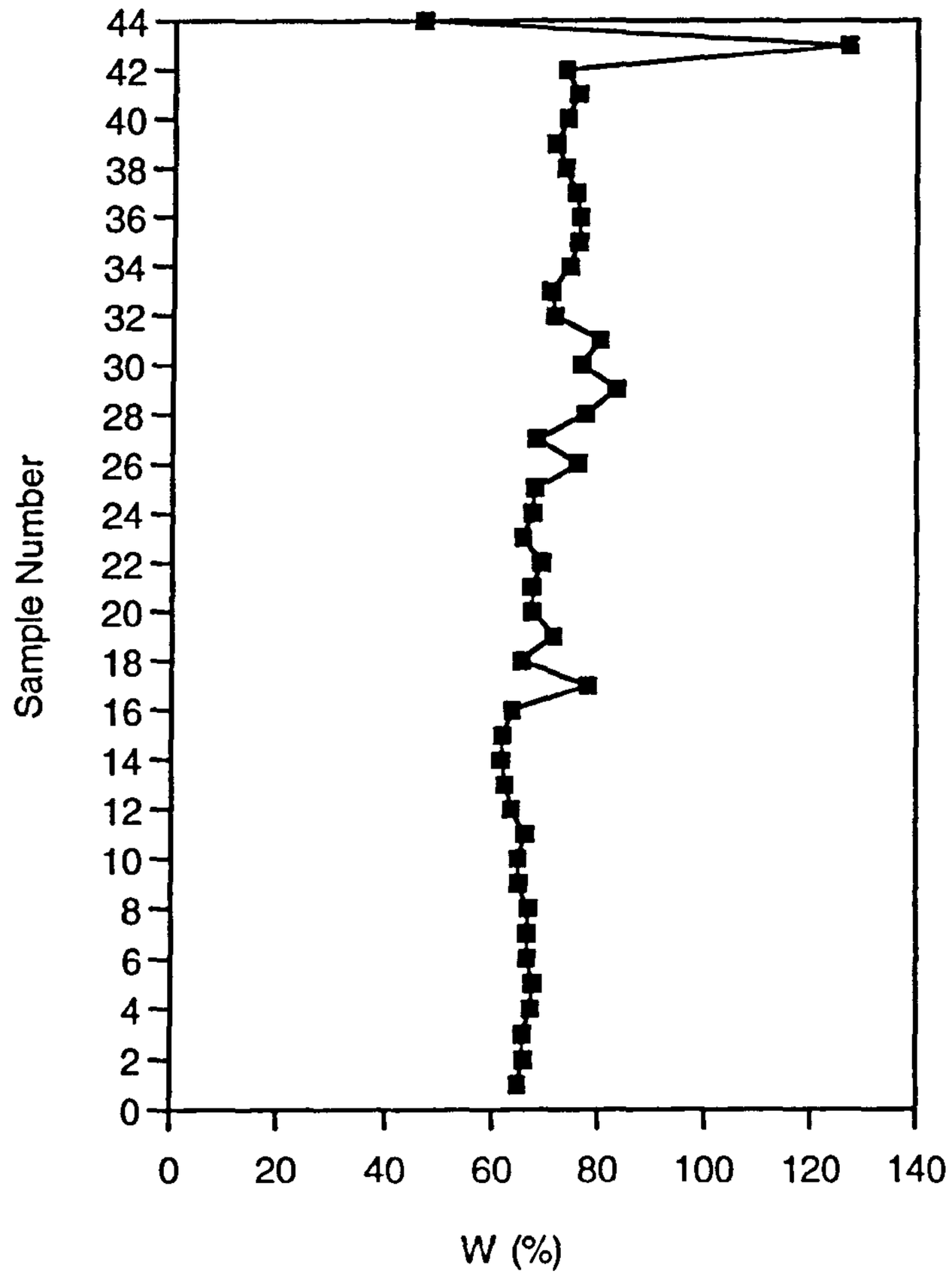

Fig. 4.7 Graph showing the normalised moisture content profile according to the new method described in this study.

This method assumes that the soil consists of just clay minerals and calcite, and that all the moisture is contained by the clays. Any layers of water that may exist adsorbed to the calcite are ignored.

Figure 4.7 displays the profile of the normalised moisture content according to the new method in this study. The shear surface is located in sample 16 and it is clear that above the shear surface, the normalised moisture content profile still shows some variation, with the majority of samples having a moisture content between approximately 62% and 83%, with an average of 76%. However, below the shear surface the normalised moisture content remains remarkably constant with an average of 65%. In addition, their appears to be a peak in the normalised moisture content at the approximate location of the shear surface.

The variation in normalised moisture content above the shear surface supports the interpretation of the standard moisture content profile and can be explained by the recently slipped material being more highly weathered and fissured so that ground waters can percolate through the sample. The clays therefore have a higher and more variable normalised moisture content. Below the shear surface the recently unslipped material, which is lithologically more consistent, is likely to have a lower permeability inhibiting the percolation of ground water. Hence, the moisture content is lower and more uniform, although it is still high due to general dilation of the soil caused by stress release. The change in moisture content at the shear surface is so sudden that the shear surface may be acting as a barrier to water moving at approximately right angles to the surface. Thus, it may prevent ground water passing from the recently slipped material to the unslipped material.

4.7 Analysis of the Shear Surface by SEM

Samples of the shear surface were viewed using a scanning electron micrograph to study the detailed structure of the clay minerals around the shear surface.

The samples were prepared for SEM analysis by partial drying at room temperature. Then, in order to view one side of the shear surface in plan section, some of the samples were snapped along the line of the shear surface; care was taken to prevent any sliding at the shear surface as this would disturb the orientation of the clay particles. In addition, some of the samples were broken across the shear surface so that a fresh cross-sectional profile was revealed.

Plate 4.5 displays six photographs from the investigation. Photographs "A", "B", "C" and "D" are plan views of the shear surface and demonstrate its smooth nature, although minor slickenside striations are visible at this scale. In general these striations were fairly shallow and ill-defined. The only deeper gouge is shown in photograph "B", however there was no evidence of the fine silt grain which may have formed it. Photographs "E" and "F" are cross-sectional views of the shear surface and the material below it. These highlight the relative smoothness of the shear surface and the horizontal orientation of the layer of platy clay minerals at the surface; below it the orientation of the clay minerals can be seen to be random. This demonstrates the change in geometry of the clay minerals immediately adjacent to the shear surface, from a random arrangement only 2 μm from it to an almost parallel arrangement at the line of failure.

The SEM examination indicates that the strain created by movement along the shear surface in the Fuller's Earth clay at Soper's Wood has caused the re-orientation of the platy clay minerals so that they are parallel to the direction of movement, creating a very smooth surface. In addition, only a few rare striations are visible. McDonald (1992) showed that silt and sand size particles in the Fuller's Earth are dominantly calcitic (although some silica is also present). Hence, the smoothness of the shear surface may be due to the percolation of acidic ground waters along it causing the dissolution of any silt and sand sized particles. However, it may simply be that at the level of the shear surface, there is a very low proportion of silt and sand sized particles due to lithological variation.

4.8 Mineralogy Across the Shear Surface

Early & Skempton (1972) report the results of x-ray diffraction analyses performed by R.E. Grim in 1962 on samples of clay obtained from the shear zone in the Walton's Wood landslide and on samples of the ambient clay. They found that there was no difference between the mineralogy of the clay samples. In order to study any variation in mineralogy across the shear surface obtained from within the landslide at Soper's Wood, particularly with respect to clay mineralogy due to increased chemical weathering at the shear surface, samples from each of the lithological units shown in Figure 4.1 were analysed by x-ray diffraction (see Appendix I for laboratory technique).

Whole "rock" powder mounts were made up from each of the lithological units and these were analysed to identify the dominant non-clay minerals present in the lithological units. The x-ray diffractograms obtained

Plate 4.5 Photograph discriptions.

A. Plan view showing the smooth nature of the shear surface. Feint striations are visible.

B. Plan view of a tool mark gouged out by movement at the shear surface.

C. Plan view highlighting a band of striations on the shear surface.

D. Plan view of the material above and below the shear surface.

E. Cross-sectional view showing a layer of platy clay particles aligned parallel to the shear surface. Below the shear surface the clay particles are randomly orientated.

F. Cross-sectional view of the shear surface. Notice the alignment of the layer of clay minerals at the shear surface.

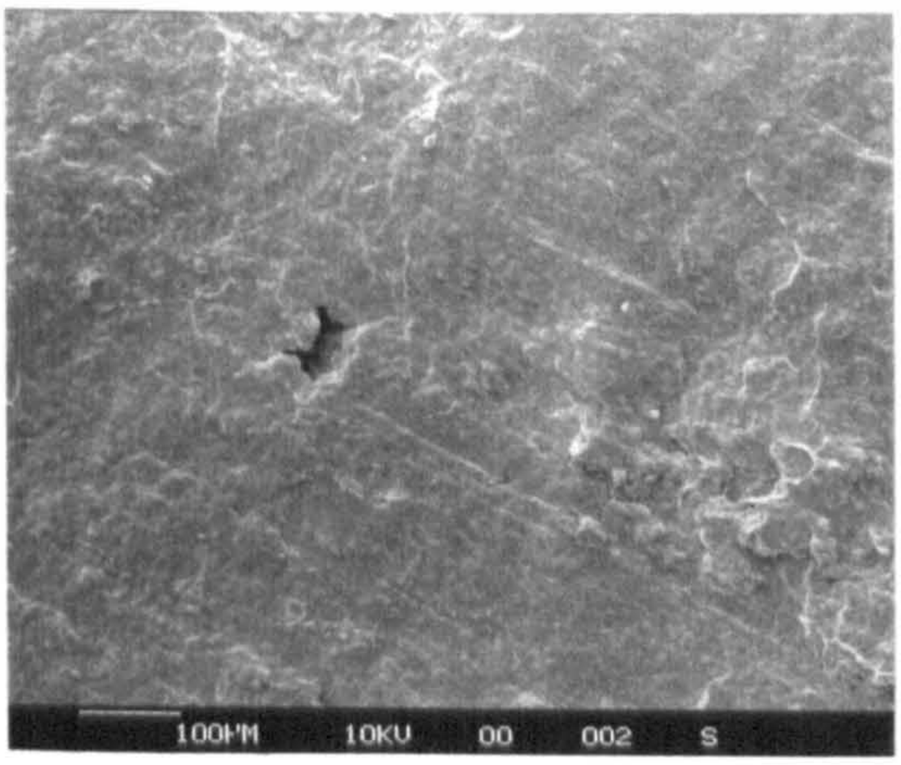

A.

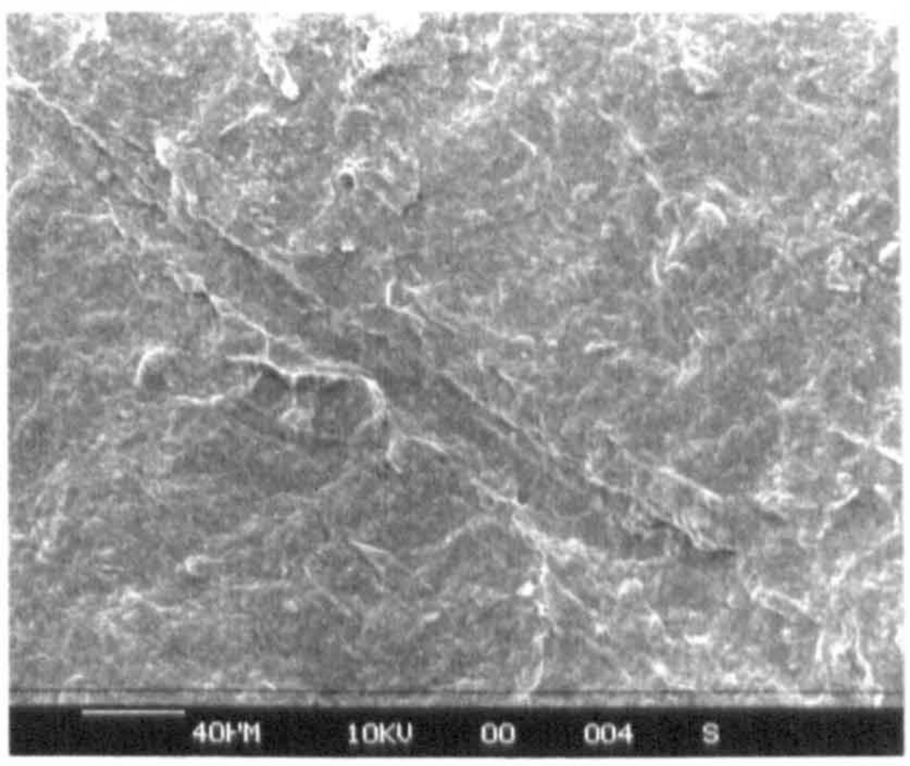

B.

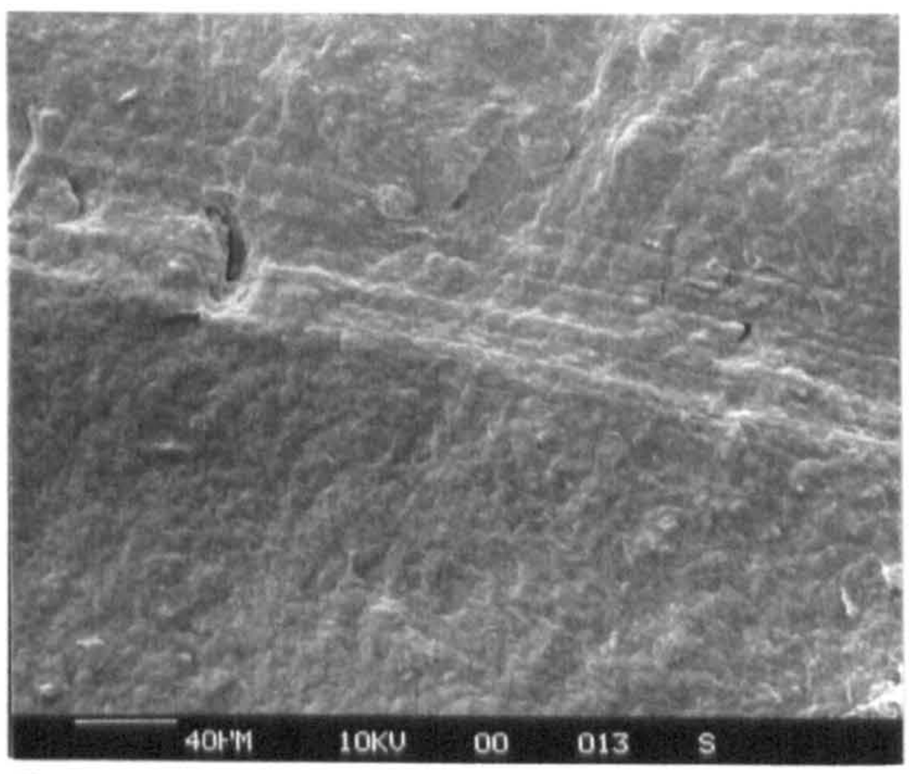

C.

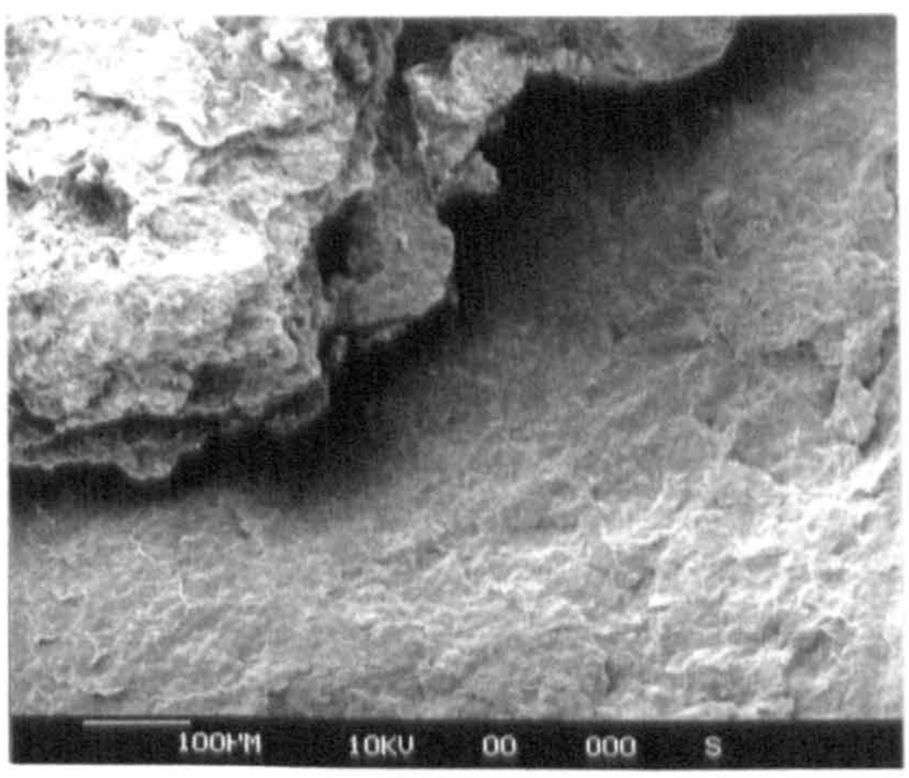

D.

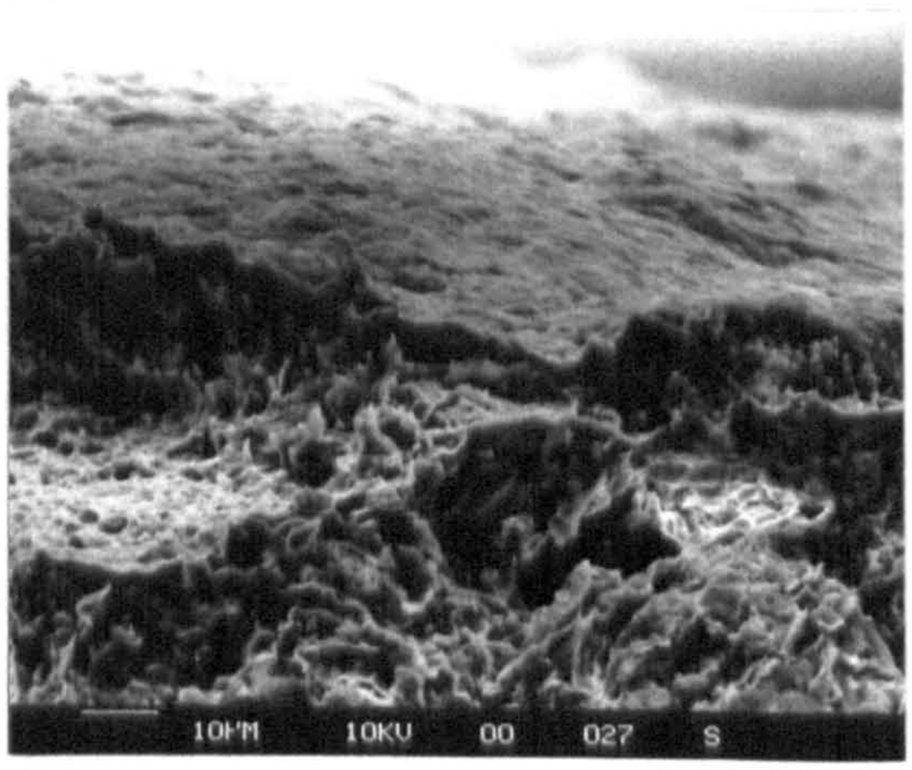

E.

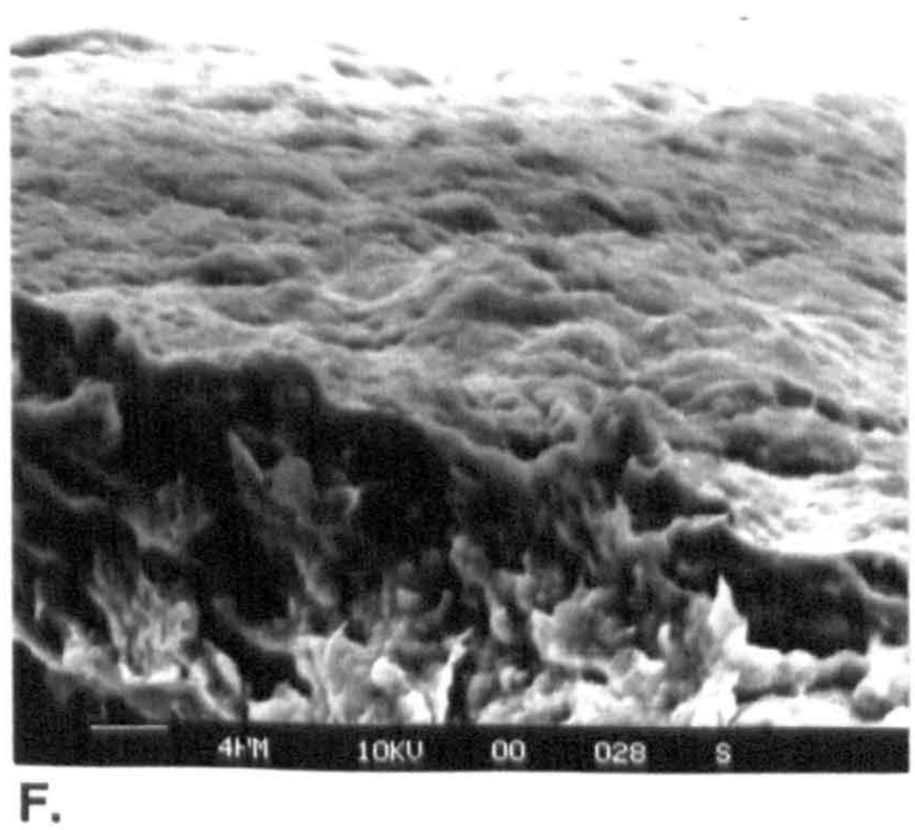

F.

Plate 4.5 Scanning electron micrographs of the shear surface obtained from the landslip at Soper's Wood, Bath.

from the whole "rock" powder mounts made up from units A and B, located below the shear surface, were dominated by quartz peaks with subordinate calcite peaks. However, the intensity of the peaks was generally relatively low, between approximately 200 and 400 counts, except for the (101) quartz reflection which was much higher at approximately 1450 counts in unit A and 1750 counts in unit B. In addition, minor peaks of feldspar, gypsum and pyrite were evident, however these were often partially masked by the more prominent peaks of quartz and calcite.

In comparison, the x-ray diffractograms from the whole "rock" powder mounts made up from units C to H, above the shear surface (unit C includes the shear surface), were dominated by calcite peaks with subordinate quartz peaks. In addition, above the shear surface, the intensity of the counts was generally higher between approximately 200 and 750 counts, except for the (104) calcite reflection which varied between approximately 900 and 2700 counts in the individual units and the (101) quartz reflection which varied between approximately 500 and 1150 counts. As found below the shear surface, minor peaks of feldspar, gypsum and pyrite were evident and again these were often partially masked by the more prominent peaks of calcite and quartz.

The variation in the observed calcite content above and below the shear surface is as expected from the calcite content profile shown in Figure 4.4. In addition, from a qualitative assessment of the relative intensity of the peak reflections, it appears that below the shear surface there is a relatively lower proportion of non-clay minerals compared to above the shear surface. This broadly correlates with the lithological description of the units and the very consistent moisture content of the material below the shear surface.

To investigate any variation in clay mineralogy across the shear surface due to weathering, the clay fraction (<2 μm) of the units was sedimented onto glass slides and air dried (see Appendix I). This technique ensures a high proportion of clay minerals are orientated with their basal (001) sections parallel to the slide, thus enhancing the clay mineral reflections. To aid the identification of the various clay minerals present the slides were then treated and analysed by x-ray diffraction in the following order; air-dried, treatment overnight with ethylene glycol at 60°C, heated to 300°C for at least 30 minutes and 550°C for a minimum of 4 hours. The order of the treatments is important as the effects of each stage are irreversible.

In each of the units analysed the following clay minerals were identified. Illite was identified in all the diffractograms by sharp well defined

reflections for (001) at approximately 10.36 Å , (002) at 5.09 Å and (003) at 3.38 Å. These peaks are unaffected by glycolation and heating.

Kaolinite was identified by reflections for (001) at 7.15 Å and (002) at 3.58 Å. The (001) and (002) reflections for kaolinite can be confused with the (002) and (004) reflections for chlorite, respectively. Heating the clay samples at 550°C causes the collapse of kaolinite to a metakaolin which shows no diffraction pattern (Brindley & Brown 1980). In all samples, the reflections at 7.15 Å and 3.58 Å totally collapsed on heating to 550°C, indicating the absence of chlorite.

Montmorillonite was identified by basal (001) spacings between 14 Å and 15.7 Å. The basal spacing of air dried samples of montmorillonite is known to depend on the interlayer cation, Grim (1953). This is supported by McAttee (1956) who noted that ideally at room temperature sodium montmorillonite would have a "single water layer" resulting in a (001) spacing of 12.4 Å, while calcium montmorillonite would have a "double water layer" and a corresponding (001) value of 15.4 Å. Hence, from the reflections of the basal spacing, the montmorillonite identified is calcium montmorillonite. This correlates with the presence of calcium rich ground waters found in the landslide at Soper's Wood (see Chapter 3). In all the units, the montmorillonite appeared to be interstratified with illite to some degree. Pure montmorillonite is identified by the presence of a regular sequence of reflections (Srodon 1980) and thus there would be a distinct (001) peak relative to the illite (001) peak. However, in all the samples there were diffuse reflections of intermediate basal spacings between the two peaks indicating a degree of interstratification. In addition, the (002) illite peak had a broad base, which on glycolation, shifted to form a low angle shoulder, characteristic of illite-smectite interstratification.

Treatment with ethylene glycol, causes the maximum expansion to about 17 Å of the basal spacing of the montmorillonite proportion of the interstratified clay mineral, whilst the illite basal spacing remains unaffected. Hence, glycolation increases the intensity of the (001) montmorillonite reflection, as well as shifting it relative to the (001) illite reflection, providing an indication of the proportion of the two component minerals. MacEwan (1949) reported a minimum requirement of a glycol saturated (001) peak at 17.7 Å for the confirmatory identification of montmorillonite. However, Srodon (1980) recorded a range of 16.5 to 17.3 Å and demonstrated that it depended on the layer charge density, the type of interlayer cation and the relative humidity. Schultz (1964) stated that heating to 300°C for at least 30

minutes volatises all the absorbed ethylene glycol and water within the montmorillonite lattice which results in a decrease in basal spacing to 10 Å, reinforcing the illite peak. However, in this study the volatisation of the adsorbed glycol and water only partially occurred at 300°C and the total collapse of the expanded montmorillonite occurred after heating to 550°C.

Srodon (1980) stated that the absence of a glycolated reflection between 5.3° and 8.7°2θ indicates that the interstratification is random. In addition, Srodon (1981) noted that, based on the work of Reynolds & Hower (1970), on glycolation where there are separate 10 Å and 17 Å peaks (characteristic of illite and montmorillonite) this is indicative of a randomly interstratified illite-smectite. All the samples analysed produced discrete illite and montmorillonite peaks on glycolation, with no intermediate reflections and hence the interstratification is likely to be random in nature, as first proposed by Lawrence (1985) and Hawkins *et al.* (1986 and 1988).

Srodon (1980) described three methods for determining the proportion of illite and montmorillonite in pure interstratified illite-montmorillonites. However, these methods are only applicable to relatively pure illite-smectites, as where there is a substantial proportion of discrete illite present (such as in naturally occurring soils), the methods cannot be used due to interference. Thus, Srodon (1981) suggested an alternative method, which uses glycolated reflections at about 15-16°2θ and 31-32°2θ. However, in this study the diffractograms did not show distinct enough signals for measurement, especially in the 31-32°2θ region. Indeed, Srodon (1981) stated:

"It may not be possible *(to use the method)* if the reflections are very diffuse (soil minerals), or if the amount of an expanding mineral in the mixture is small. Pure smectite can be identified in amounts as low as 10%. At the other end of the randomly mixed-layered series it may be difficult to identify precisely 40-45% S *(smectite)* mineral in quantities as high as 50% of a sample because at this illite-smectite layer ratio the 31-32°2θ peak becomes weak and diffuse."

Other methods for quantifying the proportions of minerals have been developed by various researchers. These use either the peak intensities of reflections or the calculation of the areas below the peaks (eg. Schultz 1964). However, due to the interference of the reflections of the clay minerals in the diffractograms obtained in this study, it becomes difficult to calculate the area beneath the peaks, or to measure an intensity of a peak above the variable general background level, and thus the results become

highly subjective. Hence, a qualitative analysis of the clay mineralogy found in the units at Soper's Wood has been carried out.

The qualitative clay mineralogy of the individual units, based on the x-ray diffraction data and diffractograms from both the untreated and treated slides, is shown in Table 4.1. The table identifies those clay minerals present in each unit and shows there approximate qualitative proportions. The calcium montmorillonite identified is randomly interstratified with illite and the approximate proportions of illite and Ca-montmorillonite are as identified from an analysis of the intensity of the (001) montmorillonite reflection and the (001) illite reflection of the glycolated samples. The proportion of illite includes that of pure illite and illite randomly interstratified with Ca-montmorillonite, as due to interference between reflections it is difficult to distinguish between the two. In addition to the clay mineralogy, minor reflections of quartz were evident in units A and B and minor reflections of calcite and quartz were evident in units C to H. However, these reflections were significantly reduced compared to the whole "rock" samples, indicating that the majority of quartz and calcite is greater in size than 2 μm.

XRD UNIT	QUALITATIVE PROPORTION OF CLAY MINERALS
H	illite>Ca-montmorillonite>kaolinite
G	Ca-montmorillonite>illite>kaolinite
F	Ca-montmorillonite>illite>kaolinite
E	Ca-montmorillonite≈illite>kaolinite
D	Ca-montmorillonite>illite>kaolinite
C	Ca-montmorillonite>>illite>kaolinite
B	Ca-montmorillonite>>>illite≈kaolinite
A	Ca-montmorillonite>>>illite≈kaolinite

Table 4.1 Qualitative proportion of clay minerals identified in the XRD units.

Units A and B are dominated by interstratified calcium montmorillonite and contain approximately equal proportions of illite and kaolinite. Unit C contains slightly less Ca-montmorillonite, but is still dominated by calcium montmorillonite and contains subordinate kaolinite. Figure 4.8 displays the diffractograms for unit C. Unit D, immediately above the shear surface, is less dominated by interstratified calcium montmorillonite but still shows a similar trend of

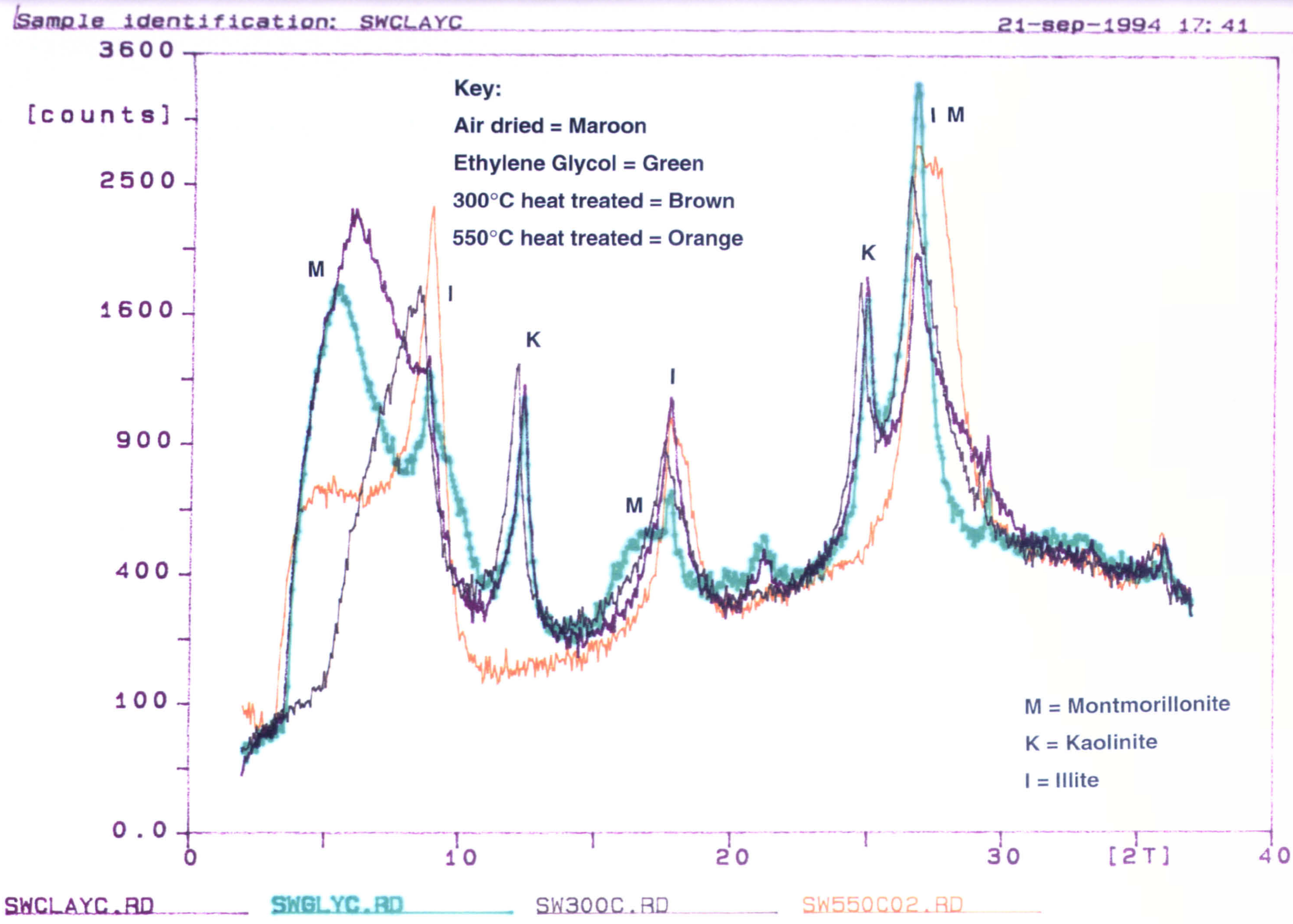

Fig. 4.8 Clay fraction (< 2μm) x-ray diffractograms for unit C.

Ca-montmorillonite>illite>kaolinite. A similar relationship is also shown by units F and G. However, unit E shows approximately equal proportions of illite and interstratified Ca-montmorillonite with sub-ordinate kaolinite and in unit H, illite is dominant, followed by interstratified Ca-montmorillonite and kaolinite. Figure 4.9 displays the diffractograms for unit E as an example.

These qualitative results indicate that there is an increased proportion of calcium montmorillonite randomly interstratified with illite in unit C, containing the shear surface, compared to in units D to H above, in the recently slipped ground. This may be interpreted to indicate that the preferential percolation of acidic ground waters along the shear surface encourages increased rates of chemical weathering at the shear surface. Hence, potassium is leached from illite at a greater rate, resulting in the formation of a higher proportion of randomly interstratified illite-Ca-montmorillonite. The analysis has shown that the montmorillonite is calcium montmorillonite, which is to be expected as the ground water has been shown to be rich in Ca^{2+} (see Chapter 3).

Above the shear surface the clay in units D to H still contains Ca-montmorillonite, but in smaller, variable proportions. This is as expected, as from the moisture content profile it was interpreted that above the shear surface the recently slipped clay would be disturbed and fractured, resulting in a secondary permeability. This allows the infiltration of surface water and hence some chemical weathering can be expected to occur.

The very high proportion of Ca-montmorillonite in those units below the shear surface is contrary to that expected. From the lithology and the moisture content profile, these units were interpreted to indicate that the recently unslipped material below the shear surface was less permeable and lithologically more uniform. In addition, it was suggested that the shear surface may act as a barrier to the vertical percolation of ground water across it. This was supported by observations made using the SEM which demonstrated the parallel orientation of clay minerals at the shear surface. One possible explanation for the increased weathering apparent in units A and B is that stress relief in this relatively near surface material has resulted in the dilation of the clay. Thus, ground water, possibly emerging from nearby limestone bands within the Fuller's Earth, is able to migrate through this more uniform recently unslipped clay and hence, over time, weathering has occurred.

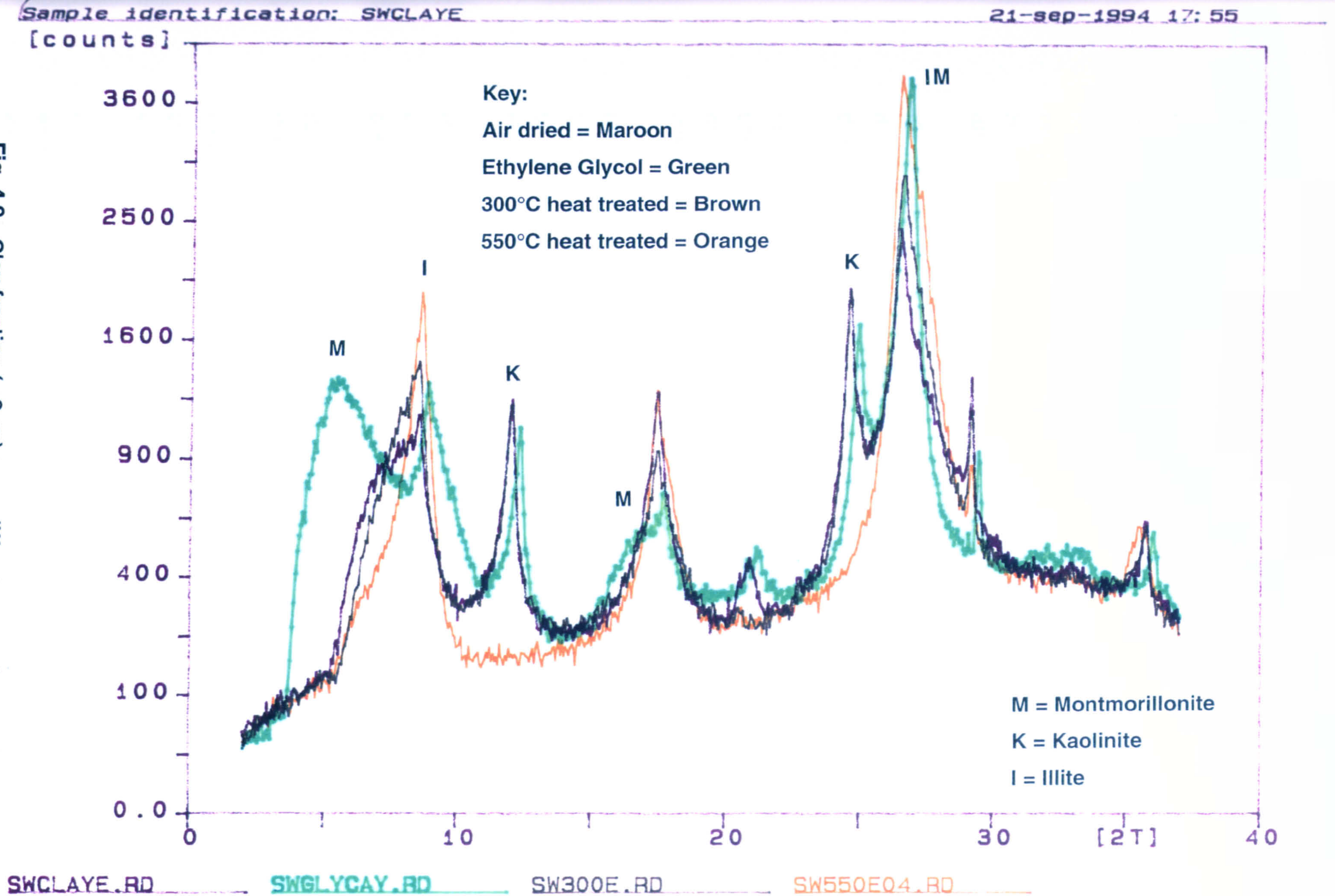

Fig. 4.9 Clay fraction (< 2μm) x-ray diffractograms for unit E.

4.9 Conclusions

(1) Moisture content analysis has demonstrated the more variable levels of moisture content in the recently slipped ground immediately above the shear surface (23% to 96%) compared to the more uniform levels in the recently unslipped material below it (60% to 66%). This is interpreted to indicate that the recently slipped material is more disturbed and permeable relative to the recently unslipped material below the shear surface. However, the values below the shear surface are still high and this is attributed to the generally dilated nature of the near surface material.

(2) Calcite content analysis provided no evidence of preferential decalcification along the shear surface. This may be due to the thickness of the samples relative to the shear surface.

(3) The study has re-emphasised the inverse relationship between calcite content and moisture content for the Fuller's Earth clay. The nature of this relationship is remarkable considering the very small sample size of this study.

(4) A new method for normalising the moisture content to a calcite content of zero has been used successfully to investigate the moisture content of the clay minerals alone. This method assumes that all the moisture present is held in the clays.

(5) The normalised moisture content profile supported conclusion (1) and showed that the moisture content of the recently slipped clays is higher compared to that of the recently unslipped clays below the shear surface.

(6) SEM examination has demonstrated the parallel alignment of clay minerals at the shear surface due to shear displacement. The anisotropic alignment may be acting as a barrier preventing ground water percolating vertically across the shear surface. Hence, the higher normalised moisture contents seen above the shear surface and the marked change in both the standard and normalised moisture content at the shear surface.

(7) Under SEM examination no silt/sand particles were observed embedded on the shear surface and it appeared remarkably smooth, indicating that shear is likely to be occurring in the sliding mode, according

to Lupini *et al.* (1981). This may be due to the dissolution of the calcitic particles at the shear surface by percolating ground waters.

(8) XRD analysis of the clay mineralogy of the shear surface and surrounding material indicates that increased rates of illitic weathering, resulting in the formation of an increased proportion of inter-stratified illite-Ca-montmorillonite, is likely to be occurring along the shear surface.

(9) The study has proved the validity of the sampling techniques and further research could be carried out on a deeper, more established, "gleyed" shear surface at an alternative site in the Fuller's Earth using these methods.

CHAPTER 5

AN INVESTIGATION INTO THE EFFECTS OF CALCIUM IN PORE WATER ON THE RESIDUAL SHEAR STRENGTH OF CLAYS

5.1 Introduction

The chemical analysis of the ground water within the landslide at Soper's Wood, described in Chapter 3, highlighted the dominance of calcium. The concentration of calcium was found to vary with location within the slip and to correlate broadly with seasonal precipitation. Chapter 2 reviews previous work carried out to investigate the effects of pore water chemistry on residual shear strength and emphasises the influence of pore water chemistry, although there is some conflict between the results of different authors. Hence, this chapter describes an investigation to study the effects of calcium in pore water on the residual shear strength of pure clays, related to the landslide at Soper's Wood.

Previous research has studied the effects of pore water chemistry on residual shear strength at one particular effective normal stress, ignoring the effects of the curvature of the residual failure envelope. In the present study, the residual failure envelopes for pure clays treated with solutions of calcium, at concentrations approximate to the levels found in the ground water in the landslide at Soper's Wood, have been defined. This has enabled an analysis of the effective residual cohesion intercept, residual shear angle and residual shear strength at various effective normal stresses. In order to interpret the results and behaviour of the clays it is important to have an understanding of clay mineralogy and its associated chemistry. Hence, these are reviewed below.

5.2 A Review of Clay Structure (based on the work by Grim 1968, van Olphen 1977, Bowles 1979 and Brady 1990)

Clay minerals are phyllosilicates formed by the interlocking of silica dominated and aluminium/magnesium dominated sheets. There are two main building blocks for the sheets, silica tetrahedra and aluminium/or magnesium octahedra, respectively. In the silica tetrahedra, each silicon atom is equidistant from four oxygens with silica at the centre, these tetrahedra are then joined horizontally to form a "tetrahedral sheet" or "silica sheet". In the second structural unit, the octahedra consist of an aluminium (or magnesium) ion surrounded by six oxygen or hydroxyl groups, these are

then linked horizontally to from an "octahedral sheet", also called the "gibbsite sheet" (aluminium) or "brucite sheet" (magnesium). Shared oxygen atoms between the sheets bind them together to form unit layers, which are stacked on one another to form the clay mineral. The specific nature and combination of the sheets within the layers allows the formation of various clay types and controls their physical and chemical properties. There are three main clay types formed by these combinations:

1: 1 Type minerals

The most commonly occurring clay mineral in this group is kaolinite. The "unit layers" of this group consist of one silica sheet and one gibbsite sheet bound tightly together by shared oxygen atoms. The unit layers are then held together by hydrogen bonding and van der Waals forces. These forces result in considerable strength, with little tendency for the interlayers to take on water and swell, and the effective surface area is restricted to its outer faces. This together with little isomorphic substitution, provide 1:1 clays with a relatively low capacity to adsorb ions. Their average specific surface area is between 5-20 m^2/g and their average size is between 0.5-5.0 μm.

2:1 Type minerals

Here the unit layers consist of one octahedral sheet sandwiched between two tetrahedral sheets. The group consists of three broad types of minerals, expanding, limited expanding and non-expanding.

In the expanding group or smectite group, of which montmorillonite is the most common member, the unit layers are held loosely together by a combination of very weak oxygen-oxygen and cation to oxygen linkages. The cations are attracted to the external and interlayer surfaces of the clay due to the isomorphic substitution of aluminium for silica in the tetrahedral sheet and magnesium for aluminium in the octahedral sheet, creating a negative charge imbalance. The cations, with there associated water molecules, cause expansion of the clay mineral. In the expanding group the large internal surface area exceeds the external surface area and the average specific surface area is between 700-800 m^2/g. Their size is between 0.01-1.0 μm.

Limited expanding clay minerals such as the vermiculites have much more isomorphic substitution in the octahedral and tetrahedral sheets and therefore have a very high negative charge imbalance. This causes the water and cations to be strongly adsorbed in the interlayer space. Hence, due to the strength of the adsorption, they bind the unit layers together and there is less expansion compared to smectites.

The non-expanding group consists of fine grained micas and illite. Here the major source of charge imbalance is caused by the isomorphous substitution of about 20% of the silica atoms in the tetrahedral layer causing a high negative charge in the interlayer space. Potassium ions are strongly attracted to the interlayer space and, as they are of the right size to fit into the spaces adjoining the tetrahedral sheets, act as a binding agent and the mineral is non expansive. Properties such as hydration, cation adsorption and swelling are less intense than in smectites but more than in kaolinite. The specific surface area and size is intermediate between kaolinite and smectite due to the tightly held interlayer potassium ions and the average is between 70-100 m^2/g and 0.2-2.0 μm, respectively.

2:1:1 Type minerals

This group is represented by the chlorites and they have a size and surface area similar to that of illite. Here 2:1 layers such as those found in vermicullites, alternate with a bruccite sheet which replaces the interlayer charge compensating cations found in vermicullites. Due to the replacement of some Mg by Al in the bruccite sheet, it carries a net positive charge which nearly compensates for the negative charge in the 2:1 layer. There is little water adsorption between the crystal units and so this type of clay is non-expansive.

5.3 Clay Mineral Chemistry (based on the work by van Olphen 1961 & 1977 and Brady 1990)

Clay minerals commonly exhibit an overall negative charge due to exposed crystal edges and isomorphous substitution. The charges caused by exposed crystal edges are due to the dissociation of the OH groups at the edge of the clay crystal. They are pH dependent, with a high pH causing increased dissociation and hence increased electronegativity, whereas at a low pH, protonation (the attachment of H^+ ions to the surface of the OH group) takes place and a positive charge is exhibited by the crystal edge. At an intermediate pH there may be no charge.

The charges caused by isomorphous substitution are constant and are much greater then those caused by broken crystal edges. The substitution may occur in both the tetrahedral and octahedral sheets and it is the ionic diameter which governs the substitution, not the pH. Under certain circumstances, eg if Al^{3+} replaces Mg^{2+}, a positive charge can result, however the substitutions leading to negative charges far outweigh those producing positive charges and so a net electronegativity results. Isomorphous substitution is common in 2:1 type clays and may occur in

certain 1:1 type clays, but to a lesser extent. In 1:1 type clays exposed crystal edge charges are the dominant cause of the electronegativity.

The negative charges associated with the clay particles attract cations which adsorb to the crystal surface. These are subject to replacement by cation exchange which depends on the valency, concentration, size and charge density of the various ions. Generally higher valency ions replace those of lower valency, however by mass action it is possible for a cation of a lower valency to replace an adsorbed cation of higher valency, if their concentration in the solution is very high. The adsorbed ions give rise to an ionic or electric double layer with the clay crystal forming the overall electronegative inner ionic layer and the adsorbed cations forming the outer layer. In addition, a large number of water molecules are attracted to the adsorbed cations which are hydrated. The adsorbed cations remain attached to the particle when the clay is dried, therefore when the dry clay is brought into contact with water a hydrated electric double layer is spontaneously created.

When clays form a dilute suspension in distilled water they disperse and the particles repel each other due to their smallness, their negative charge and diffuse double layer. In this situation the attractive van der Waals forces that exist between clay particles are unable to compete with the repulsive forces of the double layer. Highly hydrated mono-valent ions, which are not very tightly held by the clay particles, help to stabilize the dispersed solution. However, if di-valent or tri-valent ions are introduced to the solution, these are exchanged for the mono-valent ions, and are more tightly adsorbed to the crystal causing the diffuse counter ion atmosphere to be compressed towards the crystal surface. The degree of compression of the double layer is governed by the concentration and valency of the cations in solution. The higher the concentration and valency the more the double layer is compressed. Due to the compression of the double layer, the range of repulsion is considerably reduced and the attractive van der Waals forces are able to dominate and cause flocculation. The van der Waals forces remain practically the same regardless of the electrolyte concentration. The degree of flocculation is governed by the Schulze-Hardy rule which states that the higher the valence of the cations, the greater their flocculating power and hence the lower the flocculating concentration.

There is a second short range repulsive force, which should not be entirely disregarded, caused by hydration. A thin layer of water a few molecules thick is usually adsorbed to the particle surface and hence in

bringing the clay particles closer together, the work of desorption of the water is manifested as short range repulsion. The energies involved are not sufficiently large to affect the balance of the repulsive double layer forces and the van der Waals forces at the large distances from the surface of the clay, where the fate of the colliding particles is decided.

There are a number of different flocculating structures that can form depending on the charges that surround the clay particles. If the crystals have positive edges then a face to edge floc results, forming a card-house structure. However, if the crystals are a mixture of charges, then edge to edge or face to face structures may result, forming thick flakes.

5.4 A Review of Calcium Carbonate Dissolution

In pure water at 25°C calcium carbonate is only soluble to 14 mg/l, compared to gypsum 2400 mg/l, halite 370000 mg/l, and silica 5 mg/l (Drew 1985). However, in natural ground waters, concentrations of calcium carbonate of up to 450 mg/l are normal. This solvent action of natural waters depends dominantly on their acidity/aggressivity.

There are a number of sources of acidity in natural waters including sulphuric acid from 'acid rain', organic acids from decaying matter and mineral acids. However, the dissolution of calcium carbonate is dominated by carbonic acid from dissolved carbon dioxide (Gunn 1986), as it is a relatively strong acid and carbon dioxide is universally available, particularly within the unsaturated soil zone where it is generated by the decay of organic matter and by respiration from plant roots. Thus, this section will deal with the sequence of reactions caused by carbonic acid.

Picknett *et al.* (1976), Bögli (1980) and Spears (1986) provide detailed accounts of the sequence which Gunn (1986) has summarised as follows:

$$CO_{2(air)} + H_2O \rightleftharpoons CO_{2(aq)} + H_20 \qquad \textbf{Equation (5.1)}$$

Carbon dioxide in the soil atmosphere dissolves in water. Kinetically slow.

$$CO_{2(aq)} + H_20 \rightleftharpoons H_2CO_3 \qquad \textbf{Equation (5.2)}$$

Dissolved carbon dioxide hydrates to form carbonic acid. Kinetically slow.

$$H_2CO_3 \rightleftharpoons H^+ + HCO_3^- \qquad \textbf{Equation (5.3)}$$

Carbonic acid dissociates into hydrogen and hydrogen carbonate ions. Kinetically fast.

$CaCO_3 \rightleftharpoons Ca^{2+} + CO_3^{2-}$ **Equation (5.4)**

Calcium carbonate dissociates. Kinetically slow.

$H^+ + CO_3^{2-} \rightleftharpoons HCO_3^-$ **Equation (5.5)**

The CO_3^{2-} produced in equation (5.4) associates with H^+ from equation (5.3) to from hydrogen carbonate. Kinetically fast.

The reaction in equation (5.5) acts as a driving force reactivating the other four processes. The removal of the CO_3^{2-} from the solution-mineral interface drives reaction (5.4) to the right causing more calcium carbonate to dissolve. The association of H^+ with CO_3^{2-} in equation (5.5) upsets the equilibrium and drives reaction (5.3) to the right causing further dissociation of H_2CO_3. This in turn disturbs the equilibrium in equation (5.2) causing further carbon dioxide to dissolve in the water. This cycle continues until the system is in equilibrium and the forward and reverse reaction rates are equal. At this point the solution is saturated with calcium carbonate (Picknett *et al.* 1976).

The full sequence can be summarised by the equation:

$CaCO_3 + H_2CO_3 \rightleftharpoons Ca^{2+} + 2HCO_3^-$ **Equation (5.6)**

There are two main conditions for calcite dissolution, "open-system conditions" and "closed-system conditions" (Freeze & Cherry 1979). In open conditions there is an abundant supply of carbon dioxide present and the amount of dissolved carbon dioxide remains constant. This situation occurs when rain water infiltrates into the soil and dissolution of calcium carbonate occurs above the water table where abundant carbon dioxide is present in voids.

Closed systems exist when the supply of carbon dioxide is cut off before reaction with calcium carbonate and the H_2CO_3 consumed during reaction is not replenished by further dissolving of carbon dioxide. This would occur when rain water passes through a non carbonate unsaturated soil zone to the saturated zone charged with carbon dioxide. If it then encounters carbonate minerals, dissolution will occur and the concentration of dissolved carbon dioxide will decline due to the absence of any carbon dioxide containing voids in the saturated zone. Hence, the amount of calcium carbonate that can be dissolved is less than in open conditions.

Equilibrium pH's (ie at saturation) are lower, usually below 8, and the HCO_3. and Ca^{2+} concentrations are higher under open conditions, due to the increased solubility for a given initial carbon dioxide partial pressure.

However, it is important to note that ground water may proceed through both these idealised conditions during its lifetime.

In addition, water saturated with respect to calcium carbonate is unlikely to remain in equilibrium for very long. For example, water in an open system, saturated with calcium carbonate under relatively high partial pressures of carbon dioxide, will reach a state of disequilibrium if it moves into an area where there is a lower partial pressure of carbon dioxide. The dissolved carbon dioxide will degass quicker than the precipitation of calcium carbonate and the water would become supersaturated. In addition pH will rise. If the water were to remain in this zone for a period of time a new equilibrium would be reached with the precipitation of the excess calcium carbonate.

For any fixed partial pressure of carbon dioxide in contact with water, solubility increases with decreasing temperature. Hence, due to increased acidity, the solubility of calcite increases at approximately 1.3% per degree, according to Picknett *et al.* (1976). However, though this is true in experimental systems, in natural ground waters, carbon dioxide partial pressures and the nature of the system are also important controls on solute concentrations (Smith & Anderson 1976).

5.5 The Laboratory Simulation of Calcium Carbonate Dissolution

The work described in Chapter 3 indicated that in the landslide at Soper's Wood, the dissolution of calcium carbonate is likely to be a major source of calcium in the ground water. Therefore, in order to try and simulate natural ground water chemistry as closely as possible, experiments were conducted to create stable solutions of calcium ions in the laboratory from the dissolution of calcium carbonate. These solutions could then be used in ring shear tests to investigate the effects of pore water chemistry on the residual shear strength of clays.

The review of calcium carbonate equilibria highlights its instability. In addition, carbonic acid is unstable in the laboratory under normal atmospheric conditions. Thus, a technique was developed to create a system where there was abundant carbon dioxide under high partial pressures causing any calcium carbonate present in the system to dissolve. By varying the amounts of calcium carbonate in the system, it was expected that solutions of different Ca^{2+} concentrations could be created. These solutions then needed to be tested for their stability over a period of time, equivalent to the length of a ring shear test, as any precipitation of calcium

carbonate from solution during a ring shear test is likely to alter the residual shear strength of a clay sample.

5.5.1 Laboratory Technique

Three sets of experiments were conducted and the following basic technique was used, with some adaptions in the third experiment.

Heavy 100 ml polyethylene bombs, which could withstand pressures of 125 p.s.i (856 kN/m^2), were thoroughly cleaned and filled with 100 ml of "Purite" (deionised water). A predetermined amount of "analR" grade calcium carbonate was then added, together with 5 g of dry ice and the lid quickly sealed. The lids were then machine tightened to 11 N.

The bombs were thoroughly shaken and then left for 5 days to allow the system to equilibrate, after which they were opened and 10 ml aliquots pipetted off twice a day until no solution remained. The pH of the bulk solution was measured prior to each pipetting. The aliquots were then placed in evaporating dishes. Once evaporation had been completed the precipitated calcium carbonate was weighed and the amount of dissolved calcium carbonate calculated at the time of extraction of the aliquot. A profile with time of the concentration of Ca^{2+} could then be constructed to assess the stability of the solutions.

The polyethylene bombs were under intense pressure and on sealing, the safety valve of the bombs was often explosively released, indicating that 125 p.s.i (856 kN/m^2) had been exceeded.

5.5.2 Experiment 1

Three bombs were set up each containing 0.1 g $CaCO_3$, 5 g dry ice and 100 ml Purite (providing a calculated concentration of 400 mg/l Ca^{2+}). Figure 5.1 shows the change in the concentration of Ca^{2+} and pH, with time after opening, for the three bombs. Ca^{2+} concentrations may be multiplied by a factor of 2.5 to find the amount of dissolved calcium carbonate. Bombs 1 and 2 display similar patterns with an initial drop in Ca^{2+} concentration. The level then remained approximately constant until the 28th hour, when it drops off rapidly. This is supported by the appearance of a white scum of $CaCO_3$ floating on the surface of the solution, which is comparable to the rafts of $CaCO_3$ seen floating in travertine systems, described by Chafetz *et al.* (1991). The pattern is less clear for the third bomb. All the bombs show a trend of increasing pH with time, which is rapid at first, probably due to the initial rapid exsolving of dissolved carbon dioxide.

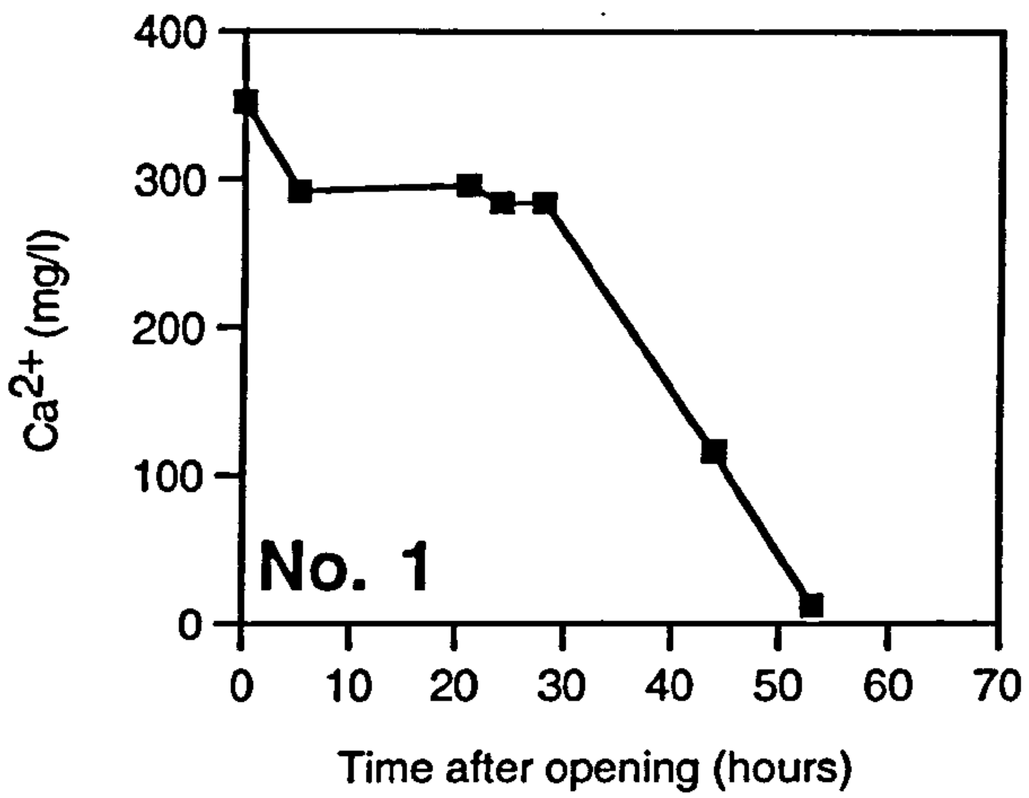

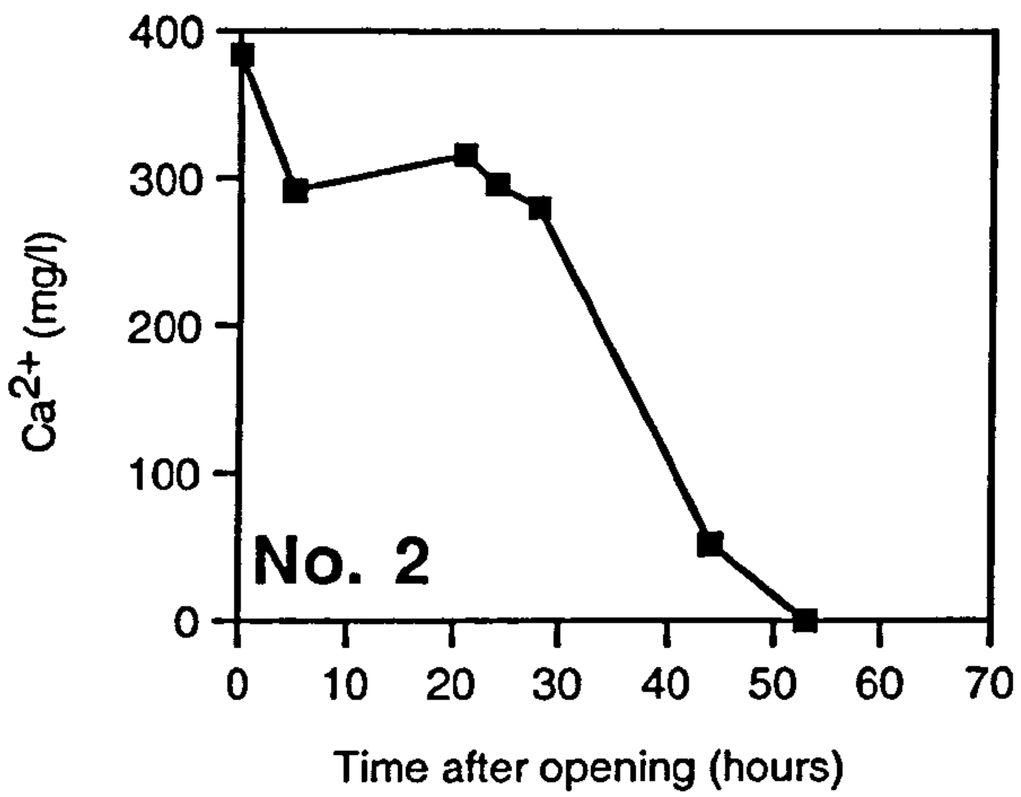

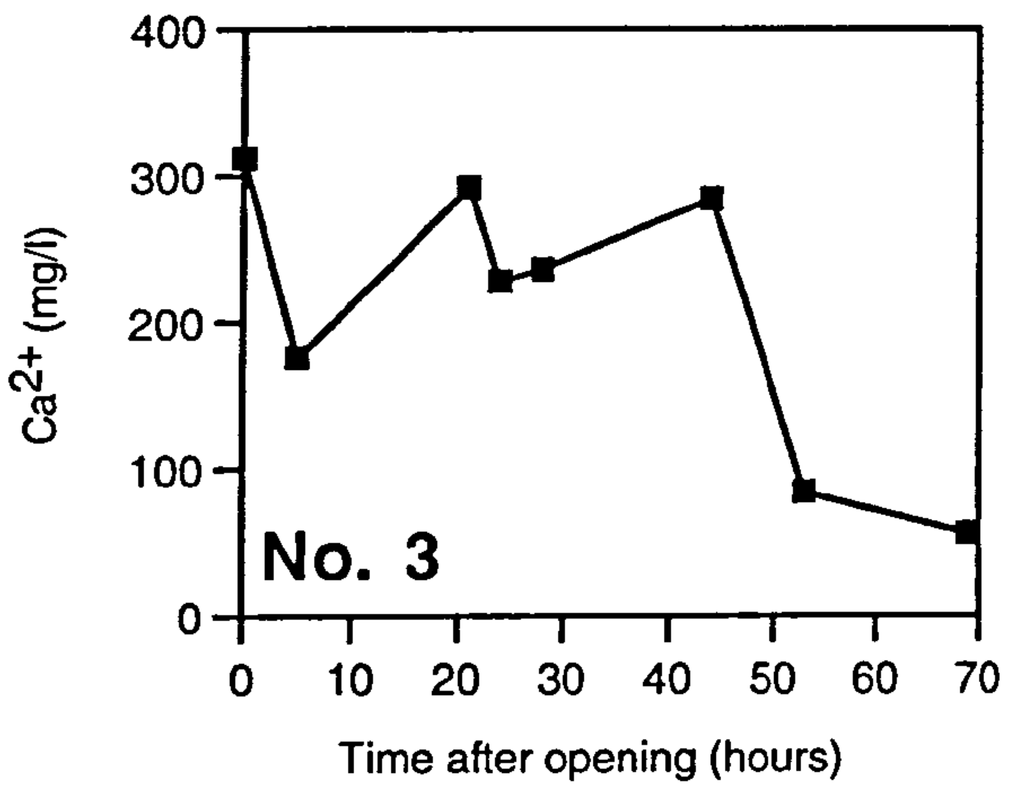

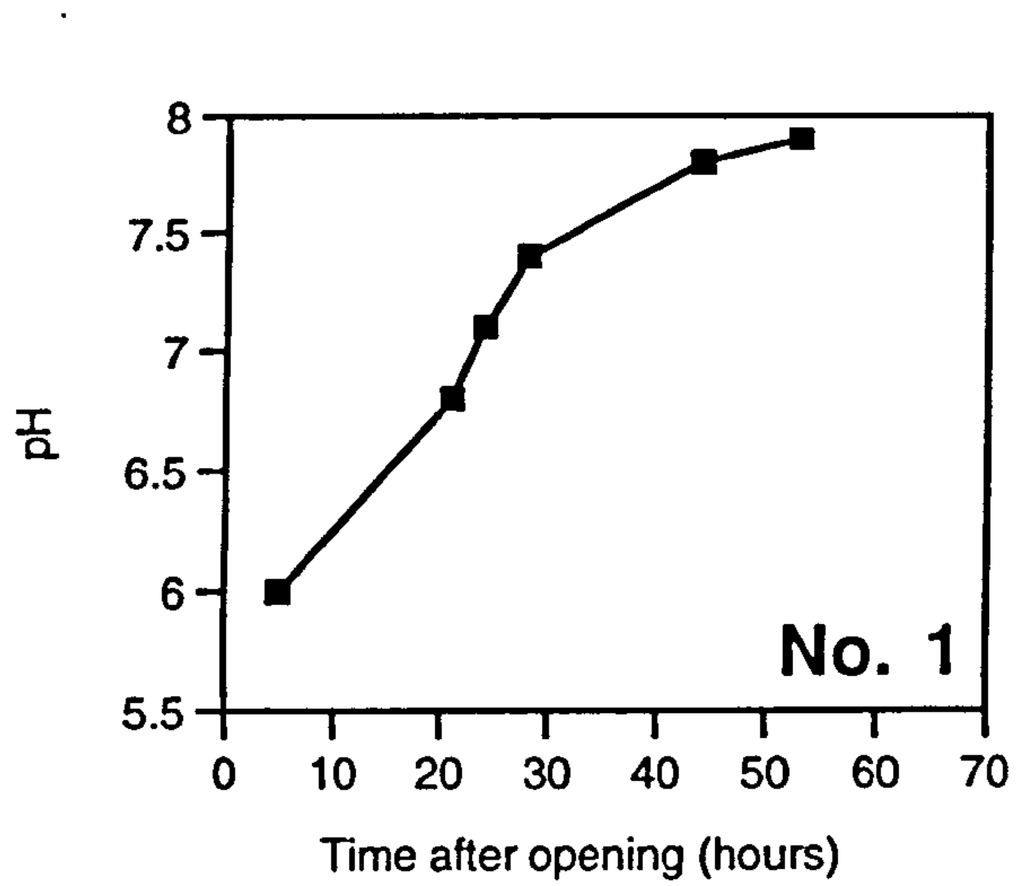

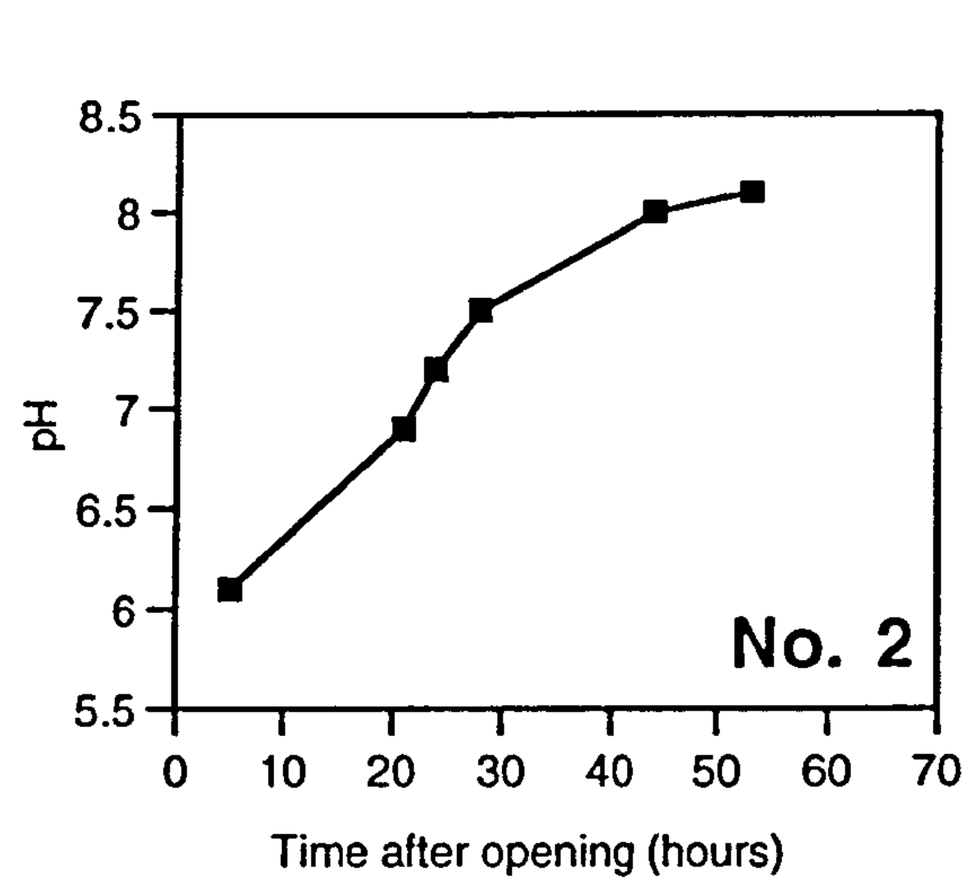

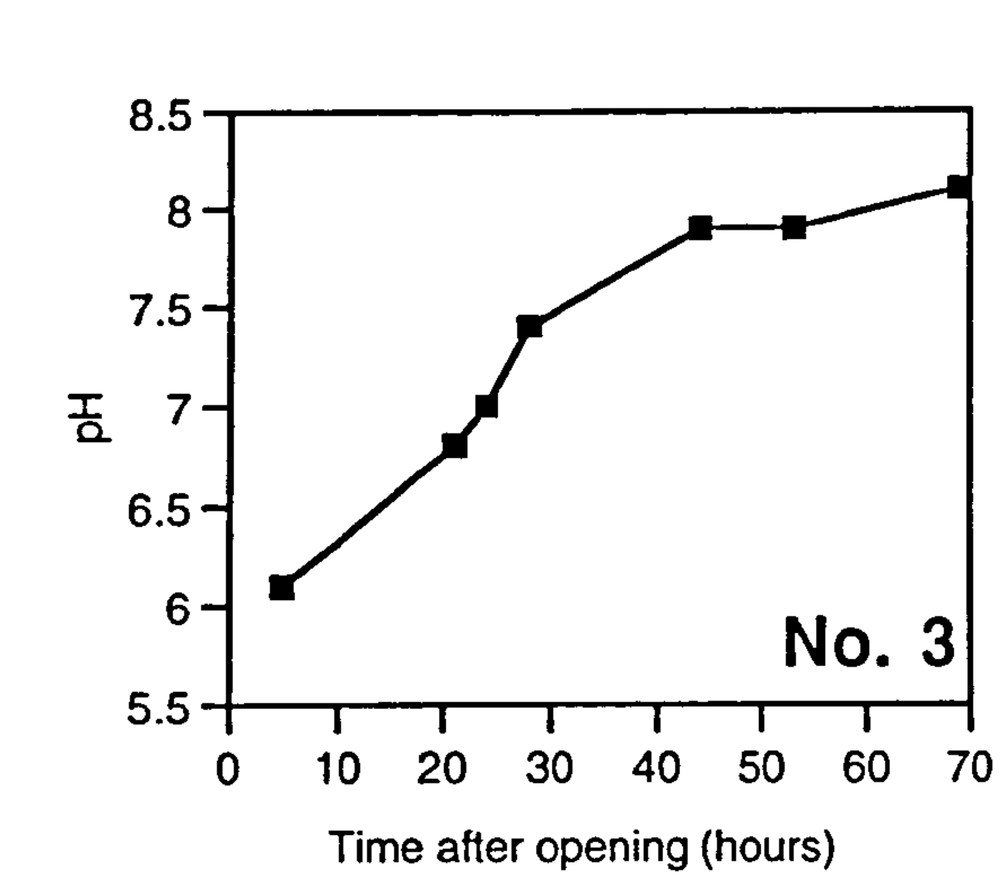

Fig. 5.1 Graphs showing the variation in calcium concentration and pH for bombs 1, 2 and 3.

The results from this initial experiment indicated that it may be possible to create stable solutions of Ca^{2+} for a 24 hour period, using this technique.

5.5.3 Experiment 2

A second, more detailed experiment was conducted to confirm and further define the stability of the Ca^{2+} solutions. Seven bombs were used, approximately representing the range of $CaCO_3$ concentrations found in the ground water at Soper's Wood:-

P =100ml Purite + 5g dry ice (control)
A =100ml Purite + 5g dry ice + 0.005g $CaCO_3$ (equivalent to 50mg/l $CaCO_3$)
B =100ml Purite + 5g dry ice + 0.01g $CaCO_3$ (equivalent to 100mg/l $CaCO_3$)
C =100ml Purite + 5g dry ice + 0.02g $CaCO_3$ (equivalent to 200mg/l $CaCO_3$)
D =100ml Purite + 5g dry ice + 0.03g $CaCO_3$ (equivalent to 300mg/l $CaCO_3$)
E =100ml Purite + 5g dry ice + 0.04g $CaCO_3$ (equivalent to 400mg/l $CaCO_3$)
F =100ml Purite + 5g dry ice + 0.05g $CaCO_3$ (equivalent to 500mg/l $CaCO_3$)
G =100ml Purite + 5g dry ice + 0.06g $CaCO_3$ (equivalent to 600mg/l $CaCO_3$)

Figure 5.2 shows how calcium ion concentration varies with time after opening, for each bomb. Most of the bombs show the same pattern, however the relationship is very different to experiment one and it is hard to draw any conclusions from the results. The pattern is also displayed by the control sample, indicating that it may be caused by experimental error.

Figure 5.3 shows the variation of solute pH with time for the various bombs. In all cases pH increases with time after opening and all show similar relationships. In addition, the pH for all the bombs is significantly higher than the control due to the dissolved $CaCO_3$ acting as a buffer, hence those bombs with greater quantities of $CaCO_3$ have higher pH's.

5.5.4 Experiment 3

The results from experiment 2 provided no clear answers and it was thought that experimental error due to the method of evaporation and weighing may have affected the results. It was therefore decided to undertake a similar experiment, but this time to analyse the concentration of calcium in the aliquots using atomic adsorption spectroscopy as this would be more accurate (see Appendix I). In addition, 8 ml aliquots were taken to further define the profiles. The temperature in the laboratory was also

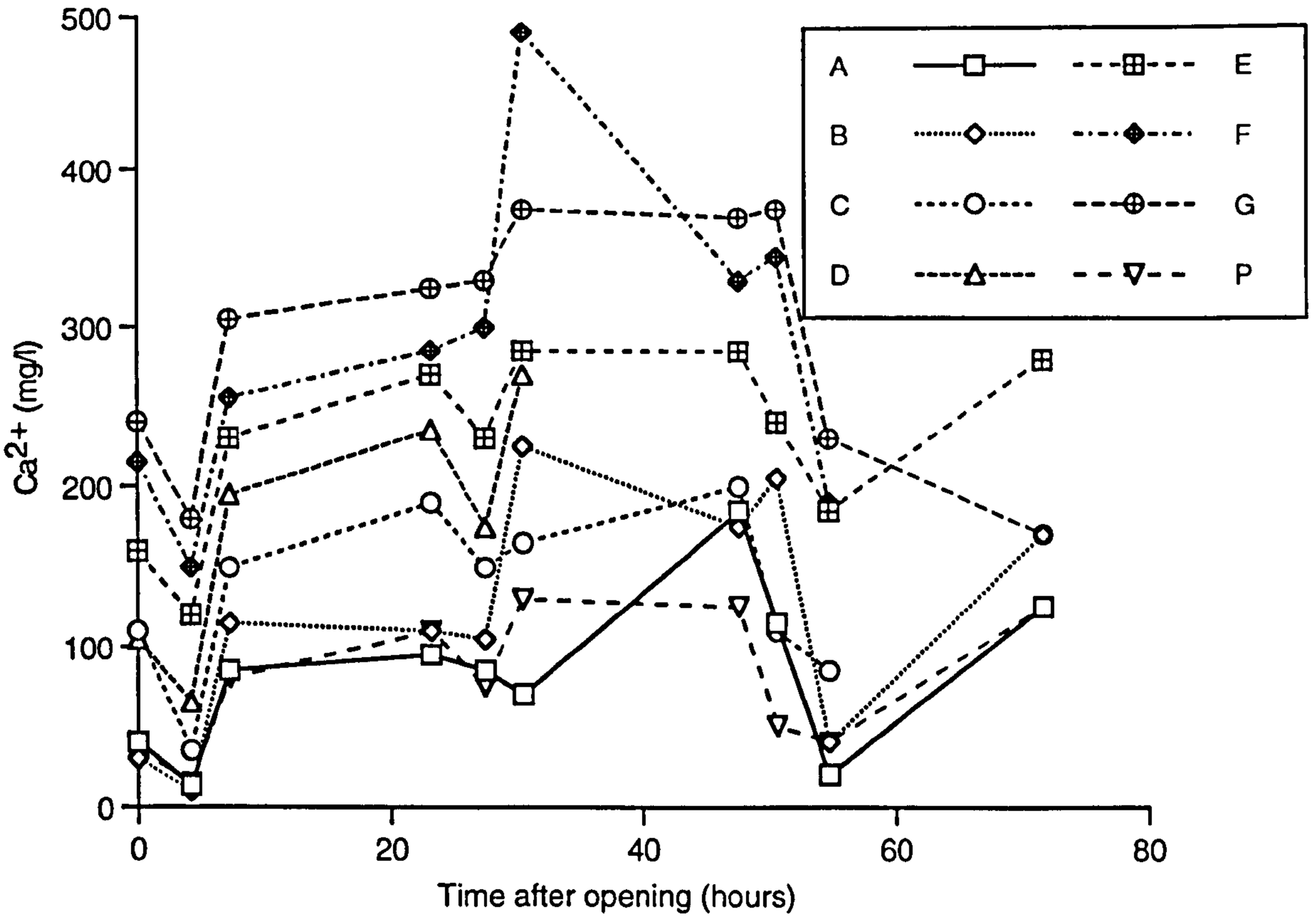

Fig. 5.2 Graph showing the variation in Ca^{2+} concentration for the second experiment.

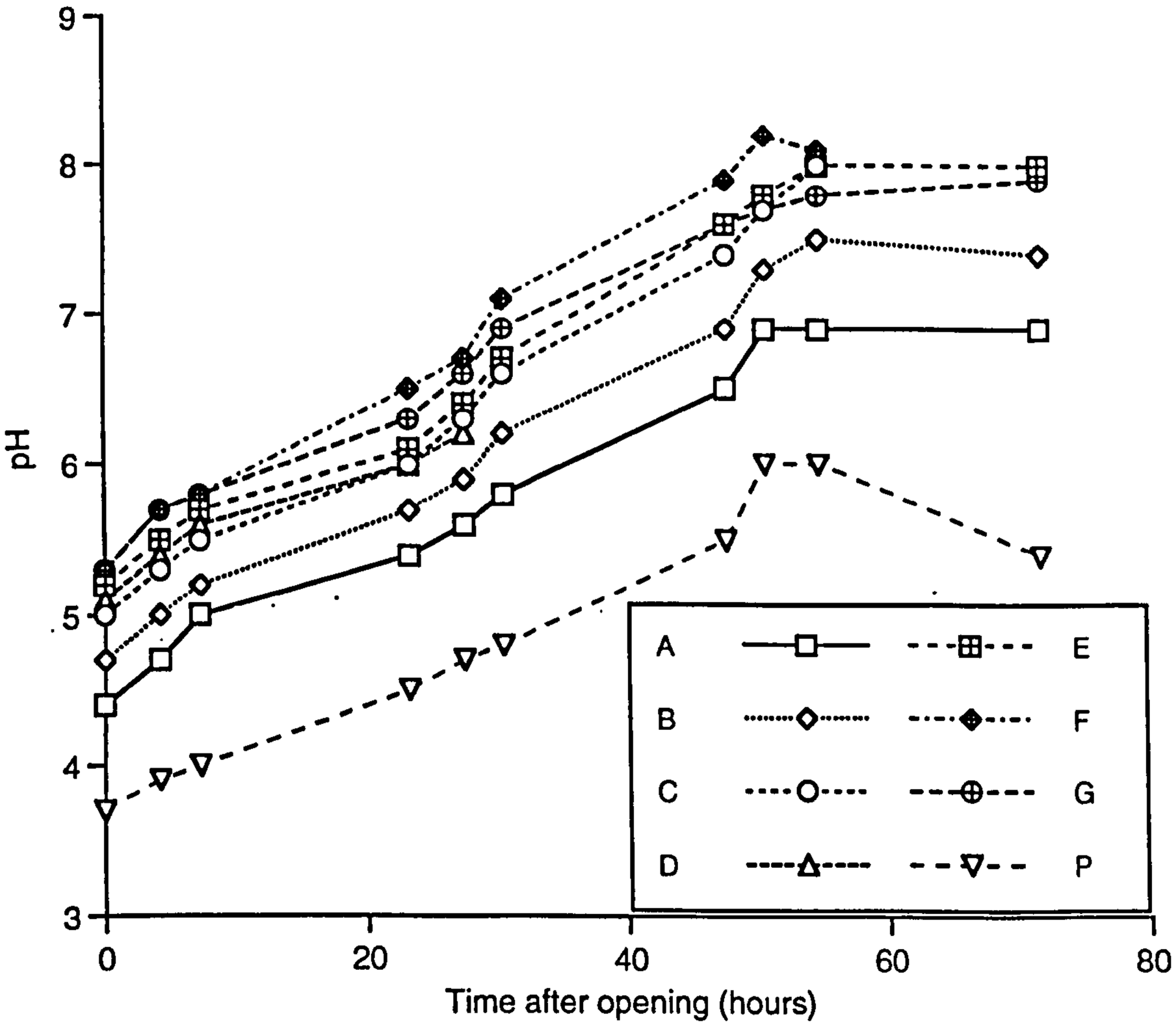

Fig. 5.3 Graph showing how pH varies with time for the second experiment.

monitored using a thermograph. Six polyethylene bombs were used, containing different amounts of calcium carbonate:-

P =100ml Purite + 5g dry ice (control)
A =100ml Purite + 5g dry ice + 0.01g $CaCO_3$ (equivalent to 100mg/l $CaCO_3$)
B =100ml Purite + 5g dry ice + 0.02g.$CaCO_3$ (equivalent to 200mg/l $CaCO_3$)
C =100ml Purite + 5g dry ice + 0.03g $CaCO_3$ (equivalent to 300mg/l $CaCO_3$)
D =100ml Purite + 5g dry ice + 0.04g $CaCO_3$ (equivalent to 400mg/l $CaCO_3$)
E =100ml Purite + 5g dry ice + 0.05g $CaCO_3$ (equivalent to 500mg/l $CaCO_3$)
F =100ml Purite + 5g dry ice + 0.06g $CaCO_3$ (equivalent to 600mg/l $CaCO_3$)

Figure 5.4 shows the variation in Ca^{2+} concentration with time and indicates that the solutions may be stable over a longer period than previously thought, however there is still some variation in the concentrations. An analysis of how solution pH varies with time in Figure 5.5 demonstrates a gradual rise in pH over the period, as seen in the first two experiments. In addition, the temperature in the laboratory was found to vary between 15°C and 26°C over the five day period.

5.5.5 Discussion of Results

The results from all three experiments show significant variation from each other, making it very difficult to say conclusively how long the solutions of calcium will be stable. In addition, the concentrations obtained are less than expected from chemical calculations. These inconsistencies would affect the results of any experiments conducted using these solutions to investigate the effect of Ca^{2+} concentration in pore water on the residual shear strength of clay. Following discussions with P. L. Smart (pers. comm., 1993), it was concluded that calcium carbonate equilibria is too unstable, being affected by carbon dioxide partial pressures, pH and temperature, which are all difficult to control during a ring shear test, as exemplified by the large variation in laboratory temperature during experiment 3. The idea of using calcium carbonate as a source of calcium ions was therefore abandoned in place of using calcium chloride as a solute, as it is highly soluble, stable and unlikely to form complexing agents in solution.

5.6 Investigation into a New Ring Shear Technique

The initial experiment indicated that the Ca^{2+} solutions may have only been stable for a 24 hour period and thus their chemical stability would have been inadequate for use in the routine ring shear test which takes

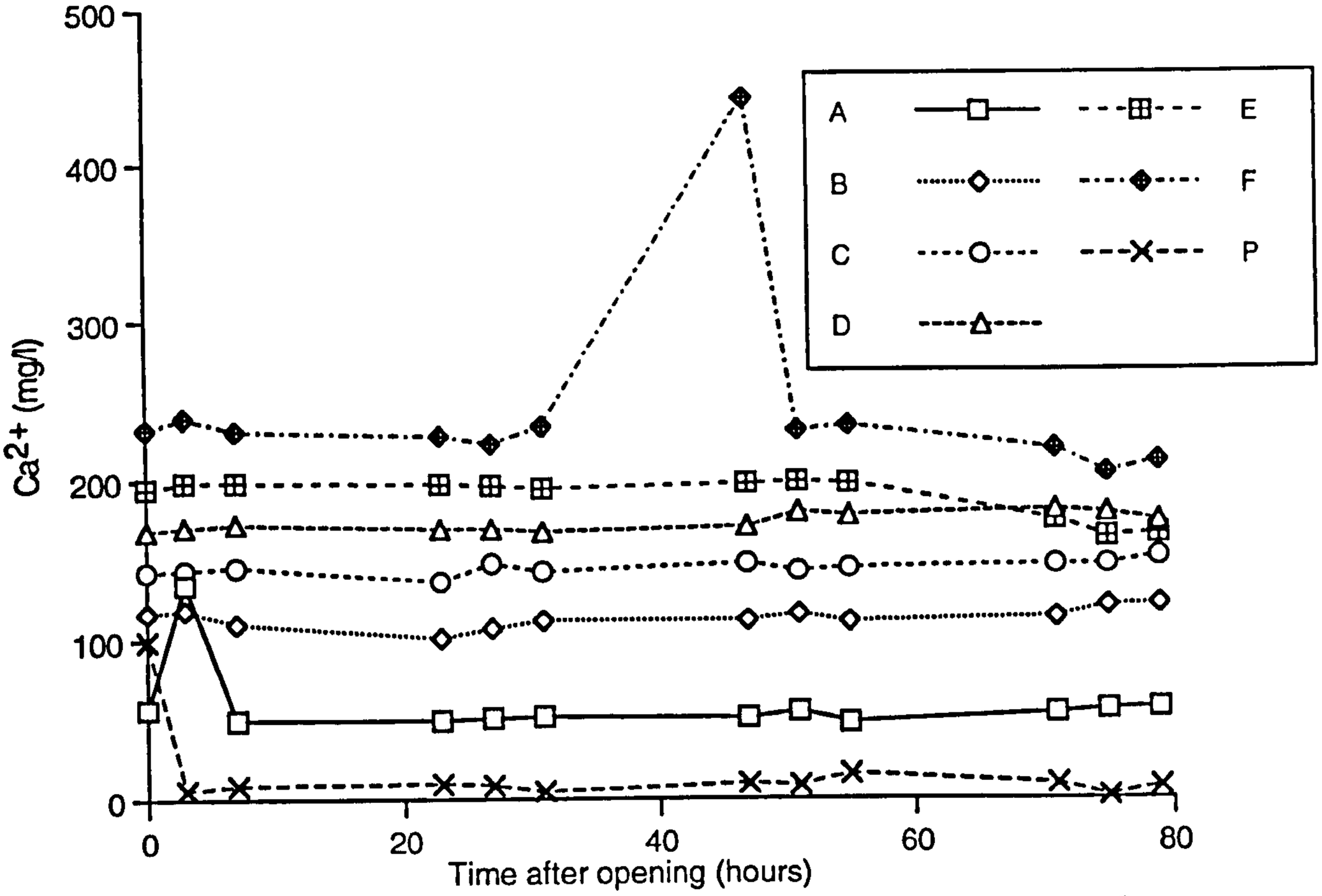

Fig. 5.4 Graph showing the variation in Ca^{2+} concentration for the third experiment.

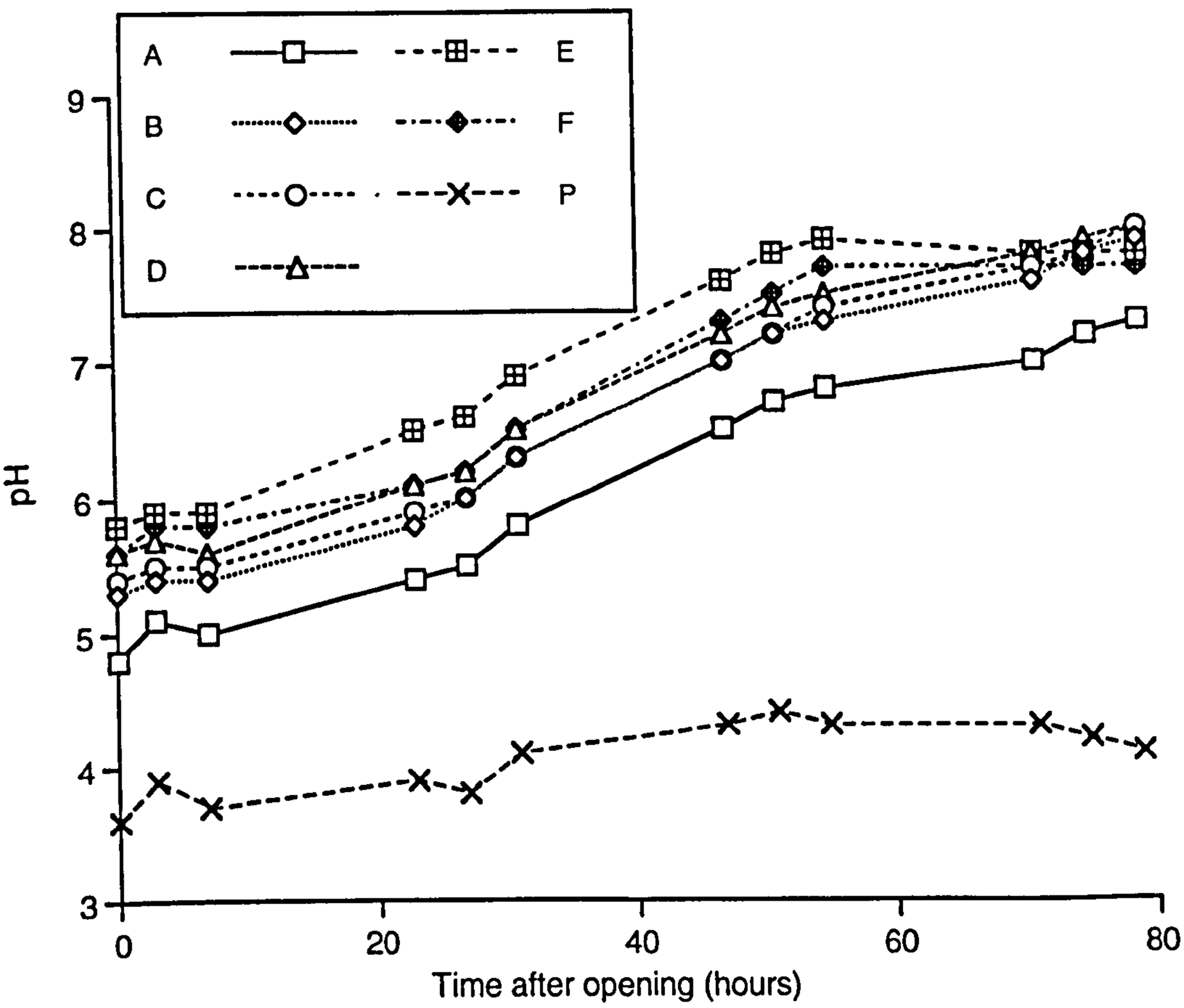

Fig. 5.5 Graph showing how pH varies with time for the third experiment.

approximately 4 days (see Appendix I). A new ring shear technique was investigated which would allow the use of a new solution of Ca^{2+} and clay sample for each normal effective stress. Thus, each solution of Ca^{2+} would be used for less than 24 hours. A series of these tests, done at a range of effective normal stresses, would allow the complete residual failure envelope to be defined for a particular clay and pore water.

5.6.1 Multiple Shear Technique

Pure "SPS" grade kaolinite, from English China Clays International Limited, was left to consolidate overnight at the required effective normal stress. The water bath was filled with deionised water. The next morning a shear surface was created by failing, under the same load, at a speed of 60°/minute (44.52 mm/minute) for 25 minutes. The sample, now in the residual condition, was then left for eight hours at a strain rate of 0.024°/minute under the same load and the residual shear strength measured at the end of this period. This procedure was done for each effective normal stress with a new kaolinite sample and solution of deionised water. All the samples came from the same homogenised batch of kaolinite.

Figure 5.6 shows the results obtained by this technique. These do not form a typical residual failure envelope created by the routine technique, described in Appendix I, and any residual shear angles taken from the envelope are likely to be inaccurate. The ultimate residual shear angle is 6°, much lower than an angle of 10.4° (see Figure 5.9) obtained by the routine method described in Appendix I. The unusual envelope is likely to be due to the large amounts of extrusion caused by the creation of a shear surface under high loads and the incomplete consolidation of the samples. On dismantling the apparatus it was found that in some cases, at least half the sample had been extruded.

5.6.2 Multiple Shear Technique with Staged Consolidation

A second approach was tried where each sample was consolidated by slowly increasing the effective normal stress up to the required level. The load was only increased once the sample appeared to have ceased consolidating. Consolidation was monitored using a vertical dial gauge and it was found that it took approximately an hour for the sample to undergo the majority of consolidation under each load. Once the full consolidation had been completed to the required effective normal stress, a shear surface was created by the previous method, but only under a load of

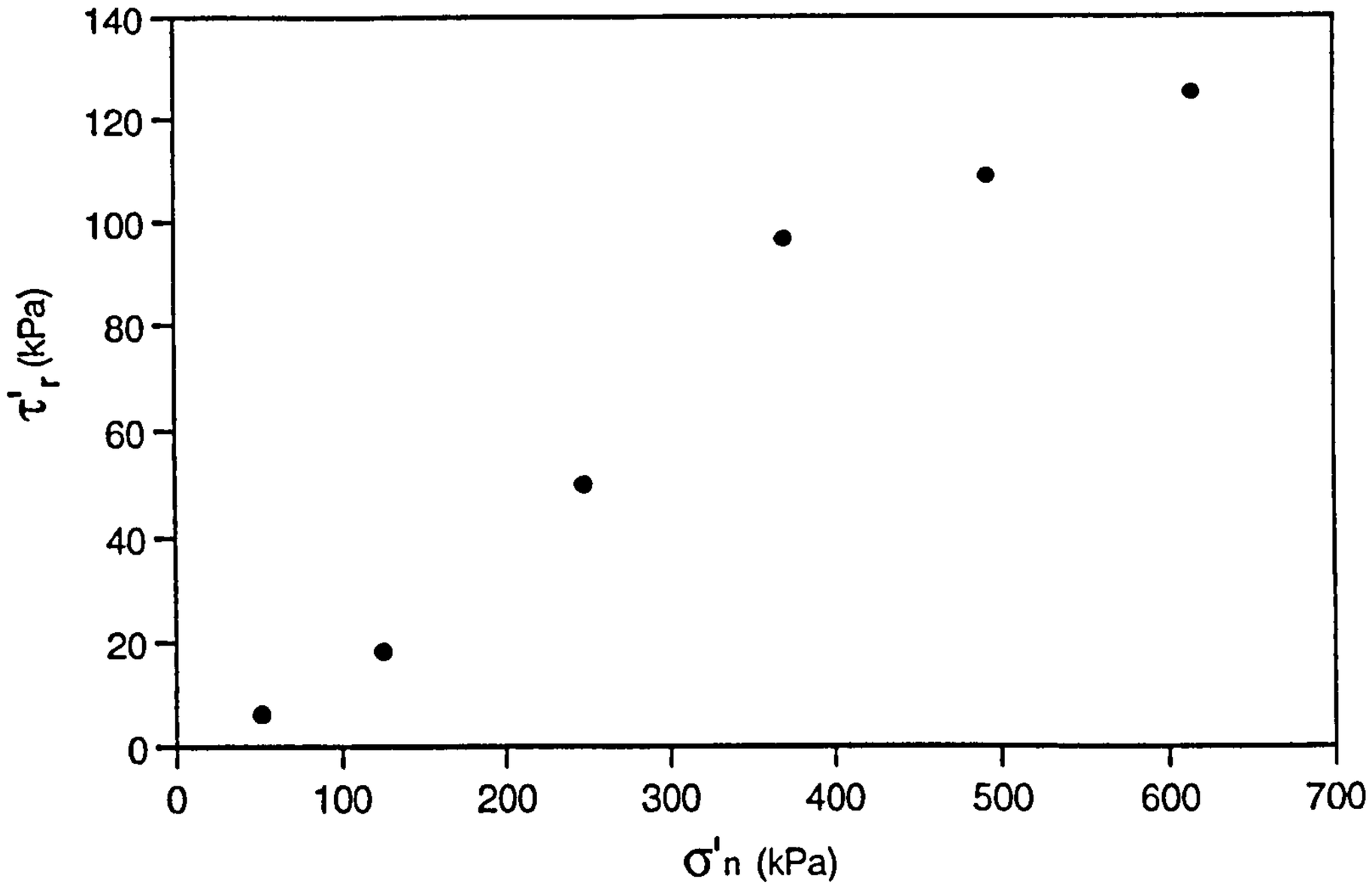

Fig. 5.6 Complete residual failure envelope for kaolinite using the multiple shear technique, with consolidation imposed by instant loading. Note the exaggerated vertical scale.

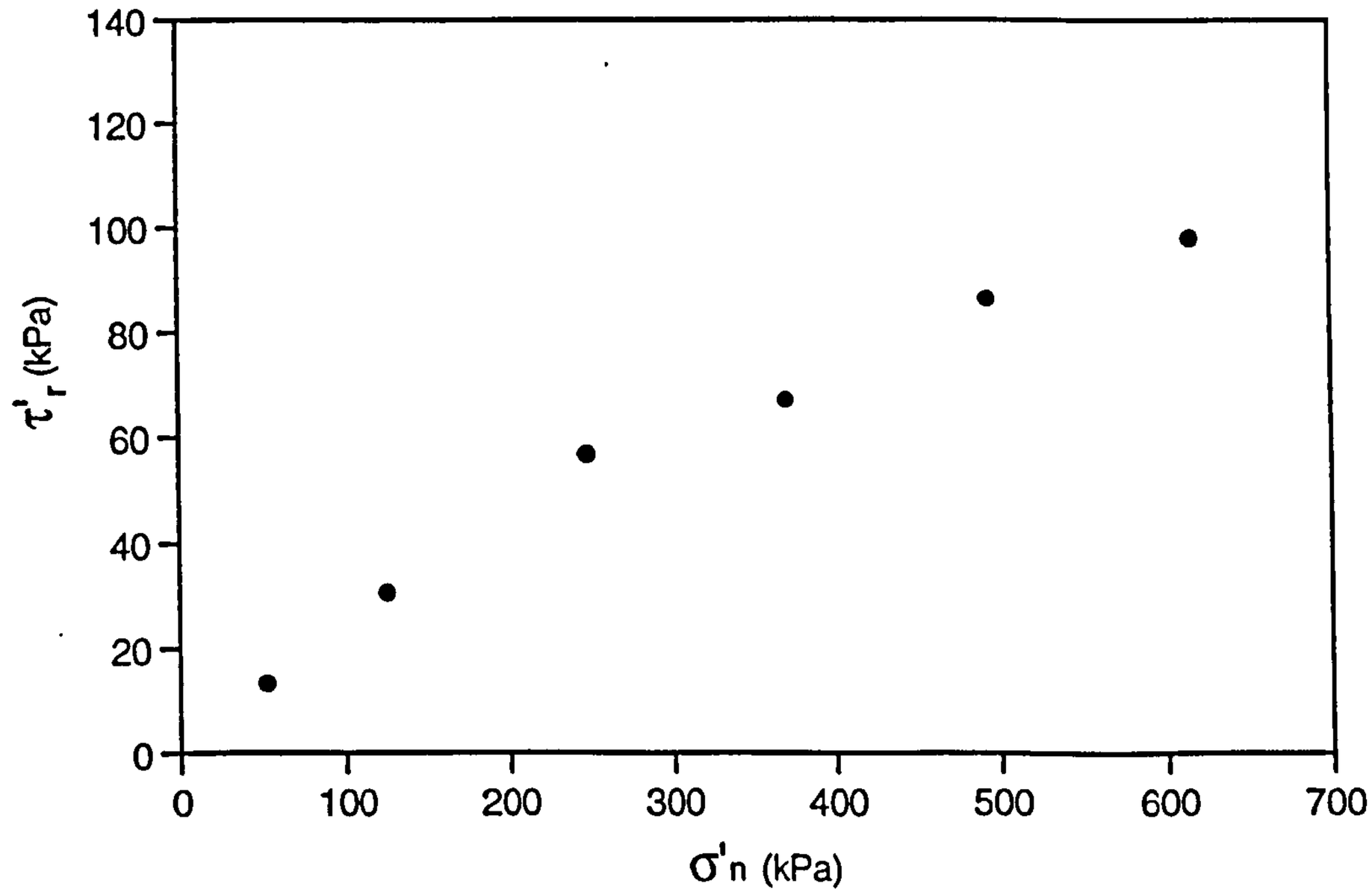

Fig. 5.7 Complete residual failure envelope for kaolinite using the multiple shear technique with staged consolidation. Note the exaggerated vertical scale.

27 kPa to avoid excessive extrusion. The sample was then left overnight at a strain rate of 0.024°/minute under the required effective normal stress and the residual shear strength measured the following morning. This processes was repeated for each effective normal stress with a new clay sample and solution of deionised water.

Figure 5.7 shows the results for this technique. Again using this technique, $\phi'_{r(ult)}$ is 6.7°, lower than 10.4° obtained by the routine method.

5.6.3 Discussion

These techniques provide different results to the routine method, described in Appendix I, most likely due to the significant amounts of sample extrusion. However, due to the lack of stability of the calcium carbonate derived solutions and the decision to use calcium chloride to create stable Ca^{2+} solutions, these techniques were not be needed and the routine method was used for the investigation.

5.7 The Effects of Calcium Ions on the Residual Shear Strength of Kaolinite and Montmorillonite

Samples of "pure" kaolinite and montmorillonite (see Section 5.7.5) were used to investigate the effects of calcium in pore water on the residual shear strength of clays, with particular reference to the landslip at Soper's Wood. Using "pure" clays reduced the number of variables which may affect the residual shear strength of the clay, such as the proportion of silt grade material. Kaolinite and montmorillonite were chosen as they are both present in the Fuller's Earth clay (interstratified illite-montmorillonite forming as a result of the weathering of illite in the Fuller's Earth) and are both readily available in a pure form. In addition, they represent the two extremes, in terms of size and behaviour (eg swelling properties), in the family of clay minerals.

5.7.1 Preparation of the Clays

5.7.1.1 Kaolinite

"SPS" grade kaolinite was obtained from English China Clays International limited. However, a chemical flocculant (polyacrylate) is used in the production process and it was necessary to remove the flocculant prior to testing. Winterkorn & Moorman (1941) treated Putnam Clay with HCl to replace all the exchangeable cations with H^+, prior to creating various homoionic clays to study the changes in the physical properties

induced by ionic substitution (see Chapter 2). However, van Olphen (1977) does not recommend this method for preparing clays, as the acid attacks the clay mineral edges, dissolving aluminium ions, which are then adsorbed in preference to H^+. Up to 40% of the exchangeable cation sites may be affected and, due to the high valency of Al^{3+}, the aluminium ions are very hard to remove or exchange. Therefore, as recommended by van Olphen (1977), the kaolinite was washed in deionised water to remove the flocculant.

Enough kaolinite for six ring shear and Atterberg tests was placed in a 10 litre bucket filled with deionised water. This was then stirred with a mixer at high speed for 15 minutes and left to stand. After 30 minutes, the kaolinite had flocculated and settled to the bottom of the bucket, leaving a chemical scum on the surface of the supernatant fluid. The fluid was syphoned off and replaced with fresh deionised water, the mixture stirred again and left to stand overnight. The clay flocculated again and the supernatant fluid was removed. The sample was then split into two 10 litre buckets of deionised water, stirred again at high speed for 15 minutes and left for a further 24 hours. The kaolinite flocculated again, but not as effectively as before. The washing process was repeated for each bucket and 48 hours later the kaolinite was still in a dispersed state. This indicated that the salts in the solution had fallen below their flocculating values and the majority of the chemical flocculant had been removed by agitation and washing.

An attempt was made to extract the kaolinite by using a large vacuum filter, this was unsuccessful as an effectively impermeable cake of clay soon formed on the filter paper. However, centrifuging the kaolinitic sol in 250 ml containers provided a solution for extracting the clay. The kaolinitic sol was centrifuged for 7 minutes at 3500 rpm. This separated out the majority of the "cleaned" kaolinite, with only a slightly milky supernatant fluid remaining which was disposed of. As a result of centrifuging, "cleaned" kaolinite was obtained. However, to check that the flocculating chemicals had effectively been removed, the kaolinite was redispersed in a 10 litre bucket and left to stand. After 24 hours, the clay was still in a dispersed state, confirming that the washing process had been successful. The centrifuge process was then repeated to extract the clay.

The centrifuged kaolinite was then placed in evaporating dishes on top of a "hot plate" and stirred every 30 minutes until a dry paste developed. This took approximately 2 days. At night, to prevent uneven drying, the evaporating dishes were removed from the "hot plate" and sealed with cling

film. The dry kaolinite paste was then thoroughly homogenised, prior to storage in clean containers.

5.7.1.2 Montmorillonite

The montmorillonite used was "Wyoming Bentonite". This is commonly assumed to consist dominantly of sodium montmorillonite and Bowels (1979) states that:

"..bags of clays of high activity, commercially available for drilling and grouting, are loosely called bentonite, although they are merely montmorillonite clays".

XRD analysis of the clay confirmed that the clay fraction was dominantly sodium montmorillonite, with some subsidiary calcium montmorillonite (see Section 5.7.5).

As for the kaolinite, the montmorillonite was washed with deionised water. Enough montmorillonite for six ring shear and Atterberg tests was placed in a 10 litre bucket filled with deionised water, stirred at high speed for 15 minutes and then left to stand. Unlike the kaolinite, the montmorillonite did not flocculate, but formed a hydrated dispersed sol, characteristic of sodium montmorillonite. The sol was left to stand overnight and then split into two 10 litre buckets which were filled to the top with deionised water, stirred for 15 minutes and left to stand. After 24 hours, the sample was found to still be in a dispersed hydrated state and was remixed.

To extract the montmorillonite from the sol, it was centrifuged for 12 minutes at 3500 rpm in 250 ml containers; again a milky supernatant fluid remained, from which it was not possible to extract the clay and it was disposed of. In addition, after centrifuging, the 250 ml containers were found to contain a layer of darker silty material adhered to their base. On emptying the bucket used for washing the clays, a similar layer was found. In order to keep the samples as homogeneous as possible, this silt grade material was removed. Again as for the kaolinite, the centrifuged montmorillonite was redispersed in deionised water, left to stand for 24 hours and then the centrifuge process repeated.

Using the same procedure as for the kaolinite, the centrifuged montmorillonite was warmed in evaporating dishes. However, it took approximately 14 days for a dry paste to develop. After the initial two days when the clay was stirred every 30 minutes, due to the very slow drying nature of the hydrated montmorillonite, the clay was only stirred 4 times a

day. The dry montmorillonite paste was then thoroughly homogenised, prior to storage in clean containers.

5.7.2 Preparation of Solutions

Three litre solutions of Ca^{2+} were prepared by weighing out the corresponding amount of $CaCl_2$ and dissolving it in deionised water. The Ca^{2+} concentrations prepared cover the range found in the ground waters at Soper's Wood and correspond to 0, 80.1, 160.2, 240.3, 320.4 and 400.5 mg/l Ca^{2+}, which equates to 0, 200, 400, 600, 800, 1000 mg/l $CaCO_3$ respectively.

5.7.3 Experimental Technique

It was important that the sample pre-treatment and geotechnical tests were undertaken following the same procedure for each clay type. This ensured that the results for a particular clay type would be relative to each other, as any variation in the procedure would have caused increased or decreased levels of cation adsorption, making it difficult to compare test results.

5.7.3.1 Kaolinite

For each concentration of Ca^{2+} solution, one full brass pot, of the type used in the cone penetrometer test, of "clean" kaolinite paste, was added to 2 litres of the corresponding Ca^{2+} solution in a plastic bucket, mixed at high speed for 5 minutes until all the kaolinite had dispersed and left to equilibrate. All the samples of kaolinite flocculated and settled to the bottom of the bucket. After 17 hours, the supernatant fluid was syphoned off from the flocculated clay. The plastic buckets containing the treated clay were then placed on a "hot plate" and any new supernatant fluid that formed was removed with a syringe. As the kaolinite thickened it was stirred frequently and warmed to a dry paste. The treated kaolinite samples were then placed in clean plastic pots for storage.

Atterberg tests were conducted on the individual treated clay samples (see Appendix I), a portion of which were used in ring shear tests. Samples were placed in the ring shear apparatus at a moisture content just above their plastic limits. The ring shear test method was routine (see Appendix I), except that the water bath was filled with the corresponding Ca^{2+} solution instead of deionised water.

5.7.3.2 Montmorillonite

A similar procedure was used to prepare the montmorillonite, except that a 3/4 full brass pot of montmorillonite (66 g), of the type used in the cone penetrometer test, was added to 2 litres of the corresponding Ca^{2+} solution in a plastic bucket. However, unlike the kaolinite, the montmorillonite treated with the weakest concentration of Ca^{2+} solution (80.1 mg/l), formed a very hydrated dispersed sol and no supernatant solution formed. This sample could be seen to have thixotropic characteristics. The remainder of the montmorillonite samples flocculated by progressively greater amounts as the concentration of the Ca^{2+} solution increased, forming a progressively denser hydrated sol and providing a greater amount of supernatant fluid. The depth of supernatant fluid was approximately 3 mm for 160.2 mg/l Ca^{2+}; 10 mm for 240.3 mg/l Ca^{2+}; 15 mm for 320.4 mg/l Ca^{2+} etc.

Following the removal of any available supernatant fluid, the plastic buckets were placed on a "hot plate" and any new supernatant fluid that formed was removed with a syringe. As the sols thickened, they were frequently stirred and warmed to a paste, prior to being placed in clean plastic containers for storage. Due to the smaller amount of supernatant fluid that formed from the samples treated with lower concentrations of Ca^{2+} solution, naturally these took longer to warm to a paste.

Unfortunately, due to the loss of some of the material during treatment, it was not possible to split the treated montmorillonite samples for ring shear tests and Atterberg tests. Thus, routine ring shear tests, with the water bath filled with the corresponding Ca^{2+} solution, were first carried out. The samples were placed in the ring shear apparatus at moisture contents just above their plastic limits. Atterberg tests were then conducted on the remoulded clay obtained from the ring shear tests. Due to the small sample size, it was not possible to use the cone penetrometer method to determine the liquid limit. Hence, the Casagrande apparatus was used following the four point method described in BS 13770 (1991).

5.7.3.3 Discussion

The individual buckets of treated montmorillonite effectively formed a flocculating series with increasing concentration of Ca^{2+} solution, as described by van Olphen (1977). The following interpretation explains these observations. For the montmorillonite treated with 80.1 mg/l Ca^{2+} solution, the concentration of Ca^{2+} ions is not great enough to cause much compression of the hydrated double layer which surrounds the clay

minerals. Thus, the individual clay platelets repel each other and a very hydrated dispersed sol forms. For the montmorillonite treated with increasing concentrations of Ca^{2+} solutions, there is progressively increased compression of the hydrated double layer. This allows the attractive van der Waals forces to dominate and there is increased bonding between the individual clay platelets and a denser, flocculated, hydrated clay results.

5.7.4 Results

5.7.4.1 Kaolinite

The results from the ring shear tests were plotted and the complete residual failure envelopes for the samples of kaolinite treated with different concentrations of Ca^{2+} are shown in Figure 5.8. In establishing the complete residual failure envelopes for the kaolinite treated with 160.2, 240.3, 320.4 and 400.5 mg/l Ca^{2+}, the value of τ'_r achieved at $\sigma'_n = 615$ kPa was ignored, as it was significantly higher relative to the values of τ'_r obtained at lower effective normal stresses. It is believed that these unusually high values of τ'_r may have been obtained as a consequence of sample extrusion during the later stages of the ring shear test. A study of the residual failure envelopes in Figure 5.8 reveals no obvious trend/differences between the various envelopes. However, the effective residual shear strength, residual cohesion intercept and residual shear angle were analysed at a range of normal effective stresses for each calcium concentration and the results are presented in Figures 5.9, 5.10 and 5.11.

Figure 5.9 illustrates the relationship between ϕ'_r and Ca^{2+} concentration at five effective normal stresses, together with the ultimate residual shear angle. The gradual lowering of ϕ'_r with increasing effective normal stresses, due to the curvature of the failure envelope, is evident. For $\sigma'_n = 25$ kPa, there is a broad trend of increasing ϕ'_r (from 14.0° to 21.8°) with Ca^{2+} concentration. However, at normal effective stresses above this level, no obvious relationship is evident. Indeed, for $\sigma'_n = 150$ kPa and above, ϕ'_r appears to be largely unaffected by Ca^{2+} concentration.

Figure 5.10 illustrates the relationship between the effective residual cohesion intercept and Ca^{2+} concentration at five effective normal stresses, together with the value of the ultimate effective residual cohesion intercept. The increase of effective residual cohesion intercept with increasing effective normal stress, due to the curvature of the envelope is evident.

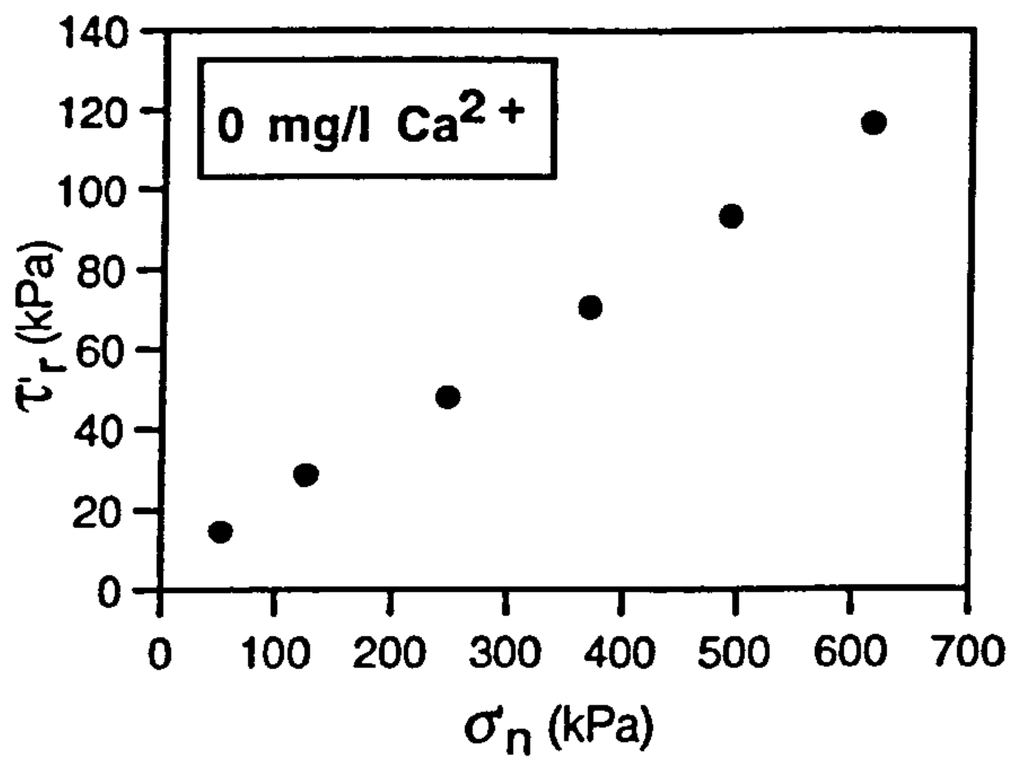

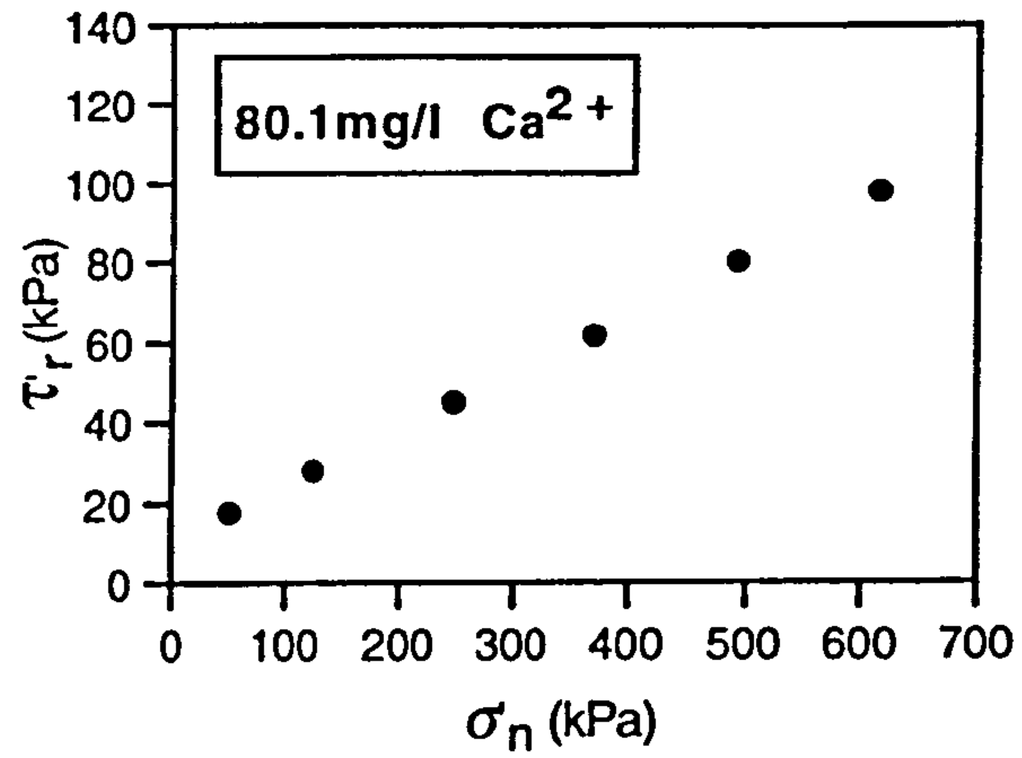

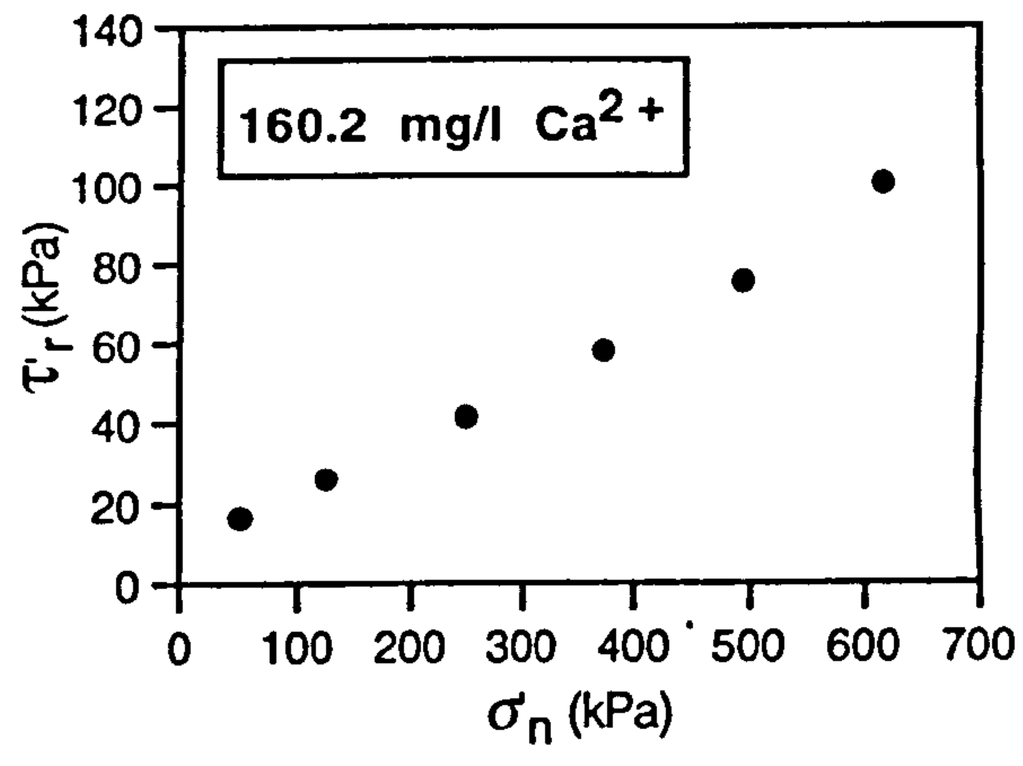

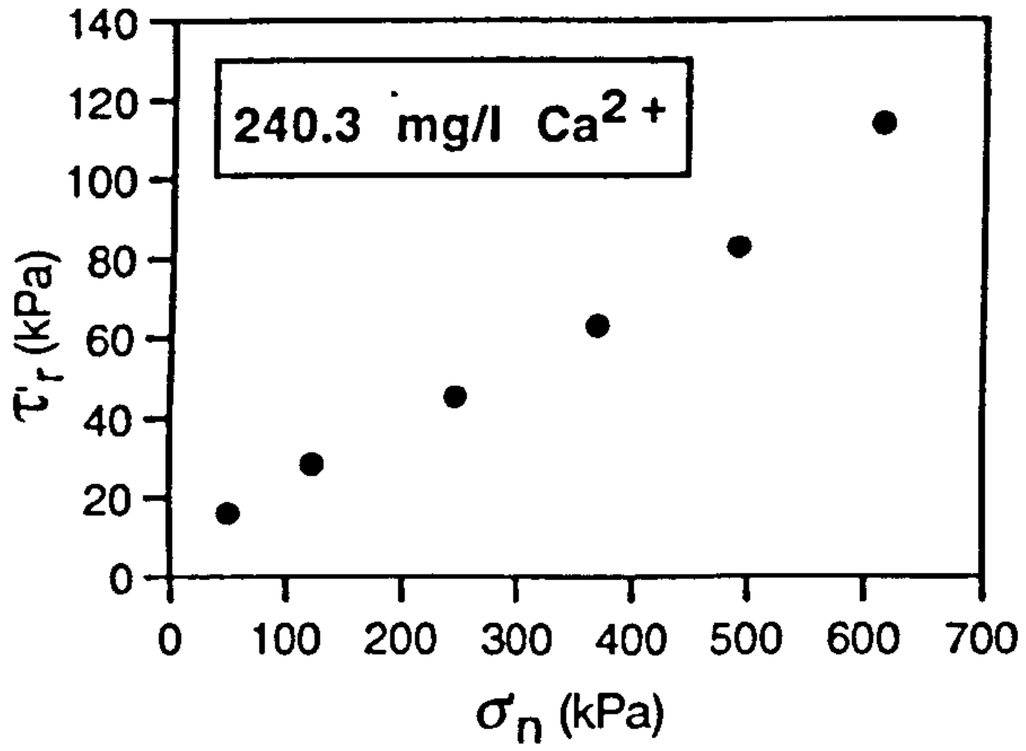

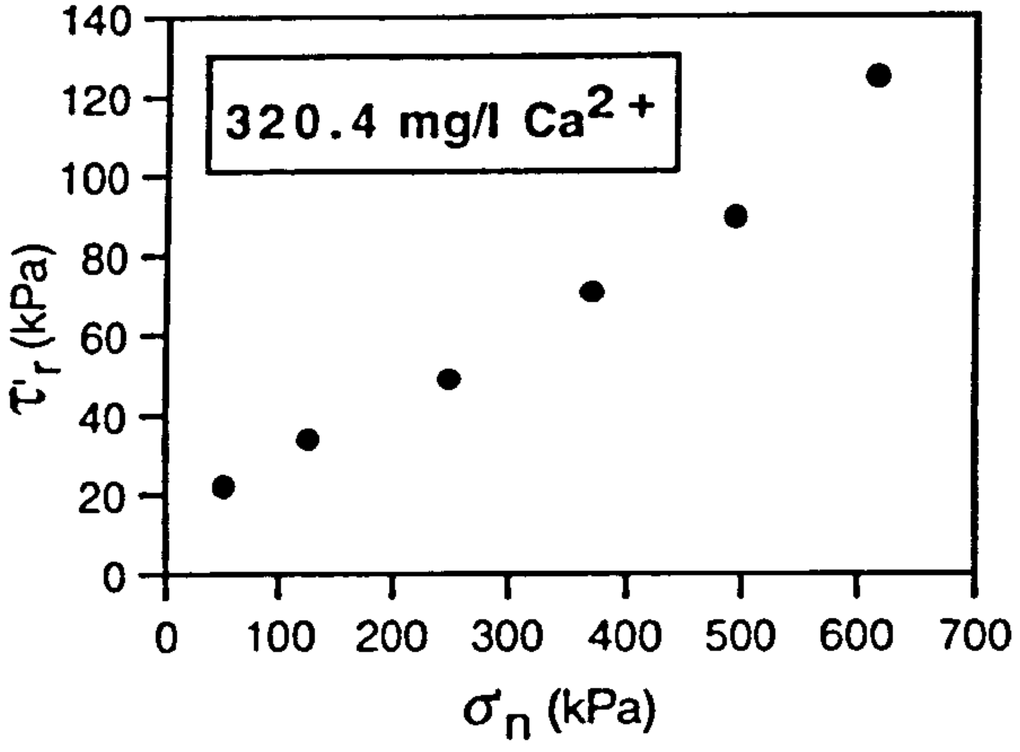

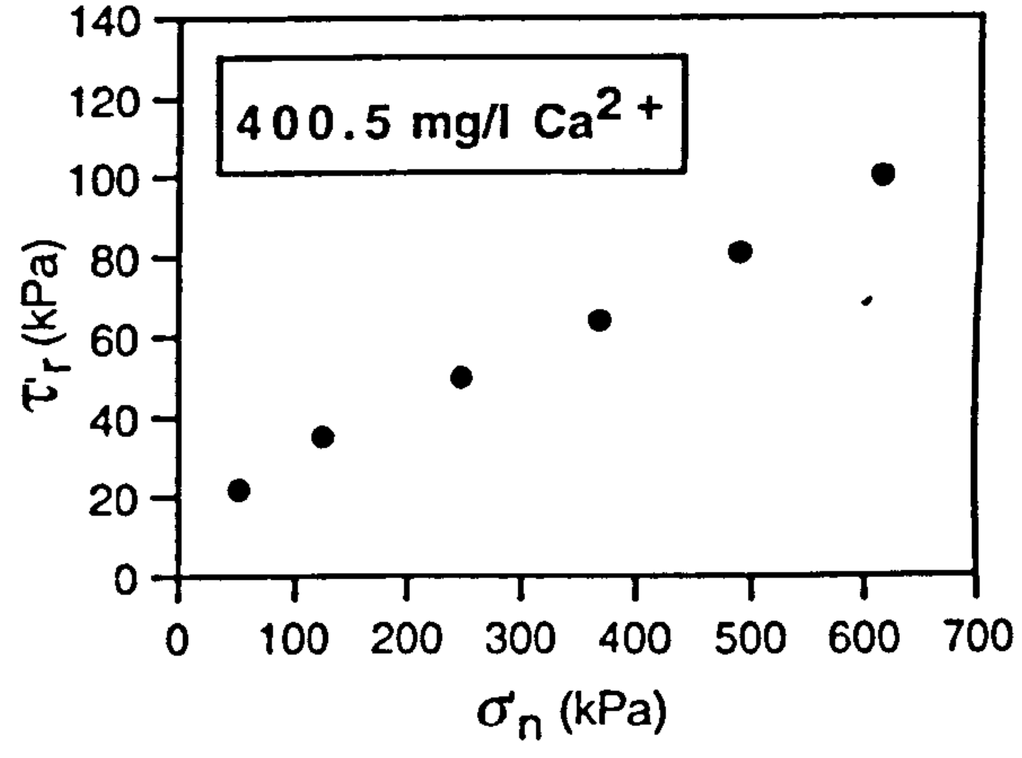

Fig. 5.8 Residual failure envelopes for kaolinite treated with solutions of calcium at the concentrations shown. Note the exaggerated vertical scale.

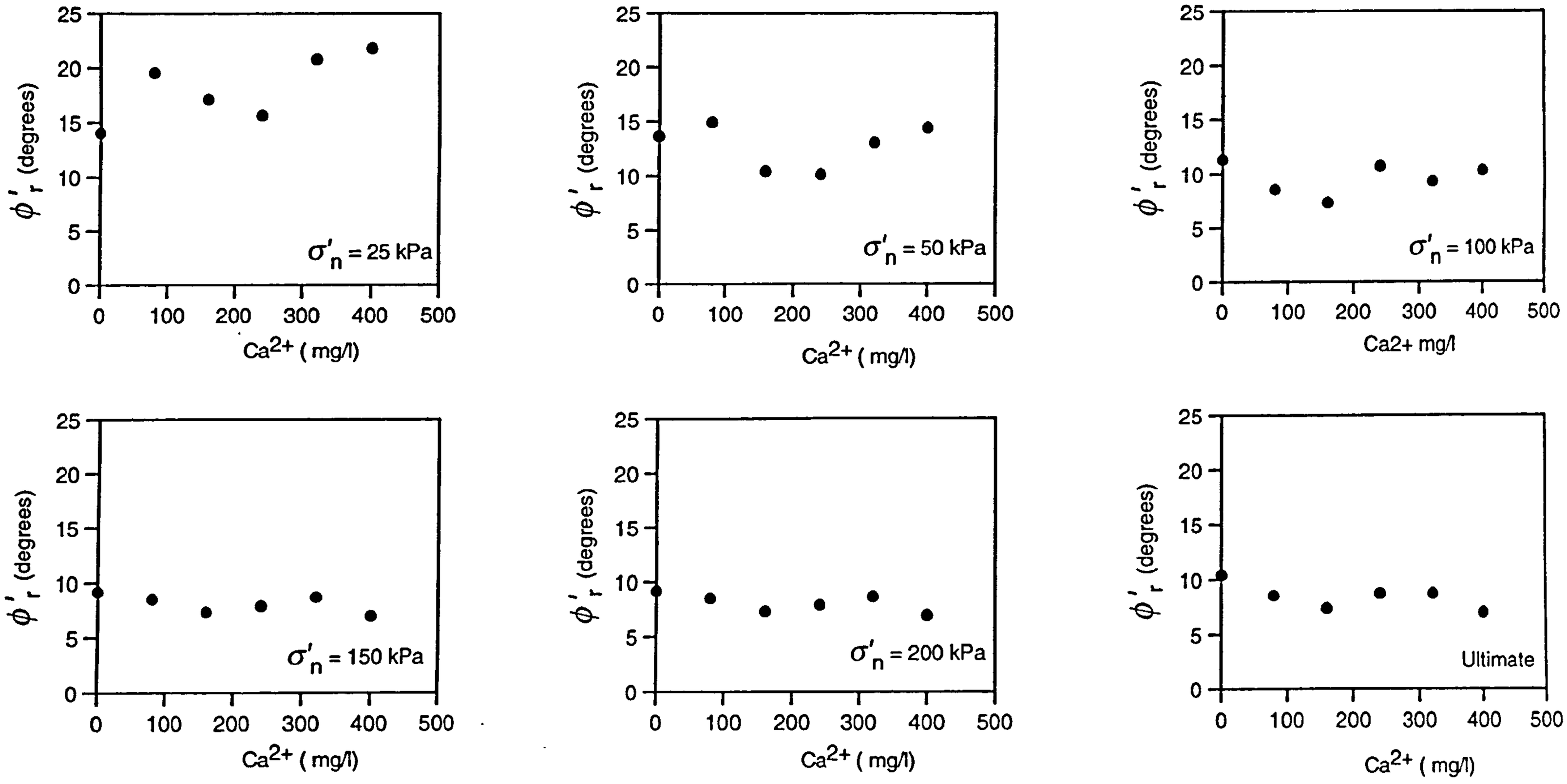

Fig. 5.9 Graphs displaying the relationship between calcium concentration and the effective residual shear angle of kaolinite at various effective normal stresses.

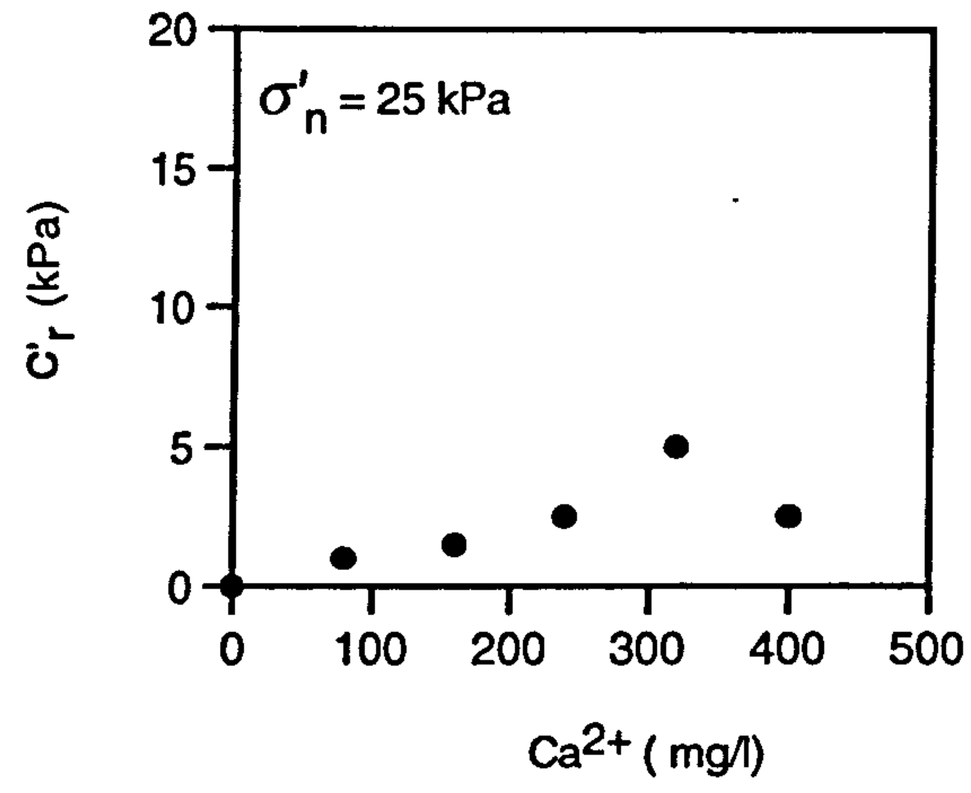

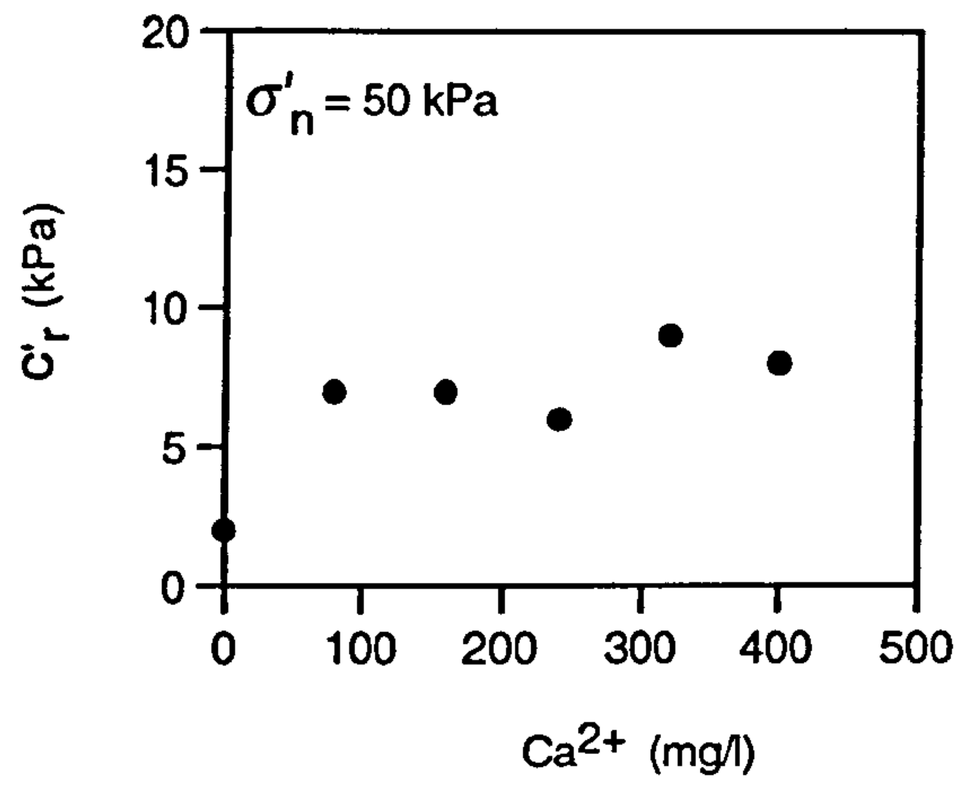

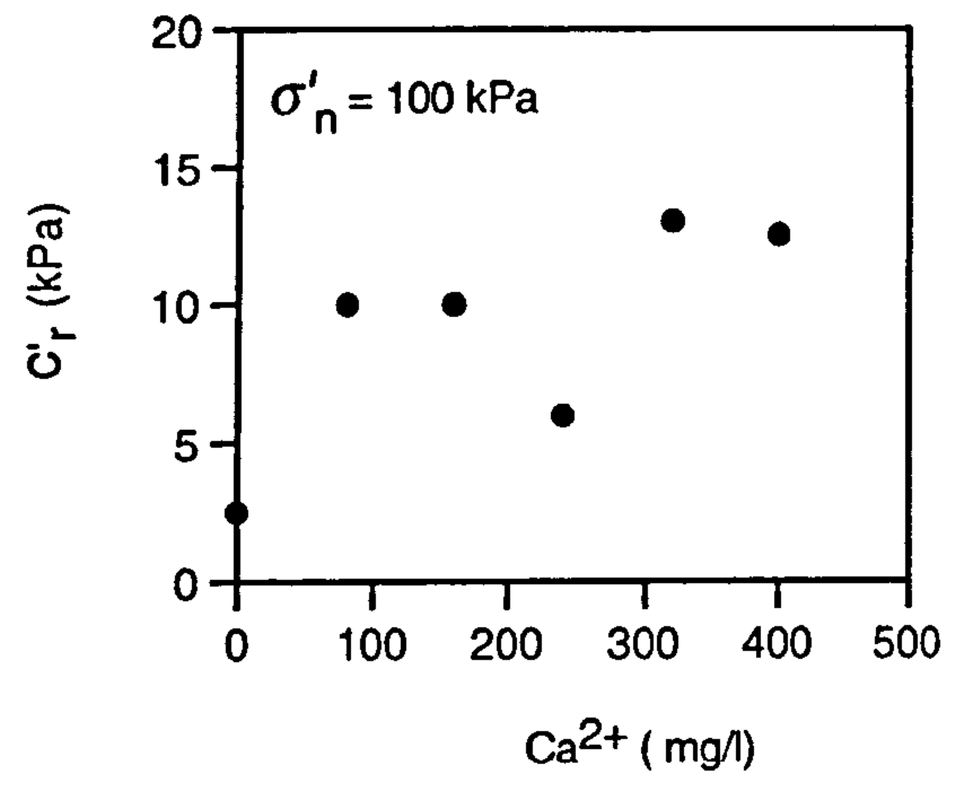

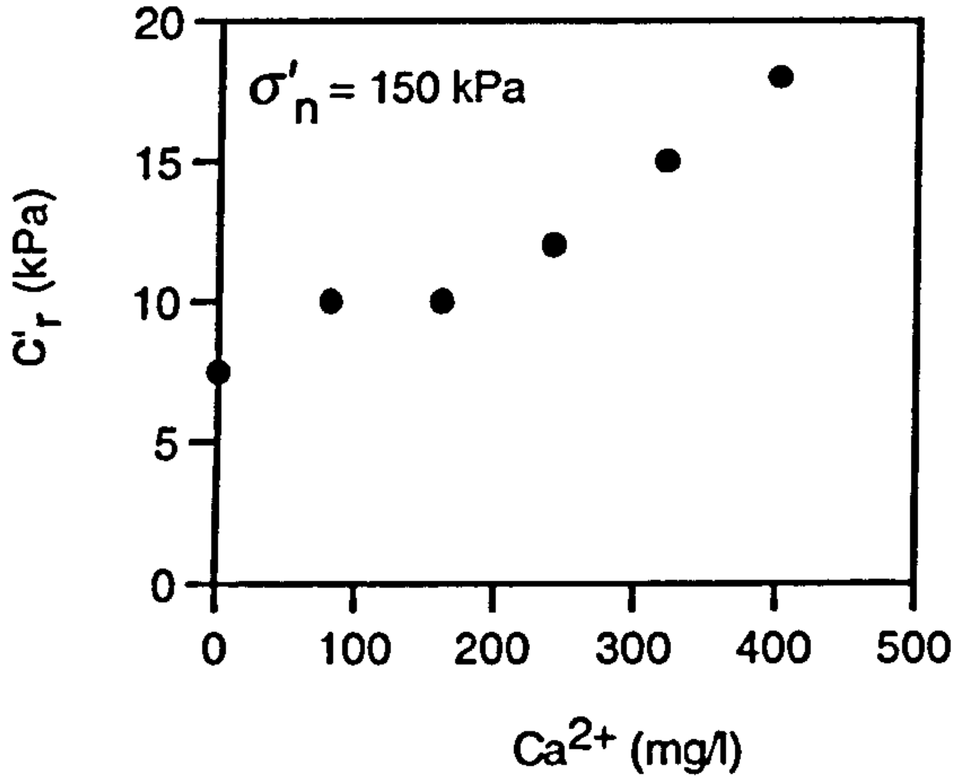

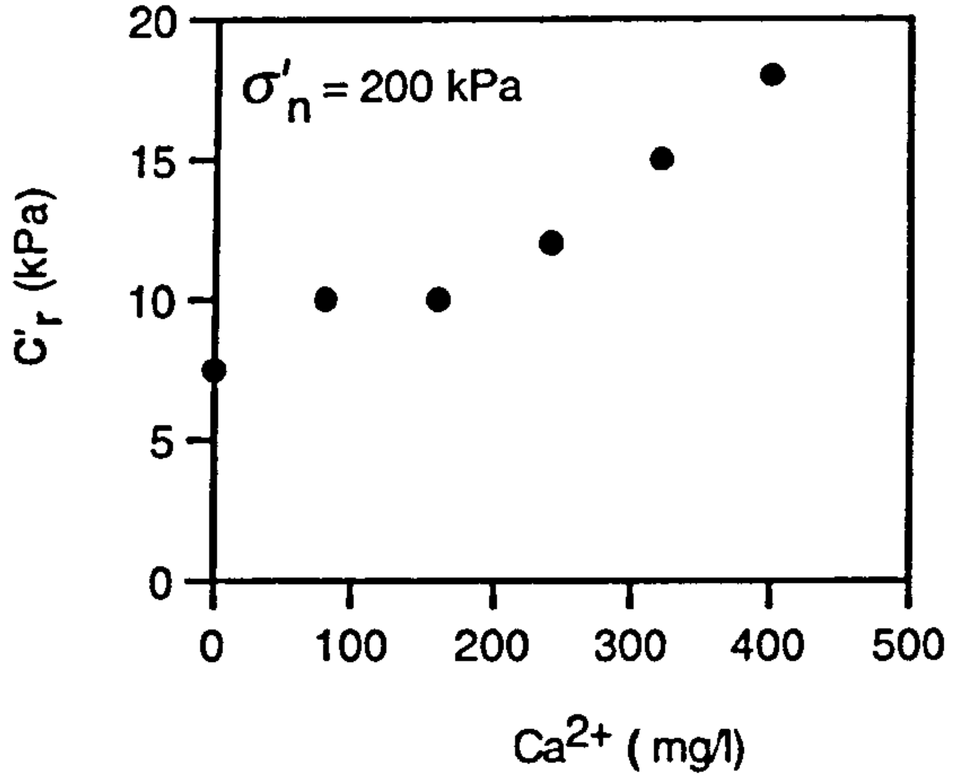

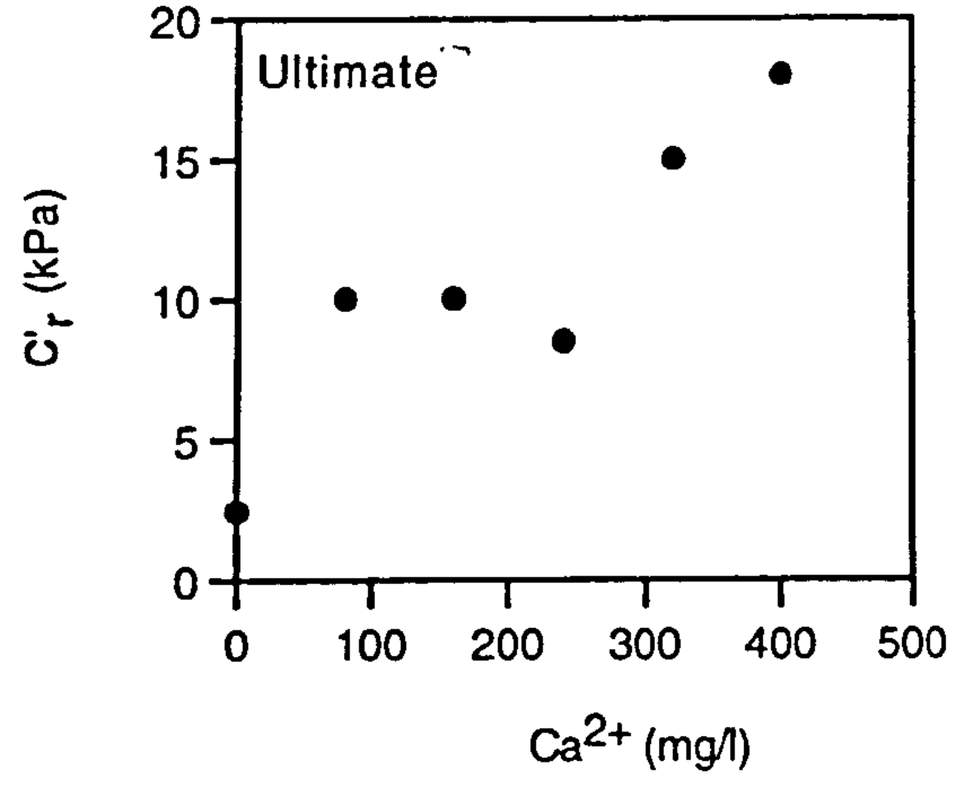

Fig. 5.10 Graphs showing the relationship between calcium concentration and the effective residual cohesion intercept of kaolinite at various effective normal stresses.

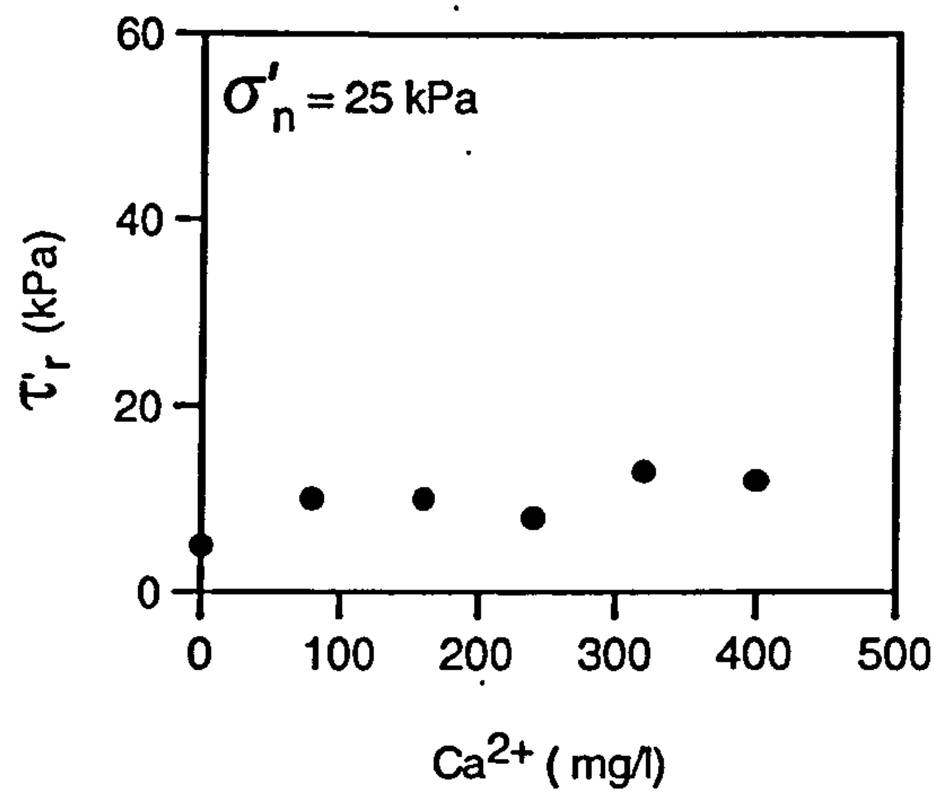

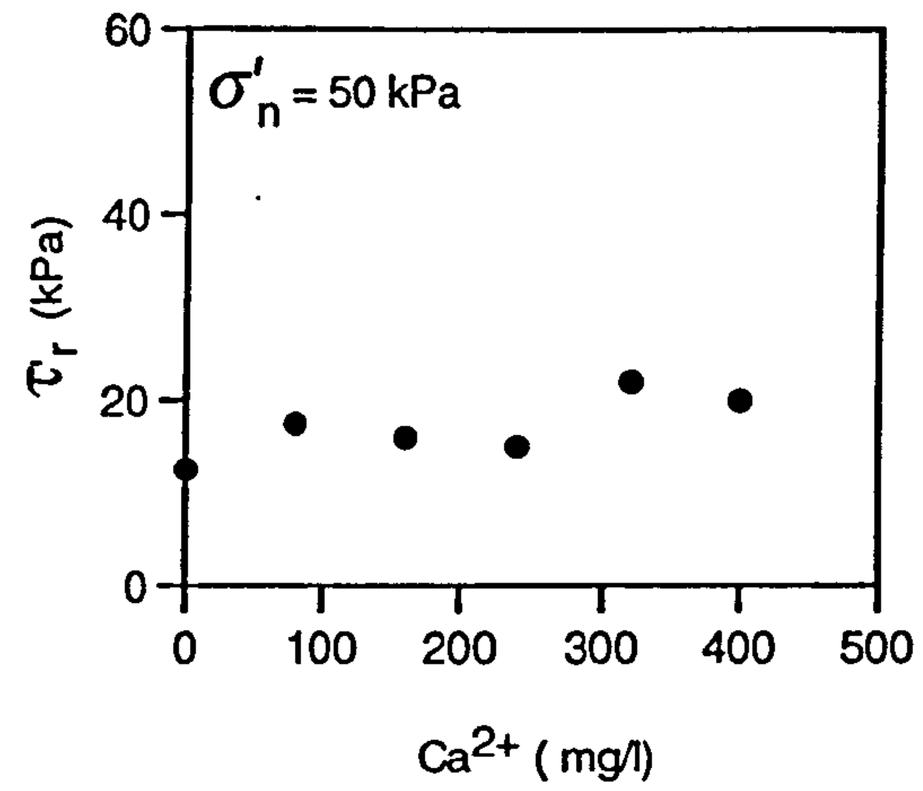

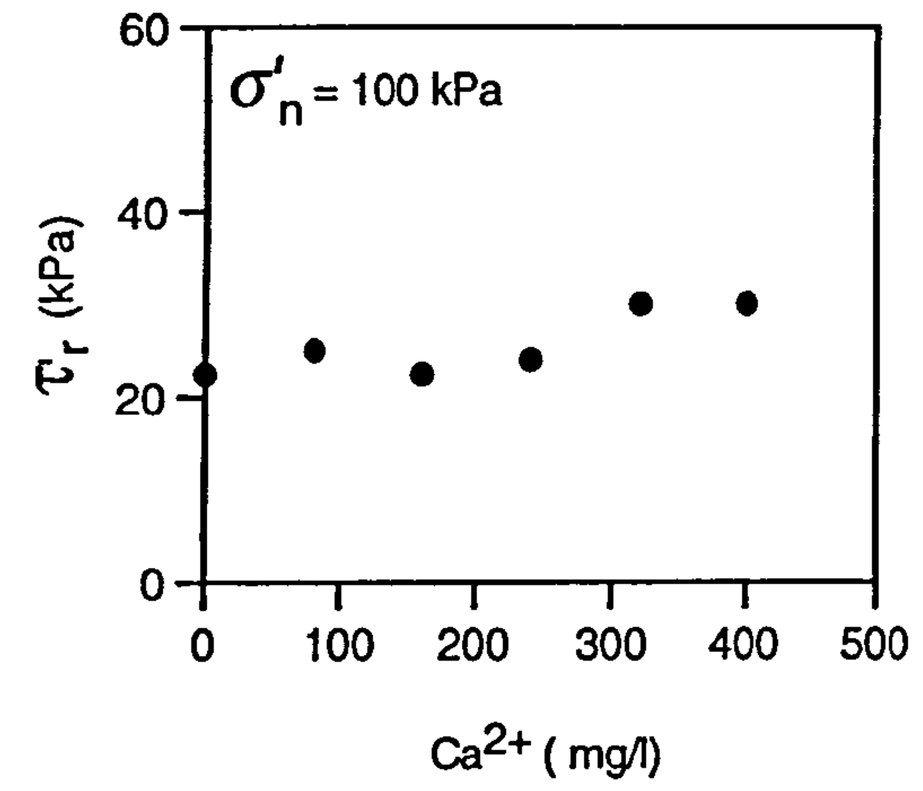

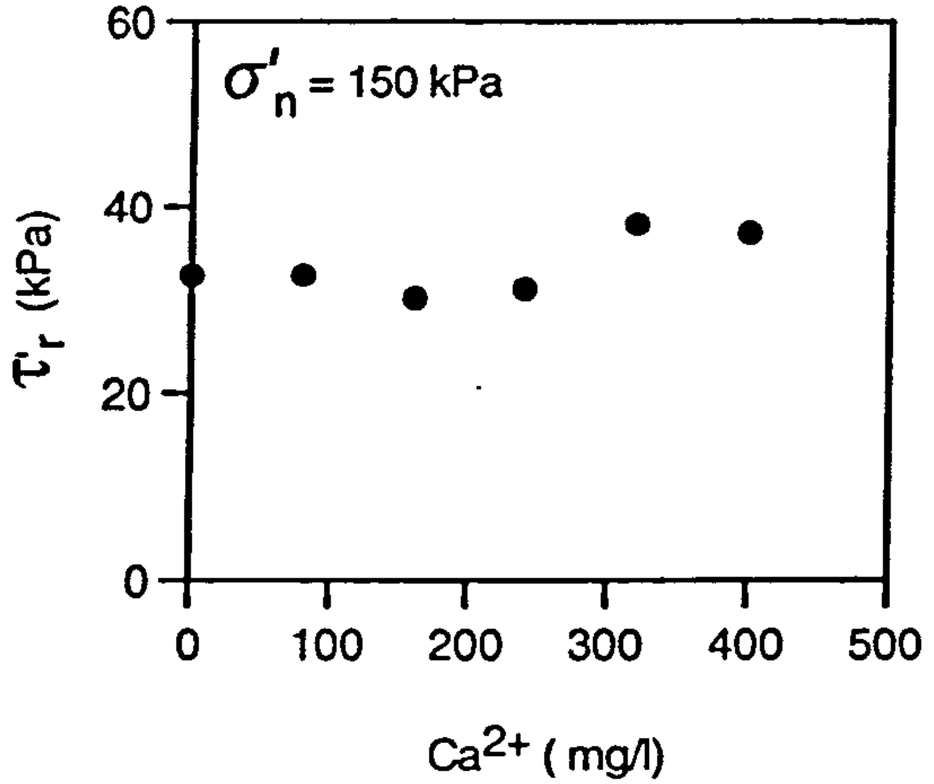

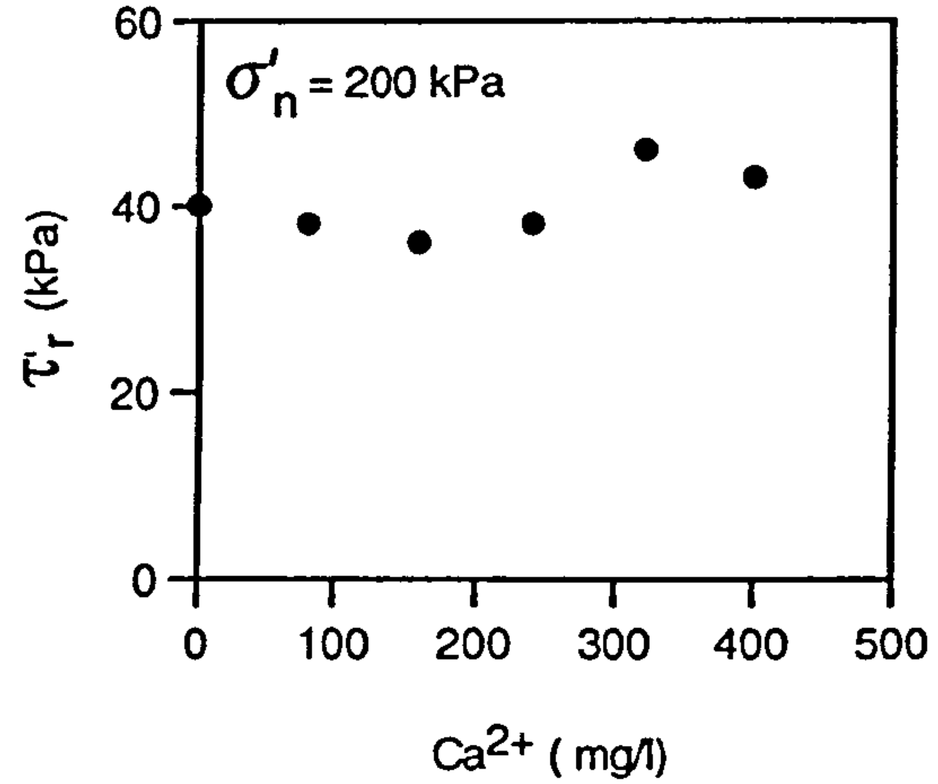

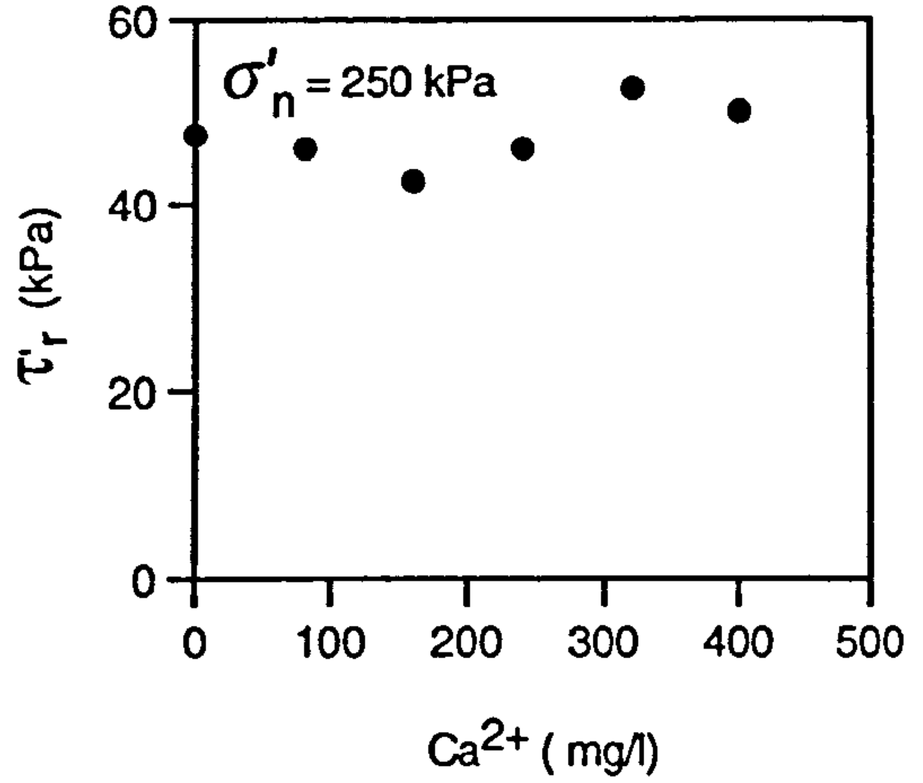

Fig. 5.11 Graphs displaying the relationship between calcium concentration and the residual shear strength of kaolinite at six effective normal stresses.

However, at each effective normal stress, an increase in Ca^{2+} concentration leads to an increase in c'_r. This is most marked when $\sigma'_n = 150$ kPa and above, where c'_r increases from 7.5 kPa to 18 kPa. In addition, a pronounced change in c'_r occurs at almost all effective normal stresses, between the samples tested using distilled water and the samples tested using a solution of 80 mg/l Ca^{2+}. Some scatter in the plots is evident, most likely due to the subjectivity involved in locating the tangent to the residual failure envelope at a particular effective normal stress.

Figure 5.11 shows plots of residual shear strength against Ca^{2+} concentration for six values of σ'_n and all the graphs show an overall increase in τ'_r with Ca^{2+} concentration. For $\sigma'_n = 150$ kPa (the clearest line on the effective normal stress diagrams in Figure 5.10), τ'_r increases from 32.5 kPa to 38 kPa. Again, due to the curvature of the residual failure envelope, residual shear strength increases with increasing effective normal stress.

The Atterberg limits for each of the treated kaolinite samples were determined and are displayed in Figure 5.12. The plot shows a clear increase in the liquid limit between the untreated kaolinite sample ($w_L = 57\%$) and the kaolinite treated with a solution of 80.1 mg/l Ca^{2+} ($w_L = 65\%$). Thereafter, there is no obvious trend with increasing Ca^{2+} concentration. There is no noticeable increase indicated by the "less sensitive" plastic limit and hence, as expected, the plasticity index of the samples mirrors the liquid limit.

5.7.4.2 Montmorillonite

The complete residual failure envelopes for the samples of montmorillonite treated with different concentrations of Ca^{2+} solutions were plotted and are displayed in Figure 5.13. In establishing the failure envelopes for the montmorillonite treated with 240.3 mg/l Ca^{2+} solution, the value of τ'_r achieved at $\sigma'_n = 615$ kPa was ignored. As for some of the kaolinite samples, this higher value of τ'_r is believed to be a consequence of sample extrusion during the later stages of the ring shear test.

A study of Figure 5.13 reveals the marked increase in the height of the complete residual failure envelope between the untreated montmorillonite sample and the sample treated with a solution of 80.1 mg/l Ca^{2+}. Thereafter, with increasing calcium concentration, there is no obvious change in the position of the complete residual failure envelopes. Some extrusion of the clay was observed during the ring shear tests. The extruded untreated clay formed a very hydrated and voluminous state in the

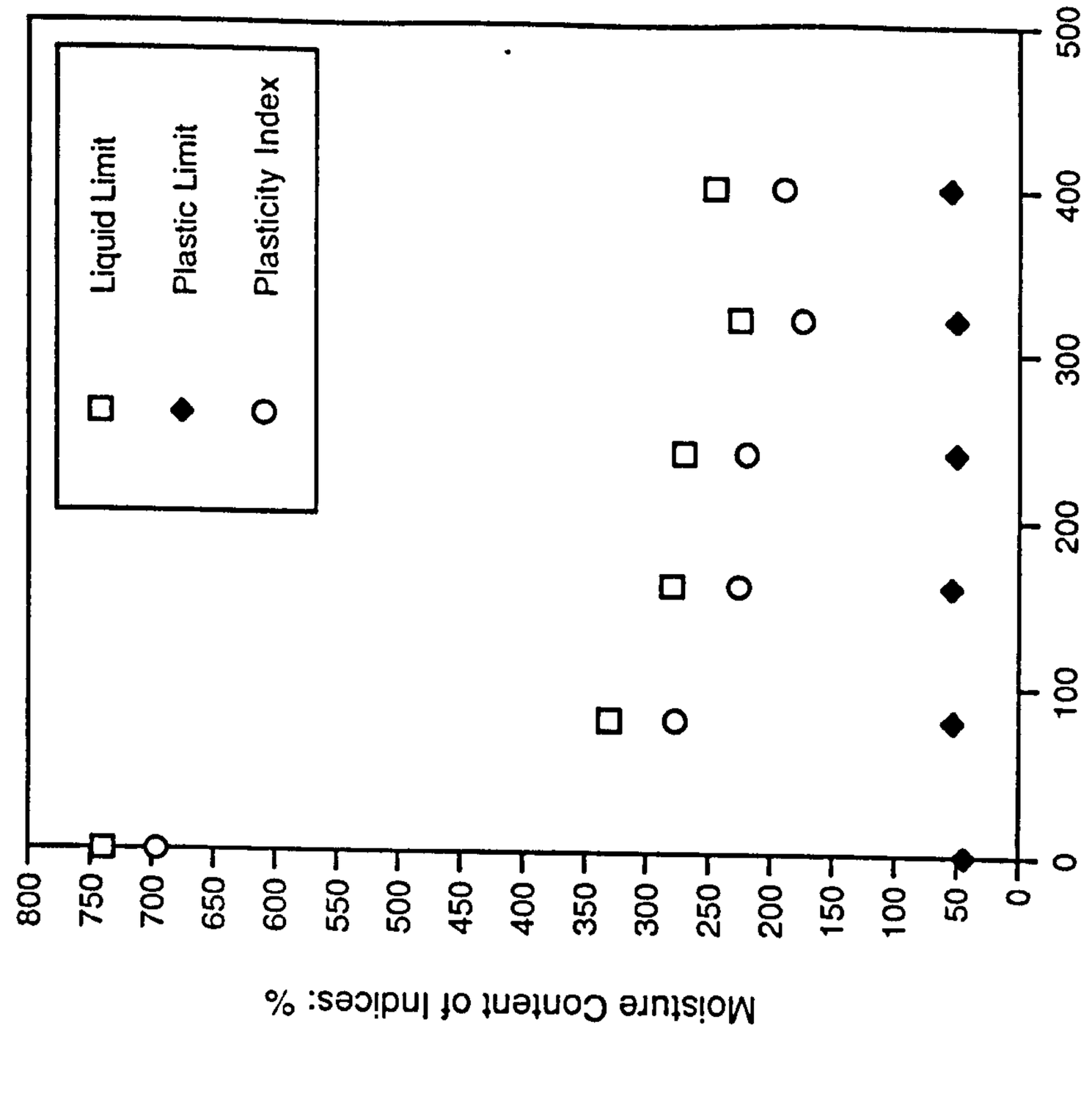

Fig. 5.17 Graph showing the relationship between calcium concentration and the Atterberg limits of montmorillonite.

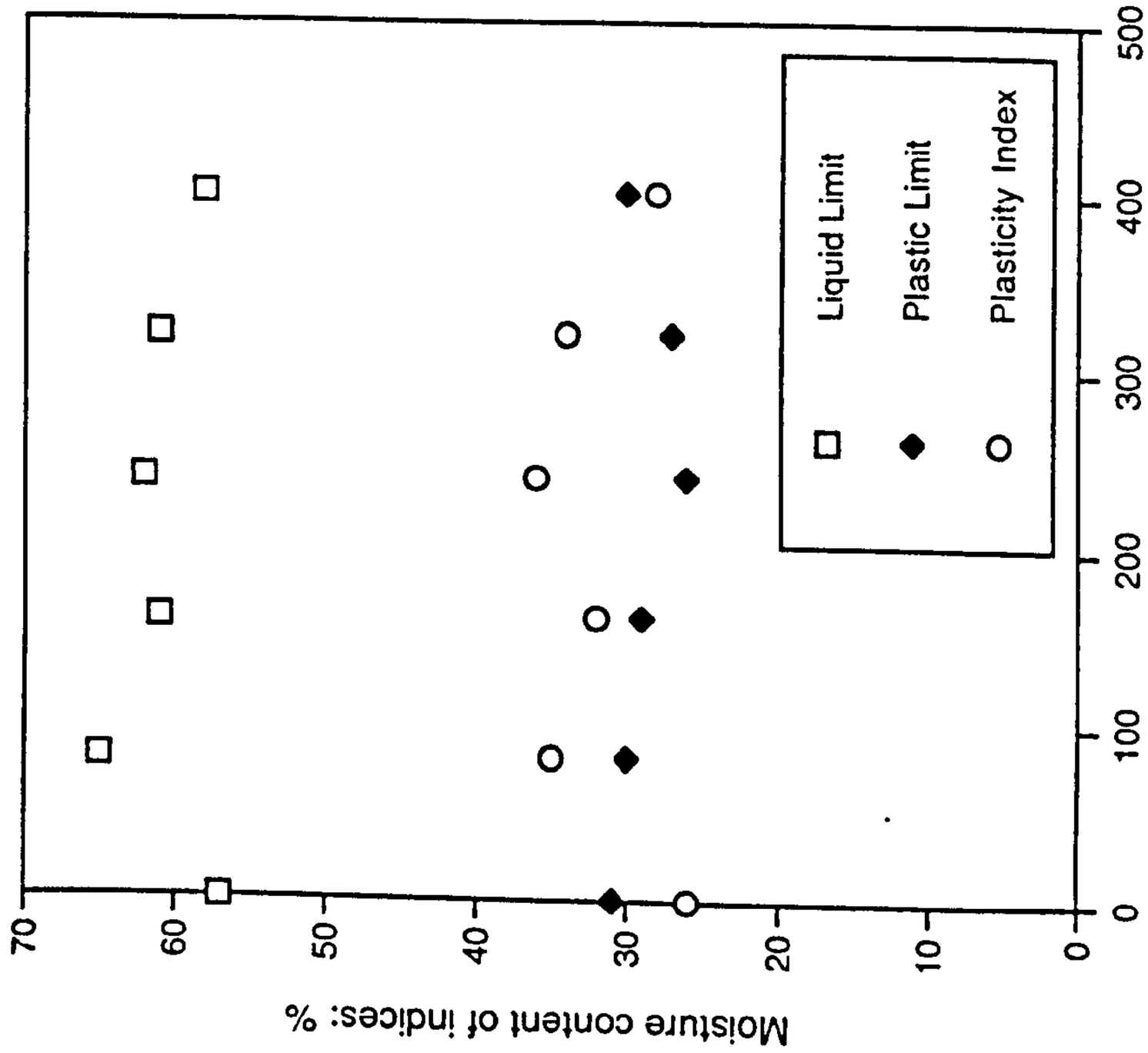

Fig. 5.12 Graph displaying the relationship between calcium concentration and the Atterberg limits of kaolinite.

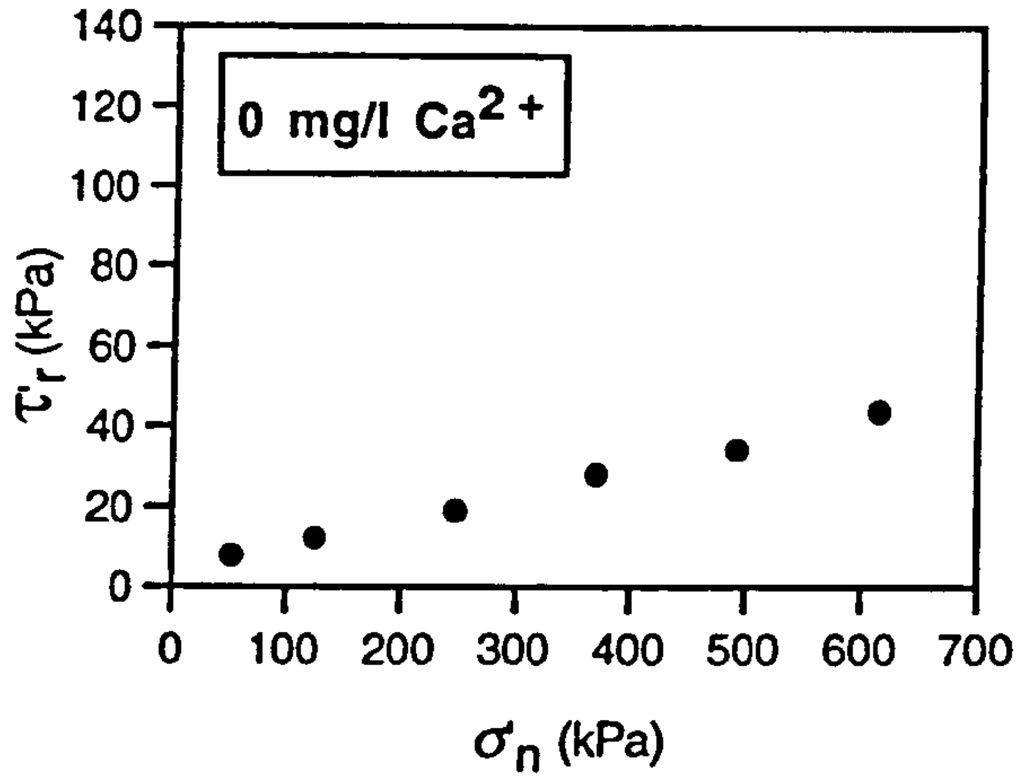

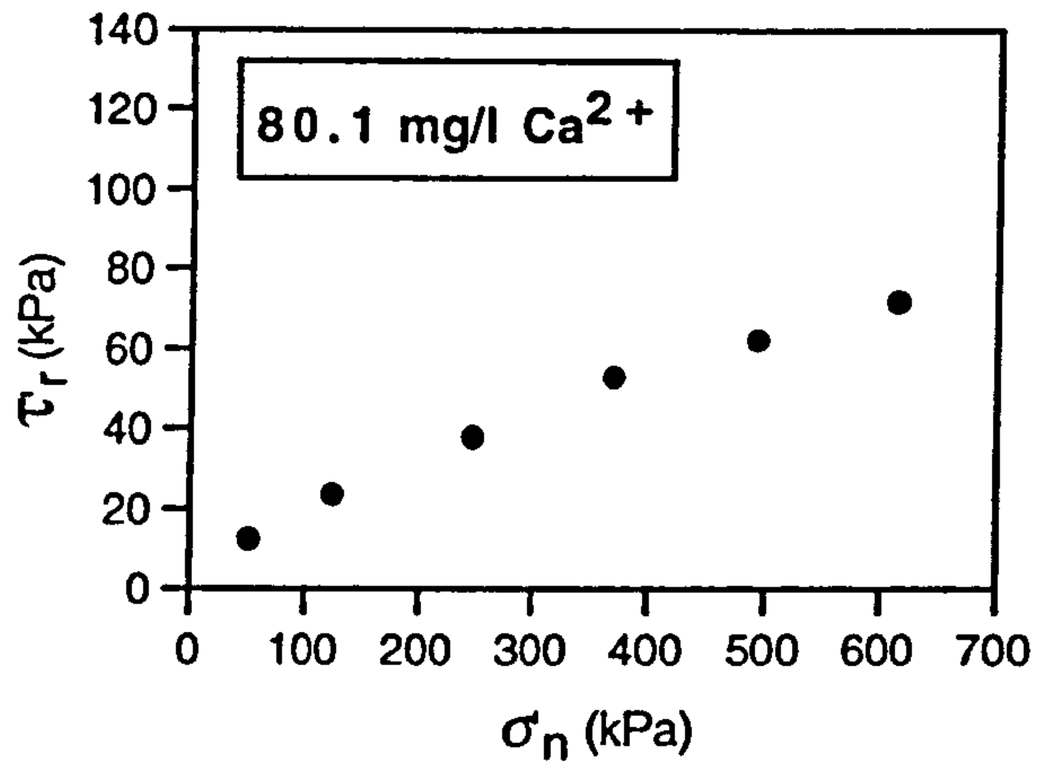

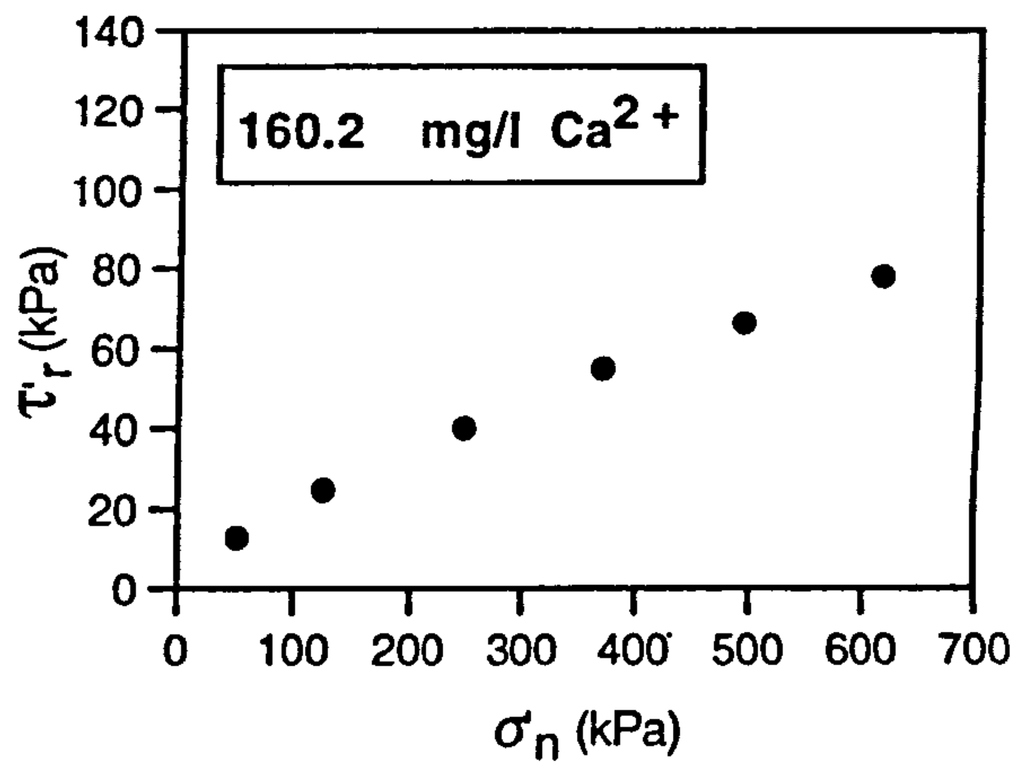

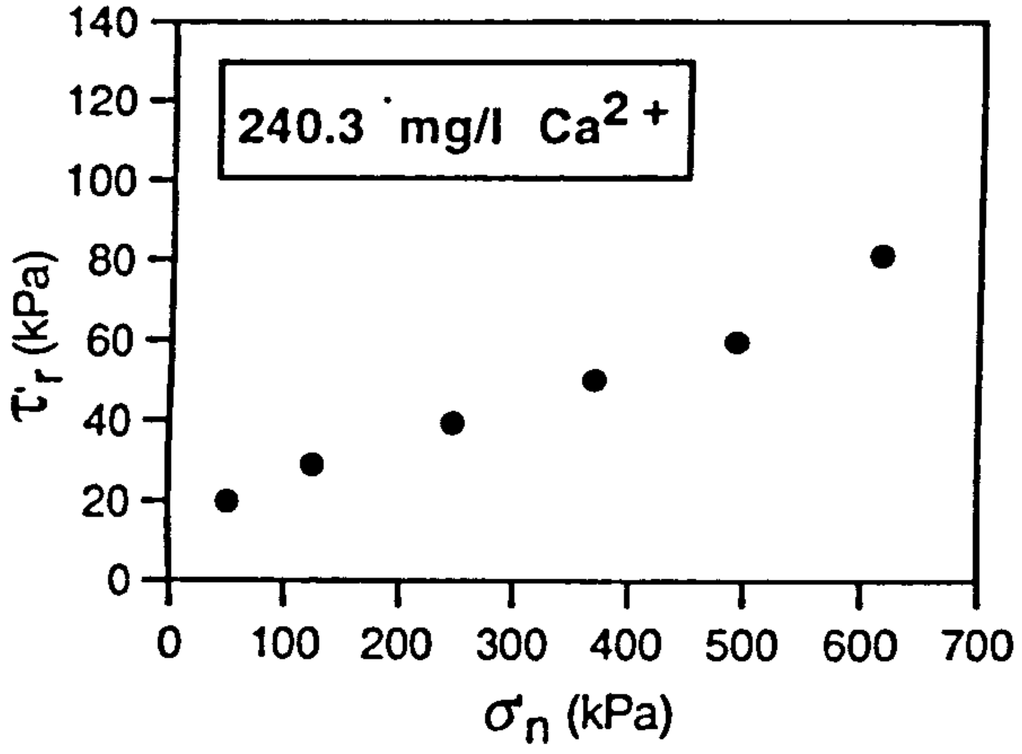

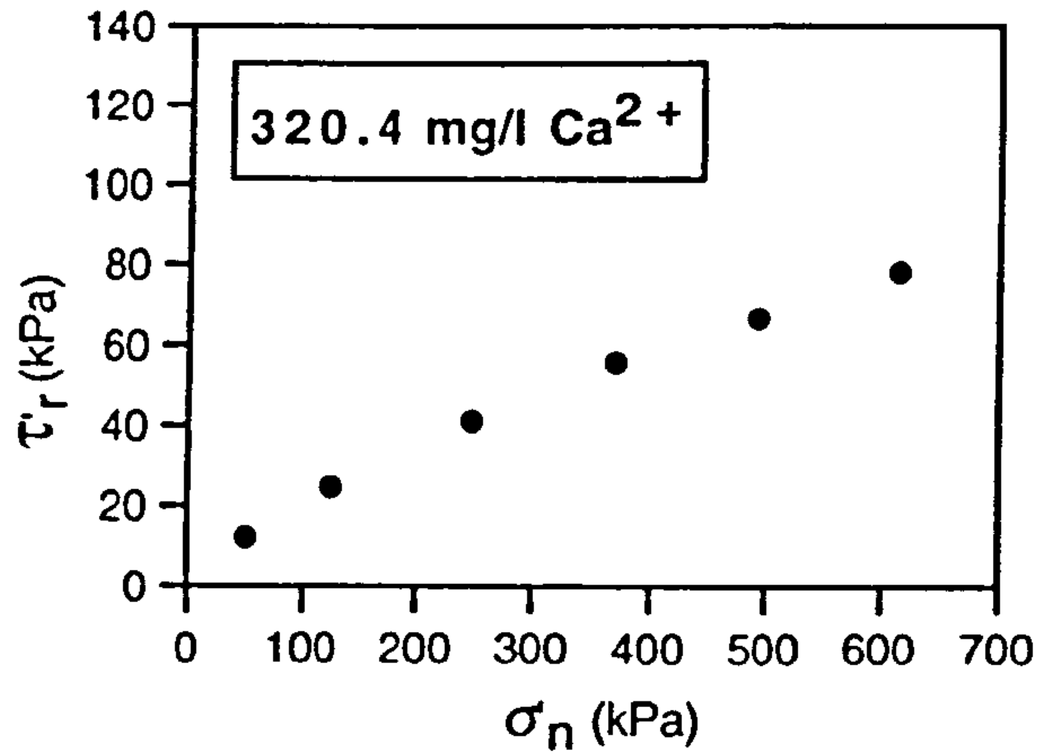

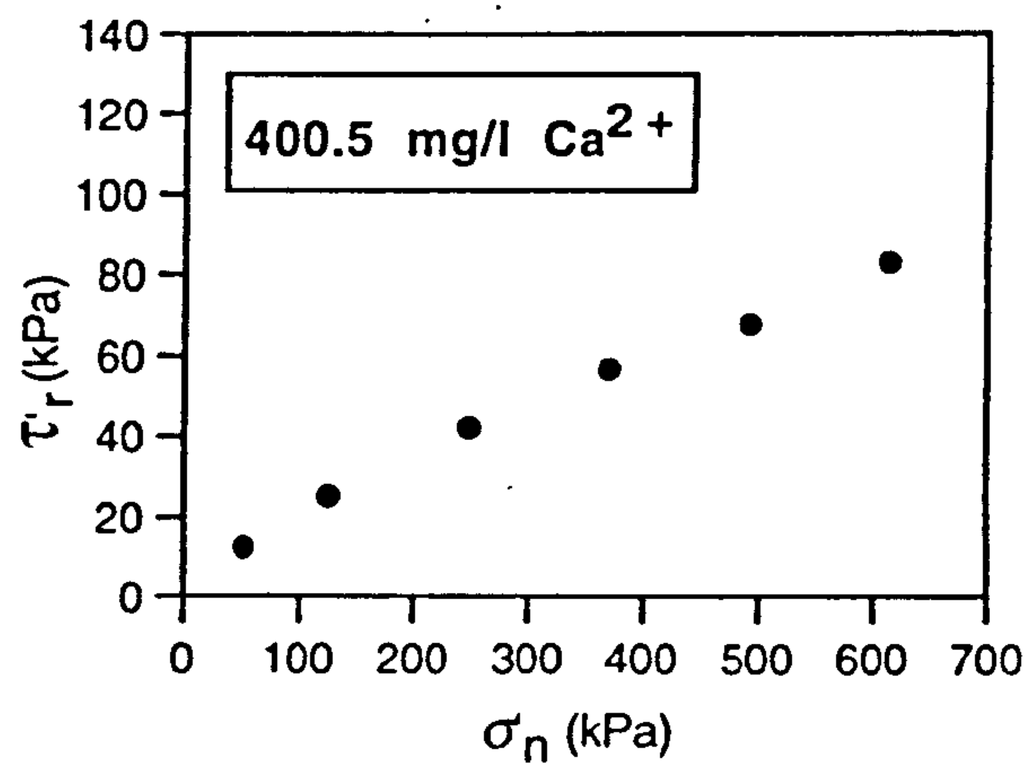

Fig. 5.13 Residual failure envelopes for montmorillonite treated with solutions of calcium at the concentrations shown. Note the exaggerated vertical scale.

water bath and had a "soapy" texture. In comparison, the extruded clay treated with 80.1 mg/l Ca^{2+} was less voluminous/hydrated. Thereafter, for each of the remaining samples (160.2, 240.3, 320.4, 400.4 mg/l Ca^{2+}), the extruded clay did not form a hydrated/voluminous state in the water bath, but had a "brittle" look to it. The change in nature of the extruded clay with increasing calcium concentration, appears to relate to the change observed in the height of the complete residual failure envelopes.

The effective residual shear strength, residual cohesion intercept and residual shear angle were analysed at a range of effective normal stresses (see Figures 5.14, 5.15, 5.16). As for the kaolinite, the change in τ'_r, c'_r and ϕ'_r, with increasing effective normal stress is evident.

Figure 5.14 displays the relationship between ϕ'_r and Ca^{2+} concentration at five effective normal stresses, along with the ultimate residual shear angle. At each effective normal stress, there is a marked increase in the value of ϕ'_r between the untreated montmorillonite and the montmorillonite treated with 80.1 mg/l Ca^{2+}. This is most noticeable at the lower effective normal stresses. At effective normal stresses of 50 kPa and above, there is a trend of increasing ϕ'_r with Ca^{2+} concentration after the initial marked increase. However, at $\sigma'_n = 200$ kPa and in the ultimate condition, this trend is less pronounced. At the very low value of effective normal stress of 25 kPa, above a concentration of 80.1 mg/l Ca^{2+}, there is no obvious trend in ϕ'_r. This may be due to the difficulties in applying a true tangent to the curved portion of the failure envelope at this very low effective normal stress. In all the plots, the value for the montmorillonite sample treated with a solution of 240.3 mg/l Ca^{2+}, forms an outlier to the trend, this is most noticeable at lower effective normal stresses. This outlier is difficult to explain and may be due to contamination during sample preparation.

Figure 5.15 illustrates the relationship between the effective residual cohesion intercept of montmorillonite and Ca^{2+} concentration at five effective normal stresses, together with the value of the ultimate effective residual cohesion intercept. Above a value of $\sigma'_n = 100$ kPa, all the plots show a broad trend of increasing c'_r with Ca^{2+} concentration and, as for ϕ'_r, there is marked increase between c'_r for the untreated montmorillonite and c'_r for the montmorillonite treated with 80.1 mg/l Ca^{2+}. Thereafter, with increasing Ca^{2+} concentration, the increase in c'_r is more gradual. The lack of any visible trend below $\sigma'_n = 100$ kPa, may again be related to the subjectivity involved in establishing the curved portion of the residual failure envelope at these low effective normal stresses and the difficulty in

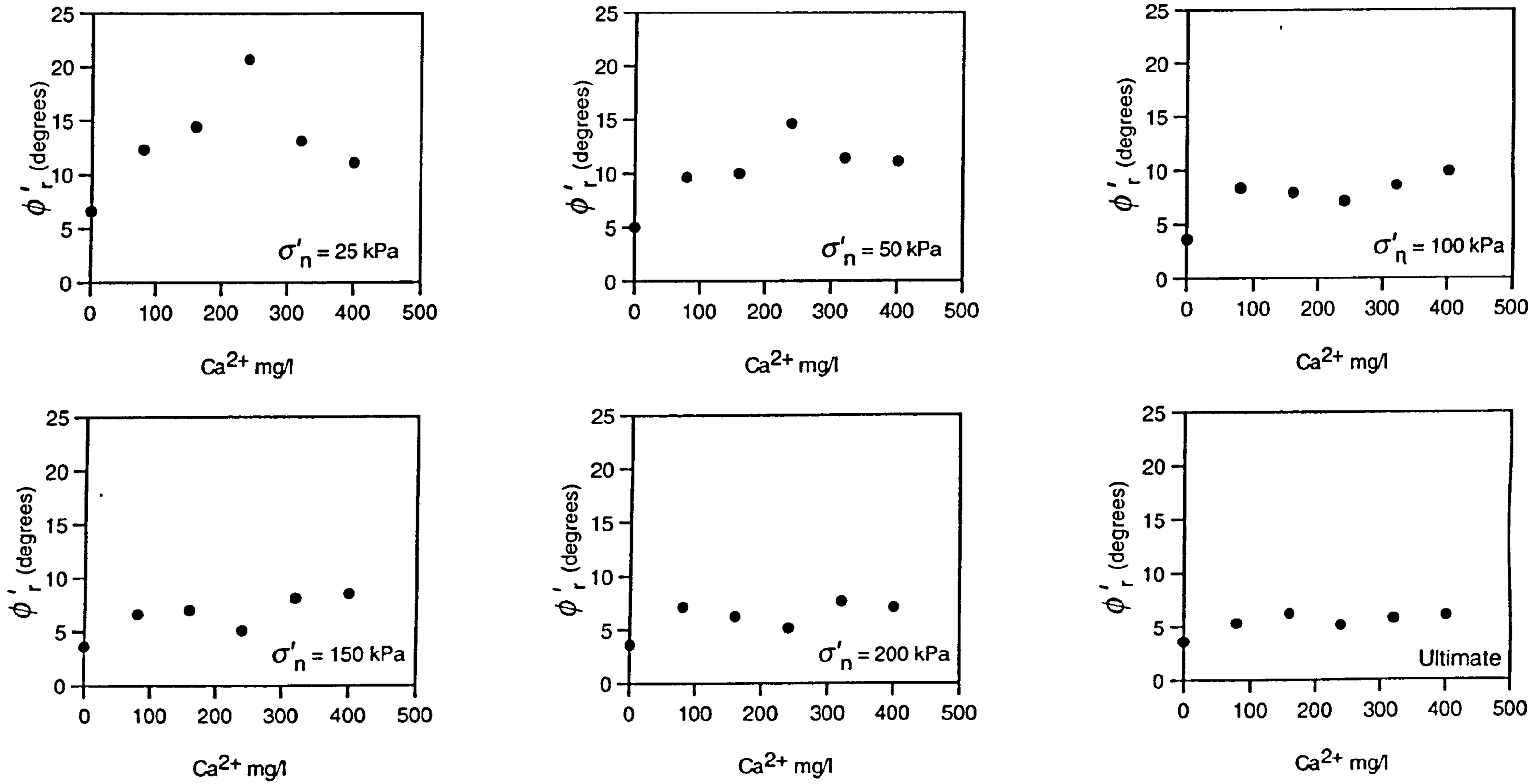

Fig. 5.14 Graphs displaying the relationship between calcium concentration and the effective residual shear angle of montmorillonite at various effective normal stresses.

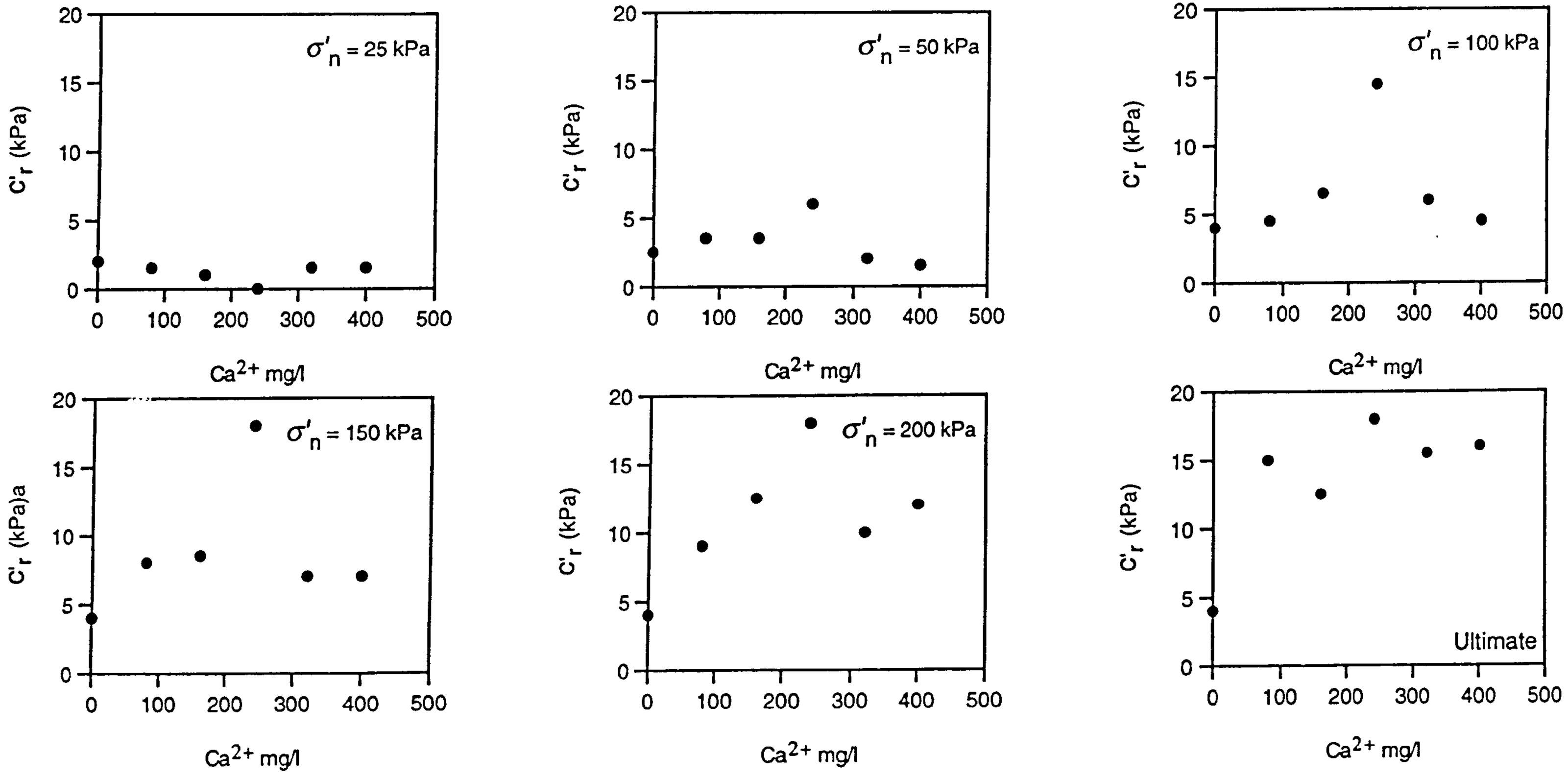

Fig. 5.15 Graphs displaying the relationship between calcium concentration and the effective residual cohesion intercept of montmorillonite at various effective normal stresses.

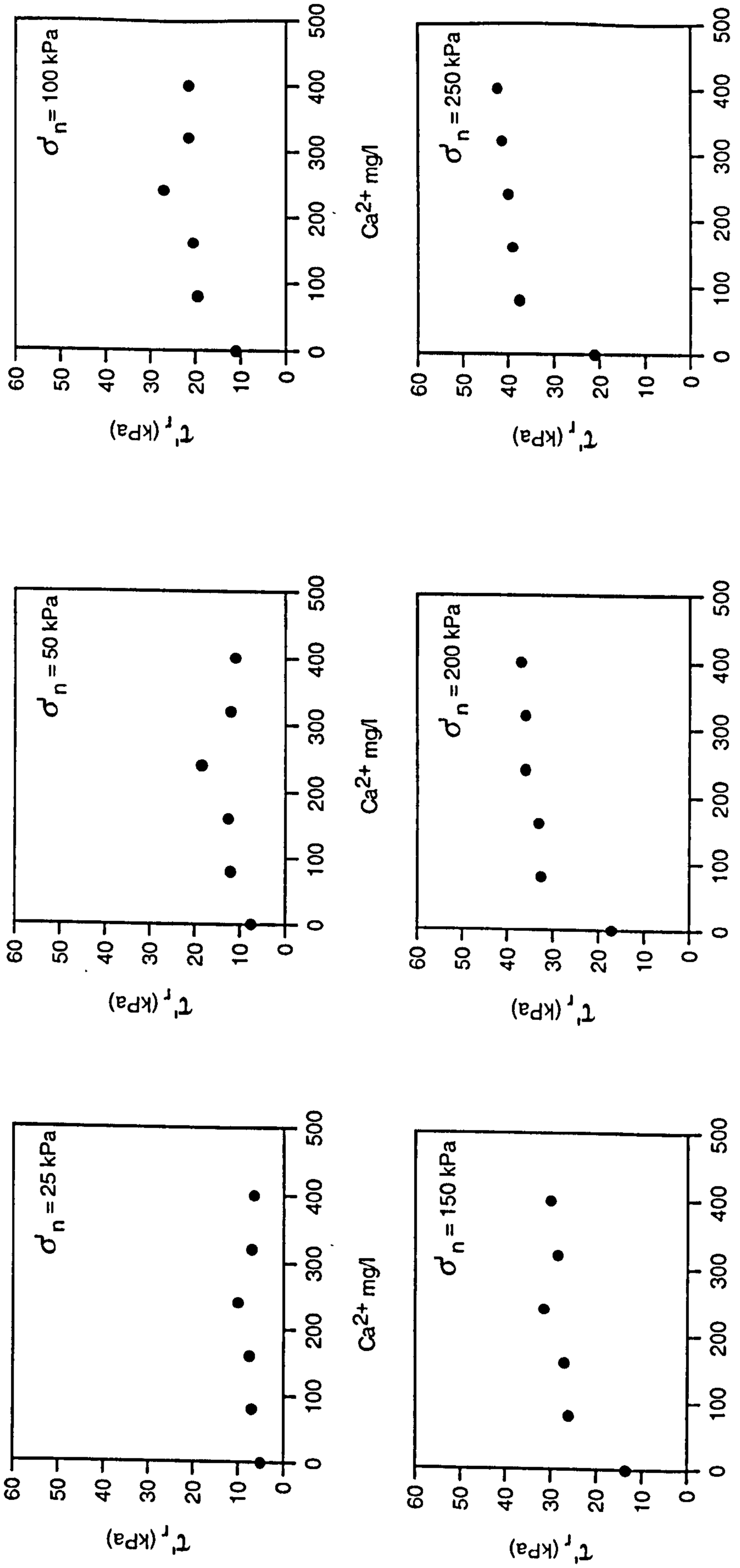

Fig. 5.16 Graphs displaying the relationship between calcium concentration and the residual shear strength of montmorillonite at six effective normal stresses.

establishing an accurate tangent. Once again, the value of c'_r for the sample treated with 240.3 mg/l Ca^{2+} forms an outlier to the trend.

Figure 5.16 displays plots of the residual shear strength of montmorillonite against Ca^{2+} concentration for 6 values of effective normal stress. All the graphs show a trend of increasing τ'_r with increasing calcium concentration, although the trend is most pronounced at higher effective normal stresses. In addition, as for ϕ'_r and c'_r, there is a marked increase between the value of τ'_r obtained for the untreated montmorillonite and that obtained for the montmorillonite treated with 80.1 mg/l. Thereafter the increase in τ'_r with increasing Ca^{2+} concentration is more gradual. Once again, the values obtained for the montmorillonite treated with 240.3 mg/l Ca^{2+} form an outlier to the trend.

The Atterberg limits for each of the treated montmorillonite samples were determined and are displayed in Figure 5.17. The plots show a significant decrease in the liquid limit obtained for the untreated montmorillonite ($w_L = 740\%$) and that obtained for the montmorillonite treated with 80.1 mg/l Ca^{2+} ($w_L = 330\%$). Thereafter, with increasing Ca^{2+} concentration, the liquid limit gradually decreases. No noticeable change is shown by the "less sensitive" plastic limit and hence, as expected, the plasticity index mirrors the liquid limit.

5.7.5 Discussion

The results indicate that both the residual shear strength and Atterberg limits of kaolinite and montmorillonite are sensitive to the concentration of calcium in pore water. However, the influence of pore water chemistry is more pronounced in montmorillonite than kaolinite. This is as expected from a consideration of the surface area to size ratios and the known behaviour of the two clay minerals (see Section 5.2).

The results compare favourably with the data reported by Kenney (1967), Steward & Cripps (1983), Steward (1984), Moore (1988 and 1991), and in part with those of Maio & Fenelli (1994), see Chapter 2. Maio & Fenelli found that the residual shear strength of bentonite increased with increasing concentrations of sodium chloride solution, however they found that kaolinite was insensitive to pore water chemistry. They suggest that where the residual shear strength of kaolinite varies with pore water chemistry, this is likely to be due to the high electrolyte concentration used, which causes a change in the clay aggregate size and micro-structure. They state that:

"The range of concentrations Moore *(who found that kaolinite was sensitive to pore water chemistry)* used gives rise to very interesting phenomena of micro-structural change, as experiments on sodium-montmorillonite suspensions by Stawinski *et al.* (1990) and Chen *et al.* (1990) seem to show".

However, the concentrations used in this study are low (maximum concentration = 400.5 mg/l Ca^{2+}) and are equivalent to the concentrations seen in natural ground waters in the landslide at Soper's Wood. Therefore, the difference between the sensitivity shown by the kaolinite in this study and the insensitivity of the kaolinite in Maio & Fenelli's study is unlikely to be explained as proposed above.

It is important to re-emphasise that these studies concern that of residual shear strength and not peak shear strength. As discussed in Chapter 1, in the sliding mode of shear (the expected mode of failure for pure clays) residual shear strength involves the re-orientation of clay particles parallel to the direction of movement, forming a discrete shear surface. Thus, as described by Skempton (1964), the residual shear strength of a clay is independent of its previous consolidation history. In addition, Chandler (1966 & 1969) and Hutchinson *et al.* (1973) noted that during shearing any silt sized aggregations of clay minerals were broken down, such that the clay fraction at the shear surface was higher than in the adjacent soil. Thus, a change in the flocculated clay micro-structure is unlikely to affect the residual shear strength of the clay.

Sridharan & Rao (1979) and Chatterji & Morgenstern (1989) proposed a "modified effective stress law", which incorporates the physico-chemical forces of interaction, in an attempt to explain the influence of clay chemistry on effectives stress and the behaviour of clays. The results obtained from the research presented in this thesis can be explained by the known physico-chemical effects of clay systems, as described in Section 5.3, and used by previous researchers (Moum & Rosenqvist 1961, Olson & Mitronovas 1962 and Warkentin & Yong 1962) to explain the effects of electrolyte solutions on the peak shear strength of "pure" clays. A similar explanation is proposed by Moore (1988 and 1991).

To confirm that the effects seen were not as a result of changing mineralogy and are indeed due to physico-chemical effects, XRD analyses were carried out on remoulded samples obtained from the ring shear apparatus (see Appendix I for technique). From the manufacturers descriptions, it was expected that the samples would be "pure" clays, hence XRD analyses were carried out on air dried samples.

Figure 5.18 displays the x-ray diffractograms for each of the kaolinite samples and, as expected, highlights the clear dominance of kaolinite. An inspection of the diffractograms indicates that they are all very similar, each showing near identical peaks. Hence, there is no variation in mineralogy between the various samples. Thus, clearly the sensitivity of the residual shear strength and Atterberg limits of the kaolinite to calcium concentration in the pore water is not related to any change in the overall mineralogy between samples.

Figure 5.19 displays the x-ray diffractograms for each of the montmorillonite samples and, as expected, emphasises the dominance of montmorillonite. Again each of the diffractograms display very similar reflections, indicating no overall change in the mineralogy of the samples. However, an inspection of the basal (001) reflection of montmorillonite indicates that the reflection migrates with increasing calcium ion concentration. McAttee (1956) notes that at room temperature, ideally sodium montmorillonite would have a single water layer resulting in a (001) spacing of 12.4 Å, while calcium montmorillonite would have a double water layer and a corresponding value of 15.4 Å. Thus, the position of the (001) montmorillonite reflection will provide a qualitative indication of the degree of substitution of sodium by calcium.

SAMPLE	(001) REFLECTION	INTERPRETATION
Untreated Montmorillonite	Dominant peak at 12.97 Å, with shoulder at 15.96 Å.	Na montmorillonite dominant, subsidiary Ca montmorillonite.
Montmorillonite + 80.1 mg/l Ca^{2+}	Broad reflection, with peaks at 12.30 and 15.94 Å	Approximately equal amounts of Na and Ca montmorillonite.
Montmorillonite + 160.2 mg/l Ca^{2+}	Broad reflection, with peaks at 15.44 and 13.46 Å.	Approximately equal amounts of Na and Ca montmorillonite; Ca slightly dominant.
Montmorillonite + 240.3 mg/l Ca^{2+}	Peaks at 15.90 and 15.59 Å.	Ca montmorillonite.
Montmorillonite + 320.4 mg/l Ca^{2+}	Broad reflection, with peaks at 15.73 and 13.71 Å.	Approximately equal amounts of Na and Ca montmorillonite; Ca slightly dominant.
Montmorillonite + 400.5 mg/l Ca^{2+}	Peak at 16.08Å.	Ca montmorillonite

Table 5.1 Qualitative analysis of (001) montmorillonite reflection.

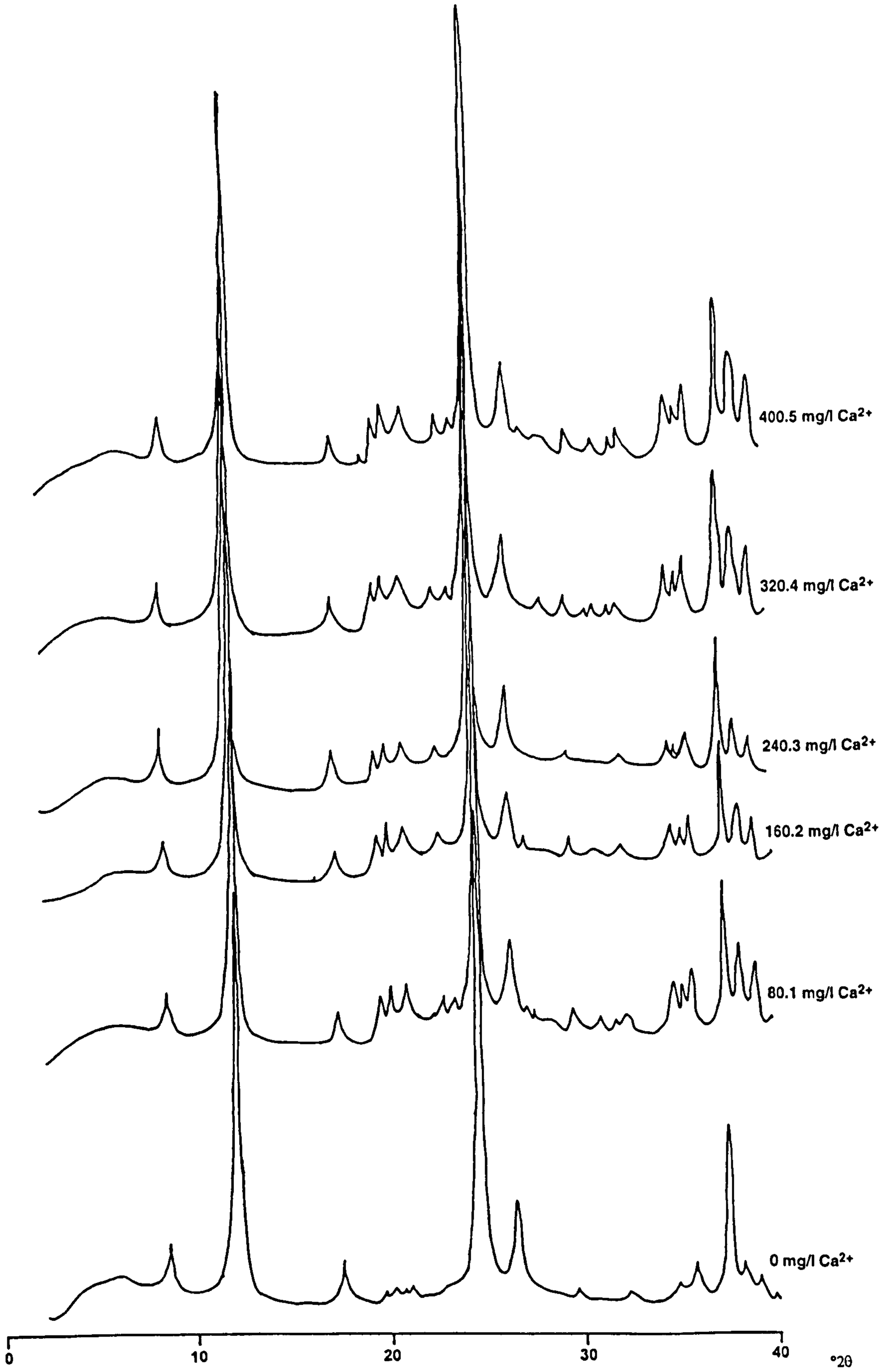

Fig. 5.18 X-ray diffractograms for the samples of kaolinite treated with solutions of calcium at the concentrations shown.

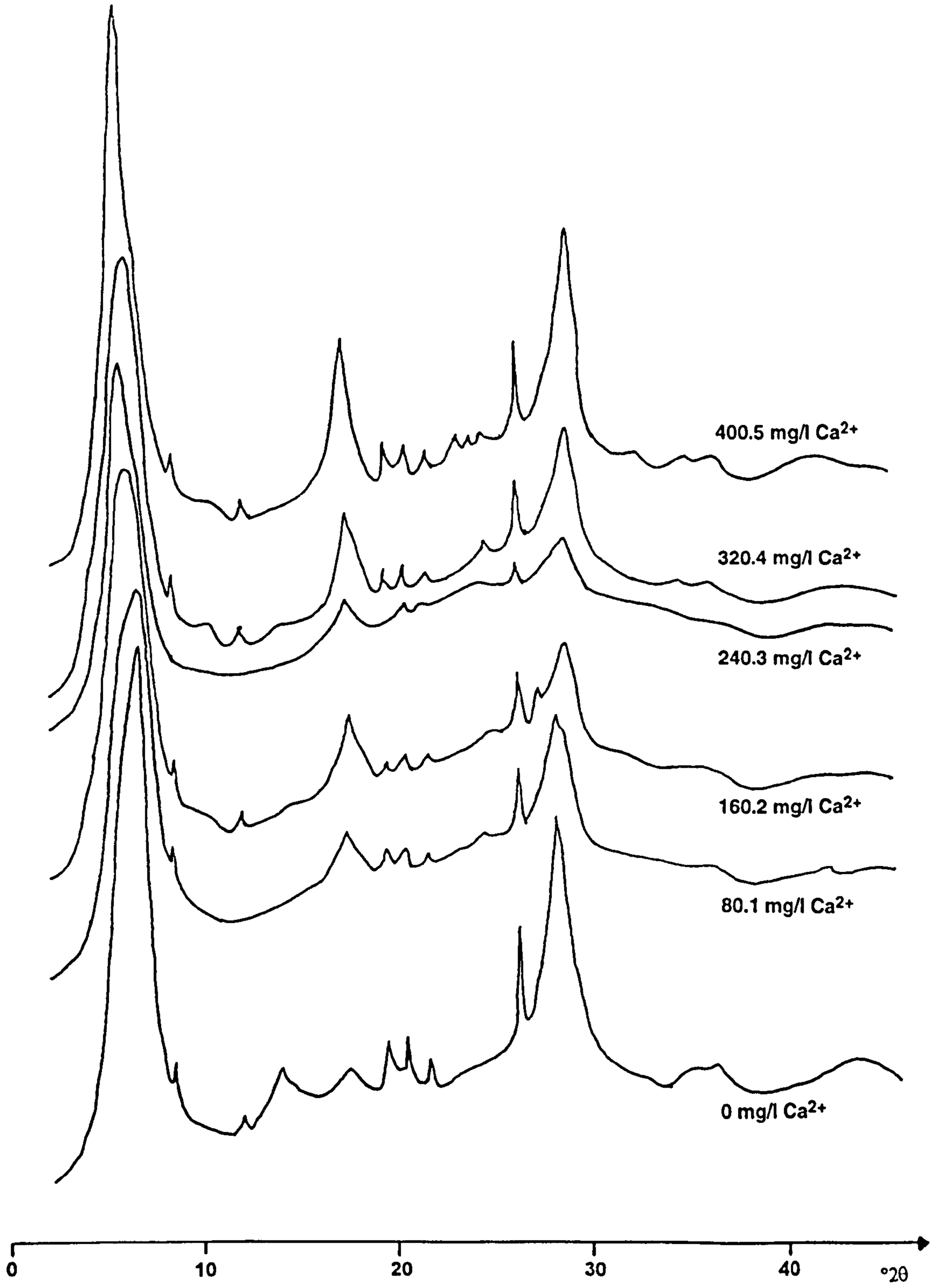

Fig. 5.19 X-ray diffractograms for the samples of montmorillonite treated with solutions of calcium at the concentrations shown.

Table 5.1 presents a qualitative analysis of the position of the (001) montmorillonite reflection and indicates that with increasing concentration of calcium there appears to be a trend of increasing substitution of calcium for sodium. The most noticeable change is between the untreated sample and the sample treated with 80.1 mg/l Ca^{2+}. In the untreated sample, Na-montmorillonite is dominant whereas in the treated sample there are approximately equal proportions of sodium and calcium montmorillonite. Only calcium montmorillonite is evident in the diffractograms for the samples treated with 400.5 mg/l Ca^{2+} and 240.3 mg/l Ca^{2+} and this may explain the behaviour of the montmorillonite treated with 240.3 mg/l Ca^{2+}. From the XRD diffractograms of the samples treated with 80.1 mg/l, 160.2 mg/l and 320.4 mg/l, it would be expected that the sample treated with 240.3 mg/l Ca^{2+} would also show approximately equal proportions of sodium and calcium montmorillonite. The dominance of calcium in the montmorillonite treated with 240.3 mg/l Ca^{2+} is contrary to the trend and may have been caused by contamination of the sample during the treatment stage.

An increase in the concentration of Ca^{2+} in the pore water will cause the compression of the diffuse hydrated double layer surrounding the individual clay particles, suppressing the repulsive forces, such that the attractive van der Waals forces are able to dominate. The degree of compression increases with increasing Ca^{2+} concentration, such that the effect of the van der Waals force is enhanced, as the range of repulsion is reduced. Thus, the bonding between clay minerals increases with increasing Ca^{2+} concentration. This accounts for the observed increase in τ'_r and c'_r. As the effects are purely physico-chemical, no change would be expected in the value of the effective residual shear angle.

The presence of Na^+ adsorbed to the untreated montmorillonite enhances the effect. Na^+ is known to stabilise the hydrated double layer, such that repulsive forces dominate and the clay platelets exist in a more dispersed state. Thus, with an increase in the concentration of Ca^{2+} in the pore water, Na^+ will be exchanged for Ca^{2+} causing compression of the double layer and allowing the attractive forces to dominate. This explains the marked increase in residual shear strength observed between the untreated montmorillonite sample and the sample treated with 80.1 mg/l Ca^{2+}.

For the kaolinite, a broad increase is noted in ϕ'_r at the very low effective normal stress of 25 kPa. This is most probably related to the curvature of the failure envelope at this low value of σ'_n. For the

montmorillonite, at all levels of σ'_n there is a notable increase in ϕ'_r between the untreated montmorillonite (which the XRD analysis has shown to be dominated by sodium montmorillonite) and the sample treated with a solution of 80.1 mg/l Ca^{2+}. In addition, after this marked increase, ϕ'_r increases gradually with increasing Ca^{2+} concentration. These two phenomena may be related to the substitution of calcium for sodium changing the character of the clay and hence its frictional properties. XRD analysis indicates that the substitution was greater between the untreated sample and the sample treated with 80.1 mg/l Ca^{2+}. This coincides with the biggest change in ϕ'_r; with increasing Ca^{2+} concentration, the XRD analyses show the substitution to be less great and hence the change in ϕ'_r is gradual. At the higher values of effective normal stress, the load applied may counteract the change in the frictional properties, such that, apart from the initial increase, the change in ϕ'_r is less pronounced.

The liquid limit and plasticity index of the kaolinite and montmorillonite samples show opposing behaviour. The liquid limit of the kaolinite shows a marked increase between the untreated sample and the sample treated with 80.1 mg/l Ca^{2+}. This correlates with Yong & Warkentin (1966) as reported by Sridharan, Rao & Murthy (1988) in their study of the liquid limit of kaolinitic soils. Yong & Warkentin (1966) observed that by saturating kaolinite with di-valent and tri-valent cations, electrostatic attraction is developed between positive and negative faces, leading to an open structured, flocculated particle arrangement. This results in a higher liquid limit, as water becomes entrapped within the void spaces of the flocculated structure.

In contrast, the liquid limit of the montmorillonite decreases with increasing Ca^{2+} concentration, markedly at first. The marked reduction in the liquid limit between the untreated montmorillonite and the montmorillonite treated with 80.1 mg/l Ca^{2+} can be explained by the change from a sodium dominated montmorillonite to a calcium/sodium montmorillonite. Thereafter, the more gradual decrease in liquid limit can be explained by the increase in bond strength between the clay particles, with increasing Ca^{2+} concentration.

The results have important implications for slope stability at Soper's Wood and at other sites. However, it must be recognised that the changes observed in the complete residual failure envelope with Ca^{2+} concentration have been demonstrated on pure clays and will undoubtedly be diluted in natural soils, where the presence of silt and sand sized particles will also affect the residual shear strength of the soil. Kenney (1977) proposed that

pore water chemistry will influence the residual shear strength of the soil as long as the behaviour of the soil is controlled by the clay mineral matrix (ie if failure is in the sliding and transitional modes of shear). Chapter 3 has shown that the concentration of calcium in the ground water at Soper's Wood varies with location within the slip and also to a certain extent with rainfall/seasonally. Thus, in the Fuller's Earth clay, pore water chemistry can be expected to play a role in determining the residual shear shear strength of the clay as long as failure occurs in the sliding or transitional modes of shear. The illite in the Fuller's Earth can be expected to show a behaviour intermediate between kaolinite and montmorillonite (see Section 5.2).

The effects of pore water chemistry on the residual shear strength of the Fuller's Earth clay are likely to be enhanced in the weathered zone. Here chemical weathering has caused the dissolution of calcite and the transformation of some of the illite to an interstratified illite-montmorillonite. Kenney (1967) found that smectites exert a greater influence on the residual shear strength of a soil than would be expected from their proportion in the dry soil mass. Chapter 4 has indicated that preferential weathering is likely to be occurring along shear surfaces within the Fullers' Earth, such that the proportion of interstratified illite-montmorillonite is increased. In addition, if the dissolution of disseminated calcite occurs at a preferential rate along the shear surface (although this was not observed during the investigation of the relatively shallow shear surface described in Chapter 4) the clay fraction will increase. Thus, pore water chemistry can be expected to play a greater role in determining the residual shear strength of the failure plane.

A knowledge of how the engineering properties of clay minerals alter with solution chemistry may be applied to slope stabilization work. Matsuo (1957) presents the results of a study on the effects of cation exchange on the stability of a landslip at Kashio, Japan. Prior to failure there was "little change in external conditions" and hence an investigation was carried out to determine whether physico-chemical factors may have caused the failure of the slope. Chemical analysis of the ground water showed it to be rich in Ca^{2+} and analyses of the cations adsorbed to the landslipped soil indicated that Ca^{2+} was dominant. However, Matsuo (1957) noted that the quantity of adsorbed Ca^{2+} was only three quarters of the total cation capacity of the soil. From these observations he proposed that the soil was originally saturated with respect to Ca^{2+} and that some of the adsorbed cations have been leached from the soil during the years preceding failure.

He reported the results of shear tests to determine the peak shear strength of both the natural soil and of the soil artificially saturated with Ca^{2+}. He found that the angle of friction for the Ca^{2+} saturated soil was higher at 0.45° compared to 0.06° for the natural soil. It is of note that these values are remarkably low. In addition, he reported the value of "apparent cohesion" to be 0.163 kg/cm^2 and 0.08 kg/cm^2, for the Ca^{2+} saturated soil and the natural soil, respectively. The results of slope stability analyses for the landslide using the strengths for both the Ca^{2+} saturated soil and the natural soil provided a factor of safety of 1.3 and 0.6, respectively. Hence, Matsuo (1957) proposed that the leaching of Ca^{2+} from the soil had brought about the failure of the slope and suggested that the slope may be stabilised by the addition of aqueous solutions of calcium salts into the soil at the head of the slip, in order to increase the shear strength of the soil.

In the 1970's work was conducted in California into the stabilization of clay slopes by ion exchange (Arora & Scott 1974). Chemical solutions were pumped into boreholes and tension cracks within a landslide. This allowed the solution to permeate through the slipped mass and along shear surfaces and, by ion exchange, stabilize the slope. Clearly, a detailed analysis of the clays to establish there chemical state was needed prior to stabilization work. This technique was evaluated by the California State Division of Highways (Mearns *et al.* 1973) who monitored an active landslide following chemical treatment. However, due to changing rainfall patterns over the time of investigation, the results were inconclusive. The simplicity and relative cost effectiveness of these ion exchange techniques, if successful, need to be balanced against the environmental consequences of pumping potentially toxic chemicals into the ground.

Further work is clearly necessary to improve the definition of these relationships and establish the repeatability of the experiments, extending them to other pure and naturally occurring clays. However, the techniques that have been used to ensure accuracy are time consuming and further investigation would make a valuable research project in itself. In addition, the use of naturally occurring clays poses certain problems due to sample heterogeneity. Steward (1984) and Moore (1988 and 1991) overcame this problem by using an adapted ring shear apparatus, although this method allows a determination of the apparent residual shear angle rather than the true residual shear angle (see Chapter 2). However, it may prove possible to use the modified apparatus to test the same sample at a range of effective normal stresses and solution concentrations over a long period of time, as long as sample extrusion is controlled by the use of a very low

strain rate. This would enable the construction of the complete residual failure envelopes for a single sample at a range of solution concentrations.

5.8 Conclusions

(1) The results indicate that the residual shear strength of kaolinite and montmorillonite increase with increasing Ca^{2+} concentration. This is most marked between the untreated samples and the samples treated with 80.1 mg/l Ca^{2+}.

(2) The influence of Ca^{2+} concentration is most pronounced in the parameters, c'_r and τ'_r.

(3) XRD analyses of the samples demonstrated that the overall mineralogy of the samples remained constant. However, the (001) montmorillonite reflection can be seen to migrate with increasing Ca^{2+} concentration. This has been interpreted to indicate that Na^+ is being exchanged for Ca^{2+}, with increasing Ca^{2+} concentration in the pore water.

(4) The behaviour of the clays can be explained by physico-chemical effects. An increase in Ca^{2+} concentration in the pore water causes compression of the hydrated double layer surrounding the clay particles. Hence, the repulsive forces between clay platelets are reduced and the attractive van der Waals forces are able to dominate. Thus, with increasing Ca^{2+} concentration, bond strength increases and c'_r and τ'_r increase.

(5) The liquid limit and plasticity index of kaolinite and montmorillonite show opposing behaviour. The liquid limit of the kaolinite shows a marked increase between the untreated sample and the sample treated with 80.1 mg/l Ca^{2+}. This is interpreted to result from a change in the arrangement of the kaolinite platelets from a dispersed state in the untreated sample, to an open flocculated structure in the presence of Ca^{2+}. In contrast, the liquid limit of the montmorillonite decreases with increasing Ca^{2+} concentration, markedly at first. This can be explained by the increase in bond strength between clay particles with increasing Ca^{2+} concentration.

(6) The results have important implications for slope stability, however the effects will undoubtedly be diluted in natural soils. Where the behaviour of a soil is controlled by the clay mineral matrix (ie in the sliding and

transitional mode of shear), pore water chemistry can be expected to play a role in determining the residual shear strength of the clay.

(7) The levels of calcium used in the ring shear test correspond to the levels found in the ground waters within the landslip at Soper's Wood. Thus, if shear is occurring in the sliding mode, pore water chemistry can be expected to play a part in determining the residual shear strength of the Fuller's Earth clay at Soper's Wood. These effects are likely to be greater in the weathered Fuller's Earth clay. Here chemical weathering has increased the proportion of interstratified illite-montmorillonite and caused the dissolution of calcite, leading to a relative increase in the clay fraction of the soil.

(8) An increased understanding of how pore water chemistry effects the complete residual failure envelope of clays may allow the further development of alternative methods for slope stabilisation using solution chemistry.

CHAPTER 6

A MODEL FOR THE STABILITY OF THE LANDSLIDE ADJACENT TO SOPER'S WOOD

6.1 Introduction

The opening chapter of this thesis describes how the combination of the geology and topography within the Swainswick valley has facilitated the development of superficial structures. This combination is characteristic of the over-steepened Avon valley and many of its tributaries in the surrounding Bath area. Beneath the plateau cap rock of the Great Oolite, the Fuller's Earth forms the upper hill slopes of these valleys and is characterised by the presence of extensive translational landslides.

This chapter attempts to incorporate the literature reviewed in Chapters 1 and 2, with the results from the investigations described in Chapters 3, 4 and 5, to produce a model for the stability of the landslide in the Fuller's Earth adjacent to Soper's Wood. This landslide is typical of the many that exist in the Fuller's Earth. Hence, although the model is derived from the investigations of the landslide adjacent to Soper's Wood, it is expected that it will apply to the many other similar landslips in the formation around Bath. It is important to recognise that this model applies to slopes which have already slipped and, as a result of pre-existing shear surfaces, are at their residual shear strength.

The stability of the landslip adjacent to Soper's Wood is considered in two ways; the "long term stability" of the landslide and the "seasonal stability" of the landslide. The long term stability is concerned with the general decrease of the residual shear strength of the shear surfaces within the slipped mass with time. Superimposed on this long term decrease are seasonal effects which cause the periodic movement of the landslide. This chapter will show that these seasonal effects are the dominant control concerning whether movement will or will not take place during a particular year; although clearly with a general decrease in residual shear strength over time, the "threshold" at which movement occurs will be reduced.

6.2 Long Term Controls on Slope Stability

The Fuller's Earth clay has been shown to have a variable calcite content (see Chapters 1 and 2, and Section 3.4.3). McDonald (1990) demonstrated that the material of greater than clay grade in size was dominantly calcitic; XRD analyses described in Section 4.8 indicated that

quartz is also present, with subsidiary feldspar, pyrite and gypsum. Chapter 2 reviews the control that the calcite content exerts on the geotechnical indices and residual shear strength of the Fuller's Earth. Hence, it is likely that in any landslide, the shear surfaces present will have propagated, where possible, through a zone of lower calcium carbonate content. This is supported by the study of the shear surface in Chapter 4, which indicated that the failure surface was located just below a zone of high calcium carbonate content.

The analysis of the ground waters from within the landslide at Soper's Wood, described in Chapter 3, indicated a dominance of calcium with subordinate potassium and magnesium (see Figure 3.23). The concentration of calcium was shown to be very high and is likely to result from the dissolution of calcium carbonate within the Fuller's Earth by acidic ground waters. It is believed that these acidic waters have also caused the chemical weathering of illite, where potassium ions are leached from the illite and exchanged for calcium ions, with the formation of a randomly interstratified illite-montmorillonite.

Natural ground water is usually acidic and, as discussed in Chapter 5, carbonic acid is probably the most important source of acidity. However, other potential sources of acidity include; sulphuric acid from pyrite degradation (Hawkins & Pinches 1987); acid rain (Henderson-Sellers 1984 and Mellanby 1988); organic acids, such as humic acid (Freeze & Cherry 1979). Of these potential subsidiary sources of acidity, sulphuric acid derived from the degradation of pyrite is likely to be the most prominent. In addition to the chemical attack of the host soil material, the sulphuric acid reacts with calcite to form gypsum. The development of gypsum on the outer edge of the core obtained from the Soper's Wood borehole (see Figure 3.3) was reported by Lawrence (1985), implying that pyrite degradation was taking place. In addition, x-ray diffractograms, described in Section 4.8, displayed minor peaks of gypsum and pyrite. However, gypsum was not recorded during the logging of the auger hole samples described in Section 3.4. This may have been due to the saturated state of the soil and the high solubility of gypsum.

These acidic ground waters will not only percolate through the dilated slipped material, but will preferentially percolate along shear surfaces, as evidenced by the outflow of water from the basal shear surface at the toe of the landslide adjacent to Soper's Wood. The investigation described in Chapter 4 demonstrated that preferential weathering of illite to form a randomly interstratified illite-montmorillonite is occurring along shear

surfaces. In addition, it is likely that the acidic ground waters will also cause the dissolution of grains of calcite along shear surfaces and adjacent calcareous cement. Hence, with time, a shear surface can be expected to show a gradually decreasing calcite content (thus an increase in clay fraction) and an increasing proportion of randomly interstratified illite-montmorillonite.

Chapter 2 has demonstrated that a decrease in the calcite content of the Fuller's Earth results in a reduction in the residual shear angle of the material to a minimum value, when failure is likely to be in the sliding mode of shear (Lupini *et al.* 1981). In addition, as reported by Kenney (1967) and Chattopadhyay (1972), montmorillonite has a lower residual shear angle compared to illite. Thus, over the long term, the shear surface can be expected to show a decrease in residual shear strength as a result of natural chemical weathering.

It is of note that Alonso *et al.* (1993), when referring to the presence of a clay band on which a large landslip took place at Cortes de Pallas, Spain, considered that this failure horizon may have been created by the preferential removal of dolomite leaving a clay rich band. As discussed by these authors, it is of vital importance to test the correct sample obtained from the field, if appropriate results are to be determined from a laboratory strength test. In the initial part of their study they took a general field sample which provided a shear strength that from stability analysis would have implied that the slope could not have failed. However, when the shear horizon was identified, the true nature of the material on which failure took place was subjected to laboratory strength tests, which provided similar results to those obtained from back analyses.

In an attempt to determine the residual shear strength of the failure surface at Soper's Wood, a residual ring shear test was undertaken on remoulded material taken from within 5 mm either side of the shear surface described in Chapter 4. The remoulded material therefore contained the weaker material on which the slip had taken place; although it is recognised that the value provided will not be the true residual shear strength of the shear surface, due to the incorporation of the additional material either side of the failure surface. Figure 6.1 displays the complete residual failure envelope for the remoulded sample and indicates that the envelope forms a straight line from σ'_n = 25 kPa and above. This provides values of $\phi'_{r(ult)}$ = 9.4° and $c'_{r\,(ult)}$ = 4 kPa. For comparison, a general homogenised sample was tested. This represented a wider zone through which the shear surface passed and hence was expected to have a higher residual shear

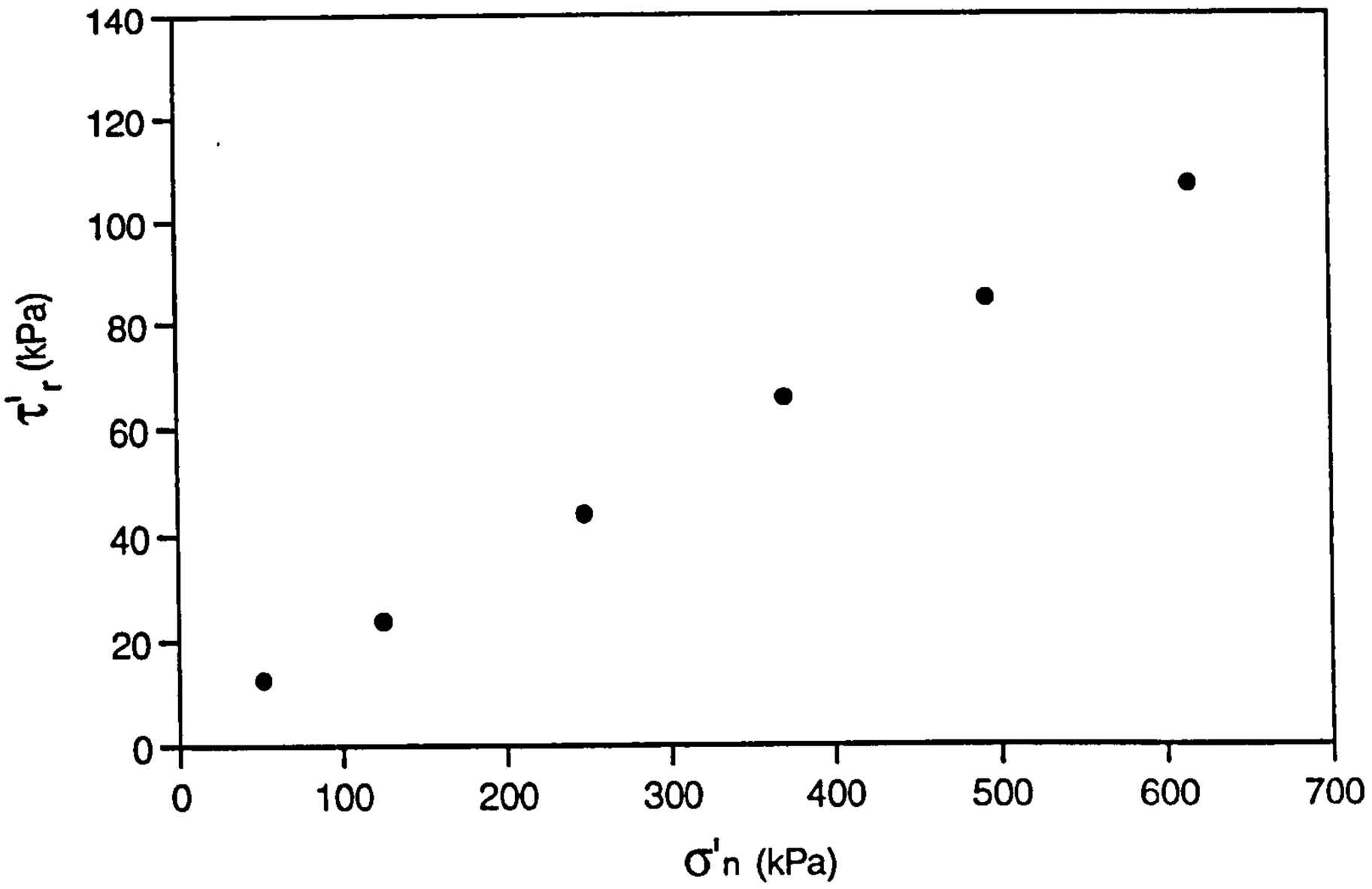

Fig. 6.1 Complete residual failure envelope for the remoulded sample of Fuller's Earth clay obtained from within 5mm either side of the shear surface described in Chapter 4.

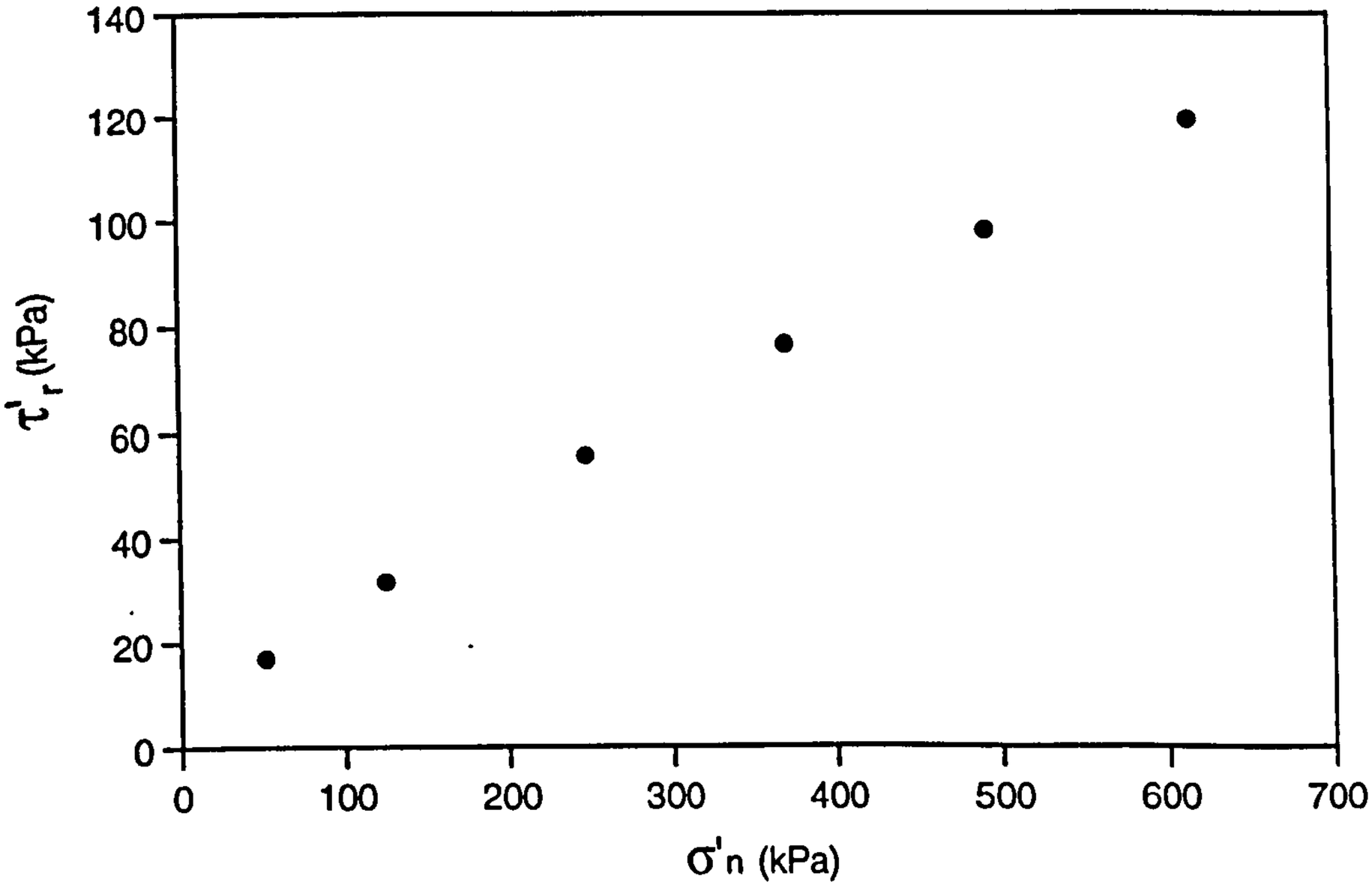

Fig. 6.2 Complete residual failure envelope for the general homogenised sample of Fuller's Earth clay taken from a wider zone of material through which the shear surface passed.

strength. Figure 6.2 displays the complete residual failure envelope for the general homogenised sample, which provides values of $\phi'_{r(ult)}$ = 10° and $c'_{r\,(ult)}$ = 12.5 kPa. It is interesting to note that the ultimate residual shear angle is only slightly higher, compared to the value of the ultimate residual cohesion intercept which is significantly higher, than the corresponding parameters obtained from the material immediately adjacent to and including the shear surface.

A comparison of $\phi'_{r(ult)}$ = 9.4°, obtained from Figure 6.1, with Figure 2.6 indicates that movement is occurring in the sliding mode. As the envelope forms a straight line above a normal effective stress of 25 kPa, it is expected that, in this case, the $\phi'_{r(ult)}$ of 9.4° will also represent the residual shear angle of the basal shear surface at Soper's Wood (see Table 6.1). It thus may be hypothesised that, due to the preferential flow of ground water, a significant amount of disseminated calcite along the shear surface has already dissolved. Hence, any further dissolution of calcite along the shear surface will not produce a significant reduction in the residual shear angle, although clearly the continued chemical weathering of illite will cause some reduction of the residual shear angle with time.

6.3 Slope Stability Analyses of the Soper's Wood Landslide

Chapter 3 stressed the close relationship between rainfall levels, ground water levels and slip movement at Soper's Wood. This section describes slope stability analyses carried out on the left side of the landslide, containing Slide A, in order to investigate these relationships by determining the factor of safety under a number of different ground water conditions.

6.3.1 Method of Analysis

The longitudinal section in Figure 3.22 indicates that the established failure surface is approximately parallel to the hill slope and is translational in nature. Thus it was appropriate to use one of the non-circular methods for slope stability analysis. Three methods were considered, which are described below; "the infinite slope procedure", "Janbu's simplified method" and "Janbu's rigorous analysis".

(A.) Infinite slope procedure (Haefili 1948 and Skempton & Delory 1957)

In this method, the slide is assumed to occur on a planar shear surface which is parallel to the ground. The slope is assumed to be infinite in extent and is treated as a single unit. The ground water conditions along

the length of the slip are assumed to be constant, with ground water seepage parallel to the shear surface. The factor of safety is calculated from the following expression which takes into account the principles of effective stress and residual shear strength:

$$F = \frac{c_r' + (\gamma.z - \gamma_w h_w)\cos^2\alpha \tan\phi'_r}{\gamma.z.\sin\alpha.\cos\alpha} \qquad \textbf{Equation (6.1)}$$

where:

γ = unit weight of soil
z = depth to shear surface
γ_w = unit weight of water
h_w = height of the ground water table above the slip surface
α = inclination of shear surface from horizontal
c_r' = effective residual cohesion intercept of soil
ϕ_r' = effective residual shear angle of soil

(B.) Janbu's simplified method. (Janbu *et al.* 1956)

This is a method for the analysis of non-circular slip surfaces. In this procedure the slipped mass is divided in to a number of slices whose normal forces act at the centre of the slice base. The factor of safety is obtained by considering the overall force equilibrium of all the slices.

Janbu *et al.* (1956) assume that the interslice forces are zero but introduced a correction factor (f_o) to compensate for this. The correction factor is related to the depth and length of the shear surface and the shear strength values (c_r' and ϕ'_r) for each slice. It can be obtained from the chart in Figure 6.3. Whilst Janbu initially used ϕ and c, this has been taken to be equivalent to effective stress and residual shear strength conditions. The factor of safety, according to this method, can be calculated using the following iterative equation:

$$F = f_o.\Sigma\left[\frac{\dfrac{c_r'l + (W-u.d).\tan\phi'_r}{\cos^2\alpha + \dfrac{\cos\alpha.\sin\alpha.\tan\phi'_r}{F(\text{assumed})}}}{\Sigma(W\tan\alpha)}\right] \qquad \textbf{Equation (6.2)}$$

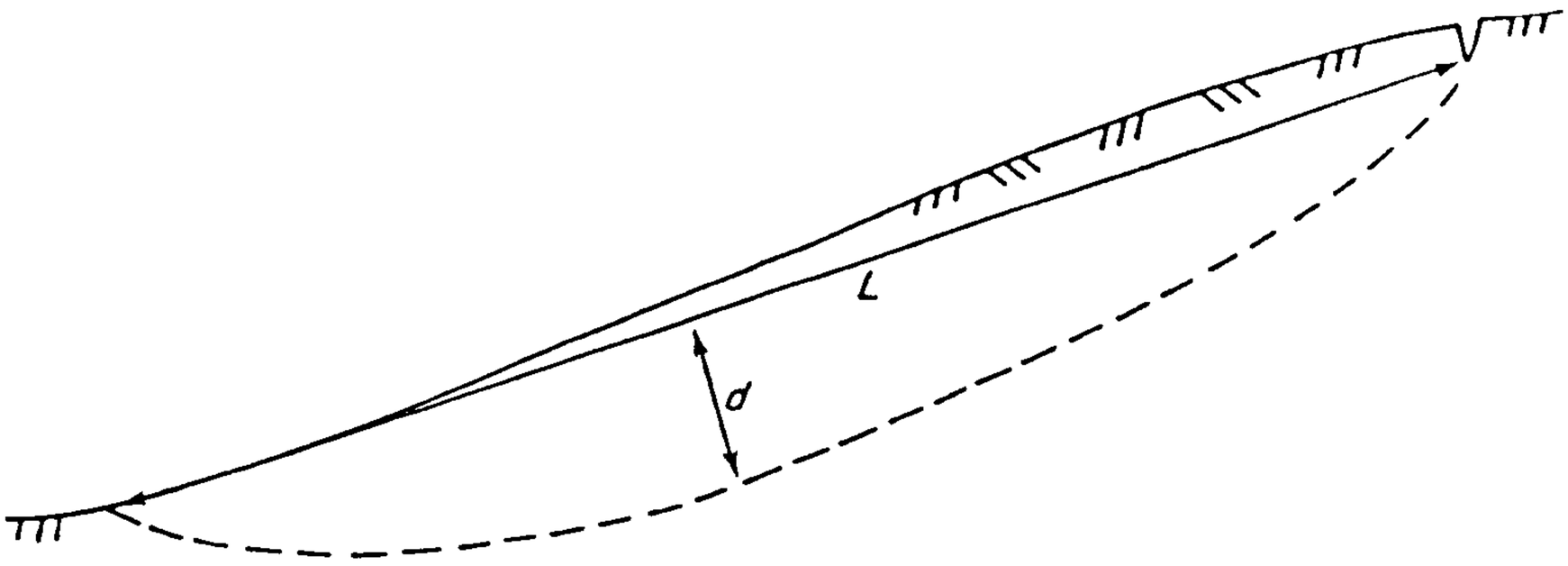

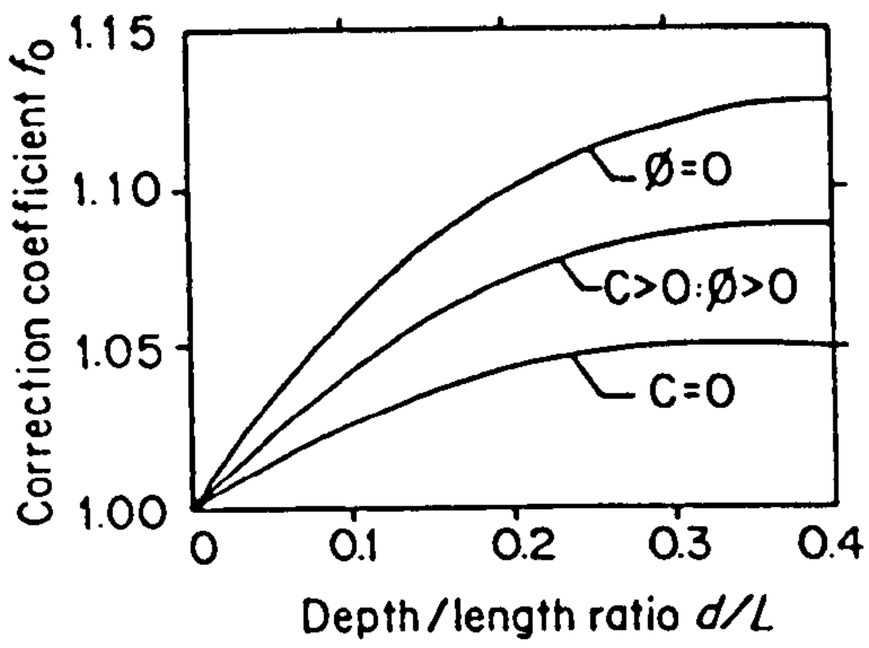

Fig. 6.3 Graph used to obtain the correction factor for use in Janbu's simplified method, after Janbu *et al.* (1956).

where:

f_o = shape correction factor
W = weight of soil slice
u = mean pore pressure on base of slice
c_r' = effective residual cohesion intercept of soil slice
ϕ'_r = effective residual shear angle of soil slice
α = inclination of slice shear surface from the horizontal
d = width of slice
l = length of slice shear surface

The mean pore pressure on the base of the slice can be calculated by:

$$u = \gamma_w h \qquad \textbf{Equation (6.3)}$$

where:

γ_w = unit weight of water
h = head of piezometric surface above slip surface ($h_w.\cos^2\alpha$)
h_w = height of the water table above the shear surface
γ = unit weight of soil
z = depth of soil slice

The weight of the soil slice (W) can be calculated by:

$$W = z.\gamma.d \qquad \textbf{Equation (6.4)}$$

(C) Janbu's Rigorous Analysis

Janbu (1954) developed this method for both circular and non-circular slip surfaces. The analysis is more accurate and less sensitive to the effects of interslice forces compared to the simplified method, as it considers both moment and force equilibrium. The position of the line of thrust of the interslice forces is assumed and moments taken about the centre of the base of each slice, satisfying overall moment equilibrium. In addition the interslice shear forces can be calculated and the factor of safety established.

Slope stability software packages are able to run Janbu's rigorous analysis. This usually involves inputting the co-ordinates of the topography, shear surface and ground water level into the programme, together with the geotechnical properties of the different strata present. The computer then

conducts either an undrained or drained analysis using Janbu's rigorous method.

Generally, although the software allows the geotechnical engineer to insert different parameters for different soil/rock horizons, which is strictly applicable to the consideration of first time failures, it does not adequately cater for the analysis of existing landslips. In these situations the soil/rock horizons will be displaced, such that the shear surface will separate materials with different geotechnical properties. The software does not easily allow this to be inserted, but clearly such phenomena are important when considering, analysing and assessing the true ground conditions related to particular slope failures. In addition, within the individual stratigraphic units, the software assumes that the shear strength parameters remain constant and does not allow for changes in the shear strength parameters related to the curved failure envelope. As a consequence, although the distance between the ground surface and shear surface changes and hence the effective overburden pressure changes, the software does not take into account the necessary change in residual shear angle.

6.3.1.1 Discussion

All three methods, by necessity, involve simplifying assumptions in order to analyse the stability of pre-existing landslides and by their nature are unable to account for; (i) the effects of friction along lateral shears, (ii) any movement which may occur by internal deformation of the material within the slide, (iii) the effects of movement along minor scarps within a slide and (iv) the retrogressive migration of scarps upslope. Clearly a knowledge of these geomorphological features is important when conducting stability analyses of pre-existing landslides. Thus, the factor of safety obtained from stability analyses should not be regarded as a true factor of safety, but should be used relatively to check the sensitivity of the parameters which control slip movement.

Bromhead (1992) recommends the infinite slope procedure for shallow translational landslides, and describes it as being: "...as useful as any other method of slope stability analysis and yields extremely good results", comments very much supported by D.F.T Nash (pers. comm., 1994). Hence, as a result of these remarks and a consideration of the various simplifying assumptions used in the analyses, for the study of the

translational landslide adjacent to Soper's Wood, the robust and simple infinite slope procedure is used.

6.3.2 Conditions and Parameters

The analyses were conducted for the northern half of the landslide containing slide A and shown in longitudinal section in Figure 3.22. For simplicity in the analyses, the depth of the basal shear surface is taken as 2.6 m, as deduced from the snapping of standpipe F (see Section 3.6). From topographic evidence, the angle of the shear surface from the horizontal was taken as 14.2°. Clearly this is an overall angle, as the shear surface has been assumed to be a straight line providing a translational slip, as discussed in Section 3.6.

The landslide is part of a long term degradation of the hillside and therefore the appropriate analysis is that for drained conditions using effective stress parameters. A mean unit weight for the landslipped Fuller's Earth of 20 kN/m^3 was used, after Chandler *et al.* (1976), when they described the eastern side of the valley.

Section 3.5.3 highlighted the importance of standpipe location within the landslide, as there was variation in the ground water level between different positions. It was concluded that the ground water levels in standpipes G and F probably most accurately represent the general ground water level in the slide for use in slope stability analyses. Hence, the ground water levels measured in standpipe F, situated in the main body of the slide, will be used for these analyses.

Section 3.5.4 indicated that when standpipe F showed that ground water levels were 0.3 m from the ground surface, the slip was unstable. Conversely, when the ground water level was seen to drop below about 0.45 m from the ground surface, movement ceased. It is rare that such detailed measurements are available. Hence, it was thought appropriate to consider whether the stability analyses would support the field observations of temporary stability/movement by providing factors of safety above and below unity, dependent upon such relatively small changes in pore water pressure. Stability analyses were therefore carried out using ground water depths of 0.3 m, 0.45 m and 0.8 m.

As discussed in Chapter 2, due to the presence of pre-existing discrete shear planes, along which the clay minerals have been shown to be aligned parallel to the direction of movement (see Chapter 4), the correct shear strength parameter for use in the analyses is that of residual shear

strength. Figure 6.1 displays the complete residual failure envelope for the remoulded material taken from within 5 mm either side of the shear surface described in Chapter 4 (see Section 6.2). The effective residual shear angle and effective residual cohesion intercept were then determined for the appropriate effective normal effective stress at the depth of the basal shear surface. This clearly will vary with ground water level. Table 6.1 illustrates the appropriate effective normal stresses for the three ground water levels, together with the effective residual shear angle and residual cohesion intercept, corresponding to these effective normal stresses. It can be seen that, as the complete failure envelope forms a straight line above σ'_n = 25 kPa, the values correspond to the ultimate condition (see Section 6.2).

GROUND WATER LEVEL	σ'_n	ϕ'_r	c'_r
0.3 m (b.g.l.)	28 kNm^{-2}	9.4°	4 kNm^{-2}
0.45 m (b.g.l.)	29 kNm^{-2}	9.4°	4 kNm^{-2}
0.8 m (b.g.l.)	32 kNm^{-2}	9.4°	4 kNm^{-2}

Table 6.1 Residual shear angle and residual cohesion intercept corresponding to the effective normal stress at the basal shear surface at Soper's Wood relating to the ground water levels shown.

There is much discussion in the literature as to what value of residual cohesion intercept should be used in slope stability analyses. Many authorities recommend that a residual cohesion intercept of zero is applied. However, studies by Chandler & Skempton (1974) have drawn attention to this unrealistically low value and they recommend a value of 1 kPa. Considering the values of c'_r obtained from the investigation described in Chapter 5 and the effects of pore water chemistry on the parameter, the value of 1 kPa suggested is still likely to underestimate the value of the residual cohesion intercept. In addition, as discussed in Chapter 2, Prior & Graham (1974) propose that c'_r is a parameter which should not be underestimated in stability calculations. As a consequence, in the following analysis the measured value of the residual cohesion intercept was used.

6.3.3 Results

Infinite slab analyses, using the parameters discussed in Section 6.3.2, provided the factors of safety displayed in Table 6.2.

DEPTH TO GROUND WATER (m)	FACTOR OF SAFETY
0.3	0.7
0.45	0.71
0.8	0.76

Table 6.2 Factors of safety obtained from infinite slab analyses for the landslide adjacent to Soper's Wood.

6.3.4 Discussion of Results

The results indicate that the slip is unstable even when the ground water is at a depth of 0.8 m. This is in contrast to the observed relationship and provides an underestimation of the factor of safety. The difference between the observed and analysed relationship, may in part be due to the approximations that have to be made in the analysis. The choice of shear surface depth and its inclination has been determined using the method discussed in section 3.6. This may have provided an incorrect estimation. The mean unit weight of the soil may be erroneous, however this is considered unlikely, although it is acknowledged that the Fuller's Earth is not uniform but contains argillaceous limestone bands and fragments of limestone.

Assuming all the other assumptions made are correct, a back analysis was undertaken to establish what value of ϕ'_r would be required if the factor of safety was unity for a ground water level of 0.45 m depth, as indicated by field observations. This analysis indicated that a value of ϕ'_r of 16.1° would be required to establish a limited equilibrium condition for a ground water depth of 0.45 m. Clearly the back analysed value of 16.1° is significantly greater than the measured residual shear angle of 9.4°. In view of the varying lithologies forming the Fuller's Earth formation, this slope stability analysis involving limited testing on the more clay rich material may not provide a realistic simulation of the actual ground conditions. However, Section 6.2 has indicated that shear is occurring in the sliding mode, such that the calcite content may be expected to have little effect on the value of the residual shear angle. Hence, from the work on pore water chemistry described in Chapter 5, and the increased montmorillonite content noted at the shear surface (see Chapter 4), it is

proposed that the difference is, in part at least, due to the effects of calcium in the ground water at Soper's Wood. The presence of the calcium rich ground water is likely to increase the residual shear strength of the shear surface, such that, as observed, the slide ceases movement when the ground water level falls below a depth of 0.45 m.

6.4 A Generalised Model for the Seasonal Control of Slope Stability

Combining the observed interaction of ground water level, rainfall, slip movement, evaporation, vegetation, and ground water chemistry, as discussed in Chapter 3, with the knowledge of the effects of calcium concentration in pore water on residual shear strength, as determined in Chapter 5, enables the construction of a generalised model for the seasonal control of movement of the landslide adjacent to Soper's Wood (see Table 6.3). It is recognised that no field observations are available for the autumn period.

During the winter period from December to March, rainfall levels are high (see Figure 3.14). Due to the combination of low evaporation rates and low vegetation levels, this results in a sustained shallow water table within the main body of the landslide (see Figure 3.17); although some variation in the ground water level between different locations within the landslip was observed. High rainfall levels and a shallow water table encourage the flow of ground water downslope through the landslipped material, as evidenced by the outflow of ground water from the toe of the slip. This results in the dissolution of calcium carbonate within the Fuller's Earth, encouraged by the lower winter ground water temperatures (see Figure 3.24), such that the ground water has a high calcium concentration. Picknett *et al.* (1976) demonstrated in the laboratory that there is increased dissolution of calcium carbonate with decreasing temperature. As discussed in Section 3.7.3, calcium in the ground water will be derived from a combination of the dissolution of calcite both from the limestone bands present within the Fuller's Earth and the dissolution of disseminated calcite within the clay.

A high calcium concentration in the ground water will result in cation exchange with the surrounding clay minerals. However, due to the high rainfall levels over this period, there will be a continual replenishment of calcium in the ground water. Ca^{2+} ions will adsorb to the clay platelets causing a reduction in the thickness of the hydrated double layer. Thus, the attractive van der Waals forces will have a greater influence and

	DEC-MAR	APRIL-MAY	JUNE-AUG	SEPT-NOV
RAINFALL LEVEL	HIGH	SPORADIC	LOW	SPORADIC
EVAPORATION LEVEL	LOW	MEDIUM	HIGH	MEDIUM
VEGETATION LEVEL	LOW	MEDIUM	HIGH	MEDIUM
GROUND WATER LEVEL	SHALLOW	FLUCTUATING	DEEP	FLUCTUATING
CALCIUM CONCENTRATION	HIGH	HIGH	LOW	LOW BECOMING HIGH
INHERENT RESIDUAL SHEAR STRENGTH	HIGH	HIGH	LOW	LOW BECOMING HIGH
SLIP MOVEMENT	CONTINUOUS GRADUAL MOVEMENT	SPORADIC "STICK-SLIP" MOVEMENT	INACTIVE	OCCASIONAL REACTIVATIONS OF SLIP MOVEMENT

Table 6.3 Generalised qualitative seasonal model illustrating controls on landslide activity in the Fuller's Earth clay.

consequently the strength of ionic bonding between individual clay platelets will increase. This is manifested as an increase in residual shear strength, as demonstrated by the laboratory testing described in Chapter 5. Hence, during this winter period, the inherent residual shear strength of the shear surfaces within the landslide will be high. However, the high levels of rainfall and the shallow water table result in high pore water pressures, such that effective stress is reduced and slip movement results, irrespective of the high inherent residual shear strength. As long as rainfall levels are high enough to sustain the shallow ground water level and high pore water pressures, slip movement is continuous; although the rate has been shown to be closely dependent on rainfall levels (see Figure 3.15).

In the spring (April and May), rainfall is more sporadic, with occasional periods of higher rainfall, such that the ground water table is subject to fluctuations (see Figures 3.14 and 3.17); a shallow ground water level corresponding to periods of higher rainfall. The sporadic nature of rainfall, combined with increased evaporation and vegetation levels, results in the ground water table rarely being sustained at a shallow level for a long period. Hence, pore water pressures are only temporarily raised. As discussed in Chapter 3, vegetation is thought to hinder the infiltration of surface water into the landslip. In addition, soil moisture is removed by roots taking in water, which is then lost to the atmosphere through evapotranspiration. During this spring period, calcium concentrations in the ground water were found to still be high (see Figure 3.24). Hence, as for the winter period the inherent residual shear strength of the shear surfaces is expected to be high. Thus, a combination of the high inherent residual shear strength and the sporadic, generally short lived periods of higher rainfall, which result in only a temporary increase in ground water level and pore water pressures, results in only small amounts of "stick-slip" style movement (see Figure 3.15).

During the summer months of June, July and August, rainfall levels are generally low (see Figure 3.14). In addition, evaporation rates are at their highest and the slope is relatively heavily vegetated. Hence, the ground water level is relatively deep (see Figure 3.17). Calcium concentrations in the ground water were found to be lower than in the winter and spring. The lower calcium concentrations are likely to result from the lower rainfalls levels and the higher summer ground water temperatures (see Figure 3.24). The lower rainfall levels result in a greatly reduced flow of ground water through the landslide and limestone bands within the Fuller's Earth. This, combined with the higher ground water temperatures,

which causes a decrease in the solubility of calcite, results in less calcium carbonate dissolution and hence calcium concentrations in the ground water are relatively low.

The more diluted ground water in the summer will cause a weakening of the close range ionic bonds and hence the inherent residual shear strength of the failure surfaces can be expected to be lower than in the winter and spring. However, due to the relative paucity of rainfall and the deeper ground water levels, pore water pressures are relatively low (and effective stress high), and thus no movement of the slip generally occurs. In addition, as discussed in Chapter 3, the presence of vegetation results in less rainfall infiltrating into the landslide to raise ground water levels. It is proposed that during this period, as a result of the low calcium concentrations in the ground water, the shear surface has its lowest inherent residual shear strength. Hence, the landslide is most vulnerable to further movement if sufficient rainfall occurred to raise ground water levels/pore pressures, despite the presence of vegetation. This in part may explain the large amounts of landslide movement that occurred during a period of exceptionally high rainfall in the summer of 1968, as reported by Hawkins (1973).

During the autumn months of September, October and November, rainfall levels increase, with occasional periods of heavy precipitation. Thus, the ground water level can be expected to slowly rise and be subject to fluctuations; peaks in the ground water level corresponding to periods of higher rainfall. Initially, evaporation rates can be expected to be relatively high and the slope vegetated, but with a decrease in temperature and insolation over the period, the rate of evaporation will decrease.

Early on during this autumn period, the inherent residual shear strength of the failure surfaces is likely to be low, as a result of the low calcium concentrations in the ground water over the summer months. Thus, when more heavy periods of rainfall occur, pore water pressures will increase and, as a result of the lower "summer" inherent residual shear strength, renewed movement of the landslip takes place. However, following a period of heavy rainfall, calcium concentrations in the ground water can be expected to increase (due to the dissolution of calcite within the Fuller's Earth). With further autumnal rainfall and a decrease in ground water temperature, calcium concentrations in the ground water will approach the higher levels of the winter and spring. Thus, due to the increase in calcium concentrations in the ground water, the inherent residual shear strength of the shear surfaces is likely to increase during the

autumnal period and approach its higher winter value. Hence, for further movement to occur during the late autumn/winter, prolonged heavy rainfall which will result in a shallower ground water level and higher pore water pressures, such as have been recorded in the winter, will be necessary to overcome the increased inherent "winter" residual shear strength of the failure surfaces.

This model may account for the three phases of renewed movement of a landslide, upslope of the active landslide studied in this thesis, which occurred during the early autumn of 1980, 1981 and 1982, see Table 3.1. However, these periods of activity may have also been affected by some regrading of the slope by the farmer. In addition, it is of note that a reactivation of the landslide studied in this thesis occurred during the autumn of 1983.

6.5 Discussion

This model has highlighted the dominance of rainfall as a control on the movement of the landslide in the Fuller's Earth adjacent to Soper's Wood. High rainfall levels result in a raised ground water level and increased pore water pressures. This reduces effective stress and slip movement occurs. However, the model has shown that the concentration of calcium in the ground water affects the inherent residual shear strength of the failure surfaces within the landslide in the Fuller's Earth. Thus, the inherent residual shear strength of the shear surfaces can be considered a dynamic property, showing seasonal variation.

This was first proposed by Moore (1988 and 1991) and used to explain coastal mudflow movement by Moore & Brunsden (1996), see Chapter 2. However, the sources of the changes in pore water chemistry which result in a change in the inherent residual shear strength of the failure surfaces are different for a coastal mudslide and the inland slide described in this study. For a coastal mudslide, the salts in the ground water are derived from sea water washed onto the landslip by storm action. Whereas, for the inland slip in the Fuller's Earth, the calcium in the ground water is derived from the dissolution of calcium carbonate within the formation.

Though this model has been derived from the field investigation of the landslip in the Fuller's Earth adjacent to Soper's Wood, it is expected that it will apply to other similar landslides in the formation around Bath. The proposition that the inherent residual shear strength of the slip is lowest in the summer and early autumn has important implications for engineering

works and the current perception of slope stability risk. It is generally perceived that slope movement occurs during the winter period. This is clearly the case, as the model has shown that the combined effect of high rainfall and shallow ground water level/high pore water pressures are the dominant control on slip movement. However, it is proposed that it is during the summer and early autumn, that the inherent residual shear strength of the shear surfaces within an inland landslide in the Fuller's Earth is at its lowest and hence the slip is most vulnerable to movement. Thus, if unusually high levels of rainfall occur during this period, large amounts of movement can be expected. Hence, when conducting stability analyses, the combination of parameters which would provide a worst case factor of safety would be those of the "summer" inherent residual shear strength and "winter" ground water levels.

In this chapter, models for the long term and seasonal controls on slope stability have been put forward. It is appreciated that much of the model is conjectural and open to discussion. However, it is hoped that the step taken to propose a model for inland slope stability in the Fuller's Earth, which includes the effects of pore water chemistry, will spur other workers into providing similar or indeed, contradictory models, for other inland slopes.

CHAPTER 7

SUMMARY AND CONCLUSIONS

The research described in this thesis was undertaken to further elucidate the instability associated with the Fuller's Earth formation around Bath. In the Bath area the formation rests conformably between the Inferior Oolite and the Great Oolite, which forms the topographic cap rock in the area. The combination of sub-horizontally interbedded competent and incompetent strata with the steeply dissected topography, characteristic of the south Cotswolds, has resulted in the development of near surface mass movement. The Fuller's Earth formation is characterised by the presence of translational landslides.

Previous work undertaken on the Fuller's Earth formation by researchers at the University of Bristol has emphasised the influence of calcite on the Atterberg limits and residual shear strength of the formation. In addition, published work, reviewed in Chapter 2, has highlighted the effects of pore water chemistry on the residual shear strength of clays. Hence, this research was carried out at both a macro and micro-scale to investigate the controls on slope stability in the Fuller's Earth; with particular emphasis on the role of calcite and ground water chemistry.

The reactivation of an active landslide in the Fuller's Earth in the fields adjacent to Soper's Wood in the Swainswick valley, approximately 3 km to the north of Bath, provided a unique opportunity. A field investigation, which included monitoring of the active slide, provided macro-scale data. This, combined with laboratory work, allowed the development of a model for the long term and seasonal stability of the landslide.

7.1 Field Investigation

A geomorphological map was produced in January 1994 which allowed comparison with previous maps. The January 1994 map indicated that the slip feature consisted of a translational landslide, about 50 m in length, which downslope extends into two distinct morphological features (see Figure 3.7). On the northern side the landslide has extended to form a well defined narrow translational landslide (Slide A), whilst on the southern side the main translational landslide has not extended so far valleyward and the lower feature is termed Slide B.

Logging of samples of the Fuller's Earth, obtained every 100 mm from auger holes drilled both inside and outside the visibly slipped mass,

has demonstrated that both the weathering grade and depth to which weathering occurs are greater in the visibly slipped material compared to in the material outside the active landslide (see Section 3.4.1). An analysis of sample moisture contents revealed that there are significant differences in the soil moisture both within the slipped zone and when the slipped zone is contrasted with the moisture content profile of the auger hole drilled outside the visibly slipped mass (see Figures 3.10a and 3.10b). The moisture content profiles for the auger holes within the slipped material show significant variation with depth; peaks in the moisture content profiles may indicate the presence of fossil shear surfaces. In contrast, the moisture content profile for the auger hole outside the slipped mass shows a smoother decrease with depth. In addition, the slipped material generally has a higher moisture content compared to the unslipped material at a similar depth.

A comparison of the geotechnical indices of samples from inside and outside the visibly slipped mass has shown the effects of the increased weathering of the slipped material on the geotechnical indices of the Fuller's Earth clay (see Figure 3.11). In addition, this study has confirmed the marked influence that calcite has on the Atterberg limits of the Fuller's Earth clay (see Figure 3.12).

In borehole B (which extended to a depth of 2.7 m), located within the landslip, the moisture content and Atterberg limit profiles increase with weathering grade and the calcite content profile decreases (see Figure 3.11). In addition, near the ground surface the moisture content is similar to the liquid limit, although below 1.1 m it starts to approach the plastic limit. However, even at the base of the borehole it is still some 10% higher than the plastic limit.

In comparison, in borehole C (which extended to a depth of 3.0 m), located outside the landslip, below a depth of 1.3 m the Atterberg limits and moisture content remain approximately constant and the moisture content is shown to be approximately equal to the plastic limit, falling below it at a depth of 2.5 m (see Figure 3.12). Above a depth of 1.3 m there is a trend of increasing Atterberg limits and moisture content and a decreasing trend of calcite content, similar to the trend seen throughout borehole B. However, unlike in borehole B, below the initial 0.3 m the moisture content more closely reflects the plastic limit of the clay.

These differences are likely to be due to the dilated and fractured nature of the slipped material, allowing the percolation of acidic ground waters through the previously less permeable Fuller's Earth clay. The

acidic ground waters increase the rate of chemical weathering within the slipped mass. Two important components of this weathering are the depotassification of illite with the formation of a randomly interstratified illite-montmorillonite and the gradual dissolution of calcite. Hence, the recently slipped material is more weathered and the increased montmorillonite content, together with a possible decrease in non-sorptive calcite, results in increased plasticity with decreasing depth/increasing weathering grade. In addition, in the slipped samples, where transverse cracks, minor scarps and lateral shears have allowed the infiltration and percolation of surface waters, the clay is hydrated. Thus, natural moisture contents tend to be high, generally above the plastic limit. Outside the slipped mass, a similar process, due to near surface stress relief, is likely to account for the increased plasticity and moisture content above 1.3 m. Below 1.3 m, less weathering has occurred such that the moisture content is approximately equal to the plastic limit and the Atterberg limits remain approximately constant with depth.

The installation of 10 survey stations within the landslide allowed regular monitoring of slip movement and highlighted the most active parts of the landslip (for locations see Figure 3.7). Surveying commenced on the 19th January 1994 and ceased on the 30th June 1994, however the majority of the measured movement was noted to have been completed by the 13th April 1994 (see Figures 3.13, 3.15 and 3.16). Along the line of survey stations A1 to A5, the portion of Slide A containing stations A2 and A3 was most active. Station A3, moved a total of 2.9 m horizontally and 0.9 m vertically downwards. Station A1, situated on the lowest toe of the slip, was effectively stationary. The upper area of the main translational landslide containing stations A4 and A5 showed much less movement.

Along the line of the B survey stations, stations B1 and B2 were the most active, with stations B3 and B4 in the upper area of the main translational slide showing less movement. Station B1 moved 2.07 m horizontally and 0.59 m vertically downwards. However, this was only in the first nine weeks of monitoring, as between the 21st March and 7th April 1994, there was an enhanced phase of movement during which time station B1 was swept away by the mudflow. Station B2 moved a total of 1.83 m horizontally and 0.46 m vertically downwards. In comparison, station B4 moved a total of 0.48 m horizontally and 0.06 m vertically downwards. In addition, the results demonstrate that in the main translational slide, up-slope of where the landslide splits into two features,

the side containing survey stations B3 and B4 has shown a greater amount of movement than the side containing stations A4 and A5.

A comparison of cumulative movement for each survey station with cumulative rainfall reveals that the two are intimately related, even with the varying amounts of movement of each station (see Figure 3.15). Once the landslide is moving any decrease or increase in the level of precipitation is reflected by the rate of movement. However, where the change in rainfall levels is dramatic, from the data presented in this thesis, there appears to be a time lag of between 3 and 6 days between the two events. In addition, a comparison of the ground water levels measured in the series of standpipes installed within the landslip, demonstrated that there is a general relationship between rainfall, ground water level and slip movement (see Figures 3.17 and 3.18).

It can be concluded that in addition to general infiltration, rainfall selectively penetrates into the soil along disturbance zones, such as shear surfaces and transverse cracks, increasing the height of the water table. Pore pressures subsequently increase, with a reduction in effective stress, encouraging further movement. This process is likely to be enhanced by the presence of in situ limestone bands within the Fuller's Earth formation. These form avenues for ground water percolation and are known to cause high pore water pressures at their exit points. It is likely that the percolation rate controls the length of delay involved between rainfall and an increase in pore water pressure. The termination of a particular rainfall event results in a decrease in the height of the ground water level. This results in a decrease in pore pressures, sufficient that movement ceases.

The majority of slip movement had been completed by the 13th April 1994, coincident with a prolonged period of very little rainfall from the 13th April 1994 to 20th May 1994. Increased levels of rainfall after the 20th May 1994 caused only comparatively small amounts of further movement (see Figure 3.15). This is likely to be due to an increase in effective stress which is in part related to a decrease in pore pressures, resulting from soil water evaporation coincident with a period of low precipitation between 13th April 1994 and 20th May 1994. In addition, indirectly vegetation may play a role in controlling slip movement.

During the late spring and summer months when vegetation levels increase, particularly on the slipped mass, the increased grass cover will collect water which will evaporate in the warm weather, reducing the amount of recorded rainfall available for infiltration. This effect may be partially balanced by the presence of desiccation cracks which will provide

further avenues for surface water infiltration. The vegetation will also take up moisture which will be lost to the atmosphere by evapotranspiration, reducing the amount available for infiltration still further. Hence, an equivalent amount of rainfall during the summer and winter will have very different effects. In the winter, due to a lack of vegetation cover, most of the recorded rainfall will penetrate into the slipped mass and thus slip movement will be sensitive to recorded rainfall. Whereas in the summer, less of the recorded rainfall will penetrate into the slipped mass and thus there is a reduced effect, with slip movement appearing to be insensitive to recorded rainfall.

A comparison of ground water levels in the standpipes within the landslip, with those in the standpipe placed outside the active landslide, revealed that the water table within the main body of the slip is shallower than outside the landslide, most likely due to selective recharge in the slipped mass (see Figure 3.17). The standpipes within the landslide had a faster initial response due to the increased disturbance and dilation of the soil within the slipped mass. In addition, the study has highlighted the importance of standpipe location within a landslide, as there is some variation in the ground water level between different locations. This is clearly important when considering slope stability analyses.

A comparison of the geomorphological map produced at the start of monitoring in January 1994, with a second map produced in May 1994 when the majority of movement appeared to have taken place, highlighted a number of morphological changes (see Figure 3.19). The morphology of slide B had changed considerably; the two mudflows existing in January 1994 had combined between the 21st March 1994 and 7th April 1994 to form one large mudflow. However, in contrast, Slide A showed little change in morphology. In the main translational slide additional transverse cracks have appeared, with some pre-existing transverse cracks being extended. In addition, some of the transverse cracks adjacent to the lateral shears have developed into minor scarps. Field observations, together with the mapping, identified two patterns of movement; transverse crack propagation and retrogressive scarp migration. From the geomorphological mapping and the snapping of the specially adapted standpipes at depth, an accurate longitudinal section of the landslide was constructed for use in slope stability analyses (see Figure 3.22).

Ground water analyses were undertaken at Soper's Wood to determine whether chemical weathering is occurring at present; with

particular emphasis on the dissolution of calcium carbonate and the depotassification of illite. The ground water at Soper's Wood was sampled from the standpipes at approximately monthly intervals between 16th March 1994 and the 3rd August 1994.

Geochemical analysis of the ground water samples revealed that the concentration of calcium varied between 61 mg/l and 335 mg/l, significantly higher than the levels found for magnesium (2.1 to 14.4 mg/l) and potassium (1.21 to 10.03 mg/l), see Figure 3.23. It is likely that the majority of calcium in the ground water originates from the dissolution of calcium carbonate within the Fuller's Earth. However, due to the high concentrations measured, some of the calcium may come from the dissolution of gypsum, although this was not recorded during the logging of the boreholes. The absence of gypsum may be a result of its high solubility. The magnesium found in the ground water samples is probably coming from the dissolution of impure calcium carbonate. The presence of potassium in the ground water is likely to originate from the depotassification of illite, as noted by Vear & Curtis (1981).

Magnesium and calcium levels found in those boreholes within the landslip were noted to be significantly higher and more variable over the period of study than the levels found in borehole C outside the visibly slipped mass. This implies enhanced dissolution of calcium carbonate within the landslide. However, the higher ground water concentrations may in part reflect ground water preferentially flowing from "in situ" limestone bands into the disturbed area, as egress here will be easier than where "in situ" clay cover is present.

In May 1994, additional standpipes were installed along the length of the slip to enable sampling of ground waters down the full length of the landslip (see Figure 3.26). Geochemical analysis of the ground water samples demonstrated the downslope variation in calcium concentration within the slip mass, which is likely to be related to the positions of the sampling standpipes within the slip relative to the flow of ground water (see Figure 3.27). Hence, at the head of the landslide, ground water concentrations of calcium are low and in general increase downslip as the ground water percolates downslope dissolving disseminated calcium carbonate within the slipped clay. However, where there are significant avenues for the infiltration of rain water, such as minor scarps, the percolating ground water is diluted by the newly infiltrated rain water so that the concentration of calcium in the ground water appears to be lower.

From the study it can be concluded that dissolution of calcium carbonate is undoubtedly occurring, however it is difficult to establish the exact levels of the dissolution of detrital calcite within the Fuller's Earth clay as the concentration of calcium in the ground water will also be affected by the dissolution of any gypsum present and the presence of "in situ" limestone bands. The significantly lower calcium concentration in the ground water sampled outside the visibly slipped mass is likely to indicate that increased dissolution rates of calcite are occurring within the more permeable, disturbed Fuller's Earth. In addition to the dissolution of calcite, this study has also shown that potassium ions are being leached from the clay minerals in the Fuller's Earth.

7.2 Small Scale Analysis of a Shear Surface

A sample of a shear surface was obtained from a trial pit within the landslide in the Fuller's Earth at Soper's Wood to investigate whether the dissolution of disseminated calcium carbonate and the chemical weathering of illite is occurring preferentially along shear planes, due to the percolation of acidic ground waters.

The shear surface was sampled by pushing a specially made steel box into the wall of the trial pit, so that it enclosed the failure surface. On return to the laboratory, a 10 mm layer was extruded from the box, providing a "slab" of Fuller's Earth clay which contained the shear surface. The slab was then divided into broad lithological units which were logged and analysed by XRD. In addition the edges of the slab were divided into 44, 5 mm wide samples for moisture content and calcite content analyses (see Figure 4.1).

Moisture content analysis (see Figures 4.2 and 4.3) revealed more variable levels of moisture content in the recently slipped ground immediately above the shear surface (23% to 96%) compared to the more uniform levels in the recently unslipped material below it (60% to 66%). This is interpreted to indicate that the recently slipped material is more disturbed and permeable relative to the soil below the shear surface, although the values are still high. This is attributed to the generally dilated nature of the near surface material. The moisture content profile was normalised to a calcite content of zero to investigate the moisture content of the clay minerals alone (see Figure 4.7). This method assumes that the soil consists of just clay minerals and calcite, with all the moisture contained by the clays. Any layers of water that may exist adsorbed to the calcite are ignored. The results obtained support the routine moisture content

analyses and there is a peak in the normalised moisture content at the approximate location of the shear surface.

A comparison of the calcite content and moisture content of the samples revealed a remarkably consistent inverse relationship, considering the very small sample size of this study (see Figures 4.4 and 4.5). These results emphasise the control that calcite content has on the moisture content of the Fuller's Earth clay, even at a very small scale. However, calcite content analyses provided no evidence of preferential decalcification along the shear surface. It is thought that this may be due to the thickness of the samples relative to the shear surface.

Samples of the shear surface were examined by SEM to gain an understanding of the nature of the shear surfaces within the landslide adjacent to Soper's Wood (see Plate 4.5). This highlighted the parallel alignment of the clay minerals at the shear surface, compared to the random orientation of the clay platelets away from the failure plane. This anisotropic alignment may be acting as a barrier preventing ground water percolating vertically across the shear surface. Hence, the higher moisture contents seen above the shear surface and the marked change in both the standard and normalised moisture content profile at the shear surface. The examination also revealed the remarkably smooth nature of the shear surface, with an absence of any silt/sand particles. Thus, it is interpreted that shear is likely to be occurring in the sliding mode and it is thought that the preferential dissolution of calcitic particles along the shear surface has already taken place.

XRD analyses of whole "rock" powder mounts made up from the lithological units indicated that the dominant non-clay minerals present were calcite and quartz, with subordinate feldspar, gypsum and pyrite. The clay mineralogy of the units was analysed by sedimenting the clay fraction onto slides and revealed a qualitative increase in the proportion interstratified illite-Ca-montmorillonite at the shear surface, compared to in the clay above it. This has been interpreted to indicate that increased rates of illitic weathering, due to the preferential percolation of acidic waters, is likely to be occurring along the shear surface.

7.3 Effects of Calcium in Pore Water on the Residual Shear Strength of Clays

The chemical analysis of the ground water within the landslide at Soper's Wood highlighted the dominance of calcium. Thus, experiments were carried out to determine the effects of calcium in pore water on the

complete residual failure envelope of clays. This enabled an analysis of the effective residual cohesion intercept, residual shear angle and residual shear strength at various effective normal stresses.

In order to try and simulate natural ground water chemistry as closely as possible, three preliminary experiments were undertaken to investigate the possibility of creating stable solutions of calcium in the laboratory from the dissolution of calcium carbonate (see Figures 5.1, 5.2, 5.3, 5.4 and 5.5). It was expected that these solutions could then be used in ring shear tests to investigate the effects of pore water chemistry on the residual shear strength of clays. Unfortunately, the results of the experiments showed significant variation, making it difficult to say conclusively how long the solutions of calcium were stable for. It was concluded that calcium carbonate equilibria is too unstable for use in ring shear tests, being affected by carbon dioxide partial pressures, pH and temperature, which are all difficult to control during a test. Hence, it was decided to use calcium chloride as a solute.

Samples of "pure" kaolinite and montmorillonite were used in the study. The kaolinite used was obtained from English China Clays International Limited and the montmorillonite used was "Wyoming Bentonite". Following XRD analyses, the "Wyoming Bentonite" was found to consist dominantly of sodium montmorillonite. Using pure clays reduced the number of variables which may affect the residual shear strength obtained from ring shear tests, such as the proportion of silt grade material. In addition, kaolinite and montmorillonite were chosen as they are both present in the Fuller's Earth and represent the two extremes in terms of size and behaviour (eg swelling properties), in the family of clay minerals. Prior to testing, the clays were washed repeatedly in distilled water to remove any remnants of chemicals used in the production of the clays.

The washed clays were then divided into six sub-samples. Each of these was then treated with solutions containing a specific concentration of calcium. The concentrations used covered the range found in the ground waters at Soper's Wood and corresponded to 0, 80.1, 160.2, 240.3, 320.4 and 400.5 mg/l Ca^{2+}, which equates to 0, 200, 400, 600, 800, 1000 mg/l $CaCO_3$ respectively. Each of the treated samples of kaolinite and montmorillonite were then subjected to Atterberg tests and residual ring shear tests.

The results indicate that the residual shear strength of kaolinite and montmorillonite are sensitive to the concentration of calcium in pore water (see Figures 5.8, 5.9, 5.10, 5.11, 5.13, 5.14, 5.15 and 5.16). However, the

influence of pore water chemistry is more pronounced in montmorillonite than kaolinite. The residual shear strength of kaolinite and montmorillonite increase with increasing calcium concentration in the pore water; this is most marked between the untreated samples and the samples treated with 80.1 mg/l Ca^{2+}. In addition, analyses of the results at various effective normal stresses indicated that the influence of Ca^{2+} concentration is most pronounced in the parameters c'_r and τ'_r.

Following the ring shear tests, samples of the clays were subjected to XRD analyses and these demonstrated that the overall mineralogy of the clays remained constant for the different calcium concentrations. However, the (001) montmorillonite reflection was observed to migrate with increasing Ca^{2+} concentration (see Figure 5.19). This was interpreted to indicate that sodium is being exchanged for calcium, with increasing calcium concentration in the pore water. This migration was most noticeable between the untreated sample and the sample treated with 80.1 mg/l Ca^{2+} and explains the marked change in residual shear strength observed between these two samples.

The observed changes in residual shear strength can be explained in terms of physico-chemical effects. An increase in Ca^{2+} concentration in the pore water causes compression of the hydrated double layer surrounding the clay particles. Hence, the repulsive forces are reduced and the attractive van der Waals forces are able to dominate. Thus, with increasing Ca^{2+} concentration, bond strength increases and c'_r and τ'_r increase.

In addition to residual shear strength, the Atterberg limits of the clays were found to be sensitive to Ca^{2+} concentration, although the montmorillonite and kaolinite displayed opposing behaviour (see Figures 5.12 and 5.17). The liquid limit of the kaolinite shows a marked increase between the untreated sample ($w_L = 57\%$) and the sample treated with 80.1 mg/l Ca^{2+} ($w_L = 65\%$). Thereafter, there is no obvious trend with increasing Ca^{2+} concentration. There is no noticeable increase indicated by the "less sensitive" plastic limit and hence, as expected, the plasticity index of the samples mirrors the liquid limit. The change in liquid limit is interpreted to result from a change in the arrangement of the kaolinite platelets from a dispersed state in the untreated sample, to an open flocculated structure in the presence of Ca^{2+}. In contrast, the liquid limit of the montmorillonite decreases with increasing Ca^{2+} concentration, markedly at first from 740% to 330%. As for the kaolinite, due to the insensitivity of the plastic limit, the plasticity index follows the trend of the

liquid limit. The decrease in liquid limit shown by the montmorillonite samples can be explained by the increase in bond strength between clay particles with increasing Ca^{2+} concentration.

The levels of calcium used in this study correspond to the levels found in the ground waters within the landslide adjacent to Soper's Wood. In addition, kaolinite and montmorillonite are present in the Fuller's Earth clay and it is expected that the behaviour of illite will be intermediate between these two "end members". Thus, pore water chemistry can be expected to play a part in determining the residual shear strength and geotechnical parameters of the Fuller's Earth clay at Soper's Wood, as long as clay grade material dominates and shear occurs in the sliding mode.

7.4 A Model for the Stability of the Landslide Adjacent to Soper's Wood

Combining the results from the field and laboratory investigations enabled the development of a model for the stability of the landslide in the Fuller's Earth adjacent to Soper's Wood. Stability is considered at two levels; long term and seasonal. Although this model is derived from the investigations of the landslide adjacent to Soper's Wood, it is expected that it will apply to many other similar landslips in the Fuller's Earth formation around Bath. It is important to recognise that this model applies to slopes which have already slipped and, as a result of pre-existing shear surfaces, have a residual shear strength.

7.4.1 Long Term Stability

It is proposed that acidic ground waters percolate through the dilated slipped material. Indeed, preferential percolation is likely to occur along shear surfaces, as evidenced by the outflow of water from the basal shear surface at the toe of the landslide. These acidic ground waters cause the dissolution of calcium carbonate within the Fuller's Earth and the chemical weathering of illite with the formation of a randomly interstratified illite-montmorillonite. Hence, with time, shear surfaces, can be expected to show a gradually decreasing calcite content and an increasing proportion of randomly interstratified illite-montmorillonite. Thus, over the long term, as a result of these two components of weathering, shear surfaces can be expected to show a decrease in residual shear strength (see Chapter 2).

However, ring shear tests conducted on the sample of the shear surface obtained from the trial pit within the landslide adjacent to Soper's Wood, indicate that shear is occurring in the sliding mode (see Figure 6.1).

In addition, SEM analyses demonstrated the smooth nature of the shear surface (see Plate 4.5). It is thus hypothesised that, due to the preferential flow of ground water, a significant amount of the dissolution of the disseminated calcite along the shear surface has already occurred. Hence, as it is thought that shear now occurs predominantly in the sliding mode, any further reduction in the calcite content along the shear surface is not expected to produce a significant further reduction in the residual shear strength. Although clearly the continued chemical weathering of illite will reduce the residual shear strength with time.

Slope stability analyses undertaken using the measured residual shear angle and cohesion of material taken from within 5 mm either side of the shear surface ($\phi'_r = 9.4°$ and $c'_r = 4$ $kNm^{-2)}$, indicated that the slip is unstable even when the ground water is at a depth of 0.8 m. This is in contrast to the observed relationship, where slip movement ceased when the ground water fell to a depth of 0.45 m, and provides an underestimation of the factor of safety. Indeed, back analyses indicate that a value of $\phi'_r = 16.1°$ would be required for the factor of safety to be unity for a ground water level of 0.45 m depth. It has been shown that shear is occurring in the sliding mode, such that the calcite content may be expected to have little effect on the value of the residual shear angle. From the work on pore water chemistry and the increased proportion of montmorillonite noted at the shear surface, it is proposed that the difference is, in part at least, due to the effects of calcium in the ground water at Soper's Wood. The presence of the calcium rich ground water is likely to increase the residual shear strength of the shear surfaces, such that, as observed, the slide ceases movement when the ground water falls below a depth of 0.45 m.

7.4.2 Seasonal Stability

Combining the field investigation data with the effects of pore water chemistry on residual shear strength allows the construction of a seasonal model for slope stability. The model highlights the dominance of rainfall and ground water level as controls on slope stability and indicates that the inherent residual shear strength of a failure surface within the landslide should be considered a dynamic property, showing seasonal variation dependent on the concentration of calcium in the ground water. There are four principal phases to the model:

December to March

Rainfall levels are high. Together with low evaporation rates and low vegetation levels, this results in the observed shallow water table and high pore water pressures. Calcium concentrations in the ground water are expected to be high, resulting in a high inherent residual shear strength. However, the raised pore water pressures induce slip movement, the rate of which has been shown to be dependent on rainfall, irrespective of the high inherent residual shear strength.

April to May

Rainfall is more sporadic. This, combined with increased evaporation and vegetation levels, results in the ground water rarely being sustained at a shallow level for a long period. Hence, pore water pressures are only temporarily raised. Calcium concentrations in the ground water were found to still be high and hence the inherent residual strength of shear surfaces is expected to be high. Thus, the combination of high inherent residual shear strength and sporadic, generally short lived periods of higher rainfall, results in only small amounts of stick-slip style movement.

June to August

Rainfall levels are low. Hence, as a result of high evaporation rates and relatively high vegetation levels, the ground water level is relatively deep. Calcium concentrations were found to be low and hence the inherent residual shear strength of the shear surfaces can be expected to be low. Thus, it is during this period that the slip is most vulnerable to movement. However, due to the relative paucity of rainfall and the deeper ground water levels, pore water pressures are relatively low and thus no movement of the slip generally occurs.

September to November

Rainfall levels start to increase after the summer low, with occasional periods of heavy rainfall. Initially, evaporation rates can be expected to be relatively high and the slope vegetated, but these will decrease over the period. Early on, the inherent residual shear strength of the failure surfaces is likely to be low, as a result of the low calcium concentrations in the ground water over the summer months. Thus, when more heavy periods of rainfall occur, pore water pressures will increase and, as a result of the lower "summer" inherent residual shear strength, renewed movement of the landslip takes place.

Following a period of heavy rainfall, calcium concentrations in the ground water can be expected to increase and, with further autumnal rainfall and a decrease in ground water temperature, calcium

concentrations in the ground water can be expected to approach the higher levels of the winter. Thus, the inherent residual shear strength of the shear surfaces is likely to increase during the autumnal period and approach its higher winter value. Hence, for further movement to occur during the late autumn/winter, prolonged heavy rainfall, which will result in a shallower ground water level and higher pore water pressures, such as have been recorded in the winter, will be necessary to overcome the increased inherent "winter" residual shear strength of the failure surfaces.

7.5 Avenues for Further Research

The research described in this thesis has enabled the development of a model for the long term and seasonal controls on inland slope stability in the Fuller's Earth. It is hoped that this model may be extended to other inland slopes in different geological and topographical settings. However, clearly further research is required to confirm or indeed contradict the model put forward in this thesis.

Ideally an active inland landslide in a different geological setting should be subjected to a similar investigation. If finances permit, this should involve; (i) the continuous recording of surface movement at a number of positions down the length of the landslide; (ii) the continuous measurement of pore water pressures using very sensitive rapid-response piezometers located at the depth of the basal shear surface; (iii) regular sampling of ground waters for chemical analyses; (iv) regular sampling of material obtained from the approximate level of the basal shear surface for exchangeable cation analysis.

Further analysis of the ground water from another landslip in the Fuller's Earth is required to differentiate between the various sources of calcium in the ground water. The use of strontium isotopes to try and source the origin of the calcium may prove to be a useful tool, enabling a qualitative estimate of the contribution from in situ limestone bands, disseminated calcite and gypsum. In addition, a detailed study of an older "gleyed" shear surface using the techniques developed in Chapter 4 will provide further information on the nature of shear surfaces in the Fuller's Earth and other formations.

This research has emphasised the effects of pore water chemistry on the complete residual failure envelopes of clays. This should be extended to include other clays, both pure and naturally occurring, to try and obtain a suite of consistent results. In addition, other pore water chemistries, applicable to different geological settings, should be considered. These

experiments are time consuming and would make a valuable research project in itself.

REFERENCES

ACKERMAN, K.J. & CAVE, R. (1967). Superficial deposits and structures, including landslip, in the Stroud district, Gloucestershire. *Proc. Geol. Assoc.*, **78**, 576-586.

ALLISON, R.J. (1992). Landslide types and processes. In: *Landslides of the Dorset coast.* (Allison, R.J., Ed.), British Geomorphological Research Group Field Guide, Geologists Association Guide no. 47, p35-39.

ALONSO, E.E., GENS, A. & LLORET, A. (1993). The landslide of Cortes de Pallas, Spain. *Géotechnique,* **43,** 507-521.

ANON. (1972). The preparation of maps and plans in terms of engineering geology. *Q. Jl. Engng Geol.*, **5,** 293-381.

ARKELL, W.J. & DONOVAN, D.T. (1952). The Fuller's Earth of the Cotswolds and its relation to the Great Oolite. *Q. Jl. Geol. Soc.*, **107,** 227-253.

ARKELL, W.J. (1933). *The Jurassic system in Great Britain.* Clarendon Press, London.

ARORA, H.S. & SCOTT, J.B. (1974). Chemical stabilization of landslides by ion exchange. *California geology,* **27,** 99-107.

ATTERBERG, A. (1911). Lerornas förhallande till vatten, deras, plasticitetsgränser och plasticitetsgrader. *Kungliga Lantbruksakademiens Handlinger och Tidskrift,* **50,** 132-158.

BALTEANU, D. (1976). Two case studies of mudflows in the Bazan SubCarpathians. *Geografiska Annaler,* **58A,** 165-171.

BINGER, W.V. & THOMPSON, T.F. (1949). Excavation slopes in the Panama Canal. *A.S.C.E. Trans.*, **114,** 734-754.

BINNIE, A.W., CLARK, J.F.F. & SKEMPTON, A.W. (1967). The effect of discontinuities in clay bedrock on the design of dams in the Mangla project. *Trans. 9th Int. Congr. Large Dams, Istanbul,* **1,** 165-183.

BISHOP, A.W., GREEN, G.E., GARGA, V.K., ANDERSON, A. & BROWN, J.D. (1971). A new ring shear apparatus and its application to the measurement of residual shear strength. *Géotechnique,* **21,** 273-328.

BJERRUM, L. (1954). Geotechnical properties of Norwegian marine clays. *Géotechnique,* **4,** 49-69.

BLONDEAU, F. & JOSSEAUME, H. (1976). Mesure de la résistance au cisaillement résiduelle en laboratoire. Bulletin de Liaison des Laboratoires des Ponts et Chaussées. *Stabilité de talus,* **1,** versants naturels, numéro spécial II, 90-106.

BLONG, R.J. (1973a). Relationships between morphometric attributes of landslides. *Zeit. Geomorph.,* **18,** 66-77.

BLONG, R.J. (1973b). A numerical classification of selected landslides of the debris slide-avalanche-flow type. *Engng. Geol.,* **7,** 66-77.

BÖGLI, A. (1980). *Karst Hydrology and Physical Speleology.* Springer - Verlag, Berlin.

BOROWICKA, H. (1965). The influence of the colloidal content on the shear strength of clay. *Proc. 6th Int. Conf. Soil Mech. Found. Engng., Montreal,* **1,** 175-178.

BOWLES, J.E. (1979). *Physical and geotechnical properties of soils.* McGraw-Hill, New York.

BRADY, N. C. (1990). *The nature and properties of soils.* Macmillan, New York. 599pp

BRINDLEY, G.W. & BROWN, G. (1980). *Crystal structures of clay minerals and their X-ray identification.* Mineralogical Society, London, 504pp.

BRITISH STANDARD 13770 (1991). Methods of testing for soils for civil engineering purposes. Part 2: classification tests.

BROMHEAD, E.N. (1979). A simple ring shear apparatus. *Ground Engng.*, **12,** 40-44.

BROMHEAD, E.N. (1992). *The stability of slopes.* Blackie, Glasgow. 411pp.

BROWN, C.J. (1991). A geotechnical study of abandoned mineworkings in the Bath area. Unpublished Ph.D. Thesis, University of Bristol.

BRUNSDEN, D. (1973). The application of systems theory to the study of mass movement. *Geologica Applicata e Idrogeologia,* **8,** 185-207.

BRUNSDEN, D. (1984). Mudslides. In: *Slope instability.* (Brunsden, D. & Prior, D.B., Eds.), John Wiley & Sons Ltd., London, p1-25.

BRUNSDEN, D. & JONES, D.K.C. (1972). The morphology of degraded landslide slopes in south-west Dorset. *Q. Jl. Engng Geol.,* **5,** 205-222.

BUCHER, F. (1975). Die Restscherfestigkeit natürlicher Böden, ihre Einflussgrössen und Beziehungen als Ergebnis experimenteller Untersuchungen. *Report No. 103. Zurich: Institutes für Grundbau und Bodenmechanik Eidgenössische Technische Hochschule.*

BUCKMAN, S.S. (1901). A Jurassic (part) time table. *Proc. Cotteswold Nat. F. C.,* **13,** 265.

CAILLEUX, A & TRICART, J. (1950). Un type de solifluction: les coulées boueuses. *Révue Géomorph. Dyn.,* **1,** 4-46.

CASAGRANDE, A. (1949). Discussion of a paper by Binger, W.V. & Thompson, T.F. "Excavation slopes in the Panama Canal". *A.S.C.E. Trans.,* **114,** 870-874.

CAVE, R. (1969). Field meeting in the Stroud district. *Proc. Geol. Assoc.,* **80,** 293-299.

CAVE, R. (1977). Geology of the Malmesbury district. *Mem. Geol Surv. G.B.* London: H.M.S.O.

CHAFETZ, H.S., RUSH, P.F. & UTECH, N.M. (1991). Microenvironmental controls on mineralogy and habitat of $CaCO_3$ precipitates: an example from an active travertine system. *Sedimentology,* **38,** 107-126.

CHANDLER R.J., KELLAWAY, G.A., SKEMPTON, A.W. & WYATT, R.J. (1976). Valley slope sections in Jurassic strata near Bath, Somerset. *Phil. Trans. R. Soc. Lond. A.,* **283,** 527-556.

CHANDLER, R.J. & SKEMPTON, A.W. (1974). The design of permanent cutting slopes in stiff fissured clays. *Géotechnique*, **24,** 457-466.

CHANDLER, R.J. (1966). The measurement of residual strength in triaxial compression. *Géotechnique,* **16,** 181-186.

CHANDLER, R.J. (1969). The effect of weathering on the shear strength properties of the Keuper Marl. *Géotechnique,* **19,** 321-334.

CHANDLER, R.J. (1970). The degradation of Lias clay slopes in an area of the east Midlands. *Q. Jl. Engng. Geol.*, **2,** 161-181.

CHANDLER, R.J. (1972). Lias clay: weathering processes and their effect on shear strength. *Géotechnique,* **22,** 403-432.

CHATTERJI, P.K. & MORGENSTERN, N.R. (1989). A modified shear strength formulation for swelling clay soils. *Proc. symp. physico-chemical aspects of soil, rock and related materials, St. Louis.*

CHATTOPADHYAY, P.K. (1972). Residual shear strength of some pure clay minerals. Unpublished Ph.D. Thesis, University of Alberta.

CHEN, J.S., CUSHMAN, J.H. & LOW, P.F. (1990). Rheological behaviour of Na-montmorillonite suspensions at low electrolyte concentration. *Clays and Clay Minerals,* **38,** 57-62.

COATES, D.R. (1977). Landslide perspectives. In: *Landslides.* (Coates, D.R., Ed.), Geological Society of America, p3-28.

COOK, D.A. (1973). Investigation of a landslip in the Fuller's Earth clay, Lansdown, Bath. *Q. Jl. Engng Geol.*, **6,** 233-240.

CRABTREE, R. W. (1986). Spatial distribution of solutional erosion. In: *Solute processes.* (Trudgill, S.T., Ed.), John Wiley & Sons Ltd., London, p167-192.

CRAIG, D. (1979). Some aspects of mudslide stability in east County Antrim, Northern Ireland. Unpublished Ph.D. Thesis, Queen's University of Belfast.

CROZIER, M.J. (1973). Techniques for the morphometric analysis of landslips. *Zeit. Geomorph. Dynamique,* **17,** 78-101.

DALWOOD, R. (1992). The effects of decalcification on slope stability in the Upper Fullers Earth clay, Soper's Wood, Bath. Unpublished final year project, University of Bristol.

DONOVAN, D.T. & KELLAWAY, G.A. (1984). *Geology of the Bristol district: the Lower Jurassic rocks.* London: H.M.S.O. 69pp.

DREW, D. (1985). *Karst processes and landforms.* (Clayton, K. & Johnson, J.H., Eds.), Macmillan, London. 63pp.

EARLY, K.R. & SKEMPTON, A.W. (1972). Investigations of the landslide at Walton's Wood, Staffordshire. *Q. Jl. Engng Geol.,* **5,** 19-41.

FLEISCHER, S. & SCHEFFLER, H. (1979). Problem-oriented shearing technologies for the determination of the drained shear strength of cohesive soils. *Proc. 7th Eur. Conf. Soil. Mech., Brighton,* **2,** 41-48.

FLEISCHER, S. (1972). Scherbruch-und Schergleitfestigkeit von Bindigen Erdstoffen. *Neue Bergbautechnil,* **2,** 98-99. Freiburg: Mining Academy.

FLEMING, S. (1878). *Reports and documents in reference to the location of the line and a western terminal harbour.* Maclean Roger & Co., Ottawa.

FREEZE, R.A. & CHERRY, J.A. (1979). *Groundwater.* Prentice-Hall, New York. 604pp.

GARGA, V.K. (1970). Residual shear strength under large strains and the effect of sample size on the consolidation of fissured clay. Unpublished Ph.D. Thesis, University of London.

GREEN, G.W. & DONOVAN, D.T. (1969). The Great Oolite of the Bath area. *Bull. Geol. Surv. G. B.*, **30,** 1-63.

GREEN, G.W. (1992). *British regional geology: Bristol and Gloucester region.* London: H.M.S.O. 173pp.

GREENWAY, D.R. (1987). Vegetation and slope stability. In: *Slope stability, geotechnical engineering and geomorphology.* (Anderson, M.G. & Richards, K.S, Eds.), John Wiley & Sons Ltd., London, p187-203.

GRIM, R.E. (1953). *Clay mineralogy.* McGraw-Hill, New York. 596pp.

GRIM, R.E. (1968). *Clay mineralogy.* 2nd Edition. McGraw-Hill, New York. 384pp.

GRIMALDI, F.S., SHAPIRO, L. & SCHNEPFE, M. (1966). Determination of carbon dioxide in limestone and dolomite acid-base titration. *U.S.Geol. Survey Prof. Paper 550 B, B186-B188.*

GUNN, J. (1986). Solute processes and karst landforms. In: *Solute processes.* (Trudgill, S.T., Ed.), John Wiley & Sons Ltd., London, p363-437.

HAEFELI, R. (1938). Mechanische Eigenshaften von Lockergesteinen. *Schweizerische Bauzeitung,* **3,** 321-325.

HAEFILI, R. (1948). The stability of slopes acted upon by parallel seepage. *Proc. 2nd Int. Conf. Soil Mech. Found. Engng., Rotterdam,* **1,** 57-62.

HAEFILI, R. (1951). Investigations and measurements of the shear strength of saturated cohesive soils. *Géotechnique,* **2,** 186-207.

HANSEN, M.J. (1984). Strategies for classification of landslides. In: *Slope instability.* (Brunsden, D. & Prior, D.B., Eds.), John Wiley & Sons Ltd., London, p1-25.

HARMER, F.W. (1907). On the origin of certain canon-like valleys associated with lake-like areas of depression. *Q. Jl. Geol. Soc.*, **63,** 470-514.

HAWKINS A.B., LAWRENCE, M.S. & PRIVETT, K.D. (1986). Clay mineralogy and plasticity of the Fuller's Earth formation Bath, UK. *Clay Minerals,* **21,** 293-310.

HAWKINS A.B., LAWRENCE, M.S. & PRIVETT, K.D. (1988). Implications of weathering on the engineering properties of the Fuller's Earth formation. *Géotechnique,* **38,** 517-532.

HAWKINS, A.B. & KELLAWAY, G.A. (1971). Field meeting at Bristol and Bath with special reference to new evidence of glaciation. *Proc. Geol. Assoc.*, **82,** 267-291.

HAWKINS, A.B. & PINCHES, G.M. (1987). Heave at Llandough Hospital, Cardiff. *Q. Jl. Engng. Geol.*, **20,** 41-57.

HAWKINS, A.B. & PRIVETT, K.D. (1979). Engineering geomorphological mapping as a technique to elucidate areas of superficial stuctures; with examples from the Bath area of the south Cotswolds. *Q. Jl. Engng. Geol.*, **12,** 221-233.

HAWKINS, A.B. & PRIVETT, K.D. (1985). Measurement and use of residual shear strength of cohesive soils. *Ground Engng.*, **22,** 22-29.

HAWKINS, A.B. (1973). The geology and slopes of the Bristol region. *Q. Jl. Engng. Geol.*, **6,** 185-205.

HAWKINS, A.B. (1977a). Jurassic rocks of the Bath area. In: *Geological excursions in the Bristol district.* (Savage, R.J.G., Ed.), University of Bristol, p119-132.

HAWKINS, A.B. (1977b). The Hedgemead landslip, Bath. In: *Large ground movements and structures.* (Geddes, J.D., Ed.), Pentech Press, p472-498.

HAWKINS, A.B. AND MCDONALD, C. (1992). Decalcification and residual shear strength reduction in Fuller's Earth clay. *Géotechnique,* **42,** 453-464.

HENDERSON-SELLERS, B. (1984). *Pollution of our atmosphere.* Adam Hilger, 210pp.

HIGGINBOTTOM, I.E. & FOOKES, P.G. (1970). Engineering aspects of periglacial features in Britain. *Q. Jl. Engng Geol.,* **3,** 83-118.

HOLLINGWORTH, S.E., TAYLOR, J.H. & KELLAWAY, G.A. (1944). Large scale superficial structures in the Northampton Ironstone Field. *Q. Jl. Geol. Soc.,* **100,** 1-44.

HORNE, H.M. & DEERE, D.U. (1962). Frictional characteristics of minerals. *Géotechnique,* **12,** 319-335.

HORSWILL, P. & HORTON, A. (1976). Cambering and valley bulging in the Gwash valley at Empingham, Rutland. *Phil. Trans. R. Soc. Lond. A.,* **283,** 427-462.

HUTCHINSON, J.N. & BHANDARI, R. (1971). Undrained loading: a fundamental mechanism of mudflows and other mass movements. *Géotechnique,* **21,** 353-358.

HUTCHINSON, J.N. (1967). The free degradation of London Clay cliffs. *Proc. Geotech. Conf., Oslo,* **1,** 113-118.

HUTCHINSON, J.N. (1968). Mass movement. In: *Encyclopaedia of earth sciences.* (Fairbridge, R.W., Ed.), Reinhold, New York, p688-695.

HUTCHINSON, J.N. (1970). A coastal mudflow on the London Clay cliffs at Beltinge, North Kent. *Géotechnique,* **20,** 412-438.

HUTCHINSON, J.N., SOMERVILLE, S.H. & PETLEY, D.J. (1973). A landslide in periglacially disturbed Etruria Marl at Bury Hill, Staffordshire. *Q. Jl. Engng. Geol.,* **6,** 377-404.

HVORSLEV, M.J. (1936). A ring shear apparatus for the determination of the shearing resistance and plastic flow of soils. *Proc. 1st Int. Conf. Soil. Mech., Boston,* **2,** 125-129.

HVORSLEV, M.J. (1937). *Über die Festigkeitseigenschaften gestörter bindiger Böden.* Thesis, published by Dansmark Naturvidenskabelige Samfund, Ingeriörvidenskabelige Skrifter, Copenhagen, Series A, No. 45. (On the strength properties of remoulded cohesive soils. In translation. Us Army Engineers, Waterways Experiment Station, Vicksburg.)

HVORSLEV, M.J. (1939). Torsion shear tests and their place in the determination of the shearing resistance of soils. *Proc. American Society for Testing Materials,* **39,** 999-1022.

HVORSLEV, M.J. (1960). Physical components of the shear strength of saturated soils. *A.S.C.E. Research Conference on Shear Strength of Cohesive Soils, Boulder, Colorado.* p615-664.

JACKSON, M.L., HSEUNG, Y., COREY, R.B., EVANS, E.J. & VANDAN HEUVEL, R.C. (1952). Weathering sequence of clay-size minerals in soils and sediments II. Chemical weathering of layer silicates. *Proc. Soil. Sci. Soc. Am.,* **16,** 3-6.

JANBU, N. (1954). Application of composite slip surfaces for stability analysis. *Eur. Conf. Stability of Earth Slopes,* Stockholme, **3,** 43-9.

JANBU, N., BJERRUM, L. & KJAERNSLI, B. (1956). Veiledning ved løsning av fundamenterings oppgaver (in Norwegian with English summary: Soil mechanics applied to some engineering problems). Norwegian Geotechnical Institute Publication 16.

JEANS, C.V., MERRIMAN, R.J. & MITCHELL, J.G. (1977). Origin of Middle Jurassic and Lower Cretaceous Fuller's Earths in England. *Clay Minerals,* **12,** 11-44.

KANJI, M.A. & WOLLE, C.M. (1977). The influence of mineral composition on the residual strength of natural soils. *Proc. 9th Int. Conf. Soil Mech. Found. Engng., Tokyo,* **1,** 153-154.

KANJI, M.A. (1974). The relationship between drained residual friction angles and Atterberg limits of natural soils. *Géotechnique*, **24,** 671-674.

KELLAWAY, G.A. & TAYLOR, J.H. (1948). *British regional geology: Bristol and Gloucester district.* London: H.M.S.O. 91pp.

KELLAWAY, G.A. & TAYLOR, J.H. (1952). Early stage physiographic evolution of a portion of the East Midlands. *Q. Jl. Geol. Soc.*, **108,** 343-375.

KELLAWAY, G.A. & TAYLOR, J.H. (1968). The influence of landslipping on the development of the city of Bath, England. *Proc. 23rd Int. Geol. Conf.*, **12,** 65-76.

KELLAWAY, G.A. & WELCH, F.B.A. (1993). *Geology of the Bristol district.* London: H.M.S.O. 199pp.

KENNEY, T.C. (1967). The influence of mineral composition on the residual strength of natural soils. *Proc. Geotech. Conf., Oslo,* **1,** 123-129.

KENNEY, T.C. (1977). Residual strengths of mineral mixtures. *Proc. 9th Int. Conf. Soil Mech. Found. Engng., Tokyo,* **1,** 155-160.

LA GATTA, D.P. (1970). Residual strength of clays and clay-shales by rotation shear tests. *Harvard Soil Mechanics series, No.86.* Cambridge, Massachusetts: Harvard Univeristy.

LADD, G.E. (1935). Landslides, subsidences and rockfalls. *Bull. Am. Railway Eng. Ass.*, **37,** 1091-1162.

LAWRENCE, M.S. (1985). The engineering geology of selected slopes on the Jurassic strata of the south Cotswolds. Unpublished Ph.D. Thesis, University of Bristol.

LICHKOV, L.S. (1938). Dopytanya pro rezhim zusovykh yavishch v raioni roztashuvanya m. Kieva i ioga okolyts (Investigation of land slide phenomena in Kiev and its surroundings). *Geol. zh.*, **4,** 145-198.

LONSDALE, W. (1832). On the Oolitic District of Bath. *Trans. Geol. Soc. London,* **3,** 241-276.

LUPINI, J.F., SKINNER, A.E. & VAUGHAN, P.R. (1981). The drained residual strength of cohesive soils. *Géotechnique,* **31,** 181-213.

MACEWAN, D.M.C. (1949). Some notes on the recording and interpretation of X-ray diagrams of soil clays. *J. Soil Sci.,* **1,** 90-103.

MAIO, C.DI. & FENELLI, G.B. (1994). Residual strength of kaolin and bentonite: the influence of their constituent pore fluid. *Géotechnique,* **44,** 217-226.

MATSUO, S. (1957). A study of the effect of cation exchange on the stability of slopes. *Proc. 4th Int. Conf. Soil Mech. Found. Engng., London,* **1,** 330-333.

MCATTEE, J.L. (1956). Determination of random interstratification in montmorillonite. *Am. Miner.,* **41,** 627-631.

MCDONALD, C. (1990). Decalcification and residual shear strength in Fuller's Earth clay. Unpublished Ph.D. Thesis, University of Bristol.

MEARNS, R., CARNEY, R. & RAYMOND, A.F. (1973). Evaluation of the ion exchange landslide correction technique. *California division of highways. Materials and research department.* Sacremento, California. 26pp.

MELLANBY, K. (1988). *Air pollution, acid rain and the environment.* Watt Committee Report No. 18, Elsevier Applied Science Publishers, London and New York.

MITCHELL, J.K. (1956). The fabric of natural clays and its relation to engineering properties. *Proc. Highw. Res. Bd.,* **35,** 693-713.

MITCHELL, J.K. (1976). *Fundamentals of soil behaviour.* J. Wiley, New York.

MOORE, C. (1880). The Hedgemead landslip. *Proc. Bath Nat. Hist. and Antiq. Field Club,* **4,** 249-258.

MOORE, R. & BRUNSDEN, D. (1996). A physico-chemical mechanism of seasonal mudsliding. In print.

MOORE, R. (1988). The clay mineralogy, weathering and mudslide behaviour of coastal cliffs. Unpublished Ph.D. Thesis, University of London.

MOORE, R. (1991). The chemical and mineralogical controls upon the residual strength of pure and natural clays. *Géotechnique,* **41,** 35-47.

MOORE, R. (1992). Discussion: the chemical and mineralogical controls upon the residual strength of pure and natural clays. *Géotechnique,* **42,** 151-153.

MORGENSTERN, N.R. & TCHALENKO, J.S. (1967). The optical determination of preferred orientation in clays and its application to the study of microstructure in consolidated kaolinite. *Proc. Royal Soc.*, **A300,** 218-250.

MOUM, J. & ROSENQVIST, I. TH. (1961). Mechanical properties of montmorillonitic and illitic clays related to electrolytes of the pore water. *Proc. 5th Int. Conf. Soil Mech. Found. Engng., Paris,* **1,** 263-267.

OLSON, R.E. & MITRONOVAS, F. (1962). Shear strength and consolidation characteristics of calcium and magnesium illite. *Clays and Clay Minerals,* **9,** 185-209.

PARRY, R.H.G. (1972). Some properties of heavily over-consolidated Oxford clay at a site near Bedford. *Géotechnique,* **2,** 485-508.

PENN, I.E., MERRIMAN, R.J. & WYATT, R.J. (1979). The Bathonian strata of the Bath-Frome area. *Rep. Inst. Geol. Sci. London*, **78,** No. 22, 88pp.

PHILLIPS, J. (1844). *Memoirs of William Smith, L.L.D.* John Murray, London.

PICKNETT, R.G., BRAY, L.F., & STENNER, R.D. (1976). The chemistry of cave waters. In: *The science of speleology.* (Ford, T.D. & Cullingford, C.H.D., Eds.), Academic Press, London, p213-266.

PRIOR, D.B. & EVE, R.M. (1975). Coastal landslide morphology at Rosneas, Denmark. *Geografisk Tidsskrift,* **74,** 12-20.

PRIOR, D.B. & GRAHAM, J. (1974). Landslides in the Magho district of Fermanagh, Northern Ireland. *Engng Geology,* **8,** 341-359.

PRIOR, D.B., STEPHENS, N. & ARCHER, D.R. (1968). Composite mudflows on the Antrim coast of north-east Ireland. *Geografiska Annaler,* **50A,** 65-78.

PRIOR, D.B., STEPHENS, N. & DOUGLAS, G.R. (1971). *Some examples of mudflow and rockfall activity in north-east Ireland.* Inst. Brit. Geogrs. Spec. Publ., **3,** 129-140.

PRIVETT, K.D. (1980). The engineering geology of slopes in the south Cotswolds. Unpublished Ph.D. Thesis, University of Bristol.

QUIGLEY, R.M., MATICH, N.A.J., HORVATH, R.G. & HOWSON, H.H. (1971). Swelling clay in two slope failures in Toronto, Canada. *Can. Geotech. Jl.,* **8,** 417-424.

RAMIAH, B.K., DAYALU, N.K. & PURUSHOTHAMARAJ, P. (1970). Influence of chemicals on residual strength of silty clay. *Soils and Foundations,* **10,** 25-36.

REYNOLDS, R.C. & HOWER, J. (1970). The nature of interlayering in mixed-layer illite-montmorillonites. *Clays & Clay Minerals,* **18,** 25-36.

ROSENQVIST, I. TH. (1946). Om leirers kvikkaktighet. Statens vegvesen. Veglaboratoriet. *Meddelelse,* **4,** 5-12.

ROSENQVIST, I. TH. (1953). Considerations on the sensitivity of Norwegian quick clays. *Géotechnique,* **3,** 195-200.

SAVIGEAR, R. A. G. (1965). A technique of morphological mapping. *Ann. Ass. Am. Geogr.,* **55,** 514-538.

SAWYER, C.N. & McCARTY, P.L. (1967). *Chemistry for sanitary engineers.* McGraw-Hill, New York, 518pp.

SCHMASSMANN, H. (1953). Die Rutschung am Sudwestabhang des Wartenberges. *Tatigkeitsberichte d. Naturfor, Gesell. Baselland,* **19,** 29-128.

SCHULTZ, L.G. (1964). Quantitative interpretation of mineralogical composition from x-ray and chemical data for the Pierre Shale. *U.S.Geol. Survey Prof. Paper,* **75,** 57-66.

SEYCEK, J. (1978). Residual shear strength of soils. *Bull. Int. Ass. Engng. Geol.,* **17,** 73-75.

SHARPE, C.F.S. (1938). *Landslides and related phenomena.* Columbia Univ. Press, New York, 137pp.

SHERWOOD, P.T. & RILEY, D.M. (1968). An examination of cone-penetrometer methods for determining the liquid limit of soils. *T. R. R. L. Report L.R. 233.*

SKEMPTON, A W. (1964). Long-term stability of clay slopes. *Géotechnique,* **14,** 75-101.

SKEMPTON, A.W. & DELORY, F.A. (1957) Stability of natural slopes in London clay. *Proc. 4th Int. Conf. Soil Mech. Found. Engng., London,* **2,** 378-381.

SKEMPTON, A.W. & NORTHEY, R.D. (1952). The sensitivity of clays. *Géotechnique,* **2,** 1-30.

SKEMPTON, A.W. & PETLEY, D.J. (1967). The strength along structural discontinuities in stiff clay. *Proc. Geotech. Conf., Oslo,* **2,** 29-46.

SKEMPTON, A.W. (1985). Residual strength of clays in landslides, folded strata and the laboratory. *Géotechnique,* **35,** 3-18.

SMITH , D.I. & ANDERSON, T.C. (1976). Process, landforms and climate in limestone regions. In: *Geomorphology and climate.* (Derbyshire, E., Ed.), John Wiley and Sons Ltd., London, p367-409.

SPEARS, D.A. & TAYLOR, R.K. (1972). The influence of weathering on the composition and engineering properties of in situ Coal Measures rocks. *Int. Jl. Rock Mech. Min. Sci.*, **9**, 729-756.

SPEARS, D.A. (1986). Mineralogical control of the chemical evolution of groundwater. In: *Solute processes*. (Trudgill, S.T., Ed.), John Wiley & Sons Ltd., London, p167-192.

SRIDHARAN, A. & VENTAKAPPA RAO, G. (1979). Shear strength behaviour of saturated clays and the role of the effective stress concept. *Géotechnique,* **29,** 177-193.

SRIDHARAN, A., RAO, S.M. & MURTHY, N.S. (1988). Liquid limit of kaolinitic soils. *Géotechnique,* **38,** 191-198.

SRODON, J. (1980). Precise identification of illite-smectite interstratifications by X-ray powder diffraction. *Clays & Clay Minerals,* **28,** 401-411.

SRODON, J. (1981). X-ray identification of randomly interstratified illite-smectite in mixtures with discrete illite. *Clay Minerals,* **16,** 297-304.

STAWINSKI, J., WIERZCHOS, J. & GARCIA-GONZALEZ, M.T. (1990). Influence of calcium and sodium concentration on the microstructure of bentonite and kaolin. *Clays and Clay Minerals,* **38,** 617-622.

STEWARD, H.E. & CRIPPS, J.C. (1983). Some engineering implications of chemical weathering of pyritic shale. *Q. Jl. Engng Geol.*, **16,** 281-289.

STEWARD, H.E. (1984). Links between geochemical and engineering properties of weathered pyritic shale. Unpublished Ph.D. Thesis, University of Sheffield.

TERZAGHI, K. (1936). Stability of slopes in natural clay. *Proc. 1st Int. Conf. Soil Mech. Found. Engng.*, **1,** 161-165.

TIEDEMANN, B. (1937). Über die Schubfestigkeit bindiger Böden. *Bautechnik,* **15,** Nos 30 and 33, 400-403 and 433-435.

TOWNSEND, F.C. & GILBERT, P.A. (1973). Tests to measure residual strength of some clay shales. *Géotechnique,* **23,** 267-271.

TOWNSEND, F.C. & GILBERT, P.A. (1974). Engineering properties of clay shales, Report 2: *Residual shear strength and classification indexes of clay shales.* Technical report S-71-6, Soils and Pavement Laboratory, U.S. Army Engineers, Waterways Experiment Station, Vicksburg.

TOWNSEND, F.C. & GILBERT, P.A. (1976). *Effects of specimen type on the residual strength of clays and clay shales.* STP 599, 43-65. Philadelphia: American Society for Testing and Materials.

TROTTER, C.M. (1993). Weathering and regolith properties of an earthflow site. *Q. Jl. Engng Geol.,* **26,** 163-178.

VAN OLPHEN, H. (1961). Ion adsorption on clays: A review. *Clays and Clay Minerals,* **8,** 115.

VAN OLPHEN, H. (1977). *An introduction to clay colloid chemistry.* John Wiley & Sons, New York. 318pp.

VARNES, D.J. (1958). Landslide types and processes. In: *Landslides and engineering practice.* (Eckel, E.B., Ed.), Highway Research Board Special Report, **29**, p20-47.

VARNES, D.J. (1978). Slope movements and types and processes. In: *Landslides: analysis and control.* Transportation Research Board Nat. Ac. Sci. Washington Special Report, **176**, p20-47.

VAUGHAN, P.R. & WALBANCKE, H.J. (1975). The stability of cut and fill slopes in boulder clay. *Proceedings of symposium on engineering behaviour of glacial materials,* 209-219. Birmingham: Midland Society Soil Mechanics.

VAUGHAN, P.R., HIGHT, D.W., SODHA, V.G. & WALBANCKE, H.J. (1978). Factors controlling the stability of caly fills in Britain. *Clay fills,* 203-217. London: Institution of Civil Engineers.

VEAR, A. & CURTIS, C.D. (1981). A quantitative evaluation of pyrite weathering. *Earth Surface Processes and Landforms*, **6**, 191-198.

VOIGHT, B. (1973). Correlation between Atterberg plasticity limits and residual shear strength of natural soils. *Géotechnique*, **23**, 265-267.

WARD, W.H. (1945). The stability of natural slopes. *Geog. Jl.*, **105**, 170-197.

WARKENTIN, B.P. & YONG, R.N. (1962). Shear strength of montmorillonite and kaolinite. *Clays and Clay Minerals*, **9**, 210-218.

WESLEY, L.D. (1977). Shear strength properties of halloysite and allophane clays in Java, Indonesia. *Géotechnique*, **27**, 125-136.

WINTERKORN, H.F. & MOORMAN, R.B.B. (1941). A study of changes in physical properties of Putnam soil induced by ionic substitution. *Proc. Highw. Res. Bd.*, **21**, 415-434.

WOODWARD, H.B. (1876). Geology of East Somerset and the Bristol Coalfields. *Mem. Geol Surv. G.B.* London: H.M.S.O.

WOODWARD, H.B. (1887). *The geology of England and Wales, with notes on the physical features of the country.* London: G.Philip.

WOODWARD, H.B. (1894). The Jurassic rocks of Britain, IV. The Lower Oolitic rocks of England (Yorkshire excepted). *Mem. Geol Surv. G.B.* London: H.M.S.O.

YONG, R.N. & WARKENTIN, B.P. (1966). *Introduction to soil behaviour.* Macmillan, New York. 451pp

YONG, R.N.A. & MCKYES, E. (1971). Failure and yield of a clay under triaxial stresses. *J. Soil. Mech. Fdns. Div., A.S.C.E.*, **97**, 159-176.

ZARUBA, Q. & MENCL, V. (1969). *Landslides and their control.* Academia & Elsevier, Prague, 205pp.

APPENDIX I

LABORATORY TECHNIQUES

This appendix describes the routine laboratory procedures used during the course of this research. New techniques developed during the research and techniques which have been adapted by the author are described in their appropriate sections.

Atterberg Limits and Moisture Content

The two index properties described by Atterberg (1911) are the liquid and plastic limits. These were determined according to British Standard 13770 (1991). Apart from for the montmorillonite samples described in Chapter 5, where the Casagrande apparatus was used, the liquid limits were determined using the falling cone penetrometer method. This method is considered superior to the Casagrande apparatus, as it is both more reliable and less prone to operator error (Sherwood & Ryley 1968).

The moisture content of a sample is defined as the mass of water in a sample divided by the mass of the dried sample, expressed as a percentage. It is found by drying the sample in an oven at 105°C for 24 hours.

Determination of Calcite Percentage

This was determined using the carbon dioxide titration method adapted from Grimaldi, Shapiro & Schnepfe (1966). 0.5 g of rock powder is weighed out accurately into a 250 ml boiling flask. 50 ml of deionised water, 1 ml of bromophenol blue indicator and 1ml of 0.2 M hydrochloric acid are then added to the flask and a yellow colour is obtained. The solution is then brought to the boil. If the solution regains the original bluish purple colour of the bromophenol blue indicator, further 1 ml measures of HCL are added until the yellow colour persists. The solution is then titrated with 0.2 M sodium hydroxide to a blue-purple end point.

The percentage of CO_2 is then calculated by

$$\frac{Z \times 2.2}{\text{sample mass}}$$

where,

Z = (molarity of HCl x vol. of HCl) - (molarity of NaOH x vol. NaOH)

Then, assuming that all the carbon dioxide liberated originates from

the digestion of calcite, the percentage of calcite is determined by

$$2.27 \times \text{percentage } CO_2 \text{ present}$$

X-ray Diffraction

The mineralogy of samples was investigated by X-ray diffraction using a Phillips PW 1800 diffractometer combined with a PW 1730/10 generator which supplied 45 kV/40 mA. To identify the dominant non-clay minerals present in samples, whole "rock" powder mounts were made up. Then, using a nickel filter, all samples were exposed to CuKα radiation and scanned between 2° and 65° at a rate of 2°/minute. The peaks of the diffractogram obtained are then attributable to probable minerals present by consulting the minerals search tables in Brindley & Brown (1980) and the JCPDS card index.

To identify the clay mineralogy of a sample, it is necessary to enhance the peak intensities of the clay minerals. Hence, the clay fraction of samples was sedimented onto glass slides and air dried. This technique ensured a high proportion of clay minerals were orientated with their basal (001) sections parallel to the slide, thus enhancing the clay mineral reflections. The slides were then exposed to CuKα radiation and scanned between 2° and either 37° or 46°, at a rate of 1°/minute. The procedure used is described below.

The disaggregated soil sample was centrifuged and the suspension containing particles less than 2 μm in size removed. The suspension was then filtered through a 0.45 μm membrane. The resultant clay slurry was sedimented onto a glass slide using distilled water and allowed to dry at room temperature. In order to identify the clay mineral groups present, x-ray traces were obtained for the following pre-treatment methods:

(1) Untreated, air-dried sample.

(2) Ethylene glycol treated sample. The samples were exposed overnight to ethylene glycol fumes at 60°C in a desiccator. This causes the lattice of expandable minerals to swell producing a peak shift to lower °2θ angles.

(3) Sample heated to 300°C for at least 30 minutes. This volatises all the absorbed ethylene glycol and water within the lattices of the swelling minerals, decreasing their basal spacing.

(4) Sample heated to 550°C for a minimum of 4 hours. This destroys any kaolinite peaks and enhances the 14.0-14.3 °2θ chlorite peak.

The order of treatment is important as the effects are not reversible.

Atomic Absorption Analysis

The elemental composition of ground water samples was analysed using a Phillips Atomic Absorption Spectrophotometer PU9000. Samples were diluted to the appropriate concentrations and lanthinum chloride added to prevent the formation of complex cations which would lead to erroneous results. The machine was then calibrated for the appropriate element using the appropriate standard at three different concentrations.

Scanning Electron Microscope Examination

The investigations were carried out using a Cambridge 250 Mk III scanning electron microscope. The clay samples were prepared for examination by first partially air drying the samples and then coating them with a film of gold. It was not possible to use very moist clay samples as the gold would not 'take' to the samples. However, partially drying the samples allowed the gold to adhere to the surface without too much visible distortion of the clay structures.

Routine Residual Shear Strength Testing

Residual shear strength was determined using the Bromhead ring shear apparatus (Wykeham Farrance WF 25850). Bromhead (1979) describes the details of the apparatus and its use is discussed extensively by Privett (1980) and Lawrence (1985). In summary, an annulus of remoulded soil (100 mm o.d. and 70 mm i.d.) is confined between two bronze annular porous plates and held in a water bath. A normal load is then applied to the upper platen and the lower platen is slowly rotated. Using two matched, calibrated proving rings and dial gauges which bear onto a cross arm on the upper platen, the shear stress is measured. The normal load is gradually increased enabling a failure envelope to be produced for the sample. The technique used is described below.

A remoulded sample, at approximately its plastic limit, was packed into the annular space of the lower platen. To enhance even consolidation during testing it is important to obtain a level upper sample surface; this was achieved by slicing off any excess soil using a sharp razor blade. The lower platen was then placed in the machine, confined by the upper platen and the water bath filled with distilled water. A normal load of 27.5 kPa was then applied to the sample via a loading system and the sample allowed to consolidate over a twelve hour period. A shear surface was then produced in the sample by failing under the same load for thirty minutes at the fastest

speed available of 60° per minute (44.52 mm/min. at median sample diameter). Following the recommendation made by Privett (1980), a few drops of light oil were smeared on the centralising pin to reduce friction.

Once a shear plane had been produced, the sample was left to shear under the same load for at least eight hours at the slowest strain rate of 0.024° per minute to obtain the residual condition, at which stage the axial gauge readings were recorded and the normal load increased. The use of this slow strain rate facilitated pore pressure dissipation and minimised sample extrusion. Past experience indicated that after eight hours the proving ring dial gauges had stabilised and the residual condition had been reached. Each sample was tested at six normal effective stress values; 51.9 kPa, 125.4 kPa, 247.9 kPa, 370.3 kPa, 492.8 kPa and 615.2 kPa. Effective normal stress was then plotted against shear stress producing good failure envelopes that usually gently curved towards the origin.

To prevent elevated shear stresses being measured due to the build up of extruded soil, it was important that any extruded soil was removed from the inner diameter of the ring shear via a small hole drilled in the upper platen using a wash bottle, as recommended by Lawrence (1985). In addition, as recommended by Privett (1980), the proving rings were tapped prior to readings being recorded. This caused the dial gauge readings to drop and then pick up slightly after a few minutes. Privett (1980) attributed this phenomena to stick-slip motion during shearing. However, as discussed by McDonald (1990), it appears to be caused by the gauge displacement arm sticking within its housing due to the presence of small amounts of dirt. Tapping the rings therefore freed the arm so that the true value of residual shear strength could be recorded.

APPENDIX II

SURVEY DATA FOR THE LANDSLIDE ADJACENT TO SOPER'S WOOD

Survey Station:A1																	
Date:	19/1/94	26/1/94	2/2/94	10/2/94	16/2/94	22/2/94	3/3/94	9/3/94	16/3/94	21/3/94	7/4/94	13/4/94	19/4/94	27/4/94	11/5/94	27/5/94	3/6/94	30/6/94
Datum:	AD	AD	AD	AD	AD	AD	AD	AD	AD	AD	AD	AD	AD	AD	AD	AD	AD	AD
Field Angle(in degrees):	166.1917	166.3189	166.1025	166.1478	166.0917	166.3768	166 3817	166.2383	166.1769	166.3594	166 3347	166 2836	166 0469	166 2994	166 3453	166.2978	166.1978	166 4014
Angle of elev. from Horiz (Degrees):	13.8083	13.6811	13.8975	13.85222	13.9083	13 6232	13.6183	13.7617	13.8231	13.6406	13.6653	13.7164	13.9531	13.7006	13.6547	13 7022	13 8022	13 5986
Field Distance (m),d1:	66 422	66.375	66.439	66 426	66 446	66.358	66.352	66.393	66.428	66.368	66 360	66 382	66.446	66 378	66 364	66 367	66.395	66 350
Field Distance (m),d2:	66.422	66 375	66.435	66.428	66.445	66.359	66.352	66.392	66.427	66.369	66 359	66.381	66 448	66.378	66.364	66 367	66 394	66 347
Field Distance (m),d3:	66.423	66 378	66.434	66.430	66 444	66.362	66.354	66 392	66.427	66 367	66 360	66 384	66 445	66 377	66 362	66.366	66 395	66 347
Field Distance (m),d4:	66.415	66.375	66.437	66.427	66 448	66 357	-	66.392	66.427	66 368	66 360	66.379	66 446	66.378	66 364	66 367	66.394	66 347
Average field distance (m),D :	66.421	66 376	66.436	66.428	66.446	66.359	66.353	66 392	66.427	66.368	66.360	66.382	66 446	66.378	66 364	66.367	66 395	66.348
Ht of geodimeter above Datum (m),x:	1.415	1.477	1.244	1.299	1 253	1 584	1.386	1.400	1.388	1.338	1.469	1.384	1.384	1.508	1 562	1 433	1 422	1 468
Ht of Prism above station (m),y:	1.407	1.303	1.230	1.326	1.348	1.326	1.125	1.310	1.381	1.106	1.262	1.246	1.528	1.347	1.344	1.274	1.376	1.180
z (m)	15.853	15 699	15.957	15.904	15.971	15 630	15.623	15.794	15.871	15 652	15.677	15.740	16.022	15 721	15.666	15.721	15 840	15 600
Vert. Ht of station from datum (m),Dv:	15.861	15.873	15.971	15.877	15.876	15.888	15.884	15.884	15.878	15.884	15.884	15.878	15.878	15.882	15.884	15.880	15.886	15.888
Horiz. Dist of station from datum (m),Dh:	64.501	64.492	64.491	64.496	64.498	64.492	64.487	64.486	64.503	64.496	64.481	64.488	64.486	64.489	64.488	64.478	64.477	64.488

Survey Station:A2																	
Date:	19/1/94	26/1/92	2/2/94	10/2/94	16/2/94	22/2/94	3/3/94	9/3/94	16/3/94	21/3/94	7/4/94	13/4/94	19/4/94	27/4/94	11/5/94	27/5/94	3/6/94	30/6/94
Datum:	AD	AD	AD	AD	AD	AD	AD	AD	AD	AD	AD	AD	AD	AD	AD	AD	AD	AD
Field Angle(in degrees):	166.4694	166.4611	166.3403	166.3483	166.1931	166.3592	166.3408	166 2900	166 2669	166.2714	166.3692	166.3297	166.2494	166.3114	166 2850	166 3086	166 2711	166 2597
Angle of elev. from Horiz (Degrees):	13.5306	13.5389	13 6597	13.6517	13 8069	13.6408	13 6592	13.71	13.7331	13.7286	13 6308	13.6703	13.7506	13 6886	13 715	13.6914	13 7289	13 7403
Field Distance (m),d1:	80.093	79 894	79.733	79.509	79.448	79.316	79 127	79 086	79 030	78 937	78 432	78.248	78 269	78 225	78 219	78.198	78 206	78 196
Field Distance (m),d2:	80 092	79 893	79.735	79.507	79 446	79 316	79.128	79.086	79 029	78 939	78.434	78 247	78 269	78.226	78 221	78 200	78 206	78 199
Field Distance (m),d3:	80.092	79 895	79.733	79 509	79.445	79.317	79.129	79 086	79.031	78.938	78.432	78.248	78.268	78.226	78 220	78 199	78 205	78 196
Field Distance (m),d4:	80.090	79 892	79.734	79.508	79 445	79 317	-	79.087	79 030	78.936	78 431	78.248	78.267	78 227	78.219	78 198	78 208	78 198
Average field distance (m),D :	80 092	79.894	79.734	79.508	79.446	79.317	79.128	79 086	79.030	78 938	78.432	78.248	78.268	78.226	78.220	78.199	78 206	78 197
Ht of geodimeter above Datum (m),x:	1.415	1.477	1.244	1 299	1.253	1.584	1.386	1.400	1.388	1.338	1 469	1.384	1.384	1.508	1.562	1 433	1.422	1 468
Ht of Prism above station (m),y:	1.360	1.234	1.119	1 129	1.274	1.381	1.157	1.232	1.259	1.182	1.115	1.218	1.233	1 258	1.322	1.194	1.244	1 299
z (m)	18.739	18.704	18.830	18.765	18 960	18.706	18 686	18.744	18.762	18.734	18 484	18 493	18 604	18.512	18 545	18 509	18 561	18 574
Vert. Ht of station from datum (m),Dv:	18.794	18.947	18.955	18.935	18.939	18.909	18.915	18.912	18.891	18.890	18.838	18.659	18.755	18.762	18.785	18.748	18.739	18.743
Horiz. Dist of station from datum (m),Dh:	77.869	77.673	77.479	77.262	77.150	77.079	76.890	76.833	76.771	76.682	76.223	76.031	76.025	76.004	75.989	75.977	75.972	75.959

Survey Station:A3																	
Date:	19/1/94	26/1/94	2/2/94	10/2/94	16/294	22/2/94	3/3/94	9/3/94	16/3/94	21/3/94	7/4/94	13/4/94	19/4/94	27/4/94	11/5/94	27/5/94	3/6/94	30/6/94
Datum:	AD	AD	AD	AD	AD	AD	AD	AD	AD	AD	AD	AD	AD	AD	AD	AD	AD	AD
Field Angle(in degrees):	166.0689	166.1097	166 0647	166.1114	166.0000	166.1386	166.2447	166.1817	166 1169	166.0814	166.3244	166.3342	166.2058	166.2711	166.3556	166.2861	166 2678	166 2406
Angle of elev. from Horiz (Degrees):	13.9311	13.8903	13.9353	13 8886	14	13.8614	13.7553	13.8183	13.8831	13.9186	13.6756	13 6658	13.7942	13 7289	13 6444	13 7139	13.7322	13 7594
Field Distance (m),d1:	90.269	89.921	89.585	89.186	88.999	88.726	88.429	88.339	88.254	88.153	87.488	87.255	87.275	87.244	87.214	87.206	87.217	87 219
Field Distance (m),d2:	90.271	89.920	89.587	89.190	88 999	88.727	88.430	88.339	88.254	88 155	87.488	87.254	87.275	87.244	87.214	87.205	87.218	87 220
Field Distance (m),d3:	90.269	89.921	89.586	89.191	88 999	88.727	88 432	88.339	88.252	88.153	87.489	87.253	87.275	87.245	87.213	87 207	87 217	87 219
Field Distance (m),d4:	90.270	89 922	89 585	89.189	89 000	88 728	88 430	88.338	88 254	88.154	87.488	87.254	87.277	87.245	87 214	87.208	87 217	87 221
Average field distance (m),D :	90.270	89.921	89 586	89.189	88.999	88 727	88.430	88 339	88.254	88.154	87.488	87.254	87 276	87.245	87.214	87.207	87 217	87 220
Ht of geodimeter above Datum (m),x:	1.415	1.477	1.244	1.299	1.253	1 584	1.386	1 400	1.388	1 338	1 469	1 384	1.384	1.508	1 562	1 433	1 422	1 468
Ht of Prism above station (m),y:	1.454	1.324	1.152	1.167	1 310	1 439	1.130	1.249	1.372	1.393	1.160	1 179	1.377	1 401	1 325	1 306	1 328	1 421
z (m)	21.733	21.587	21 575	21.408	21.531	21.257	21.027	21.099	21 176	21.205	20 684	20 614	20 810	20.706	20 573	20 674	20 704	20 745
Vert. Ht of station from datum (m),Dv:	21.694	21.740	21.667	21.540	21.474	21.402	21.283	21.250	21.192	21.150	20.993	20.819	20.817	20.813	20.810	20.801	20.798	20.792
Horiz. Dist of station from datum (m),Dh:	87.615	87.291	86.949	86.581	86.356	86.143	85.894	85.782	85.675	85.565	85.008	84.784	84.758	84.752	84.752	84.720	84.724	84 717

Survey Station:A4																	
Date:	19/1/94	26/1/94	2/2/94	10/2/94	16/2/94	22/2/94	3/3/94	9/3/94	16/3/94	21/3/94	7/4/94	13/4/94	19/4/94	27/4/94	11/5/94	27/5/94	3/6/94	30/6/94
Datum:	AD	AD	AD	AD	AD	AD	AD	AD	AD	AD	AD	AD	AD	AD	AD	AD	AD	AD
Field Angle(in degrees):	165.8658	165.9753	165.9608	165.9561	165.8847	166 0319	165.9425	165 9467	165.9561	165.9075	165 9639	165.9644	165.9453	166 0031	166.0256	165 9950	165 9261	165 9539
Angle of elev. from Horiz (Degrees):	14.1342	14.0247	14.0392	14.0439	14.1153	13.9681	14.0575	14.0533	14.0439	14.0925	14 0361	14.0356	14 0547	13 9969	13.97444	14 005	14 0739	14 0461
Field Distance (m),d1:	111.783	111.695	111.652	111.594	111.605	111.511	111.494	111.499	111 475	111.459	111.185	111.131	111.136	111.095	111.086	111.088	111.107	111 104
Field Distance (m),d2:	111.786	111.692	111.654	111.596	111.605	111.512	111.495	111.498	111.476	111.457	111.186	111.130	111 135	111 096	111 085	111 088	111 108	111 104
Field Distance (m),d3:	111.791	111.692	111 653	111.595	111 605	111 513	111 496	111.496	111 475	111 457	111.187	111.131	111.135	111 096	111.087	111.088	111 107	111 102
Field Distance (m),d4:	111.788	111.690	111.654	111 596	111.603	111.513	-	111.497	111 476	111.457	111.187	111.129	111 135	111 096	111 087	111.087	111 108	111.102
Average field distance (m),D :	111.787	111.692	111.653	111.595	111.605	111.512	111 495	111.498	111.476	111.458	111.186	111.130	111 135	111 096	111.086	111 088	111.108	111 103
Ht of geodimeter above Datum (m),x:	1.415	1.477	1.244	1.299	1.253	1.584	1 386	1.400	1.388	1 338	1.469	1.384	1 384	1 508	1.562	1 433	1.422	1 468
Ht of Prism above station (m),y:	1.530	1.360	1.143	1.205	1.292	1.322	1.309	1 312	1.270	1.337	1.305	1.218	1.255	1.265	1.278	1.198	1.331	1 322
z (m)	27.298	27.068	27.085	27.080	27.217	26.917	27.082	27.074	27.051	27.139	26.966	26.952	26.989	26 871	26 826	26 884	27 018	26 965
Vert. Ht of station from datum (m),Dv:	27.183	27.185	27.186	27.174	27.178	27.179	27.159	27.162	27.169	27.140	27.130	27.118	27.118	27.114	27.110	27.119	27.109	27.111
Horiz. Dist of station from datum (m),Dh:	108.403	108.363	108.318	108.260	108.235	108.215	108.156	108.160	108.144	108.103	107.867	107.812	107.808	107.797	107.798	107.786	107.772	107.781
Survey Station:A5																		
Date:	19/1/94	26/1/95	2/2/94	10/2/94	16/2/94	22/2/94	3/3/94	9/3/94	16/3/94	21/3/94	7/4/94	13/4/94	19/4/94	27/4/94	11/5/94	27/5/94	3/6/94	30/6/94
Datum:	AD	AD	AD	AD	AD	AD	AD	AD	AD	AD	AD	AD	AD	AD	AD	AD	AD	AD
Field Angle(in degrees):	166.1953	166.1875	166.1908	166.1178	166.1072	166.2528	166.1625	166.1083	166.2108	166.1944	166.2222	166.1814	166.1481	166.1525	166 2453	166 2292	166.1525	166.1242
Angle of elev. from Horiz (Degrees):	13.8047	13.8125	13.8092	13.8822	13 8928	13.7472	13.8375	13.8917	13.7892	13.8056	13.7778	13.8186	13.8519	13 8475	13.7547	13.7708	13 8475	13 8758
Field Distance (m),d1:	133.187	133.177	133.165	133 174	133.170	133.080	133.103	133.117	133.085	133.076	132.954	132.933	132.947	132.937	132.895	132 882	132 934	132 941
Field Distance (m),d2:	133.187	133.175	133.165	133.173	133.167	133.081	133.103	133.117	133.086	133.076	132.954	132.930	132.946	132.935	132.893	132.881	132.933	132 940
Field Distance (m),d3:	133.188	133.173	133.164	133.175	133.167	133 082	133.102	133.118	133.085	133.076	132.953	132 931	132.945	132 936	132 894	132 880	132.935	132 941
Field Distance (m),d4:	133.188	133.175	133.162	133.172	133.168	133.082	133 100	133.116	133.084	133.077	132.951	132.931	132.949	132.937	132.897	132.882	132.937	132.944
Average field distance (m),D :	133.188	133.175	133.164	133.174	133.168	133.081	133.102	133.117	133.085	133.076	132.953	132.931	132.947	132 936	132 895	132 881	132 935	132 942
Ht of geodimeter above Datum (m),x:	1.415	1.477	1.244	1.299	1.253	1.584	1.386	1.400	1.388	1.338	1.469	1.384	1.384	1.508	1.562	1.433	1 422	1 468
Ht of Prism above station (m),y:	1.308	1.394	1.155	1.390	1.355	1.336	1.346	1.487	1.245	1.217	1.262	1.276	1.362	1.378	1.307	1.207	1.373	1 495
z (m)	31.780	31.795	31.785	31.952	31.974	31.625	31.834	31.960	31.721	31.756	31 664	31.750	31.829	31 817	31.598	31.631	31.816	31 882
Vert. Ht of station from datum (m),Dv:	31.887	31.878	31.874	31.861	31.872	31.873	31.874	31.873	31.864	31.877	31.871	31.858	31.851	31.947	31.853	31.857	31.865	31.855
Horiz. Dist of station from datum (m),Dh:	129.340	129.324	129.315	129.284	129.272	129.269	129.239	129.223	129.249	129.232	129.127	129.084	129.080	129.073	129.084	129.062	129.071	129.062
Survey Station:B1																		
Date:	19/1/94	26/1/94	2/2/94	10/2/94	16/2/94	22/2/94	3/3/94	9/3/94	16/3/94	21/3/94	7/4/94	13/4/94	19/4/94	27/4/94	11/5/94	27/5/94	3/6/94	30/6/94
Datum:	BD	BD	BD	BD	BD	BD	BD	BD	BD	BD	BLOCK	BLOCK	REINSERT	BD	BD	BD	BD	BD
Field Angle(in degrees):	166.1578	166.1717	166.2597	166.2658	166.2525	166.3358	166.2700	166.3492	166.3656	166.3431	TILTED	TILTED	166.3453	166.3642	166 4258	166.4881	166.3308	166 4883
Angle of elev. from Horiz (Degrees):	13.8422	13.8283	13.7403	13.7342	13 7475	13 6642	13.7300	13 6508	13 6344	13.6569	OVER	OVER	13.6547	13.6358	13.5742	13.5119	13 6692	13 5117
Field Distance (m),d1:	90.027	89.660	89.279	88.884	88.719	88.585	88.261	88 070	87.972	87.826			86.820	86.805	86.777	86.744	86.812	86 739
Field Distance (m),d2:	90.030	89 660	89.282	88.881	88.719	88.584	88.261	88 071	87.975	87.826			86.819	86.804	86.776	86.745	86 815	86 743
Field Distance (m),d3:	90.027	89 661	89.281	88.881	88.721	88 584	88.264	88 071	87.975	87.825			86 820	86 806	86 775	86.745	86.814	86 737
Field Distance (m),d4:	90.028	89 660	89.282	88 883	88.721	88.586	88.264	88.071	87.973	87.825			86 821	86 807	86.776	86 743	86 813	86 740
Average field distance (m),D :	90 028	89.660	89.281	88 882	88.720	88.585	88.263	88.071	87 974	87.826	0 000	0.000	86.820	86 806	86.776	86 744	86 814	86 740
Ht of geodimeter above Datum (m),x:	1.436	1.469	1.344	1.291	1.285	1.346	1.257	1.387	1.388	1.395	0.000	0.000	1.537	1.554	1 578	1 477	1 433	1 592
Ht of Prism above station (m),y:	1.465	1.519	1.280	1.278	1.293	1.235	1.256	1.223	1.181	1.210	0 000	0 000	1.415	1.426	1.350	1.147	1.362	1 253
z (m)	21.539	21.430	21.206	21.102	21 084	20.926	20.949	20.785	20.738	20.736	#VALUE!	#VALUE!	20.496	20 464	20 367	20.268	20.515	20 266
Vert. Ht of station from datum (m),Dv:	21.510	21.380	21.270	21.115	21.078	21.037	20.950	20.949	20.945	20.921	#VALUE!	#VALUE!	20.618	20.592	20.595	20.598	20.586	20 605
Horiz. Dist of station from datum (m),Dh:	87.413	87.062	86.726	86.341	86.178	86.078	85.740	85.583	85.495	85.342	#VALUE!	#VALUE!	84.366	84.359	84.352	84.343	84.355	84 339

Survey Station:B2																	
Date:	19/1/94	26/1/94	2/2/94	10/2/94	16/2/94	22/2/94	3/3/94	9/3/94	16/3/94	21/3/94	7/4/94	13/4/94	19/4/94	27/4/94	11/5/94	27/5/94	3/6/94	30/6/94
Datum:	BD	BD	BD	BD	BD	BD	BD	BD	BD	BD	BD	BD	BD	BD	BD	BD	BD	BD
Field Angle(in degrees):	165 8661	165.9261	165 9106	165.8006	165 8008	165.9094	165.7942	165 8642	165.7944	165.8236	165.9400	165.8500	165.8819	165 9692	165 9611	165.9931	165 8403	166 0581
Angle of elev. from Horiz (Degrees):	14.1339	14.0739	14.0894	14.1994	14.1992	14.0906	14.2058	14.1358	14.2056	14.1764	14 06	14.15	14.1181	14.0308	14.0389	14.00694	14 1597	13 9419
Field Distance (m),d1:	99 318	99.226	99.116	98.988	98.935	98.812	98 677	98.626	98 567	98 439	97.776	97.600	97.601	97.550	97.554	97.413	97 447	97.347
Field Distance (m),d2:	99 317	99 225	99.119	98 993	98 934	98 812	98.676	98 625	98.569	98.439	97.775	97.600	97.603	97.548	97.554	97.413	97 449	97 345
Field Distance (m),d3:	99 315	99.222	99.118	98 991	98.934	98.812	98 678	98 627	98 567	98 439	97.774	97.601	97.599	97 551	97.553	97 414	97 447	97 343
Field Distance (m),d4:	99 314	99.222	99 118	98.994	98.937	98 811	98.674	98 627	98.567	98.439	97.775	97.602	97 601	97 550	97 556	97 417	97 446	-
Average field distance (m),D :	99 316	99.224	99.118	98.992	98.935	98 812	98 676	98.626	98.568	98.439	97.775	97.601	97 601	97.550	97.554	97.414	97 447	97 345
Ht of geodimeter above Datum (m),x:	1.436	1.469	1.344	1.291	1.285	1.346	1 257	1.387	1.388	1.395	1.452	1.355	1 537	1 554	1.578	1 477	1 433	1 592
Ht of Prism above station (m),y:	1.366	1.286	1.175	1.322	1.298	1.170	1.290	1.295	1.421	1 372	1.226	1.302	1 428	1.298	1 340	1.184	1.421	1.188
z (m)	24.252	24.129	24.129	24.282	24.268	24.056	24.216	24.087	24.189	24.109	23.753	23.860	23.807	23.650	23 665	23.578	23 838	23 454
Vert. Ht of station from datum (m),Dv:	24.322	24.312	24.298	24.251	24.255	24.232	24.183	24.179	24.156	24.132	23.979	23.913	23.916	23.906	23.903	23.871	23.850	23.858
Horiz. Dist of station from datum (m),Dh:	96.309	96.245	96.136	95.967	95.912	95.839	95.659	95.640	95.553	95.441	94.846	94.639	94.653	94.639	94.640	94.518	94.487	94.477

Survey Station:B3																	
Date:	19/1/94	26/1/94	2/2/94	10/2/94	16/2/94	22/2/94	3/3/94	9/3/94	16/3/994	21/3/94	7/4/94	13/4/94	19/4/94	27/4/94	11/5/94	27/5/94	3/6/94	30/6/94
Datum:	BD	BD	BD	BD	BD	BD	BD	BD	BD	BD	BD	BD	BD	BD	BD	BD	BD	BD
Field Angle(in degrees):	165.9764	166.0881	166.0400	166.0364	165.9531	166.1339	166.0236	165.9681	165 9833	165 9928	166.1253	166.1194	166 1347	166.1475	166.1350	166.1983	166 0653	166 2100
Angle of elev. from Horiz (Degrees):	14.0236	13.9119	13.96	13.9636	14.0469	13 8661	13.9764	14.0319	14 0167	14 0072	13 8747	13 8806	13 8653	13.8525	13 865	13 8017	13 9347	13 79
Field Distance (m),d1:	109 939	109.813	109.743	109.596	109.609	109 447	109.359	109.365	109.312	109 201	108.666	108 546	108.531	108 514	108 527	108.424	108 457	108 375
Field Distance (m),d2:	109.939	109 820	109.747	109.598	109.611	109.445	109.360	109.366	109 313	109.199	108.666	108.547	108.531	108.516	108 526	108 424	108.457	108 373
Field Distance (m),d3:	109 933	109.822	109.743	109.597	109 611	109 446	109.358	109.367	109 311	109 199	108.667	108.545	108 532	108.515	108 526	108.423	108 458	108 378
Field Distance (m),d4:	109.941	109.820	109.747	109.600	109.610	109.446	109.362	109.367	109.311	109 201	108.670	108 548	108.528	108.516	108 524	108.423	108 458	-
Average field distance (m),D :	109.938	109.819	109.745	109.598	109.610	109 446	109 360	109.366	109.312	109.200	108.667	108.547	108 531	108 515	108.526	108.424	108 458	108 375
Ht of geodimeter above Datum (m),x:	1.436	1.469	1.344	1.291	1.285	1.346	1 257	1.387	1.388	1.395	1.452	1.355	1.537	1.554	1.578	1.477	1 433	1 592
Ht of Prism above station (m),y:	1.476	1.288	1.274	1.223	1.396	1.101	1.261	1.502	1.481	1.473	1 322	1.256	1.410	1.402	1.457	1.234	1.465	1.325
z (m)	26.640	26.404	26.475	26 447	26.604	26.229	26.413	26.517	26.476	26.431	26 058	26 040	26 008	25 981	26.007	25.866	26 118	25 833
Vert. Ht of station from datum (m),Dv:	26.600	26.585	26.545	26.515	26.493	26.474	26.409	26.402	26.383	26.353	26.188	26.139	26.135	26.133	26.128	26.109	26.086	26.100
Horiz. Dist of station from datum (m),Dh:	106.661	106.597	106.504	106.359	106.333	106.257	106.122	106.103	106.057	105.953	105.497	105.377	105.368	105.359	105.364	105.293	105.266	105.252

Survey Station:B4																	
Date:	19/1/94	26/1/94	2/2/94	10/2/94	16/2/94	22/2/94	3/3/94	9/3/94	16/3/94	21/3/94	7/4/94	13/4/94	19/4/94	27/4/94	11/5/94	27/5/94	3/6/94	30/6/94
Datum:	BD	BD	BD	BD	BD	BD	BD	BD	BD	BD	BD	BD	BD	BD	BD	BD	BD	BD
Field Angle(in degrees):	166.4489	166.4242	166.4008	166.2839	166.2406	166.3831	166.3539	166.2886	166.3847	166.3586	166 4189	166.3844	166.4456	166.4361	166.4261	166.4733	166.3817	166.3286
Angle of elev. from Horiz (Degrees):	13.5511	13.5758	13.5992	13.7161	13.7594	13 6169	13.6461	13.7114	13.6153	13.6414	13.5811	13.6156	13.5544	13.5639	13.5739	13.5267	13.6183	13 6714
Field Distance (m),d1:	130.596	130.587	130.563	130 576	130.638	130.484	130 474	130.495	130 443	130.431	130.195	130.168	130.114	130.114	130.135	130.074	130.114	130 175
Field Distance (m),d2:	130.597	130.584	130 564	130.578	130 638	130.484	130 472	130.496	130.445	130.431	130.195	130.165	130.113	130.114	130.136	130 072	130.114	130 171
Field Distance (m),d3:	130.596	130.582	130.562	130.578	130.637	130.482	130.472	130.494	130.442	130 431	130.194	130.168	130.112	130.114	130.136	130.074	130.113	130.169
Field Distance (m),d4:	130.595	130.587	130.563	130 578	130 640	130.485	130.470	130.494	130.444	130.431	130.195	130.167	130.114	130.113	130.138	130 074	130.116	-
Average field distance (m),D :	130.596	130.585	130.563	130.578	130.638	130.484	130 472	130.495	130.444	130.431	130.195	130.167	130 113	130.114	130.136	130 074	130.114	130.172
Ht of geodimeter above Datum (m),x:	1.436	1.469	1.344	1.291	1.285	1.346	1.257	1.387	1.388	1.395	1.452	1.355	1.537	1.554	1.578	1 477	1 433	1.592
Ht of Prism above station (m),y:	1.229	1.311	1.228	1.380	1.553	1.272	1.226	1.513	1.306	1.364	1.266	1.251	1.291	1.335	1.382	1.168	1 348	1.607
z (m)	30 600	30 652	30 699	30 961	31.072	30.720	30.781	30.931	30.707	30.761	30.573	30.642	30.494	30.516	30.543	30 424	30 636	30.766
Vert. Ht of station from datum (m),Dv:	30.807	30.810	30.815	30.872	30.804	30.794	30.812	30.805	30.789	30.792	30.759	30.746	30.740	30.735	30.739	30.733	30.721	30.751
Horiz. Dist of station from datum (m),Dh:	126.960	126.936	126.903	126.854	126.889	126.816	126.789	126.776	126.778	126.752	126.554	126.509	126.489	126.485	126.501	126.465	126.456	126.484

Summary

DATE:	19/1/94	26/1/94	2/2/94	10/2/94	16/2/94	22/2/94	3/3/94	9/3/94	16/3/94	21/3/94	7/4/94	13/4/94	19/4/94	27/4/94	11/5/94	27/5/94	3/6/94	30/6/94
A1 Vert. Ht (m) from datum AD:	15.861	15.873	15.971	15.877	15 876	15 888	15.884	15 884	15.878	15.884	15.884	15 878	15.878	15 882	15 884	15.880	15 886	15 888
A1 Horiz. Dist (m) from datum AD:	64 501	64.492	64 491	64 496	64.498	64 492	64.487	64 486	64.503	64.496	64.481	64 488	64 486	64 489	64 488	64 478	64 477	64 488
A2 Vert. Ht (m) from datum AD:	18.794	18.947	18.955	18 935	18.939	18 909	18 915	18.912	18 891	18.890	18 838	18.659	18 755	18.762	18.785	18.748	18 739	18 743
A2 Horiz. Dist (m) from datum AD:	77.869	77.673	77 479	77.262	77.150	77.079	76.890	76.833	76.771	76 682	76.223	76 031	76 025	76.004	75 989	75 977	75.972	75 959
A3 Vert. Ht (m) from datum AD:	21.694	21.740	21.667	21 540	21.474	21.402	21.283	21.250	21.192	21.150	20.993	20 819	20.817	20 813	20 810	20 801	20.798	20 792
A3 Horiz. Dist (m) from datum AD:	87.615	87.291	86.949	86 581	86 356	86.143	85.894	85.782	85.675	85.565	85.008	84 784	84.758	84 752	84.752	84.720	84 724	84 717
A4 Vert. Ht (m) from datum AD:	27.183	27.185	27.186	27 174	27.178	27.179	27.159	27.162	27.169	27.140	27.130	27.118	27.118	27.114	27.110	27.119	27.109	27 111
A4 Horiz. Dist (m) from datum AD:	108 403	108.363	108.318	108.260	108.235	108.215	108.156	108.160	108.144	108.103	107.867	107.812	107.808	107.797	107.798	107.786	107.772	107 781
A5 Vert. Ht (m) from datum AD:	31.887	31.878	31.874	31.861	31.872	31.873	31.874	31.873	31.864	31.877	31.871	31 858	31.851	31.947	31 853	31 857	31.865	31 855
A5 Horiz. Dist (m) from datum AD:	129.340	129.324	129.315	129.284	129.272	129.269	129.239	129.223	129.249	129.232	129.127	129 084	129.080	129 073	129 084	129.062	129.071	129 062
B1 Vert. Ht (m) from datum BD:	21.510	21.380	21.270	21.115	21.076	21.037	20.950	20.949	20.945	20.921	#VALUE!	#VALUE!	20 618	20 592	20.595	20.598	20.586	20 605
B1 Horiz. Dist (m) from datum BD:	87.413	87.062	86.726	86.341	86.178	86.078	85 740	85.583	85.495	85.342	#VALUE!	#VALUE!	84.366	84.359	84.352	84 343	84 355	84 339
B2 Vert. Ht (m) from datum BD:	24.322	24 312	24.298	24.251	24.255	24.232	24.183	24.179	24.156	24.132	23.979	23.913	23.916	23.906	23 903	23 871	23.850	23 858
B2 Horiz. Dist (m) from datum BD	96.309	96.245	96.136	95.967	95.912	95.839	95.659	95.640	95.553	95.441	94.846	94.639	94.653	94 639	94 640	94 518	94.487	94.477
B3 Vert. Ht (m) from datum BD:	26.600	26 585	26.545	26.515	26.493	26.474	26.409	26 402	26.383	26.353	26.188	26.139	26.135	26 133	26.128	26.109	26.086	26 100
B3 Horiz. Dist (m) from datum BD:	106.661	106.597	106.504	106 359	106.333	106.257	106.122	106.103	106.057	105.953	105.497	105 377	105.368	105.359	105.364	105.293	105 266	105.252
B4 Vert. Ht (m) from datum BD:	30.807	30 810	30.815	30 872	30.804	30.794	30.812	30.805	30.789	30.792	30.759	30.746	30.740	30.735	30.739	30.733	30.721	30.751
B4 Horiz. Dist (m) from datum BD:	126.960	126.936	126.903	126 854	126.889	126 816	126 789	126.776	126.778	126 752	126 554	126 509	126 489	126 485	126 501	126 465	126 456	126 484

Cummulative Movement

Total Movement from 19/1 to:-	26/1/94	2/2/94	10/2/94	16/2/94	22/2/94	3/3/94	9/3/94	16/3/94	21/3/94	7/4/94	13/4/94	19/4/94	27/4/94	11/5/94	27/5/94	3/6/94	30/6/94
A1 Vert. Movement (m)	-0.012	-0.11	-0.016	-0.015	-0.027	-0.023	-0.023	-0.017	-0.023	-0.023	-0.017	-0.017	-0.021	-0.023	-0.019	-0.025	-0 027
A1 Horiz. Movement (m)	0.009	0.01	0.005	0.003	0.009	0.014	0.015	-0.002	0.005	0.020	0.013	0.015	0.012	0.013	0.023	0.024	0.013
A2 Vert. Movement (m)	-0.153	-0.161	-0.141	-0.145	-0.115	-0.121	-0.118	-0.097	-0.096	-0.044	0.135	0.039	0.032	0.009	0.046	0.055	0.051
A2 Horiz. Movement (m)	0.196	0.39	0.607	0.719	0.79	0.979	1.036	1.098	1.187	1.646	1.838	1.844	1.865	1.880	1.892	1.897	1.910
A3 Vert. Movement (m)	-0.046	0.027	0.154	0.22	0.292	0.411	0.444	0.502	0.544	0.701	0.875	0.877	0.881	0.884	0.893	0.896	0.902
A3 Horiz. Movement (m)	0.324	0.666	1.034	1.259	1.472	1.721	1.833	1.94	2.050	2.607	2.831	2.857	2.863	2.863	2.895	2.891	2.898
A4 Vert. Movement (m)	-0.002	-0.003	0.009	0.005	0.004	0.024	0.021	0.014	0.043	0.053	0.065	0.065	0.069	0.073	0.064	0.074	0.072
A4 Horiz. Movement (m)	0.040	0.085	0.143	0.168	0.188	0.247	0.243	0.259	0.300	0.536	0.591	0 595	0.606	0.605	0 617	0.631	0 622
A5 Vert. Movement (m)	0.009	0.013	0.026	0.015	0.014	0.013	0.014	0.023	0.010	0.016	0.029	0.036	-0.060	0.034	0.030	0.022	0.032
A5 Horiz. Movement (m)	0.016	0.025	0.056	0.068	0.071	0.101	0.117	0.091	0.108	0.213	0.256	0.260	0.267	0.256	0.278	0.269	0.278
B1 Vert. Movement (m)	0.130	0.24	0.395	0.434	0.473	0.56	0.561	0.565	0.589	#VALUE!	#VALUE!	0 000	0.026	0.023	0.020	0.032	0.013
B1 Horiz. Movement (m)	0.351	0.687	1.072	1.235	1.335	1.673	1.83	1.918	2.071	#VALUE!	#VALUE!	0.000	0.007	0.014	0.023	0.011	0.027
B2 Vert. Movement (m)	0.010	0.024	0.071	0.067	0.09	0.139	0.143	0.166	0.190	0.343	0.409	0.406	0.416	0.419	0.451	0.472	0.464
B2 Horiz. Movement (m)	0.064	0.173	0.342	0.397	0.47	0.65	0.669	0.756	0.868	1.463	1.670	1.656	1.670	1.669	1.791	1.822	1.832
B3 Vert. Movement (m)	0.015	0.055	0.085	0.107	0.126	0.191	0.198	0.217	0.247	0.412	0.461	0.465	0.467	0.472	0.491	0.514	0.500
B3 Horiz. Movement (m)	0.064	0.157	0.302	0.328	0.404	0.539	0.558	0.604	0.708	1.164	1.284	1.293	1.302	1.297	1.368	1.395	1.409
B4 Vert. Movement (m)	-0.003	-0.008	-0.065	0.003	0.013	-0.005	0.002	0.018	0.015	0.048	0.061	0.067	0.072	0.068	0.074	0.086	0.056
B4 Horiz. Movement (m)	0.024	0.057	0.106	0.071	0.144	0.171	0.184	0.182	0.208	0.406	0.451	0.471	0.475	0.459	0.495	0 504	0.476

Spreadsheet showing weekly movements

(NB Negative = rise/moving further away)

Movement Between:	19/1/94 26/1/94	26/1/94 2/2/94	2/2/94 10/2/94	10/2/94 16/2/94	16/2/94 22/2/94	22/2/94 3/3/94	3/3/94 9/3/94	9/3/94 16/3/94	16/3/94 21/3/94	21/3/94 7/4/94	7/4/94 13/4/94	13/4/94 19/4/94	19/4/94 27/4/94	27/4/94 11/5/94	11/594 27/5/94	27/5/94 3/6/94	3/6/94 30/6/94
A1 Vert. Movement (m)	-0.012	-0.098	0.094	0.001	-0.012	0.004	0.000	0.006	-0.006	0.000	0.006	0.000	-0.004	-0.002	0.004	-0.006	-0.002
A1 Horiz. Movement (m)	0.009	0.001	-0.005	-0.002	0.006	0.005	0.001	-0.017	0.007	0.015	-0.007	0.002	-0.003	0 001	0.010	0.001	-0.011
A2 Vert. Movement (m)	-0.153	-0.008	0.020	-0.004	0.030	-0.006	0.003	0.021	0.001	0.052	0.179	-0.096	-0.007	-0.023	0.037	0.009	-0 004
A2 Horiz. Movement (m)	0.196	0.194	0.217	0.112	0.071	0.189	0.057	0.062	0.089	0.459	0.192	0.006	0.021	0.015	0.012	0.005	0 013
A3 Vert. Movement (m)	-0.046	0.073	0.127	0.066	0.072	0.119	0.033	0.058	0.042	0.157	0.174	0.002	0.004	0 003	0.009	0.003	0 006
A3 Horiz. Movement (m)	0.324	0.342	0.368	0.225	0.213	0.249	0.112	0.107	0.110	0.557	0.224	0.026	0.006	0.000	0.032	-0.004	0.007
A4 Vert. Movement (m)	-0.002	-0.001	0.012	-0.004	-0.001	0.020	-0.003	-0.007	0.029	0.010	0.012	0.000	0.004	0.004	-0.009	0.010	-0.002
A4 Horiz. Movement (m)	0.040	0.045	0.058	0.025	0.020	0.059	-0.004	0.016	0.041	0.236	0.055	0.004	0.011	-0.001	0.012	0.014	-0.009
A5 Vert. Movement (m)	0.009	0.004	0.013	-0.011	-0.001	-0.001	0.001	0.009	-0.013	0.006	0.013	0.007	-0.096	0.094	-0.004	-0.008	0 010
A5 Horiz. Movement (m)	0.016	0.009	0.031	0.012	0.003	0.030	0.016	-0.026	0.017	0.105	0.043	0.004	0.007	-0.011	0.022	-0.009	0.009
B1 Vert. Movement (m)	0.130	0.110	0.155	0.039	0.039	0.087	0.001	0.004	0.024	n/a	n/a	REINSERT	0.026	-0.003	-0.003	0.012	-0.019
B1 Horiz. Movement (m)	0.351	0.336	0.385	0.163	0.100	0.338	0.157	0.088	0.153	n/a	n/a	REINSERT	0.007	0.007	0.009	-0.012	0.016
B2 Vert. Movement (m)	0.010	0.014	0.047	-0.004	0.023	0.049	0.004	0.023	0.024	0.153	0.066	-0.003	0.010	0.003	0.032	0.021	-0.008
B2 Horiz. Movement (m)	0.064	0.109	0.169	0.055	0.073	0.180	0.019	0.087	0.112	0.595	0.207	-0.014	0.014	-0.001	0.122	0.031	0.010
B3 Vert. Movement (m)	0.015	0.040	0.030	0.022	0.019	0.065	0.007	0.019	0.030	0.165	0.049	0.004	0.002	0.005	0.019	0.023	-0.014
B3 Horiz. Movement (m)	0.064	0.093	0.145	0.026	0.076	0.135	0.019	0.046	0.104	0.456	0.120	0.009	0.009	-0.005	0.071	0.027	0.014
B4 Vert. Movement (m)	-0.003	-0.005	-0.057	0.068	0.010	-0.018	0.007	0.016	-0.003	0.033	0.013	0.006	0.005	-0.004	0.006	0.012	-0.030
B4 Horiz. Movement (m)	0.024	0.033	0.049	-0.035	0.073	0.027	0.013	-0.002	0.026	0.198	0.045	0.020	0.004	-0.016	0.036	0.009	-0.028

APPENDIX III

RECORDS OF GROUND WATER LEVELS FOR THE LANDSLIDE ADJACENT TO SOPER'S WOOD

Borehole A

(emplaced on 18/1/94)

Depth at Emplacement:	c 2.5m																
Date:	26/1/94	2/2/94	10/2/94	16/2/94	22/2/94	3/3/94	9/3/94	16/3/94	23/3/94	7/4/94	13/4/94	19/4/94	27/4/94	5/5/94	27/5/94	3/6/94	30/6/94	3/8/94
Depth to base from tube top,m:	2.70	2.70	2.10	2.13	2.10	2.06	2 00	2.06	2.11	2 07	2.06	1 95	1.97	1.94	2 00	2.00	2 00	2 00
Amnt tube above ground,m:	1.50	1.30	1 05	1.05	1.05	1 06	1.05	1 06	1 05	1.04	0 98	0.96	0.98	0 99	1 01	0 98	0 98	0 98
Depth to water from tube top,m:	1.49	1.44	1.46	1.36	1.39	1.40	1.38	1 36	1.64	1.34	1.34	1.37	1.37	1.59	1.33	1 47	1 64	1 95
Base below ground,m:	1.20	1.40	1.05	1.08	1.05	1.00	0.95	1.00	1.06	1.03	1.08	0.99	0.99	0.95	0.99	1.02	1.02	1.02
Water Table below ground,m:	-0.01	0.14	0.41	0.31	0.34	0.34	0.33	0.30	0.59	0.30	0.36	0.41	0.39	0.60	0.32	0.49	0.66	0.97

Borehole B

(emplaced on 22/1/94)

Depth at Emplacement:	c.2.65m																
Date:	26/1/94	2/2/94	10/2/94	16/2/94	22/2/94	3/3/94	9/3/94	16/3/94	23/3/94	7/4/94	13/4/94	19/4/94	27/4/94	5/5/94	27/5/94	3/6/94	30/6/94	3/8/94
Depth to base from tube top,m:	4.00	1.90	1.69	1.66	1.50	1.18	1.18	2.55	2 39	1 97	2 06	2 03	1.95	2 04	1.98	1.98	1.98	1 98
Amnt tube above ground,m:	1.37	1.28	1.09	0.97	0 88	0.62	0 57	1.99	1.81	1.30	1.33	1.31	1.32	1.32	1.27	1.28	1.33	1 27
Depth to water from tube top,m:	1.93	1 87	1.58	1.31	1.22	0 87	0.75	2.25	No access	1.30	1.34	1.31	1.31	1.51	1 27	1.28	1 58	1 73
Base below ground,m:	2.63	0.62	0.60	0.69	0.62	0.56	0.61	0.56	0.58	0.67	0.73	0.72	0.63	0.72	0.71	0.70	0.65	0.71
Water Table below ground,m:	0.56	0.59	0.49	0.34	0.34	0.25	0.18	0.26	No Reading	0.00	0.01	0.00	-0.01	0.19	0.00	0.00	0.25	0.46

Borehole C

(emplaced on 26/1/94)

Depth at Emplacement:	c 3.0m																
Date:	26/1/93	2/2/94	10/2/94	16/2/94	22/2/94	3/3/94	9/3/94	16/3/94	23/3/94	7/4/94	13/4/94	19/4/94	27/4/94	5/5/94	27/5/94	3/6/94	30/6/94	3/8/94
Depth to base from tube top,m:	just drilled	3 89	3 95	3.77	3.70	3.62	3 60	3 60	3.66	3 50	3 44	3 44	3 60	3.60	3 60	3 60	3 60	2 44
Amnt tube above ground,m:	n/a	1.13	1.12	1.11	1.10	1.13	1.14	1.10	1.12	1 12	1.14	1.13	1.16	1.16	1 16	1.16	1 16	0 00
Depth to water from tube top,m:	n/a	3.28	2.44	2 01	1.65	2.13	2.22	1 46	2.17	dry	1 96	2 44	3 12	3 40	2.21	2 85	dry	1 51
Base below ground,m:	#VALUE!	2.76	2.83	2.66	2.60	2.49	2.46	2.50	2.54	2.38	2.30	2.31	2.44	2.44	2.44	2.44	2.44	2.44
Water Table below ground,m:	#VALUE!	2.15	1.32	0.90	0.55	1.00	1.08	0.36	1.05	faulty reading ?	0.82	1.31	1.96	2.24	1.05	1.69	dry	1.51

Borehole D

(emplaced on 4/2/94)

Depth at Emplacement:	c.2 8m																
Date:	26/1/94	2/2/94	10/2/94	16/2/94	22/2/94	3/3/94	9/3/94	16/3/94	23/3/94	7/4/94	13/4/94	19/4/94	27/4/94	5/5/94	27/5/94	3/6/94	30/6/94	3/8/94
Depth to base from tube top,m:	not drilled	not drilled	2.27	2.29	2.24	2.22	2 24	2.22	2.17	2 21	2 22	2 20	2 20	2.22	2 22	2 22	2 22	0 81
Amnt tube above ground,m:	n/a	n/a	1.35	1.36	1.33	1.37	1.34	1 34	1.35	1.42	1 40	1 37	1 39	1.38	1 36	1 36	1 36	0 00
Depth to water from tube top,m:	n/a	n/a	dry	dry	1 81	1.44	1.40	1.58	1 92	1 93	1 93	dry	dry	dry	1 68	2 09	dry	dry
Base below ground,m:	#VALUE!	#VALUE!	0.92	0.93	0.91	0.85	0.90	0.88	0.82	0.79	0.82	0.83	0.81	0.84	0.86	0.86	0.86	0.81
Water Table below ground,m:	#VALUE!	#VALUE!	dry	dry	0.48	0.07	0.06	0.24	0.57	0.51	0.53	dry	dry	dry	0.32	0.73	dry	dry

Borehole E	(emplaced on 22/1/94)																
Depth at Emplacement:	c.2.6m																
Date:	26/1/94	2/2/94	10/2/94	16/2/94	22/2/94	3/3/94	9/3/94	16/3/94	23/3/94	7/4/94	13/4/94	19/4/94	27/4/94	5/5/94	27/5/94	3/6/94	30/6/94	3/8/94
Depth to base from tube top,m:	3.80	3 61	3.45	3.32	3.19	3.17	3.12	3.11	3 25	3 07	3.07	3 04	3 04	3 04	3 04	3 04	3 04	3 04
Amnt tube above ground,m:	1.47	1.51	1.47	1.47	1 54	1.46	1 45	1.48	1 50	1 54	1.53	1 49	1 55	1 55	1 46	1 46	0 00	0 00
Depth to water from tube top,m:	2 20	2.20	2.19	2.15	2.20	2 23	2.22	2 32	2.34	2.36	2 33	2 39	2.52	2 54	2 27	2 49	1 15	1 21
Base below ground,m:	2.33	2.10	1.98	1.85	1.65	1.71	1.67	1.63	1.75	1.53	1.54	1.55	1.49	1.49	1.58	1.58	3.04	3.04
Water Table below ground,m:	0.73	0.69	0.72	0.68	0.66	0.77	0.77	0.84	0.84	0.82	0.80	0.90	0.97	0.99	0.81	1.03	1.15	1.21
Borehole F	(emplaced on 26/1/94)																	
Depth at Emplacement:	c.3.2m																	
Date:	26/1/94	2/2/94	10/2/94	16/2/94	22/2/94	3/3/94	9/3/94	16/3/94	23/3/94	7/4/94	13/4/94	19/4/94	27/4/94	5/5/94	27/5/94	3/6/94	30/6/94	3/8/94
Depth to base from tube top,m:	just drilled	3 50	3.41	3 30	3.25	3 23	3.16	3.32	3.42	2.21	2.16	2 10	2 09	2 04	2.13	2 13	2 13	2 13
Amnt tube above ground,m:	n/a	0.92	0.93	0.92	0.94	0.91	0 92	0.92	0 92	0 84	0 83	0.83	0 81	0 84	0 82	0 82	0 82	0 82
Depth to water from tube top,m:	n/a	1.26	1.29	1.20	1.28	1 27	1.19	1.23	1.20	1.14	1.12	1 29	1.54	1.73	1.19	1.38	1 02	dry
Base below ground,m:	#VALUE!	2.58	2.48	2.38	2.31	2.32	2.24	2.40	2.50	1.37	1.33	1.27	1.28	1.20	1.31	1.31	1.31	1.31
Water Table below ground,m:	#VALUE!	0.34	0.36	0.28	0.34	0.36	0.27	0.31	0.28	0.30	0.29	0.46	0.73	0.89	0.37	0.56	0.20	dry
Borehole G	(emplaced on 4/2/94)																	
Depth at Emplacement:	c.2.2m																	
Date:	26/1/92	2/2/94	10/2/94	16/2/94	22/2/94	3/3/94	9/3/94	16/3/94	23/3/94	7/4/94	13/4/94	19/4/94	27/4/94	5/5/94	27/5/94	3/6/94	30/6/94	3/8/94
Depth to base from tube top,m:	not drilled	not drilled	4.03	4 00	2.07	1.94	1.96	1.97	2.06	2.05	0 90	0 89	0 90	0 89	0 89	0 89	0 89	0 89
Amnt tube above ground,m:	n/a	n/a	1.89	1.90	0.00	0.00	0.00	0.00	0 00	0.00	0 00	0 00	0 00	0 00	0 00	0 00	0 00	0 00
Depth to water from tube top,m:	n/a	n/a	2.78	2 08	0.22	No access	0 22	0 23	0 28	0 30	0 22	0 34	0 48	0 63	0 21	0 49	dry	dry
Base below ground,m:	#VALUE!	#VALUE!	2.14	2.10	2.07	1.94	1.96	1.97	2.06	2.05	0.90	0.89	0.90	0.89	0.89	0.89	0.89	0.89
Water Table below ground,m:	#VALUE!	#VALUE!	0.89	0.18	0.22	No Reading	0.22	0.23	0.28	0.30	0.22	0.34	0.48	0.63	0.21	0.49	dry	dry
Borehole X	(emplaced on 5/5/94)																	
Depth at Emplacement:	2.28m																	
Date:	26/1/92	2/2/94	10/2/94	16/2/94	22/2/94	3/3/94	9/3/94	16/3/94	23/3/94	7/4/94	13/4/94	19/4/94	27/4/94	5/5/94	27/5/94	3/6/94	30/6/94	3/8/94
Depth to base from tube top,m:	not drilled	not drilled	not drilled	not drilled	not drilled	not drilled	not drilled	not drilled	not drilled	not drilled	not drilled	not drilled	not drilled	not drilled	3 81	3 81	3 81	3 81
Amnt tube above ground,m:	n/a	n/a	n/a	n/a	n/a	n/a	n/a	n/a	n/a	n/a	n/a	n/a	n/a	n/a	1 52	1 52	1 53	1 53
Depth to water from tube top,m:	n/a	n/a	n/a	n/a	n/a	n/a	n/a	n/a	n/a	n/a	n/a	n/a	n/a	n/a	2 29	2 92	3 51	dry
Base below ground,m:	#VALUE!	#VALUE!	#VALUE!	#VALUE!	#VALUE!	#VALUE!	#VALUE!	#VALUE!	#VALUE!	#VALUE!	#VALUE!	#VALUE!	#VALUE!	#VALUE!	2.29	2.29	2.28	2.28
Water Table below ground,m:	#VALUE!	#VALUE!	#VALUE!	#VALUE!	#VALUE!	#VALUE!	#VALUE!	#VALUE!	#VALUE!	#VALUE!	#VALUE!	#VALUE!	#VALUE!	#VALUE!	0.77	1.40	1.98	dry

Borehole Y	(emplaced on 5/5/94)																	
Depth at Emplacement:	c.2 8m																	
Date:	26/1/92	2/2/94	10/2/94	16/2/94	22/2/94	3/3/94	9/3/94	16/3/94	23/3/94	7/4/94	13/4/94	19/4/94	27/4/94	5/5/94	27/5/94	3/6/94	30/6/94	3/8/94
Depth to base from tube top,m:	not drilled	not drilled	not drilled	not drilled	not drilled	not drilled	not drilled	not drilled	not drilled	not drilled	not drilled	not drilled	not drilled	not drilled	3 98	3 98	3 98	3 98
Amnt tube above ground,m:	n/a	n/a	n/a	n/a	n/a	n/a	n/a	n/a	n/a	n/a	n/a	n/a	n/a	n/a	1.21	1.22	1 22	1 22
Depth to water from tube top,m:	n/a	n/a	n/a	n/a	n/a	n/a	n/a	n/a	n/a	n/a	n/a	n/a	n/a	n/a	1 59	1.61	dry	dry
Base below ground,m:	#VALUE!	#VALUE!	#VALUE!	#VALUE!	#VALUE!	#VALUE!	#VALUE!	#VALUE!	#VALUE!	#VALUE!	#VALUE!	#VALUE!	#VALUE!	#VALUE!	2.77	2.76	2.76	2.76
Water Table below ground,m:	#VALUE!	#VALUE!	#VALUE!	#VALUE!	#VALUE!	#VALUE!	#VALUE!	#VALUE!	#VALUE!	#VALUE!	#VALUE!	#VALUE!	#VALUE!	#VALUE!	0.38	0.39	dry	dry

Borehole Z	(emplaced on 6/5/94)																	
Depth at Emplacement:	c.2.78m																	
Date:	26/1/92	2/2/94	10/2/94	16/2/94	22/2/94	3/3/94	9/3/94	16/3/94	23/3/94	7/4/94	13/4/94	19/4/94	27/4/94	5/5/94	27/5/94	3/6/94	30/6/94	3/8/94
Depth to base from tube top,m:	not drilled	not drilled	not drilled	not drilled	not drilled	not drilled	not drilled	not drilled	not drilled	not drilled	not drilled	not drilled	not drilled	not drilled	3.98	3 98	3 53	3 53
Amnt tube above ground,m:	n/a	n/a	n/a	n/a	n/a	n/a	n/a	n/a	n/a	n/a	n/a	n/a	n/a	n/a	1.23	1 24	1 25	1 26
Depth to water from tube top,m:	n/a	n/a	n/a	n/a	n/a	n/a	n/a	n/a	n/a	n/a	n/a	n/a	n/a	n/a	1 49	1 79	2 26	2 36
Base below ground,m:	#VALUE!	#VALUE!	#VALUE!	#VALUE!	#VALUE!	#VALUE!	#VALUE!	#VALUE!	#VALUE!	#VALUE!	#VALUE!	#VALUE!	#VALUE!	#VALUE!	2.75	2.74	2.28	2.27
Water Table below ground,m:	#VALUE!	#VALUE!	#VALUE!	#VALUE!	#VALUE!	#VALUE!	#VALUE!	#VALUE!	#VALUE!	#VALUE!	#VALUE!	#VALUE!	#VALUE!	#VALUE!	0.26	0.55	1.01	1.10

Borehole W	(emplaced on 6/5/94)																	
Depth at Emplacement:	c.2 55m																	
Date:	26/1/92	2/2/94	10/2/94	16/2/94	22/2/94	3/3/94	9/3/94	16/3/94	23/3/94	7/4/94	13/4/94	19/4/94	27/4/94	5/5/94	27/5/94	3/6/94	30/6/94	3/8/94
Depth to base from tube top,m:	not drilled	not drilled	not drilled	not drilled	not drilled	not drilled	not drilled	not drilled	not drilled	not drilled	not drilled	not drilled	not drilled	not drilled	3 98	3 98	3 98	3 98
Amnt tube above ground,m:	n/a	n/a	n/a	n/a	n/a	n/a	n/a	n/a	n/a	n/a	n/a	n/a	n/a	n/a	1.45	1 50	1 47	1 47
Depth to water from tube top,m:	n/a	n/a	n/a	n/a	n/a	n/a	n/a	n/a	n/a	n/a	n/a	n/a	n/a	n/a	1 61	2.30	3 02	dry
Base below ground,m:	#VALUE!	#VALUE!	#VALUE!	#VALUE!	#VALUE!	#VALUE!	#VALUE!	#VALUE!	#VALUE!	#VALUE!	#VALUE!	#VALUE!	#VALUE!	#VALUE!	2.53	2.48	2.51	2.51
Water Table below ground,m:	#VALUE!	#VALUE!	#VALUE!	#VALUE!	#VALUE!	#VALUE!	#VALUE!	#VALUE!	#VALUE!	#VALUE!	#VALUE!	#VALUE!	#VALUE!	#VALUE!	0.16	0.80	1.55	dry

Borehole U	(emplaced on 6/5/94)																	
Depth at Emplacement:	2 86m																	
Date:	26/1/92	2/2/94	10/2/94	16/2/94	22/2/94	3/3/94	9/3/94	16/3/94	23/3/94	7/4/94	13/4/94	19/4/94	27/4/94	5/5/94	27/5/94	3/6/94	30/6/94	3/8/94
Depth to base from tube top,m:	not drilled	not drilled	not drilled	not drilled	not drilled	not drilled	not drilled	not drilled	not drilled	not drilled	not drilled	not drilled	not drilled	not drilled	3 98	3 98	3 98	3 98
Amnt tube above ground,m:	n/a	n/a	n/a	n/a	n/a	n/a	n/a	n/a	n/a	n/a	n/a	n/a	n/a	n/a	1 11	1 11	1 11	1 11
Depth to water from tube top,m:	n/a	n/a	n/a	n/a	n/a	n/a	n/a	n/a	n/a	n/a	n/a	n/a	n/a	n/a	2 40	dry	dry	dry
Base below ground,m:	#VALUE!	#VALUE!	#VALUE!	#VALUE!	#VALUE!	#VALUE!	#VALUE!	#VALUE!	#VALUE!	#VALUE!	#VALUE!	#VALUE!	#VALUE!	#VALUE!	2.87	2.87	2.87	2.87
Water Table below ground,m:	#VALUE!	#VALUE!	#VALUE!	#VALUE!	#VALUE!	#VALUE!	#VALUE!	#VALUE!	#VALUE!	#VALUE!	#VALUE!	#VALUE!	#VALUE!	#VALUE!	1.29	dry	dry	dry

Borehole T	(emplaced on 7/5/94)																	
Depth at Emplacement:	c.2 0m																	
Date:	26/1/92	2/2/94	10/2/94	16/2/94	22/2/94	3/3/94	9/3/94	16/3/94	23/3/94	7/4/94	13/4/94	19/4/94	27/4/94	5/5/94	27/5/94	3/6/94	30/6/94	3/8/94
Depth to base from tube top,m:	not drilled	not drilled	not drilled	not drilled	not drilled	not drilled	not drilled	not drilled	not drilled	not drilled	not drilled	not drilled	not drilled	not drilled	2 70	2 70	2 70	2 70
Amnt tube above ground,m:	n/a	n/a	n/a	n/a	n/a	n/a	n/a	n/a	n/a	n/a	n/a	n/a	n/a	n/a	0 71	0 71	0 74	0 74
Depth to water from tube top,m:	n/a	n/a	n/a	n/a	n/a	n/a	n/a	n/a	n/a	n/a	n/a	n/a	n/a	n/a	0 91	0 92	1 43	1 60
Base below ground,m:	#VALUE!	#VALUE!	#VALUE!	#VALUE!	#VALUE!	#VALUE!	#VALUE!	#VALUE!	#VALUE!	#VALUE!	#VALUE!	#VALUE!	#VALUE!	#VALUE!	1.99	1.99	1.96	1 96
Water Table below ground,m:	#VALUE!	#VALUE!	#VALUE!	#VALUE!	#VALUE!	#VALUE!	#VALUE!	#VALUE!	#VALUE!	#VALUE!	#VALUE!	#VALUE!	#VALUE!	#VALUE!	0.20	0.21	0.69	0 86

APPENDIX IV

ENGINEERING GEOMORPHOLOGICAL MAP OF THE LANDSLIDE ADJACENT TO SOPER'S WOOD

UNIVERSITY OF BRISTOL LIBRARY

ENGINEERING GEOMORPHOLOGICAL MAP OF THE LANDSLIDE AT SOPER'S WOOD JANUARY 1994

COLLIERS LANE

FENCE

GATE

N

0 20m

A1 A2 A3 A4 A5

B1 B2 B3 B4

C

D

E

F

G

FENCE